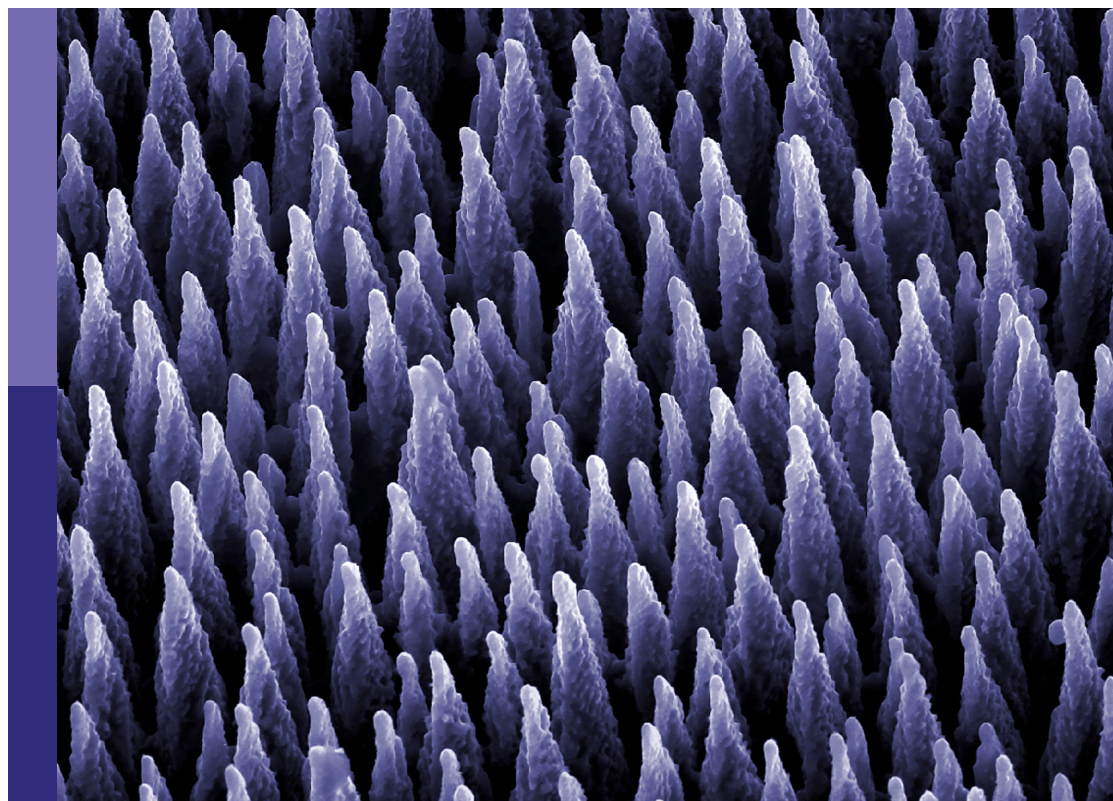# Sustainable fiber reinforced cementitious composites for construction and building materials

Edited by
Li Li, Mehran Khan, Xi Jiang, Pshtiwan Shakor and
Yangyang Zhang

Published in
Frontiers in Materials

About Frontiers

Frontiers is more than just an open access publisher of scholarly articles: it is a pioneering approach to the world of academia, radically improving the way scholarly research is managed. The grand vision of Frontiers is a world where all people have an equal opportunity to seek, share and generate knowledge. Frontiers provides immediate and permanent online open access to all its publications, but this alone is not enough to realize our grand goals.

Frontiers journal series

The Frontiers journal series is a multi-tier and interdisciplinary set of open-access, online journals, promising a paradigm shift from the current review, selection and dissemination processes in academic publishing. All Frontiers journals are driven by researchers for researchers; therefore, they constitute a service to the scholarly community. At the same time, the *Frontiers journal series* operates on a revolutionary invention, the tiered publishing system, initially addressing specific communities of scholars, and gradually climbing up to broader public understanding, thus serving the interests of the lay society, too.

Dedication to quality

Each Frontiers article is a landmark of the highest quality, thanks to genuinely collaborative interactions between authors and review editors, who include some of the world's best academicians. Research must be certified by peers before entering a stream of knowledge that may eventually reach the public – and shape society; therefore, Frontiers only applies the most rigorous and unbiased reviews. Frontiers revolutionizes research publishing by freely delivering the most outstanding research, evaluated with no bias from both the academic and social point of view. By applying the most advanced information technologies, Frontiers is catapulting scholarly publishing into a new generation.

What are Frontiers Research Topics?

Frontiers Research Topics are very popular trademarks of the *Frontiers journals series*: they are collections of at least ten articles, all centered on a particular subject. With their unique mix of varied contributions from Original Research to Review Articles, Frontiers Research Topics unify the most influential researchers, the latest key findings and historical advances in a hot research area.

Find out more on how to host your own Frontiers Research Topic or contribute to one as an author by contacting the Frontiers editorial office: frontiersin.org/about/contact

Sustainable fiber reinforced cementitious composites for construction and building materials

Topic editors

Li Li — Northwest A & F University, China

Mehran Khan — Hong Kong Polytechnic University, SAR China

Xi Jiang — The University of Tennessee, Knoxville, United States

Pshtiwan Shakor — Sulaimani Polytechnic University, Iraq

Yangyang Zhang — Yanshan University, China

Table of
contents

Editorial: Sustainable fiber reinforced cementitious composites for construction and building materials

Li Li[1,2]*, Mehran Khan[3]*, Xi Jiang[4], Pshtiwan Shakor[5] and Yangyang Zhang[6]

[1]Shaanxi Key Laboratory of Safety and Durability of Concrete Structures, Xijing University, Xi'an, China, [2]College of Water Resources and Architectural Engineering, Northwest A&F University, Yangling, China, [3]School of Civil Engineering, University College Dublin, Dublin, Ireland, [4]Department of Civil and Environmental Engineering, University of Tennessee, Knoxville, TN, United States, [5]Technical College of Engineering, Sulaimani Polytechnic University, Sulaymaniyah, Iraq, [6]State Key Laboratory of Metastable Materials Science and Technology, Yanshan University, Qinhuangdao, China

Editorial on the Research Topic
Sustainable fiber reinforced cementitious composites for construction and building materials

Sustainable composites reinforced with fibers have gained significant attention in the construction sector, owing to their remarkable strength, long-lasting properties, and positive environmental impact. This editorial presents a summary of recent scientific papers focusing on diverse facets of sustainable composites.

Progress in the realm of ultra-high-performance concrete (UHPC) technology has led to notable enhancements in its characteristics, including exceptional compressive and tensile strength, ductility, and durability (Alkadhim et al.). Nevertheless, there are still hurdles to overcome concerning the cost-effectiveness and sustainability of UHPC when incorporating steel fibers. Sustainable fibrous high-strength concrete (SFHSC) demonstrates promise as a material, although additional research is necessary to understand the impact of thermal cycles on its engineering properties and long-term durability (Hakeem et al.).

The utilization of machine learning algorithms in construction materials research is on the rise (Qian et al.). Khan et al. have demonstrated that these algorithms have the capability to effectively forecast the ultrasonic pulse velocity of hybrid fiber-reinforced concrete that has been modified with nano-silica. Moreover, they can be employed to assess the performance of high-strength concrete in challenging environments (Chen et al.).

The application of scientometric analysis offers valuable insights into the patterns and advancements within a specific research domain. A recent study conducted by Mohamad Moasas et al. examining mineral fiber reinforced concrete (MFRC) revealed a consistent growth in research activities related to this field over the last decade. Nevertheless, further research is warranted to enhance the durability and sustainability aspects of MFRC.

In the context of environmental sustainability, the significance of recycling plastic waste is steadily rising. A recent research study by Qaidi et al. delved into the application of recycled polyethylene terephthalate (PET) plastic waste as a substitute for sand in high-strength concrete. The findings revealed that this substitution positively impacted the mechanical and durability properties of the concrete. Likewise Nikhade et al. (2023) have explored the viability of sugar cane bagasse ash (SCBA) as an environmentally friendly substitute for conventional concrete materials. SCBA is a by-product of the sugar cane industry and shows promise as a sustainable alternative. In recent studies, the performance of a composite geomaterial incorporating SCBA has been examined under compressive and flexural loading conditions. The research findings indicated notable enhancements in the mechanical properties of the composite material.

Concrete structures are often reinforced using carbon fiber reinforced polymer (CFRP), a widely adopted fiber material. Current research efforts are concentrated on constructing models specific to CFRP-confined concrete-filled steel columns featuring elliptical cross-sections (Isleem et al.). The aim is to enhance the precision of predicting the structural behavior under diverse loading conditions for such columns. Ahmad et al. have explored bio-deposition techniques as a potential method for integrating recycled aggregates into concrete structures. The findings have shown promise in enhancing the strength and durability of concrete made with recycled aggregates.

Ternary hybrid fibers have emerged as a promising substitute for conventional fiber materials in reinforcing concrete structures. Abed et al. have demonstrated that the inclusion of ternary hybrid fibers resulted in notable improvements in both the strength and ductility of ultrahigh strength concrete. In grouting materials, the use of mineral admixtures is widespread to augment their strength and durability. Current research endeavors have focused on examining the influence of various mineral admixtures on the operational and mechanical characteristics of grouting materials (Shen et al.).

In summary, the articles addressed in this editorial underscore the necessity for continued research in multiple areas. These include the exploration of sustainable alternatives to conventional materials, the enhancement of durability in sustainable composites under challenging circumstances, the optimization of recycled material utilization, and the improvement of cost-effectiveness and sustainability in material practices. Applying machine learning algorithms and employing scientometric analysis can yield valuable insights into the aforementioned research domains. Promising alternatives to traditional materials include recycling plastic waste and utilizing by-products like sugar cane bagasse ash. Furthermore, innovative methodologies like bio-deposition and the utilization of ternary hybrid fibers demonstrate promising potential for enhancing the strength and durability of sustainable composites. Ultimately, persistent research and development within this realm have the capacity to yield more resilient and sustainable structures that positively impact both the environment and society.

Author contributions

Conceptualization, methodology, investigation, formal analysis, writing—original draft, writing—review and editing, supervision, funding acquisition, LL; methodology, investigation, formal anal-ysis, writing—original draft, writing—review and editing, supervision. MK; resources, XJ; resources. PS; resources, YZ. All authors contributed to the article and approved the submitted version.

Acknowledgments

Conflict of interest

The authors declare that the research was conducted in the absence of any commercial or financial relationships that could be construed as a potential conflict of interest.

Publisher's note

All claims expressed in this article are solely those of the authors and do not necessarily represent those of their affiliated organizations, or those of the publisher, the editors and the reviewers. Any product that may be evaluated in this article, or claim that may be made by its manufacturer, is not guaranteed or endorsed by the publisher.

Reference

Nikhade, H., Birali, R. R. L., Ansari, K., Khan, M. A., Najm, H. M., Anas, S., et al. (2023). Behavior of geomaterial composite using sugar cane bagasse ash under compressive and flexural loading. *Front. Mater.* 10, 1108717. doi:10.3389/fmats.2023.1108717

An overview of progressive advancement in ultra-high performance concrete with steel fibers

Hassan Ali Alkadhim[1], Muhammad Nasir Amin[1]*,
Waqas Ahmad[2], Kaffayatullah Khan[1], Umbreen-us-Sahar[3],
Mohammed Najeeb Al-Hashem[1] and Abdullah Mohamed[4]

[1]Department of Civil and Environmental Engineering, College of Engineering, King Faisal University, Al-Ahsa, Saudi Arabia, [2]Department of Civil Engineering, COMSATS University Islamabad, Abbottabad, Pakistan, [3]Civil Engineering Department, University of Engineering and Technology, Lahore, Pakistan, [4]Research Centre, Future University in Egypt, New Cairo, Egypt

A progressive advance in the construction sector is attained by employing ultra-high performance concrete (UHPC) technology. Rigorous efforts have been made in this research domain to have remarkable quality levels with 150 MPa or more strength and significant durability, which was impossible previously. Steel fiber incorporation in UHPC is vital in improving its mechanical characteristics. This review on the incorporation of steel fibers in UHPC evaluates, identifies, and synthesizes research outcomes for creating a summary of current evidence that can contribute to evidence-based practice. This study summarized a review of the literature on steel fibers' effect on UHPC, intending to explore its essential aspects. The aim is to summarize the literature in this research domain and provide guidance for future research. Moreover, the basic requirements and materials, mixing and casting, mechanical properties, modern applications, advantages and disadvantages, and future perspectives associated with steel fibers reinforced UHPC in the construction sector are discussed. It is revealed from the conducted analysis that the most widely applied keyword is "steel fibers." Due to the graphical illustration of the contributing studies, the current work may benefit academic scholars in sharing novel techniques and ideas and establishing collaborative efforts. Furthermore, the present work reveals that steel fibers have the potential to enhance the mechanical properties of UHPC; however, the large-scale production and applications of steel fiber-reinforced UHPC are controlled by parameters like fiber content and geometry.

KEYWORDS

steel fiber, mechanical properties, concrete, fiber, fiber-reinforced composite

Introduction

Concrete is among the most frequently and widely utilized building construction materials globally. However, due to the natural properties of concrete, it bears a few shortcomings like less tensile resistance, more brittleness, lower strain capacity, and less resistance toward crack initiation and propagation (Huang et al., 2022). To cater such issues, the addition of fibers like synthetic fibers (Qin et al., 2019; Ahmed and Lim, 2021b; Rezaie et al., 2021; Meng et al., 2022), metallic/steel fibers (Zhang et al., 2020), natural fibers (Khan et al., 2018b; Farooqi and Ali, 2019; Ahmad W. et al., 2020; Farooqi and Ali, 2022), and mineral fibers (Khan et al., 2018a; Ahmed and Lim, 2021a; Akbar and Liew, 2021; Khan et al., 2021; Khan et al., 2022a), in concrete is usually made (Cao et al., 2020; Li et al., 2020; Ye et al., 2021) to improve its toughness (Khan et al.). The fiber incorporation into concrete started back in the early 1960s. The fiber-reinforced concrete (FRC) concept with a theory of fiber spacing was first proposed by Batson (Zollo, 1997). With the growing demand for durable and high-strength concrete, ultra-high performance concrete (UHPC), introduced in the 1990s, has excellent mechanical characteristics and a highly dense microstructure (Shi et al., 2015). The significant resistance against crack generation and further propagation are offered by adding fibers in concrete (Ahmad J. et al., 2020; Shi et al., 2022). Figure 1 depicts the different shapes of steel fibers considered dispersed reinforcement in UHPC by various researchers, as presented by Sidodikromo et al. (2019).

UHPC is a cementitious material with higher strength and durability. It is a potentially practical solution to enhance the performance and sustainability of building elements and infrastructure components (Bahari et al., 2018; Bahari et al., 2021; Dabbaghi et al., 2021; Bahari et al., 2022). In the last 2 decades, UHPC has gained attention in several countries with its possible applications in bridges, building components, repair and rehabilitation, architectural features, cladding, and vertical elements like windmill and utility towers, offshore structures, the oil and gas industry, overlay materials, and hydraulic structures (Tayeh et al., 2013a; Voo et al., 2017; Zhang et al., 2021). In all these mentioned applications, bridge and road construction using UHPC is more frequent in practice. UHPC is utilized in various countries like the United States (US), China, Austria, Canada, the Czech Republic, Australia, Germany, France, Italy, Malaysia, Japan, New Zealand, the Netherlands, South Korea, and Switzerland (Voo et al., 2017; Aisheh et al., 2022; Aslam et al., 2022). The available design codes for typical concrete manufacturing are not meant for UHPC. Different countries, including Australia (Gowripalan and Gilbert, 2000), Germany (Brühwiler, 2016), Spain (López et al., 2017), Canada (Perry and Habel, 2017), Japan (JSCE, 2004), and Switzerland (Brühwiler, 2016), are developing UHPC design guidelines. The non-availability of design codes, insufficient information on raw materials and manufacturing methods, and higher overall

FIGURE 1
Steel fiber shapes considered for incorporation in UHPC (Sidodikromo et al., 2019).
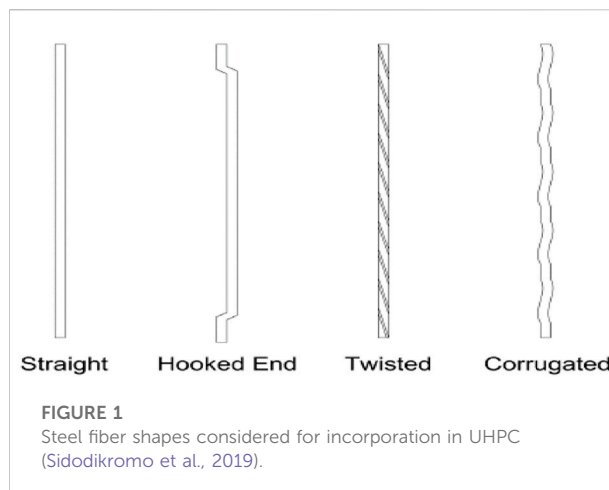
costs seem to restrict the practical implementation of this exceptional material in addition to already developed projects (Vande Voort et al., 2008; Lei et al., 2012; Nematollahi et al., 2012; Voo et al., 2017). The public and private sectors are paying significant attention to extensive efforts to utilize this promising material (Alwesabi et al., 2020; Abadel et al., 2022; Alwesabi et al., 2022).

The current study's review is conducted to explore the steel fibers' effect on the UHPC key characteristics. The steel fiber characteristics that influence the UHPC matrix to fiber bonding mechanism include the orientation of fibers and their distribution, resistance to pullout, and the bonding zone microstructure are elaborated in addition to the impact of shapes, length, and hybridization of steel fibers on mechanical properties, failure mode, durability, and autogenous shrinkage of UHPC. As research on steel fibers reinforced UHPC enhances an urge to achieve high-strength concrete, researchers face limitations on the information that restricts novel research and collaborations. Therefore, it is critical to establish and execute a scheme that aids researchers in acquiring important and necessary information from highly authentic sources. The current study focuses on the review of bibliographic published data on steel fiber-reinforced UHPC. The present study's findings would help young researchers exchange state-of-the-art ideas and procedures and establish joint ventures. In light of the conducted literature review, the current research discusses and emphasizes the steel fiber-reinforced UHPC basic requirements and materials, mixing and casting, mechanical properties, modern applications, advantages and disadvantages, and its future perspectives.

Review strategy

In this study, a detailed review methodology is carried out to retrieve data from the available relevant literature for keyword

FIGURE 2
Sequence of the review method.

TABLE 1 Leading 20 frequently used keywords in the relevant research domain.

S/N	Keyword	Occurrence
1	Steel fiber	645
2	Ultra-high performance concrete	302
3	Compressive strength	248
4	Ultra-high performance concrete (UHPC)	218
5	UHPC	179
6	Concretes	108
7	Steel fiber	83
8	Mechanical properties	78
9	Bending strength	72
10	Silica fume	53
11	Durability	52
12	Fiber-reinforced concrete	48
13	Mixtures	48
14	Cements	47
15	Aggregates	46
16	Ultra-high performance fiber-reinforced concrete	43
17	Microstructure	39
18	Bond strength	39
19	Scanning electron microscopy	36
20	Flexural behavior	30

analysis. Numerous publications relevant to the steel fiber-reinforced UHPC domain are available, and difficulty is usually faced in the selection of a reliable search engine. Scopus and Web of Science are the two most reliable and dependent search engines (Zhang et al., 2022). The highly recommended search engine, that is, Scopus (Amin et al., 2022), is used in this research to retrieve the bibliographic data on steel fiber-reinforced UHPC. The needless documents are excluded by using several screening filters. An inclusive methodical flowchart representing all the performed steps is shown in Figure 2. It is interesting to see the progressive concentration of academic research on using steel fibers in UHPC. Furthermore, in pursuance of a review study regarding most related articles and critical review analysis, the primary elements of steel fiber-reinforced UHPC research are highlighted and illustrated in the succeeding sections. Keywords are vital in research as they distinguish and emphasize the primary theme of a particular research study (Song et al., 2021). The keyword minimum repetition criteria are set at 30. A total of 20 keywords are shortlisted this way, as provided in Table 1. Steel fibers, ultra-high performance concrete, and compressive strength are the three frequently used keywords in the steel fiber-reinforced UHPC research field. It is extracted from keyword analysis that steel fibers in UHPC have been studied to achieve enhanced compressive strength.

Figure 3 shows a map for occurrence frequency based on connections and density. Here again, the dimensions of the frame for a specific keyword (Figure 3A) depict the frequency of the keyword, and the frame position shows its co-occurrence in papers. Furthermore, the frame size is comparatively larger for leading keywords than others, as shown in the graph, indicating their importance for the exploration of research on steel fiber-reinforced UHPC. The representation of keyword co-occurrences in different publications is made by clustering. Multiple colors are allocated to every individual cluster to signify the keywords' co-occurrences in published articles. The different color shades are used to illustrate four distinct groups (Figure 3A). Similarly, different unique colors represent keyword density concentrations (Figure 3B). The color shades are organized according to density, with red being employed for maximum density followed by yellow, green, and blue shades depicting subsequently lesser densities. Steel fibers, ultra-high performance concrete, UHPC, and other noteworthy keywords are shown in red or yellow shades, indicating their higher density of occurrences. This conclusion will aid young scientists in opting for keywords that can minimize the efforts required for exploring this specific research area-related publication.

Basic requirements of UHPC

Figure 4 shows the basic requirements of UHPC, as reported by Mishra and Singh (2019). Shi et al. (2015) reported the main factors for preparing UHPC: porosity reduction, enhanced fresh
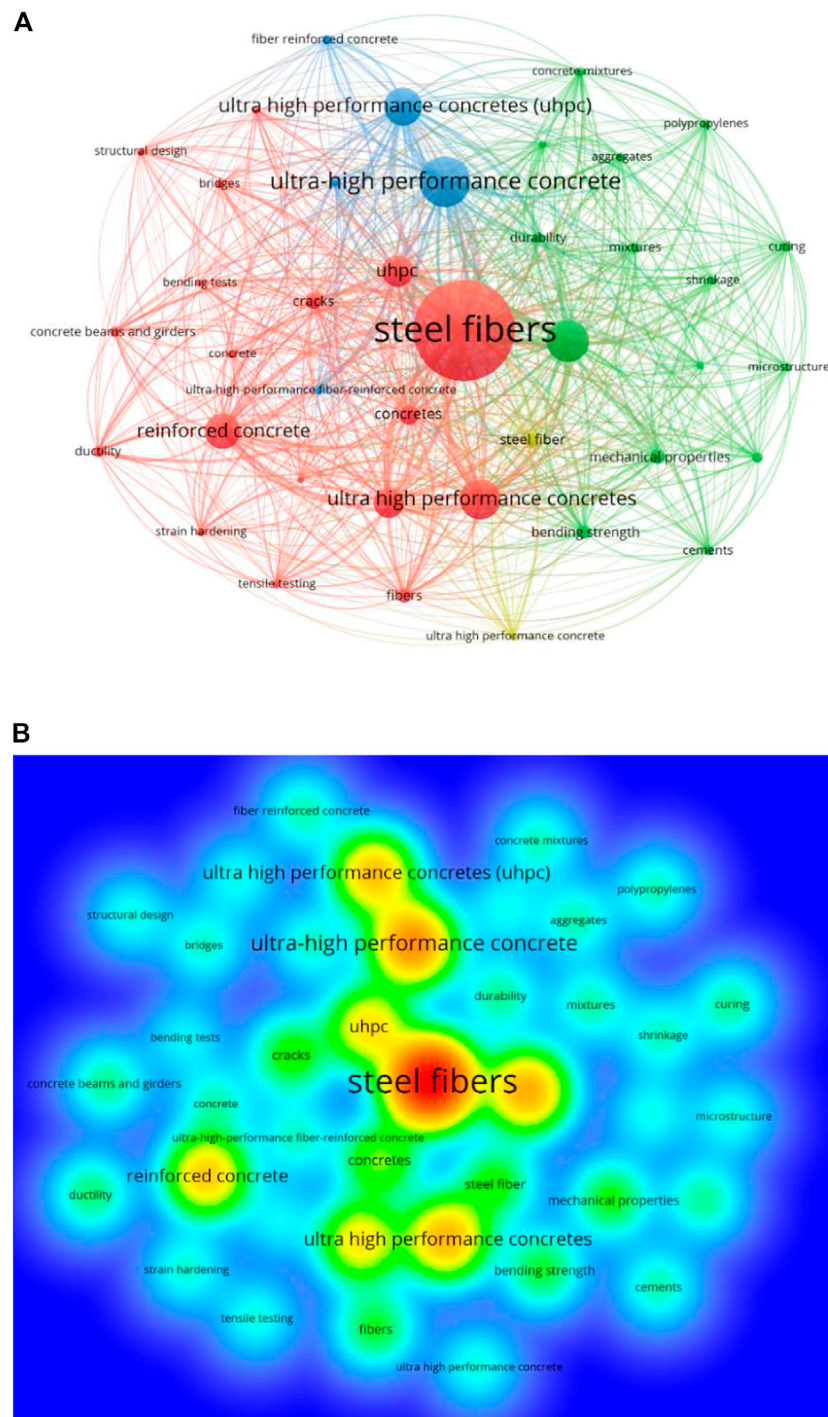
FIGURE 3
Keyword analysis: **(A)** scientific visualization and **(B)** density visualization.

paste homogeneity, and improved microstructure. The parameters are closely linked with the raw materials and mix design for UHPC. The impact of additives, like silica fume (Yazıcı, 2007), rice husk ash (Van Tuan et al., 2011b), nano-

particle (Rong et al., 2015; Wu et al., 2017a), limestone powder (Yu et al., 2015a), and fly ash (Chen et al., 2019; Li G. et al., 2022), in addition to raw materials, on UHPC has been extensively investigated in various studies. For UHPC mix design, several

FIGURE 4
Basic requirements of UHPC.
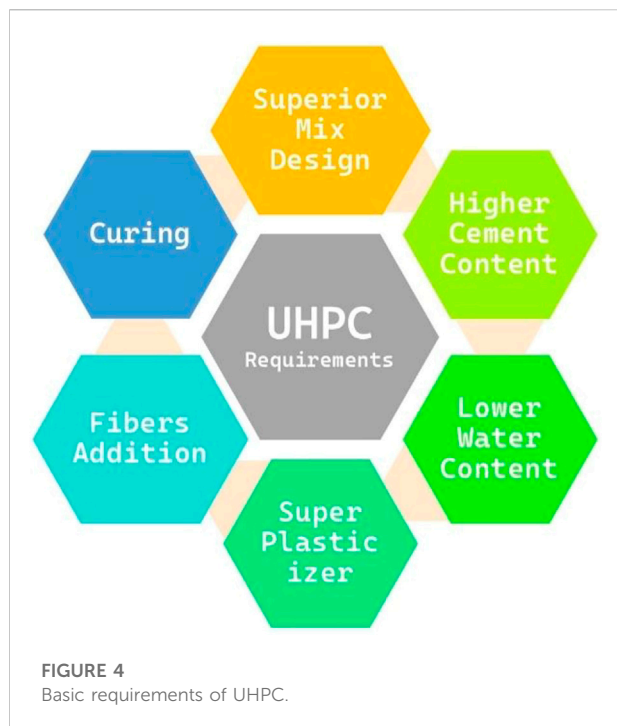
techniques are suggested, such as the compressive packing model (CPM) (De Larrard and Sedran, 2002), the linearly packing density model (LPDM) (Stovall et al., 1986), and the Aim and Goff model (Sohail et al., 2018). In recent years, the most famous UHPC mix design model is the Andreasen and Andersen model (AAM) (Yu et al., 2014b; Yu et al., 2015a; Dingqiang et al., 2021; Du et al., 2021). Figure 5 shows the dense particle packing mechanism in UHPC, as presented by Abu-Lebdeh et al. (2022).

Furthermore, in terms of materials for UHPC, its compressive strength is more highly influenced by the variation in cement than any other ingredient. Cement of higher quality is an important requirement for consistently manufacturing uniform UHPC (Ahmad et al., 2021). In addition to cement, silica fume also possesses pozzolanic characteristics, making it vital for manufacturing UHPC. It is extracted from ferrocenium alloy production (Wetzel and Middendorf, 2019). Silica fume results in an enhanced interfacial transition zone (ITZ) between aggregates and cement paste (Rossignolo, 2007). The optimum content of silica fume is dependent on the water–binder ratio (Máca et al., 2014), which is reported to be between 20% and 30% by mass of cement, by Chan and Chu (2004). To improve the rheology of UHPC, nano-particles such as nano-silica (nano-SiO_2), nano-iron (nano-Fe_2O_3), nano-titanium oxide (nano-TiO_2), and nano-$CaCO_3$ are used to fill the spaces among paste agglomerates and physical contact sites (Qian, 2017). High-range polycarboxylate-based water-reducing agents are also considered for UHPC to have a lower water–binder ratio (Schröfl et al., 2012). The suitable range of these polycarboxylate-based superplasticizers is 2.0%–3.5% by weight of the binder. As far as aggregates are concerned for UHPC, the mineralogy, surface texture, and shape of aggregates influence the overall requirement for mixing water. The coarse aggregates larger than 4.75 mm are usually avoided for UHPC to sidestep the negative influence of their angularity on particle packing density and to achieve a stronger interfacial transition zone (Richard and Cheyrezy, 1995; Alkaysi et al., 2016; Li et al., 2018). In UHPC, the quartz sand should preferably be replaced with river sand (Soliman and Tagnit-Hamou, 2016). However, in river sand, the size range of particles is 0–4.75 mm, in which the maximum particle size is 5–8 times that of quartz sand, which may lead to reduced particle packing density. In this scenario, the finer masonry sand with a size of up to 2 mm extracted by grinding and crushing the coarse aggregates, was recommended by Meng et al. (2017) for improving the packing of particles. The higher particle angularity of river sand may reduce the UHPC's workability (Yang et al., 2009). Hence, the packing particles should be optimized using the aforementioned fine aggregates. The percentage distribution of aggregates in conventional concrete and UHPC is shown in Figure 6, as presented by Sidodikromo et al. (2019).

FIGURE 5
Particle packing mechanism in the UHPC (Abu-Lebdeh et al., 2022).

FIGURE 6
Percentage contents of aggregates in normal strength concrete (NSC) and UHPC (Sidodikromo et al., 2019).

FIGURE 7
Schematic composition (not to scale) of fiber-reinforced UHPC (taken from Park et al. (2015)).
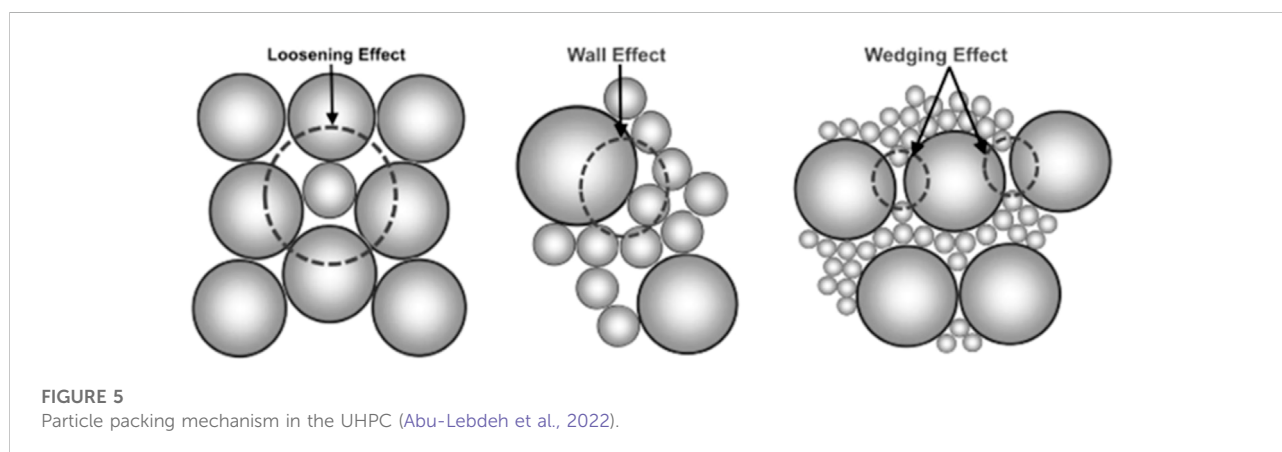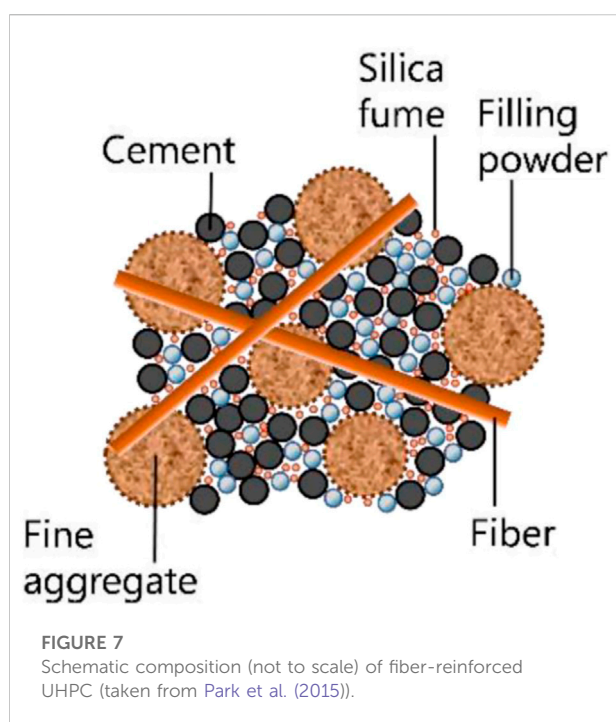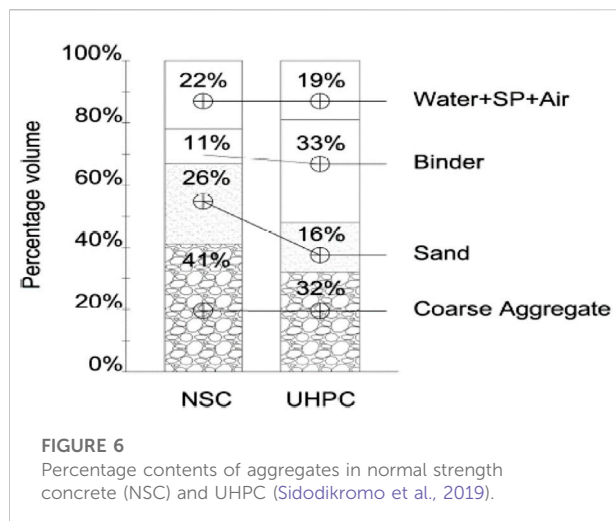
The fiber addition in UHPC is important for attaining improved mechanical characteristics (Li et al., 2021). The schematic composition of fiber-reinforced UHPC, as devised by the Korea Institute of Civil Engineering and Building Technology (KCI-M-12-003, 2012), is shown in Figure 7. Out of all fibers, the most widely utilized fibers in UHPC are steel fibers due to their exceptional mechanical characteristics. UHPC is exceptionally brittle due to its high homogeneity and strength, so this brittleness may be reduced by incorporating steel fibers (Wang et al., 2015). Abbas et al. (2015) reported improved compressive properties, such as tensile behavior and peak load, of UHPC with more steel fiber content. Wille, Naaman [47] concluded that UHPC's 28-day compressive strength was enhanced up to 292 MPa upon incorporating steel fibers up to 8% volumetric content. Significant improvements in deflection under peak flexural loading and corresponding strength were observed in UHPC upon the incorporation of steel fibers (Niu et al., 2019). Incorporating steel fibers in UHPC with up to 3% volumetric content provides uniform fiber dispersion and acceptable workability. The UHPC flowability was improved by incorporating quartz and limestone as replacements, as investigated by Yu et al. (2014b). It was reported in the study that with the increasing content of steel fibers, the flowability decreased. Similarly, in a study by Wu et al. [38], a 21.4% reduction in UHPC flowability was reported upon adding straight steel fibers upon enhancing the volumetric fiber content from 1% to 3% having 0.02% content of the superplasticizer. It might be because more steel fiber content enhanced the contact surface between fibers and matrix, resulting in reduced workability and cohesive force (Yu et al., 2014b; Xu et al., 2019; Gul et al., 2021). Moreover, the flowability reduction is more significant when incorporating steel fibers with a higher aspect ratio (Cao et al., 2019).

In past research, it has been reported that the fiber shapes also considerably influence the UHPC flowability (Soliman and Nehdi, 2014; Abbas et al., 2015; Meng and Khayat, 2018). Table 2 illustrates the four unique steel fiber shapes usually incorporated in UHPC. The UHPC flowability can be further decreased by using deformed steel fibers instead of straight ones. Wu et al. (2016b) reported a 21.1% and 10.9% reduction in UHPC flowability with 3% volumetric content of corrugated and hooked-end steel fibers, respectively, compared with straight steel fibers. It might be due to 1) the friction between aggregates and hooked-end steel fibers being higher than other considered fiber shapes, 2) the added mechanical anchorage in the case of deformed steel fibers within the matrix-fiber bonding region, and 3) the comparatively easy bundling of deformed fibers compared to straight fibers (Wang et al., 2012; Yu et al., 2014b). There is a critical steel fiber content value, and the UHPC flowability may be considerably decreased. It might be agglomerating, and balls forming steel fibers exceed the fiber content from critical value (Khayat et al., 2019). The UHPC workability is usually improved by adding a vital superplasticizer, as reported by Shi et al. (2015) and Wang et al. (2017). However, the direct incorporation of water and superplasticizer led to the cement particles' absorption by the superplasticizer, and subsequently, effective dispersion cannot be attained while mixing (Shi et al., 2015). Hence, in Schachinger et al. (2004), Graybeal (2006), Yu et al. (2014a), Zhao et al. (2014), Abbas et al. (2015), Yu et al. (2015a), Meng W. and Khayat K. (2017), and Huang et al. (2018), the stepwise process is proposed to add steel fibers that improve the superplasticizer dispersion in UHPC. The UHPC yield viscosity enhanced up to 53 Pa s upon increasing the

TABLE 2 Steel fiber types and geometry (Park et al., 2012; Wu et al., 2016a; 2017b; Yoo et al., 2017b; Wu et al., 2019b; Yoo et al., 2019).

Type of the steel fiber	Straight				Twisted			Corrugated		Hooked-end		
Shape of the steel fiber												
Length of the steel fiber (mm)	6	12	13	30	13	18	30	13	30	13	20	30
Diameter of the steel fiber (μm)	0.16	0.20	0.16/0.20	0.30	0.20	0.30	0.30/0.50	0.20	0.30	0.20	0.25/0.35	0.38

viscosity-modified admixture content to 1% (Meng W. and Khayat K. H., 2017). In parallel, the workability of steel fibers reinforced UHPC is also dependent on mixing time. Generally, additional time and energy for mixing are vital for fiber uniform distribution in UHPC. Instead, the UHPC temperature is enhanced because of the extended time for mixing and air bubble formation, leading to strength reduction (Dils et al., 2012; ACI 239R-18, 2018). As per the literature, the UHPC mixing time is usually controlled between 10 and 20 min.

Mixing and casting of steel fiber-reinforced UHPC

In the past 60 years, there has been continuous improvement in FRCs. An advanced form of FRC is UHPC, which is composed of higher cement contents, superplasticizer (SP), fibers, silica fume, and other supplementary cementitious materials. The design of UHPC is a way to achieve dense packing of solid materials by limiting water content (w/c) below 0.2 (Meng et al., 2020). Such features result in UHPC's higher compressive strength, even more than 150 MPa (C/CM-17, 2017; Qin et al., 2022), which is almost 3–16 times more than conventional concrete (Yoo and Banthia, 2016; Xu S. et al., 2021), and excellent energy absorption capability and ductility. As per standards, multiple criteria are there for describing UHPC, for example, the American Society for Testing and Materials (ASTM) C185 (C/CM-17, 2017), the American Concrete Institute (ACI) committee 239 (ACI 239R-18, 2018), the Japan Society of Civil Engineers (JSCE) (JSCE, 2004), and the U.S. Department of Transportation Federal Highway Administration (FHWA) (Graybeal, 2006). As per the main definitions, the suggested compressive strength and tensile ductility for UHPC are 150 MPa and 5 MPa, respectively. With such excellent mechanical characteristics, the UHPC structures have 1/2 to 2/3 times less weight than conventional concrete without compromising the loading requirements (Schmidt and Fehling, 2005).

UHPC is similar to conventional concrete; therefore, the traditional procedure of casting remains usable and relevant. The standard concrete mixer is used for mixing UHPC. Figure 8 shows the steps of UHPC mixing, as presented by Zheng et al.

(2022), similar to conventional concrete. The superplasticizer and water are added after mixing powdered ingredients for almost 10 min, and the mixing process is repeated for another 5–10 min. The addition of steel fibers is performed as per the mix design on the satisfactory flowability of the mortar to have optimum workability. It should be noted that in the case of UHPC, more energy is consumed than conventional concrete, so the mixing process requires more time. Due to the additional energy input and lesser contents of water and coarse aggregates, additional care is used to avoid overheating during the mixing process. Cooling ingredients, utilizing a high-energy mixer, and replacing water partially or completely with ice may solve this overheating issue. Such UHPC can then be mixed in a conventional concrete mixer and in ready-mix trucks (Graybeal, 2011). Casting steel fibers incorporated in UHPC requires special attention regarding placement methods. In this case, the internal vibration is not recommended for UHPC; a slight external vibration can be applied to exclude the entrapped air.

Flowability of steel fiber-reinforced UHPC

The workability of concrete is basically an effort to manipulate a fresh concrete mix with maximum uniformity (homogeneity) (ASTM, 2018; Abetua and Kebedeb, 2021; Aisheh et al., 2022). This manipulation subjects to the placing, compaction, and concrete finishing (Li Z. et al., 2022). Concrete's workability is affected by adding fibers to it to improve the concrete's characteristics and performance (Cao et al., 2018a; Cao et al., 2018b). Usually, the viscosity of UHPC is more than conventional concrete (Sadrmomtazi et al., 2018). This is due to the dense packing of the finer ingredients in UHPC and the significantly lower water-to-binder ratio. Moreover, the UHPC's durability and mechanical characteristics are primarily based on its fresh state (Askar et al., 2013; Tayeh et al., 2013b; Tayeh et al., 2013d; Soliman and Nehdi, 2014). During the manufacturing of steel fiber-reinforced UHPC, its flowability is influenced by the surface area, geometry, shape, and volumetric content (Wang et al., 2017). The steel fiber incorporation in the UHPC mix enhances the air content in the fresh mix and decreases the
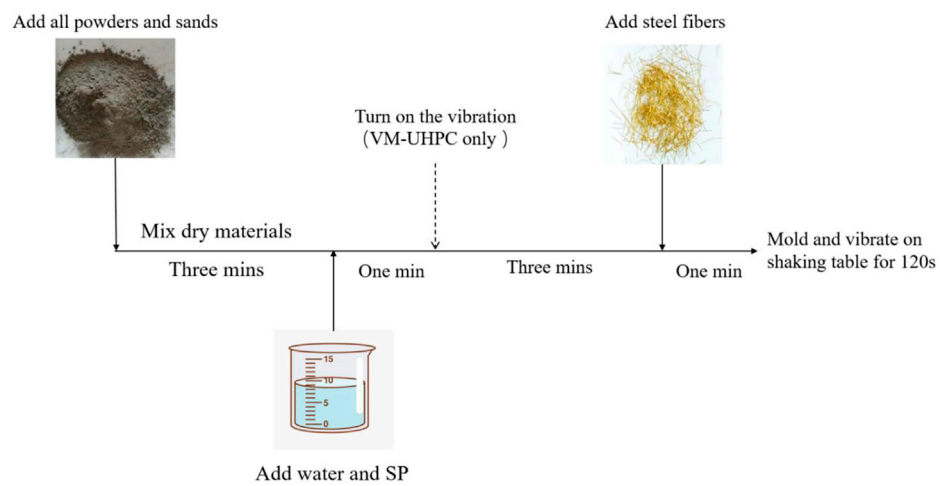
FIGURE 8
Steel fiber-reinforced UHPC mixing process (Zheng et al., 2022).
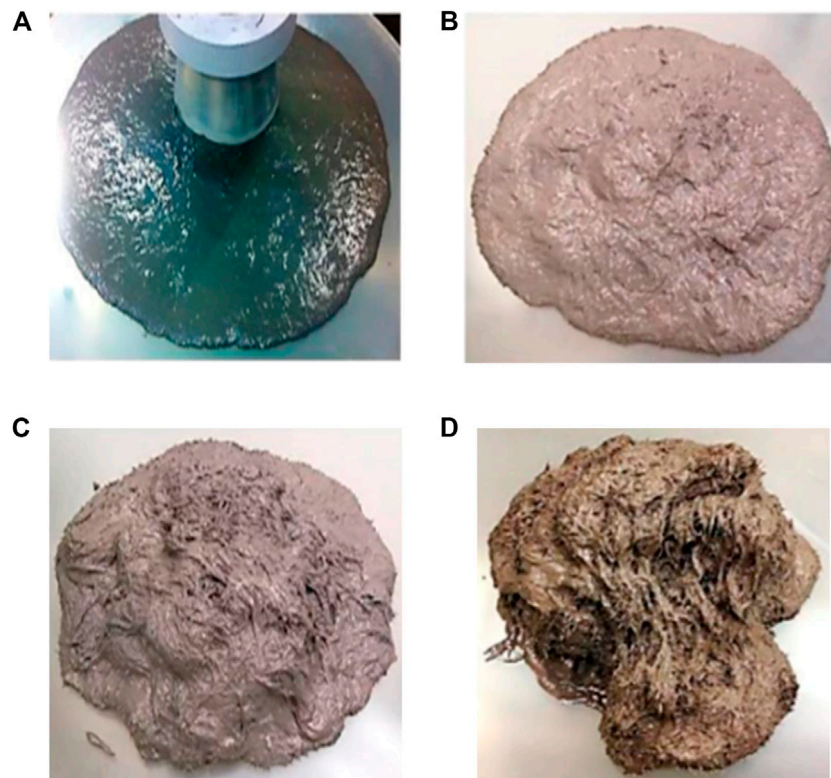
FIGURE 9
UHPC flowability having **(A)** 4%, **(B)** 5%, **(C)** 6%, and **(D)** 8% fiber contents (Biswas et al., 2021).

relative droop (Akeed et al., 2022a). Biswas et al. (2021) also reported a decrease in the flowability of fiber-reinforced UHPC with increasing fiber contents, as also illustrated in Figure 9.

Furthermore, the enhancement in cohesive force among steel fibers and paste also reduces the flowability of respective UHPC (Yu et al., 2015b). Kwon et al. (2014) proposed an equation, that

is, $\chi_f = V_f \times l_f/d_f$, for computing the factor named fiber factor to estimate the flowability of fiber-reinforced UHPC, where the fiber factor is shown by χ_f; V_f is notated for fiber volume, and d_f and l_f show the diameter and length of the fiber, respectively. It was revealed from the conducted study that with the increasing fiber factor, the fiber-reinforced UHPC slump tends to decrease. Similar types of results were also reported by Naaman and Wille (2010) and Marković (2006).

Mechanical properties of steel fiber-reinforced UHPC

The flexural and compressive strengths are the two vital mechanical factors in UHPC mix design to evaluate ductility and strength. However, the nature of UHPC is brittle. To cater to this issue, the incorporation of uniformly dispersed steel fibers with higher ultimate elongation and tensile strength is reported with enhanced strength and ductility of UHPC. Such concrete is considered ultra-high performance steel fiber-reinforced concrete by Qu et al. (2018). The role of steel fibers in UHPC is to enhance the cohesive forces among matrix and fibers, alter the granular skeleton, and enhance the length of anchorage among fibers and the UHPC matrix (Grünewald, 2004; Zdeb, 2017). Moreover, as frequently reported in the literature, the steel fibers provide a bridging mechanism in case of cracking and resist the crack propagation (Lan et al., 2022), ultimately enhancing the steel fiber-reinforced UHPC strength and ductility (Yu et al., 2014b). It may also be noted that the steel fiber content in UHPC is also of significant importance as the incorporation of steel fibers in bulk quantities can lead to their interlocking and inter-wrapping with each other, influencing the workability of the respective composite, which ultimately results in strength reduction (Qu et al., 2018). So, this review on the utilization of steel fibers in UHPC may assist in adopting the appropriate composition and characteristics like length, diameter, and content, for improving the mechanical properties of respective composites.

Compressive strength

UHPC compressive strength is a vital characteristic that is usually determined with respect to conventional concrete (Russell H. G. et al., 2013). The steel fibers are incorporated in UHPC to have bridging behavior (Alsalman et al., 2017; Khan et al., 2019). Compared with conventional concrete, the steel fiber-reinforced UHPC's compressive behavior is not considerably different. The main difference is in stiffness and compressive strength, which are significantly higher in UHPC. The ingredients influence the compressive strength of UHPC, mix design, fiber content, and curing (Russell H. G. et al., 2013). Researchers have reported different results for the compressive

strength of steel fiber-reinforced UHPC. Bae et al. (2016) reported a slight effect (i.e., <10%) on the compressive strength of UHPC upon the incorporation of steel fibers. Arora et al. (2019) reported that the UHPC compressive strength is primarily based on aggregates' packing density and the amount of hydration products. However, Ibrahim et al. (2017) reported considerable influence (i.e., >50% enhancement) in UHPC compressive strength upon the addition of steel fibers. This might be due to steel fibers capacity to delay fracture development and propagation (Ibrahim et al., 2017). The increasing content of fiber tends to have enhanced compressive strength (Wu et al., 2016b; Ibrahim et al., 2017). Compared with straight steel fibers, deformed steel fibers offer enhanced pullout strength, ultimately bridging the cracks more effectively (Meng and Khayat, 2018). However, this increased pullout strength does not considerably influence the UHPC compressive strength. Liu et al. (2016) reported a slight variation in UHPC compressive strength between macro and micro hooked-end steel fibers. Yoo et al. (2017a) reported that straight steel fibers have a comparatively lesser enhancement in UHPC compressive strength than macro-deformed steel fibers. The reported compressive strengths of UHPC are shown in Figure 10, as summarized from the literature (Wang et al., 2012; Yu et al., 2014a; Wu et al., 2016b; Shafieifar et al., 2017; Wu et al., 2019a; Hung et al., 2020; Mo et al., 2020; Teng et al., 2020).

Flexural Strength

The incorporation of steel fibers in UHPC offers the achievement of structural integrity through load transference across cracks (Gu et al., 2022) through the crack bridging phenomenon. Pakravan and Ozbakkaloglu (2019) reported the enhancement in UHPC flexural strength as a fiber content function. As reported in the literature, the UHPC flexural tensile strength is generally increased with increasing fiber content. Abbas et al. (2015) associated this enhancement in UHPC flexural strength with more closely spaced fibers in cases of higher content. In this scenario, each crack is spanned by more fibers, thus offering more area for bonding between fibers and matrix [54] and more resistance against crack propagation (Abbas et al., 2015; Yoo et al., 2017c). Park et al. (2017) reported three times more peak strength for the UHPC matrix, having 2% volumetric content of steel fibers than a matrix with 0.5% volumetric content. It is also reported in the literature that UHPC flexural strength did not improve continuously with increasing fiber content (Gesoglu et al., 2016; Meng and Khayat, 2018). Meng and Khayat (2018) reported the agglomeration of steel fibers in cases of higher contents (i.e., >3%), resulting in an adverse impact on flexural strength. However, Abbas et al. (2015) concluded with slightly decreased workability even in the case of higher fiber contents (i.e., up to 6%) and significant enhancement

FIGURE 10
Reported compressive strengths of steel fiber-reinforced UHPC.
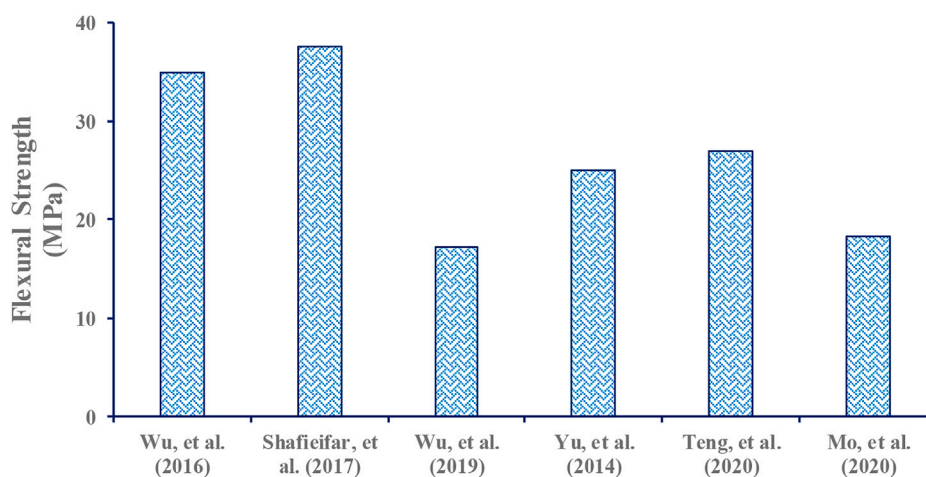
FIGURE 11
Reported flexural strengths of steel fiber-reinforced UHPC.

in peak load. The prolonged curing might offer a higher degree of hydration and more dense microstructure, resulting in improved bond strength among steel fibers and the surrounding matrix (Wu et al., 2016c). The incorporation of more content of coarse aggregates in UHPC may result in microstructure defects, thus weakening the fiber–matrix bond strength. Furthermore, fiber dispersion may also be impaired by using more coarse aggregates, resulting in lower flexural strength (Liu et al., 2016). Kim et al. (2011) reported 20%–40% enhanced flexural strength in UHPC with 1% deformed steel fibers than that of straight steel fibers. Numerous researchers have reported that the flexural strength of UHPC can be enhanced by more than 20% by incorporating longer steel fibers (Yoo et al., 2016; Yoo et al., 2017a; Wu et al., 2017b; Yoo et al., 2017c; Park et al., 2017; Pourbaba et al., 2018).

The reported flexural strengths of UHPC are shown in Figure 11, as summarized from the literature (Yu et al., 2014b; Wu et al., 2016b; Shafieifar et al., 2017; Wu et al., 2019a; Mo et al., 2020; Teng et al., 2020).

Steel fiber bonding and bridging effect in UHPC

An essential constituent in UHPC is discontinuous fiber reinforcement. The fiber incorporation in UHPC is vital for enhancing the ductility under compressive loading, as needed to attain structural safety. The addition of fibers can reduce the brittleness of concrete and enhance numerous material
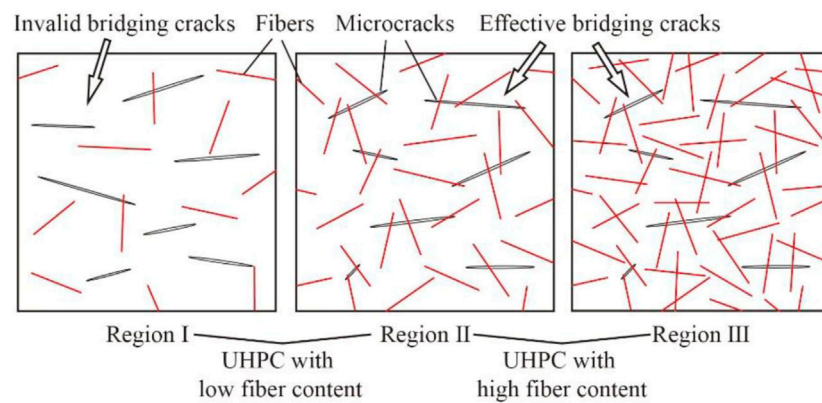
FIGURE 12
Effective bridging mechanism due to higher fiber contents in UHPC (taken from He et al. (2021)).
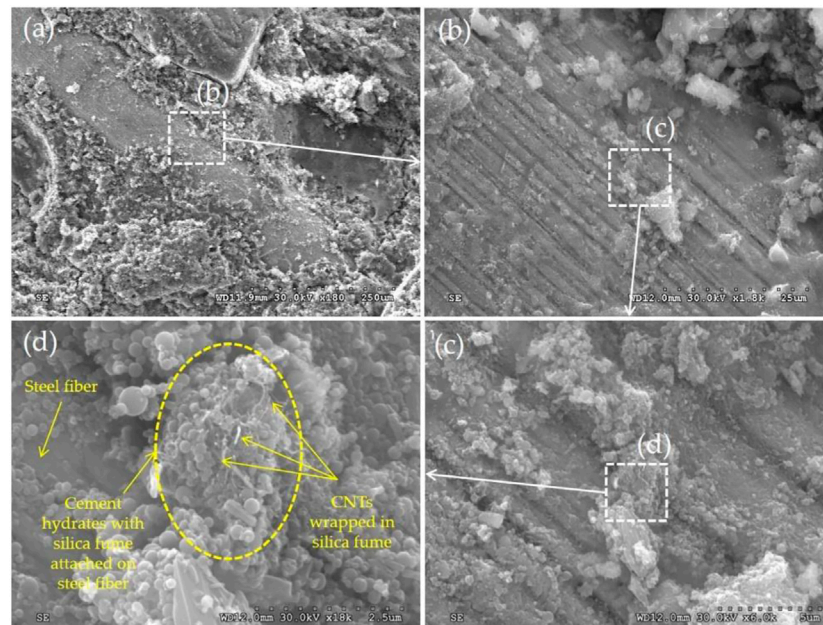
FIGURE 13
SEM images for steel fiber-reinforced UHPC (taken from You et al. (2017)).

characteristics, like enhanced energy absorption capability and provision of significant tensile strength. Different fiber types can be made based on material, shape, and size. As far as steel fiber incorporation in UHPC is concerned, its reinforcing effect is evaluated through adhesion bonding among matrix and fibers. The bonding characteristics, determined *via* a pullout test (single), are associated with the UHPC manufacturing method, the shape of the steel fiber, the friction coefficient, fiber content, orientation, and distribution (Gong et al., 2022; Huang, 2022). The bridging effect in UHPC due to steel fibers can

be enhanced by optimizing the content (≤3%), orientation (<45°), and distribution of steel fibers to evade the accumulation of fibers in a way to prevent stress from transferring from the matrix to the steel fibers (Gong et al., 2022). This bridging phenomenon due to addition of fibers is illustrated in Figure 12, as presented by He et al. (2021). The scanning electronic microscopic view of the interfacial transition zone (ITZ) of steel fiber-reinforced concrete UHPC is illustrated in Figure 13, as presented by You et al. (2017). These SEM images show a durable bond between the steel fiber and the surrounding concrete matrix, depicting its

capability to decrease stress concentrations and prevent internal degradation, ultimately leading to enhanced mechanical properties. The complexity of the UHPC structural design may be due to the varied content, combination, geometry, orientation, and distribution of fibers. Steel fibers may also be the reason behind UHPC's more carbon footprint and costs. Accordingly, enhancing the information regarding steel fibers' effects on UHPC is a crucial step for devising generally accepted UHPC applications and standard design codes.

Applications of steel fiber-reinforced UHPC

In the last two decades, researchers/academics and engineers around the globe have performed wide-ranging research to industrialize the technology of UHPC as a potential sustainable construction material in the future (Voo and Poon, 2009). It is extracted from a detailed literature search that almost 200 bridges have incorporated UHPC into their elements (Voo et al., 2017). Some other applications of UHPC include structural strengthening, building, precast elements, and retrofitting (Vande Voort et al., 2008). The resources and efforts of both the private and public sectors are focused on exploiting UHPC for practical implementation as a sustainable construction material (Ng et al., 2012; Akeed et al., 2022a; Akeed et al., 2022b; Akeed et al., 2022c). The superior mechanical characteristics of UHPC offer the design/manufacturing of aesthetically good, light, and slim architectural elements. The European and Mediterranean Civilizations Museum in France is an example where UHPC was used substantially for the very first time in the world. UHPC was utilized in creating perimeter footbridge decks and brackets, roof lattices, and prestressing anchorage points' protective covers. Various studies have been conducted for optimum designs of UHPC components, concluding in the construction of UHPC bridges around the globe. Some of the other possible applications of UHPC comprise security infrastructure or basic infrastructure elements. Furthermore, extensive research has also been conducted on UHPC mechanical properties subjected to penetration resistance, blast resistance (Wu et al., 2009), and high strain loading rate (Habel and Gauvreau, 2008; Millard et al., 2010). Moreover, UHPC has also been frequently used as a repair overlay for existing concrete structures because of its excellent properties that require less maintenance work (Hajar et al., 2013; Moreillon and Menétrey, 2013). UHPC overlay was reported to be first applied on a bridge in Switzerland over the La Morge River (Denarié, 2005). The UHPC utilization was also found in cover plates throughout the high-speed railroads in China (Gu et al., 2013) and in retrofitting containment walls for a nuclear reactor in France (Corvez and Masson, 2013). Further than bridges and buildings, the UHPC can also be utilized in wind turbine towers, nuclear power plants, and tunnels. Gamarra (2016) reported that

UHPC could also be utilized in developing more effective tunnel systems by reducing the thickness of tunnel elements. Hence, it can be summarized that the improved UHPC composite incorporating steel fibers may be utilized in pavements, tunnel and canal linings, bridge decks, airport runways and aprons, hydraulic structures, pipes, and slope stabilization, as also illustrated in Figure 14.

Discussion

Compared to conventional cementitious concrete, ultra-high performance concrete (UHPC) is one of the advanced cementitious composites that have significantly enhanced durability and mechanical characteristics (Russell H. et al., 2013). The interest in commercial applications and research on UHPC is growing daily. Despite UHPC's acceptability in various countries, there are still limitations, such as a lack of information on its material categorization procedures, structural capability for extensive usage, and design codes for general acceptability. The points of attention toward its enhanced utilization are the designing of slender/lightweight structures (Yoo and Banthia, 2016; Zhang and Ali, 2021), low maintenance, decreased environmental footprint, and overall cost. Depending on the results of the detailed literature review, the following advantages and disadvantages of steel fiber-reinforced UHPC are summarized as follows.

Advantages of steel fiber-reinforced UHPC: The compressive strengths of UHPC are reported in the literature (Tayeh et al., 2013c; Tayeh et al., 2013d; Qaidi et al., 2022) from 150 to 810 MPa which is almost 3–16 times more than that the in case of conventional concrete. The energy absorption capability and ductility of UHPC are conventionally increased by 300 times upon incorporation of steel fibers. CO_2, sulfates, and chlorides are almost non-permeable (Abetua and Kebedeb, 2021) to UHPC. Its improved durability comes with a prolonged service life that requires low maintenance. Industrial floors and bridge decks benefit from enhanced resistance against abrasion, whereas spots with harsh or poor climatic conditions benefit from enhanced resistance against corrosion (Tam et al., 2012). Un-hydrated cement's substantial percentage in the finished product during the cracking mechanism offers self-healing capability. Due to their exceptionally higher compressive strengths, buildings having UHPC weigh only 1/3rd or ½ of their conventional concrete components under similar loading conditions. This weight reduction comes out with thinner construction, additional serviceable floor space in case of multi-storey buildings, and reduced overall cost. The steel reinforcement bar exclusion enhances architectural freedom and reduces labor costs. Moreover, it also offers designers and architects the forms and shapes of structural members without virtual limits (Tam et al., 2012; Tayeh et al., 2014).
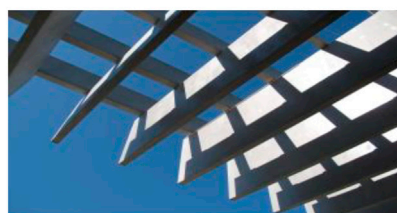
FIGURE 14
Possible applications of UHPC.

Disadvantages of steel fiber-reinforced UHPC: The UHPC disadvantages comprise its higher contents of cement (i.e., 950–1,000 kg/m³) and silica fume (i.e., 100–250 kg/m³) which enhance its manufacturing costs and CO_2 emissions, ultimately contributing toward ozone layer depletion and global warming (Aitcin, 2000; Mostofinejad et al., 2016; Almeshal et al., 2022; Faraj et al., 2022). Moreover, the sensitivity in case of quantities for water-to-binder materials, superplasticizers-to-binder, material chemical characteristics, and fine particle distribution (requires high-speed mixers) are UHPC's additional disadvantages. Furthermore, in the absence of fibers, the brittleness of UHPC would be significantly higher, as in the case of high-strength concrete possessing a higher elastic modulus (i.e., around 45–60 GPa), which is not desirable. These issues might be resolved effectively by incorporating metakaolin (Huang et al., 2017; Amin et al., 2020; Mansour and Tayeh, 2020) and rice husk ash, slag, fly ash, and zeolite, as partial substitution for cement (Sobuz et al., 2016). Also, the SCMs may also be utilized in UHPC to reduce the manufacturing cost to encourage the potential customer for more wide-ranging applications.

Conclusion and recommendations

A literature review-based research is an appropriate practice to recognize the growing trend in literature volume concentrating on steel fiber-reinforced UHPC-relevant evaluation, which may aid young academics. The primary objective of this research is to conduct a detailed review of steel fiber-reinforced UHPC's available literature for exploring the different aspects. The following conclusions are drawn:

- The evaluation of steel fiber-reinforced UHPC research shows that steel fibers, ultra-high performance concrete, and compressive strength are the three most widely adopted keywords. This assessment also shows that steel fibers in UHPC have primarily been investigated to achieve high-strength concrete.
- The reported cement quantity incorporated in different types of concrete was 16% for HPC, 33% for UHPC, and 20% for SCC. Accordingly, in the steel fiber-reinforced UHPC, a significant cement quantity (i.e., 800–1,300 kg/

m^3) was reported. The partial replacement of cement with readily available SCMs like slag and fly ash and the utilization of silica fume come out with certain benefits in terms of improved mechanical properties like higher compressive strength (i.e., up to 150–200 MPa), lower shrinkage, and reduced overall cost. The content of polycarboxylate-based superplasticizers has a significant influence on calcium silicate reactivity.

- Steel fiber effectiveness in UHPC, which enhances the energy absorption capability, toughness, and tensile strength is evident from the literature. The hooked-end steel fibers are reported to be more effective than straight steel fibers. It might be due to (i) the friction between aggregates and hooked-end steel fibers being more than other considered fiber shapes, (ii) the added mechanical anchorage in the case of deformed steel fibers within the matrix–fiber bonding region, and (iii) the comparatively easier bundling of deformed fibers than straight fibers. The reinforcing effect of steel fibers is endorsed through adhesion bonding between the UHPC matrix and steel fibers. Steel fiber types such as micro or macro steel fibers, and straight and deformed (twisted, hooked-end, or corrugated), have been explored for UHPC.

- The basic concept for the design of steel fiber-reinforced UHPC is to achieve improved microstructure, reduced porosity, and enhanced toughness and homogeneity. The UHPC properties are considerably affected by the raw ingredients, method of preparation, and curing treatments.

- The overall outcomes for UHPC compressive strength depict that incorporating deformed steel fibers instead of straight fibers does not have a considerable impact. However, in the case of UHPC flexural strength, deformed fibers positively impact the lower contents of steel fibers. On the other hand, the higher content of straight steel fibers results in better performance.

- As revealed from the reported SEM analysis, the durable bond between the steel fiber and the surrounding concrete matrix can decrease stress concentrations and prevent internal degradation of the material, ultimately leading to enhanced mechanical properties of steel fiber-reinforced UHPC.

- Around the globe, accomplishments in steel fiber-reinforced UHPC can be seen. At the same time, UHPC is progressing slowly with limitations that restrict its applications. Higher initial costs, non-availability of design codes, complex manufacturing approaches, design challenges, and inadequate availability of resources obstructed its development at the commercial level and utilization in modern structures of buildings in developing countries.

- The applications and significant production of steel fiber-reinforced UHPC depend on parameters like fiber content, geometry, mix design, w/c ratio, and supplementary cementitious material contents Furthermore, there is limited knowledge on durability, steel fiber

hybridization, life cycle assessment (LCA), bonding mechanisms, and life cycle cost analysis (LCCA) for steel fiber-reinforced UHPC. Hence, steel fiber-reinforced UHPC should be further explored in detail.

Based on the review conducted on steel fiber-reinforced UHPC, the following prospects for this research domain are proposed:

- For a better comprehensive understanding from the joint efforts of the research community, the future evaluation of all variables and testing mechanisms, in parallel, should be explored.

- It is also evident that researchers from different cultures would not agree to utilize a single standard among the already available guides. Therefore, considering the development of multiple standards for UHPC, the comparison studies among different proposed standards, by keeping all other parameters constant, will benefit scientific discussions by relating the novel research with existing ones (Larsen and Thorstensen, 2020).

- Furthermore, for the provision of a scientific basis for improving the performance, the UHPC load–slip modeling should also be explored comprehensively in terms of steel fiber effects regarding matrix age and compressive strength, fracture, damage of the matrix along the fiber and at the anchorage end, concrete macro-properties, slip-hardening, and incomplete straightening (Deng et al., 2022).

- In the literature, some recent studies show the feasibility of using steel fiber-reinforced UHPC in 3D printing (Van Tuan et al., 2011a; Arunothayan et al., 2020). Arunothayan et al. (2020) concluded that utilizing fiber-reinforced UHPC has enhanced shape retention ability compared to conventional concrete. Despite the available data on the 3D printing of UHPC, its manufacturing is still dependent on dedicated printing with specific configurations, such as the flow rate, nozzle type, and pumping specifications. It might not be feasible for various printing configurations and cementitious mixes (Arunothayan et al., 2020). As practitioners over the globe find it difficult to create 3D printing with UHPC, much effort is required to gain accessible information on utilizing steel fiber-reinforced UHPC for large-scale production of structural components using 3D printing technology.

- Additionally, a detailed, in-depth analysis of the bonding mechanism between steel fibers and the UHPC matrix should also be made to get a clear idea of UHPC's mechanical characteristics for its structural applications.

- The durability evaluation in extreme ageing/ environmental/climatic conditions is also required, with numerous coupling effects to have an insight into UHPC's full utilization throughout the structure's design life.

- Although the effect of deformed steel fibers in UHPC shows better bonding, as revealed from single pullout strength testing, the mechanical characteristics in the case of deformed fibers are less than those of straight fibers in some scenarios (Gong et al., 2022). Therefore, further investigation should also be conducted to validate the deformed steel fibers' effectiveness.

- Cracks in UHPC usually resulted in debonding among steel and the surrounded UHPC matrix that may damage the inert coating on surface of steel and accelerate corrosion. So, to address this issue, the concept of self-healing cracks is important in UHPC to attain long-term durability. The cement hydration low degree may be attributed to self-healing of UHPC. Moreover, the fibers, other than steel, like carbon fibers, mineral fibers, and synthetic fibers, possess unique impacts on UHPC performance. Hence, incorporating such fibers to avoid corrosion in the case of steel and to improve UHPC performance as per their properties needs to be explored.

- Further research on the treatment of fibers, both chemically and physically, for enhancing the bonding mechanism between the fiber and matrix is highly recommended in the future.

- Although some studies have been carried out on using hybrid fibers in UHPC, analytical and experimental investigations to explore the effect of hybrid fibers on UHPC are still lacking. The synergistic mechanism of hybrid fibers is still not clear. Therefore, further research is required to optimize the combination of the hybrid fiber to enhance the UHPC's mechanical characteristics, microstructure, and durability.

- The concept of hybridization of steel fibers in a way to incorporate a combination of steel fibers of varying lengths and shapes (Khan et al., 2022b) should also be further explored to resist the initiation and propagation of cracks in UHPC.

- Furthermore, various researchers like Wang et al. (2022) and Khan et al. (2022c) used various machine learning (ML) techniques under the concept of artificial intelligence (AI) to predict the mechanical properties (i.e., compressive and flexural strengths) of UHPC. However, there is still a gap in the employment of ML approaches for optimization of different variables, such as the fiber length, shape, content, mix design, w/c ratio, and supplementary cementitious material contents, considered in the design of steel fiber-reinforced UHPC to conserve natural resources and reduce the consumption of time, efforts, and cost, which is necessary to be covered (Xu Y. et al., 2021; Farooq et al., 2021; Wang et al., 2022).

- In the recent two decades, UHPC has been utilized in various countries for structural and non-structural applications. However, due to the higher cost of UHPC and the non-availability of its design codes, the application of UHPC in the construction industry is still limited. Therefore, future studies are required to reduce the UHPC cost for its wide-ranging practical implementation. Furthermore, the life cycle cost analysis (LCCA) of steel fiber-reinforced UHPC is also necessary before its applicability on large-scale production.

- Lastly, multiple studies were carried out to balance material mixes by adopting locally available raw and waste materials to reduce the quantity of cement, SP, and steel fibers [208]. With lesser environmental impacts, UHPC would be much more effective to implement by the construction industry. Hence, the knowledge of steel fiber-reinforced UHPC life cycle assessment (LCA) is also important to be explored before its practical applicability in the construction sector.

Author contributions

HA: visualization, funding acquisition, and writing—reviewing and editing. MA: conceptualization, validation, investigation, project administration, funding acquisition, and writing—reviewing and editing. WA: conceptualization, methodology, resources, supervision, software, validation, investigation, writing—original draft, and writing—reviewing and editing. KK: data curation, methodology, visualization, and writing—reviewing and editing. U-u-S: data curation, formal analysis, and writing—reviewing and editing. MA-H: investigation, formal analysis, and writing—reviewing and editing. AM: resources, validation, investigation, and writing—reviewing and editing.

Funding

Acknowledgments

Conflict of interest

The authors declare that the research was conducted in the absence of any commercial or financial relationships that could be construed as a potential conflict of interest.

Publisher's note

All claims expressed in this article are solely those of the authors and do not necessarily represent those of their affiliated organizations, or those of the publisher, the editors, and the reviewers. Any product that may be evaluated in this article, or claim that may be made by its manufacturer, is not guaranteed or endorsed by the publisher.

References

Abadel, A., Abbas, H., Almusallam, T., Alshaikh, I. M. H., Khawaji, M., Alghamdi, H., et al. (2022). Experimental study of shear behavior of CFRP strengthened ultra-high-performance fiber-reinforced concrete deep beams. *Case Stud. Constr. Mater.* 16, e01103. doi:10.1016/j.cscm.2022.e01103

Abbas, S., Soliman, A. M., and Nehdi, M. L. (2015). Exploring mechanical and durability properties of ultra-high performance concrete incorporating various steel fiber lengths and dosages. *Constr. Build. Mater.* 75, 429–441. doi:10.1016/j.conbuildmat.2014.11.017

Abetua, A. G., and Kebedeb, A. B. (2021). Crushed concrete as adsorptive material for removal of phosphate ions from aqueous solutions. *Water Conserv. Manag.* 2 (5), 40–46.

Abu-Lebdeh, T. M., Damptey, R., Ungureanu, L. M., and Petrescu, F. I. T. (2022). A ternary model for particle packing optimization. *J. Compos. Sci.* 6 (4), 113. doi:10.3390/jcs6040113

ACI 239R-18 (2018). *Ultra-high-performance concrete: An emerging technology report*. American Concrete Institute. ACI 239R-18).

Ahmad, J., Manan, A., Ali, A., Khan, M. W., Asim, M., and Zaid, O. (2020a). A study on mechanical and durability aspects of concrete modified with steel fibers (SFs). *cea.* 8, 814–823. doi:10.13189/cea.2020.080508

Ahmad, J., Zaid, O., Shahzaib, M., Abdullah, M. U., Ullah, A., and Ullah, R. (2021). Mechanical properties of sustainable concrete modified by adding marble slurry as cement substitution. *AIMS Mat. Sci.* 8, 343–358. doi:10.3934/matersci.2021022

Ahmad, W., Farooq, S. H., Usman, M., Khan, M., Ahmad, A., Aslam, F., et al. (2020b). Effect of coconut fiber length and content on properties of high strength concrete. *Materials* 13 (5), 1075. doi:10.3390/ma13051075

Ahmed, W., and Lim, C. W. (2021a). Coupling effect assessment of vacuum based pozzolana slurry encrusted recycled aggregate and basalt fiber on mechanical performance of fiber reinforced concrete. *Constr. Build. Mater.* 300, 124032. doi:10.1016/j.conbuildmat.2021.124032

Ahmed, W., and Lim, C. W. (2021b). Production of sustainable and structural fiber reinforced recycled aggregate concrete with improved fracture properties: A review. *J. Clean. Prod.* 279, 123832. doi:10.1016/j.jclepro.2020.123832

Aisheh, Y. I. A., Atrushi, D. S., Akeed, M. H., Qaidi, S., and Tayeh, B. A. (2022). Influence of steel fibers and microsilica on the mechanical properties of ultra-high-performance geopolymer concrete (UHP-GPC). *Case Stud. Constr. Mater.* 17, e01245. doi:10.1016/j.cscm.2022.e01245

Aitcin, P.-C. (2000). Cements of yesterday and today: Concrete of tomorrow. *Cem. Concr. Res.* 30 (9), 1349–1359. doi:10.1016/S0008-8846(00)00365-3

Akbar, A., and Liew, K. (2021). Multicriteria performance evaluation of fiber-reinforced cement composites: An environmental perspective. *Compos. Part B Eng.* 218, 108937. doi:10.1016/j.compositesb.2021.108937

Akeed, M. H., Qaidi, S., Ahmed, H. U., Emad, W., Faraj, R. H., Mohammed, A. S., et al. (2022a). Ultra-high-performance fiber-reinforced concrete. Part III: Fresh and hardened properties. *Case Stud. Constr. Mater.* 17, e01265. doi:10.1016/j.cscm.2022.e01265

Akeed, M. H., Qaidi, S., Ahmed, H. U., Faraj, R. H., Mohammed, A. S., Emad, W., et al. (2022b). Ultra-high-performance fiber-reinforced concrete. Part IV: Durability properties, cost assessment, applications, and challenges. *Case Stud. Constr. Mater.* 17, e01271. doi:10.1016/j.cscm.2022.e01271

Akeed, M. H., Qaidi, S., Ahmed, H. U., Faraj, R. H., Mohammed, A. S., Emad, W., et al. (2022c). Ultra-high-performance fiber-reinforced concrete. Part II: Hydration and microstructure. *Case Stud. Constr. Mater.* 17, e01289. doi:10.1016/j.cscm.2022.e01289

Alkaysi, M., El-Tawil, S., Liu, Z., and Hansen, W. (2016). Effects of silica powder and cement type on durability of ultra high performance concrete (UHPC). *Cem. Concr. Compos.* 66, 47–56. doi:10.1016/j.cemconcomp.2015.11.005

Almeshal, I., Al-Tayeb, M. M., Qaidi, S. M. A., Abu Bakar, B. H., and Tayeh, B. A. (2022). Mechanical properties of eco-friendly cements-based glass powder in aggressive medium. *Mater. Today Proc.* 58, 1582–1587. doi:10.1016/j.matpr.2022.03.613

Alsalman, A., Dang, C. N., and Hale, W. M. (2017). Development of ultra-high performance concrete with locally available materials. *Constr. Build. Mater.* 133, 135–145. doi:10.1016/j.conbuildmat.2016.12.040

Alwesabi, E. A. H., Abu Bakar, B. H., Alshaikh, I. M. H., Abadel, A. A., Alghamdi, H., and Wasim, M. (2022). An experimental study of compressive toughness of Steel–Polypropylene hybrid Fibre-Reinforced concrete. *Structures* 37, 379–388. doi:10.1016/j.istruc.2022.01.025

Alwesabi, E. A. H., Bakar, B. H. A., Alshaikh, I. M. H., and Akil, H. M. (2020). Experimental investigation on mechanical properties of plain and rubberised concretes with steel–polypropylene hybrid fibre. *Constr. Build. Mater.* 233, 117194. doi:10.1016/j.conbuildmat.2019.117194

Amin, M. N., Ahmad, W., Khan, K., and Sayed, M. M. (2022). Mapping research knowledge on rice husk ash application in concrete: A scientometric review. *Materials* 15 (10), 3431. doi:10.3390/ma15103431

Amin, M., Tayeh, B. A., and Agwa, I. S. (2020). Effect of using mineral admixtures and ceramic wastes as coarse aggregates on properties of ultrahigh-performance concrete. *J. Clean. Prod.* 273, 123073. doi:10.1016/j.jclepro.2020.123073

Arora, A., Yao, Y., Mobasher, B., and Neithalath, N. (2019). Fundamental insights into the compressive and flexural response of binder-and aggregate-optimized ultra-high performance concrete (UHPC). *Cem. Concr. Compos.* 98, 1–13. doi:10.1016/j.cemconcomp.2019.01.015

Arunothayan, A. R., Nematollahi, B., Ranade, R., Bong, S. H., and Sanjayan, J. (2020). Development of 3D-printable ultra-high performance fiber-reinforced concrete for digital construction. *Constr. Build. Mater.* 257, 119546. doi:10.1016/j.conbuildmat.2020.119546

Askar, L. K., Tayeh, B. A., and Abu Bakar, B. H. (2013). Effect of different curing conditions on the mechanical properties of UHPFC. *Iran. J. Energy & Environ.* 4 (3). doi:10.5829/idosi.ijee.2013.04.03.18

Aslam, F., Zaid, O., Althoey, F., Alyami, S. H., Qaidi, S. M., de Prado Gil, J., et al. (2022). *Evaluating the influence of fly ash and waste glass on the characteristics of coconut fibers reinforced concrete*. New Jersey, NJ: Structural Concrete.

ASTM (2018). *ASTM C125-standard terminology relating to concrete and concrete aggregates*. Pennsylvania: ASTM International West Conshohocken.

Aubry, S., Bompas, P., Vaudeville, B., Corvez, D., Lagrange, T., Mazzacane, P., et al. (2013). "A UHPFRC cladding challenge: The fondation louis vuitton pour la création" iceberg," in *2nd RILEM-fib-AFGC international Symposium on ultra-high performance fibre-reinforced concrete*.

Bae, B.-I., Choi, H.-K., Lee, B.-S., and Bang, C.-H. (2016). Compressive behavior and mechanical characteristics and their application to stress-strain relationship of steel fiber-reinforced reactive powder concrete. *Adv. Mater. Sci. Eng.* 2016, 1–11. doi:10.1155/2016/6465218

Bahari, A., Sadeghi-Nik, A., Cerro-Prada, E., Sadeghi-Nik, A., Roodbari, M., and Zhuge, Y. (2021). One-step random-walk process of nano-particles in cement-based materials. *J. Cent. South Univ.* 28 (6), 1679–1691. doi:10.1007/s11771-021-4726-6

Bahari, A., Sadeghi-Nik, A., Roodbari, M., Sadeghi-Nik, A., and Mirshafiei, E. (2018). Experimental and theoretical studies of ordinary Portland cement composites contains nano LSCO perovskite with Fokker-Planck and chemical reaction equations. *Constr. Build. Mater.* 163, 247–255. doi:10.1016/j.conbuildmat.2017.12.073

Bahari, A., Sadeghi-Nik, A., Shaikh, F. U. A., Sadeghi-Nik, A., Cerro-Prada, E., Mirshafiei, E., et al. (2022). Experimental studies on rheological, mechanical, and microstructure properties of self-compacting concrete containing perovskite nanomaterial. *Struct. Concr.* 23 (1), 564–578. doi:10.1002/suco.202000548

Biswas, R. K., Bin Ahmed, F., Haque, M. E., Provasha, A. A., Hasan, Z., Hayat, F., et al. (2021). Effects of steel fiber percentage and aspect ratios on fresh and harden properties of ultra-high performance fiber reinforced concrete. *Appl. Mech.* 2 (3), 501–515. doi:10.3390/applmech2030028

Brühwiler, E. (2016). *Recommendation: Ultra-high performance fibre reinforced cement-based composites (UHPFRC) construction material, dimensioning and application*. Zurich: EPFL.

C/Cm-17, A. (2017). *Standard practice for fabricating and testing specimens of ultra-high performance concrete*. West Conshohocken, PA: ASTM International.

Cao, M., Li, L., and Khan, M. (2018a). Effect of hybrid fibers, calcium carbonate whisker and coarse sand on mechanical properties of cement-based composites. *Mat. construcc.* 68 (330), e156. doi:10.3989/mc.2018.01717

Cao, M., Xie, C., Li, L., and Khan, M. (2019). Effect of different PVA and steel fiber length and content on mechanical properties of CaCO<sub>3</sub> whisker reinforced cementitious composites. *Mat. construcc.* 69 (336), e200. doi:10.3989/mc.2019.12918

Cao, M., Xie, C., Li, L., and Khan, M. (2018b). The relationship between reinforcing index and flexural parameters of new hybrid fiber reinforced slab. *Comput. Concr. Int. J.* 22 (5), 481–492.

Cao, Y., Liu, G., Brouwers, H., and Yu, Q. (2020). Enhancing the low-velocity impact resistance of ultra-high performance concrete by an optimized layered-structure concept. *Compos. Part B Eng.* 200, 108221. doi:10.1016/j.compositesb.2020.108221

Chan, Y.-W., and Chu, S.-H. (2004). Effect of silica fume on steel fiber bond characteristics in reactive powder concrete. *Cem. Concr. Res.* 34 (7), 1167–1172. doi:10.1016/j.cemconres.2003.12.023

Chen, X., Wan, D.-w., Jin, L.-z., Qian, K., and Fu, F. (2019). Experimental studies and microstructure analysis for ultra high-performance reactive powder concrete. *Constr. Build. Mater.* 229, 116924. doi:10.1016/j.conbuildmat.2019.116924

Corvez, D., and Masson, B. (2013). "UHPFRC solutions for the retrofit of nuclear reactor containment walls," in *Proceedings UHPFRC*, 147–156.

Dabbaghi, F., Sadeghi-Nik, A., Libre, N. A., and Nasrollahpour, S. (2021). Characterizing fiber reinforced concrete incorporating zeolite and metakaolin as natural pozzolans. *Structures* 34, 2617–2627. doi:10.1016/j.istruc.2021.09.025

De Larrard, F., and Sedran, T. (2002). Mixture-proportioning of high-performance concrete. *Cem. Concr. Res.* 32 (11), 1699–1704. doi:10.1016/s0008-8846(02)00861-x

Denarié, E. (2005). *Samaris D22 - full scale application of UHPFRC for the rehabilitation of bridges – from the lab to the field*. SAMARIS.

Deng, Y., Zhang, Z., Shi, C., Wu, Z., and Zhang, C. (2022). *Steel fiber–matrix interfacial bond in ultra-high performance concrete: A review*. Engineering.

Dils, J., De Schutter, G., and Boel, V. (2012). Influence of mixing procedure and mixer type on fresh and hardened properties of concrete: A review. *Mat. Struct.* 45 (11), 1673–1683. doi:10.1617/s11527-012-9864-8

Dingqiang, F., Yu, R., Kangning, L., Junhui, T., Zhonghe, S., Chunfeng, W., et al. (2021). Optimized design of steel fibres reinforced ultra-high performance concrete (UHPC) composites: Towards to dense structure and efficient fibre application. *Constr. Build. Mater.* 273, 121698. doi:10.1016/j.conbuildmat.2020.121698

Du, J., Meng, W., Khayat, K. H., Bao, Y., Guo, P., Lyu, Z., et al. (2021). New development of ultra-high-performance concrete (UHPC). *Compos. Part B Eng.* 224, 109220. doi:10.1016/j.compositesb.2021.109220

Faraj, R. H., Ahmed, H. U., Rafiq, S., Sor, N. H., Ibrahim, D. F., and Qaidi, S. M. A. (2022). Performance of self-compacting mortars modified with nano-particles: A systematic review and modeling. *Clean. Mater.* 4, 100086. doi:10.1016/j.clema.2022.100086

Farooq, F., Ahmed, W., Akbar, A., Aslam, F., and Alyousef, R. (2021). Predictive modeling for sustainable high-performance concrete from industrial wastes: A comparison and optimization of models using ensemble learners. *J. Clean. Prod.* 292, 126032. doi:10.1016/j.jclepro.2021.126032

Farooqi, M. U., and Ali, M. (2022). A study on natural fibre reinforced concrete from materials to structural applications. *Arab. J. Sci. Eng.* doi:10.1007/s13369-022-06977-1

Farooqi, M. U., and Ali, M. (2019). Effect of pre-treatment and content of wheat straw on energy absorption capability of concrete. *Constr. Build. Mater.* 224, 572–583. doi:10.1016/j.conbuildmat.2019.07.086

Gamarra, J. (2016). *Potential application of ultra-high performance fiber-reinforced concrete with wet-mix shotcrete system in tunneling*.

Gesoglu, M., Güneyisi, E., Muhyaddin, G. F., and Asaad, D. S. (2016). Strain hardening ultra-high performance fiber reinforced cementitious composites: Effect of fiber type and concentration. *Compos. Part B Eng.* 103, 74–83. doi:10.1016/j.compositesb.2016.08.004

Gong, J., Ma, Y., Fu, J., Hu, J., Ouyang, X., Zhang, Z., et al. (2022). *Utilization of fibers in ultra-high performance concrete: A review*. Engineering: Composites Part B, 109995.

Gowripalan, N., and Gilbert, R. (2000). *Design guidelines for ductal prestressed concrete beams. Reference Artical*. Sydney, NSW: The University of NSW.

Graybeal, B. A. (2006). *Material property characterization of ultra-high performance concrete*. United States: Federal Highway Administration. Office of Infrastructure.

Graybeal, B. (2011). *Ultra-high performance concrete*.

Grünewald, S. (2004). *Performance-based design of self-compacting fibre reinforced concrete*.

Gu, C., Zhao, S., Sun, W., and Wang, Q. (2013). "Production of precast UHPFRC pavement cover plates in high-speed railway construction," in *Proceedings of international symposium on ultra-high performance fiber-reinforced concrete*. Editors F. Toutlemonde and J. Resplendino (Marseille, France, 463–470.

Gu, M., Mo, H., Qiu, J., Yuan, J., and Xia, Q. (2022). Behavior of floating stone columns reinforced with geogrid encasement in model tests. *Front. Mat.* 9, 980851. doi:10.3389/fmats.2022.980851

Gul, A., Alam, B., Iqbal, M. J., Ahmed, W., Shahzada, K., Javed, M. H., et al. (2021). Impact of length and percent dosage of recycled steel fibers on the mechanical properties of concrete. *Civ. Eng. J.* 7 (10), 1650–1666. doi:10.28991/cej-2021-03091750

Habel, K., and Gauvreau, P. (2008). Response of ultra-high performance fiber reinforced concrete (UHPFRC) to impact and static loading. *Cem. Concr. Compos.* 30 (10), 938–946. doi:10.1016/j.cemconcomp.2008.09.001

Hajar, Z., Novarin, M., Servant, C., Généreux, G., Przybyla, D., and Bitar, D. (2013). ""Innovative solution for strengthening orthotropic decks using UHPFRC: The Illzach bridge," in *Proceedings of international symposium on ultra-high performance fiber-reinforced concrete*, 117–126.

He, J., Chen, W., Zhang, B., Yu, J., and Liu, H. (2021). The mechanical properties and damage evolution of UHPC reinforced with glass fibers and high-performance polypropylene fibers. *Materials* 14 (9), 2455. doi:10.3390/ma14092455

Huang, H., Gao, X., Li, L., and Wang, H. (2018). Improvement effect of steel fiber orientation control on mechanical performance of UHPC. *Constr. Build. Mater.* 188, 709–721. doi:10.1016/j.conbuildmat.2018.08.146

Huang, H., Yao, Y., Liang, C., and Ye, Y. (2022). Experimental study on cyclic performance of steel-hollow core partially encased composite spliced frame beam. *Soil Dyn. Earthq. Eng.* 163, 107499. doi:10.1016/j.soildyn.2022.107499

Huang, W., Kazemi-Kamyab, H., Sun, W., and Scrivener, K. (2017). Effect of replacement of silica fume with calcined clay on the hydration and microstructural development of eco-UHPFRC. *Mater. Des.* 121, 36–46. doi:10.1016/j.matdes.2017.02.052

Huang, Y. (2022). Three-dimensional numerical investigation of mixed-mode debonding of FRP-concrete interface using a cohesive zone model. *Constr. Build. Mater.* 350, 128818. doi:10.1016/j.conbuildmat.2022.128818

Hung, C.-C., Chen, Y.-T., and Yen, C.-H. (2020). Workability, fiber distribution, and mechanical properties of UHPC with hooked end steel macro-fibers. *Constr. Build. Mater.* 260, 119944. doi:10.1016/j.conbuildmat.2020.119944

Ibrahim, M. A., Farhat, M., Issa, M. A., and Hasse, J. A. (2017). Effect of material constituents on mechanical and fracture mechanics properties of ultra-high-performance concrete. *ACI Mater. J.* 114 (3). doi:10.14359/51689717

Jsce, F. (2004). *Recommendations for design and construction of ultra-high strength fiber reinforced concrete structures (Draft)*. Japan: Japan Society of Civil Engineers Tokyo.

Kci-M-12-003 (2012). *Design recommendations for ultra-high performance concrete K-UHPC*. Seoul: Korea Concrete Institute Seoul.

Khan, M., Cao, M., and Ali, M. (2018a). Effect of basalt fibers on mechanical properties of calcium carbonate whisker-steel fiber reinforced concrete. *Constr. Build. Mater.* 192, 742–753. doi:10.1016/j.conbuildmat.2018.10.159

Khan, M., Cao, M., and Ali, M. (2018b). "Influence of CaCO3 whiskers, steel fibers and basalt fibers hybridization on flexural toughness of concrete," in *Proceedings of the fifth international conference on sustainable construction materials and technologies* (London, UK), 14–17.

Khan, M., Cao, M., Chu, S., and Ali, M. (2022a). Properties of hybrid steel-basalt fiber reinforced concrete exposed to different surrounding conditions. *Constr. Build. Mater.* 322, 126340. doi:10.1016/j.conbuildmat.2022.126340

Khan, M., Cao, M., Xie, C., and Ali, M. (2022b). Effectiveness of hybrid steel-basalt fiber reinforced concrete under compression. *Case Stud. Constr. Mater.* 16, e00941. doi:10.1016/j.cscm.2022.e00941

Khan, M., Cao, M., Xie, C., and Ali, M. (2021). Efficiency of basalt fiber length and content on mechanical and microstructural properties of hybrid fiber concrete. *Fatigue Fract. Eng. Mat. Struct.* 44 (8), 2135–2152. doi:10.1111/ffe.13483

Khan, M., Lao, J., and Dai, J.-G. (2022c). Comparative study of advanced computational techniques for estimating the compressive strength of UHPC. *J. Asian Concr. Fed.* 8, 51–68. doi:10.18702/acf.2022.6.8.1.51

Khan, U. A., Jahanzaib, H. M., Khan, M., and Ali, M. (2019). "Improving the tensile energy absorption of high strength natural fiber reinforced concrete with fly-ash for bridge girders," in *Key engineering materials*. Switzerland: Trans Tech Publ, 335–342.

Khayat, K. H., Meng, W., Vallurupalli, K., and Teng, L. (2019). Rheological properties of ultra-high-performance concrete—an overview. *Cem. Concr. Res.* 124, 105828. doi:10.1016/j.cemconres.2019.105828

Kim, D. J., Park, S. H., Ryu, G. S., and Koh, K. T. (2011). Comparative flexural behavior of hybrid ultra high performance fiber reinforced concrete with different macro fibers. *Constr. Build. Mater.* 25 (11), 4144–4155. doi:10.1016/j.conbuildmat.2011.04.051

Kwon, S., Nishiwaki, T., Kikuta, T., and Mihashi, H. (2014). Development of ultra-high-performance hybrid fiber-reinforced cement-based composites. *ACI Mater. J.* 111 (3), 309. doi:10.14359/51686890

Lan, Y., Zheng, B., Shi, T., Ma, C., Liu, Y., and Zhao, Z. (2022). Crack resistance properties of carbon nanotube-modified concrete. *Mag. Concr. Res.* 74, 1165–1175. doi:10.1680/jmacr.21.00227

Larsen, I. L., and Thorstensen, R. T. (2020). The influence of steel fibres on compressive and tensile strength of ultra high performance concrete: A review. *Constr. Build. Mater.* 256, 119459. doi:10.1016/j.conbuildmat.2020.119459

Lei, V.-Y., Nematollahi, B., Said, A. B. M., Gopal, B. A., and Yee, T. S. (2012). Application of ultra high performance fiber reinforced concrete – the Malaysia perspective. *Int. J. Sustain. Constr. Eng. Technol.* 3 (1), 26–44.

Li, G., Zhou, C., Ahmad, W., Usanova, K. I., Karelina, M., Mohamed, A. M., et al. (2022a). Fly ash application as supplementary cementitious material: A review. *Materials* 15 (7), 2664. doi:10.3390/ma15072664

Li, P., Sluijsmans, M. J., Brouwers, H., and Yu, Q. (2020). Functionally graded ultra-high performance cementitious composite with enhanced impact properties. *Compos. Part B Eng.* 183, 107680. doi:10.1016/j.compositesb.2019.107680

Li, P., Yu, Q., and Brouwers, H. (2018). Effect of coarse basalt aggregates on the properties of Ultra-high Performance Concrete (UHPC). *Constr. Build. Mater.* 170, 649–659. doi:10.1016/j.conbuildmat.2018.03.109

Li, S., Jensen, O. M., Wang, Z., and Yu, Q. (2021). Influence of micromechanical property on the rate-dependent flexural strength of ultra-high performance concrete containing coarse aggregates (UHPC-CA). *Compos. Part B Eng.* 227, 109394. doi:10.1016/j.compositesb.2021.109394

Li, Z., Zhou, X., Ma, H., and Hou, D. (2022b). *Advanced concrete technology.* John Wiley & Sons.

Liu, J., Han, F., Cui, G., Zhang, Q., Lv, J., Zhang, L., et al. (2016). Combined effect of coarse aggregate and fiber on tensile behavior of ultra-high performance concrete. *Constr. Build. Mater.* 121, 310–318. doi:10.1016/j.conbuildmat.2016.05.039

López, J. A., Serna, P., and Navarro-Gregori, J. (2017). "Advances in the development of the first UHPFRC recommendations in Spain: Material classification, design and characterization," in *UHPFRC 2017 Designing and Building with UHPFRC: New large-Scale implementations, recent technical advances, experience and standards.* Editors F. Toutlemonde and J. T. Ch. Resplendino (France: RILEM Publications SAR), 565–574.

Máca, P., Sovják, R., and Konvalinka, P. (2014). Mix design of UHPFRC and its response to projectile impact. *Int. J. Impact Eng.* 63, 158–163. doi:10.1016/j.ijimpeng.2013.08.003

Mansour, W., and Tayeh, B. A. (2020). Shear behaviour of RC beams strengthened by various ultrahigh performance fibre-reinforced concrete systems. *Adv. Civ. Eng.* 2020, 1–18. doi:10.1155/2020/2139054

Marković, I. (2006). *High-performance hybrid-fibre concrete: Development and utilisation.* (Amsterdam, NH: IOS Press).

Mazzacane, P., Ricciotti, R., Lamoureux, G., and Corvez, D. (2013a). "Roofing of the stade jean bouin in UHPFRC," in *Proceedings of international Symposium on ultra-high performance fibre-reinforced concrete,* 59–68.

Mazzacane, P., Ricciotti, R., Teply, F., Tollini, E., and Corvez, D. (2013b). "Mucem: The builder's perspective," in *Proceedings UHPFRC,* 3–16.

Ménétrey, P. (2013). "UHPFRC cladding for the Qatar national Museum," in *Proceedings of the international symposium on ultra-high performance fiber-reinforced concrete* (Marseille, France, 1–3.

Meng, Q., Wu, C., Li, J., Liu, Z., Wu, P., Yang, Y., et al. (2020). Steel/basalt rebar reinforced Ultra-High Performance Concrete components against methane-air explosion loads. *Compos. Part B Eng.* 198, 108215. doi:10.1016/j.compositesb.2020.108215

Meng, W., and Khayat, K. (2017a). Effects of saturated lightweight sand content on key characteristics of ultra-high-performance concrete. *Cem. Concr. Res.* 101, 46–54. doi:10.1016/j.cemconres.2017.08.018

Meng, W., and Khayat, K. H. (2018). Effect of hybrid fibers on fresh properties, mechanical properties, and autogenous shrinkage of cost-effective UHPC. *J. Mat. Civ. Eng.* 30 (4), 04018030. doi:10.1061/(asce)mt.1943-5533.0002212

Meng, W., and Khayat, K. H. (2017b). Improving flexural performance of ultra-high-performance concrete by rheology control of suspending mortar. *Compos. Part B Eng.* 117, 26–34. doi:10.1016/j.compositesb.2017.02.019

Meng, W., Valipour, M., and Khayat, K. H. (2017). Optimization and performance of cost-effective ultra-high performance concrete. *Mat. Struct.* 50 (1), 29–16. doi:10.1617/s11527-016-0896-3

Meng, Z., Li, L., Farooqi, M. U., Feng, L., and Wang, L. (2022). Fiber factor for fresh and hardened properties of polyethylene fiber-reinforced geopolymer mortar. *J. Build. Eng.* 53, 104556. doi:10.1016/j.jobe.2022.104556

Millard, S. G., Molyneaux, T. C. K., Barnett, S. J., and Gao, X. (2010). Dynamic enhancement of blast-resistant ultra high performance fibre-reinforced concrete under flexural and shear loading. *Int. J. Impact Eng.* 37 (4), 405–413. doi:10.1016/j.ijimpeng.2009.09.004

Mishra, O., and Singh, S. (2019). An overview of microstructural and material properties of ultra-high-performance concrete. *J. Sustain. Cement-Based Mater.* 8 (2), 97–143. doi:10.1080/21650373.2018.1564398

Mo, Z., Wang, R., and Gao, X. (2020). Hydration and mechanical properties of UHPC matrix containing limestone and different levels of metakaolin. *Constr. Build. Mater.* 256, 119454. doi:10.1016/j.conbuildmat.2020.119454

Moreillon, L., and Ménétrey, P. (2013). "Rehabilitation and strengthening of existing RC structures with UHPFRC: Various applications," in *RILEM-fib-AFGC int. Symposium on ultra-high performance fibre-reinforced concrete* (France: RILEM Publication SARL), 136.

Mostofinejad, D., Nikoo, M. R., and Hosseini, S. A. (2016). Determination of optimized mix design and curing conditions of reactive powder concrete (RPC). *Constr. Build. Mater.* 123, 754–767. doi:10.1016/j.conbuildmat.2016.07.082

Naaman, A., and Wille, K. (2010). Some correlation between high packing density, ultra-high performance, flow ability, and fiber reinforcement of a concrete matrix. *BAC2010—2nd Iber. Congr. Self Compact.*

Nematollahi, B., Saifulnaz, R. M., Jaafar, M. S., and Voo, Y. L. (2012). A review on ultra high performance'ductile'concrete (UHPdC) technology. *Int. J. Civ. Struct. Eng.* 2 (3), 994. doi:10.6088/ijcser.00202030026

Ng, T. S., Voo, Y. L., and Foster, S. J. (2012). "Sustainability with ultra-high performance and geopolymer concrete construction," in *Innovative materials and techniques in concrete construction.* Editor M. N. Fardis (Springer Netherlands), 81–100.

Niu, Y., Huang, H., Zhang, J., Jin, W., Wei, J., and Yu, Q. (2019). Development of the strain field along the crack in ultra-high-performance fiber-reinforced concrete (UHPFRC) under bending by digital image correlation technique. *Cem. Concr. Res.* 125, 105821. doi:10.1016/j.cemconres.2019.105821

Pakravan, H. R., and Ozbakkaloglu, T. (2019). Synthetic fibers for cementitious composites: A critical and in-depth review of recent advances. *Constr. Build. Mater.* 207, 491–518. doi:10.1016/j.conbuildmat.2019.02.078

Park, J.-J., Yoo, D.-Y., Park, G.-J., and Kim, S.-W. (2017). Feasibility of reducing the fiber content in ultra-high-performance fiber-reinforced concrete under flexure. *Materials* 10 (2), 118. doi:10.3390/ma10020118

Park, J.-S., Kim, Y. J., Cho, J.-R., and Jeon, S.-J. (2015). Early-age strength of ultra-high performance concrete in various curing conditions. *Materials* 8 (8), 5537–5553. doi:10.3390/ma8085261

Park, S. H., Kim, D. J., Ryu, G. S., and Koh, K. T. (2012). Tensile behavior of ultra high performance hybrid fiber reinforced concrete. *Cem. Concr. Compos.* 34 (2), 172–184. doi:10.1016/j.cemconcomp.2011.09.009

Perry, V., and Habel, K. (2017). *Standardization of ultra-high performance concrete the Canadian perspective.* Paris: UHPFRC.

Pokorný, P., Kolísko, J., Čítek, D., and Kostelecká, M. (2020). Effect of elevated temperature on the bond strength of prestressing reinforcement in UHPC. *Materials* 13 (21), 4990. doi:10.3390/ma13214990

Pourbaba, M., Asefi, E., Sadaghian, H., and Mirmiran, A. (2018). Effect of age on the compressive strength of ultra-high-performance fiber-reinforced concrete. *Constr. Build. Mater.* 175, 402–410. doi:10.1016/j.conbuildmat.2018.04.203

Qaidi, S. M. A., Mohammed, A. S., Ahmed, H. U., Faraj, R. H., Emad, W., Tayeh, B. A., et al. (2022). Rubberized geopolymer composites: A comprehensive review. *Ceram. Int.* 48 (17), 24234–24259. doi:10.1016/j.ceramint.2022.06.123

Qian, Y. (2017). *Characterization of structural rebuilding and shear migration in cementitious materials in consideration of thixotropy.* Columbia University.

Qin, J., Dai, F., Ma, H., Dai, X., Li, Z., Jia, X., et al. (2022). Development and characterization of magnesium phosphate cement based ultra-high performance concrete. *Compos. Part B Eng.* 234, 109694. doi:10.1016/j.compositesb.2022.109694

Qin, Y., Zhang, X., Chai, J., Xu, Z., and Li, S. (2019). Experimental study of compressive behavior of polypropylene-fiber-reinforced and polypropylene-fiber-fabric-reinforced concrete. *Constr. Build. Mater.* 194, 216–225. doi:10.1016/j.conbuildmat.2018.11.042

Qu, D., Cai, X., and Chang, W. (2018). Evaluating the effects of steel fibers on mechanical properties of ultra-high performance concrete using artificial neural networks. *Appl. Sci.* 8 (7), 1120. doi:10.3390/app8071120

Rezaie, A. B., Liebscher, M., Ranjbarian, M., Simon, F., Zimmerer, C., Drechsler, A., et al. (2021). Enhancing the interfacial bonding between PE fibers and

cementitious matrices through polydopamine surface modification. *Compos. Part B Eng.* 217, 108817. doi:10.1016/j.compositesb.2021.108817

Richard, P., and Cheyrezy, M. (1995). Composition of reactive powder concretes. *Cem. Concr. Res.* 25 (7), 1501–1511. doi:10.1016/0008-8846(95)00144-2

Rong, Z., Sun, W., Xiao, H., and Jiang, G. (2015). Effects of nano-SiO2 particles on the mechanical and microstructural properties of ultra-high performance cementitious composites. *Cem. Concr. Compos.* 56, 25–31. doi:10.1016/j.cemconcomp.2014.11.001

Rossignolo, J. A. (2007). Effect of silica fume and SBR latex on the pasteaggregate interfacial transition zone. *Mat. Res.* 10, 83–86. doi:10.1590/s1516-14392007000100018

Russell, H. G., Graybeal, B. A., and Russell, H. G. (2013b). *Ultra-high performance concrete: A state-of-the-art report for the bridge community". United states*. New Jersey, NJ: Federal Highway Administration. Office of Infrastructure.

Russell, H., Graybeal, B., and Russell, H. (2013a). *Ultra-high performance concrete: A state-of-the-art report for the bridge community*. Washington, DC: Federal Highway Administration. Rep. No". FHWA-HRT-13-060.

Sadrmomtazi, A., Tajasosi, S., and Tahmouresi, B. (2018). Effect of materials proportion on rheology and mechanical strength and microstructure of ultra-high performance concrete (UHPC). *Constr. Build. Mater.* 187, 1103–1112. doi:10.1016/j.conbuildmat.2018.08.070

Schachinger, I, Schubert, J., and Mazanec, O. (2004). "Effect of mixing and placement methods on fresh and hardened ultra high performance concrete (UHPC)," in *International Symposium on ultra high performance concrete*, 575–586.

Schmidt, M., and Fehling, E. (2005). Ultra-high-performance concrete: Research, development and application in europe. *ACI Spec. Publ.* 228 (1), 51–78.

Schröfl, C., Gruber, M., and Plank, J. (2012). Preferential adsorption of polycarboxylate superplasticizers on cement and silica fume in ultra-high performance concrete (UHPC). *Cem. Concr. Res.* 42 (11), 1401–1408. doi:10.1016/j.cemconres.2012.08.013

Shafieifar, M., Farzad, M., and Azizinamini, A. (2017). Experimental and numerical study on mechanical properties of ultra high performance concrete (UHPC). *Constr. Build. Mater.* 156, 402–411. doi:10.1016/j.conbuildmat.2017.08.170

Shi, C., Wu, Z., Xiao, J., Wang, D., Huang, Z., and Fang, Z. (2015). A review on ultra high performance concrete: Part I. Raw materials and mixture design. *Constr. Build. Mater.* 101, 741–751. doi:10.1016/j.conbuildmat.2015.10.088

Shi, T., Liu, Y., Zhao, X., Wang, J., Zhao, Z., Corr, D. J., et al. (2022). Study on mechanical properties of the interfacial transition zone in carbon nanofiber-reinforced cement mortar based on the PeakForce tapping mode of atomic force microscope. *J. Build. Eng.* 61, 105248. doi:10.1016/j.jobe.2022.105248

Sidodikromo, E. P., Chen, Z., and Habib, M. (2019). Review on the cement-based composite ultra-high-performance concrete (UHPC). *Open Civ. Eng. J.* 13 (1), 147–162. doi:10.2174/1874149501913010147

Sobuz, H. R., Visintin, P., Mohamed Ali, M. S., Singh, M., Griffith, M. C., and Sheikh, A. H. (2016). Manufacturing ultra-high performance concrete utilising conventional materials and production methods. *Constr. Build. Mater.* 111, 251–261. doi:10.1016/j.conbuildmat.2016.02.102

Sohail, M. G., Wang, B., Jain, A., Kahraman, R., Ozerkan, N. G., Gencturk, B., et al. (2018). Advancements in concrete mix designs: High-performance and ultrahigh-performance concretes from 1970 to 2016. *J. Mat. Civ. Eng.* 30 (3), 04017310. doi:10.1061/(asce)mt.1943-5533.0002144

Soliman, A., and Nehdi, M. (2014). Effects of shrinkage reducing admixture and wollastonite microfiber on early-age behavior of ultra-high performance concrete. *Cem. Concr. Compos.* 46, 81–89. doi:10.1016/j.cemconcomp.2013.11.008

Soliman, N., and Tagnit-Hamou, A. (2016). Development of ultra-high-performance concrete using glass powder–Towards ecofriendly concrete. *Constr. Build. Mater.* 125, 600–612. doi:10.1016/j.conbuildmat.2016.08.073

Song, H., Liu, J., He, K., and Ahmad, W. (2021). A comprehensive overview of jute fiber reinforced cementitious composites. *Case Stud. Constr. Mater.* 15, e00724. doi:10.1016/j.cscm.2021.e00724

Stovall, T., De Larrard, F., and Buil, M. (1986). Linear packing density model of grain mixtures. *Powder Technol.* 48 (1), 1–12. doi:10.1016/0032-5910(86)80058-4

Tam, C. M., Tam, V. W. Y., and Ng, K. M. (2012). Assessing drying shrinkage and water permeability of reactive powder concrete produced in Hong Kong. *Constr. Build. Mater.* 26 (1), 79–89. doi:10.1016/j.conbuildmat.2011.05.006

Tayeh, B. A., Abu Bakar, B. H., and Megat Johari, M. A. (2013a). Characterization of the interfacial bond between old concrete substrate and ultra high performance fiber concrete repair composite. *Mat. Struct.* 46 (5), 743–753. doi:10.1617/s11527-012-9931-1

Tayeh, B. A., Abu Bakar, B. H., Megat Johari, M. A., and Zeyad, A. M. (2014). Microstructural analysis of the adhesion mechanism between old concrete substrate and UHPFC. *J. Adhesion Sci. Technol.* 28 (18), 1846–1864. doi:10.1080/01694243.2014.925386

Tayeh, B. A., Bakar, B. A., Johari, M. M., and Ratnam, M. M. (2013b). The relationship between substrate roughness parameters and bond strength of ultra high-performance fiber concrete. *J. Adhesion Sci. Technol.* 27 (16), 1790–1810. doi:10.1080/01694243.2012.761543

Tayeh, B. A., Bakar, B. H. A., Johari, M. A. M., and Voo, Y. L. (2013c). Utilization of ultra-high performance fibre concrete (UHPFC) for rehabilitation – a review. *Procedia Eng.* 54, 525–538. doi:10.1016/j.proeng.2013.03.048

Tayeh, B. A., Bakar, B. H. A., Megat Johari, M. A., and Zeyad, A. (2013d). "Flexural strength behavior of composite UHPFC-existing concrete," in Advanced materials research: *Trans tech publ*, 32–36.

Teng, L., Meng, W., and Khayat, K. H. (2020). Rheology control of ultra-high-performance concrete made with different fiber contents. *Cem. Concr. Res.* 138, 106222. doi:10.1016/j.cemconres.2020.106222

Van Tuan, N., Ye, G., van Breugel, K., and Copuroglu, O. (2011a). Hydration and microstructure of ultra high performance concrete incorporating rice husk ash. *Cem. Concr. Res.* 41 (11), 1104–1111. doi:10.1016/j.cemconres.2011.06.009

Van Tuan, N., Ye, G., Van Breugel, K., Fraaij, A. L., and Dai Bui, D. (2011b). The study of using rice husk ash to produce ultra high performance concrete. *Constr. Build. Mater.* 25 (4), 2030–2035. doi:10.1016/j.conbuildmat.2010.11.046

Vande Voort, T. L., Suleiman, M. T., and Sritharan, S. (2008). *Design and performance verification of ultra-high performance concrete piles for deep foundations*.

Voo, Y., Foster, S., and Pek, L. (2017). "Ultra-high performance concrete—Technology for present and future," in *Proceedings of the high tech concrete: Where technology and engineering meet* (Maastricht, Netherlands, 12–14.

Voo, Y., and Poon, W. (2009). "Ultra High performance ductile concrete (UHPdC) for Bridge engineering," in *Proceedings of the international Conference and Exhibition on bridge engineering*.

Wang, C., Yang, C., Liu, F., Wan, C., and Pu, X. (2012). Preparation of ultra-high performance concrete with common technology and materials. *Cem. Concr. Compos.* 34 (4), 538–544. doi:10.1016/j.cemconcomp.2011.11.005

Wang, D., Shi, C., Wu, Z., Xiao, J., Huang, Z., and Fang, Z. (2015). A review on ultra high performance concrete: Part II. Hydration, microstructure and properties. *Constr. Build. Mater.* 96, 368–377. doi:10.1016/j.conbuildmat.2015.08.095

Wang, Q., Hussain, A., Farooqi, M. U., and Deifalla, A. F. (2022). Artificial intelligence-based estimation of ultra-high-strength concrete's flexural property. *Case Stud. Constr. Mater.* 17, e01243. doi:10.1016/j.cscm.2022.e01243

Wang, R., Gao, X., Huang, H., and Han, G. (2017). Influence of rheological properties of cement mortar on steel fiber distribution in UHPC. *Constr. Build. Mater.* 144, 65–73. doi:10.1016/j.conbuildmat.2017.03.173

Wetzel, A., and Middendorf, B. (2019). Influence of silica fume on properties of fresh and hardened ultra-high performance concrete based on alkali-activated slag. *Cem. Concr. Compos.* 100, 53–59. doi:10.1016/j.cemconcomp.2019.03.023

Wu, C., Oehlers, D. J., Rebentrost, M., Leach, J., and Whittaker, A. S. (2009). Blast testing of ultra-high performance fibre and FRP-retrofitted concrete slabs. *Eng. Struct.* 31 (9), 2060–2069. doi:10.1016/j.engstruct.2009.03.020

Wu, Z., Khayat, K. H., and Shi, C. (2019a). Changes in rheology and mechanical properties of ultra-high performance concrete with silica fume content. *Cem. Concr. Res.* 123, 105786. doi:10.1016/j.cemconres.2019.105786

Wu, Z., Khayat, K. H., and Shi, C. (2017a). Effect of nano-SiO2 particles and curing time on development of fiber-matrix bond properties and microstructure of ultra-high strength concrete. *Cem. Concr. Res.* 95, 247–256. doi:10.1016/j.cemconres.2017.02.031

Wu, Z., Shi, C., He, W., and Wang, D. (2017b). Static and dynamic compressive properties of ultra-high performance concrete (UHPC) with hybrid steel fiber reinforcements. *Cem. Concr. Compos.* 79, 148–157. doi:10.1016/j.cemconcomp.2017.02.010

Wu, Z., Shi, C., He, W., and Wang, D. (2016a). Uniaxial compression behavior of ultra-high performance concrete with hybrid steel fiber. *J. Mat. Civ. Eng.* 28 (12), 06016017. doi:10.1061/(asce)mt.1943-5533.0001684

Wu, Z., Shi, C., He, W., and Wu, L. (2016b). Effects of steel fiber content and shape on mechanical properties of ultra high performance concrete. *Constr. Build. Mater.* 103, 8–14. doi:10.1016/j.conbuildmat.2015.11.028

Wu, Z., Shi, C., and Khayat, K. H. (2019b). Investigation of mechanical properties and shrinkage of ultra-high performance concrete: Influence of steel fiber content and shape. *Compos. Part B Eng.* 174, 107021. doi:10.1016/j.compositesb.2019.107021

Wu, Z., Shi, C., and Khayat, K. (2016c). Influence of silica fume content on microstructure development and bond to steel fiber in ultra-high strength cement-based materials (UHSC). *Cem. Concr. Compos.* 71, 97–109. doi:10.1016/j.cemconcomp.2016.05.005

Xu, L., Wu, F., Chi, Y., Cheng, P., Zeng, Y., and Chen, Q. (2019). Effects of coarse aggregate and steel fibre contents on mechanical properties of high performance concrete. *Constr. Build. Mater.* 206, 97–110. doi:10.1016/j.conbuildmat.2019.01.190

Xu, S., Zhou, F., Li, Q., and Wu, P. (2021a). A novel dynamic cavity expansion model to predict the resistance of reactive powder concrete (RPC) against projectile impact. *Compos. Part B Eng.* 223, 109107. doi:10.1016/j.compositesb.2021.109107

Xu, Y., Ahmad, W., Ahmad, A., Ostrowski, K. A., Dudek, M., Aslam, F., et al. (2021b). Computation of high-performance concrete compressive strength using standalone and ensembled machine learning techniques. *Materials* 14 (22), 7034. doi:10.3390/ma14227034

Yang, S., Millard, S., Soutsos, M., Barnett, S., and Le, T. T. (2009). Influence of aggregate and curing regime on the mechanical properties of ultra-high performance fibre reinforced concrete (UHPFRC). *Constr. Build. Mater.* 23 (6), 2291–2298. doi:10.1016/j.conbuildmat.2008.11.012

Yazıcı, H. (2007). The effect of curing conditions on compressive strength of ultra high strength concrete with high volume mineral admixtures. *Build. Environ.* 42 (5), 2083–2089. doi:10.1016/j.buildenv.2006.03.013

Ye, J., Cui, C., Yu, J., Yu, K., and Xiao, J. (2021). Fresh and anisotropic-mechanical properties of 3D printable ultra-high ductile concrete with crumb rubber. *Compos. Part B Eng.* 211, 108639. doi:10.1016/j.compositesb.2021.108639

Yoo, D.-Y., and Banthia, N. (2016). Mechanical properties of ultra-high-performance fiber-reinforced concrete: A review. *Cem. Concr. Compos.* 73, 267–280. doi:10.1016/j.cemconcomp.2016.08.001

Yoo, D.-Y., Kang, S.-T., and Yoon, Y.-S. (2016). Enhancing the flexural performance of ultra-high-performance concrete using long steel fibers. *Compos. Struct.* 147, 220–230. doi:10.1016/j.compstruct.2016.03.032

Yoo, D.-Y., Kim, J.-J., and Chun, B. (2019). Dynamic pullout behavior of half-hooked and twisted steel fibers in ultra-high-performance concrete containing expansive agents. *Compos. Part B Eng.* 167, 517–532. doi:10.1016/j.compositesb.2019.03.022

Yoo, D.-Y., Kim, M. J., Kim, S.-W., and Park, J.-J. (2017a). Development of cost effective ultra-high-performance fiber-reinforced concrete using single and hybrid steel fibers. *Constr. Build. Mater.* 150, 383–394. doi:10.1016/j.conbuildmat.2017.06.018

Yoo, D.-Y., Kim, S.-W., and Park, J.-J. (2017b). Comparative flexural behavior of ultra-high-performance concrete reinforced with hybrid straight steel fibers. *Constr. Build. Mater.* 132, 219–229. doi:10.1016/j.conbuildmat.2016.11.104

Yoo, D.-Y., Kim, S., Park, G.-J., Park, J.-J., and Kim, S.-W. (2017c). Effects of fiber shape, aspect ratio, and volume fraction on flexural behavior of ultra-high-performance fiber-reinforced cement composites. *Compos. Struct.* 174, 375–388. doi:10.1016/j.compstruct.2017.04.069

You, I., Yoo, D.-Y., Kim, S., Kim, M.-J., and Zi, G. (2017). Electrical and self-sensing properties of ultra-high-performance fiber-reinforced concrete with carbon nanotubes. *Sensors* 17 (11), 2481. doi:10.3390/s17112481

Yu, R., Spiesz, P., and Brouwers, H. (2015a). Development of an eco-friendly Ultra-High Performance Concrete (UHPC) with efficient cement and mineral admixtures uses. *Cem. Concr. Compos.* 55, 383–394. doi:10.1016/j.cemconcomp.2014.09.024

Yu, R., Spiesz, P., and Brouwers, H. (2015b). Development of ultra-high performance fibre reinforced concrete (UHPFRC): Towards an efficient utilization of binders and fibres. *Constr. Build. Mater.* 79, 273–282. doi:10.1016/j.conbuildmat.2015.01.050

Yu, R., Spiesz, P., and Brouwers, H. (2014a). Effect of nano-silica on the hydration and microstructure development of Ultra-High Performance Concrete (UHPC) with a low binder amount. *Constr. Build. Mater.* 65, 140–150. doi:10.1016/j.conbuildmat.2014.04.063

Yu, R., Spiesz, P., and Brouwers, H. (2014b). Mix design and properties assessment of ultra-high performance fibre reinforced concrete (UHPFRC). *Cem. Concr. Res.* 56, 29–39. doi:10.1016/j.cemconres.2013.11.002

Zdeb, T. (2017). An analysis of the steam curing and autoclaving process parameters for reactive powder concretes. *Constr. Build. Mater.* 131, 758–766. doi:10.1016/j.conbuildmat.2016.11.026

Zhang, B., Ahmad, W., Ahmad, A., Aslam, F., and Joyklad, P. (2022). A scientometric analysis approach to analyze the present research on recycled aggregate concrete. *J. Build. Eng.* 46, 103679. doi:10.1016/j.jobe.2021.103679

Zhang, C., and Ali, A. (2021). The advancement of seismic isolation and energy dissipation mechanisms based on friction. *Soil Dyn. Earthq. Eng.* 146, 106746. doi:10.1016/j.soildyn.2021.106746

Zhang, Y., Li, X., Zhu, Y., and Shao, X. (2020). Experimental study on flexural behavior of damaged reinforced concrete (RC) beam strengthened by toughness-improved ultra-high performance concrete (UHPC) layer. *Compos. Part B Eng.* 186, 107834. doi:10.1016/j.compositesb.2020.107834

Zhang, Z., Yang, F., Zhang, H., Zhang, T., Wang, H., Xu, Y., et al. (2021). Influence of CeO2 addition on forming quality and microstructure of TiC-reinforced CrTi4-based laser cladding composite coating. *Mater. Charact.* 171, 110732. doi:10.1016/j.matchar.2020.110732

Zhao, S., Fan, J., and Sun, W. (2014). Utilization of iron ore tailings as fine aggregate in ultra-high performance concrete. *Constr. Build. Mater.* 50, 540–548. doi:10.1016/j.conbuildmat.2013.10.019

Zheng, Y., Zhou, Y., Nie, F., Luo, H., and Huang, X. (2022). Effect of a novel vibration mixing on the fiber distribution and mechanical properties of ultra-high performance concrete. *Sustainability* 14 (13), 7920. doi:10.3390/su14137920

Zollo, R. F. (1997). Fiber-reinforced concrete: An overview after 30 years of development. *Cem. Concr. Compos.* 19 (2), 107–122. doi:10.1016/s0958-9465(96)00046-7

Machine learning techniques to evaluate the ultrasonic pulse velocity of hybrid fiber-reinforced concrete modified with nano-silica

Kaffayatullah Khan[1]*, Muhammad Nasir Amin[1], Umbreen Us Sahar[2], Waqas Ahmad[3], Kamran Shah[4] and Abdullah Mohamed[5]

[1]Department of Civil and Environmental Engineering, College of Engineering, King Faisal University, Al-Ahsa, Saudi Arabia, [2]Civil Engineering Department, University of Engineering and Technology, Lahore, Pakistan, [3]Department of Civil Engineering, COMSATS University Islamabad, Abbottabad, Pakistan, [4]Department of Mechanical Engineering, College of Engineering, King Faisal University, Al-Ahsa, Saudi Arabia, [5]Research Centre, Future University in Egypt, New Cairo, Egypt

It is evident that preparing materials, casting samples, curing, and testing all need time and money. The construction sector will benefit if these problems can be handled using cutting-edge techniques like machine learning. Also, a material's ultrasonic pulse velocity (UPV) is affected by various variables, and it is difficult to study their combined effect experimentally. This research used machine learning to assess the UPV and SHapley Additive ExPlanations techniques to study the impact of input parameters of hybrid fiber-reinforced concrete modified with nano-silica (HFRNSC). Three ML algorithms were employed, i.e., gradient boosting regressor, adaptive boosting regressor, and extreme gradient boosting, for ultrasonic pulse velocity evaluation. The accuracy of machine learning models was measured *via* the coefficient of determination (R^2), k-fold analysis, statistical tests, and comparing the predicted and actual ultrasonic pulse velocity. This study determined that the gradient boosting and adaptive boosting models had a good level of accuracy for ultrasonic pulse velocity, but the extreme gradient boosting method estimated the ultrasonic pulse velocity of HFRNSCs with a greater degree of precision. Also, from the statistical checks and k-fold approach, it was discovered that the extreme gradient boosting method is more exact in estimating the ultrasonic pulse velocity of HFRNSCs. The SHapley Additive ExPlanations analysis revealed that the age of the specimen and nano-silica had a greater positive impact on the ultrasonic pulse velocity of HFRNSCs, whereas the coarse aggregate to fine aggregate ratio had a negative impact. In addition, fiber volume was found to have both positive and negative effects. By aiding the development of rapid and low-cost methods for determining material properties and the influence of input parameters, the construction industry may profit from the use of such technologies.

1 Introduction

Concrete is a commonly used building material (AMIN et al., 2019; KHAN et al., 2022F; KHAN et al., 2022G). To lower the brittleness of concrete, scholars are investigating fiber-reinforced concrete (FRC), which is significantly more ductile than conventional concrete (KHAN et al., 2018; LI AND DENG, 2021; XIE et al., 2021; ZAID et al., 2021). The onset of concrete failure is the emergence of cracks (CAO et al., 2019; XUPENG et al., 2021). The introduction of hybrid FRC, which is comprised of multiple fibers (glass, steel, and polypropylene), is proposed to enhance the mechanical performance and energy absorption capacity of concrete (CAO et al., 2018A; HUANG et al., 2021; XUE AND YILMAZ, 2022; ZHAO et al., 2022). Fibers restrict the growth of cracks in concrete, thereby allowing structural elements to withstand greater deformations following the development of early cracks (cao et al., 2018B; ABIRAMI et al., 2020; CHUN et al., 2022; ZHANG et al., 2022). Nanoparticles, such as nano-silica (NS), have been shown to fill holes in cement paste and improve the mechanical performance and durability of concrete (BAHARI et al., 2016; CAO et al., 2020; MURAD, 2021; KHAN et al., 2022E). Consequently, using nanoparticles in FRC might result in a material with enhanced performance that is perfect for constructing durable, high-performance structures (HAO et al., 2021). NS decreases the setting time of the mix and increases its early-age strength. A crucial characteristic of NS is its nanostructure, which offers an exceptionally greater specific surface area (SSA) and thus works as an aggregate-cement binder (WANG et al., 2018). The strong pozzolanic effect of NS is due to its nanoparticle size (ARDALAN et al., 2017; YING et al., 2017). The interfacial transition zone (ITZ), which is considered a weak region in concrete, is also strengthened because these nanoparticles cover all gaps and voids, hence decreasing permeability (XU et al., 2017; SHARKAWI et al., 2018). NS is a highly effective ingredient for accelerating the hydration and producing more calcium-silicate-hydrate (C-S-H) gel in concrete, which is responsible for the achievement of concrete strength (NIEWIADOMSKI et al., 2017; NORHASRI et al., 2017; MOHAMMED et al., 2018; REN et al., 2018; ZAHIRI AND ESKANDARI-NADDAF, 2019). In cementitious materials, the quantity of portlandite-$Ca(OH)_2$ reduces when NS and $Ca(OH)_2$ combine to form a denser product (MASSANA et al., 2018). Certain prior research suggests that replacing NS for up to 4% of the cement can improve the material's durability and strength under adverse conditions like corrosion and high temperatures (ERDEM et al., 2018; MAHAPATRA AND BARAI, 2019). The excessive quantity of NS might cause particle aggregation due to non-uniform dispersal, thus reducing workability (ZAREEI et al.,

2019). To improve the macroscopic characteristics and performance of cementitious composites, several nanoparticles are utilized as additives, and NS has become frequent among these nanoparticles. Notwithstanding, the limited practical applications of NS in the building industry are a result of their higher costs, which are approximately 1,000 times more expensive than ordinary cement (RECHES, 2018; FANG et al., 2021).

From the standpoint of evaluating the structural health of concrete structures, ultrasonic pulse velocity (UPV) has been identified as an essential measure (BOLBOREA et al., 2021; KARIMAEI et al., 2021). Numerous research was conducted to comprehend the correlation between UPV and concrete compressive strength (YAN et al., 2021; ZHANG AND ASLANI, 2021). Similarly to compressive strength, the UPV of concrete likewise increases with age and is inversely related to the pore volume in the matrix (KOU et al., 2012). The rate of change of UPV with time may be utilized not only to estimate the setting of a mix but also to show distinct phases of microstructural changes in the matrix (LATIF AL-MUFTI AND FRIED, 2012; BARLUENGA et al., 2015). It was also shown that UPV is impacted by microstructural differences in the mortar and may be utilized to efficiently assess sand concentration in a mortar (MOLERO et al., 2009). Additionally, the UPV of concrete was explored to identify deterioration within the concrete (OULD NAFFA et al., 2002; LENCIS et al., 2021).

In two ways, the UPV test findings of FRC vary from those of plain concrete. Firstly, since the observed velocity is directly related to the concentration of the medium through which it is propagated, the insertion of different fibers might vary the density of the concrete and, therefore, the UPV findings (ASHRAFIAN et al., 2018). For instance, recent studies observed that the UPV of steel FRC was higher than the plain concrete; however, the UPV of FRC with low-density fibers, like polyphenylene sulfide or recycled polyethylene terephthalate, was less than plain concrete (RAHMANI et al., 2013; SADEGHI NIK AND LOTFI OMRAN, 2013). Secondly, the introduction of varying amounts of fibers might affect the concrete's compaction level and, subsequently, its porosity (LI et al., 2022A; QIN et al., 2022; ZHENG et al., 2022). Previously, it was demonstrated that the slightly increased porosity of concrete resulting from the integration of 1% fibers by volume reduced the UPV of FRC samples, including polypropylene and steel fibers, by 4% and 3%, respectively (SUKONTASUKKUL et al., 2010). The number of parameters impacting concrete and the length of time necessary to establish the characteristics of hardened concrete motivate the search for alternate estimation techniques. UPV, which relies on ultrasonic wave speed transmission through the matrix, has been used to determine

the characteristics of hardened concrete (TRTNIK et al., 2009; HUANG et al., 2011; DÜĞENCI et al., 2015; MOBINI et al., 2015). As previously demonstrated, the UPV of concrete mixes is an excellent indicator of their mechanical characteristics, including compressive and flexural strength and modulus of elasticity (TRTNIK et al., 2009). Large, thin, and difficult-to-access elements make it difficult to assess the UPV of the concrete. Not only do data-driven models assist minimize the time and expense of testing by supplying designers with vital data, but they also aid in avoiding complications that emerge during the assessment of the many hardened characteristics of FRC. The progress of innovative formula-based models with high precision to forecast this essential attribute can greatly minimize concrete waste by reducing the number of trial mixes necessary to get the ideal blend (KHAN et al., 2022H). Artificial intelligence-based practices, like machine learning (ML), are among the highly modern prediction procedures used in the present issue area (NAFEES et al., 2021; KHAN et al., 2022A; NAFEES et al., 2022A; NAFEES et al., 2022B; ILYAS et al., 2022). These methods imitate results based on the input dataset, and resultant models are validated by testing. The utilization of ML techniques to anticipate the characteristics of construction materials is gaining prominence (SHAFABAKHSH et al., 2015; AWOYERA et al., 2020; KHAN et al., 2022D). The most of past ML-based researches centered on estimating the strength of traditional concrete (QI et al., 2022; SHAH et al., 2022; SHARMA et al., 2022), while few research has been published on predicting the UPV of FRC. Therefore, it is vital to study the effectiveness of ML methods in estimating the UPV of FRC.

This research utilized the data sample to estimate the UPV of hybrid fiber-reinforced concrete modified with NS, hereinafter called HFRNSC, by employing ML methods. Three ML methods from boosting family were employed, i.e., gradient boosting regressor (GBR), Adaptive boosting regressor (ABR), and extreme gradient boosting (XGB), to achieve the study's aims. Coefficient of determination (R^2), k-fold technique, statistical tests, and comparing estimated and actual results were used to assess and evaluate the performance of each model. It is obvious that conducting experiments requires a great deal of time, money, and effort due to the necessity of gathering materials, casting samples, curing, and testing. These issues might be resolved using cutting-edge methods like ML, which will be a benefit for the building industry. Moreover, the UPV and strength of HFRNSCs depend on a number of factors, and it is challenging to measure their combined influence using experimental methods. The influencing factors include fiber volume (Vf), coarse aggregate to fine aggregate ratio (CA/FA), superplasticizer to binder ratio (SP/B), water to binder ratio (w/b), NS, and age of specimen ((A). To investigate the relationship between the input characteristics and the UPV of HFRNSCs, a SHapley Additive exExplanations (SHAP) analysis was conducted. The literature may be mined for a data sample to use with ML methods. As a result, the information gathered may be used to run ML methods,

estimate material characteristics, and evaluate the influence of input factors. In this work, a dataset was used to evaluate the performance of several ML methods for predicting the UPV of HFRNSCs and to determine the relative importance of various input variables in producing accurate predictions.

2 Materials and methods

In order to get desired findings, ML methods require a wide collection of input variables (SUFIAN et al., 2021). For this purpose, a literature search was performed using six input parameters, including Vf, CA/FA, w/b, NS, SP/B, and the age of the specimen. To avoid bias, data samples were collected arbitrarily from previous studies (SADRMOMTAZI AND FASIHI, 2010; ASHRAFIAN et al., 2018), and data points containing UPV results were collected for algorithm execution. In this research, 132 data samples were recorded from the literature and employed to train ML techniques. The combination's proportions and the desired outcome were considered when obtaining the data since models called for similar input variables for each mixture to estimate the required results. Three types of fiber, including glass, steel, and polypropylene, were used in the samples as hybrid fibers. The length and diameter of steel fibers were 36 mm and 0.7 mm, respectively, while the length and diameter of polypropylene and glass fibers were 12 mm and 0.1 mm, respectively. For the ML algorithms to run, all six features were used as inputs, with UPV serving as the result. The statistical details of inputs and outcomes are summarized in Table 1. The standard deviation, maximum, and minimum, show the range of values, whereas the mode, mean, and median show the basic tendencies.

The UPV of HFRNSCs was analyzed by employing published research data. The goals of the study were attained by employing ML strategies using *Python* code and Spyder (version 5.1.5) tool from the Anaconda Navigator software. The UPV of HFRNSCs was evaluated using GBR, ABR, and XGB ML techniques. In practice, these ML techniques are typically employed to approximate outputs from given inputs (YUAN et al., 2022). ML techniques are being employed to predict the strength, durability, and temperature resistance of materials (AMIN et al., 2022; KHAN et al., 2022C). Nevertheless, there are some limitations associated with the use of ML methods. Specifically, challenges associated with dataset generation, model validation, and model deployment, as reported by (LI et al., 2022B). The allocation of testing and training data samples utilized for the model was 30% and 70%, respectively. The precision of a model may be noted from the R^2 value of the predicted result. Values closer to zero imply more variance, whereas values closer to one indicate that the prediction model and experimental findings are nearly completely matched (AHMAD et al., 2022). The k-fold method and statistical measures, including mean absolute error (MAE),

TABLE 1 Statistical parameters of input and output parameters.

Parameter	Vf (%)	CA/FA	W/b	NS (kg/m³)	SP/B	Age (days)	UPV (km/s)
Mean	0.23	0.88	0.39	23.95	0.02	40.76	5.23
Standard Error	0.02	0.00	0.00	1.61	0.00	3.00	0.02
Median	0.20	0.87	0.39	24.00	0.02	28.00	5.23
Mode	0.20	0.87	0.39	0.00	0.02	7.00	5.15
Standard Deviation	0.20	0.01	0.01	18.50	0.00	34.48	0.22
Minimum	0.00	0.87	0.39	0.00	0.02	7.00	4.49
Maximum	0.90	0.91	0.43	49.60	0.03	90.00	5.61

FIGURE 1
Flowchart of research methods.
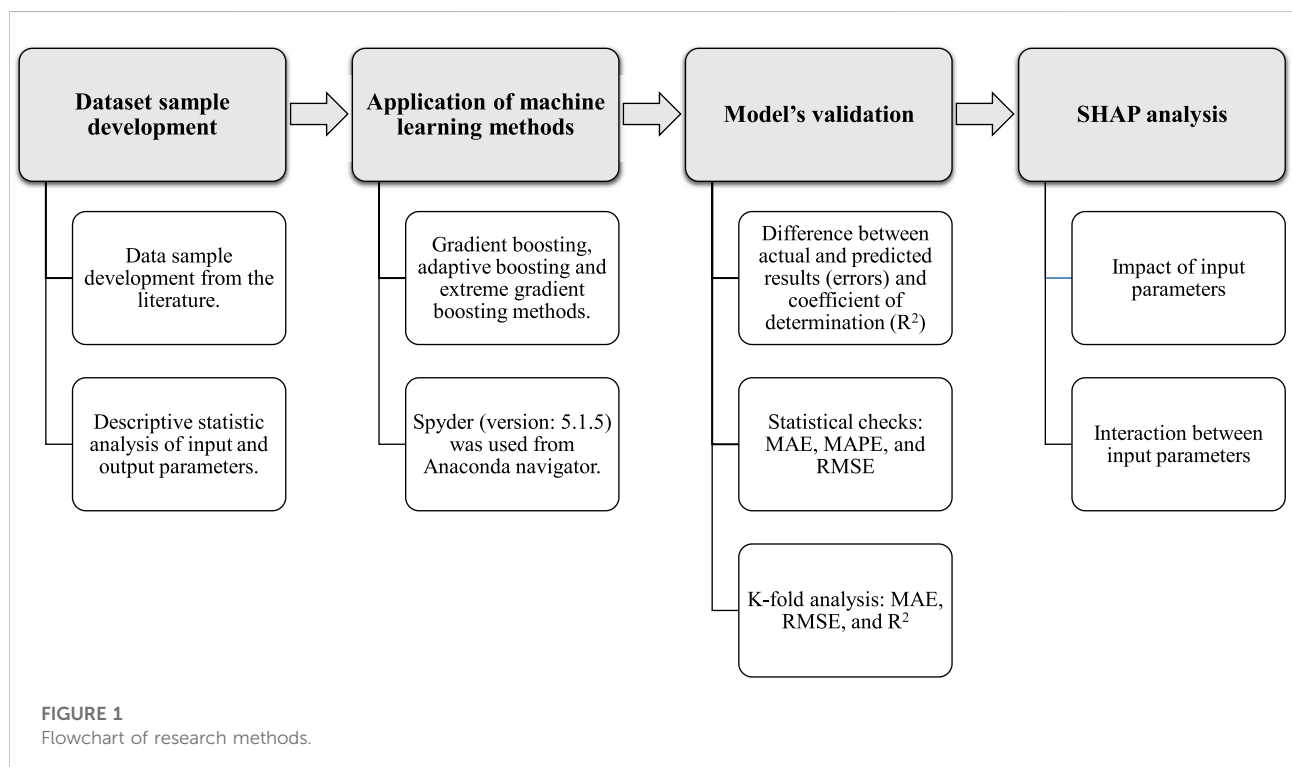
root mean squared error (RMSE) and mean absolute percentage error (MAPE), were employed to measure the exactness of a model. The sequence of study methods is shown in Figure 1. The subsequent sub-sections elaborate on the ML techniques and validation strategies that were put to use in this study.

2.1 Gradient boosting regressor (GBR)

The GBR ensemble method of regression and classification was first proposed by FRIEDMAN (2001). GBR is similar to other boosting techniques, except it can only be used for regression. As can be seen in Figure 2, the strategy randomly selects repetitions from the training set and then verifies them using the base model. As a result, preventing overfitting may be achieved by arbitrarily subsampling the training data sample, which can increase GBR's accuracy and speed. The rate of regression to fit tends to increase as the sample size of the training data decreases. Tuning factors for GBR include the shrinkage rate and n-trees, where n-trees is the total number of trees produced. In this case, n trees are not a small enough number; therefore, the learning rate (shrinkage factor) is applied to each expansion tree individually.
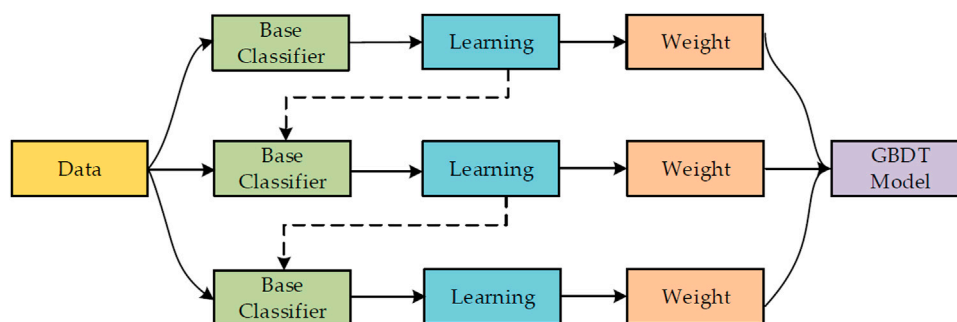
FIGURE 2
Structure of GBR training method (YAO et al., 2019).
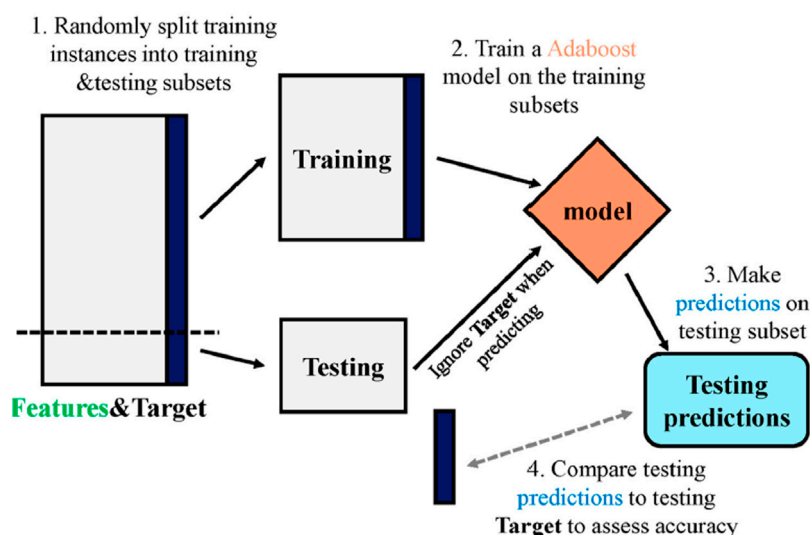
FIGURE 3
Structure of ABR training method (WANG et al., 2021).

2.2 Adaptive boosting regressor (ABR)

Figure 3 depicts the procedure for making an ABR-based estimation. The term "multi-classifiers" refers to the ensemble that is created when many algorithms are combined. An educational community of about a thousand people working together to find a solution to the situation. Ensemble learning, effectively a supervised ML methodology, is one way to tackle ABR. In adaptive boosting, weights are linked to each occurrence, with greater weights attached to examples that were incorrectly categorized. It is common practice in supervised machine learning to employ boosting algorithms in order to mitigate bias and reduce variance. Assisting struggling pupils through the use of ensemble strategies. It takes in as many decision trees as you like during the training process. Incorrectly classified data inside the core model are revealed during the decision tree

building phase. Another model uses the same set of data records as inputs. This process would continue until enough number of novice learners were produced. For problems involving binary classification, ABR facilitates the growth of the decision tree's operational capabilities. It's also used to make the ML model more efficient. It's a great tool for those who study slowly. These ensemble methods see extensive use in the field of materials science, particularly in the estimation of concrete's mechanical properties (YANG et al., 2022).

2.3 Extreme gradient boosting (XGB)

The XGB technique was developed by CHEN AND GUESTRIN (2016) and is regarded as a trustworthy tool for
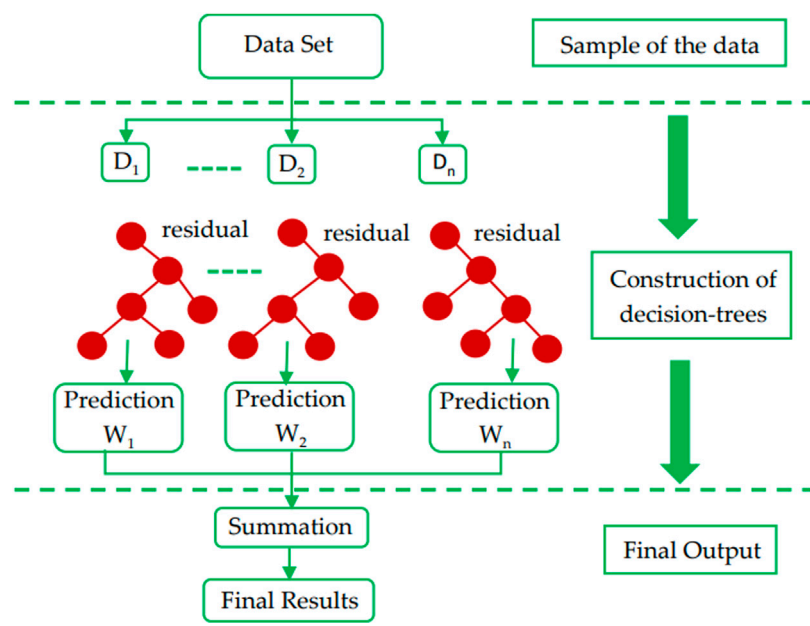
FIGURE 4
Schematic illustration of XGB procedure (AMJAD et al., 2022).
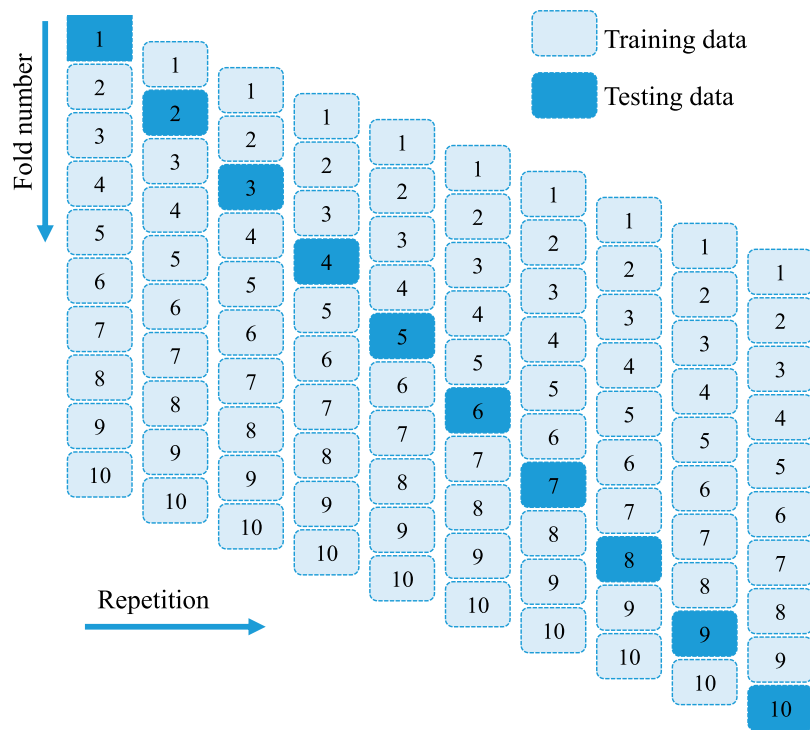
FIGURE 5
K-fold validation process.

FIGURE 6
GBR model: **(A)** Relationship amongst actual and estimated UPV; **(B)** Dispersal of actual and estimated UPV and error values.

FIGURE 7
ABR model: **(A)** Relationship amongst actual and estimated UPV; **(B)** Dispersal of actual and estimated UPV and error values.
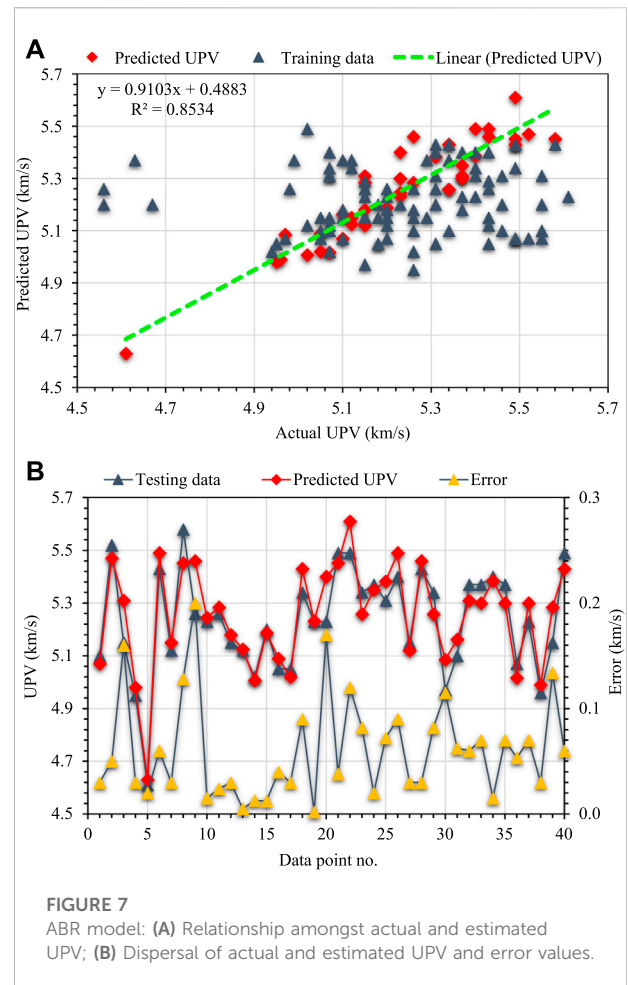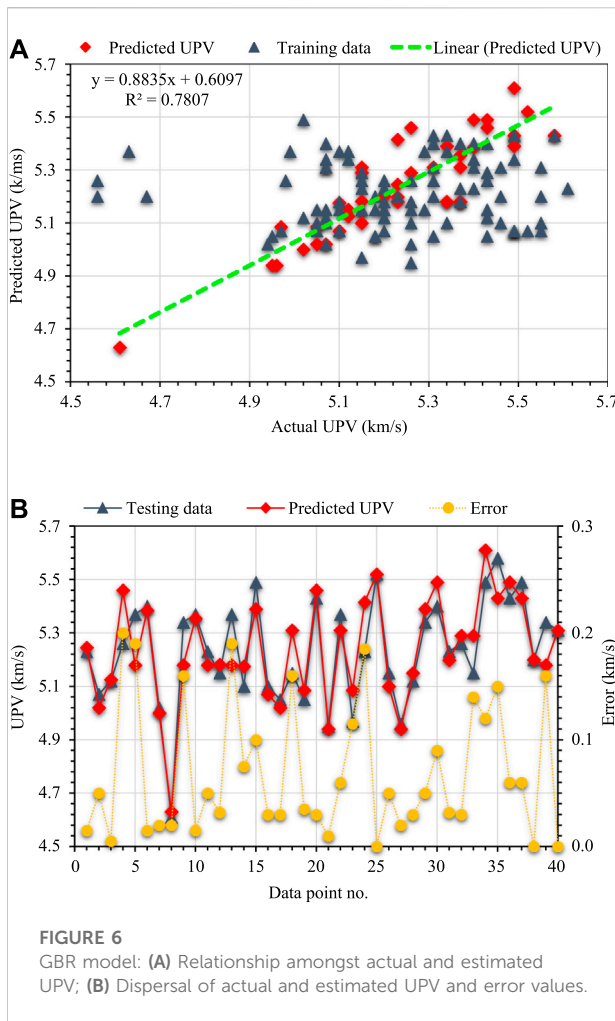
data science scholars since it uses a tree-based ensemble learning approach. XGB is built on the GBR architecture, which involves using several functions to estimate outcomes according to Eq. 1 (FRIEDMAN, 2001).

$$\bar{y}_i = y_i^0 + \eta \sum\nolimits_{K=1}^{n} f_k (U_i).$$ (1)

The anticipated output is represented by $\bar{y}_i$ with i^{th} data and U_i as the variable vector; η represents the estimator quantity in connection with separate tree structures next to each f_k With k ranging from 1 to n; and y_i^0 is the null hypothesis represents the learning rate to improve the accuracy of the model, as well as the connection of new trees to prevent overfitting. Building a model with minimum overfitting is a significant difficulty in ML. The training phase of the XGB model is assessed in a complementary manner.

According to Eq. 1, at the kth level, the kth predictor is associated with the model and the prediction of kth y_i^{-k} is

calculated using the expected output $y_i^{-(k-1)}$, with the respective produced f_k against the kth corresponding predictor supplied in Eq. 2.

$$y_i^{-k} = y_i^{-(k-1)} + \eta f_k$$ (2)

Where f_k is leave's weight formed by minimizing the kth tree factual task Eq. 3.

$$f_{obj} = \gamma Z + \sum\nolimits_{a=1}^{Z} \left[g_a \omega_a + \frac{1}{2} (h_a + \lambda) \omega_a^2 \right]$$ (3)

Where leaf node fraction is indicated by Z, complexity factor by γ, constant coefficient by λ, and leaf weight by ω_a^2, λ and γ are controlling parameters used to prevent overfitting and enhance the model. h_a and g_a are the summation factors for the whole data sample associated with the prior and initial gradient leaf loss functions, respectively. For the construction of the kth tree, a leaf is divided into many leaves. Such a system is implemented using gain parameters, as shown in Eq. 4.

FIGURE 8
XGB model: **(A)** Relationship amongst actual and estimated UPV; **(B)** Dispersal of actual and estimated UPV and error values.
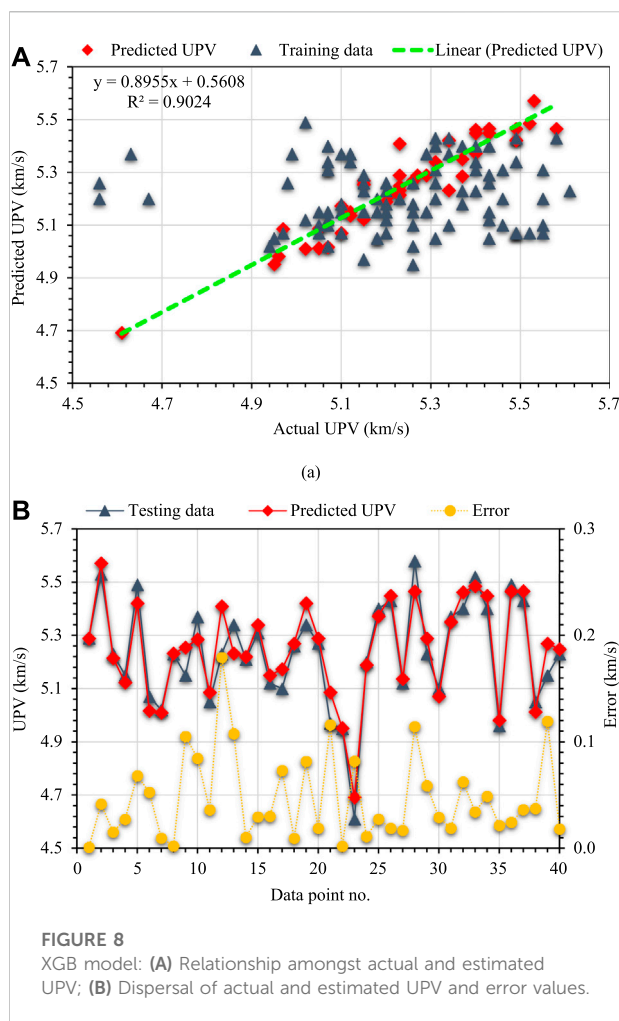
TABLE 2 Error assessments of the build ML-based models using statistical tests.

Model	MAE (km/s)	MAPE (%)	RMSE (km/s)
GBR	0.070	1.30	0.093
ABR	0.061	1.20	0.077
XGB	0.047	0.90	0.062

$$G = \frac{1}{2}\left[\frac{O_L^2}{P_L + \lambda} + \frac{O_R^2}{P_R + \lambda} + \frac{(O_L + O_R)^2}{P_L + P_R + \lambda}\right] \qquad (4)$$

Where gain parameters are represented by **G**, the right and left leaves are designated by P_R and O_R and P_L & O_L, respectively. In general, the division criterion is assumed while the approximation of the gain parameter to zero. λ is a regulating variable that is indirectly reliant on gain settings. For instance, a bigger regularization value might significantly reduce the gain parameter, hence stopping the leaf convolution process. However, the performance of the model when incorporating training data would also be diminished. Figure 4 depicts the fundamental level-wise structure of the XGB tree model.

2.4 Validation of models

The ML algorithms were verified using statistical tests and k-fold approaches. The k-fold technique is commonly used to assess a model's performance by randomly dividing samples of relevant data into 10 groups (AHMAD et al., 2021). Figure 5 illustrates how nine classes are utilized to train ML models, whereas just one is used for testing. The ML method performs better when errors are lower, and R^2 is higher. In addition, this approach needs to be repeated 10 times, which results in the model's exceptional accuracy. Errors assessment (MAE, RMSE, and MAPE) was also used statistically to assess the accuracy of each ML method. Statistical analysis was performed on the projections made by the ML approaches using Eqs 5–7, which were obtained from prior work (ASLAM et al., 2020; FAROOQ et al., 2021).

$$\text{MAE} = \frac{1}{n}\sum_{i=1}^{n}|P_i - Ti| \qquad (5)$$

$$\text{RMSE} = \sqrt{\sum \frac{(P_i - T_i)^2}{n}} \qquad (6)$$

$$\text{MAPE} = \frac{100\%}{n}\sum_{i=1}^{n}\frac{|P_i - Ti|}{T_i} \qquad (7)$$

where n = number of data points, P_i = predicted findings, and T_i = actual results.

3 Results and analysis

3.1 GBR model

Figure 6 shows the outcomes of the GBR model for estimating the HFRNSC's UPV. Figure 6A displays the relation among actual and estimated UPV. The GBR approach estimated UPV with a moderate level of accuracy and divergence among actual and estimated findings. The R^2 of 0.78 suggests that the GBR method for calculating the UPV of HFRNSCs is satisfactory, and the actual and estimated results reasonably agree. Figure 6B presents the actual, estimated, and error values distribution for the GBR model. The error values varied up to 0.200 km/s, with a mean of 0.070 km/s. Additionally, the percentage variance of errors was evaluated, and it was found that 47.5% of the error readings were lower than 0.05 km/s, 22.5% fell among 0.05–0.1 km/s, and 30.0% were higher than 0.1 km/s. The analysis of errors indicated that the GBR strategy estimated the UPV of HFRNSCs reasonably.

Fold no.	GBR			ABR			XGB		
	MAE (km/s)	RMSE (km/s)	R^2	MAE (km/s)	RMSE (km/s)	R^2	MAE (km/s)	RMSE (km/s)	R^2
1	0.09	0.10	0.74	0.08	0.11	0.72	0.07	0.07	0.76
2	0.07	0.09	0.63	0.06	0.09	0.63	0.08	0.07	0.82
3	0.11	0.12	0.61	0.09	0.12	0.58	0.09	0.08	0.71
4	0.09	0.11	0.57	0.08	0.10	0.65	0.08	0.10	0.90
5	0.10	0.08	0.72	0.10	0.08	0.78	0.05	0.07	0.83
6	0.09	0.09	0.64	0.08	0.08	0.81	0.05	0.07	0.85
7	0.07	0.19	0.73	0.07	0.09	0.84	0.07	0.11	0.86
8	0.18	0.29	0.32	0.06	0.15	0.76	0.09	0.17	0.39
9	0.07	0.14	0.78	0.07	0.22	0.85	0.06	0.06	0.88
10	0.16	0.19	0.45	0.08	0.13	0.33	0.05	0.18	0.52

3.2 ABR model

Figure 7 presents the findings of the ABR model in forecasting the UPV of the HFRNSCs. The relation amongst actual and forecasted UPV is seen in Figure 7A. In comparison with the GBR approach, the ABR technique produced more accurate results and the minimum difference among actual and estimated findings. Compared to other models, the ABR model is more precise, as seen by its R^2 score of 0.85. The distribution of real, estimated, and error values generated by the ABR approach are depicted in Figure 7B. The lowest error was 0.002 km/s, the mean error was 0.061 km/s, and the highest error was 0.200 km/s. The distribution of error values was: 47.5% were below 0.05 km/s, 35.0% were between 0.05 and 0.1 km/s, and 17.5% were over 0.1 km/s. Since the ABR model had a smaller deviation of errors, it was concluded that it was more accurate than the GBR model. Due to the usage of an endless number of decision trees during training and its initial decision tree's emphasis on incorrectly categorized input, the ABR model achieves better accuracy. Another model also makes use of the same data. This process is repeated until enough number of basic learners have been created. Additionally, ABR improves the effectiveness of decision trees for classifying data into two categories.

3.3 XGB model

Figure 8 exhibits the results of the XGB method to foretell the UPV of HFRNSCs. A connection among actual and forecasted UPV is shown in Figure 8A. The XGB method produced the fewest discrepancies amongst real and anticipated data as compared to the other models used. The higher R^2 of 0.90 for the XGB model reflects its improved

accuracy. The XGB method's actual, estimated, and errors are shown in Figure 8B. The average error was calculated to be 0.047 km/s, while the maximum error was calculated to be 0.179 km/s. Nearly 65.0% of the errors were found to be less than 0.05 km/s, 20.0% were found to be between 0.05 and 0.1 km/s, and 15.0% were found to be larger than 0.1 km/s. The error distribution showed that the XGB model was more accurate than the GBR and ABR models. But the accuracy of the other models used is equally satisfactory. The XGB model is more precise because it employs a tree-based ensemble learning strategy that optimizes output by generating submodels.

3.4 Model's validation

Table 2 displays the results of the error evaluations (MAE, RMSE, and MAPE) utilizing the aforementioned Eqs.s 5-7 for UPV estimation models. The MAE for predicting UPVs were found to be 0.070 km/s for GBR, 0.061 km/s for ABR, and 0.047 km/s for XGB. According to the calculations, the MAPE for GBR was 1.30%, ABR was 1.20%, and XGB was 0.90%. In addition, it was found that the RMSE for GBR, ABR, and XGB were 0.093, 0.077, and 0.062 km/s, respectively. These evaluations also showed that the XGB method had a lower error rate than the GBR and the ABR, making it more exact. Table 3 displays the results of calculating the k-fold method's validity using R^2, RMSE, and MAE. The k-fold analysis for the UPV prediction was compared using the various ML approaches used, and the results are depicted in Figure 9, Figure 10, and Figure 11. The MAE for the UPV estimation using the GBR method ranged from 0.07 to 0.18 km/s, with a mean of 0.10 km/s. The MAE for the ABR model was 0.06–0.10 km/s, with an average of 0.08 km/s. The XGB model had an MAE
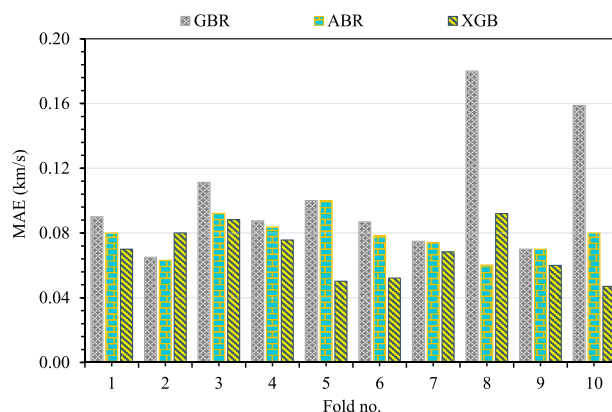
FIGURE 9
MAE values for all models from the k-fold analysis.
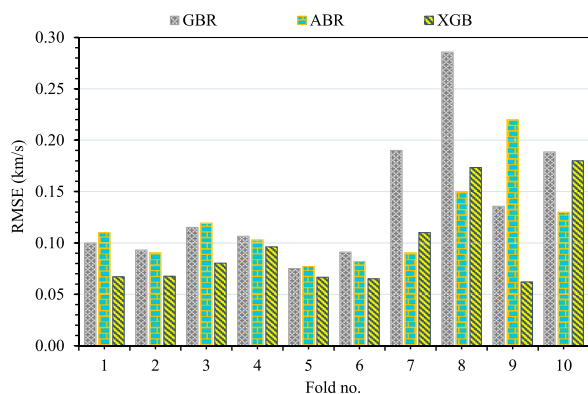
FIGURE 10
RMSE values for all models from the k-fold analysis.
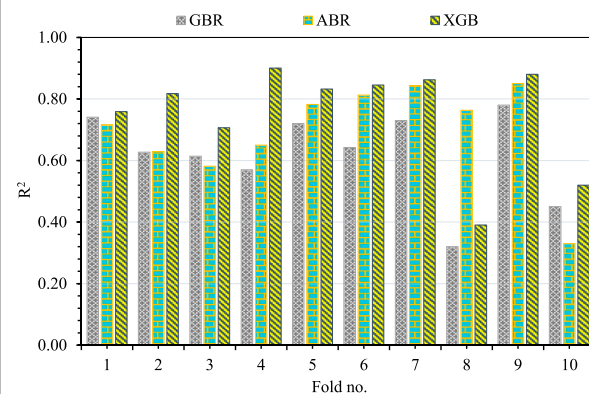
FIGURE 11
R^2 values for all models from the k-fold analysis.

distribution from 0.05 to 0.09 km/s, with an average of 0.07 km/s. Similar results were found when comparing the RMSE of the GBR, ABR, and XGB methods. The average RMSE for GBR, ABR, and XGB was 0.14, 0.12, and 0.10 km/s, respectively. However, the average R^2 values for GBR, ABR, and XGB were 0.62, 0.70, and 0.75, respectively. The XGB model predicted the UPV of HFRNSCs with the fewest errors, and the highest R^2 was the most reliable. However, both the ABR and GBR models achieved reasonable levels of accuracy. Therefore, all of the models might be used to precisely evaluate the UPV of HFRNSCs.

3.5 Impact of input features on UPV

This study looked at how different input characteristics affected the UPV of HFRNSCs. SHAP tree explainer is used

across the board to include local SHAP explanations into a more comprehensive narrative of global feature impacts. Input-by-input, the violin SHAP plot shows how HFRNSCs' UPV responds to all stimuli (see Figure 12). The x-axis represents the final SHAP value after all parameters have been adjusted, and the y-axis represents the contribution of each individual parameter. The positive correlation among the age of specimen A) and UPV of HFRNSCs was bigger than that of any other characteristic (more red points on the positive side). It was determined that UPV rises as specimen age A) rise. It was also demonstrated that the impact of NS on the UPV was more positive. It might be because NS acts as a filler, decreasing the porosity of the matrix and leading to an increase in UPV. In contrast, it was shown that CA/FA had a larger negative effect on UPV, suggesting that CA/FA should be kept low to get a higher UPV. One probable explanation is that UPV is inversely

FIGURE 12
SHAP plot signifying the effect of input features on UPV.
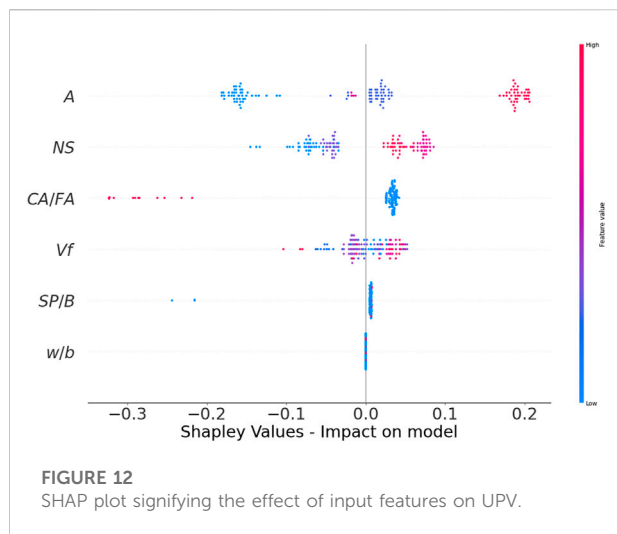
proportional to matrix porosity (MOHAMMED AND RAHMAN, 2016); thus, when CA/FA increases, UPV decreases. It was shown that Vf had both positive and negative effects, suggesting that utilizing Vf up to an optimal amount can improve the UPV but that at larger Vf

concentrations, the UPV would decrease. The impact of SP/B and w/b could not be determined due to the absence of input value variation in the used dataset. Using a bigger data sample with more varied input features can better interpret their impact.

Figure 13 displays the relation amongst prominent input parameters and their effect on the UPV of HFRNSCs. Figure 13A shows the interaction of specimen age A). The plot demonstrates that as the specimen age A) increases, the UPV rises and mainly interacts with the NS. It can be established that with increasing age, the reaction between NS and $Ca(OH)_2$ takes place, resulting in the formation of dense microstructure, increasing the UPV of the sample. Likewise, incorporating NS in FRC has a favorable effect on UPV (Figure 13B) and interacts mostly with specimen age A). However, utilizing NS up to the optimal quantity will help improve the UPV of HFRNSCs. Hence, NS may be employed in the range of 30–40 kg/m³ to achieve higher UPV. Furthermore, as depicted in Figure 13C, increasing CA/FA has a detrimental effect on UPV. Therefore, the CA/FA should be maintained lower to get a higher UPV. The UPV of the HFRNSC is also affected by Vf, as shown in Figure 13D. UPV rises with Vf concentration up to 0.5%, then drops and largely interacts with the NS. For getting a high UPV for HFRNSC under these

FIGURE 13
Interaction of input parameters and their impact on UPV: **(A)** Age of specimen; **(B)** Nano-silica; **(C)** Coarse aggregate to fine aggregate ratio; **(D)** Fiber volume.
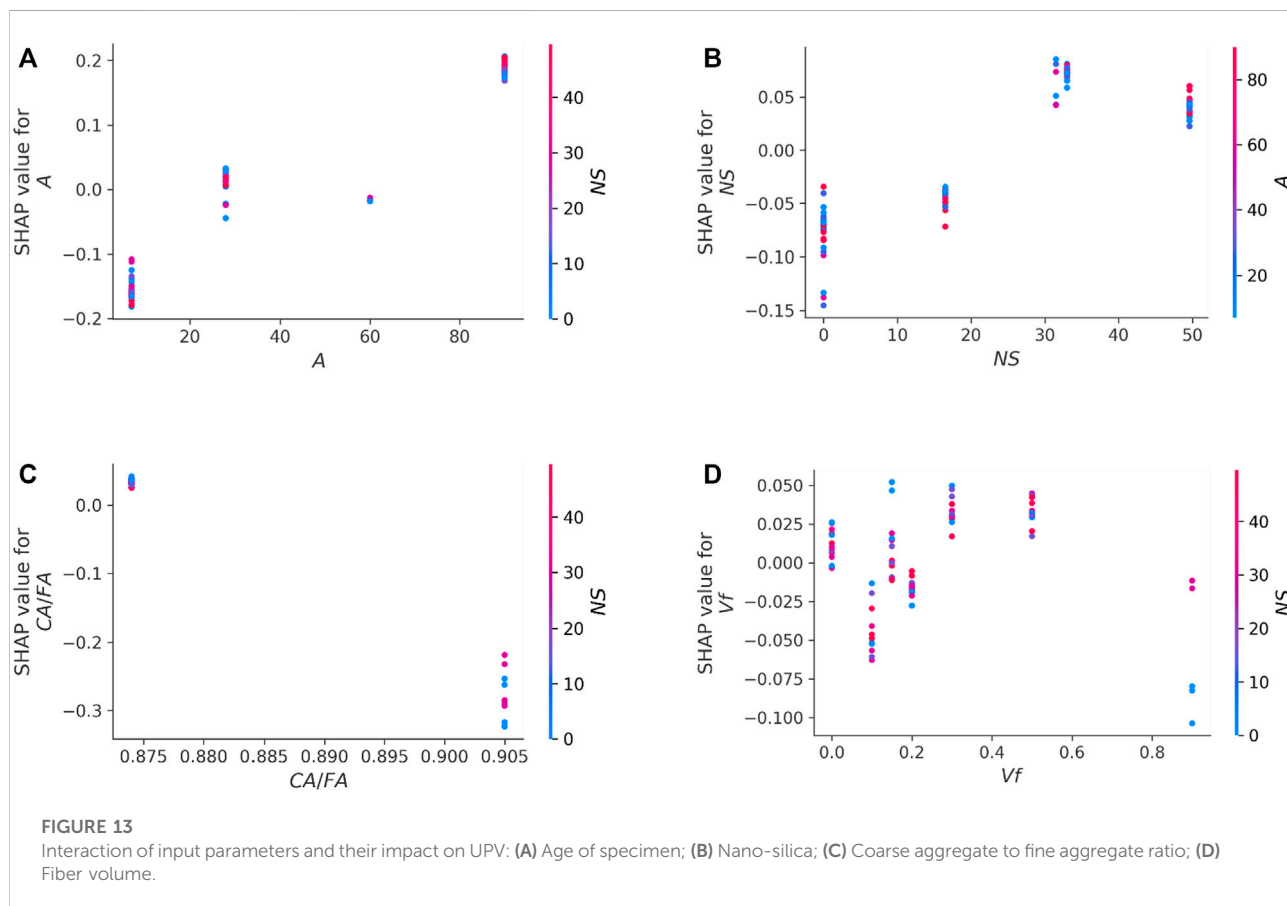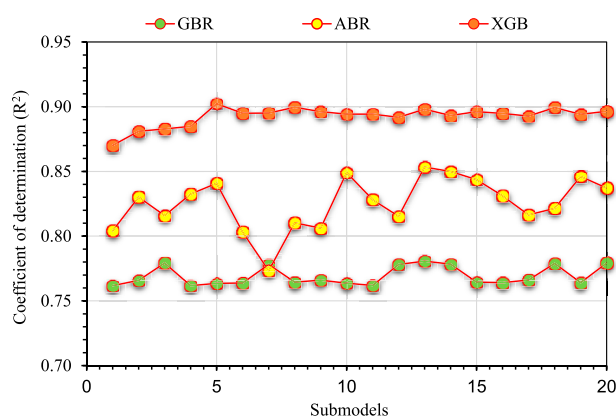
FIGURE 14
Distribution of R² for the XGB UPV and FS models.

TABLE 4 Best ML techniques recommended in past studies.

Study	Material studied	Properties predicted	ML method used	Best ML technique reported
ZHENG et al. (2022)	Steel fiber -reinforced concrete	Flexural strength	GBR, random forest, and XGB	XGB
KHAN et al. (2022b)	Geopolymer concrete	Compressive strength	Support vector machine, GBR, and XGB	XGB
WANG et al. (2022)	Geopolymer concrete	Compressive strength	Decision tree, ABR, and random forest	ABR
SHANG et al. (2022)	Recycled aggregate concrete	Compressive and split-tensile strength	Decision tree and ABR	ABR
AL-HASHEM et al. (2022)	Steel fiber-reinforced concrete	Compressive and flexural strength	Multiple-layer perceptron neural network and ABR	ABR
ANJUM et al. (2022)	Fiber reinforced concrete	Compressive strength	Bagging, random forest, GBR, and ABR	ABR

circumstances while employing the same components as in the current study, a Vf of almost 0.5% is ideal. These findings heavily rely on the nature of the inputs used and the scope of the dataset used in this analysis. Depending on the parameters and data used, the results may change.

4 Discussions

In this study, GBR, ABR, and XGB ML methods were utilized to evaluate the HFRNSCs' UPV. Each method was tested for precision to determine which one was the most reliable indicator. The XGB approach yielded more precise findings, with an R^2 of 0.90, for UPV prediction than the GBR and ABR methods, which had R^2 of 0.78 and 0.85, respectively. The error readings provided additional proof of the XGB method's better accuracy. The error analysis reveals

that the XGB models had a better agreement between real and estimated values than the GBR and ABR methods. Table 4 is generated to compare the optimum ML methods of the present study with the literature. Previous studies have proven the XGB method's superior accuracy in forecasting the strength of cementitious materials (FAROOQ et al., 2021; KHAN et al., 2022b; ZHENG et al., 2022). Similarly, the ABR method was also noted to be the best suitable in several studies (AL-HASHEM et al., 2022; ANJUM et al., 2022; SHANG et al., 2022; WANG et al., 2022).

Additionally, k-fold and statistical methods were utilized to evaluate the models' precision. The accuracy of a model increases when the R^2 is high and the degrees of divergence (MAE, RMSE, and MAPE) are minimum. Because the precision of an ML approach is so dependent on the amount of inputs and data samples used to run algorithms (FAROOQ et al., 2021), it is challenging to define and suggest

the best ML technique for prediction in different fields of research. With ensemble ML techniques, the weak learner is used over and over again to build submodels that are trained on the data sample and then fine-tuned to improve accuracy. In this way, the ensemble ML models produce more precise results than any of the individual models could have on their own. The variation in R^2 for the GBR, ABR, and XGB submodels is displayed in Figure 14. For GBR submodels, R^2 varied from 0.762 to 0.781, with a mean of 0.769. The average R^2 for the ABR models was 0.825, with a range of 0.773–0.853. Furthermore, the XGB submodels' R^2 ranged from 0.870 to 0.902, with an average of 0.893. Based on these results, it can be said that the XGB submodels are the most accurate of the three. More specifically, a SHAP analysis was run to learn how various input factors affected the UPV of HFRNSCs and how they interacted with one another. In a greater positive correlation with the UPV of the HFRNSC, specimen age was shown to be a highly useful parameter. The impact of NS on the UPV was also revealed to be more beneficial. It could be relied on by the filler action of NS, which lowers matrix porosity and ultimately raises UPV. However, it was shown that the impact of CA/FA on UPV was more adverse, indicating that a low CA/FA must be maintained to get a higher UPV. Also, it was determined that Vf had both positive and negative effects, suggesting that utilizing Vf up to an optimum amount can improve the UPV, while at larger Vf contents, the UPV may decline. The increasing matrix porosity, which is inversely correlated with matrix porosity (MOHAMMED AND RAHMAN, 2016), may cause decreased UPV at greater CA/FA and Vf. Because of the dearth of alteration in SP/B and w/b in the dataset used, their influence was unclear, and a broader data sample with more inputs and variations might result in better findings.

5 Conclusion

This research aimed to expand the knowledge on how machine learning (ML) models might be used to estimate the ultrasonic pulse velocity (UPV) of hybrid fiber-reinforced concrete modified with nano-silica (HFRNSCs). Three ML methods, including gradient boosting regressor (GBR), adaptive boosting regressor (ABR), and extreme gradient boosting (XGB), were used to evaluate the UPV. Also, SHapley Additive ExPlanations (SHAP) analysis was performed to examine the effect of input features on the UPV of HFRNSCs. The conclusions of this research are as follows:

- Modeling methods showed that the GBR and ABR techniques had a satisfactory level of accuracy with an R^2 of 0.78 and 0.85 for UPV estimation, respectively, while

the XGB method had a better level of accuracy with an R^2 of 0.90 for UPV prediction.
- The average difference among actual and estimated UPV (error) in GBR, ABR, and XGB techniques was found to be 0.070, 0.061, and 0.047 km/s, respectively. The error analysis also validated the reasonable accuracy of the GBR and ABR approaches and the superior precision of the XGB model in predicting the UPV of HFRNSCs.
- The SHAP analysis showed that specimen age was a crucial parameter, with a superior positive relationship to the material's UPV. It was also discovered that the effect of nano-silica (NS) on the UPV was more favorable. Nonetheless, it was discovered that the effect of coarse aggregate to fine aggregate ratio (CA/FA) on UPV was more negative, indicating that a low CA/FA must be maintained to increase UPV. In addition, it was revealed that fiber volume (Vf) had both positive and negative impacts, suggesting that incorporating Vf up to the optimal level can increase the UPV; however, at higher Vf concentrations, the UPV may fall.
- The construction sector will benefit from the development of more efficient and cost-effective methods for assessing material properties and the influence of different factors by using novel methods like ML and SHAP analysis.

This study utilized data for which controlled-environment experiments were conducted (laboratory). It is proposed that in future research, actual on-site circumstances, such as humidity, temperature, curing, *etc.*, should be integrated into the modeling phase in order to investigate their effect on the material's strength.

Data availability statement

The original contributions presented in the study are included in the article/supplementary material, further inquiries can be directed to the corresponding author.

Author contributions

KK: conceptualization, methodology, project administration, writing, reviewing, and editing. MA: investigation, resources, writing, reviewing, and editing. US: data acquisition, visualization, writing, reviewing, and editing. WA: conceptualization, software, methodology, validation, investigation, supervision, writing original draft, reviewing, and editing. MF: methodology, resources, writing, reviewing, and editing. AM: data curation, visualization, writing, reviewing, and editing.

Funding

Acknowledgments

Conflict of interest

The authors declare that the research was conducted in the absence of any commercial or financial relationships that could be construed as a potential conflict of interest.

Publisher's note

All claims expressed in this article are solely those of the authors and do not necessarily represent those of their affiliated organizations, or those of the publisher, the editors and the reviewers. Any product that may be evaluated in this article, or claim that may be made by its manufacturer, is not guaranteed or endorsed by the publisher.

References

Abirami, R., Vijayan, D. S., John, S. J., Albert, A., and Alex, A. K. (2020). Experimental study on concrete properties using pineapple leaf fiber. *Int. J. Adv. Res. Eng. Technol.* 11 (6), 913–920.

Ahmad, A., Ahmad, W., Aslam, F., and Joyklad, P. (2022). Compressive strength prediction of fly ash-based geopolymer concrete via advanced machine learning techniques. *Case Stud. Constr. Mater.* 16, e00840. doi:10.1016/j.cscm.2021.e00840

Ahmad, A., Chaiyasarn, K., Farooq, F., Ahmad, W., Suparp, S., and Aslam, F. (2021). Compressive strength prediction via gene expression programming (GEP) and artificial neural network (ANN) for concrete containing RCA. *Buildings* 11, 324. doi:10.3390/buildings11080324

Al-Hashem, M. N., Amin, M. N., Ahmad, W., Khan, K., Ahmad, A., Ehsan, S., et al. (2022). Data-driven techniques for evaluating the mechanical strength and raw material effects of steel fiber-reinforced concrete. *Materials* 15, 6928. doi:10.3390/ma15196928

Amin, M. N., Hissan, S., Shahzada, K., Khan, K., and Bibi, T. (2019). Pozzolanic reactivity and the influence of rice husk ash on early-age autogenous shrinkage of concrete. *Front. Mat.* 6, 150. doi:10.3389/fmats.2019.00150

Amin, M. N., Khan, K., Ahmad, W., Javed, M. F., Qureshi, H. J., Saleem, M. U., et al. (2022). Compressive strength estimation of geopolymer composites through novel computational approaches. *Polymers* 14, 2128. doi:10.3390/polym14102128

Amjad, M., Ahmad, I., Ahmad, M., Wróblewski, P., Kamiński, P., and Amjad, U. (2022). Prediction of pile bearing capacity using XGBoost algorithm: Modeling and performance evaluation. *Appl. Sci.* 12, 2126. doi:10.3390/app12042126

Anjum, M., Khan, K., Ahmad, W., Ahmad, A., Amin, M. N., and Nafees, A. (2022). Application of ensemble machine learning methods to estimate the compressive strength of fiber-reinforced nano-silica modified concrete. *Polymers* 14, 3906. doi:10.3390/polym14183906

Ardalan, R. B., Jamshidi, N., Arabameri, H., Joshaghani, A., Mehrinejad, M., and Sharafi, P. (2017). Enhancing the permeability and abrasion resistance of concrete using colloidal nano-SiO2 oxide and spraying nanosilicon practices. *Constr. Build. Mater.* 146, 128–135. doi:10.1016/j.conbuildmat.2017.04.078

Ashrafian, A., Taheri Amiri, M. J., Rezaie-Balf, M., Ozbakkaloglu, T., and Lotfi-Omran, O. (2018). Prediction of compressive strength and ultrasonic pulse velocity of fiber reinforced concrete incorporating nano silica using heuristic regression methods. *Constr. Build. Mater.* 190, 479–494. doi:10.1016/j.conbuildmat.2018.09.047

Aslam, F., Farooq, F., Amin, M. N., Khan, K., Waheed, A., Akbar, A., et al. (2020). Applications of gene expression programming for estimating compressive strength of high-strength concrete. *Adv. Civ. Eng.* 2020, 1–23. doi:10.1155/2020/8850535

Awoyera, P. O., Kirgiz, M. S., Viloria, A., and Ovallos-Gazabon, D. (2020). Estimating strength properties of geopolymer self-compacting concrete using machine learning techniques. *J. Mater. Res. Technol.* 9, 9016–9028. doi:10.1016/j.jmrt.2020.06.008

Bahari, A., Berenjian, J., and Sadeghi-Nik, A. (2016). Modification of portland cement with nano SiC. *Proc. Natl. Acad. Sci. India Sect. A. Phys. Sci.* 86, 323–331. doi:10.1007/s40010-015-0244-y

Barluenga, G., Puentes, J., and Palomar, I. (2015). Early age monitoring of self-compacting concrete with mineral additions. *Constr. Build. Mater.* 77, 66–73. doi:10.1016/j.conbuildmat.2014.12.033

Bolborea, B., Baera, C., Dan, S., Gruin, A., Burduhos-Nergis, D.-D., and Vasile, V. (2021). Concrete compressive strength by means of ultrasonic pulse velocity and moduli of elasticity. *Materials* 14, 7018. doi:10.3390/ma14227018

Cao, M., Khan, M., and Ahmed, S. (2020). Effectiveness of calcium carbonate whisker in cementitious composites. *Period. Polytech. Civ. Eng.* 64, 265. doi:10.3311/ppci.14288

Cao, M., Li, L., and Khan, M. (2018a). Effect of hybrid fibers, calcium carbonate whisker and coarse sand on mechanical properties of cement-based composites. *Mat. construcc.* 68, e156. doi:10.3989/mc.2018.01717

Cao, M., Xie, C., Li, L., and Khan, M. (2018b). The relationship between reinforcing index and flexural parameters of new hybrid fiber reinforced slab. *Comput. Concr. Int. J.* 22, 481–492.

Cao, S., Xue, G., and Yilmaz, E. (2019). Flexural behavior of fiber reinforced cemented tailings backfill under three-point bending. *IEEE Access* 7, 139317–139328. doi:10.1109/access.2019.2943479

Chen, T., and Guestrin, C. X (2016). A scalable tree boosting systemProceedings of the 22nd acm sigkdd international conference on knowledge discovery and data mining. New York, NY. 13 August 2016 New York: Association for Computing Machinery. 785–794. doi:10.1145/2939672.2939785

Chun, B., Kim, S., and Yoo, D.-Y. (2022). Reinforcing effect of surface-modified steel fibers in ultra-high-performance concrete under tension. *Case Stud. Constr. Mater.* 16, e01125. doi:10.1016/j.cscm.2022.e01125

Düğenci, O., Haktanir, T., and Altun, F. (2015). Experimental research for the effect of high temperature on the mechanical properties of steel fiber-reinforced concrete. *Constr. Build. Mater.* 75, 82–88. doi:10.1016/j.conbuildmat.2014.11.005

Erdem, S., Hanbay, S., and Güler, Z. (2018). Micromechanical damage analysis and engineering performance of concrete with colloidal nano-silica and demolished concrete aggregates. *Constr. Build. Mater.* 171, 634–642. doi:10.1016/j.conbuildmat.2018.03.197

Fang, Y., Wang, J., Ma, H., Wang, L., Qian, X., and Qiao, P. (2021). Performance enhancement of silica fume blended mortars using bio-functionalized nano-silica. *Constr. Build. Mater.* 312, 125467. doi:10.1016/j.conbuildmat.2021.125467

Farooq, F., Ahmed, W., Akbar, A., Aslam, F., and Alyousef, R. (2021). Predictive modeling for sustainable high-performance concrete from industrial wastes: A comparison and optimization of models using ensemble learners. *J. Clean. Prod.* 292, 126032. doi:10.1016/j.jclepro.2021.126032

Friedman, J. H. (2001). Greedy function approximation: A gradient boosting machine. *Ann. statistics*, 1189–1232.

Hao, X., Wei, Y., Chen, Z., Zhang, H., Niu, Y., Chen, K., et al. (2021). Mechanical modification of nanomaterials on fully saturated concrete in groundwater reservoir under long-term water immersion. *Front. Mat.* 8. doi:10.3389/fmats.2021.702308

Huang, Q., Gardoni, P., and Hurlebaus, S. (2011). Predicting concrete compressive strength using ultrasonic pulse velocity and rebound number. *ACI Mater. J.* 108.

Huang, Z., Cao, S., and Yilmaz, E. (2021). Investigation on the flexural strength, failure pattern and microstructural characteristics of combined fibers reinforced cemented tailings backfill. *Constr. Build. Mater.* 300, 124005. doi:10.1016/j.conbuildmat.2021.124005

Ilyas, I., Zafar, A., Afzal, M. T., Javed, M. F., Alrowais, R., Althoey, F., et al. (2022). Advanced machine learning modeling approach for prediction of compressive strength of FRP confined concrete using multiphysics genetic expression programming. *Polymers* 14, 1789. doi:10.3390/polym14091789

Karimaei, M., Dabbaghi, F., Dehestani, M., and Rashidi, M. (2021). Estimating compressive strength of concrete containing untreated coal waste aggregates using ultrasonic pulse velocity. *Materials* 14, 647. doi:10.3390/ma14030647

Khan, K., Ahmad, A., Amin, M. N., Ahmad, W., Nazar, S., and Arab, A. M. A. (2022a). Comparative study of experimental and modeling of fly ash-based concrete. *Materials* 15, 3762. doi:10.3390/ma15113762

Khan, K., Ahmad, W., Amin, M. N., Ahmad, A., Nazar, S., and Al-Faiad, M. A. (2022b). Assessment of artificial intelligence strategies to estimate the strength of geopolymer composites and influence of input parameters. *Polymers* 14, 2509. doi:10.3390/polym14122509

Khan, K., Ahmad, W., Amin, M. N., Ahmad, A., Nazar, S., and Alabdullah, A. A. (2022c). Compressive strength estimation of steel-fiber-reinforced concrete and raw material interactions using advanced algorithms. *Polymers* 14, 3065. doi:10.3390/polym14153065

Khan, K., Ahmad, W., Amin, M. N., Aslam, F., Ahmad, A., and Al-Faiad, M. A. (2022d). Comparison of prediction models based on machine learning for the compressive strength estimation of recycled aggregate concrete. *Materials* 15, 3430. doi:10.3390/ma15103430

Khan, K., Ahmad, W., Amin, M. N., and Nazar, S. (2022e1989). Nano-silica-modified concrete: A bibliographic analysis and comprehensive review of material properties. *Nanomaterials* 12, 1989. doi:10.3390/nano12121989

Khan, M., Cao, M., Chaopeng, X., and Ali, M. (2022f). Experimental and analytical study of hybrid fiber reinforced concrete prepared with basalt fiber under high temperature. *Fire Mater.* 46, 205–226. doi:10.1002/fam.2968

Khan, M., Cao, M., Xie, C., and Ali, M. (2022g). Effectiveness of hybrid steel-basalt fiber reinforced concrete under compression. *Case Stud. Constr. Mater.* 16, e00941. doi:10.1016/j.cscm.2022.e00941

Khan, M., Lao, J., and Dai, J.-G. (2022h). Comparative study of advanced computational techniques for estimating the compressive strength of UHPC. *J. Asian Concr. Fed.* 8, 51–68. doi:10.18702/acf.2022.6.8.1.51

Khan, U. A., Jahanzaib, H. M., Khan, M., and Ali, M. (2018). Improving the tensile energy absorption of high strength natural fiber reinforced concrete with fly-ash for bridge girders. *Key Eng. Mat.* 765, 335–342. doi:10.4028/www.scientific.net/kem.765.335

Kou, S.-C., Poon, C.-S., and Wan, H.-W. (2012). Properties of concrete prepared with low-grade recycled aggregates. *Constr. Build. Mater.* 36, 881–889. doi:10.1016/j.conbuildmat.2012.06.060

Latif Al-Mufti, R., and Fried, A. N. (2012). The early age non-destructive testing of concrete made with recycled concrete aggregate. *Constr. Build. Mater.* 37, 379–386. doi:10.1016/j.conbuildmat.2012.07.058

Lencis, U., Udris, A., and Korjakins, A. (2021). Frost influence on the ultrasonic pulse velocity in concrete at early phases of hydration process. *Case Stud. Constr. Mater.* 15, e00614. doi:10.1016/j.cscm.2021.e00614

Li, J., and Deng, Z. (2021). Tensile behavior of hybrid fiber-reinforced ultra-high-performance concrete. *Front. Mat.* 8. doi:10.3389/fmats.2021.769579

Li, Y., Zhang, Q., Kamiński, P., Deifalla, A. F., Sufian, M., Dyczko, A., et al. (2022a). Compressive strength of steel fiber-reinforced concrete employing supervised machine learning techniques. *Materials* 15, 4209. doi:10.3390/ma15124209

Li, Z., Yoon, J., Zhang, R., Rajabipour, F., Srubar, W. V., III, Dabo, I., et al. (2022b). Machine learning in concrete science: Applications, challenges, and best practices. *npj Comput. Mat.* 8, 127. doi:10.1038/s41524-022-00810-x

Mahapatra, C. K., and Barai, S. V. (2019). Temperature impact on residual properties of self-compacting based hybrid fiber reinforced concrete with fly ash

and colloidal nano silica. *Constr. Build. Mater.* 198, 120–132. doi:10.1016/j.conbuildmat.2018.11.155

Massana, J., Reyes, E., Bernal, J., León, N., and Sánchez-Espinosa, E. (2018). Influence of nano- and micro-silica additions on the durability of a high-performance self-compacting concrete. *Constr. Build. Mater.* 165, 93–103. doi:10.1016/j.conbuildmat.2017.12.100

Mobini, M. H., Khaloo, A., Hosseini, P., and Esrafili, A. (2015). Mechanical properties of fiber-reinforced high-performance concrete incorporating pyrogenic nanosilica with different surface areas. *Constr. Build. Mater.* 101, 130–140. doi:10.1016/j.conbuildmat.2015.10.032

Mohammed, B. S., Liew, M. S., Alaloul, W. S., Khed, V. C., Hoong, C. Y., and Adamu, M. (2018). Properties of nano-silica modified pervious concrete. *Case Stud. Constr. Mater.* 8, 409–422. doi:10.1016/j.cscm.2018.03.009

Mohammed, T. U., and Rahman, M. N. (2016). Effect of types of aggregate and sand-to-aggregate volume ratio on UPV in concrete. *Constr. Build. Mater.* 125, 832–841. doi:10.1016/j.conbuildmat.2016.08.102

Molero, M., Segura, I., Izquierdo, M. A. G., Fuente, J. V., and Anaya, J. J. (2009). Sand/cement ratio evaluation on mortar using neural networks and ultrasonic transmission inspection. *Ultrasonics* 49, 231–237. doi:10.1016/j.ultras.2008.08.006

Murad, Y. (2021). Compressive strength prediction for concrete modified with nanomaterials. *Case Stud. Constr. Mater.* 15, e00660. doi:10.1016/j.cscm.2021.e00660

Nafees, A., Amin, M. N., Khan, K., Nazir, K., Ali, M., Javed, M. F., et al. (2022a). Modeling of mechanical properties of silica fume-based green concrete using machine learning techniques. *Polymers* 14, 30. doi:10.3390/polym14010030

Nafees, A., Javed, M. F., Khan, S., Nazir, K., Farooq, F., Aslam, F., et al. (2021). Predictive modeling of mechanical properties of silica fume-based green concrete using artificial intelligence approaches: MLPNN, ANFIS, and GEP. *Materials* 14, 7531. doi:10.3390/ma14247531

Nafees, A., Khan, S., Javed, M. F., Alrowais, R., Mohamed, A. M., Mohamed, A., et al. (2022b). Forecasting the mechanical properties of plastic concrete employing experimental data using machine learning algorithms: DT, MLPNN, SVM, and RF. *Polymers* 14, 1583. doi:10.3390/polym14081583

Niewiadomski, P., Stefaniuk, D., and Hoła, J. (2017). Microstructural analysis of self-compacting concrete modified with the addition of nanoparticles. *Procedia Eng.* 172, 776–783. doi:10.1016/j.proeng.2017.02.122

Norhasri, M. S. M., Hamidah, M. S., and Fadzil, A. M. (2017). Applications of using nano material in concrete: A review. *Constr. Build. Mater.* 133, 91–97. doi:10.1016/j.conbuildmat.2016.12.005

Ould Naffa, S., Goueygou, M., Piwakowski, B., and Buyle-Bodin, F. (2002). Detection of chemical damage in concrete using ultrasound. *Ultrasonics* 40, 247–251. doi:10.1016/s0041-624x(02)00146-4

Qi, C., Huang, B., Wu, M., Wang, K., Yang, S., and Li, G. (2022). Concrete strength prediction using different machine learning processes: Effect of slag, fly ash and superplasticizer. *Materials* 15, 5369. doi:10.3390/ma15155369

Qin, D., Gao, P., Aslam, F., Sufian, M., and Alabduljabbar, H. (2022). A comprehensive review on fire damage assessment of reinforced concrete structures. *Case Stud. Constr. Mater.* 16, e00843. doi:10.1016/j.cscm.2021.e00843

Rahmani, E., Dehestani, M., Beygi, M. H. A., Allahyari, H., and Nikbin, I. M. (2013). On the mechanical properties of concrete containing waste PET particles. *Constr. Build. Mater.* 47, 1302–1308. doi:10.1016/j.conbuildmat.2013.06.041

Reches, Y. (2018). Nanoparticles as concrete additives: Review and perspectives. *Constr. Build. Mater.* 175, 483–495. doi:10.1016/j.conbuildmat.2018.04.214

Ren, J., Lai, Y., and Gao, J. (2018). Exploring the influence of SiO2 and TiO2 nanoparticles on the mechanical properties of concrete. *Constr. Build. Mater.* 175, 277–285. doi:10.1016/j.conbuildmat.2018.04.181

Sadeghi Nik, A., and Lotfi Omran, O. (2013). Estimation of compressive strength of self-compacted concrete with fibers consisting nano-SiO2 using ultrasonic pulse velocity. *Constr. Build. Mater.* 44, 654–662. doi:10.1016/j.conbuildmat.2013.03.082

Sadrmomtazi, A., and Fasihi, A. (2010). Influence of polypropylene fibers on the performance of NANO-SIO$_2$-INCORPORATED mortar. *Iran. J. Sci. Technol. TRANSACTION B- Eng.* 34, 385–395.

Shafabakhsh, G. H., Ani, O. J., and Talebsafa, M. (2015). Artificial neural network modeling (ANN) for predicting rutting performance of nano-modified hot-mix asphalt mixtures containing steel slag aggregates. *Constr. Build. Mater.* 85, 136–143. doi:10.1016/j.conbuildmat.2015.03.060

Shah, H. A., Yuan, Q., Akmal, U., Shah, S. A., Salmi, A., Awad, Y. A., et al. (2022). Application of machine learning techniques for predicting compressive, splitting

tensile, and flexural strengths of concrete with metakaolin. *Materials* 15, 5435. doi:10.3390/ma15155435

Shang, M., Li, H., Ahmad, A., Ahmad, W., Ostrowski, K. A., Aslam, F., et al. (2022). Predicting the mechanical properties of RCA-based concrete using supervised machine learning algorithms. *Materials* 15, 647. doi:10.3390/ma15020647

Sharkawi, A. M., Abd-Elaty, M. A., and Khalifa, O. H. (2018). Synergistic influence of micro-nano silica mixture on durability performance of cementious materials. *Constr. Build. Mater.* 164, 579–588. doi:10.1016/j.conbuildmat.2018.01.013

Sharma, N., Thakur, M. S., Sihag, P., Malik, M. A., Kumar, R., Abbas, M., et al. (2022). Machine learning techniques for evaluating concrete strength with waste marble powder. *Materials* 15, 5811. doi:10.3390/ma15175811

Sufian, M., Ullah, S., Ostrowski, K. A., Ahmad, A., Zia, A., Śliwa-Wieczorek, K., et al. (2021). An experimental and empirical study on the use of waste marble powder in construction material. *Materials* 14, 3829. doi:10.3390/ma14143829

Sukontasukkul, P., Pomchiengpin, W., and Songpiriyakij, S. (2010). Post-crack (or post-peak) flexural response and toughness of fiber reinforced concrete after exposure to high temperature. *Constr. Build. Mater.* 24, 1967–1974. doi:10.1016/j.conbuildmat.2010.04.003

Trtnik, G., Kavčič, F., and Turk, G. (2009). Prediction of concrete strength using ultrasonic pulse velocity and artificial neural networks. *Ultrasonics* 49, 53–60. doi:10.1016/j.ultras.2008.05.001

Wang, C., Xu, S., and Yang, J. (2021). Adaboost algorithm in artificial intelligence for optimizing the IRI prediction accuracy of asphalt concrete pavement. *Sensors* 21, 5682. doi:10.3390/s21175682

Wang, Q., Ahmad, W., Ahmad, A., Aslam, F., Mohamed, A., and Vatin, N. I. (2022). Application of soft computing techniques to predict the strength of geopolymer composites. *Polymers* 14, 1074. doi:10.3390/polym14061074

Wang, X. F., Huang, Y. J., Wu, G. Y., Fang, C., Li, D. W., Han, N. X., et al. (2018). Effect of nano-SiO2 on strength, shrinkage and cracking sensitivity of lightweight aggregate concrete. *Constr. Build. Mater.* 175, 115–125. doi:10.1016/j.conbuildmat.2018.04.113

Xie, C., Cao, M., Guan, J., Liu, Z., and Khan, M. (2021). Improvement of boundary effect model in multi-scale hybrid fibers reinforced cementitious composite and prediction of its structural failure behavior. *Compos. Part B Eng.* 224, 109219. doi:10.1016/j.compositesb.2021.109219

Xu, J., Kong, F., Song, S., Cao, Q., Huang, T., and Cui, Y. (2017). Effect of Fenton pre-oxidation on mobilization of nutrients and efficient subsequent bioremediation of crude oil-contaminated soil. *Chemosphere* 180, 1–10. doi:10.1016/j.chemosphere.2017.03.087

Xue, G., and Yilmaz, E. (2022). Strength, acoustic, and fractal behavior of fiber reinforced cemented tailings backfill subjected to triaxial compression loads. *Constr. Build. Mater.* 338, 127667. doi:10.1016/j.conbuildmat.2022.127667

Xupeng, C., Zhuowen, S., and Jianyong, P. (2021). Study on metakaolin impact on concrete performance of resisting complex ions corrosion. *Front. Mat.* 8. doi:10.3389/fmats.2021.788079

Yan, D., Tian, Y., Liu, K., Chen, S., Zeng, Q., and Ruan, S. (2021). Evaluation of mechanical properties of concrete after exposure to elevated temperatures using ultrasonic pulse velocity measurement and a split-Hopkinson pressure bar. *J. Mat. Civ. Eng.* 33, 04021352. doi:10.1061/(asce)mt.1943-5533.0003983

Yang, D., Zhao, J., Suhail, S. A., Ahmad, W., Kamiński, P., Dyczko, A., et al. (2022). Investigating the ultrasonic pulse velocity of concrete containing waste marble dust and its estimation using artificial intelligence. *Materials* 15, 4311. doi:10.3390/ma15124311

Yao, M., Zhu, Y., Li, J., Wei, H., and He, P. (2019). Research on predicting line loss rate in low voltage distribution network based on gradient boosting decision tree. *Energies* 12, 2522. doi:10.3390/en12132522

Ying, J., Zhou, B., and Xiao, J. (2017). Pore structure and chloride diffusivity of recycled aggregate concrete with nano-SiO2 and nano-TiO2. *Constr. Build. Mater.* 150, 49–55. doi:10.1016/j.conbuildmat.2017.05.168

Yuan, X., Tian, Y., Ahmad, W., Ahmad, A., Usanova, K. I., Mohamed, A. M., et al. (2022). Machine learning prediction models to evaluate the strength of recycled aggregate concrete. *Materials* 15, 2823. doi:10.3390/ma15082823

Zahiri, F., and Eskandari-Naddaf, H. (2019). Optimizing the compressive strength of concrete containing micro-silica, nano-silica, and polypropylene fibers using extreme vertices mixture design. *Front. Struct. Civ. Eng.* 13, 821–830. doi:10.1007/s11709-019-0518-6

Zaid, O., Ahmad, J., Siddique, M. S., and Aslam, F. (2021). Effect of incorporation of rice husk ash instead of cement on the performance of steel fibers reinforced concrete. *Front. Mat.* 8. doi:10.3389/fmats.2021.665625

Zareei, S. A., Ameri, F., Bahrami, N., Shoaei, P., Moosaei, H. R., and Salemi, N. (2019). Performance of sustainable high strength concrete with basic oxygen steel-making (BOS) slag and nano-silica. *J. Build. Eng.* 25, 100791. doi:10.1016/j.jobe.2019.100791

Zhang, N., Yan, C., Li, L., and Khan, M. (2022). Assessment of fiber factor for the fracture toughness of polyethylene fiber reinforced geopolymer. *Constr. Build. Mater.* 319, 126130. doi:10.1016/j.conbuildmat.2021.126130

Zhang, Y., and Aslani, F. (2021). Compressive strength prediction models of lightweight aggregate concretes using ultrasonic pulse velocity. *Constr. Build. Mater.* 292, 123419. doi:10.1016/j.conbuildmat.2021.123419

Zhao, Z., Cao, S., and Yilmaz, E. (2022). Effect of layer thickness on the flexural property and microstructure of 3D-printed rhomboid polymer-reinforced cemented tailing composites. *Int. J. Minerals, Metallurgy Mater.* 30, 1–14.

Zheng, D., Wu, R., Sufian, M., Kahla, N. B., Atig, M., Deifalla, A. F., et al. (2022). Flexural strength prediction of steel fiber-reinforced concrete using artificial intelligence. *Materials* 15, 5194. doi:10.3390/ma15155194

Bibliographic trends in mineral fiber-reinforced concrete: A scientometric analysis

Abdulrhman Mohamad Moasas[1], Muhammad Nasir Amin[1]*, Waqas Ahmad[2], Kaffayatullah Khan[1], Mohammed Najeeb Al-Hashem[1], Hisham Jahangir Qureshi[1] and Abdullah Mohamed[3]

[1]Department of Civil and Environmental Engineering, College of Engineering, King Faisal University, Al-Ahsa, Saudi Arabia, [2]Department of Civil Engineering, COMSATS University Islamabad, Abbottabad, Pakistan, [3]Research Centre, Future University in Egypt, New Cairo, Egypt

In the construction industry, pursuing sustainable development by using sustainable materials necessitates using renewable resources. Among different renewable materials, mineral-derived natural fibers are relatively cheaper and abundantly available in various countries. This study summarizes the research advancements on concrete reinforced with mineral-derived natural fibers. This review on the incorporation of mineral fibers in concrete evaluates, identifies, and synthesizes research outcomes for creating a summary of current evidence which can contribute to evidence-based practice. Mapping knowledge, c/o-occurrence, and co-citation are hard gears for innovative research. Accordingly, the present study is aimed at exploring the literature on key features of mineral fiber-reinforced concrete by performing a scientometric analysis. The current study implemented an advanced approach for mining, processing, and analyzing data, interpretation, and presentation of available bibliographic data on mineral fibers in concrete. Furthermore, the discussion on the applications and limitations of using mineral fiber-reinforced concrete in the construction industry is also made. The current research may aid academics in exchanging new ideas and techniques and developing collective efforts.

KEYWORDS

concrete, mineral fiber, construction material, natural fiber, scientometric analysis

1 Introduction

Establishing novel/alternative construction materials focuses on enhanced properties (i.e., physical/mechanical) and the performance of concrete and relative structures. Generally, concrete is weaker under flexural loading than under compressive loading. To cater to this issue, the concept of short, discrete fibers as dispersed reinforcement is introduced, enhancing the mechanical properties of concrete and improving the resistance against deformation and cracks, ultimately contributing to the durability of concrete (Pukharenko, 2012; de Azevedo et al., 2021a; de Azevedo et al., 2021b; Azevedo

et al., 2022; Ali et al., 2022c; Meng et al., 2022). During the past three decades, the emerging concern toward environmental problems arising from conventional concrete manufacturing has gained the attention of researchers in civil engineering to pursue alternative approaches for discovering environment-friendly construction materials (Cabeza et al., 2010; Väntsi and Kärki, 2014; de Azevedo et al., 2017; de Azevedo et al., 2018; Ahmed et al., 2021; Arooj and Ali, 2021; de Azevedo et al., 2021b; de Azevedo et al., 2022a; de Azevedo et al., 2022b; Raza et al., 2022). In 2019, the WGBC reported techniques/standards to design environment-friendly structures to reduce 40% of carbon footprints by 2030 and eliminate CO_2 emissions by 2050 (Alhawat et al., 2022). Utilization of substitute fuels, engrossing CO_2, enhancing energy efficiency within the boiler, and replacing ordinary Portland cement with waste/supplementary materials such as silica fume, sugarcane bagasse ash, plastic waste fibers, recycled tires, etc., to produce green/environment-friendly cementitious concrete are the advised measures (Kaïkea et al., 2014; Pogorelov and Semenyak, 2016; Li and Cao, 2018; Ali et al., 2021; Nafees et al., 2021; Thomas et al., 2021; Ali, 2022; Ali et al., 2022e; Li et al., 2022; Nafees et al., 2022).

The fibers are usually classified as metallic, organic, and mineral (Ali et al., 2022d). The selection of these fibers is made based on distinct dominant properties. The literature reported that the concrete strength could be improved by enhancing the modular ratio, aspect ratio, degree of alignment, and content of fiber (Aydın, 2013; Farooqi and Ali, 2019; Ali et al., 2022a; Azevedo et al., 2022). The specific fiber property is only emphasized at the molecular level (Ali et al., 2022b; Farooqi and Ali, 2022). Figure 1 reveals that the incorporation of mineral fibers in concrete will help in terms of both the economy and environment, as these fibers are naturally available and would result in reduced amounts of conventional materials such as cement and aggregates, for conventional cementitious concrete, ultimately conserving natural resources and reducing CO_2 emissions (Khan et al.; Mechtcherine et al., 2016; Khan et al., 2018; Cao et al., 2019b; Li et al., 2019a). Mineral fibers such as basalt fiber are categorized as raw materials that meet the technical requirements and environmental aspects (Khan et al., 2018; Khan et al., 2021b; John and Dharmar, 2021). These fibers have the following excellent properties: 1) effective mechanical properties; 2) substantial bond behavior among epoxies, glues, and metals; and 3) extra-ordinary electrical, thermal, and acoustic properties (Khan et al., 2021a; Khan and Cao, 2021). These mineral basalt/wool/$CaCO_3$ whisker fibers are famous for their energy-absorption capability and binding ability (Jerman and Černý, 2012; Luo et al., 2014; Xin et al., 2015; Stonys et al., 2016; Khan et al., 2018; Yliniemi et al., 2018; Cao et al., 2019a; Li et al., 2019b; Cao et al., 2019c; Li L. et al., 2020; Khan et al., 2022; Khan et al., 2022f). After replacement with natural/mineral fibers, conventional fibers reduce the damage

to different industry zones and social aspects (Farooqi and Ali, 2018a; Farooqi and Ali, 2018b; Farooqi and Ali, 2018c; Li et al., 2019c; Li et al., 2021; Khan et al., 2022a; Khan et al., 2022e).

As the mineral fiber-reinforced concrete research is enhanced due to rising concerns against environmental issues resulting from conventional cementitious concrete, researchers are facing restrictions in terms of information available, which may limit the innovation in academic and research collaborations. Therefore, it is critical to establish and execute a process that aids academicians in obtaining necessary information from the most authentic sources. Employing a software tool, a scientometric approach can aid in overcoming the said lacking factors (Figure 2). Accordingly, the current study is focused on performing a scientometric analysis on published bibliographic data in the mineral fiber-reinforced concrete research area up to December 2022. A scientometric evaluation may conduct a quantitative investigation of a bulk volume of the bibliographic database by applying a suitable software tool. Typical review-based research studies show a deficiency in its capability to comprehensively and precisely connect different literature aspects. Scientific visualization, co-occurrence, and co-citations are the main complex features of modern research (Udomsap and Hallinger, 2020; Yang et al., 2022). It is from the scientometric analysis that revealed sources and authors with maximum publications, keyword co-occurrences, actively contributing countries, and publications with maximum citations in mineral fiber-reinforced concrete research. The Scopus search engine is made for attaining abstracts, keywords, bibliographies, citations, funding, and other relevant data from 912 related articles. VOSviewer tool is applied to process these data afterward. The statistical and graphical mappings of countries and scientists/researchers in this work would help research scholars exchange novel ideas and approaches and establish collaborative research-based activities. As the scientometric analysis demonstrates subject-relevant

FIGURE 1
Benefits of mineral fiber-reinforced concrete.
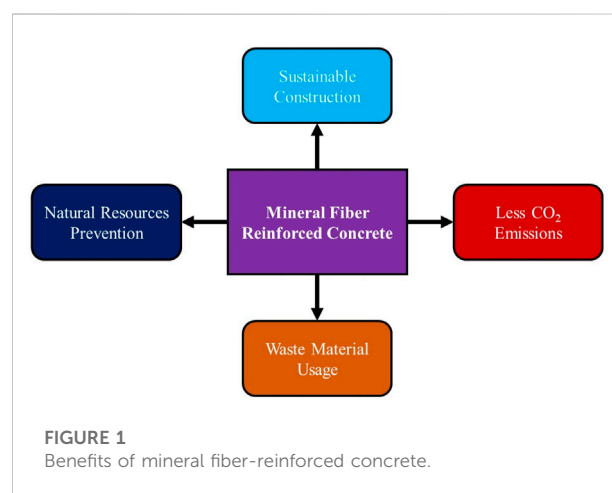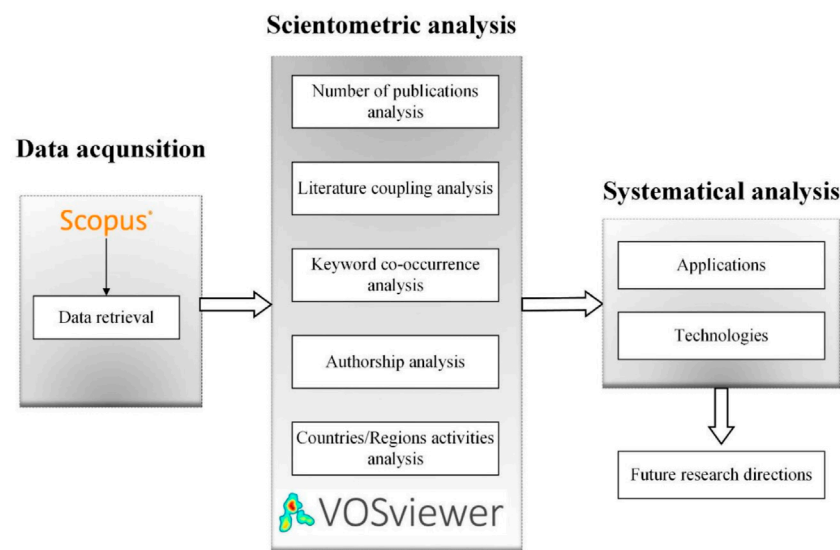
FIGURE 2
Scientometric review process (Zheng et al., 2021a).
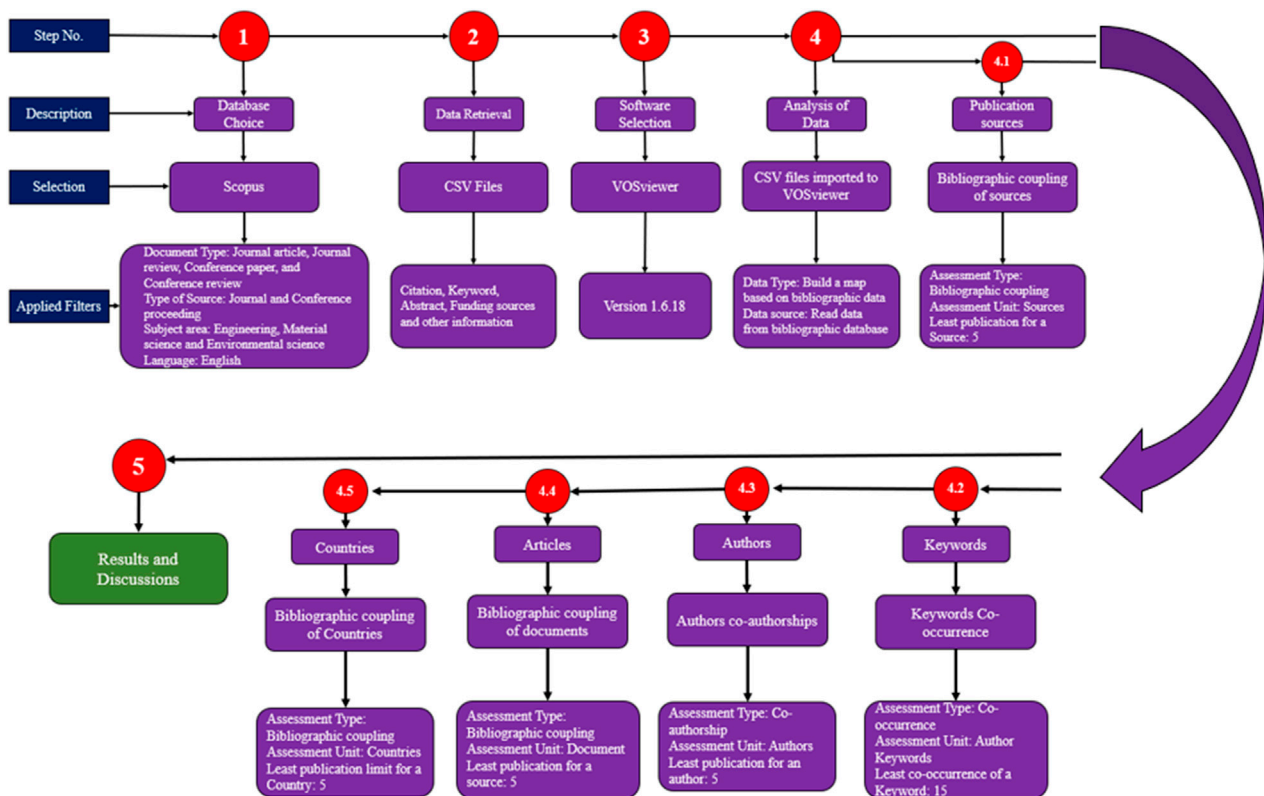
FIGURE 3
Sequential flowchart of the review strategy.
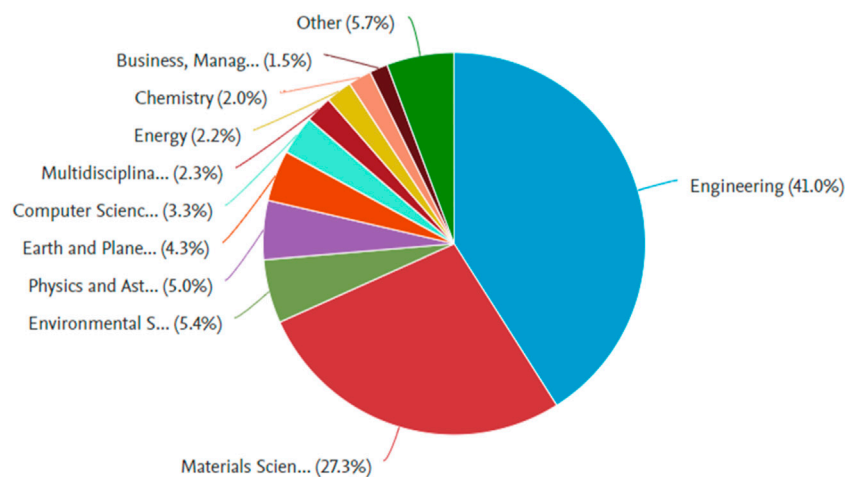
FIGURE 4
Domains of documents in mineral fiber-reinforced concrete research.
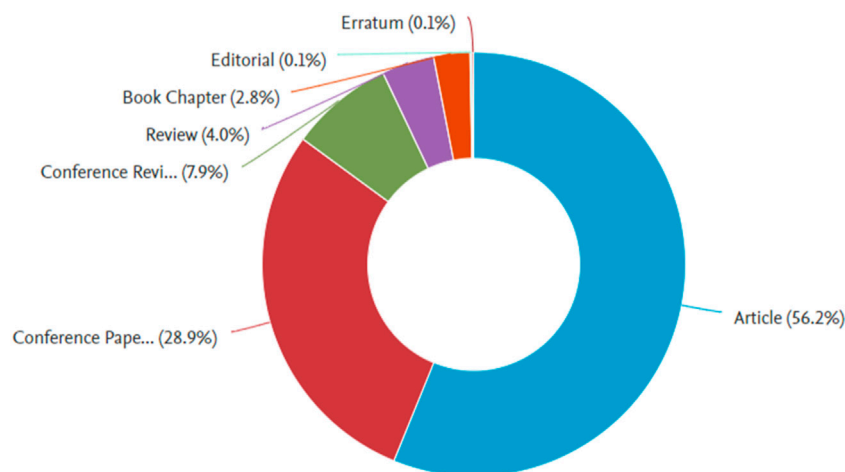
FIGURE 5
Published document types on mineral fiber-reinforced concrete research.

keywords and the most appropriate literature review, the current research discussed and emphasized the latest applications of mineral fiber-reinforced concrete, the limitations related to the application and production of mineral fiber-reinforced concrete and possible solutions. This research will help engineering field academicians who belong to different areas/regions/locations establish joint ventures, exchange innovative and novel techniques/ ideas, and develop research collaborations resulting from the statistical and graphical depictions of authors and countries.

2 Review strategy

In the current research, scientometric analysis is performed on bibliographic data (Xu et al., 2018; Darko et al., 2019; Xiao et al., 2019) to quantify several properties of said bibliographic data. Scientific mapping is utilized in the scientometric study, an approach developed by academics to analyze bibliometric data (Markoulli et al., 2017; Amin et al., 2022). Abundant publications have been found on the subject; therefore, it is vital to employ a reliable search engine. Scopus and Web of Science are two highly accurate databases perfectly suitable for said objective (Afgan and
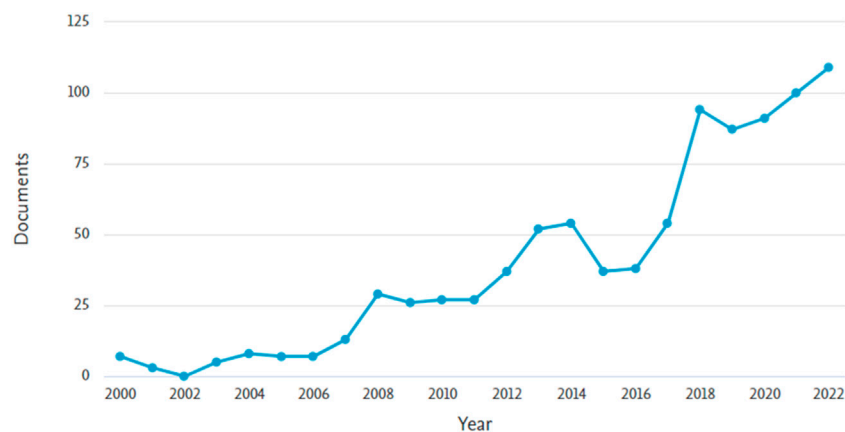
FIGURE 6
Annual publication trend of published articles on mineral fiber-reinforced concrete research till December 2022.

TABLE 1 Publication sources having a minimum of 10 publications on mineral fiber-reinforced concrete research.

S/N	Source of publication	Publication count	Total citations received
1	Construction and Building Materials	62	2158
2	Advanced Materials Research	29	1120
3	Materials Today: Proceedings	25	793
4	Lecture Notes in Civil Engineering	22	256
5	Applied Mechanics and Materials	17	166
6	Materials	17	160
7	Arabian Journal for Science and Engineering	16	146
8	International Journal of Civil Engineering and Technology	16	96
9	Cement and Concrete Composites	13	92
10	Matec Web of Conferences	10	63
11	Materials Science Forum	10	53

Bing, 2021; Huang S. et al., 2022). The highly recommended database, i.e., Scopus, is employed to gather information regarding the bibliography for current research on mineral fiber-reinforced concrete. As of today, a search of mineral fibers in concrete on Scopus yielded 912 results. Several filters are employed to scrutinize needless papers. A comprehensive procedural flowchart showing the steps such as retrieval of data, analysis, and different filters used while performing the study are shown in Figure 3.

Moreover, other researchers have also reported on the same technique (Oraee et al., 2017; Jin et al., 2018; Park and Nagy, 2018). Applying the said filters on the Scopus database, 912 results remained. These records are stored in a Comma Separated Values (CSV) format for evaluation by a relevant tool. VOSviewer (version 1.6.18) is employed to develop the attained material's quantitative assessment and scientific visualization. VOSviewer is an open-source and freely accessible mapping tool usually used in discrete research areas (Zuo and Zhao, 2014; Darko et al., 2017; Ahmad et al., 2021). The subsequent CSV file is uploaded on VOSviewer for additional assessment while keeping the data consistent and reliable. In the scientometric analysis, the most widely used keywords, the publishing sources, the contribution of different states, and the publications having the highest citations are evaluated. The aspects, co-occurrences, and interrelationships are demonstrated with the help of maps. Furthermore, the respective quantitative data are provided in tables. Colors are assigned to the
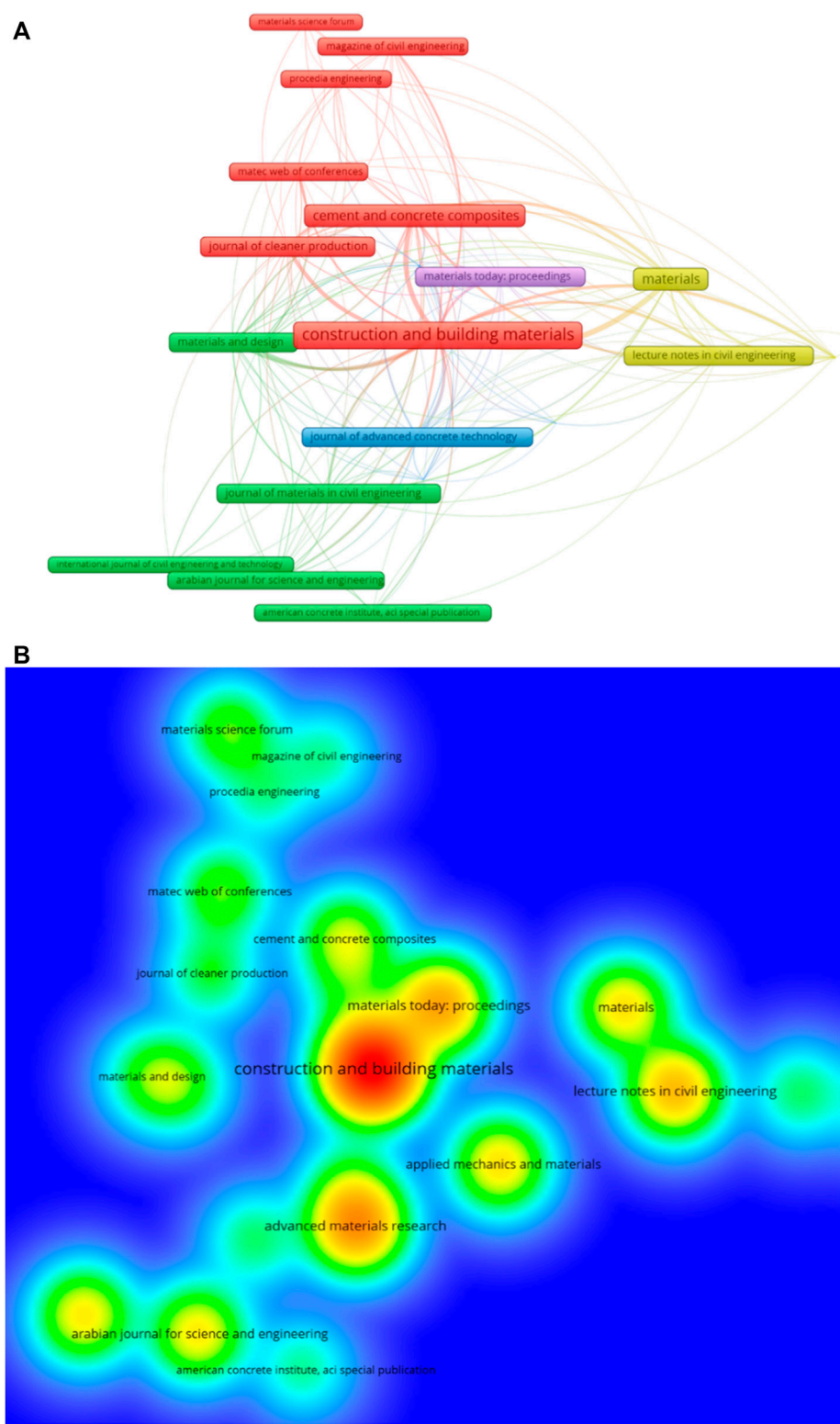
FIGURE 7
Mapping of sources having at least 10 publications. **(A)** Network visualization; **(B)** density.

TABLE 2 List of the top twenty most-used keywords in the research of mineral fiber-reinforced concrete.

S/N	Keyword	Occurrences
1	Mechanical Properties	80
2	Fiber-Reinforced Concrete	77
3	Natural Fibers	72
4	Minerals	72
5	Basalt Fiber	69
6	Silicate Minerals	64
7	Bending Strength	49
8	Mineral Fibers	39
9	Mineral Wool	33
10	Cementitious Composites	32
11	Concrete Construction	30
12	Fiber-Reinforced Concretes	30
13	Sustainable Development	30
14	Basalt	29
15	Fiber-Reinforced Concrete	28
16	Construction Industry	24
17	Flexural Strength	22
18	Mechanical Performance	21
19	Cementitious Materials	19
20	Mineral Additives	19

clusters for the identification of a particular item on the map. In addition, different color schemes, such as plasma, viridis, and rainbow, are used for density visualization, and the rainbow option is used in the current work for density mapping.

3 Results and discussion

3.1 Subject area and yearly publication of documents

A Scopus analyzer is utilized to perform this assessment to identify the most relevant research areas. Figure 4 shows that Engineering, Materials Science, and Environmental Science are the three leading disciplines in the generation of documents, having almost 41%, 27%, and 6% of documents, respectively. As a whole, these three disciplines contribute 74% of papers. Moreover, the analysis on the Scopus database is also made to assess the publication types having subject research area documents (Figure 5). This assessment revealed that there are almost 56% of journal papers, around 29% of conference articles, 8% of conference

reviews, and nearly 4% of journal reviews. The annual trend of published articles in the considered research area from 2011 to December 2022 is illustrated in Figure 6. Until 2014, a slight rise was observed in mineral fiber-reinforced concrete research publications. Following that, the publication trend was reduced to less than 40 articles in a year for two years, i.e., 2015 and 2016. The number of publications was enhanced considerably from 2016 to 2018. Again, from 2019–2020, the publications were slightly comprised, followed by a significant increase afterward. In the current year, the number of articles on the considered study field is more than 100 so far (as of December 2022). It is interesting to note that the attention of researchers is focused on using mineral fibers in concrete to have sustainable construction materials.

3.2 Publication sources

The sources of the publication are assessed by employing the VOSviewer on the bibliographic data. A minimum of ten papers from one source is specified, and 11 out of the 912 sources met the requirement. The publication sources have at least ten publications on mineral fibers in concrete research up to December 2022, and the received number of citations is enlisted in Table 1. The top three publication sources are "Construction and building materials", "Advanced materials research", and "Materials today: proceedings", having 62, 29, and 25 papers, respectively, and 2,158, 1,120, and 793 citations up to December 2022, respectively. Exceptionally, *via* this assessment, a foundation is attained for upcoming scientometric analysis on mineral fibers in concrete research. Furthermore, the recent typical review-based research was incapable of providing systematic graphs. The visualization of publication sources having a minimum of ten articles is depicted in Figure 7. The frame size in Figure 7A shows the influence of the source on the current study research field as per document count, which means that the bigger the frame size, the more significant the impact. For example, the frame size for "Construction and building materials" is more than the others, depicting the significance of this journal in the considered research area. The formation of five groups is made, and a unique color represents each one on the map (red, yellow, green, purple, and blue). Group development is done based on publication source-extent or the co-citation frequency with comparable publications (Wuni et al., 2019). VOSviewer establishes the groups as per the co-citation tendencies in research publications. Seven journals in the red cluster are frequently co-cited in the same research. Furthermore, the link among closely placed publication sources in a particular group is more when compared to widely spread frames, for example, "Cement and concrete composites" majorly correlates with "Journal of cleaner production" than with "Procedia engineering" or "Construction and building materials". As
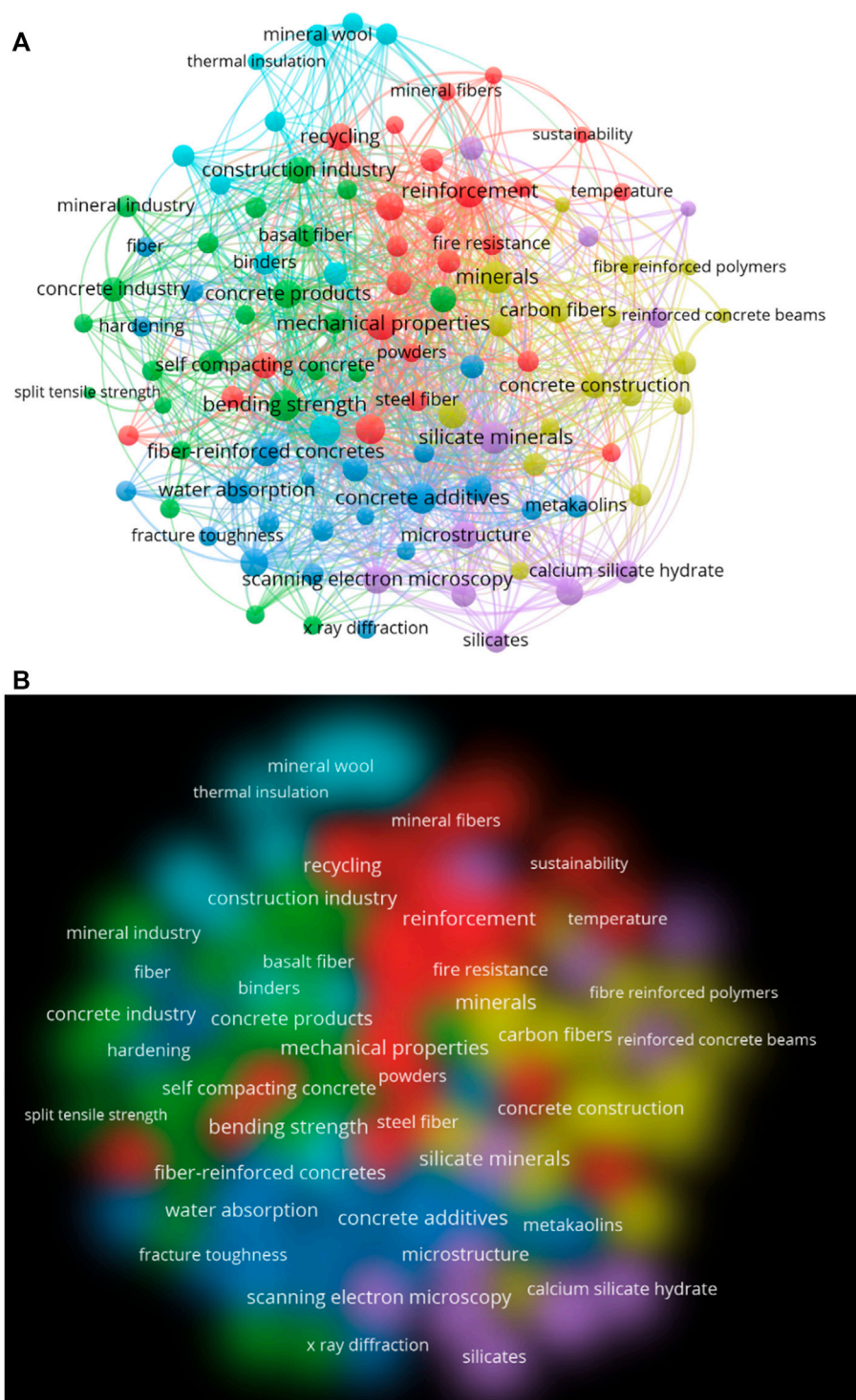
FIGURE 8
Mapping of keywords having at least 15 publications. **(A)** Network visualization; **(B)** density.

evident from Figure 7B, several tints correspond to different journal-density concentrations. Red color has the highest concentration. Blue, green, and yellow colors are afterward.

"Construction and building materials" depict a red shade indicating its higher involvement in the mineral fiber-reinforced concrete research.
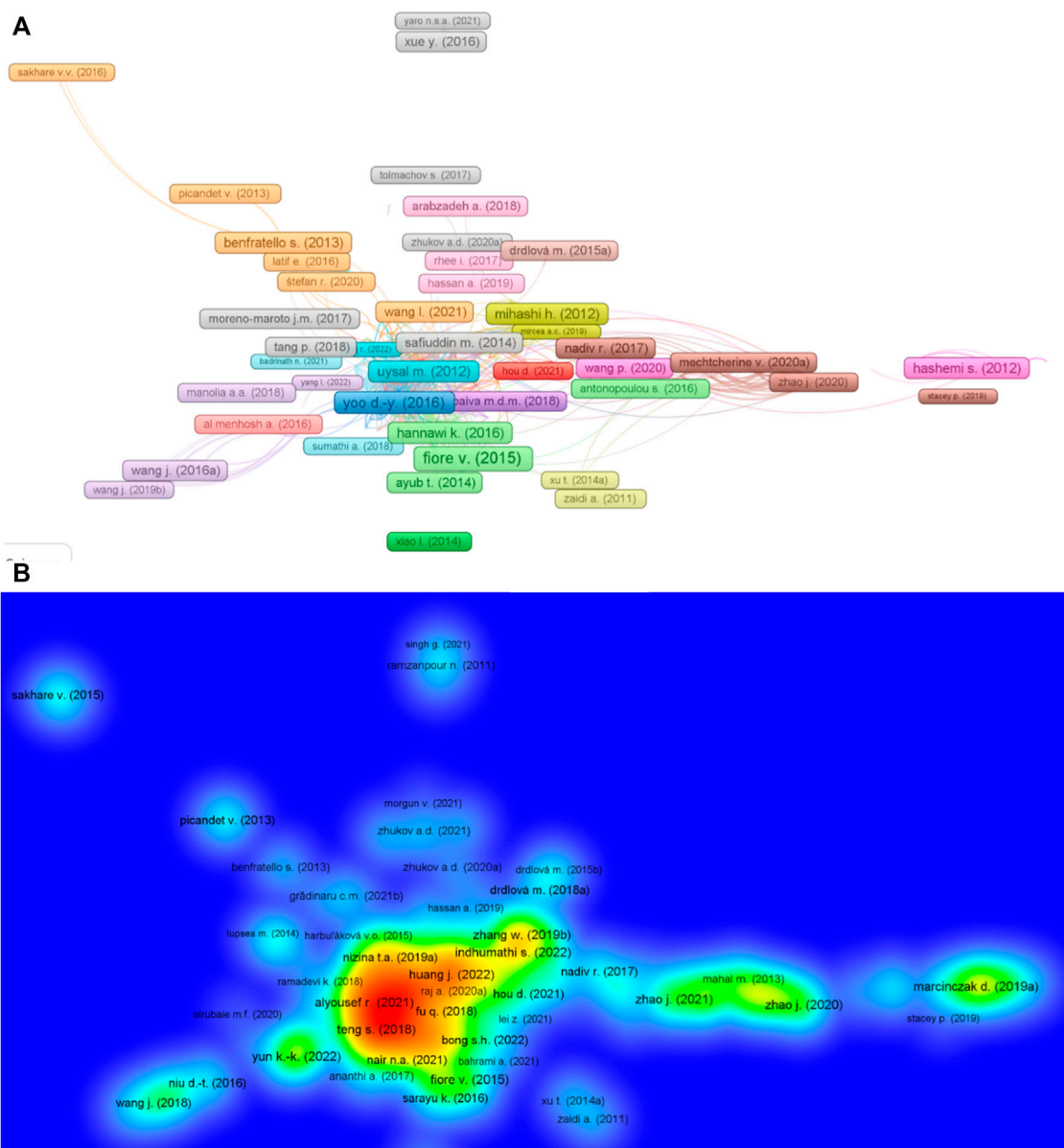
FIGURE 9
Systematic map of articles; **(A)** citation, base-linked articles; **(B)** density of connected articles.

3.3 Keyword co-occurrence

In research, keywords are important as the main subject of the research study domain is emphasized and distinguished by them (Song et al., 2021). The keyword recurrence requirement is set to at least 15. In this way, 20 keywords are preserved, as enlisted in Table 2. Mechanical properties, fiber-reinforced concrete, natural fibers, minerals, and basalt fiber are the five most widely occurring keywords in the considered research field. The keyword analysis revealed that mineral fibers in concrete have mainly been

explored to have an alternative sustainable construction material. Depending upon the co-occurrences, density, and connections related to their frequency of occurrence, a graph is presented in Figure 8. The frame size of a keyword in Figure 8A indicates its frequency, where the position of the frame represents the co-occurrence. Moreover, the top keywords show larger frames than the rest, indicating that these are important keywords to investigate the reinforced concrete research of the mineral fibers. The clustering is also done to represent the co-occurrences of keywords in various published articles, as seen from the graph. Different colors are assigned to

TABLE 3 Countries with at least 10 papers in the mineral fiber-reinforced concrete research.

S/N	Country	Documents published	Overall citations
1	India	166	538
2	China	138	1,754
3	Russian Federation	48	291
4	United States	34	834
5	Germany	32	296
6	Poland	25	356
7	Australia	24	456
8	France	21	662
9	Malaysia	21	416
10	Turkey	20	351
11	United Kingdom	18	280
12	Czech Republic	16	68
13	Italy	15	1,031
14	Canada	14	674
15	Algeria	13	196
16	Brazil	13	189
17	Iran	12	193
18	Spain	12	176
19	South Korea	11	389
20	Iraq	10	88
21	Pakistan	10	173

each group to represent keyword recurrences. In Figure 8A, the diverse shades of the five clusters are shown. The density concentrations for different keywords are also represented by unique colors, as shown in Figure 8B. The shades yellow, red, blue, and green show their densities. Mechanical properties, mineral fibers, sustainability, concrete construction, and other significant keywords show red or yellow tints representing more occurrences of density. This outcome would assist determined scientists in selecting keywords, reducing the effort to discover published articles on a definite topic.

3.4 Documents

The impact of a certain paper in a specific research area is depicted by its citations. Articles with higher citations pioneer in a particular research area. The scientific visualization of citations based on inter-connected publications and concentration of published papers in considered research areas, i.e., mineral fibers in concrete, is presented in Figure 9. Figure 9A

represents the interlinked publications *via* citations, evaluated using VOSviewer analysis. The size of the frame for a particular document is directly proportional to the impact of that specific article in the considered research domain, i.e., mineral fibers in concrete. Moreover, in Figure 9B, the density mapping reveals the enhanced density concentration of the leading articles as per citations.

3.5 Countries

Several countries have produced articles in the considered domain, and these countries aim to keep contributing. A systematic plot is developed for bibliophiles to assess the countries enthusiastic about researching mineral fibers in concrete to predict their properties. For this analysis, the criteria of minimum articles per nation are set as 10, and 21 countries have met this requirement, as listed in Table 3. Among all the countries, India, China, and the Russian Federation have contributed the maximum articles having 166, 138, and 48 articles, respectively. Moreover, China received
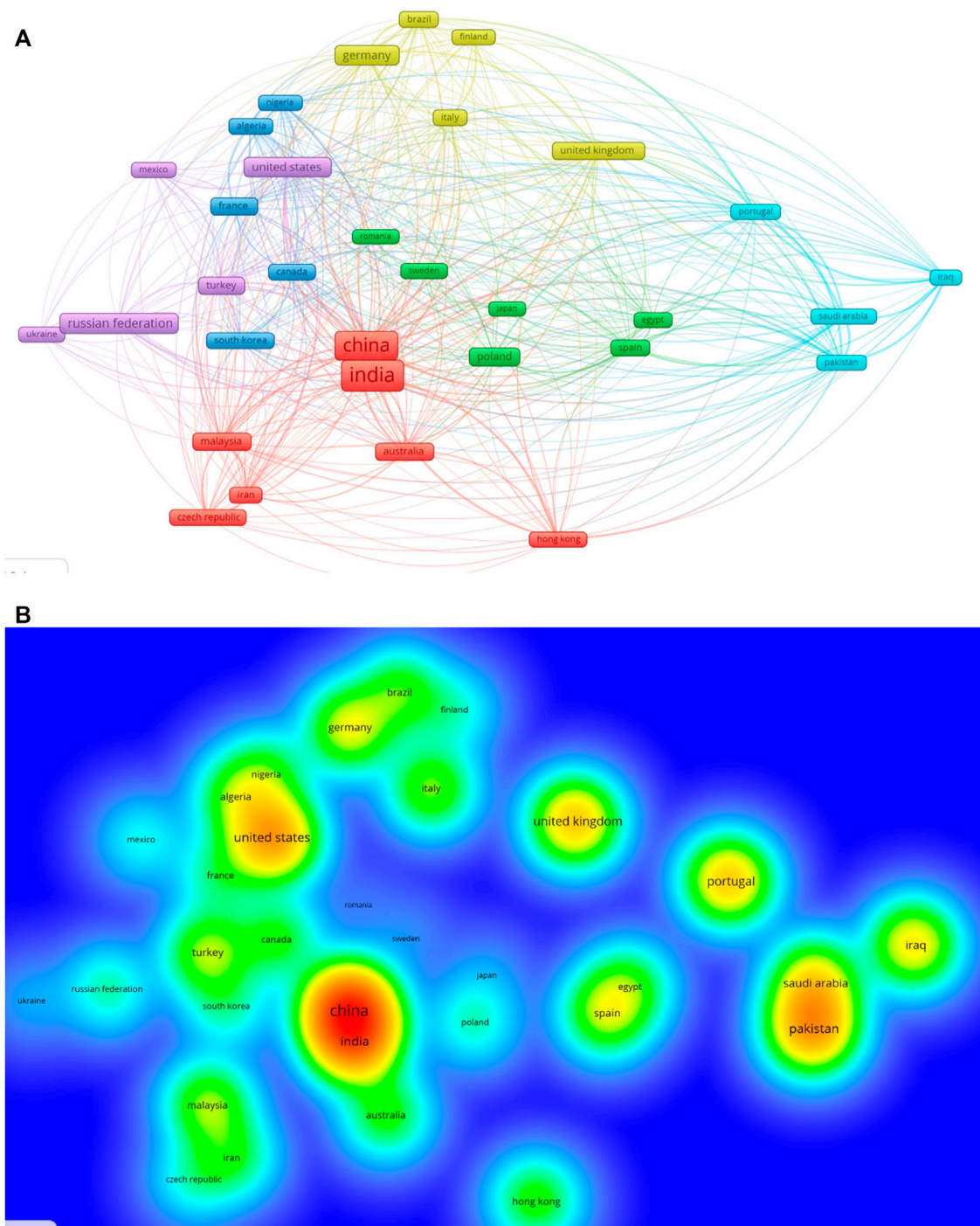
FIGURE 10
Systematic mapping of countries having at least 10 publications. **(A)** network map; **(B)** density.

1,754 citations, followed by Italy and the United States with 1,031 and 834 citations, respectively. The systemic map and density concentrations for citation-based linked countries are presented in Figure 10. The impact of a specific country in terms of article quantity on the subject-research domain is depicted from the frame size of that particular country (Figure 10A). As shown in Figure 10B, the countries with the most publications have more density. The quantitative output and graphical representation of the contributing countries would help young researchers establish scientific associations, initiate joint ventures, and exchange

FIGURE 11
Basalt fiber's typical chemical composition (Liu H. et al., 2022).
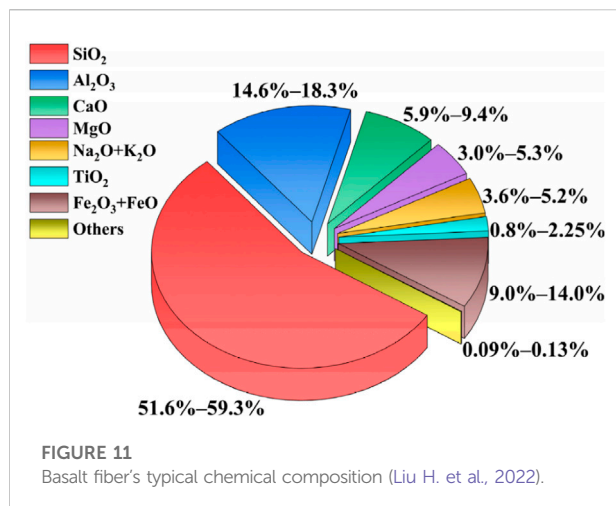
inventive approaches and ideas. Researchers from countries concerned with establishing research on mineral fibers in concrete may work with experts in this domain to yield aid from their expertise.

4 Discussion

4.1 Incorporation of mineral fibers in concrete

The remarkable enhancement in concrete's mechanical properties due to the incorporation of mineral fibers is mainly due to its capability of forming an even spatial net structure in concrete, improvement in internal stress redistribution and mode of damage, enhancement in concrete's internal mechanical stability, and improvement in the microstructure (Gao et al., 2021). Hence, it is vital to develop linkages to damages at the macroscopic level by the fiber distribution response properties and pore structure to demonstrate its mechanical performance. Accordingly, a generalized summary regarding mineral fiber-reinforced microstructure is also discussed in this study. The

incorporation of mineral fibers in manufacturing dispersed fiber-reinforced cementitious concrete is promising for multiple reasons. Basalt roving and thin-staple fiber are examples of mineral fibers, primarily formed by using the centrifugal-spinneret technique and categorized by even characteristics, diameter uniformity, and lesser waste content. The mineral fibers are attained using an electro-thermal process to melt raw materials (Buyantuev et al., 2012). The chemical resemblance of mineral fibers enables their interaction with Portland cement. The typical chemical composition and physical appearance of basalt fibers are shown in Figure 11 and Figure 12, respectively, as reported by Liu H. et al. (2022). But, this feature might badly affect the mineral fibers and decrease the reinforcing effect. Saraikina et al. (2012) reported various methods for resolving this issue and summarized the primary ways for the protection of mineral fibers from the alkaline-medium effects of cement: 1) utilization of cement-less binders in concrete having fibers; 2) alteration in the surfaces of mineral fibers; 3) modification in the structure of mineral fibers; and 4) the incorporation of admixtures that decrease the alkalinity of fiber-reinforced concrete medium. Globally, the popularity of mineral fiber-reinforced concrete is gaining popularity in the research field with a possibility of coming out as one of the most sustainable construction materials. As incorporating mineral fibers in concrete is a comparatively new approach, it lacks in guidelines for design than typical concrete; therefore, more experimental studies are important to fill the research gaps in this field (Khan et al., 2022d; Kirthika and Singh, 2018; Yang et al., 2019; Gebremariam et al., 2021; Khan et al., 2018).

4.2 Durability of mineral fiber-reinforced concrete

In case of mineral fiber-reinforced concrete, the durability is considered in the form of impermeability, wear resistance, freeze–thaw resistance, and chloride-corrosion resistance (Zheng et al., 2021b). It has been observed that concrete has

FIGURE 12
Basalt fiber's physical appearance, **(A)** sheet, **(B)** short fibers, and **(C)** SEM image of basalt fiber (Liu H. et al., 2022).
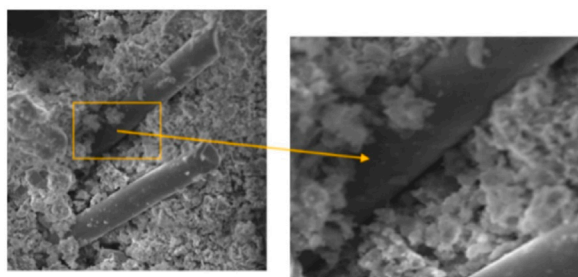
FIGURE 13
SEM image of mineral-derived basalt fiber-reinforced concrete (Li Y. et al., 2020).
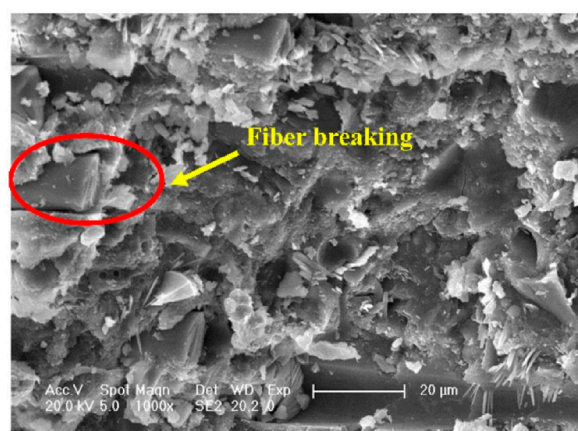
FIGURE 14
SEM image of mineral-derived basalt fiber fracture in concrete (Liu M. et al., 2022).

considerable susceptibility toward plastic cracking during the processes of setting and hardening (Huang Y. et al., 2022), that would adversely impact the respective project's long-term durability due to cement species, additives, water–cement ratio, aggregate grading, and the construction environment (Xiaomei et al., 2019). Khan et al., 2018 evaluated the durability of mineral-based basalt fiber-reinforced concrete after its exposure to different accelerated environmental conditions. The weight loss, water absorption, and compressive strength of basalt fiber-reinforced concrete were determined experimentally after undergoing ageing conditions, i.e., immersion in sulphate and acidic solutions, for 90 days after 28 days of curing. The incorporation of basalt fibers resulted in improved concrete properties, i.e., water absorption and compressive strength, even after exposure to sulfate and acidic attacks. Zhang Z. et al. (2021) reported that the addition of CeO_2 may also resist crack formation. Furthermore, the utilization of curing with moisture retaining (i.e., (e.g., steam curing or film

curing) (Wei and Pengcheng, 2020), expansion agents like additives (Guoxin et al., 2018), or the incorporation of an adequate content of fibers may effectively reduce or may even resist the early plastic cracks-occurrence in concrete (Shi et al., 2022). There would be as lesser chances for occurrence of plastic-cracking in concrete as earlier as the conservation of moisture starts (Li et al., 2004). In case of more aspect ratio of fiber, the volume fraction would be higher and, subsequently, the adhesion strength at the fiber–matrix interface would be more (Sheng et al., 2021), which would enhance the repressive strength to resist plastic-cracking in concrete and ultimately improve the durability performance of the respective concrete (Jia et al., 2021). In case of durability of conventional concrete, steel fiber-reinforced concrete, and polymer fiber-reinforced concrete, the research has already been the subject of multiple reports (Zhang P. et al., 2021); however, in case of durability of mineral fiber-reinforced concrete, the research is still relatively small.

4.3 Microstructure of mineral fiber-reinforced concrete

The SEM analysis is very important to explore the microstructure of concrete having mineral fibers. Li Y. et al. (2020) examined the mineral-derived basalt fiber-reinforced concrete by using SEM (Figure 13). Instead of fiber slippage, a cement paste coating was observed on the fiber surface, depicting an effective bonding among the mineral fiber and cement slurry (Figure 13). The cementitious material stuck on the fibers indicates its proper bonding, ultimately resulting in fiber fracture, as shown in Figure 14. It may be noted that crack propagation/expansion is limited due to proper bridging and bonding of embedded mineral-derived basalt fiber in the cementitious matrix. So, it can be said, based on the findings mentioned previously, that mineral fibers have considerably enhanced the concrete mechanical properties and thus, it can offer a stable structure in terms of load-bearing in concrete and resist the initiation and propagation of micro-cracks. Furthermore, adding mineral fibers in concrete can increase the pore and capillary contents, improve pore connectivity, and prevent the deterioration of the concrete-pore structure.

4.4 Environmental aspect of mineral fiber-reinforced concrete

Nowadays, sustainable development is in demand. Global warming resulting from swift ozone layer depletion due to bad environmental impacts is a severe problem. Ecological disintegration is due to the extreme consumption of fossil fuels and natural resources. So, leading toward sustainable development, the contributing factors toward ozone layer depletion must be

FIGURE 15
Concept of using mineral fibers to achieve sustainable development.
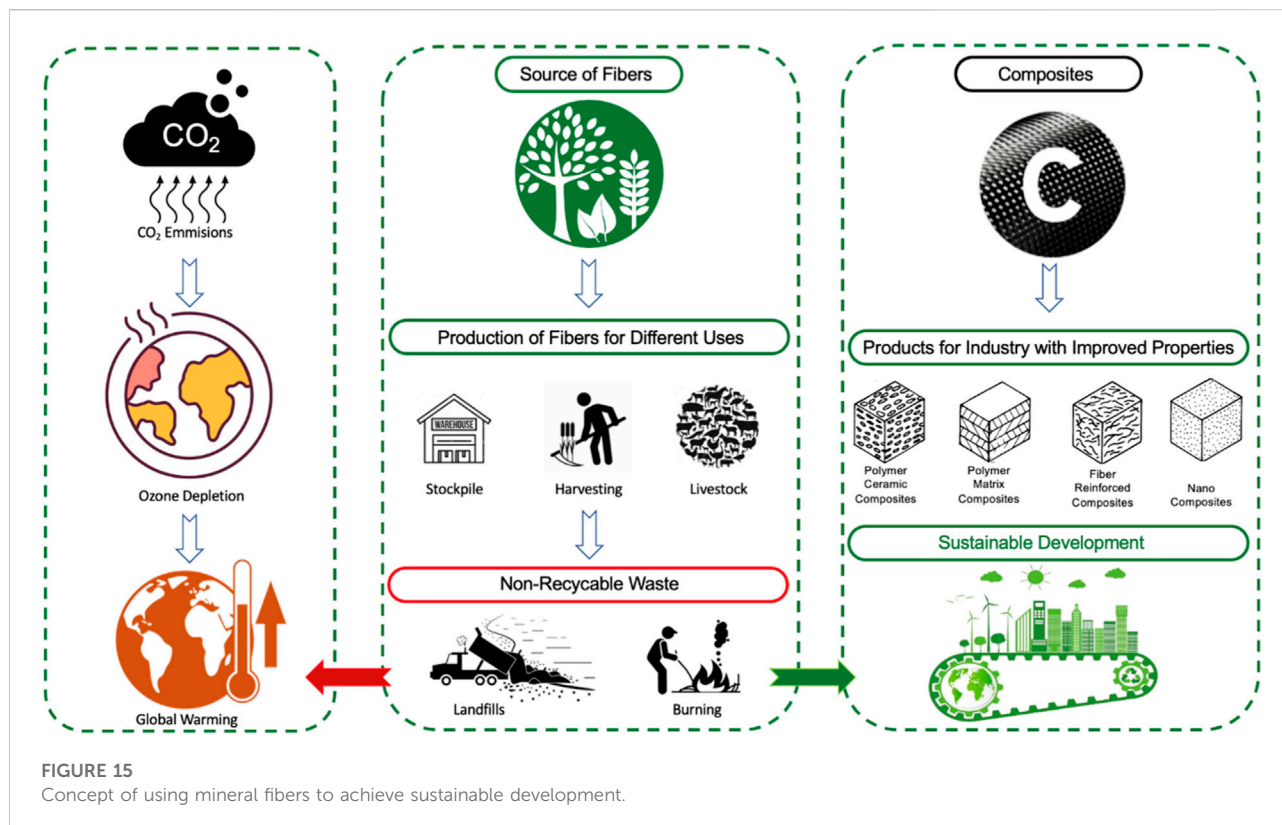
eliminated as per the sustainable development goals. Waste mineral fibers are one of the major contributors. Furthermore, the increasing demand for fossil fuel and natural resources to meet the construction industries' requirement has also accumulated toward ecological degradation. Therefore, incorporating such mineral fibers in concrete can significantly play its role in achieving UNDP's sustainable development goals (Figure 15). This incorporation would not only contribute toward a reduction in the overall cost of the respective concrete, but it would also decline the conventional material consumption, ultimately leading to a reduction of natural resource consumption. In addition, the environmental pollution caused by CO_2 emissions from these waste fibers (such as mineral fibers) may also be decreased significantly. Hence, green, sustainable, and economic development can be achieved by utilizing mineral fibers as reinforcement in cementitious concrete.

5 Conclusion

Research on cementitious concrete reinforced with mineral-derived natural fibers is evolving due to enhancing demand for the utilization of sustainable materials, as well as the strength, low density, low cost, and abundant local availability of these fibers. In recent years, the abundantly produced scientific information,

in addition to new communication channels, encouraged the research community to suggest the metric which provided the basis for the novel bibliometrics field. It employs statistical and mathematical analytic approaches to attain reliable quality gauges. Hence, there is a feasibility to evaluate the number of published documents by a nation, institution, individual, or research group having the highest scientific outcome. Bibliometric research is a suitable technique to identify the literature growth trend and volume, focusing on mineral fiber-reinforced concrete-related examinations that will benefit young scholars. The main aim of the current study is to perform a scientometric analysis of the literature available on mineral fiber-reinforced concrete to assess multiple aspects. The obtained conclusions are as follows:

- Mineral fibers are categorized as natural materials and are one such material that meets the technical requirements and environmental needs. These fibers have excellent properties such as 1) effective mechanical properties; 2) substantial bond behavior; and 3) extra-ordinary reinforcing, thermal, and acoustic properties. Mineral fibers considerably enhance the concrete mechanical properties and thus, offer a stable structure in terms of load-bearing in concrete and resist the initiation and propagation of micro-cracks.

- It is revealed from the assessment of publication sources of a search on mineral fibers in concrete that "Construction and building materials," "Advanced materials research," and "Materials today: proceedings" are the leading three sources, with 62, 29, and 25 publications, respectively. As far as total citations are concerned, here again, the top three sources are "Construction and building materials" with 2,158 citations, "Advanced materials research" with 1,120 citations, and "Materials today: proceedings" with 793 citations.

- Keywords assessment in the mineral fiber-reinforced concrete research domain reveals that mechanical properties, fiber-reinforced concrete, natural fibers, minerals, and basalt fibers are the most frequently occurring five terms. This analysis also reveals that mineral fibers in concrete have mainly been explored to have sustainable construction materials.

- The leading countries are determined by the contribution of mineral fiber-reinforced concrete research, and it is summarized that 32 countries have published at least five articles. Among all the nations, India, China, and the Russian Federation have contributed the maximum number of articles having 166, 138, and 48 articles, respectively. Moreover, China received 1,754 citations, followed by Italy and the United States with 1,031 and 834 citations, respectively.

- The incorporation of mineral fibers in cementitious concrete decreases their brittleness and significantly improves their properties, including toughness, energy-absorption capacity, and tensile strength. Mineral fibers endorse the reinforcing effect *via* adhesion bonding among cementitious matrix and mineral fibers. The bonding mechanism is based on the respective concrete manufacturing method and content, orientation, dimension, and distribution of mineral fibers.

- The appropriate proportion of mineral fibers may significantly improve the impermeability, resistance against sulfate and chloride erosion, resistance against the freeze–thaw cycle, and high-temperature durability of mineral fiber-reinforced concrete. Furthermore, adding mineral fibers to concrete can increase the pore and capillary contents, improve pore connectivity, and prevent the deterioration of the concrete's pore structure. However, it is important to explore the in-depth durability of concrete having mineral fibers and to develop specific test procedures for this purpose.

- It is evident from the reported SEM analysis that the string bonding among mineral fibers and the surrounding cementitious matrix offers an effective bridging mechanism that shows its ability to reduce stress concentrations and eliminates the probable internal degradation, ultimately leading to an improved mechanical performance of mineral fiber-reinforced concrete.

- This incorporation of mineral fibers in concrete would not only contribute toward a reduction in the overall cost, but it would also decline the consumption of conventional materials, ultimately leading toward sustainable development by reducing the adverse environmental impacts.

- The large-scale production and corresponding applications of mineral fiber-reinforced concrete are limited due to lacking information on various aspects such as long-term durability, Life Cycle Cost Analysis (LCCA), and Life Cycle Assessment (LCA) for mineral fiber-reinforced concrete. Therefore, mineral fiber-reinforced concrete needs to be further investigated in depth in terms of the aspects mentioned previously before its large-scale production and applicability.

6 Future recommendations

The bibliographic mapping and statistical analysis of research data on mineral fiber-reinforced concrete fields are conducted in this systematic review. The already available conventional, i.e., manual, review-based research studies are insufficient to comprehensively and accurately relate different literature aspects. The most widely-adopted keywords, publications (journals), and sources having the most published articles, the most contributing countries in the form of publications and the authors having maximum citations in the mineral fiber-reinforced concrete research field are identified in the current research. As per the keyword's evaluation, mechanical properties have been widely used to develop sustainable construction materials. Moreover, the literature and citation-based linkages are used to recognize the most participating and highly committed countries depending on the number of publications. The quantitative analysis and graphical representation of contributing countries and researchers would aid young researchers in establishing scientific collaborations, sharing progressive concepts and techniques, and developing joint ventures. Researchers from countries contributing to escalating the research on mineral fiber-reinforced concrete applications may collaborate with experts of the same discipline to benefit from their expertise. After evaluating the keywords in the considered research area with the help of scientometric analysis and reviewing the closely related literature, the current research emphasized the future perspectives of mineral fiber-reinforced concrete. Usually, research on mineral fiber wastes is not as deep as on other waste materials. For more efficiency and commercial feasibility in reusing after repurposing and recycling waste minerals, the following perspectives are proposed for the future:

- Before developing an appropriate technique to cater for the waste, a transparent classification of mineral-waste fibers from multiple sources is to be done. The said classification should mainly cover the mineral fiber type, prior usage, source, contaminant types, chemical composition, and physical conditions.
- The currently employed comminution method does not cost much and is energy-effective for treating waste–rock–mineral–wool fibers. This method seems to be a critical parameter in reducing the overall cost and developing more attention toward research development (Yap et al., 2021).
- The incorporation of additional admixtures such as; air-entraining agents, superplasticizers, and pozzolanic materials such as fly ash and silica fume also need to be explored to improve the mechanical properties and flow of concrete.
- Further enhancement in mineral fiber-reinforced cementitious concrete demands thorough research to assess the durability of concrete having mineral fibers (Awoyera et al., 2022).
- In the future, the aim of research should be toward optimizing and altering building materials, including simplified environmental analysis at a minimum level, as the ecological effect mitigation signifies a significant challenge to the current society. The efficiency of the existing building in terms of eco-friendly links less-energy requirement maintenance and embodied energy (Fořt et al., 2021; Zhang et al., 2022).
- Moreover, manual mixing for concrete preparation is hectic in the case of fiber-incorporation, resulting in a non-homogeneous mix. Therefore, the specific chemical addition may also be explored to replace manual and machine mixing.
- Further research is also suggested for the large-scale production of mineral fiber-reinforced concrete and the construction of a relevant structure to ensure the actual capability of mineral fibers in concrete and to portray the application of this sustainable material in the construction industry.
- The structural applications, such as pavements, bridge girders, etc., of mineral fiber-reinforced concrete should also be explored in detail if its long-term durability evaluation provides satisfactory outcomes.
- Furthermore, nowadays, researchers are giving significant attention to the 3D-printing technique to determine the performance of structures made by different types of cementitious concrete for optimizing their materials to get improved mechanical properties by conserving natural resources. Hence, the exploration of mineral fibers for 3D-printing concrete would be an exciting horizon to explore.
- Moreover, the exploration of concrete incorporating different fiber (i.e., mineral and synthetic) combinations, i.e., hybrid fiber-reinforced cementitious concrete, should also be made in parallel with the employment of novel techniques for producing said concrete.
- Although the incorporation of waste mineral fibers in concrete tends to decrease the overall cost of material, as reported in the literature, Life Cycle Cost Analysis (LCCA) should also be performed before its application in real-life structures.
- The reported reduced CO_2 emissions in the case of mineral fiber-reinforced concrete should also be validated by conducting Life Cycle Assessment (LCA), from the cradle to the grave, for mineral fiber-reinforced concrete when intended to be used in bulk quantities.

Author contributions

AM: visualization, funding acquisition, writing, reviewing, and editing. MA: conceptualization, validation, investigation, project administration, funding acquisition, writing, reviewing, and editing. WA: conceptualization, data acquisition, methodology, validation, software, supervision, writing–original draft, reviewing, and editing. KK: conceptualization, methodology, resources, supervision, software, validation, investigation, writing original draft, reviewing, and editing. MA-H: data curation, methodology, visualization, writing, reviewing, and editing. HQ: investigation, formal analysis, writing, reviewing, and editing. AM: resources, validation, investigation, writing, reviewing, and editing.

Funding

Acknowledgments

Conflict of interest

The authors declare that the research was conducted in the absence of any commercial or financial relationships that could be construed as a potential conflict of interest.

Publisher's note

All claims expressed in this article are solely those of the authors and do not necessarily represent those of their affiliated organizations, or those of the publisher, the editors, and the reviewers. Any product that may be evaluated in this article, or claim that may be made by its manufacturer, is not guaranteed or endorsed by the publisher.

References

Afgan, S., and Bing, C. (2021). Scientometric review of international research trends on thermal energy storage cement based composites via integration of phase change materials from 1993 to 2020. *Constr. Build. Mater.* 278, 122344. doi:10.1016/j.conbuildmat.2021.122344

Ahmad, W., Khan, M., and Smarzewski, P. (2021). Effect of short fiber reinforcements on fracture performance of cement-based materials: A systematic review approach. *Materials* 14 (7), 1745. doi:10.3390/ma14071745

Ahmed, T., Farooqi, M., and Ali, M. (2020). "Compressive behavior of rice straw-reinforced concrete for rigid pavements," in Proceeding of the IOP conference series: Materials science and engineering (IOP Publishing), 012004.

Alhawat, M., Ashour, A., Yildirim, G., Aldemir, A., and Sahmaran, M. (2022). Properties of geopolymers sourced from construction and demolition waste: A review. *J. Build. Eng.* 50, 104104. doi:10.1016/j.jobe.2022.104104

Ali, B., Azab, M., Ahmed, H., Kurda, R., El Ouni, M. H., and Elhag, A. B. (2022a). Investigation of physical, strength, and ductility characteristics of concrete reinforced with banana (Musaceae) stem fiber. *J. Build. Eng.* 61, 105024. doi:10.1016/j.jobe.2022.105024

Ali, B. (2022). Development of environment-friendly and ductile recycled aggregate concrete through synergetic use of hybrid fibers. *Environ. Sci. Pollut. Res.* 29 (23), 34452–34463. doi:10.1007/s11356-022-18627-y

Ali, B., Farooq, M. A., El Ouni, M. H., Azab, M., and Elhag, A. B. (2022b). The combined effect of coir and superplasticizer on the fresh, mechanical, and long-term durability properties of recycled aggregate concrete. *J. Build. Eng.* 59, 105009. doi:10.1016/j.jobe.2022.105009

Ali, B., Farooq, M. A., Kurda, R., Alyousef, R., Noman, M., and Alabduljabbar, H. (2022c). Effect of type and volume fraction of recycled-tire steel fiber on durability and mechanical properties of concrete. *Eur. J. Environ. Civ. Eng.*, 1–22. doi:10.1080/19648189.2022.2103590

Ali, B., Hawreen, A., Ben Kahla, N., Talha Amir, M., Azab, M., and Raza, A. (2022d). A critical review on the utilization of coir (coconut fiber) in cementitious materials. *Constr. Build. Mater.* 351, 128957. doi:10.1016/j.conbuildmat.2022.128957

Ali, B., Kurda, R., Ahmed, H., and Alyousef, R. (2022e). Effect of recycled tyre steel fiber on flexural toughness, residual strength, and chloride permeability of high-performance concrete (HPC). *J. Sustain. Cement-Based Mater.*, 1–17. doi:10.1080/21650373.2021.2025165

Ali, B., Raza, S. S., Hussain, I., and Iqbal, M. (2021). Influence of different fibers on mechanical and durability performance of concrete with silica fume. *Struct. Concr.* 22 (1), 318–333. doi:10.1002/suco.201900422

Amin, M. N., Ahmad, W., Khan, K., and Sayed, M. M. (2022). Mapping research knowledge on rice husk ash application in concrete: A scientometric review. *Materials* 15 (10), 3431. doi:10.3390/ma15103431

Arooj, K., and Ali, M. (2021). Mechanical, dynamic and absorption properties of hybrid fiber reinforced concrete for rigid pavements application. *Masters Civ. Eng.* Capital University of Science & technology.

Awoyera, P. O., Oduguwa, O. L., Effiong, J. U., De Jesus Silvera Sarmiento, A., Mortazavi, S. J., and Hu, J. W. (2022). Development of fibre-reinforced cementitious mortar with mineral wool and coconut fibre. *Materials* 15 (13), 4520. doi:10.3390/ma15134520

Aydın, S. (2013). Effects of fiber strength on fracture characteristics of normal and high strength concrete. *Per. Pol. Civ. Eng.* 57 (2), 191–200. doi:10.3311/ppci.7174

Azevedo, A. R., Lima, T. E., Reis, R. H., Oliveira, M. S., Candido, V. S., and Monteiro, S. N. (2022). Guaruman fiber: A promising reinforcement for cement-based mortars. *Case Stud. Constr. Mater.* 16, e01029. doi:10.1016/j.cscm.2022.e01029

Buyantuev, S., Mognonov, D., and Badmayev, B. (2012). The mini plant producing thermal insulation materials from basalt on the basis of electromagnetic melting units with low energy consumption. *Bull. East Sib. State Univ. Technol. Manag.* 1 (36), 16–20.

Cabeza, L. F., Castell, A., Medrano, M., Martorell, I., Pérez, G., and Fernández, I. (2010). Experimental study on the performance of insulation materials in Mediterranean construction. *Energy Build.* 42 (5), 630–636. doi:10.1016/j.enbuild.2009.10.033

Cao, M., Li, L., Yin, H., and Ming, X. (2019a). Microstructure and strength of calcium carbonate (CaCO3) whisker reinforced cement paste after exposed to high temperatures. *Fire Technol.* 55 (6), 1983–2003. doi:10.1007/s10694-019-00839-3

Cao, M., Ming, X., Yin, H., and Li, L. (2019b). Influence of high temperature on strength, ultrasonic velocity and mass loss of calcium carbonate whisker reinforced cement paste. *Compos. Part B Eng.* 163, 438–446. doi:10.1016/j.compositesb.2019.01.030

Cao, M., Xie, C., Li, L., and Khan, M. (2019c). Effect of different PVA and steel fiber length and content on mechanical properties of $CaCO_3$ whisker reinforced cementitious composites. *Mat. construcc.* 69 (336), e200. doi:10.3989/mc.2019.12918

Darko, A., Chan, A. P., Huo, X., and Owusu-Manu, D.-G. (2019). A scientometric analysis and visualization of global green building research. *Build. Environ.* 149, 501–511. doi:10.1016/j.buildenv.2018.12.059

Darko, A., Zhang, C., and Chan, A. P. (2017). Drivers for green building: A review of empirical studies. *Habitat Int.* 60, 34–49. doi:10.1016/j.habitatint.2016.12.007

de Azevedo, A. R., Alexandre, J., Xavier, G. d. C., and Pedroti, L. G. (2018). Recycling paper industry effluent sludge for use in mortars: A sustainability perspective. *J. Clean. Prod.* 192, 335–346. doi:10.1016/j.jclepro.2018.05.011

de Azevedo, A. R., Costa, A. M., Cecchin, D., Pereira, C. R., Marvila, M. T., and Adesina, A. (2022a). Economic potential comparative of reusing different industrial solid wastes in cementitious composites: A case study in Brazil. *Environ. Dev. Sustain.* 24 (4), 5938–5961. doi:10.1007/s10668-021-01630-7

de Azevedo, A. R. G., Alexandre, J., Zanelato, E. B., and Marvila, M. T. (2017). Influence of incorporation of glass waste on the rheological properties of adhesive mortar. *Constr. Build. Mater.* 148, 359–368. doi:10.1016/j.conbuildmat.2017.04.208

de Azevedo, A. R., Marvila, M. T., Antunes, M. L. P., Rangel, E. C., and Fediuk, R. (2021a). Technological perspective for use the natural pineapple fiber in mortar to repair structures. *Waste Biomass Valorization* 12 (9), 5131–5145. doi:10.1007/s12649-021-01374-5

de Azevedo, A. R., Marvila, M. T., Tayeh, B. A., Cecchin, D., Pereira, A. C., and Monteiro, S. N. (2021b). Technological performance of açaí natural fibre reinforced cement-based mortars. *J. Build. Eng.* 33, 101675. doi:10.1016/j.jobe.2020.101675

de Azevedo, A. R., Nascimento, M., do Carmo, D., Marvila, M. T., Xavier, G. d. C., and Monteiro, S. N. (2022b). *Environmental and durability perspective of the use of curaua fiber treated in mortars.*

Farooqi, M. U., and Ali, M. (2022). A study on natural fibre reinforced concrete from materials to structural applications. *Arab. J. Sci. Eng.* doi:10.1007/s13369-022-06977-1

Farooqi, M. U., and Ali, M. (2018a). Contribution of plant fibers in improving the behavior and capacity of reinforced concrete for structural applications. *Constr. Build. Mater.* 182, 94–107. doi:10.1016/j.conbuildmat.2018.06.041

Farooqi, M. U., and Ali, M. (2018b). "Effect of fibre content on compressive strength of wheat straw reinforced concrete for pavement applications," in Proceeding of the IOP Conference Series: Materials Science and Engineering (United Kingdom: IOP Publishing), 012014.

Farooqi, M. U., and Ali, M. (2018c). "Effect of fibre content on splitting-tensile strength of wheat straw reinforced concrete for pavement applications," in *Key engineering materials* (Switzerland: Trans Tech Publ), 349–354.

Farooqi, M. U., and Ali, M. (2019). Effect of pre-treatment and content of wheat straw on energy absorption capability of concrete. *Constr. Build. Mater.* 224, 572–583. doi:10.1016/j.conbuildmat.2019.07.086

Fořt, J., Kočí, J., and Černý, R. (2021). Environmental efficiency aspects of basalt fibers reinforcement in concrete mixtures. *Energies* 14 (22), 7736. doi:10.3390/en14227736

Gao, L., Adesina, A., and Das, S. (2021). Properties of eco-friendly basalt fibre reinforced concrete designed by Taguchi method. *Constr. Build. Mater.* 302, 124161. doi:10.1016/j.conbuildmat.2021.124161

Gebremariam, A. T., Vahidi, A., Di Maio, F., Moreno-Juez, J., Vegas-Ramiro, I., Łagosz, A., et al. (2021). Comprehensive study on the most sustainable concrete design made of recycled concrete, glass and mineral wool from C&D wastes. *Constr. Build. Mater.* 273, 121697. doi:10.1016/j.conbuildmat.2020.121697

Guoxin, Z., Yi, L., Youzhi, L., Songhui, L., and Lei, Z. (2018). Reviews on temperature control and crack prevention of high concrete dam. *J. Hydraulic Eng.* 49 (09), 1068–1078.

Huang, S., Wang, H., Ahmad, W., Ahmad, A., Ivanovich Vatin, N., Mohamed, A. M., et al. (2022a). Plastic waste management strategies and their environmental aspects: A scientometric analysis and comprehensive review. *Int. J. Environ. Res. Public Health* 19 (8), 4556. doi:10.3390/ijerph19084556

Huang, Y., Zhang, W., and Liu, X. (2022b). Assessment of diagonal macrocrack-induced debonding mechanisms in FRP-strengthened RC beams. *J. Compos. Constr.* 26 (5), 04022056. doi:10.1061/(asce)cc.1943-5614.0001255

Jerman, M., and Černý, R. (2012). Effect of moisture content on heat and moisture transport and storage properties of thermal insulation materials. *Energy Build.* 53, 39–46. doi:10.1016/j.enbuild.2012.07.002

Jia, F., Yao, Y., and Wang, J. (2021). Influence and mechanism research of hydration heat inhibitor on low-heat portland cement. *Front. Mat.* 8. doi:10.3389/fmats.2021.697380

Jin, R., Gao, S., Cheshmehzangi, A., and Aboagye-Nimo, E. (2018). A holistic review of off-site construction literature published between 2008 and 2018. *J. Clean. Prod.* 202, 1202–1219. doi:10.1016/j.jclepro.2018.08.195

John, V. J., and Dharmar, B. (2021). Influence of basalt fibers on the mechanical behavior of concrete—a review. *Struct. Concr.* 22 (1), 491–502. doi:10.1002/suco.201900086

Kaïkea, A., Achoura, D., Duplan, F., and Rizzuti, L. (2014). Effect of mineral admixtures and steel fiber volume contents on the behavior of high performance fiber reinforced concrete. *Mater. Des.* 63, 493–499. doi:10.1016/j.matdes.2014.06.066

Khan M, M., Cao, M., Chaopeng, X., and Ali, M. (2022). Experimental and analytical study of hybrid fiber reinforced concrete prepared with basalt fiber under high temperature. *Fire Mater.* 46 (1), 205–226. doi:10.1002/fam.2968

Khan, M., Cao, M., Ai, H., and Hussain, A. (2022a). Basalt fibers in modified whisker reinforced cementitious composites. *Period. Polytech. Civ. Eng.* 66 (2), 344–354. doi:10.3311/ppci.18965

Khan, M., Cao, M., and Ali, M. (2018). Effect of basalt fibers on mechanical properties of calcium carbonate whisker-steel fiber reinforced concrete. *Constr. Build. Mater.* 192, 742–753. doi:10.1016/j.conbuildmat.2018.10.159

Khan, M., Cao, M., and Ali, M. (2018). *Experimental and empirical study of basalt fibber reinforced concrete*. Building Tomorrow's Society. Paper ID–MA39_0610035833.

Khan, M., Cao, M., and Ali, M. (2022b). "Influence of CaCO3 whiskers, steel fibers and basalt fibers hybridization on flexural toughness of concrete," in Proceeding of the Fifth International Conference on Sustainable Construction Materials and Technologies, London.

Khan, M., Cao, M., Chu, S., and Ali, M. (2022d). Properties of hybrid steel-basalt fiber reinforced concrete exposed to different surrounding conditions. *Constr. Build. Mater.* 322, 126340. doi:10.1016/j.conbuildmat.2022.126340

Khan, M., and Cao, M. (2021). Effect of hybrid basalt fibre length and content on properties of cementitious composites. *Mag. Concr. Res.* 73 (10), 487–498. doi:10.1680/jmacr.19.00226

Khan, M., Cao, M., Hussain, A., and Chu, S. (2021a). Effect of silica-fume content on performance of CaCO3 whisker and basalt fiber at matrix interface in cement-based composites. *Constr. Build. Mater.* 300, 124046. doi:10.1016/j.conbuildmat.2021.124046

Khan, M., Cao, M., Xie, C., and Ali, M. (2022e). Effectiveness of hybrid steel-basalt fiber reinforced concrete under compression. *Case Stud. Constr. Mater.* 16, e00941. doi:10.1016/j.cscm.2022.e00941

Khan, M., Cao, M., Xie, C., and Ali, M. (2021b). Efficiency of basalt fiber length and content on mechanical and microstructural properties of hybrid fiber concrete. *Fatigue Fract. Eng. Mat. Struct.* 44 (8), 2135–2152. doi:10.1111/ffe.13483

Khan, M., Cao, M., Xie, C., and Ali, M. (2022f). Hybrid fiber concrete with different basalt fiber length and content. *Struct. Concr.* 23 (1), 346–364. doi:10.1002/suco.202000472

Kirthika, S., and Singh, S. (2018). Experimental investigations on basalt fibre-reinforced concrete. *J. Inst. Eng. India. Ser. A* 99 (4), 661–670. doi:10.1007/s40030-018-0325-4

Li, J., Peng, X., Cao, J., Chen, G., Tian, J., Wang, X., et al. (2004). Research of high belite cement dam concrete with low-heat and high carack resistance. *JOURNAL-CHINESE Ceram. Soc.* 32 (3), 364–371.

Li, L., and Cao, M. (2018). Influence of calcium carbonate whisker and polyvinyl alcohol-steel hybrid fiber on ultrasonic velocity and resonant frequency of cementitious composites. *Constr. Build. Mater.* 188, 737–746. doi:10.1016/j.conbuildmat.2018.08.154

Li, L., Cao, M., Ming, X., Yin, H., and Sun, Y.-n. (2019a). Microstructure of calcium carbonate whisker reinforced cement paste after elevated temperature exposure. *Constr. Build. Mater.* 227, 116609. doi:10.1016/j.conbuildmat.2019.07.335

Li, L., Cao, M., Xie, C., and Yin, H. (2019b). Effects of CaCO3 whisker, hybrid fiber content and size on uniaxial compressive behavior of cementitious composites. *Struct. Concr.* 20 (1), 506–518. doi:10.1002/suco.201800185

Li, L., Cao, M., and Yin, H. (2019c). Comparative roles between aragonite and calcite calcium carbonate whiskers in the hydration and strength of cement paste. *Cem. Concr. Compos.* 104, 103350. doi:10.1016/j.cemconcomp.2019.103350

Li, L., Gao, D., Li, Z., Cao, M., Gao, J., and Zhang, Z. (2020a). Effect of high temperature on morphologies of fibers and mechanical properties of multi-scale fiber reinforced cement-based composites. *Constr. Build. Mater.* 261, 120487. doi:10.1016/j.conbuildmat.2020.120487

Li, L., Li, Z., Cao, M., Tang, Y., and Zhang, Z. (2021). Nanoindentation and porosity fractal dimension of calcium carbonate whisker reinforced cement paste after elevated temperatures (up to 900◦C). *Fractals* 29 (02), 2140001. doi:10.1142/s0218348x21400016

Li, L., Xie, C., Cao, M., Zhou, X., and Li, Z. (2022). Synergistic effect between CaCO 3 whisker and steel-PVA fiber cocktail in cement-based material at elevated temperature. *J. Mat. Civ. Eng.* 34 (2), 04021415. doi:10.1061/(asce)mt.1943-5533.0004103

Li, Y., Shen, A., and Wu, H. (2020b). Fractal dimension of basalt fiber reinforced concrete (BFRC) and its correlations to pore structure, strength and shrinkage. *Materials* 13 (14), 3238. doi:10.3390/ma13143238

Liu, H., Yu, Y., Liu, Y., Zhang, M., Li, L., Ma, L., et al. (2022a). A review on basalt fiber composites and their applications in clean energy sector and power grids. *Polymers* 14 (12), 2376. doi:10.3390/polym14122376

Liu, M., Dai, W., Zhong, C., and Yang, X. (2022b). Study on mechanical properties and microstructure of basalt fiber reactive powder concrete. *Buildings* 12 (10), 1734. doi:10.3390/buildings12101734

Luo, X., Xu, J.-y., Bai, E.-l., and Li, W. (2014). Study on the effect of basalt fiber on the energy absorption characteristics of porous material. *Constr. Build. Mater.* 68, 384–390. doi:10.1016/j.conbuildmat.2014.06.072

Markoulli, M. P., Lee, C. I., Byington, E., and Felps, W. A. (2017). Mapping human resource management: Reviewing the field and charting future directions. *Hum. Resour. Manag. Rev.* 27 (3), 367–396. doi:10.1016/j.hrmr.2016.10.001

Mechtcherine, V., Schneider, K., and Brameshuber, W. (2016). "Mineral-based matrices for textile-reinforced concrete," in *Textile fibre composites in civil engineering* (Elsevier), 25–43.

Meng, Z., Li, L., Farooqi, M. U., Feng, L., and Wang, L. (2022). Fiber factor for fresh and hardened properties of polyethylene fiber-reinforced geopolymer mortar. *J. Build. Eng.* 53, 104556. doi:10.1016/j.jobe.2022.104556

Nafees, A., Amin, M. N., Khan, K., Nazir, K., Ali, M., Javed, M. F., et al. (2021). Modeling of mechanical properties of silica fume-based green concrete using machine learning techniques. *Polymers* 14 (1), 30. doi:10.3390/polym14010030

Nafees, A., Khan, S., Javed, M. F., Alrowais, R., Mohamed, A. M., Mohamed, A., et al. (2022). Forecasting the mechanical properties of plastic concrete employing experimental data using machine learning algorithms: DT, MLPNN, SVM, and RF. *Polymers* 14 (8), 1583. doi:10.3390/polym14081583

Oraee, M., Hosseini, M. R., Papadonikolaki, E., Palliyaguru, R., and Arashpour, M. (2017). Collaboration in BIM-based construction networks: A bibliometric-qualitative literature review. *Int. J. Proj. Manag.* 35 (7), 1288–1301. doi:10.1016/j.ijproman.2017.07.001

Park, J. Y., and Nagy, Z. (2018). Comprehensive analysis of the relationship between thermal comfort and building control research-A data-driven literature review. *Renew. Sustain. Energy Rev.* 82, 2664–2679. doi:10.1016/j.rser.2017.09.102

Pogorelov, S., and Semenyak, G. (2016). Frost resistance of the steel fiber reinforced concrete containing active mineral additives. *Procedia Eng.* 150, 1491–1495. doi:10.1016/j.proeng.2016.07.088

Pukharenko, Y. (2012). Restoration and construction: The potential of fiber reinforced materials and products. *Mod. problems Sci. Educ.* 4, 1–7.

Raza, S. S., Amir, M. T., Azab, M., Ali, B., Abdallah, M., El Ouni, M. H., et al. (2022). Effect of micro-silica on the physical, tensile, and load-deflection characteristics of micro fiber-reinforced high-performance concrete (HPC). *Case Stud. Constr. Mater.* 17, e01380. doi:10.1016/j.cscm.2022.e01380

Saraikina, K., Golubev, V., and Semkova, E. (2012). Alkali resistance of basalt fiber and methods of its improvement. *Constr. Archit.* 1, 185–192. Bulletin of Perm National Research Polytechnic University.

Sheng, C., He, G., Hu, Z., Chou, C., Shi, J., Li, J., et al. (2021). Yarn on yarn abrasion failure mechanism of ultrahigh molecular weight polyethylene fiber. *J. Eng. Fibers Fabr.* 16, 155892502110527. doi:10.1177/15589250211052766

Shi, T., Liu, Y., Zhao, X., Wang, J., Zhao, Z., Corr, D. J., et al. (2022). Study on mechanical properties of the interfacial transition zone in carbon nanofiber-reinforced cement mortar based on the PeakForce tapping mode of atomic force microscope. *J. Build. Eng.* 61, 105248. doi:10.1016/j.jobe.2022.105248

Song, H., Liu, J., He, K., and Ahmad, W. (2021). A comprehensive overview of jute fiber reinforced cementitious composites. *Case Stud. Constr. Mater.* 15, e00724. doi:10.1016/j.cscm.2021.e00724

Stonys, R., Kuznetsov, D., Krasnikovs, A., Škamat, J., Baltakys, K., Antonovič, V., et al. (2016). Reuse of ultrafine mineral wool production waste in the manufacture of refractory concrete. *J. Environ. Manag.* 176, 149–156. doi:10.1016/j.jenvman.2016.03.045

Thomas, B. S., Yang, J., Bahurudeen, A., Abdalla, J. A., Hawileh, R., Hamada, H. M., et al. (2021). Sugarcane bagasse ash as supplementary cementitious material in concrete–A review. *Mater. Today Sustain.* 15, 100086. doi:10.1016/j.mtsust.2021.100086

Udomsap, A. D., and Hallinger, P. (2020). A bibliometric review of research on sustainable construction, 1994–2018. *J. Clean. Prod.* 254, 120073. doi:10.1016/j.jclepro.2020.120073

Väntsi, O., and Kärki, T. (2014). Mineral wool waste in europe: A review of mineral wool waste quantity, quality, and current recycling methods. *J. Mat. Cycles Waste Manag.* 16 (1), 62–72. doi:10.1007/s10163-013-0170-5

Wei, H., and Pengcheng, W. (2020). Key methods for non-cover-weight consolidation grouting of super high dam foundations. *J. Tsinghua Univ. Sci. Technol.* 60 (7), 582–588.

Wuni, I. Y., Shen, G. Q., and Osei-Kyei, R. (2019). Scientometric review of global research trends on green buildings in construction journals from 1992 to 2018. *Energy Build.* 190, 69–85. doi:10.1016/j.enbuild.2019.02.010

Xiao, X., Skitmore, M., Li, H., and Xia, B. (2019). Mapping knowledge in the economic areas of green building using scientometric analysis. *Energies* 12 (15), 3011. doi:10.3390/en12153011

Xiaomei, W., Qiang, G., Hao, D., and Yueming, F. (2019). Flexural fatigue performance of concrete prepared with low-heat portland cement. *J. Southwest Jiaot. Univ.* 54 (2).

Xin, L., Jin-Yu, X., Weimin, L., and Zhi-Kun, W. (2015). Comparative study of the effect of basalt fiber on dynamic damage characteristics of ceramics cement–based porous material. *J. Mat. Civ. Eng.* 27 (8), 04014224. doi:10.1061/(asce)mt.1943-5533.0001178

Xu, Y., Zeng, J., Chen, W., Jin, R., Li, B., and Pan, Z. (2018). A holistic review of cement composites reinforced with graphene oxide. *Constr. Build. Mater.* 171, 291–302. doi:10.1016/j.conbuildmat.2018.03.147

Yang, H., Liu, L., Yang, W., Liu, H., Ahmad, W., Ahmad, A., et al. (2022). A comprehensive overview of geopolymer composites: A bibliometric analysis and literature review. *Case Stud. Constr. Mater.* 16, e00830. doi:10.1016/j.cscm.2021.e00830

Yang, Y., Zhou, Q., Li, X., Lum, G. C., and Deng, Y. (2019). Uniaxial compression mechanical property and fracture behavior of hybrid inorganic short mineral fibers reinforced cement-based material. *Cem. Concr. Compos.* 104, 103338. doi:10.1016/j.cemconcomp.2019.103338

Yap, Z. S., Khalid, N. H. A., Haron, Z., Mohamed, A., Tahir, M. M., Hasyim, S., et al. (2021). Waste mineral wool and its opportunities—a review. *Materials* 14 (19), 5777. doi:10.3390/ma14195777

Yliniemi, J., Laitinen, O., Kinnunen, P., and Illikainen, M. (2018). Pulverization of fibrous mineral wool waste. *J. Mat. Cycles Waste Manag.* 20 (2), 1248–1256. doi:10.1007/s10163-017-0692-3

Zhang, P., Wang, J., Li, Q., Wan, J., and Ling, Y. (2021a). Mechanical and fracture properties of steel fiber-reinforced geopolymer concrete. *Sci. Eng. Compos. Mater.* 28(1), 299–313. doi:10.1515/secm-2021-0030

Zhang, Z., Liang, G., Niu, Q., Wang, F., Chen, J., Zhao, B., et al. (2022). A Wiener degradation process with drift-based approach of determining target reliability index of concrete structures. *Qual. Reliab. Eng. Int.* 38 (7), 3710–3725. doi:10.1002/qre.3168

Zhang, Z., Yang, F., Zhang, H., Zhang, T., Wang, H., Xu, Y., et al. (2021b). Influence of CeO2 addition on forming quality and microstructure of TiC -reinforced CrTi4-based laser cladding composite coating. *Mater. Charact.* 171, 110732. doi:10.1016/j.matchar.2020.110732

Zheng, Y., Zhang, W., Baca Lopez, D. M., and Ahmad, R. (2021a). Scientometric analysis and systematic review of multi-material additive manufacturing of polymers. *Polymers* 13 (12), 1957. doi:10.3390/polym13121957

Zheng, Y., Zhang, Y., and Zhang, P. (2021b). Methods for improving the durability of recycled aggregate concrete: A review. *J. Mater. Res. Technol.* 15, 6367–6386. doi:10.1016/j.jmrt.2021.11.085

Zheng, Y., Zhuo, J., Zhang, Y., and Zhang, P. (2022). Mechanical properties and microstructure of nano-SiO2 and basalt-fiber-reinforced recycled aggregate concrete. *Nanotechnol. Rev.* 11 (1), 2169–2189. doi:10.1515/ntrev-2022-0134

Zuo, J., and Zhao, Z.-Y. (2014). Green building research–current status and future agenda: A review. *Renew. Sustain. energy Rev.* 30, 271–281. doi:10.1016/j.rser.2013.10.021

Application of machine learning algorithms to evaluate the influence of various parameters on the flexural strength of ultra-high-performance concrete

Yunfeng Qian[1], Muhammad Sufian[2]*, Ahmad Hakamy[3], Ahmed Farouk Deifalla[4] and Amr El-said[5]

[1]School of Civil Engineering, Changsha University of Science and Technology, Changsha, China, [2]School of Civil Engineering, Southeast University, Nanjing, China, [3]Department of Physics, Umm Al-Qura University, Mecca, Saudi Arabia, [4]Structural Engineering and Construction Management Department, Future University in Egypt, New Cairo, Egypt, [5]Department of Civil Engineering, The Higher Institute of Engineering, El Shrouk, Cairo, Egypt

The effect of various parameters on the flexural strength (FS) of ultra-high-performance concrete (UHPC) is an intricate mechanism due to the involvement of several inter-dependent raw ingredients. In this digital era, novel artificial intelligence (AI) approaches, especially machine learning (ML) techniques, are gaining popularity for predicting the properties of concrete composites due to their better precision than typical regression models. In addition, the developed ML models in the literature for FS of UHPC are minimal, with limited input parameters. Hence, this research aims to predict the FS of UHPC considering extensive input parameters (21) and evaluate each their effect on its strength by applying advanced ML approaches. Consequently, this paper involves the application of ML approaches, i.e., Support Vector Machine (SVM), Multi-Layer Perceptron (MLP), and Gradient Boosting (GB), to predict the FS of UHPC. The GB approach is more effective in predicting the FS of UHPC precisely than the SVM and MLP algorithms, as evident from the outcomes of the current study. The ensembled GB model determination coefficient (R^2) is 0.91, higher than individual SVM with 0.75 and individual MLP with 0.71. Moreover, the precision of applied models is validated by employing the k-fold cross-validation technique. The validity of algorithms is ensured by statistical means, i.e., mean absolute error and root mean square errors. The exploration of input parameters (raw materials) impact on FS of UHPC is also made with the help of SHAP analysis. It is revealed from the SHAP analysis that the steel fiber content feature has the highest influence on the FS of UHPC.

Abbreviations: AI, Artificial Intelligence; ANN, Artificial Neural Network; FA, Fly Ash; FS, Flexural Strength; GB, Gradient Boosting; GEP, Gene Expression Programming; GGBFS, Ground Granulated Blast Slag Furnace; MAE, Mean Absolute Error; ML, Machine Learning; MLP, Multi-Layer Perceptron; R^2, Determination Coefficient; RMSE, Root Mean Square Error; SCM, Supplementary Cementitious Material; SHAP, SHapley Additive exPlanations; SVM, Support Vector Machine; UHPC, Ultra-High-Performance Concrete.

Introduction

The development of a new generation of concrete named ultra-high-performance concrete (UHPC) is based on four principles that include 1. Microstructure improvement; ii. Reduction in porosity; iii. Enhancement in toughness; and iv. Increase in homogeneity (Shi et al., 2015; Wu et al., 2016). The significantly higher strength (i.e., more than 150 MPa) of UHPC, superior durability, and toughness are well known (Habel et al., 2006; Park et al., 2012). Hence, UHPC is potentially applicable as a precast structural component in bridges and various industrial products to have lightweight, durable, flexible, and aesthetic structures (Schmidt and Fehling, 2005; Wang et al., 2015). For achieving these superior properties of UHPC, low water-to-cement ratio, higher cement content, fine powders (silica fume, quartz, etc.), high-range water-reducing admixtures, and well-graded aggregates are deployed to get minimum lowest porosity with good consolidation and flow, and more particle packing density (Zhang and Ali, 2021; Ali et al., 2022b). Various studies have been conducted in the recent past to determine UHPC mechanical properties having different mix designs and ingredients (Yu et al., 2014; Yoo and Banthia, 2016; Zhou et al., 2018). Precisely, the incorporation of eco-friendly supplementary cementitious materials (SCMs), like; ground granulated blast slag furnaces (GGBFS), fly ash (FA) etc., has gained the attention of researchers (Chen et al., 2018; Khan et al., 2018; Khan and Ali, 2019; Zhang et al., 2019; Jiang et al., 2020a; Arshad et al., 2020; Jiang et al., 2020b; Jiang et al., 2022a; Jiang et al., 2022b; Tariq et al., 2022). Plain UHPC has brittle nature that may restrict its applications (Wang et al., 2015; Le Hoang and Fehling, 2017; Jiang et al., 2020b; Larsen and Thorstensen, 2020; Raza et al., 2022b). Hence different fibers, including artificial and steel fibers, have been commonly incorporated to enhance composites' impact resistance and ductility (Zhang and Huang, 2022). Multiple researchers have explored the addition of steel/synthetic/natural fibers to concrete as reinforcement for improving characteristics like fatigue resistance, toughness, ductility, and resist propagation of cracks in concrete (Cao et al., 2018; Ali et al., 2021; Li et al., 2021b; Cao and Khan, 2021; Deifalla et al., 2021; Khan et al., 2021; Xie et al., 2021; Ali et al., 2022a; Khan et al., 2022a; Li et al., 2022b; Ali et al., 2022c; Ali et al., 2022d; Farooqi and Ali, 2022; Hu et al., 2022; Meng et al., 2022; Zhang N et al., 2022). Steel fibers are incorporated into concrete to enhance its post-cracking phenomenon and toughness (Deifalla, 2020; Li et al., 2021a; Li et al., 2022a; Raza et al., 2022a; Khan et al., 2022b; Khan et al., 2022c; Khan et al., 2022d). However, researchers have also reported that fibers do not help improve the UHPC compressive strength, whereas the matrix particle packing density and cement hydration degree have a more significant role in the development of UHPC strength (Liang et al., 2018; Arora et al., 2019; Larsen and Thorstensen, 2020; Baili et al., 2022; El Ouni et al., 2022; Zheng et al., 2022). Such research findings highlight the information lacking to predict the UHPC behavior having different mixture ingredients. So, there is a need of modelling for developing a relationship among input parameters and the outcomes (Huang et al., 2022).

Recently, due to the recent advancements in Artificial Intelligence (AI), Machine Learning (ML) techniques have come out as an interesting tool for modelling that is suitable for a wide-ranging variety of scientific domains such as materials engineering (Worden and Manson, 2007; Cao and Li, 2018; Cui et al., 2018; Musumeci et al., 2018; Ebid and Deifalla, 2021; Andalib et al., 2022; Nawaz et al., 2022; Pandey et al., 2022). Keeping this in mind, an inclination has recently been made towards employing ML approaches for concrete strength prediction (Aiyer et al., 2014; Asteris et al., 2016; Sonebi et al., 2016; Dutta et al., 2017; Bayrami, 2022; Sarkhani Benemaran et al., 2022; Shah et al., 2022; Wang et al., 2022; Wang and Wu, 2022). These approaches may be used for numerous applications such as classification, regression, clustering, and correlation (Nehdi et al., 2001; Nguyen et al., 2020; Asri et al., 2022; De-Prado-Gil et al., 2022; Kumar and Kumar, 2022). Due to the development in ML techniques, it is thus easier to determine the concrete strength (Balf et al., 2021; Kovačević et al., 2021; Zhang Z et al., 2022). Mahjoubi et al. (2022a) performed an auto-tune learning framework for UHPC prediction and considered different multiple-function models (Mahjoubi et al., 2021; Mahjoubi et al., 2022b). Marani et al. (2020) employed the Gradient Boosting (GB) ML approach for the compressive strength prediction of UHPC. The research was conducted on 28 days of concrete strength prediction in significantly less time. The study concluded with the highly precise prediction of UHPC compressive strength, having an R^2 of 0.96. Lu et al. (2019) have applied the Support Vector Machine (SVM) modelling approach to determine the lithium-slag effect on the properties of cementitious mortar and resulted in an 11% enhanced and improved prediction performance of SVM with respect to other ML models. Similarly, Solhmirzaei et al. (2020) also reported the effective prediction of SVM modelling in the case of shear capacity for UHPC beams. Abellán-García (2020) employed the four-layer Multi-Layer Perceptron (MLP) for predicting the UHPC compressive strength and resulted in the satisfactory capability of MLP for strength prediction. A similar type of finding was also found in the literature for MLP modelling prediction (Abellán-García et al., 2020; Fan et al., 2021; Abellán-García and García-Castaño, 2022). Although, the application of these algorithms for UHPC compressive strength is reported several times in the literature; however, the employment of these models for predicting the flexural strength of UHPC has limited. Further, the available studies have considered a limited number of variables for prediction modelling. Moreover, applying a *post hoc* model-agnostic technique called SHapley Additive exPlanations (SHAP) provides insight into ML algorithms (Lundberg and Lee, 2017; Lauritsen et al., 2020; Johnsen et al., 2021). The interpretation of correlation among characteristics and a structure in different domains like; material science (Lauritsen et al., 2020; Johnsen et al., 2021), nanophotonic structures behavior (Yeung et al., 2020), low-alloy steel corrosion rate (Yan et al., 2020), inorganic materials synthesis (Tang et al., 2020), finances (Mokhtari et al., 2019), text classification (Zhao et al., 2020), and biomedical engineering (Lundberg et al., 2018), may be achieved effectively by the application of SHAP. But the employment of ML with SHAP for the flexural properties of UHPC is not common enough yet.

Importance of current study

For evaluating the superior properties of UHPC, the laboratory procedures for its manufacturing and testing, such as specimen
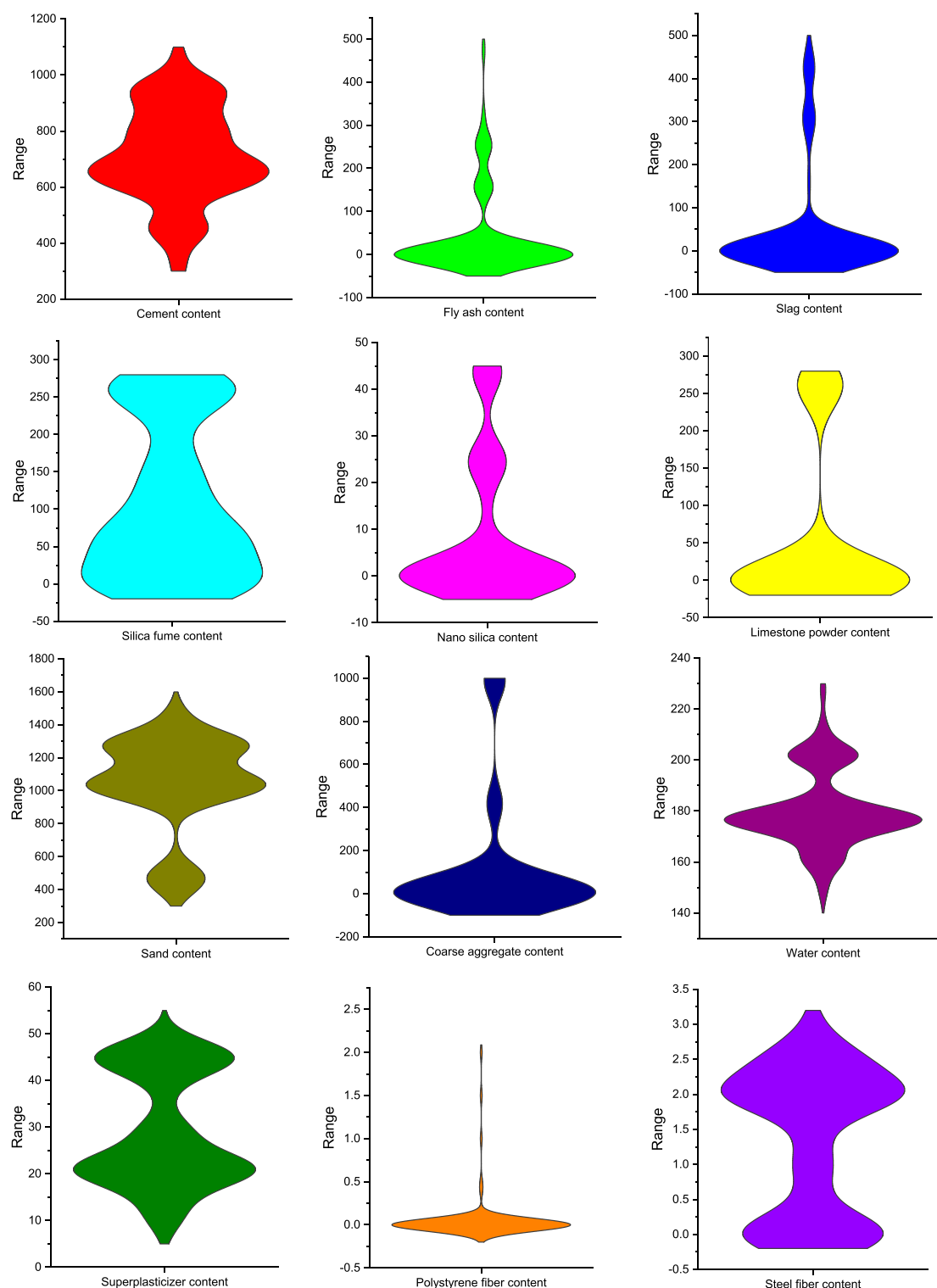
FIGURE 1
Violin plots distribution of the input parameters.

casting, curing, and testing, are a major concern in terms of high cost and time consumption. Modern methods of ML are now gaining attention to predict the UHPC mechanical behavior to avoid the issues mentioned above. The current study focuses on the FS prediction of UHPC considering extensive input parameters (21) by employing ML techniques which are still limited in the literature. The importance of this study is the prediction of UHPC FS by using both ensemble ML techniques (i.e., Gradient Boosting) and individual ML techniques (i.e., SVM and MLP) along with the exploration of raw ingredients effect and
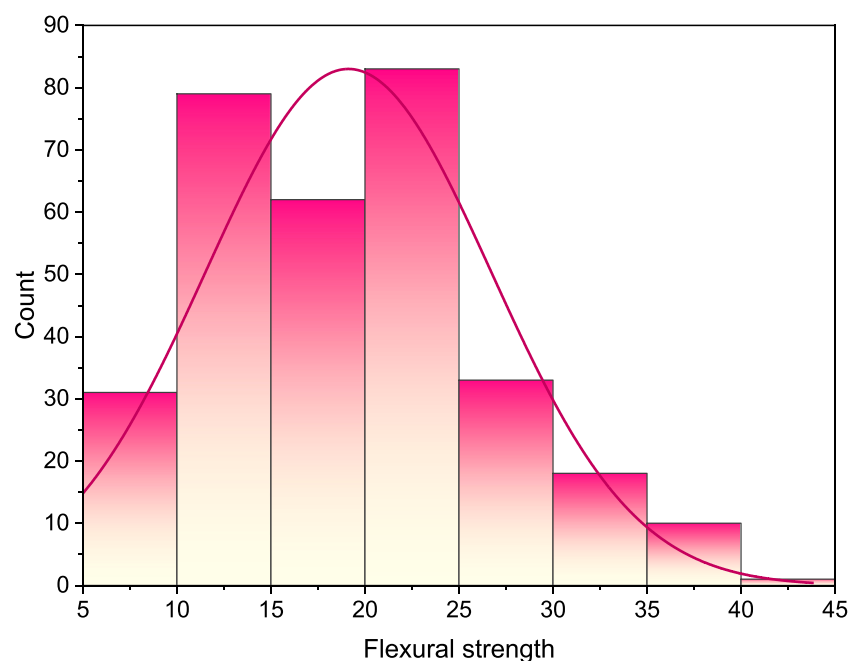
FIGURE 2
Relative distribution of output parameter.

interaction by applying SHAP analysis. A total of 21 input factors, i.e., the content and type of cement, its compressive strength and strength class, the content of fine and coarse aggregates, the content of fly ash, slag, silica fume, limestone powder, nano silica, quartz powder and super-plasticizer, the maximum size of aggregates, water content, content, length and diameter of polystyrene and steel fiber, and time of curing, are considered for FS as an output parameter. The anaconda navigator software is used with Python programming to execute the required prediction models. The data training of twenty boosting sub-models is done for ensembled ML models to achieve maximum precision. Moreover, the test data is confirmed by employing k-Fold cross-validation in combination with MAE, R², and RMSE. Further, the performance of statistical checks is used to compare individual and ensemble models. At last, the SHAP analysis is also included to analyze the contribution level for every input factor toward the FS of UHPC. This is aimed at ensuring the accuracy of this study. The effective, efficient and economical design for durable structures can be achieved by precisely predicting concrete properties, which would ultimately reduce the time consumption in selecting adequate materials. Also, the application of SHAP analysis is significant for illustrating raw ingredients' impact on the FS of UHPC. The employed prediction approaches enable researchers to devise novel materials smartly."

and Bao, 2021). A total of 21 input factors, i.e., (i) the cement content (kg/m^3), (ii) cement type and strength class, (iii) cement compressive strength (MPa), (iv) fine aggregates content (kg/m^3), (v) coarse aggregates content (kg/m^3), (vi) fly ash content (kg/m^3), (vii) slag content (kg/m^3), (viii) silica fume content (kg/m^3), (ix) limestone powder content (kg/m^3), (x) nano silica content (kg/m^3), (xi) quartz powder content (kg/m^3), (xii) super-plasticizer content (kg/m^3), (xiii) the maximum size of aggregates (mm), (xiv) water content (kg/m^3), (xv) polystyrene fiber content (%), (xvi) steel fiber content (%), (xvii) polystyrene fiber length (mm), (xviii) steel fiber length (mm), (xix) polystyrene fiber diameter (mm), (xx) steel fiber diameter (mm), and (xxi) time of curing (days), are considered for flexural strength as an output parameter. Figure 1 illustrates the violin plot distribution against considered input parameters. Furthermore, the graphs provide the output parameter's relative frequency dispersion, as presented in Figure 2. Relative frequency distributions are essential in recognizing a database's typical value. In regression analysis, the VIF, i.e., Variance Inflation Factor, is the multicollinearity severity. In current data, the correlation was weak (i.e., less than 0.5) for most of the input parameters; therefore, in this situation, there would be no multicollinearity issues as the result of microscopic differences. In the case of stronger correlation (i.e., near to 1), the multicollinearity issues would be higher, and the input variables would have a significantly higher impact that ultimately would influence the outcomes and may offer less precise findings (Amin et al., 2022; Pan et al., 2022).

Dataset description

A total of 317 data points are used for running the employed algorithms. The UHPC database used to run the algorithms for predicting its FS is extracted from the available literature (Soroush

Brief methodology and employed machine learning algorithms

Anaconda navigator software python coding plays a significant role in running all the applied algorithms. The data was split into two

FIGURE 3
SVM model implementation process (Muzzammel and Raza, 2020).

Support vector machine

Support Vector Machine (SVM) is an algorithm used to connect learning models employed for data evaluation in the case of both classification and regression. An S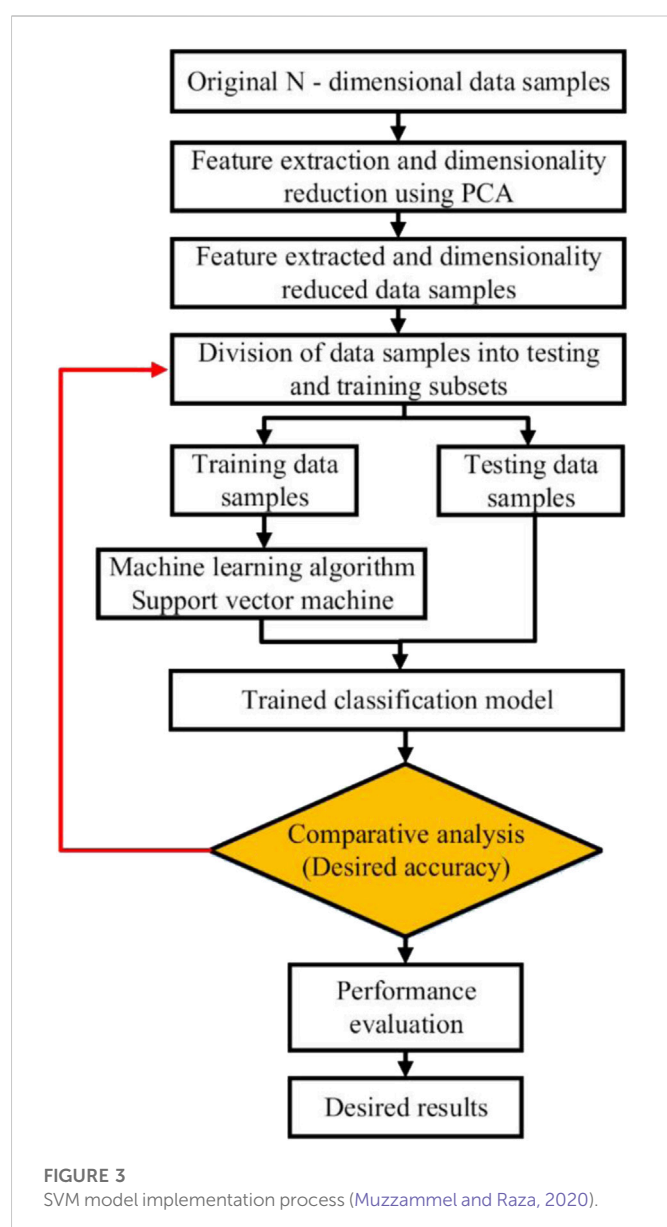VM approach describes the samples as space points drawn so that a distinct vector bifurcates the different classification patterns with the highest possible gap. Figure 3 shows the execution technique for the SVM model. This algorithm is utilized to evaluate the strength of the material, considering the impact of various parameters. The optimization technique is adopted to determine the SVM model's parameters.

Multi-layer perceptron

A Multi-Layer Perceptron (MLP) is an ANN type which converts a set of input parameters into an output. A targeted graph connects many input-node layers among input and output layers (Umeonyiagu and Nwobi-Okoye, 2015a; Umeonyiagu and Nwobi-Okoye, 2015b; Abubakar and Tabra, 2020). Backpropagation is used in MLP to train the network (Boukhatem et al., 2012). It may also use for connecting several loops in a targeted graph, with unidirectional moving signals across the nodes. Each entity (except input nodes) owns its distinct non-linear activation function (Abellán-García, 2020). MLPs use backpropagation during learning methods (Boukhatem et al., 2012). MLP is usually regarded as an AI technique due to using several neuron layers (Bikku, 2020). MLP is generally utilized in studies of imputation, supervised learning, pure science, and parallel distributed processing. Image recognition, machine translation, and speech recognition are their applications. To start with, the selection of predictors is made by the algorithm utilized during the whole phase of regression for locating the Variance Inflation Factor (VIF). VIF then identifies the change in the predicted regression coefficient due to collinearity (Lin et al., 2011; Kroll and Song, 2013). The MLP model procedural flowchart is shown in Figure 4.

Gradient boosting

Friedman (2001) recommended this ensemble technique, i.e., gradient boosting (GB), for regression and classification. The GB approach is similar to other boosting approaches, but the regression is limited. In this approach, the random selection for each iteration of the training set is made, and its validation by the base model is done, as shown in Figure 5. In the case of GB, the precision level of execution and speed may be improved by sub-sampling of the training set randomly, which aids in avoiding overfitting. A more regression speed for fitting more minor model data on every iteration can be achieved by having a smaller fraction of training data. GB regression requires n-trees and shrinkage rate tuning factors, where n-trees express the grown trees' quantity. It may be noted here that the value of n trees must not be minimal, and the learning rate, i.e., shrinkage factor, is applicable in the case of every expansion tree.

parts, i.e., 70% as training data and 30% as model testing data. The k-fold cross-validation technique is adopted for the validation of the required algorithm. For the reduction in data complexity, the data pre-processing approach is adopted. The pre-processing of data for data mining resolves a critical issue from the renowned knowledge discovery out of data procedure. Data preparation involves data reduction techniques for decreasing the complexity of data by identifying and eliminating noisy and inappropriate data items. The analysis model is made with the help of error distribution and regression methods. In addition, the SHAP analysis was also performed because the considered input factors have a significant effect on output. Consequently, the impact of all the input factors is evaluated to estimate the FS of UHPC *via* SHAP analysis. Statistical checks have also been applied to assess the level of accuracy of employed algorithms. The implementation processes for the employed algorithms are presented below.

FIGURE 4
MLP model implementation process (Isabona et al., 2022).
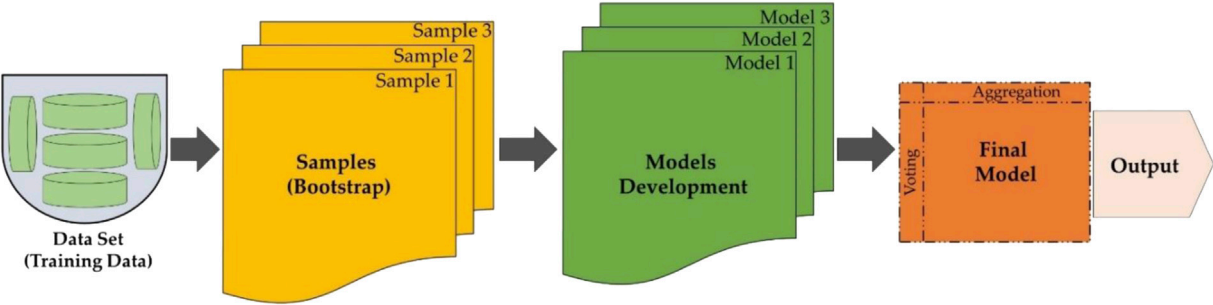
FIGURE 5
Bagging model implementation process.
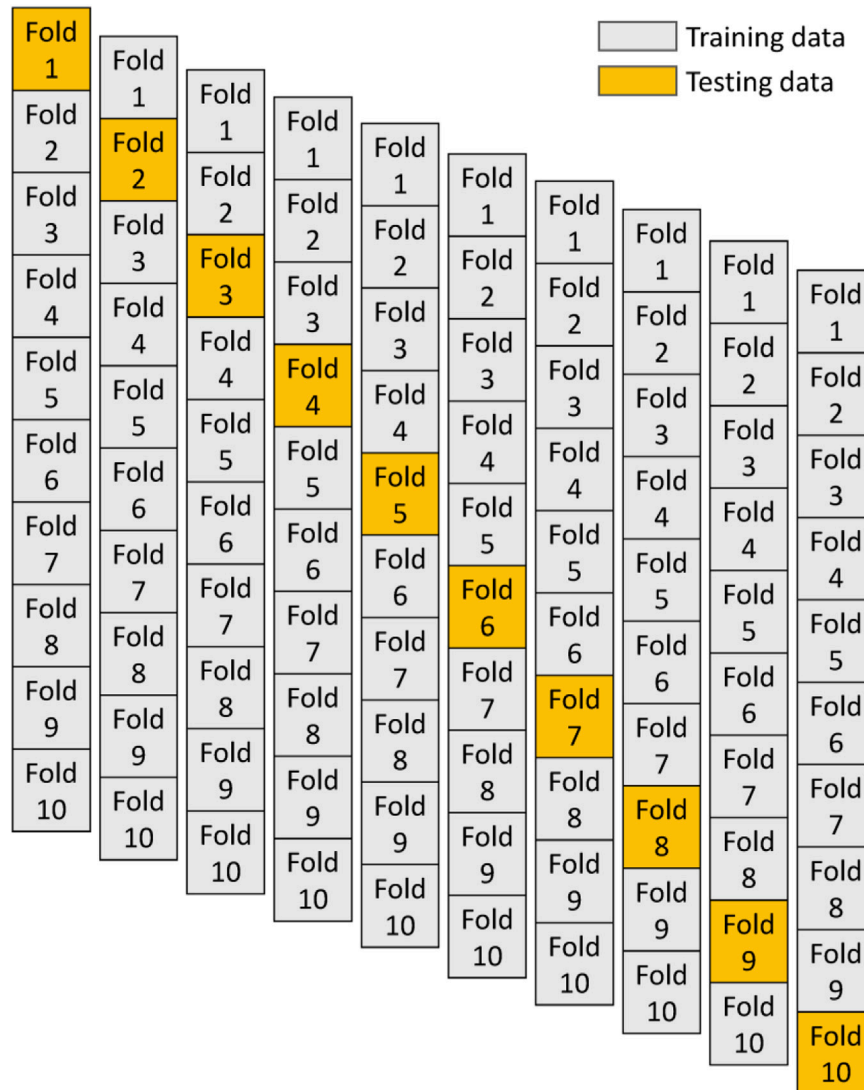
FIGURE 6
K-fold cross-validation approach (Zou et al., 2022).

K-fold cross-validation outcomes and statistical metrics

The application of k-fold and statistical checks is also made for validating ML models in use (Figure 6). Conventionally, the k-fold cross-validation method is employed to evaluate the practicability of an approach by randomly dividing and distributing the related data into ten sub-groups. Nine groups are utilized for training ML models, whereas one is used for their validation. The ML method is highly precise when there are fewer errors, i.e., MAPE, RMSE, and MAE, and higher R^2 value. Furthermore, this method must be repeated ten times to attain the desired result. This bulk quantity work is a major reason behind the highly precise model. In addition, Nazar et al. (2022) derived the below-mentioned equations, i.e., Eq. 1 and Eq. 2, to evaluate the performance of prediction approaches statistically. These equations are also applied in the current study.

$$MAE = \frac{1}{n}\sum_{i=1}^{n}|P_i - Ti| \tag{1}$$

$$RMSE = \sqrt{\sum \frac{(P_i - T_i)^2}{n}} \tag{2}$$

Where; P_i = anticipated values; n = number of data points; T_i = experimental values; A = actual values; and.F = predicted values.

Results and discussion

Support vector machine model output

Figure 7 depicts that the SVM model offers a more precise relationship between the experimental and predicted UHPC FS results upon comparison with the MLP algorithm, which results in a 0.75 R^2 value. It may be noted here that the vertical and horizontal

FIGURE 7
Experimental and predicted results for UHPC FS—SVM model.
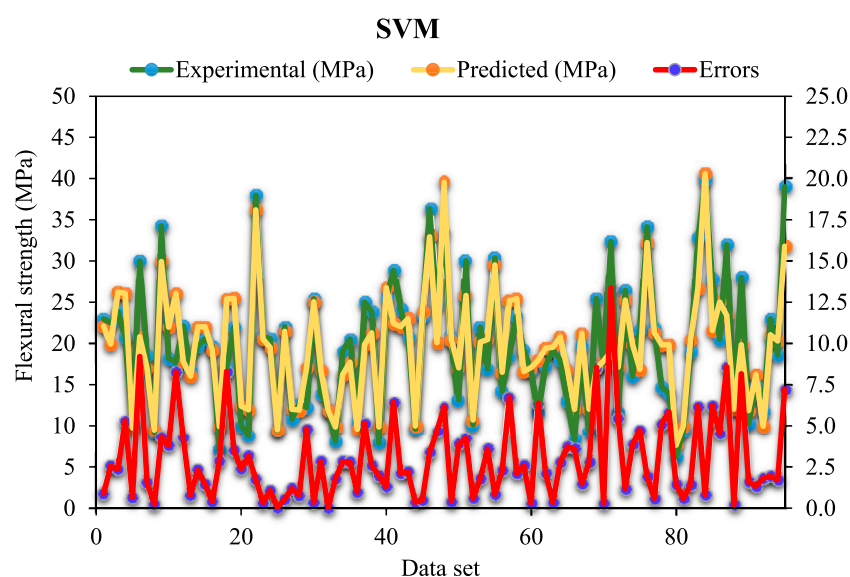
FIGURE 8
Difference of errors among actual and predicted UHPC FS—SVM model.

axes depict the predicted and experimental values, respectively, in the case of FS. Figure 8 illustrates data distribution, representing the difference between the actual and predicted outcomes. Here, the horizontal axis depicts the dataset for testing or training the models, whereas the predicted FS values are shown on the vertical axis. Based on this distribution, the highest, lowest, and average values are 13.3, 2.99, and 0.02 MPa, respectively. Moreover, 63.16% of values are found from 0.02 to 3 MPa, 22.11% of values are found from 3 MPa to 6 MPa, and the remaining 14.74% of values are more than 6 MPa. Furthermore, in Figure 9, the additional statistics like the lowest, mean, highest, median, first, and third quartile values for predicted

and experimental outcomes from the test data set are shown. It is evident from the graph data that a difference is there between the actual and predicted results. Jueyendah et al. (2021) also reported similar findings for SVM with a higher correlation coefficient and lesser errors in the FS prediction of cementitious mortar.

Multi-layer perceptron model outcome

Figure 10 depicts the relationships between the actual and predicted UHPC FS values. This relationship provides 0.71 as the

FIGURE 9
Box plot for actual and predicted results—SVM model.

FIGURE 10
Experimental and predicted results for UHPC FS—MLP model.

FIGURE 11
Difference of errors among actual and predicted UHPC FS—MLP model.

FIGURE 12
Box plot for actual and predicted results—MLP model.
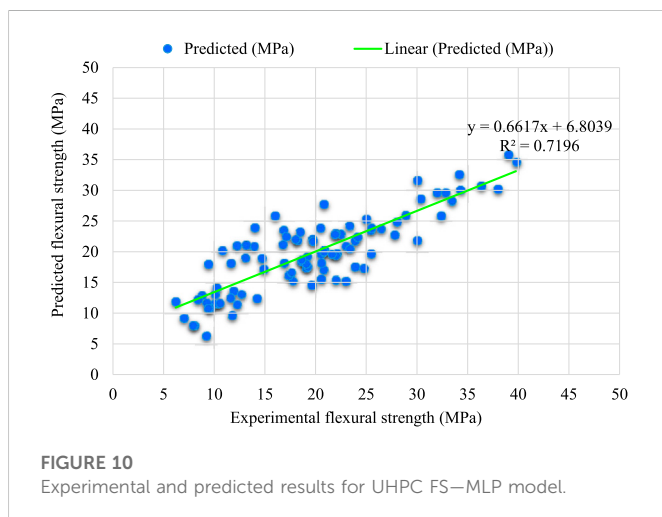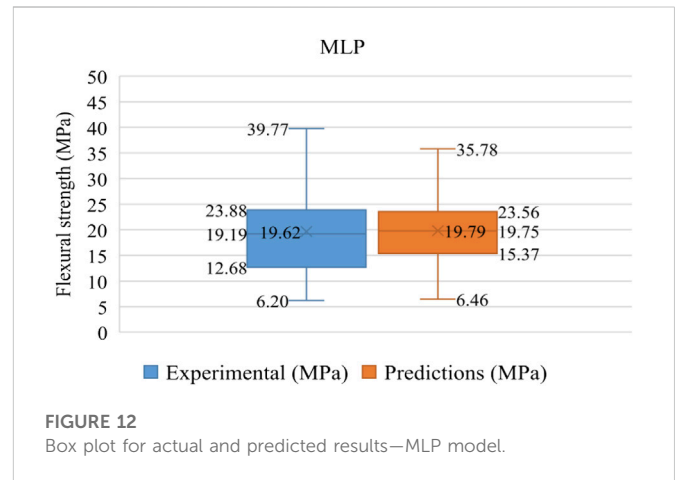
determination coefficient (R^2) value. It may be noted here that the vertical and horizontal axes depict the predicted and experimental values, respectively, in the case of FS. Figure 11 shows the difference between the actual and predicted outcomes. Here, the horizontal axis depicts the dataset for testing or training the models, whereas the predicted FS values are shown on the vertical axis. The difference shows the higher values, i.e., 9.96 MPa, and lower values, i.e., 0.04 MPa. Furthermore, it is found that the 57.89% difference in data lies from 0.04 to 3 MPa, and 22.11% of data lies from 3 to 6 MPa. Where only 20% of data is found which is more 6 MPa. In Figure 12, the box plot depicts the statistical information like the maximum, mean, minimum, first and third quartile and median values for the experimental and estimated results from the test dataset. The difference between actual and predicted outcomes can be seen from the values on the graph. Abellán-García (2020) performed MLP analysis demonstrating an acceptable precision for the compressive strength of UHPC.

Gradient boosting model outcome
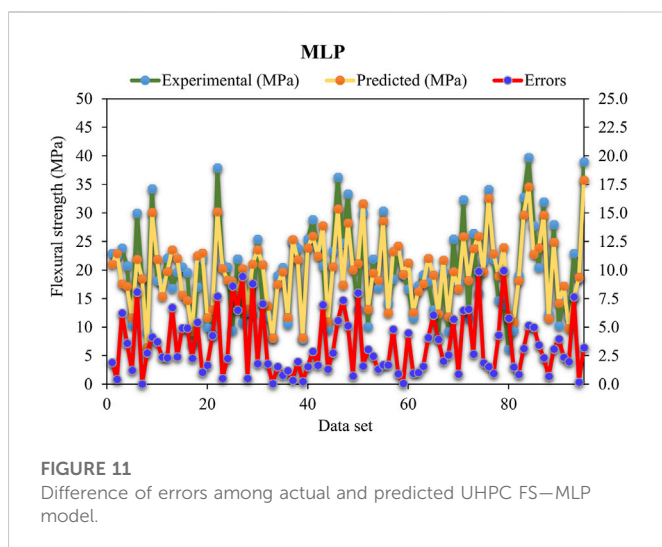
Figure 13 shows the outcome of the GB model depicting a strengthened and improved relation with experimental results in the case of UHPC FS as compared to SVM and MLP prediction models. It may be noted here that the vertical and horizontal axes depict the predicted and experimental values, respectively, in the case of FS. Also, it comes out with a 0.97 R^2 value, which contrasts with SVM and MLP predictions. The visuals for error distribution are presented in Figure 14, an additional point of interest. Here, the horizontal axis depicts the dataset for testing or training the models, whereas the predicted FS values are shown on the vertical axis. The variation gives data with a minimum of 0 MPa, an average of 1.71 MPa, and a maximum of 11 MPa. Furthermore, it is observed that 91.58% of data lies from 0 to 3 MPa, 5.26% of data lies from 3 to 6 MPa, and the remaining 3.16% of data is found to be more than 6 MPa. Additionally, more statistical information is illustrated in the Box Plot shown in Figure 15, showing the lowest, mean, highest, median, first, and third quartile values for predicted and experimental test set outcomes. The difference between the expected and actual
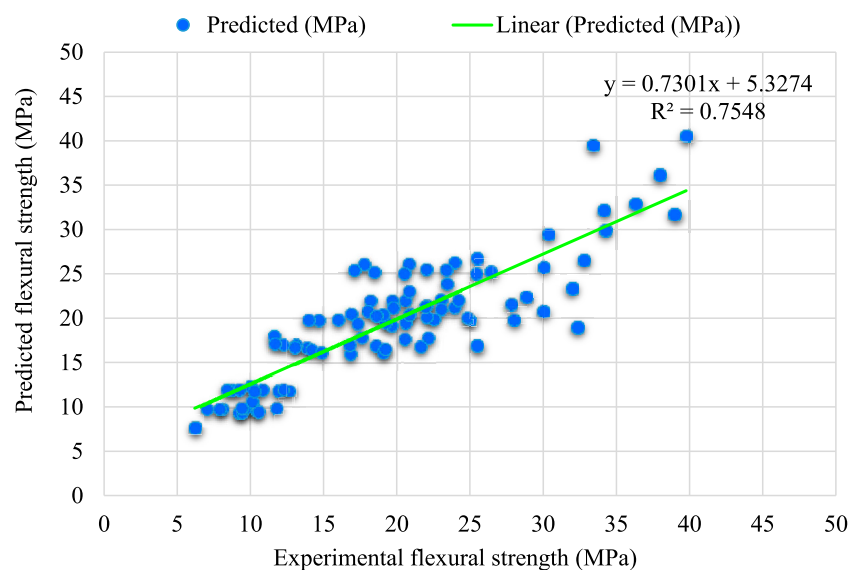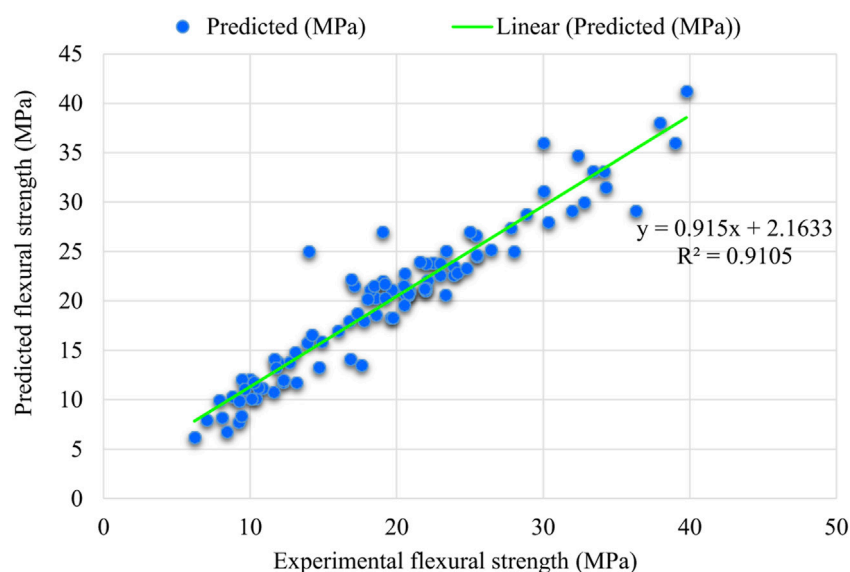
FIGURE 13
Experimental and predicted results for UHPC FS—GB model.
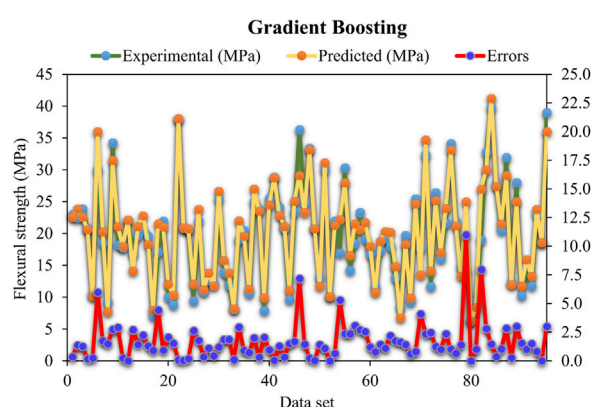
FIGURE 14
Difference of errors among actual and predicted UHPC FS—GB model.

results is represented graphically. Marani and Nehdi (2020) also employed the GB algorithm for predicting the compressive strength of cementitious composites integrated with phase change materials. It was concluded that the GB model shows the maximum precision among all the considered algorithms. In the current study, the output precision from the GB algorithm is higher for flexural strength, contrary to both SVM and MLP algorithms.
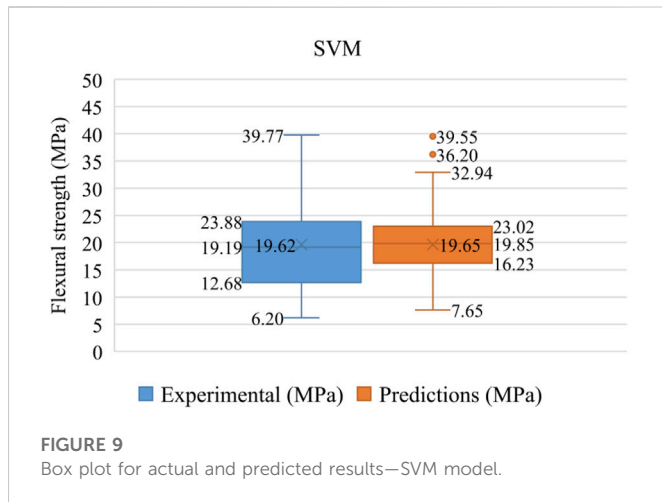
K-statistical checks and k-fold analysis

The statistics extracted from the algorithms are provided in Table 1. A check named the k-fold cross-validation test is applied as a standard for determining of model's legitimacy. For the investigation of outcomes, the statistical checks, i.e., R^2, RMSE, and

MAE, are considered. Likewise, the highest RMSE and MAE in SVM models come out as 9.76 and 7.85 MPa, as presented in Figure 16. As per this check, the RMSE and MAE values in the case of MLP models are higher, i.e., 9.82 and 8.68 MPa, respectively, as shown in Figure 17. But, in the case of boosting, the higher RMSE and MAE values come out as 6.14 MPa and 4.45 MPa, respectively, as illustrated in Figure 18.

Discussion

The current work explains the flexural strength performance in prediction for 3 ML models. The support vector machine (SVM), multi-layer perceptron (MLP), and gradient boosting (GB) are employed for the analysis. Although SVM and MLP come under the umbrella of individual machine learning approaches, the accuracy of their prediction outcomes is observed to be in an acceptable range. The GB comes under the umbrella of ensemble machine learning techniques, which usually undergo the splitting process of the model into twenty sub-models to optimize the accurate result. Figure 19 shows the boosting sub-model outcome. It is observed that the input factors and data points numbers have a considerable effect on desired results. Accordingly, the input data's relative frequency distribution and descriptive statistics to determine their impact on the outcome are incorporated into the study. A satisfactory correlation is observed between experimental and predicted results for UHPC FS from all the models employed. The k-fold cross-validation method assesses the legitimacy of models.

The application of advanced machine learning techniques is gaining attention nowadays in various engineering fields (Chen et al., 2022). In the recent past, several studies have been conducted by employing different algorithms to predict various properties of other cementitious materials such as Recycled Aggregate Concrete, Geopolymer Concrete, Rice Husk Ash Concrete, and Fly Ash-Based Concrete etc. The number of considered input parameters was from 5 to 9, and the minimum number of considered dataset points was 98. It may be noted from
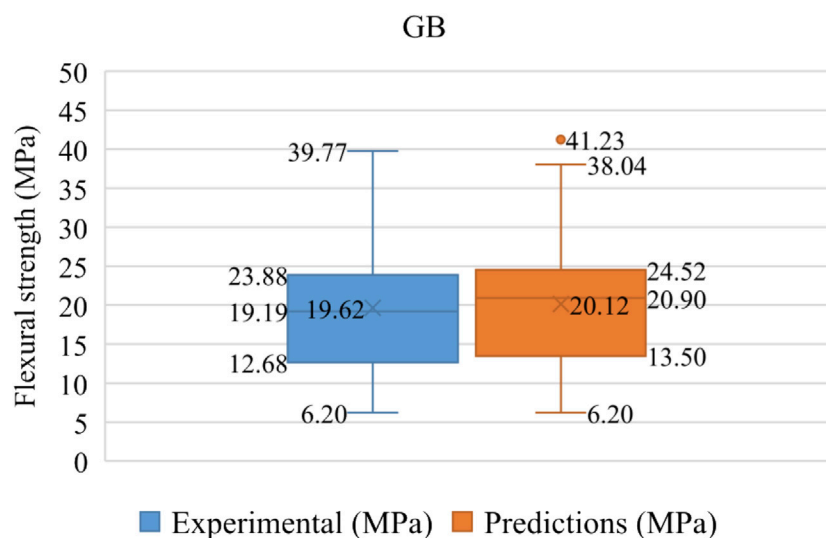
FIGURE 15
Box plot for actual and predicted results—GB model.
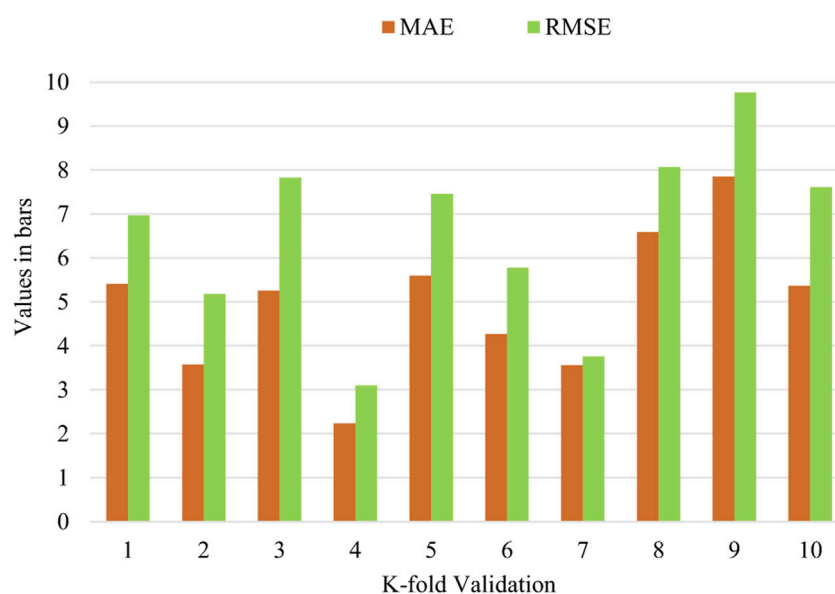
FIGURE 16
SVM model statistical analysis.

TABLE 1 Statistics derived from the employed models.

Statistical checks	Algorithms		
	SVM	MLP	GB
R^2	0.75	0.71	0.91
RMSE (MPa)	3.0	4.2	2.4
MAE (MPa)	3.9	3.4	1.7

Table 2 that the dataset points range from 98 to 357 in numbers. The details from the different studies regarding the employment of ML algorithms (GEP, Bagging Regressor, AdaBoost, Random Forest) for predicting various properties of different cementitious composites (compressive, splitting-tensile and shear strengths) are summarized in the literature and are presented in Table 2. The maximum data points and the number of input parameters extracted from this literature-based summary in Table 2 are 357 and 9, respectively. However, in the current study, as also demonstrated in the first row of Table 2 in
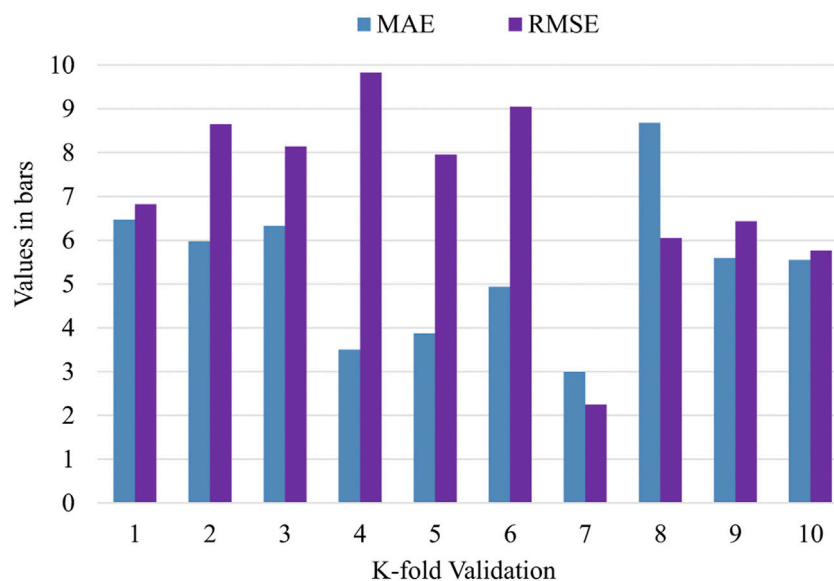
FIGURE 17
MLP model statistical analysis.
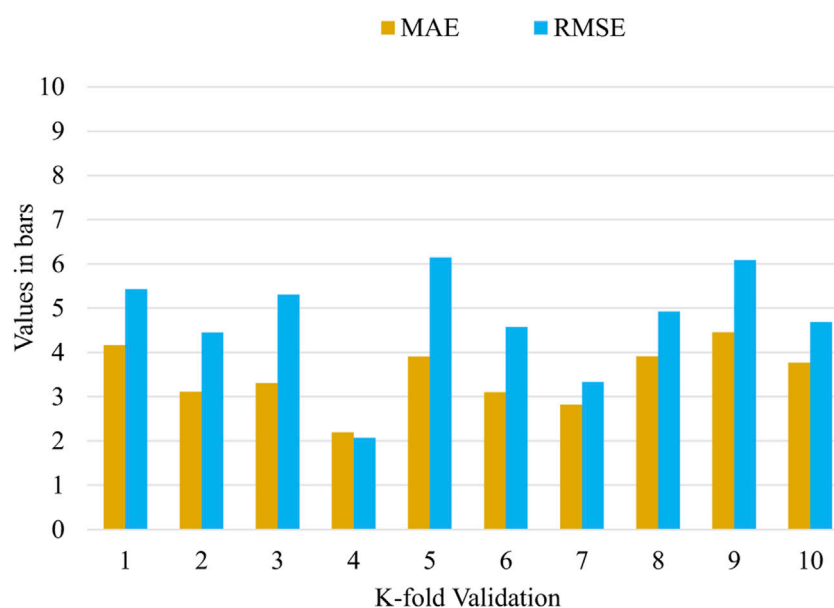
FIGURE 18
GB model statistical analysis.

comparison with other reported studies, a total of 317 data points are considered, and 21 input parameters are taken for the flexural strength prediction of UHPC which is in the acceptable range of prediction.

SHAP analysis

The current research provides an in-depth explanation of the ML algorithm and interactions and dependencies for every feature.

The application of the SHAP tree explainer on the entire dataset and an enhanced illustration of influences of global features by merging SHAP local explanations are also provided. The tree-like SHAP prediction technique, named TreeExplainer, is applied (Lundberg et al., 2019). In this method, the interior structure of tree-based models is explored, which is summing up of a calculations set linked with the tree model leaf node, leading to low-order complexity (Lundberg et al., 2019). The model interpretation is made for UHPC FS by applying SHAP. The

FIGURE 19
Boosting sub-models result.
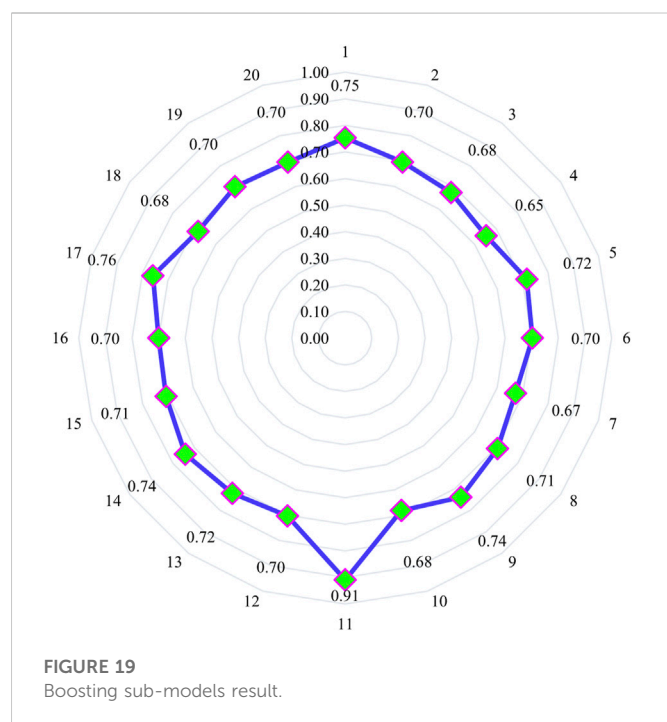
value, which is more or less the same as curing time, which is in third place in terms of more SHAP value, as shown in Figure 20. In cementitious concrete composites, more curing time would come up with improved bonds and strengths of the matrix, thus contributing to its better mechanical characteristics. It may be due to the more binders in UHPC, i.e., fly ash, silica fume, slag etc., due to which more curing time is required by the process of hydration, which would ultimately result in improved FS. Subsequently, the water and super-plasticizer contents have the fourth and fifth highest SHAP values, respectively. The strength of UHPC mainly depends on the theory of particle packing density; hence there is a requirement to have limited water content, and the super-plasticizer plays the main role in the development of strength. Meanwhile, the quarts and silica fume also influence UHPC FS. Other features like limestone powder content, coarse aggregate content, contents of slag, nano-silica, sand and fly-ash fine/coarse aggregates, and steel fibers length influence the UHPC FS slightly. All the mentioned features have a specific impact on UHPC FS.

Similarly, Figure 21 illustrates the correlation for the importance of features UHPC FS. It can be noted that the enhancing steel fiber content is increasing the UHPC FS and *vice versa*. As far as the water content is concerned, it is

TABLE 2 Literature-based summary of ML models with details of parameters.

Recommended ML approach	Predicted properties	Material type	Data points	No. of input parameters	Reference
GB	Flexural Strength	UHPC	317	21	Current Study
GEP	Ultimate Axial Capacity	Concrete-Filled Steel Tubes	227	6	Javed et al. (2020)
Bagging Regressor	Compressive Strength	Geopolymer Concrete	371	9	Zou et al. (2022)
Bagging Regressor	Split-Tensile Strength	Recycled Aggregate Concrete	166	9	Zhu et al. (2022)
GEP	Compressive Strength	Rice Husk Ash Concrete	192	6	Iftikhar et al. (2022)
AdaBoost	Compressive and Split-Tensile Strength	Recycled Aggregate Concrete	344	9	Shang et al. (2022)
Bagging Regressor	Compressive Strength	Geopolymer Concrete	154	9	Ahmad et al. (2022)
Bagging Regressor	Compressive Strength	Fly Ash-Based Concrete	98	7	Song et al. (2021)
Bagging Regressor	Compressive Strength	Fly Ash-Based Concrete	270	8	Ahmad et al. (2021)
Random Forest	Compressive Strength	High-Strength Concrete	357	5	Farooq et al. (2020)

relationship of different features with UHPC FS is depicted by the SHAP values, as presented in Figure 20. It is observed that the highest SHAP value is for steel fiber content for UHPC FS prediction. It is renowned that the bridging mechanism is achieved by incorporating steel fibers, ultimately enhancing the strength factors (Deifalla et al., 2021). Consequently, enhancing steel fiber content would produce a higher FS of UHPC. In the second place, the maximum aggregate size has the highest SHAP

influencing negatively, as it can be seen from Figure 21 that the increasing water content results in the reduction of UHPC FS. However, in the case of cement content, it shows a positive influence which means the more the content of cement is, the higher will be the FS of UHPC. Similarly, enhancing silica fume content results in more FS of UHPC. The dataset employed in this study is the basis for the conducted prediction, and highly accurate outcomes may be achieved by having more data points.
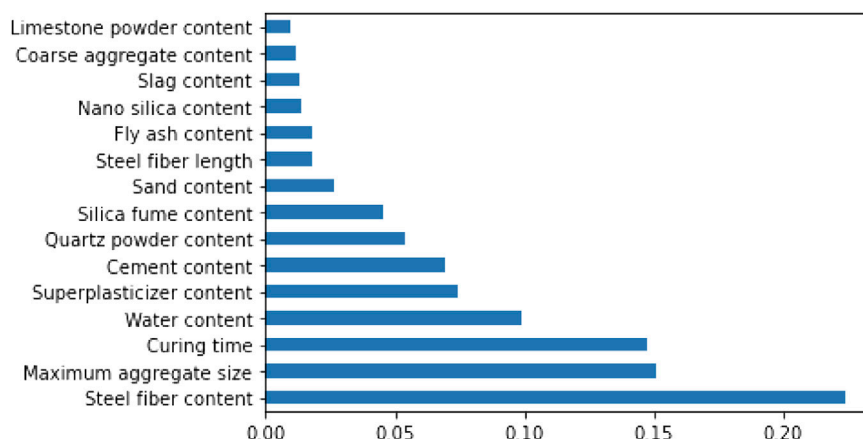
FIGURE 20
Influence of the input parameters towards the predicted output.

FIGURE 21
SHAP plot for UHPC FS.

Conclusion

To assess the improved properties of UHPC, the laboratory procedures for its manufacturing and testing, such as specimen casting, curing, and testing, are a major concern point in terms of excessive cost and time consumption. Modern AI methods especially machine learning (ML) are now gaining attention to predict the mechanical behavior of UHPC. In this study, flexural strength (FS) estimation of UHPC is done by applying both ensemble techniques (i.e., gradient boosting) and individual techniques (i.e., SVM and MLP) along with the exploration of raw ingredients effect and interaction by applying SHAP analysis. A total of 21 input parameters are considered, i.e., the cement content (kg/m^3), cement type and strength class, cement compressive strength (MPa), fine aggregates content (kg/m^3), coarse aggregates content (kg/m^3), fly ash content (kg/m^3), slag content (kg/m^3), silica fume content (kg/m^3), limestone powder content (kg/m^3), nano silica content (kg/m^3), quartz powder content (kg/m^3), super-plasticizer content (kg/m^3), the maximum size of aggregates (mm), water content (kg/m^3), polystyrene fiber content (%), steel fiber content (%), polystyrene fiber length (mm), steel fiber length (mm), polystyrene fiber diameter (mm), steel fiber diameter (mm), and time of curing (days). The following conclusions are drawn based on the study findings:

- The employed ensemble machine learning algorithm (Gradient boosting) successfully predicted FS of UHPC using python coding with higher accuracy of R^2 value than that of individual algorithms (SVM and MLP). Twenty sub models with 10–200 predictors are used to optimize the FS prediction of UHPC.

- The gradient boosting (GB) algorithm is superior in precision with a low error rate (MAE = 1.7) as to that of SVM (MAE = 3.9) and MLP (MAE = 3.4) algorithms.
- The higher R^2 of 0.91 is attained through a relationship of experimental and predicted values in the GB algorithm, which depicts its higher precision for FS of UHPC than that of SVM (R^2 = 0.75) and MLP (R^2 = 0.71) algorithms.
- The validity of the applied algorithms is also ensured with the help of RMSE and k-fold cross-validation. It is found that RMSE for the GB algorithm is 2.4, which is lower than that of the SVM (RMSE = 3.0) and MLP (RMSE = 4.2) algorithms
- The influence of all the considered input factors on the FS of UHPC is determined by SHAP analysis, which reveals that the steel fiber content feature has the highest impact on UHPC FS. This is due to the bridging effect of steel fibers that ultimately results in improved FS.
- In general, employing ensembled machine learning approaches provides a cost-effective and better way to analyze the characteristics of complex materials like ultra-high-performance concrete. The current research would give academics in civil engineering in-depth insight into adopting adequate ML models to predict the strength properties of any concrete type. Further, this work explains the importance of input parameters for the targeted outcome using ML approaches.

UHPC is a modern cementitious composite with enhanced mechanical properties compared to conventional concrete. The research interest towards the exploration of UHPC is gaining popularity day by day. However, based on this study's outcomes, the following future recommendations are proposed:

- The nature of the correlation between the raw components of UHPC mix design and its characteristics is a major parameter influencing the model selection. This non-linear relation requires the application of ML algorithms. But optimizing applied algorithms through metaheuristic models is an effective way to attain more accurate results and enhanced processes.
- Although a suitable dataset is being considered in this research; however, a further extended dataset should be taken to improve the effectiveness of applied algorithms.
- Furthermore, increasing the dataset quantity through experimental evaluations can enhance the performance of ML algorithms for highly accurate prediction.
- Moreover, increasing the type of input parameters, like the chemical formation of raw components and the climatic impacts (i.e., humidity and temperature), can result in more precision of ML models. Additionally, this study aimed to predict UHPC flexural strength, so its other parameters would also be taken in ML prediction.
- The application of hybrid ANN and SVM models can also be explored for predicting UHPC characteristics regarding the process and precision. Although it will improve the computation time, applying these models on an expanded database with appropriate feature selection will provide highly accurate results.
- The detailed exploration of UHPC load–slip modelling in terms of steel fibers impacts regarding the age of the matrix and strength needs to be explored.

Data availability statement

The original contributions presented in the study are included in the article/Supplementary Material, further inquiries can be directed to the corresponding author.

Author contributions

YQ: Conceptualization, methodology, investigation, validation, writing-original draft, supervision, writing—reviewing and editing. MS: Methodology, formal analysis, validation, visualization, writing—reviewing and editing. AH: Funding acquisition, data curation, writing—reviewing and editing. AF: Funding acquisition, resources, software, visualization, writing—reviewing and editing. AE: Formal analysis, resources, software, writing—review and editing, validation.

Conflict of interest

The authors declare that the research was conducted in the absence of any commercial or financial relationships that could be construed as a potential conflict of interest.

Publisher's note

All claims expressed in this article are solely those of the authors and do not necessarily represent those of their affiliated organizations, or those of the publisher, the editors and the reviewers. Any product that may be evaluated in this article, or claim that may be made by its manufacturer, is not guaranteed or endorsed by the publisher.

References

Abellán-García, J., and García-Castaño, E. (2022). Development and research on ultra-high-performance concrete dosages in Colombia: A review. *ACI Mater. J.* 119, 209–221. doi:10.14359/51734617

Abellán-García, J., Fernández-Gómez, J. A., Torres-Castellanos, N., and Núñez-López, A. M. (2020). "Machine learning prediction of flexural behavior of UHPFRC," in *RILEM-Fib international symposium on fibre reinforced concrete* (Germany: Springer), 570–583.

Abellán-García, J. (2020). Four-layer perceptron approach for strength prediction of UHPC. *Constr. Build. Mater.* 256, 119465. doi:10.1016/j.conbuildmat.2020.119465

Abubakar, A., and Tabra, M. (2020). Predictive capabilities of Multilayer Perceptron (MLP) in WEKA algorithm for high strength concrete with steel fiber addition. *Cem. Based Compos* 2, 13–18. doi:10.36937/cebacom.2020.002.003

Ahmad, A., Farooq, F., Niewiadomski, P., Ostrowski, K., Akbar, A., Aslam, F., et al. (2021). Prediction of compressive strength of fly ash based concrete using individual and ensemble algorithm. *Materials* 14, 794. doi:10.3390/ma14040794

Ahmad, A., Ahmad, W., Aslam, F., and Joyklad, P. (2022). Compressive strength prediction of fly ash-based geopolymer concrete via advanced machine learning techniques. *Case Stud. Constr. Mater.* 16, e00840. doi:10.1016/j.cscm.2021.e00840

Aiyer, B. G., Kim, D., Karingattikkal, N., Samui, P., and Rao, P. R. (2014). Prediction of compressive strength of self-compacting concrete using least square support vector machine and relevance vector machine. *KSCE J. Civ. Eng.* 18, 1753–1758. doi:10.1007/s12205-014-0524-0

Ali, A. H., Mohamed, H. M., Chalioris, C. E., and Deifalla, A. (2021). Evaluating the shear design equations of FRP-reinforced concrete beams without shear reinforcement. *Eng. Struct.* 235, 112017. doi:10.1016/j.engstruct.2021.112017

Ali, B., Azab, M., Ahmed, H., Kurda, R., El Ouni, M. H., and Elhag, A. B. (2022a). Investigation of physical, strength, and ductility characteristics of concrete reinforced with banana (Musaceae) stem fiber. *J. Build. Eng.* 61, 105024. doi:10.1016/j.jobe.2022.105024

Ali, B., Farooq, M. A., El Ouni, M. H., Azab, M., and Elhag, A. B. (2022b). The combined effect of coir and superplasticizer on the fresh, mechanical, and long-term durability properties of recycled aggregate concrete. *J. Build. Eng.* 59, 105009. doi:10.1016/j.jobe.2022.105009

Ali, B., Farooq, M. A., Kurda, R., Alyousef, R., Noman, M., and Alabduljabbar, H. (2022c). Effect of type and volume fraction of recycled-tire steel fiber on durability and mechanical properties of concrete. *Eur. J. Environ. Civ. Eng.*, 1–22. doi:10.1080/19648189.2022.2103590

Ali, B., Hawreen, A., Kahla, N. B., Amir, M. T., Azab, M., and Raza, A. (2022d). A critical review on the utilization of coir (coconut fiber) in cementitious materials. *Constr. Build. Mater.* 351, 128957. doi:10.1016/j.conbuildmat.2022.128957

Amin, M. N., Ahmad, W., Khan, K., Ahmad, A., Nazar, S., and Alabdullah, A. A. (2022). Use of artificial intelligence for predicting parameters of sustainable concrete and raw ingredient effects and interactions. *Materials* 15, 5207. doi:10.3390/ma15155207

Andalib, A., Aminnejad, B., and Lork, A. (2022). Grey wolf optimizer-based ANNs to predict the compressive strength of self-compacting concrete. *Appl. Comput. Intell. Soft Comput.* 2022, 1–17. doi:10.1155/2022/9887803

Arora, A., Yao, Y., Mobasher, B., and Neithalath, N. (2019). Fundamental insights into the compressive and flexural response of binder-and aggregate-optimized ultra-high performance concrete (UHPC). *Cem. Concr. Compos.* 98, 1–13. doi:10.1016/j.cemconcomp.2019.01.015

Arshad, S., Sharif, M. B., Irfan-Ul-Hassan, M., Khan, M., and Zhang, J.-L. (2020). Efficiency of supplementary cementitious materials and natural fiber on mechanical performance of concrete. *Arabian J. Sci. Eng.* 45, 8577–8589. doi:10.1007/s13369-020-04769-z

Asri, Y. E., Aicha, M. B., Zaher, M., and Alaoui, A. H. (2022). Prediction of compressive strength of self-compacting concrete using four machine learning technics. *Mater. Today Proc.* 57, 859–866. doi:10.1016/j.matpr.2022.02.487

Asteris, P., Kolovos, K., Douvika, M., and Roinos, K. (2016). Prediction of self-compacting concrete strength using artificial neural networks. *Eur. J. Environ. Civ. Eng.* 20, s102–s122. doi:10.1080/19648189.2016.1246693

Baili, J., Raza, A., Azab, M., Ali, K., El Ouni, M. H., Haider, H., et al. (2022). Experiments and predictive modeling of optimized fiber-reinforced concrete columns having FRP rebars and hoops. *Mech. Adv. Mater. Struct.*, 1–20. doi:10.1080/15376494.2022.2108527

Balf, F. R., Kordkheili, H. M., and Kordkheili, A. M. (2021). A New method for predicting the ingredients of self-compacting concrete (SCC) including fly ash (FA) using data envelopment analysis (DEA). *Arabian J. Sci. Eng.* 46, 4439–4460. doi:10.1007/s13369-020-04927-3

Bayrami, B. (2022). Estimation of splitting tensile strength of modified recycled aggregate concrete using hybrid algorithms. *Available at SSRN 3992623* 44, 375–392.

Bikku, T. (2020). Multi-layered deep learning perceptron approach for health risk prediction. *J. Big Data* 7, 50–14. doi:10.1186/s40537-020-00316-7

Boukhatem, B., Kenai, S., Hamou, A., Ziou, D., and Ghrici, M. (2012). Predicting concrete properties using neural networks(NN) with principal component analysis(PCA) technique. *Comput. Concr.* 10, 557–573. doi:10.12989/cac.2012.10.6.557

Cao, M., and Khan, M. (2021). Effectiveness of multiscale hybrid fiber reinforced cementitious composites under single degree of freedom hydraulic shaking table. *Struct. Concr.* 22, 535–549. doi:10.1002/suco.201900228

Cao, M., and Li, L. (2018). New models for predicting workability and toughness of hybrid fiber reinforced cement-based composites. *Constr. Build. Mater.* 176, 618–628. doi:10.1016/j.conbuildmat.2018.05.075

Cao, M., Mao, Y., Khan, M., Si, W., and Shen, S. (2018). Different testing methods for assessing the synthetic fiber distribution in cement-based composites. *Constr. Build. Mater.* 184, 128–142. doi:10.1016/j.conbuildmat.2018.06.207

Chen, T., Gao, X., and Ren, M. (2018). Effects of autoclave curing and fly ash on mechanical properties of ultra-high performance concrete. *Constr. Build. Mater.* 158, 864–872. doi:10.1016/j.conbuildmat.2017.10.074

Chen, J., Tong, H., Yuan, J., Fang, Y., and Gu, R. (2022). Permeability prediction model modified on kozeny-carman for building foundation of clay soil. *Buildings* 12, 1798. doi:10.3390/buildings12111798

Cui, L., Yang, S., Chen, F., Ming, Z., Lu, N., and Qin, J. (2018). A survey on application of machine learning for Internet of Things. *Int. J. Mach. Learn. Cybern.* 9, 1399–1417. doi:10.1007/s13042-018-0834-5

Deifalla, A. F., Zapris, A. G., and Chalioris, C. E. (2021). Multivariable regression strength model for steel fiber-reinforced concrete beams under torsion. *Materials* 14, 3889. doi:10.3390/ma14143889

Deifalla, A. (2020). "Torsion design of lightweight concrete beams without or with fibers: A comparative study and a refined cracking torque formula," in *Structures* (Netherland: Elsevier), 786–802.

De-Prado-Gil, J., Palencia, C., Silva-Monteiro, N., and Martínez-García, R. (2022). To predict the compressive strength of self compacting concrete with recycled aggregates utilizing ensemble machine learning models. *Case Stud. Constr. Mater.* 16, e01046. doi:10.1016/j.cscm.2022.e01046

Dutta, S., Murthy, A. R., Kim, D., and Samui, P. (2017). Prediction of compressive strength of self-compacting concrete using intelligent computational modeling. *Comput. Mater. Contin.* 53, 167–185. doi:10.3970/cmc.2017.053.167

Ebid, A. M., and Deifalla, A. (2021). Prediction of shear strength of FRP reinforced beams with and without stirrups using (GP) technique. *Ain Shams Eng. J.* 12, 2493–2510. doi:10.1016/j.asej.2021.02.006

El Ouni, M. H., Raza, A., Elhadi, K. M., Azab, M., and Arshad, M. (2022). "Parametric investigation of GFRP-RCC jute fibre-reinforced recycled aggregate concrete elements," in *Structures* (Netherland: Elsevier), 1043–1061.

Fan, D., Yu, R., Fu, S., Yue, L., Wu, C., Shui, Z., et al. (2021). Precise design and characteristics prediction of Ultra-High Performance Concrete (UHPC) based on artificial intelligence techniques. *Cem. Concr. Compos.* 122, 104171. doi:10.1016/j.cemconcomp.2021.104171

Farooq, F., Nasir Amin, M., Khan, K., Rehan Sadiq, M., Faisal Javed, M., Aslam, F., et al. (2020). A comparative study of random forest and genetic engineering programming for the prediction of compressive strength of high strength concrete (HSC). *Appl. Sci.* 10, 7330. doi:10.3390/app10207330

Farooqi, M. U., and Ali, M. (2022). A study on natural fibre reinforced concrete from materials to structural applications. *Arabian J. Sci. Eng.*, 1–21. doi:10.1007/s13369-022-06977-1

Friedman, J. H. (2001). Greedy function approximation: A gradient boosting machine. *Ann. statistics*, 1189–1232. doi:10.1214/aos/1013203451

Habel, K., Viviani, M., Denarié, E., and Brühwiler, E. (2006). Development of the mechanical properties of an ultra-high performance fiber reinforced concrete (UHPFRC). *Cem. Concr. Res.* 36, 1362–1370. doi:10.1016/j.cemconres.2006.03.009

Hu, C.-F., Li, L., and Li, Z. (2022). Effect of fiber factor on the workability and mechanical properties of polyethylene fiber-reinforced high toughness geopolymers. *Ceram. Int.* 48, 10458–10471. doi:10.1016/j.ceramint.2021.12.254

Huang, Y., Zhang, W., and Liu, X. (2022). Assessment of diagonal macrocrack-induced debonding mechanisms in FRP-strengthened RC beams. *J. Compos. Constr.* 26, 04022056. doi:10.1061/(asce)cc.1943-5614.0001255

Iftikhar, B., Alih, S. C., Vafaei, M., Elkotb, M. A., Shutaywi, M., Javed, M. F., et al. (2022). Predictive modeling of compressive strength of sustainable rice husk ash concrete: Ensemble learner optimization and comparison. *J. Clean. Prod.* 348, 131285. doi:10.1016/j.jclepro.2022.131285

Isabona, J., Imoize, A. L., Ojo, S., Karunwi, O., Kim, Y., Lee, C.-C., et al. (2022). Development of a multilayer perceptron neural network for optimal predictive modeling in urban microcellular radio environments. *Appl. Sci.* 12, 5713. doi:10.3390/app12115713

Javed, M. F., Farooq, F., Memon, S. A., Akbar, A., Khan, M. A., Aslam, F., et al. (2020). New prediction model for the ultimate axial capacity of concrete-filled steel tubes: An evolutionary approach. *Crystals* 10, 741. doi:10.3390/cryst10090741

Jiang, X., Xiao, R., Zhang, M., Hu, W., Bai, Y., and Huang, B. (2020a). A laboratory investigation of steel to fly ash-based geopolymer paste bonding behavior after exposure to elevated temperatures. *Constr. Build. Mater.* 254, 119267. doi:10.1016/j.conbuildmat.2020.119267

Jiang, X., Zhang, Y., Xiao, R., Polaczyk, P., Zhang, M., Hu, W., et al. (2020b). A comparative study on geopolymers synthesized by different classes of fly ash after exposure to elevated temperatures. *J. Clean. Prod.* 270, 122500. doi:10.1016/j.jclepro.2020.122500

Jiang, X., Xiao, R., Bai, Y., Huang, B., and Ma, Y. (2022a). Influence of waste glass powder as a supplementary cementitious material (SCM) on physical and mechanical properties of cement paste under high temperatures. *J. Clean. Prod.* 340, 130778. doi:10.1016/j.jclepro.2022.130778

Jiang, X., Zhang, Y., Zhang, Y., Ma, J., Xiao, R., Guo, F., et al. (2022b). Influence of size effect on the properties of slag and waste glass-based geopolymer paste. *J. Clean. Prod.* 383, 135428. doi:10.1016/j.jclepro.2022.135428

Johnsen, P. V., Riemer-Sørensen, S., Dewan, A. T., Cahill, M. E., and Langaas, M. (2021). A new method for exploring gene–gene and gene–environment interactions in GWAS with tree ensemble methods and SHAP values. *BMC Bioinforma.* 22, 230–329. doi:10.1186/s12859-021-04041-7

Jueyendah, S., Lezgy-Nazargah, M., Eskandari-Naddaf, H., and Emamian, S. A. (2021). Predicting the mechanical properties of cement mortar using the support vector machine approach. *Constr. Build. Mater.* 291, 123396. doi:10.1016/j.conbuildmat.2021.123396

Khan, M., and Ali, M. (2019). Improvement in concrete behavior with fly ash, silica-fume and coconut fibres. *Constr. Build. Mater.* 203, 174–187. doi:10.1016/j.conbuildmat.2019.01.103

Khan, U. A., Jahanzaib, H. M., Khan, M., and Ali, M. (2018). "Improving the tensile energy absorption of high strength natural fiber reinforced concrete with fly-ash for bridge girders," in *Key engineering materials* (Switzerland: Trans Tech Publ), 335–342.

Khan, M., Cao, M., Hussain, A., and Chu, S. (2021). Effect of silica-fume content on performance of CaCO3 whisker and basalt fiber at matrix interface in cement-based composites. *Constr. Build. Mater.* 300, 124046. doi:10.1016/j.conbuildmat.2021.124046

Khan, M., Cao, M., Ai, H., and Hussain, A. (2022a). Basalt fibers in modified whisker reinforced cementitious composites. *Period. Polytech. Civ. Eng.* 66, 344–354. doi:10.3311/ppci.18965

Khan, M., Cao, M., Chu, S., and Ali, M. (2022b). Properties of hybrid steel-basalt fiber reinforced concrete exposed to different surrounding conditions. *Constr. Build. Mater.* 322, 126340. doi:10.1016/j.conbuildmat.2022.126340

Khan, M., Cao, M., Xie, C., and Ali, M. (2022c). Effectiveness of hybrid steel-basalt fiber reinforced concrete under compression. *Case Stud. Constr. Mater.* 16, e00941. doi:10.1016/j.cscm.2022.e00941

Khan, M., Cao, M., Xie, C., and Ali, M. (2022d). Hybrid fiber concrete with different basalt fiber length and content. *Struct. Concr.* 23, 346–364. doi:10.1002/suco.202000472

Kovačević, M., Lozančić, S., Nyarko, E. K., and Hadzima-Nyarko, M. (2021). Modeling of compressive strength of self-compacting rubberized concrete using machine learning. *Materials* 14, 4346. doi:10.3390/ma14154346

Kroll, C. N., and Song, P. (2013). Impact of multicollinearity on small sample hydrologic regression models. *Water Resour. Res.* 49, 3756–3769. doi:10.1002/wrcr.20315

Kumar, B. N., and Kumar, P. P. (2022). Prediction on flexural strength of high strength hybrid fiber self compacting concrete by using artificial intelligence. *J. Artif. Intell.* 4, 1–16. doi:10.36548/jaicn.2022.1.001

Larsen, I. L., and Thorstensen, R. T. (2020). The influence of steel fibres on compressive and tensile strength of ultra high performance concrete: A review. *Constr. Build. Mater.* 256, 119459. doi:10.1016/j.conbuildmat.2020.119459

Lauritsen, S. M., Kristensen, M., Olsen, M. V., Larsen, M. S., Lauritsen, K. M., Jørgensen, M. J., et al. (2020). Explainable artificial intelligence model to predict acute critical illness from electronic health records. *Nat. Commun.* 11, 3852–3911. doi:10.1038/s41467-020-17431-x

Le Hoang, A., and Fehling, E. (2017). Influence of steel fiber content and aspect ratio on the uniaxial tensile and compressive behavior of ultra high performance concrete. *Constr. Build. Mater.* 153, 790–806. doi:10.1016/j.conbuildmat.2017.07.130

Li, L., Khan, M., Bai, C., and Shi, K. (2021a). Uniaxial tensile behavior, flexural properties, empirical calculation and microstructure of multi-scale fiber reinforced cement-based material at elevated temperature. *Materials* 14, 1827. doi:10.3390/ma14081827

Li, L., Sun, H.-X., Zhang, Y., and Yu, B. (2021b). Surface cracking and fractal characteristics of bending fractured polypropylene fiber-reinforced geopolymer mortar. *Fractal Fract.* 5, 142. doi:10.3390/fractalfract5040142

Li, L., Cao, M., Li, Z., Zhang, W., Shi, D., and Shi, K. (2022a). Uniaxial tensile behavior and mechanism characterization of multi-scale fiber-reinforced cementitious materials. *Mater. Construcción* 72, e271. doi:10.3989/mc.2022.05521

Li, L., Tao, J.-C., Zhang, Y., Sun, H.-X., Yuen, K.-V., and You, P.-B. (2022b). Crack fractal analysis of fractured polyethylene fiber reinforced alkali activated mortar under flexural load. *Constr. Build. Mater.* 345, 128428. doi:10.1016/j.conbuildmat.2022.128428

Liang, X., Wu, C., Su, Y., Chen, Z., and Li, Z. (2018). Development of ultra-high performance concrete with high fire resistance. *Constr. Build. Mater.* 179, 400–412. doi:10.1016/j.conbuildmat.2018.05.241

Lin, D., Foster, D. P., and Ungar, L. H. (2011). VIF regression: A fast regression algorithm for large data. *J. Am. Stat. Assoc.* 106, 232–247. doi:10.1198/jasa.2011.tm10113

Lu, J., Yu, Z., Zhu, Y., Huang, S., Luo, Q., and Zhang, S. (2019). Effect of lithium-slag in the performance of slag cement mortar based on least-squares support vector machine prediction. *Materials* 12, 1652. doi:10.3390/ma12101652

Lundberg, S. M., and Lee, S.-I. (2017). A unified approach to interpreting model predictions. *Adv. neural Inf. Process. Syst.* 30.

Lundberg, S. M., Nair, B., Vavilala, M. S., Horibe, M., Eisses, M. J., Adams, T., et al. (2018). Explainable machine-learning predictions for the prevention of hypoxaemia during surgery. *Nat. Biomed. Eng.* 2, 749–760. doi:10.1038/s41551-018-0304-0

Lundberg, S. M., Erion, G., Chen, H., Degrave, A., Prutkin, J. M., Nair, B., et al. (2019). Explainable AI for trees: From local explanations to global understanding. *arXiv preprint arXiv:1905.04610*.

Mahjoubi, S., Barhemat, R., Guo, P., Meng, W., and Bao, Y. (2021). Prediction and multi-objective optimization of mechanical, economical, and environmental properties for strain-hardening cementitious composites (SHCC) based on automated machine learning and metaheuristic algorithms. *J. Clean. Prod.* 329, 129665. doi:10.1016/j.jclepro.2021.129665

Mahjoubi, S., Meng, W., and Bao, Y. (2022a). Auto-tune learning framework for prediction of flowability, mechanical properties, and porosity of ultra-high-performance concrete (UHPC). *Appl. Soft Comput.* 115, 108182. doi:10.1016/j.asoc.2021.108182

Mahjoubi, S., Meng, W., and Bao, Y. (2022b). Logic-guided neural network for predicting steel-concrete interfacial behaviors. *Expert Syst. Appl.* 198, 116820. doi:10.1016/j.eswa.2022.116820

Marani, A., and Nehdi, M. L. (2020). Machine learning prediction of compressive strength for phase change materials integrated cementitious composites. *Constr. Build. Mater.* 265, 120286. doi:10.1016/j.conbuildmat.2020.120286

Marani, A., Jamali, A., and Nehdi, M. L. (2020). Predicting ultra-high-performance concrete compressive strength using tabular generative adversarial networks. *Materials* 13, 4757. doi:10.3390/ma13214757

Meng, Z., Li, L., Farooqi, M. U., Feng, L., and Wang, L. (2022). Fiber factor for fresh and hardened properties of polyethylene fiber-reinforced geopolymer mortar. *J. Build. Eng.* 53, 104556. doi:10.1016/j.jobe.2022.104556

Mokhtari, K. E., Higdon, B. P., and Başar, A. (2019). ""Interpreting financial time series with SHAP values," in Proceedings of the 29th Annual International Conference on Computer Science and Software Engineering, 166–172.

Musumeci, F., Rottondi, C., Nag, A., Macaluso, I., Zibar, D., Ruffini, M., et al. (2018). An overview on application of machine learning techniques in optical networks. *IEEE Commun. Surv. Tutorials* 21, 1383–1408. doi:10.1109/comst.2018.2880039

Muzzammel, R., and Raza, A. (2020). A support vector machine learning-based protection technique for MT-HVDC systems. *Energies* 13, 6668. doi:10.3390/en13246668

Nawaz, M. N., Qamar, S. U., Alshameri, B., Karam, S., Çodur, M. K., Nawaz, M. M., et al. (2022). Study using machine learning approach for novel prediction model of liquid limit. *Buildings* 12, 1551. doi:10.3390/buildings12101551

Nazar, S., Yang, J., Ahmad, A., and Shah, S. F. A. (2022). Comparative study of evolutionary artificial intelligence approaches to predict the rheological properties of fresh concrete. *Mater. Today Commun.* 32, 103964. doi:10.1016/j.mtcomm.2022.103964

Nehdi, M., El Chabib, H., and El Naggar, M. H. (2001). Predicting performance of self-compacting concrete mixtures using artificial neural networks. *Mater. J.* 98, 394–401.

Nguyen, T. T., Pham Duy, H., Pham Thanh, T., and Vu, H. H. (2020). Compressive strength evaluation of fiber-reinforced high-strength self-compacting concrete with artificial intelligence. *Adv. Civ. Eng.* 2020, 1–12. doi:10.1155/2020/3012139

Pan, X., Xiao, Y., Suhail, S. A., Ahmad, W., Murali, G., Salmi, A., et al. (2022). Use of artificial intelligence methods for predicting the strength of recycled aggregate concrete and the influence of raw ingredients. *Materials* 15, 4194. doi:10.3390/ma15124194

Pandey, P. K., Aggarwal, P., Aggarwal, Y., and Aggarwal, S. (2022). "Prediction of compressive strength of self-compacting concrete containing silica's using soft computing techniques," in *Applications of computational intelligence in concrete technology* (Florida: CRC Press), 163–181.

Park, S. H., Kim, D. J., Ryu, G. S., and Koh, K. T. (2012). Tensile behavior of ultra high performance hybrid fiber reinforced concrete. *Cem. Concr. Compos.* 34, 172–184. doi:10.1016/j.cemconcomp.2011.09.009

Raza, S. S., Ali, B., Noman, M., Fahad, M., and Elhadi, K. M. (2022a). Mechanical properties, flexural behavior, and chloride permeability of high-performance steel fiber-reinforced concrete (SFRC) modified with rice husk ash and micro-silica. *Constr. Build. Mater.* 359, 129520. doi:10.1016/j.conbuildmat.2022.129520

Raza, S. S., Amir, M. T., Azab, M., Ali, B., Abdallah, M., El Ouni, M. H., et al. (2022b). Effect of micro-silica on the physical, tensile, and load-deflection characteristics of micro fiber-reinforced high-performance concrete (HPC). *Case Stud. Constr. Mater.* 17, e01380. doi:10.1016/j.cscm.2022.e01380

Sarkhani Benemaran, R., Esmaeili-Falak, M., and Javadi, A. (2022). Predicting resilient modulus of flexible pavement foundation using extreme gradient boosting based optimised models. *Int. J. Pavement Eng.*, 1–20. doi:10.1080/10298436.2022.2095385

Schmidt, M., and Fehling, E. (2005). Ultra-high-performance concrete: Research, development and application in europe. *ACI Spec. Publ.* 228, 51–78.

Shah, S. a. R., Azab, M., Seif Eldin, H. M., Barakat, O., Anwar, M. K., and Bashir, Y. (2022). Predicting compressive strength of blast furnace slag and fly ash based sustainable concrete using machine learning techniques: An application of advanced decision-making approaches. *Buildings* 12, 914. doi:10.3390/buildings12070914

Shang, M., Li, H., Ahmad, A., Ahmad, W., Ostrowski, K. A., Aslam, F., et al. (2022). Predicting the mechanical properties of RCA-based concrete using supervised machine learning algorithms. *Materials* 15, 647. doi:10.3390/ma15020647

Shi, C., Wu, Z., Xiao, J., Wang, D., Huang, Z., and Fang, Z. (2015). A review on ultra high performance concrete: Part I. Raw materials and mixture design. *Constr. Build. Mater.* 101, 741–751. doi:10.1016/j.conbuildmat.2015.10.088

Solhmirzaei, R., Salehi, H., Kodur, V., and Naser, M. (2020). Machine learning framework for predicting failure mode and shear capacity of ultra high performance concrete beams. *Eng. Struct.* 224, 111221. doi:10.1016/j.engstruct.2020.111221

Sonebi, M., Cevik, A., Grünewald, S., and Walraven, J. (2016). Modelling the fresh properties of self-compacting concrete using support vector machine approach. *Constr. Build. Mater.* 106, 55–64. doi:10.1016/j.conbuildmat.2015.12.035

Song, H., Ahmad, A., Farooq, F., Ostrowski, K. A., Maślak, M., Czarnecki, S., et al. (2021). Predicting the compressive strength of concrete with fly ash admixture using machine learning algorithms. *Constr. Build. Mater.* 308, 125021. doi:10.1016/j.conbuildmat.2021.125021

Soroush, M., and Bao, Y. (2021). The key material properties of ultra-high-performance concrete (UHPC). *Mendeley Data* V1. doi:10.17632/dd62d5hyzr.11

Tang, B., Lu, Y., Zhou, J., Chouhan, T., Wang, H., Golani, P., et al. (2020). Machine learning-guided synthesis of advanced inorganic materials. *Mater. Today* 41, 72–80. doi:10.1016/j.mattod.2020.06.010

Tariq, H., Siddique, R. M. A., Shah, S. a. R., Azab, M., Qadeer, R., Ullah, M. K., et al. (2022). Mechanical performance of polymeric ARGF-based fly ash-concrete composites: A study for eco-friendly circular economy application. *Polymers* 14, 1774. doi:10.3390/polym14091774

Umeonyiagu, I., and Nwobi-Okoye, C. (2015a). Predicting flexural strength of concretes incorporating river gravel using multi-layer perceptron networks: A case study of eastern Nigeria. *Niger. J. Technol.* 34, 12–20. doi:10.4314/njt.v34i1.2

Umeonyiagu, I. E., and Nwobi-Okoye, C. C. (2015b). Modelling compressive strength of concretes incorporating termite mound soil using multi-layer perceptron networks: A case study of eastern Nigeria. *Int. J. Res. Rev. Appl. Sci.* 24, 19.

Wang, J., and Wu, F. (2022). New hybrid support vector regression methods for predicting fresh and hardened properties of self-compacting concrete. *J. Intelligent Fuzzy Syst.*, 1–15. doi:10.3233/jifs-220744

Wang, D., Shi, C., Wu, Z., Xiao, J., Huang, Z., and Fang, Z. (2015). A review on ultra high performance concrete: Part II. Hydration, microstructure and properties. *Constr. Build. Mater.* 96, 368–377. doi:10.1016/j.conbuildmat.2015.08.095

Wang, Q., Hussain, A., Farooqi, M. U., and Deifalla, A. F. (2022). Artificial intelligence-based estimation of ultra-high-strength concrete's flexural property. *Case Stud. Constr. Mater.* 17, e01243. doi:10.1016/j.cscm.2022.e01243

Worden, K., and Manson, G. (2007). The application of machine learning to structural health monitoring. *Philosophical Trans. R. Soc. A Math. Phys. Eng. Sci.* 365, 515–537. doi:10.1098/rsta.2006.1938

Wu, Z., Shi, C., He, W., and Wang, D. (2016). Uniaxial compression behavior of ultra-high performance concrete with hybrid steel fiber. *J. Mater. Civ. Eng.* 28, 06016017. doi:10.1061/(asce)mt.1943-5533.0001684

Xie, C., Cao, M., Guan, J., Liu, Z., and Khan, M. (2021). Improvement of boundary effect model in multi-scale hybrid fibers reinforced cementitious composite and prediction of its structural failure behavior. *Compos. Part B Eng.* 224, 109219. doi:10.1016/j.compositesb.2021.109219

Yan, L., Diao, Y., Lang, Z., and Gao, K. (2020). Corrosion rate prediction and influencing factors evaluation of low-alloy steels in marine atmosphere using machine learning approach. *Sci. Technol. Adv. Mater.* 21, 359–370. doi:10.1080/14686996.2020.1746196

Yeung, C., Tsai, J.-M., King, B., Kawagoe, Y., Ho, D., Knight, M. W., et al. (2020). Elucidating the behavior of nanophotonic structures through explainable machine learning algorithms. *ACS Photonics* 7, 2309–2318. doi:10.1021/acsphotonics.0c01067

Yoo, D.-Y., and Banthia, N. (2016). Mechanical properties of ultra-high-performance fiber-reinforced concrete: A review. *Cem. Concr. Compos.* 73, 267–280. doi:10.1016/j.cemconcomp.2016.08.001

Yu, R., Spiesz, P., and Brouwers, H. (2014). Mix design and properties assessment of ultra-high performance fibre reinforced concrete (UHPFRC). *Cem. Concr. Res.* 56, 29–39. doi:10.1016/j.cemconres.2013.11.002

Zhang, C., and Ali, A. (2021). The advancement of seismic isolation and energy dissipation mechanisms based on friction. *Soil Dyn. Earthq. Eng.* 146, 106746. doi:10.1016/j.soildyn.2021.106746

Zhang, W., and Huang, Y. (2022). Three-dimensional numerical investigation of mixed-mode debonding of FRP-concrete interface using a cohesive zone model. *Constr. Build. Mater.* 350, 128818. doi:10.1016/j.conbuildmat.2022.128818

Zhang, X., Zhao, S., Liu, Z., and Wang, F. (2019). Utilization of steel slag in ultra-high performance concrete with enhanced eco-friendliness. *Constr. Build. Mater.* 214, 28–36. doi:10.1016/j.conbuildmat.2019.04.106

ZhangN, ., Yan, C., Li, L., and Khan, M. (2022). Assessment of fiber factor for the fracture toughness of polyethylene fiber reinforced geopolymer. *Constr. Build. Mater.* 319, 126130. doi:10.1016/j.conbuildmat.2021.126130

ZhangZ, ., Liang, G., Niu, Q., Wang, F., Chen, J., Zhao, B., et al. (2022). A Wiener degradation process with drift-based approach of determining target reliability index of concrete structures. *Qual. Reliab. Eng. Int.* 38, 3710–3725. doi:10.1002/qre.3168

Zhao, W., Joshi, T., Nair, V. N., and Sudjianto, A. (2020). Shap values for explaining cnn-based text classification models. *arXiv preprint arXiv:2008.11825*.

Zheng, D., Wu, R., Sufian, M., Kahla, N. B., Atig, M., Deifalla, A. F., et al. (2022). Flexural strength prediction of steel fiber-reinforced concrete using artificial intelligence. *Materials* 15, 5194. doi:10.3390/ma15155194

Zhou, M., Lu, W., Song, J., and Lee, G. C. (2018). Application of ultra-high performance concrete in bridge engineering. *Constr. Build. Mater.* 186, 1256–1267. doi:10.1016/j.conbuildmat.2018.08.036

Zhu, Y., Ahmad, A., Ahmad, W., Vatin, N. I., Mohamed, A. M., and Fathi, D. (2022). Predicting the splitting tensile strength of recycled aggregate concrete using individual and ensemble machine learning approaches. *Crystals* 12, 569. doi:10.3390/cryst12050569

Zou, Y., Zheng, C., Alzahrani, A. M., Ahmad, W., Ahmad, A., Mohamed, A. M., et al. (2022). Evaluation of artificial intelligence methods to estimate the compressive strength of geopolymers. *Gels* 8, 271. doi:10.3390/gels8050271

Investigation of the physical-mechanical properties and durability of high-strength concrete with recycled PET as a partial replacement for fine aggregates

Shaker Qaidi[1,2]*, Yaman Al-Kamaki[1], Ibrahim Hakeem[3]*,
Anmar F. Dulaimi[4,5], Yasin Özkılıç[6], Mohanad Sabri[7] and
Vitaly Sergeev[7]

[1]Department of Civil Engineering, College of Engineering, University of Duhok, Duhok, Iraq, [2]Department of
Civil Engineering, College of Engineering, Nawroz University, Duhok, Iraq, [3]Department of Civil Engineering,
College of Engineering, Najran University, Najran, Saudi Arabia, [4]College of Engineering, University of Warith
Al-Anbiyaa, Karbala, Iraq, [5]School of Civil Engineering and Built Environment, Liverpool John Moores
University, Liverpool, United Kingdom, [6]Department of Civil Engineering, Faculty of Engineering, Necmettin
Erbakan University, Konya, Turkey, [7]Peter the Great St. Petersburg Polytechnic University, StPetersburg,
Russia

In this study, PET plastic waste, which is a type of polymer commonly used in the manufacture of plastic bottles, has been incorporated into concrete by partially replacing the natural fine aggregate. An experimental study was conducted by casting and testing 90 concrete cylinders and 54 concrete cubes. A concrete mixture was designed in which the natural fine aggregate was substituted partially with PET plastic waste (PW) at a ratio of 0%, 25%, and 50%, with various w/c ratios of .40, .45, and .55. Physical, mechanical, and durability properties were assessed. The downside of the test results show degradation in each of the following characteristics: slump, compressive strength, splitting tensile strength, ultrasonic pulse velocity, water absorption, and porosity. The degradation of these characteristics increased with the increase in the volume of plastic aggregate (PA) and the w/c ratio. While the positive side of the results showed that with the increase of the PA volume and the w/c ratio, the fresh and dry densities decreased further, and by using 50% PET, the dry density became below 2000 kg/m^3. Therefore, it is classified as lightweight concrete. Moreover, the fracture of concrete changed from brittle to more ductile compared to control concrete. Also, the thermal conductivity decreased significantly (11%−47%), and by using 50% of PET, the thermal conductivity became less than .71 W/mK, and accordingly, classified as a bearing insulator.

KEYWORDS

plastic waste, polyethylene terephthalate, mechanical properties, durability properties, functional properties

1 Introduction

Concrete is one of the most popular and used building materials in the world (Kılıç et al., 2003; Topçu and Uygunoğlu, 2007; Akçaözoğlu et al., 2010; Khan et al., 2021b; Kumar et al., 2021; Khan et al., 2022d). Per year, "around 12 billion tonnes of concrete are produced worldwide, which is approximately 10 billion tonnes of rock (Shah and Wang, 2004). Besides, the concrete demand is estimated to grow to 18 billion tonnes by 2050 (Khoshkenari et al., 2014). The concrete industry has a significant environmental impact. Virtually, the use of concrete cannot be restricted, but there are different approaches to reduce its environmental impact. On the other hand, the human lifestyle and the new technology have led to the development of PW products, for which the enquiry of disposal perseveres (Khan et al., 2022a; Khan et al., 2022b). The majority of this solid PW is deposited in waste dump sites. This management of waste is unfavorable because most wastes are non-biodegradable and stay in the natural environment for hundreds and thousands of centuries (Rahmani et al., 2013; Barreto et al., 2021; de Azevedo et al., 2021; Room et al., 2021; Fediuk and Ali, 2022; Lesovik et al., 2022). Accordingly, the environmental friendliness of this process decreases" (Qaidi et al., 2022a).

However, "since earthquake forces are directly proportional to building mass, lightweight aggregate is a critical component in reducing the unit weight of concrete to make earthquake-resistant structures" (Kılıç et al., 2003; Qaidi et al., 2022b). Lightweight aggregates are often used in place of traditional aggregates to reduce the unit weight of concrete. There are various lightweight concrete applications that use natural or manufactured lightweight aggregates in the literature today. The cost of making artificial lightweight aggregate, on the other hand, is considerable due to the requirement of a high incineration temperature or heat treatment. As a result, unlike other materials, scientists are interested in using waste plastic granules as lightweight aggregate in the creation of lightweight concrete. This method enables the low-cost recycling of plastic trash as well as the manufacturing of lightweight concrete (Qaidi et al., 2022c; Tayeh et al., 2022a; Tayeh et al., 2022b).

According to Plastic-Europe (2019), plastics can usually be classified into two groups: thermoplastic and thermosetting. Thermoplastics, for example, PET, polyethylene (PE), polystyrene (PS), polypropylene (PP), and high-density polyethylene (HDPE), can be frequently reheated, reshaped, and frozen. In contrast,

thermosets cannot be reformed after heated and formed, such as epoxy, silicone, melamine, phenolic, and polyurethane (PU). PET is the most common plastic around the world as it is frequently utilized for containers and bottles for various purposes. Bottles are discarded at a rate of almost half a billion each year; a million bottles are discarded every minute worldwide, and this rate is predicted to rise by 23% by 2025 (Qaidi and Al-Kamaki, 2021). Figure 1 shows the chemical compositions of the major types of polymers, as well as the global market share for each type, with C-O polymers (PET, PU, etc.) covering more than 18% of the worldwide market share (Ali et al., 2021; Khan, 2023).

Because of the benefits of plastics, such as their versatility and low cost, there is an increasing need for plastics all over the world. As a consequence, the world generated 368 million tonnes (Mt) of plastics in 2019, out of which 57.9 Mt were generated in Europe (Zulkernain et al., 2021). In the European Union, according to Plastic-Europe (2019) for post-consumer PW, as shown in Figure 2, about 39.5% of post-consumer plastic was recycled, and 43% of this waste was recovered for fuel and the rest of it is deposited in the landfill. While globally, only about 25% of PW is recycled and it is estimated that more than 33% of the PW produced will be recycled by 2050 (Babafemi et al., 2018; Almeshal et al., 2022; Emad et al., 2022; Faraj et al., 2022; He et al., 2022). Even if this estimate is correct, the volume of non-recycled waste remains highly undesirable and inefficient. As a result, millions of tonnes of plastic end up every year in oceans and landfills (Khan et al., 2019; Khan, 2022).

The common techniques for treating PWs are varied, like burial, incinerate, and recycling. An undesirable effect of the burial method is the fact that plastic products slowly dissolve, and it takes hundreds of years to come back to the natural cycle. While the heat generated during the incinerate can be beneficial in the incinerate method. However, the burning of other forms of waste such as PET will release toxic gases. So, recycling appears to be the safest path for compliance with the ecosystem and economic gains (Albano et al., 2009). As a result, the recycling rate will be improving, and demand for natural raw material production will decrease. Thus, the environmental pressure on the concrete sector is reduced and eliminates the demand for capital assets, and as a result, contributes to sustainable production (Khan et al., 2021a; Khan, 2021). For these reasons, several papers have been conducted to use this waste in concrete and it is still ongoing. However, studies clearly indicated that not all of them are acceptable as concrete aggregates, as the types of PW that rely on resin and PET had
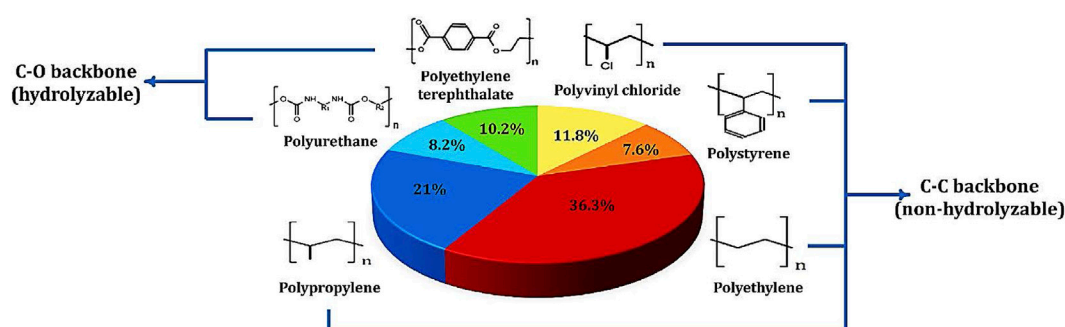
FIGURE 1
Forms of synthetic plastics and percentage distribution of their market share (Ali et al., 2021).

been stated to have the greatest utilization rate for concrete production (Kore, 2018; Akeed et al., 2022; Al-Tayeb et al., 2022). Recycling PET into concrete, on the other hand, reduces quarrying operations and is a big step toward sustainability due to its economic and environmental benefits, therefore substituting PET for aggregates is a mutualistic solution to both concerns. Thus, the goal of the study is to investigate the behavior of concrete that contains a considerable amount of recycled PW of type PET as a fine aggregate.

1.1 Significance of study

Building materials such as cement and aggregate are in high demand as the construction sector increases. "As is well known, concrete mixes comprise 60 to 80 percent aggregate by volume, despite the fact that aggregate is a non-renewable resource. Continuous quarrying has a negative environmental impact as well as a scarcity of aggregate. As a result, aggregate replacement is preferred to reduce demand for quarries. PET, on the other hand, is a type of PW derived from human waste. As a result, there will be fewer landfills in the coming years. However, because recycling PET into concrete reduces quarrying operations and is a big step toward sustainability due to its economic and environmental benefits, replacing PET for aggregates is a mutualistic solution to both concerns". Thus, the goal of the study is to understand the performance of concrete that contains a considerable amount of recycled PW of type PET as a fine aggregate.

2 Materials and methods

2.1 Cement

Ordinary Portland cement (OPC) Type I which conformed with the Iraqi standard specification (I.O.S.) (No. 5/1984) (COSQC, 1984a)

was used as the only binder in this study. The chemical properties and physical and mechanical properties of the OPC are presented in Table 1 and Table 2, respectively.

2.2 Aggregates

2.2.1 Fine aggregate

The primary fine aggregate used in this study is natural sand which was sourced from the Khabor region of Dahok city in Iraq. The natural sand was sieved to ensure the natural sand used to have a maximum particle size of 4.75 mm. The natural fine sand possesses a fineness modulus of 2.81, specific gravity of 2.7, absorption of 1.14%, and bulk density of 1,634 kg/m^3. The sieve analysis evaluation of the fine aggregates indicates they conform to the I.Q.S. No. 45/1984 Zone 2 (COSQC, 1984b).

2.2.2 Coarse aggregate

Natural crushed aggregate from the Sejia district of Dahok city in Iraq was used as the coarse aggregate to produce the concrete mixtures. The crushed aggregates were sieved to ensure the maximum aggregate size is 19 mm. The aggregates were then washed to remove impurities and dried in the open air before use in the production of the concrete mixtures. The analysis of the properties of the aggregates showed that it conforms with the I.O.S. No. 45/1984 (COSQC, 1984b). The specific gravity, absorption, and bulk density of the coarse aggregate used are 2.67, .68%, and 1,540 kg/m^3, respectively.

2.2.3 PET aggregate

PET waste bottles (type BC210) were "processed and reused as partial replacement of the fine aggregate in this study. These PET bottles were supplied by the Light Plastic Factory. The properties of the PET waste bottles are presented in Table 3. After receiving the PET waste bottles, they were processed as follows: (i) removal of

FIGURE 2
Recycling, energy recovery, and landfill percentages for plastic post-consumer waste in the EU in 2018 (Plastic-Europe, 2019).
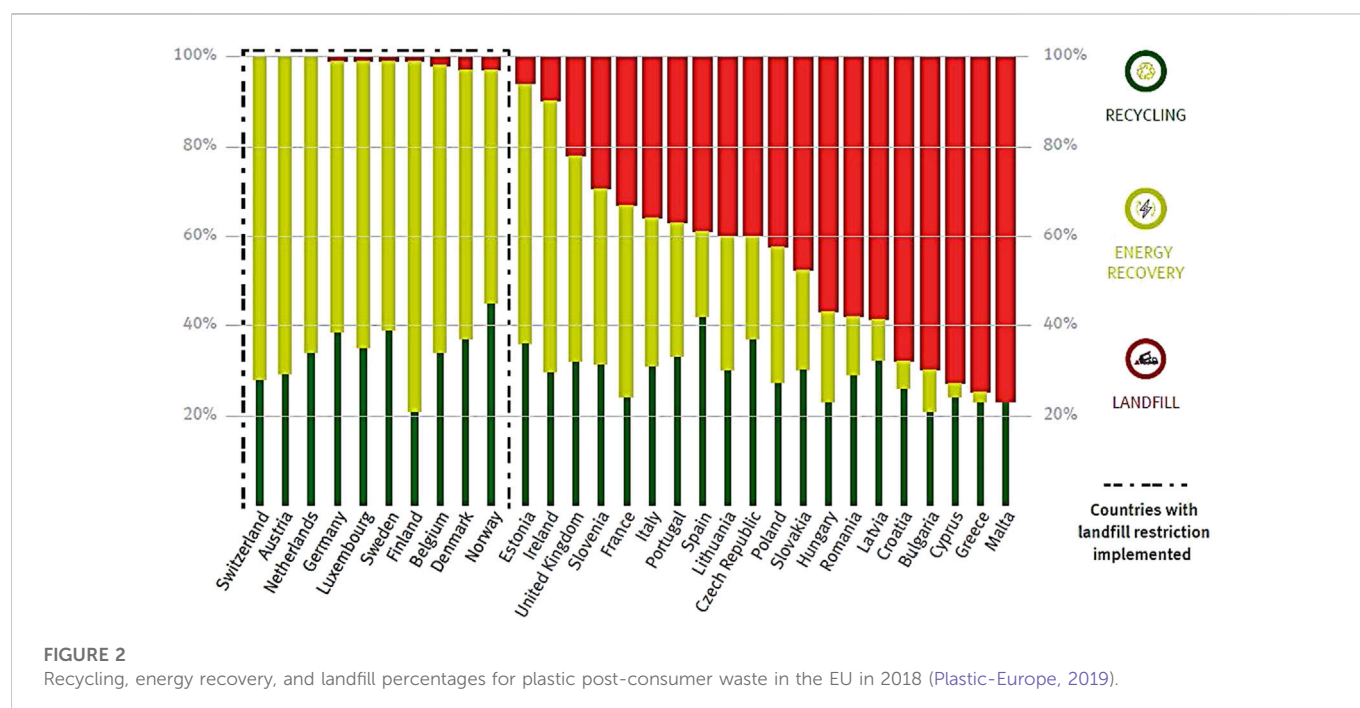
TABLE 1 The chemical characteristics of OPC.

Chemical requirements	Test result (%)	Limitation (I.O.S.) (No. 5/1984) COSQC. (1984a)
SO_3	2.24	2.5 if C_3A < 3.5
		2.8 if C_3A > 3.5
SiO_2	19.11	—
Al_2O_3	6.42	—
MgO	3.82	<5.0
Fe_2O_3	3.73	—
CaO	66.26	—
C_2S	19.91	—
C_3S	50.40	—
C_3A	7.67	—
C_4AF	10.03	—
Insoluble residue	.96	Not more than 1.5
Loss on ignition	2.2	Not more than 4
Lime saturation factor	.91	.66–1.02
Chloride Quantity	.01	—

TABLE 2 The physical and mechanical characteristics of OPC Qaidi et al. (2022a).

Physical & mechanical requirements	Test result	Limitation (I.O.S.) (No. 5/1984) COSQC. (1984a)
Initial setting time (minute)	190	≥45 min
Final setting time (minute)	240	≤600 min
Fineness (Blaine) (cm²/g)	3,470	≥2,300
Compressive strength (3 days) (MPa)	25	≥15 MPa
Compressive strength (7 days) (MPa)	35	≥23 MPa

TABLE 3 "Physical and mechanical characteristics of used PET" Qaidi et al. (2022a).

Property	Results
Specific gravity	1.38
Water absorption (24 h)	Nil
Shape of particles	Flaky
Thickness	.34 mm
Bulk density	855 ± 10 kg/m³
Color	Crystalline white
Melting temperature	230°C–255°C
Tensile strength	79.3 MPa
Tensile modulus	4.0 GPa

bottle caps followed by the washing and drying of the bottles, (ii) shredding and grinding of the PET waste bottles using a plastic granulator machine, and (iii) sieving the grinded PET waste bottles

to obtain PET aggregate with a maximum aggregate size of 4.75 mm" (Qaidi et al., 2022a). Figure 3 shows the processed PET used as aggregates. It can be observed from Figure 3 that the PET aggregates possess flaky and angular morphology. The sieve analysis of all the aggregate used in this study is presented in Figure 4.

2.3 Mixing solution

For all concrete mixtures, potable water free of impurities was utilized as the mixing solution.

2.4 Admixtures

Superplasticizer (SP) with trading name "Sika ViscoCrete Hi-Tech 1,316 conforming to ASTM C494 (ASTM-International, 2015) type D and G was added into the concrete mixtures to improve the workability. Furthermore, several testing were carried out in order to determine the optimal dosage of SP, which impacts
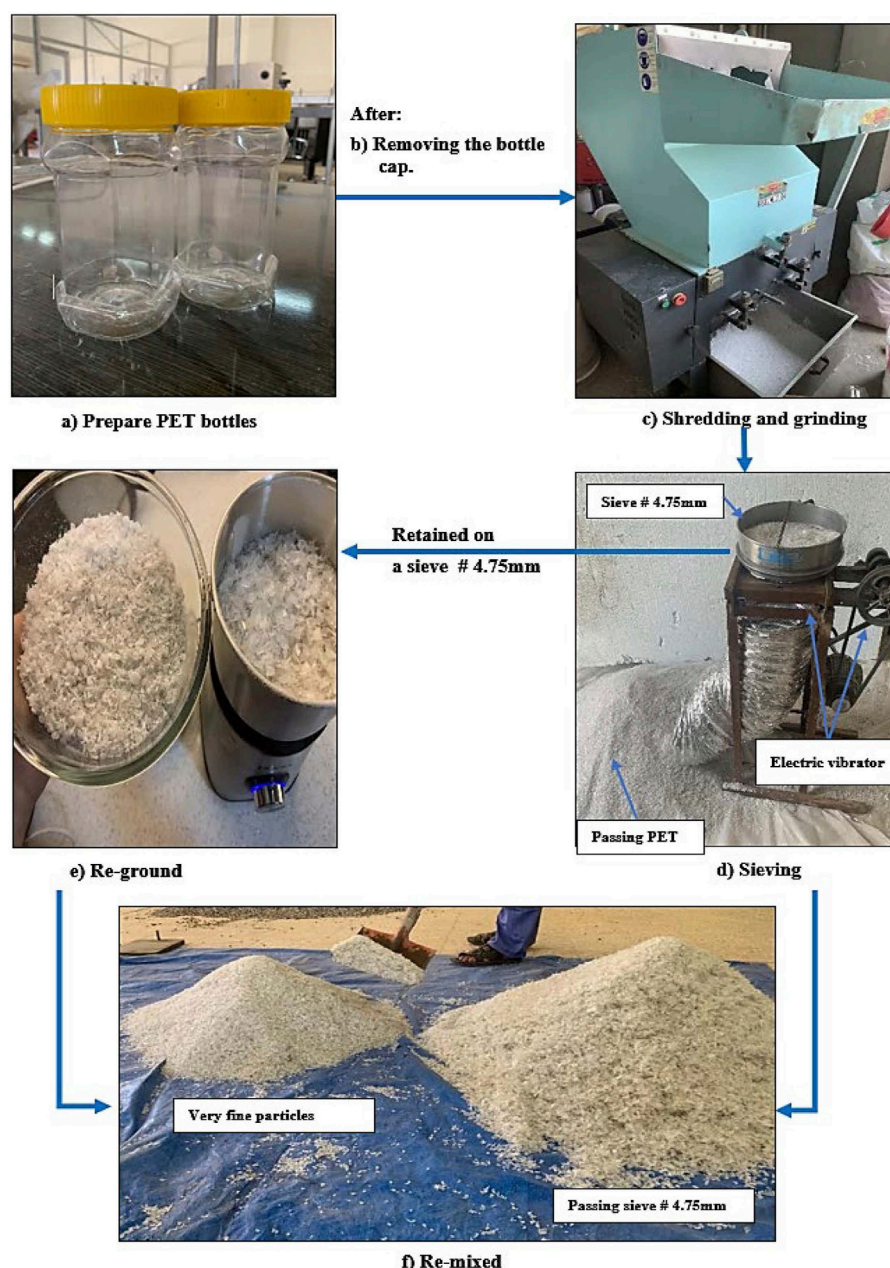
FIGURE 3
Processing of PET aggregates.

the fresh and mechanical properties of concrete mixes" (Qaidi et al., 2022a). The properties of the SP are presented in Table 4.

2.5 Mixture proportion

The concrete mixtures made in this study were designed by ACI 211.1-91-R-02 (Aci-211-1-91, 2002) with w/c of .40, .45, and .55. The PET aggregates were used to replace the natural fine sand up to 50% at an increment of 25% (i.e., 0%, 25%, and 50%). Table 5 presents a detailed composition of the nine concrete mixtures made and evaluated. The mixture ID in Table 5 represents the content of PET aggregate used as a replacement of the fine aggregate and the w/c used.

2.6 Sample preparation and curing

The concrete mixtures were prepared as per ASTM-C192/C192M (2009) by using an electrical rotary tilting drum mixer with a capacity of .1 m³. The concrete mixtures were prepared by mixing the aggregates and OPC for 3 minutes followed by the addition of potable water premixed with the SP. After the mixing process was completed, the slump of the concrete mixtures was evaluated followed by casting of the samples for the properties to be evaluated. After casting the samples, the surfaces of the moulds were covered with a plastic sheet to avoid the loss of water from the samples. At approximately 24 h after casting the concrete samples, the samples were removed from the moulds and cured in water until the testing

TABLE 4 Specification of superplasticizer Qaidi et al. (2022a).

"Characteristics	Description
Appearance	Brownish liquid
Specific gravity	1.123 ± .01 kg/L
Chloride quantity	Max. .1% Chloride-free
Chemical base	Modified polycarboxylates based polymer"

age. Furthermore, Superplasticizer (Polycarboxylic acid water-reducing agent) complying to ASTM C494 type D and G was added to the concrete mixtures to increase workability and eliminate the problem of PET floating in the mix.

2.7 Tests

The details of the tests carried out are outlined in Table 6.

2.8 Instrumentation

Sandpaper was used to "smooth the surface of the cylinders and then cleaned with isopropyl alcohol. Then, two strain gauges (Model PL-60-11-3LJC-F) were installed, one horizontally and one vertically as T-shaped and equally spaced in the mid-height of all samples. The strain gauges were connected to the digital collector (data logger) for data collection during the compression test" (Qaidi et al., 2022a) as shown in Figure 5.

TABLE 5 Concrete mixture proportions (kg/m³).

Mixture ID	R0WC40	R25WC40	R50WC40	R0WC45	R25WC45	R50WC45	R0WC55	R25WC55	R50WC55
w/c	.40			.45			.55		
PET content	0%	25%	50%	0%	25%	50%	0%	25%	50%
Cement	460	460	460	387	387	387	320	320	320
Water	174	174	174	174	174	174	174	174	174
Gravel	955	955	955	955	955	955	955	955	955
Sand	861	645.7	430.5	880	660	440	940	705	470
PET	0	110.8	221.6	0	113.2	226.5	0	120.9	241.9
SP	4.14	4.14	4.14	3.29	3.29	3.29	2.81	2.81	2.81

FIGURE 4
Sieve analysis of aggregates.

TABLE 6 Details of experimental tests.

Test	Standards	Remarks
Slump	ASTM-C142 (2015)	Only for each control concrete mixture of w/c (.40, .45, and .55), the SP ratio was modified to have a slump of 100 ± 10 mm)
Fresh Density	ASTM-C138 (2015)	—
Dry Density	ASTM-C642 (2015)	These tests were performed at 28 days old by using cubic samples (100 mm)
Water Absorption		
Porosity		
Compressive Strength	ASTM-C39 (2012)	The test was executed on concrete cylinder specimens of (150 × 300) mm. The test was carried out with a universal test machine (walter + bai ag) with a capacity of 3,000 kN, and a loading rate of .33 MPa/s
Stress-Strain Curves	—	The stress-strain curves of the concrete cylinders were carefully investigated during the compression tests at 90 days only. For each load increment, the corresponding axial and lateral strains were recorded
Splitting Tensile Strength	ASTM-C496 (2008)	The test was executed on concrete cylinder specimens of (150 × 300) mm. The load was continuously applied at a rate of 1.2 MPa/min to failure
Ultrasonic Pulse Velocity (UPV)	ASTM-C597 (2009)	The test was performed on concrete cubes specimens (100 mm). A transducer with a vibration frequency of 52 kHz was also utilized
Theoretical Thermal Conductivity	ACI-122R (2002)	The test is carried theoretically according to the exponential equation provided by (ACI-122R, 2002)
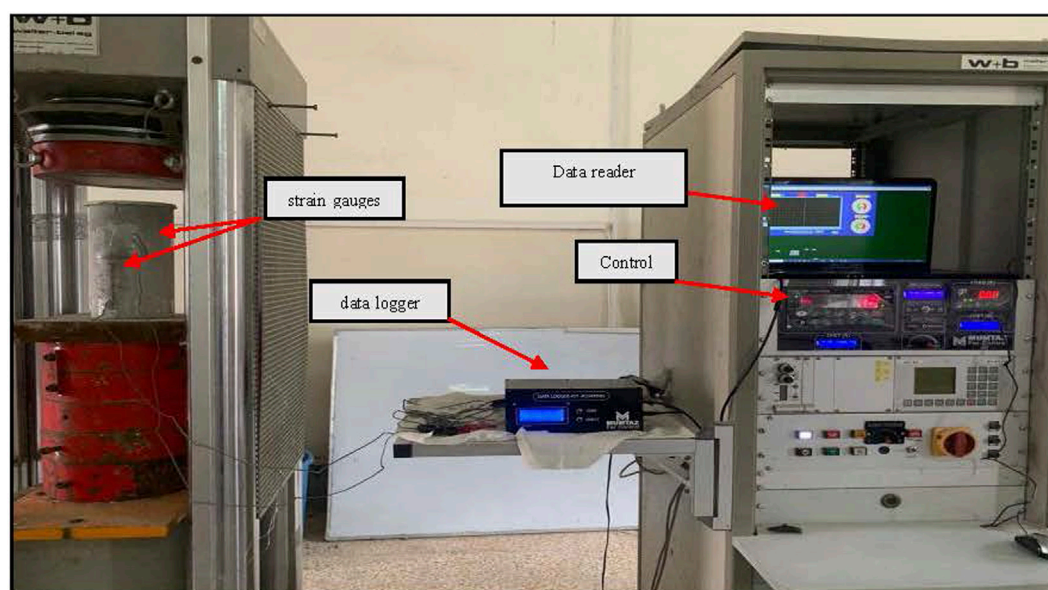
FIGURE 5
Compression testing with equipment.

3 Results and discussion

3.1 Workability (slump test)

The workability of the mixture was evaluated in terms of the slump. Figure 6 shows the effect of PET content and w/c on the resulting workability of the concrete mixtures. "It can be noted that the slump reduced with higher content of PET regardless of the w/c ratio used. For example, compared to the control mix, at the 25% replacement, the reduction rate is 33.33% (w/c of .40), 38.1% (w/c of .45), and 41.28% (w/c of .55). While, at 50% replacement, the

reduction rate is 79.9% (w/c of .40), 82.86% (w/c of .45), and 90.83% (w/c of .55). Nevertheless, all mixtures evaluated were still workable to some extent. The reduction in the workability of the concrete with the incorporation of PET can be attributed to the flat and irregular shape of PET particles which embodied them with a larger surface area compared to that of the natural sand. As a result, there would be further friction among the particles resulting in less workability of the concrete mixtures" (Qaidi et al., 2022a).

The detrimental impact of the PET aggregate on the workability of the concrete mixture is more significant in mixtures made with higher w/c. This significant impact of the PET aggregate at higher
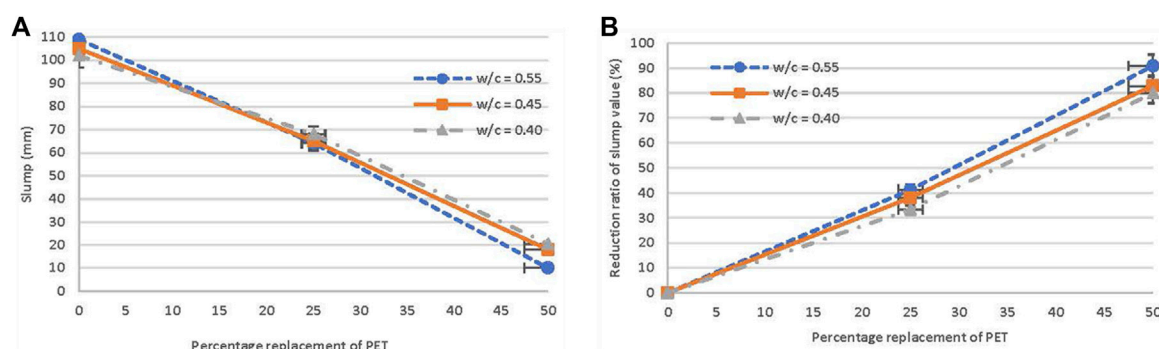
FIGURE 6
Slump test results for different ratios of PET and w/c: **(A)** slump value; and **(B)** reduction ratio.
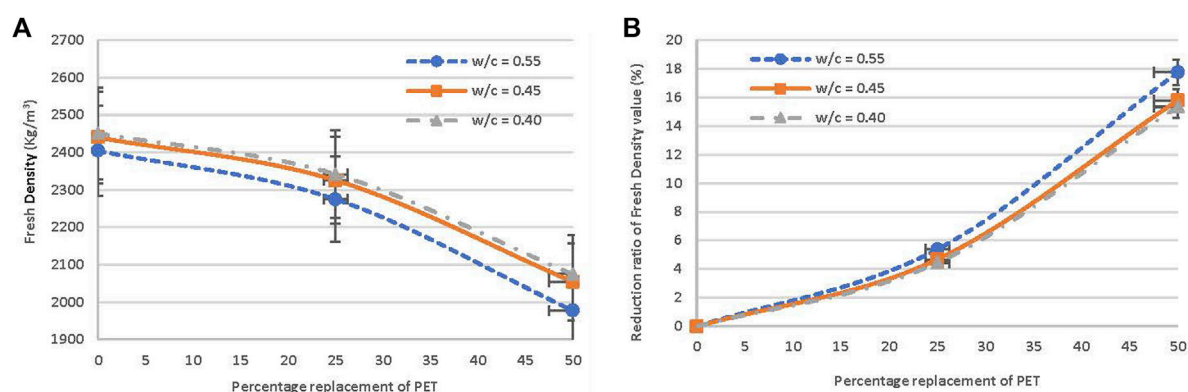
FIGURE 7
Fresh density test results for different ratios of PET and w/c: **(A)** fresh density value; and **(B)** reduction ratio.

w/c can be linked to bleeding as the interface between PET particles and the hydrated Portland cement becomes more porous at higher w/c. This behavior occurred as a result of the inability to water absorption and the flat form of the PET particles (Xie et al., 2021; Khan et al., 2022c). Thus, lowering the workability of the mixture. Similar observations have been reported by other studies where PET aggregates were used (Albano et al., 2009; Rahmani et al., 2013).

3.2 Fresh and dry densities

Figures 7, 8 present the fresh and dry densities results with different proportions of PET particles and w/c ratios. The results showed that the fresh and dry densities of all mixtures decreased with higher PET content. For fresh density, a maximum reduction of 17.75% was observed for concrete made with w/c of .55 and PET aggregate as a 50% replacement of the natural sand. For the dry density, the maximum reduction was 21.63% when the concrete was made with a w/c of .55 and PET as a 50% replacement of the natural sand. The reduction in the density of the concrete when PET aggregates were incorporated can be ascribed to the lower density of PET aggregates compared to that of natural sand.

The decline in concrete density is "more pronounced when higher w/c especially for the dry density, as shown in Figures 7, 8. This has been related to the excess water in the concrete samples that does not take part in the water and cement reactions. Thus, so small canals are formed that can create pores after drying. Therefore, lower unit weights are achieved for higher w/c ratios, as confirmed by Choi et al. (2005). Moreover, values of dry density for mixtures including 0% of PET PAs decreased from 2,388 kg/m³ (w/c of .40), 2,376 kg/m³ (w/c of .45), and 2,347 kg/m³ (w/c of .55) to 1993 kg/m³, 1964 kg/m³, and 1839 kg/m³, respectively, for mixtures including 50% of PET PAs. Thus, all dry density values, at the replacement ratio of 50%, were below 2000 kg/m³ [minimum dry density needed for lightweight concrete as per the classification of RILEM-LC2 (1978)]. Accordingly, these concretes are classified as lightweight concretes" (Qaidi et al., 2022a). This result is also within the scope of the results obtained by Azhdarpour et al. (2016).

3.3 Water absorption and porosity

Water absorption refers to the gradation of material porosity by measuring the ratios of water absorbed under a particular state (Farhana et al., 2015; Babafemi et al., 2018). Figures 9, 10 show the
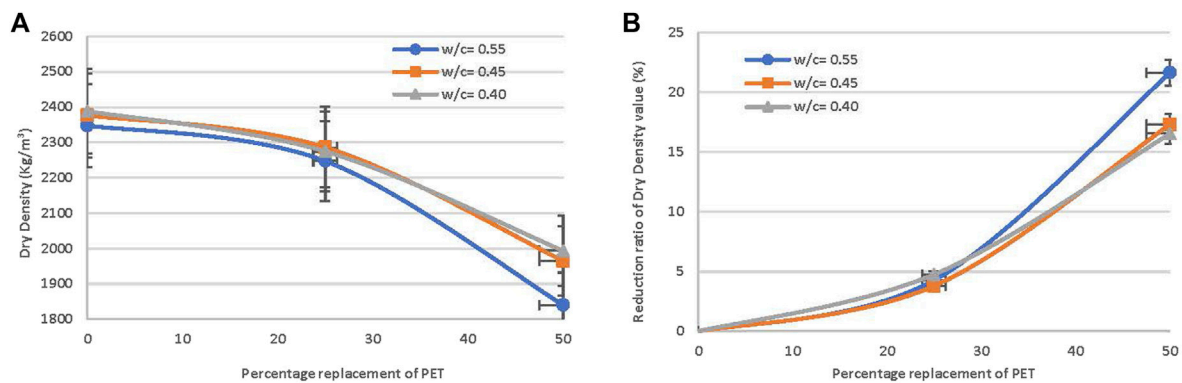
FIGURE 8
Dry density test results for different ratios of PET and w/c: **(A)** dry density value; and **(B)** reduction ratio.
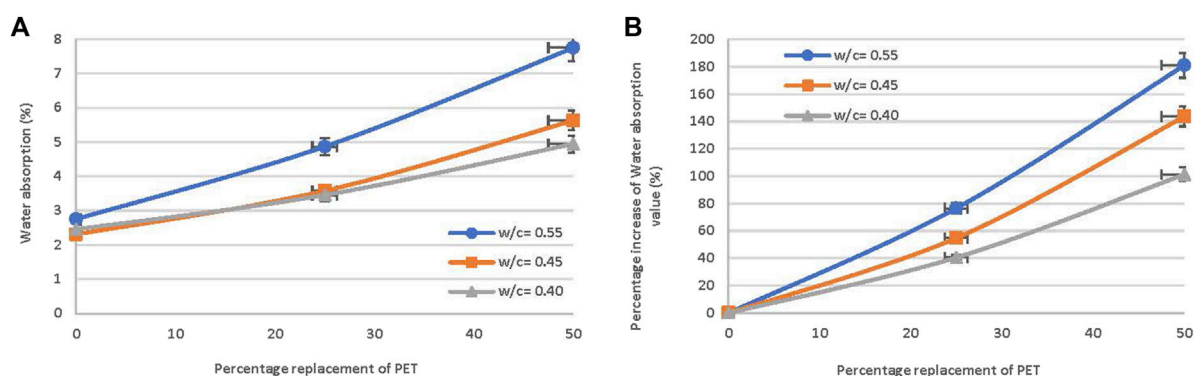
FIGURE 9
Water absorption test results for various ratios of PET and w/c: **(A)** water absorption value; and **(B)** increase the percentage.

influence of w/c and PET aggregate content on the water absorption and the porosity of concrete mixtures evaluated. The values presented for each mixture represent the average value. From the data presented, the water absorption and porosity of concrete, irrespective of the w/c ratio, increased significantly with higher PET aggregate content. For example, compared to the reference mixture, at the 50% replacement, the increased rate of water absorption and porosity was, respectively, 101.25% and 69.32% (w/c of .40), 143.6% and 89.96% (w/c of .45), and 181% and 95.85% (w/c of .55). This behavior occurred because of the fact that natural aggregates and plastic are not sufficiently combined in the concrete matrix, leading to a porous matrix. This could be attributed to two factors: (i) the smooth surface and irregular shape of most PAs weakens the bond between the aggregates and the matrix of cement; and (ii) PAs almost have no absorption capacity for water, this will cause water to accumulate in the ITZ. Consequently, after these samples have dried, they create blank cavities. Accordingly, allowing the water absorption to increase when the specimens are exposed to water (Ahmed et al., 2021; Cao and Khan, 2021; Maglad et al., 2022).

From the data presented in Figures 9, 10, "it can be observed that the water absorption and porosity increased with higher w/c. This is because the coated surface of the aggregate (surface-coating

pozzalanics materials around aggregate) is smaller in case of a higher w/c ratio. So, as the volume of paste is decreased, the pores in the concrete increase, and the water absorption increases. Moreover, as this study mentioned before, the extra water in the concrete samples that has not reacted with the cement and has not been absorbed by the waste PET particles creates cavities after drying" (Qaidi et al., 2022a). Therefore, higher water absorption and porosity are achieved for higher w/c ratios, as confirmed by Albano et al. (2009); Heredia (2018).

3.4 Compressive strength

The influence of the PET aggregate content and w/c on the compressive strength of concrete is presented in Table 7. "The presented results are the average of three specimens whose individual values are (±2.0 MPa) relevant to the average mentioned in Table 7. Generally, and at all test ages, while the substitution rate of PET particles increases, the trend of compressive strength is further reduced. For example, compared to the control mix, at the 25% replacement at 90-day, the reduction rate in strength was 43.46% (w/c of .40), 40.96% (w/c of .45) and
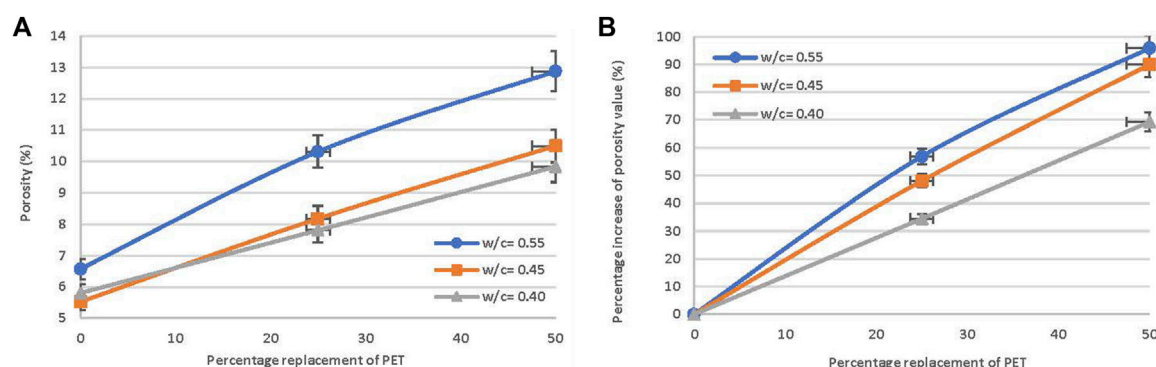
FIGURE 10
Porosity test results for different ratios of PET and w/c: **(A)** porosity value; and **(B)** increase percentage.

TABLE 7 Compressive strength and splitting tensile strength testing results.

w/c	Symbols	Compressive strength (MPa)								Splitting tensile strength (MPa)	
		7 d	Variation (%)	SD*	28 d	Variation (%)	SD	90 d	Variation (%)	90 d	Variation (%)
.40	R0WC40	64.14	—	2.40	77.08	-	2.91	80.13	—	6.07	—
	R25WC40	38.28	−40.31	2.97	44.48	−42.29	3.08	45.31	−43.46	4.23	−30.22
	R50WC40	17.14	−73.27	2.69	18.86	−75.53	3.01	19.14	−76.12	2.48	−59.11
.45	R0WC45	51.51	—	2.62	64.09	—	3.11	66.83	-	5.41	—
	R25WC45	32.16	−37.57	2.33	38.62	−39.74	3.18	39.46	−40.96	3.88	−28.20
	R50WC45	12.90	−74.96	2.90	15.26	−76.19	3.04	15.49	−76.82	2.18	−59.68
.55	R0WC55	34.26	—	2.12	44.48	—	2.90	47.73	—	4.38	—
	R25WC55	27.81	−18.83	2.47	34.79	−21.78	3.11	35.70	−25.20	3.49	−20.23
	R50WC55	10.03	−70.71	2.26	11.98	−73.07	2.83	12.21	−74.41	1.89	−56.87

*SD: standard deviation.

25.2% (w/c of .55). While, at the 50% replacement, the reduction rate was 76.12% (w/c of .40), 76.82% (w/c of .45), and 74.41% (w/c of .55). This strength lessening can be labelled by the following reasons: The bonding strength between cement paste and PW surfaces is diminished as a consequence of the smooth surface and flat shape of the plastic particles acting as a barrier and preventing cement paste from adhering to the natural aggregate. As a consequence, the ITZ in concrete containing PET particles is weaker than in control concrete, lowering the resulting compressive strength. Also, the water that did not get absorbed by the PET and did not take part in the reaction between water and cement surrounded these aggregates. This made the bonding weaker and led to the formation of tiny channels that, when dry, could turn into pores" (Qaidi et al., 2022a).

On the other hand, "it is noticed that when increasing the ratio of w/c, the compressive strength decreases, similar to the conventional concrete mixtures. Because, in the case of higher ratios of w/c, the coated surface of the aggregates (surface-coating pozzalanics materials around aggregate) is smaller, and as a result of lower paste volume,

higher bleeding water quantity occurs (Xie et al., 2021; Khan et al., 2022b). The latter (excess water), which is mainly located around PET particles, does not participate in the reaction with the cement, generates a weaker connection between the cement paste and the PET particles, also, generates some small channels which can form pores after drying, causing a decrease in strength" (Ahmad et al., 2022; Al-Tayeb et al., 2022; Tayeh et al., 2022c).

3.5 Splitting tensile strength

To understand the impact of replacing a natural aggregate with a PA with various w/c ratios on the behavior of splitting tensile strength of concrete at 90 days, the experimental results are shown in Table 7. Generally, the results show performance reductions of tensile strength for any pattern of substitution, like compressive strength but with less severe due to the flexible nature of plastic. Accordingly, decreases in split tensile strength can be related to the same reasons as decreases in compressive strength.

FIGURE 11
Stress-strain curve for cylinders with different ratio of PET and: **(A)** .40 w/c; **(B)** .45 w/c; and **(C)** .55 w/c.

3.5.1 Splitting tensile test failure modes

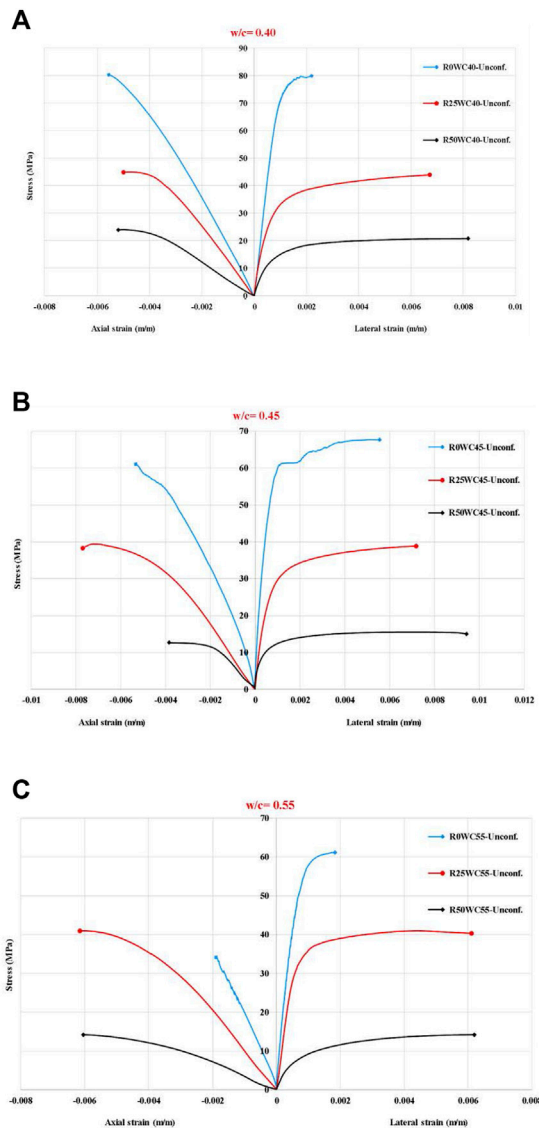From the failure patterns for both PET-containing and non-containing concrete, the splitting failures of PA concrete specimens did not show the typical brittle failure that was noted in the control concrete case. In other words, the inclusion of PW aggregates in concrete changed the concrete specimen fracture mode from brittle to more ductile failure. It was also noted that the concrete control specimens had a sudden breakage accompanied by sound. In contrast, the failure occurred smoothly without sound during breaking for specimens with PAs. This behavior is possible because of (i) according to Azhdarpour et al., 2016, the existence of flexible plastic particles at failure starting points. In this location (at the surfaces of failure), a part of the shear stress is transformed into tensile stress to beat the tensile strength of the PW. Also, plastic particles withstand part of the stress applied before being isolated from other materials. In other words, the plastic aggregates having angular

and flat form can serve as a bridge between the two split parts. In contrast, fine aggregates are semi-spherical and brittle, causing them to separate from the surrounding cement before failure; and (ii) in specimens without PW, a failure occurs in the matrix around the aggregates and through coarse aggregate in the ITZ. Whereas in PET-concrete, failure mainly occurs around PET particles because of the elastic modulus mismatch and, also, the poor bond strength between cement paste and PET PW aggregate. This remark is compatible with the observation of Kou et al. (2009). Besides, the pores and cavities have appeared on the specimen external surface in honeycomb form. These observations are in line with those of Albano et al. (2009).

3.6 Stress-strain behavior

The stress-strain curves governed from compression tests, with different percentages of PET quantity and w/c, are plotted in Figure 11. From the data presented, "for a constant w/c ratio, it can be noticed that: (i) PET-concrete achieved the highest strain increase; and (ii) the peak compressive stress is less at a high PA level, but the corresponding strains are higher. In other words, due to the high flexibility of plastic, the ductility behavior will be enhanced at high PA substitutions. But, compared to the control concrete, the peak compressive stress was lower. Consequently, these reductions impact the stress-strain graph and lead to a decrease in the gradient of the graph during its linear elastic phase" (Qaidi et al., 2022a).

3.7 UPV

UPV is a non-destructive test to verify concrete uniformity and quality. Durability and concrete strength are evaluated *via* the concrete specimen by determining the speed of an ultrasonic pulse through the concrete. Mostly, pulse velocity is influenced by the moisture quantity, density, and elasticity of the material (Akçaözoğlu et al., 2013). Figure 12 presents the UPV performance at different curing ages (7, 28, 90 days) for concrete specimens with different PET quantity and w/c ratios. Each value shown is an average of three cubes. Results indicate that UPV decreases by increasing the PET quantity in the mix. Such behavior can be attributed to: (i) the incorporation of PET directly affects the porosity of the concrete (cavities are formed), which in turn attenuates the velocity of the ultrasonic waves: and (ii) plastic particles have a plate structure (flat and angular shape), which has a role in becoming the refractive limit of ultrasonic waves. In contrast, as shown in Figure 12, it can be gotten that the UPV raised with curing age due to improving the chemical and physical characteristics of concrete as a result of continuing the hydration reactions. On the other hand, one can recognize from Figure 12, that the UPV declines as the w/c ratio increases. This is attributable to extra water stored in the pores which leave empty holes in the concrete upon hardening. Such outcomes have already been confirmed by Albano et al. (2009); Rahmani et al. (2013).

3.8 Theoretical thermal conductivity

To increase understanding of the impact of the substitute of normal fine aggregate with a PA with various w/c ratios on the
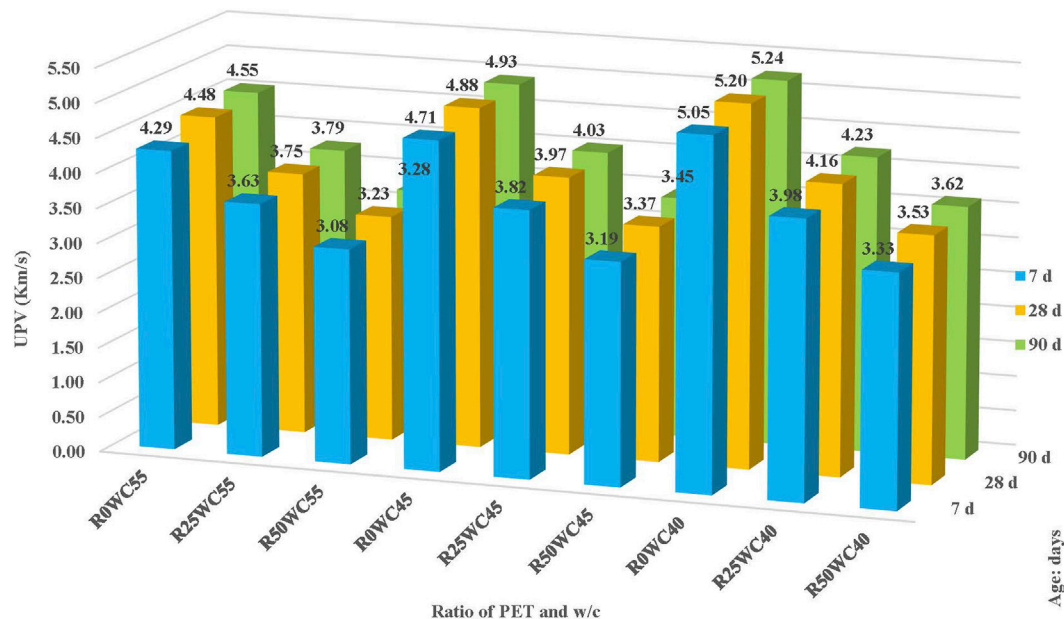
FIGURE 12
UPV test results.

TABLE 8 Thermal conductivity test results.

w/c	PET (%)	Dry density (kg/m³)		Theoretical thermal conductivity (W/mK)	
		28 days	Ref	ACI-122R (2002)	
			$k_c =$	$0.072e^{0.00125d}$	Variation (%)
.40	0	2,388.19	—	1.424	—
	25	2,274.49	—	1.236	−13.25
	50	1993.40	—	.867	−38.95
.45	0	2,376.14	—	1.403	—
	25	2,285.93	—	1.253	−10.66
	50	1964.92	—	.839	−40.19
.55	0	2,347.49	—	1.354	—
	25	2,247.09	—	1.194	−11.79
	50	1839.77	—	.717	−46.99

k_c = the coefficient of thermal conductivity for concrete (W/mK); d = oven-dry density (kg/m 3).

thermal conductivity (k_c) behavior of concrete, the theoretical results obtained by the exponential equation provided by ACI-122R (2002) are presented in Table 8. Moreover, as this study mentioned earlier, the coefficient of Kc of this equation depends on the form of aggregate utilized in the mixtures of concrete. From the data presented, it can be found that with an increase in the quantity of PET aggregates, at a constant ratio of w/c, a significant decrease in Kc occurs. The reason for this decrease is attributed to (i) the PET aggregate had lower Kc (.15–.24 W/mK), compared with natural aggregate (2 W/mK), as stated by Hannawi

et al. (2010). "Therefore, the PET aggregates act to slow thermal heat spread, causing a decline in Kc; and (ii) the presence of a large number of pores in the structure of PET-concrete, which reduces the Kc as a result of the low Kc of the air in these voids" (Akçaözoğlu et al., 2013).

On the other hand, from the data presented in Table 8, one can notice that the maximum reduction in Kc value is 46.99% (kc = .71 W/mK) for 50% replacement of PET (w/c ratio of .55), in comparison with control concrete (kc = 1.35 W/mK). Consequently, these composites (50% PET with .55 w/c) could be utilized as a bearing
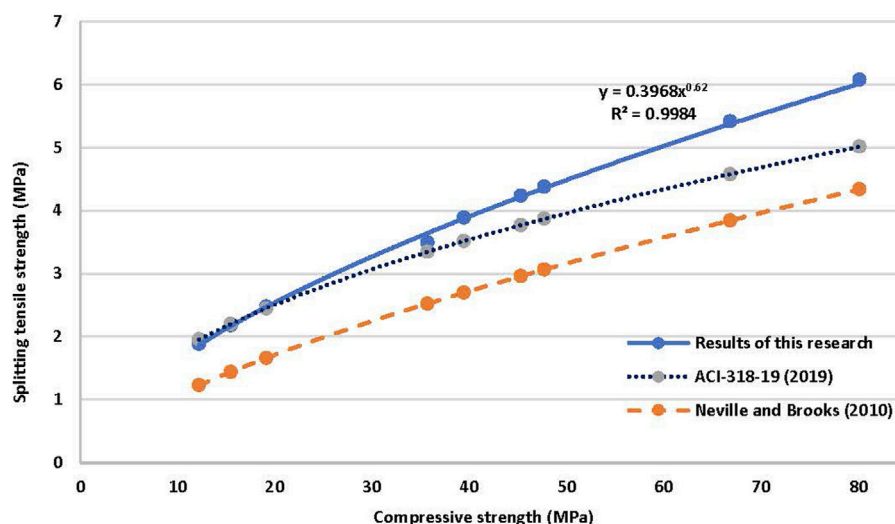
FIGURE 13
The relationship between the concrete compressive strength and split tensile strength at 90 days.
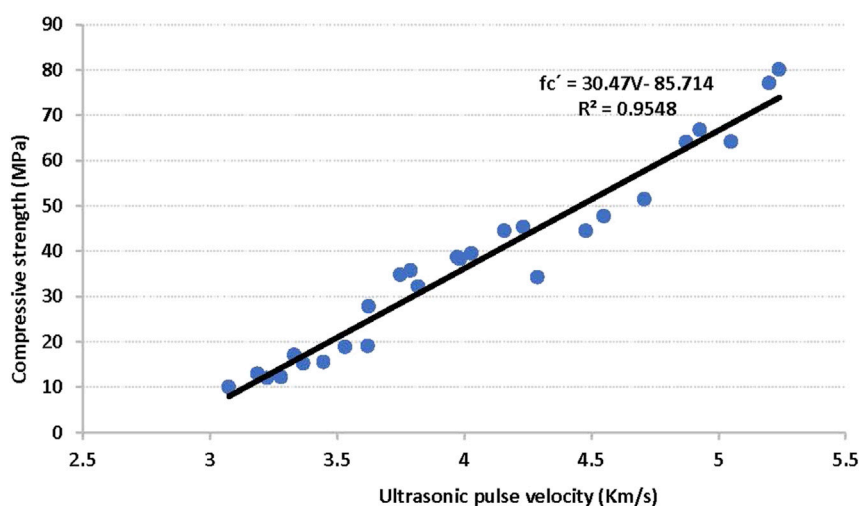
FIGURE 14
The relationship between the properties of concrete for its compressive strength and UPV at 7, 28, and 90 days.

insulator according to RILEM-LC2 (1978) (kc sample <.75 W/mK,; $f_c' > 3.5$ MPa).

3.9 Relationship between PET-Concrete characteristics

3.9.1 Relationship between compressive and splitting tensile strengths

Figure 13 presents the relationship between the concrete compressive strength and split tensile strength at 90 days for several PET proportions and w/c ratios. Besides, the presented figure compares the relationship with that of other studies by

Neville and Brooks (2010); ACI-318-19 (2019). Based on Figure 13, correlation follows a direct relationship. The related experimental expression derived from this analysis is:

$$f_t = 0.3968 f_c^{0.62} \qquad (1)$$

The empirical relations of Neville and Brooks (2010); ACI-318-19 (2019), respectively, are expressed as:

$$f_t = 0.23 f_c^{0.67} \qquad (2)$$

$$f_t = 0.56 f_c^{0.5} \qquad (3)$$

As shown in Figure 13, it was observed that the ACI Building Code Eq. 3 ACI-318-19 (2019) gives a ratio closer to Eq. 1, as it appears to have
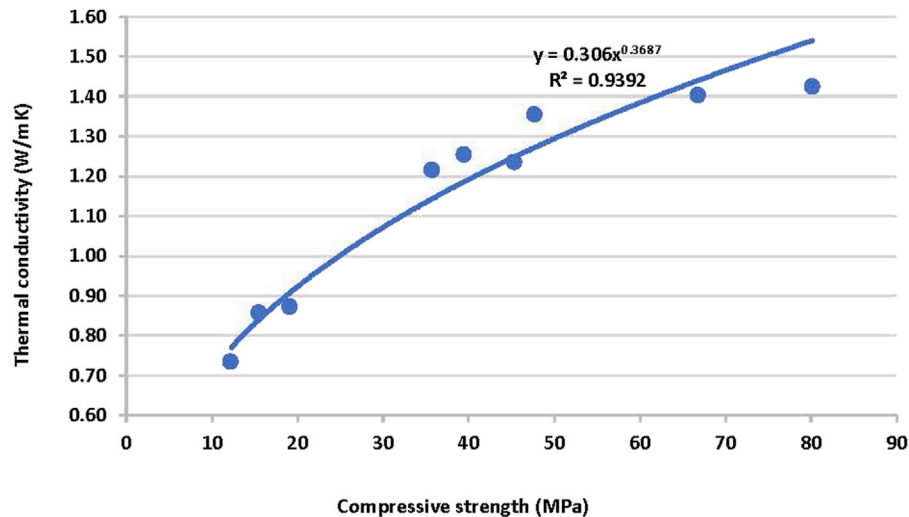
FIGURE 15
Relationship between compressive strength and thermal conductivity.
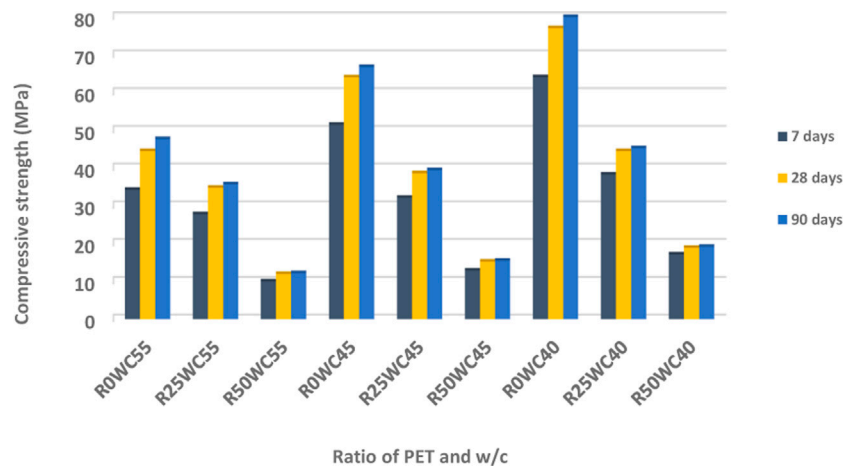
FIGURE 16
Relationship between compressive strength and curing time.

reduced the tensile strength of the split. While Eq. 2 that proposed by Neville and Brooks (2010) underestimates considerably the split tensile strength of the respective PET substitution.

3.9.2 Relationship between compressive strength and UPV

Figure 14 presents the relationship between the concrete compressive strength and UPV at 7, 28, and 90 days, for several PET proportions and w/c ratios. It can be remarked that the compression strength increases with an increase in ultrasonic speed for all w/c ratios. The experimental data are correlated to Eq. 4 where (V) is the UPV, and (fc′) is the compressive strength. Moreover, the coefficient of determination (R2) equals .95, thereby indicating a strong correlation.

$$f_c{}' = 30.47V - 85.714 \qquad (4)$$

3.9.3 Relationship between compressive strength and thermal conductivity

Figure 15 presents the relationship between compressive strengths and thermal conductivity at 28 days, for several PET proportions and w/c ratios. It remarks a direct relationship between them since R2 is .955.

3.9.4 Relationship between compressive strength and curing time

Figure 16 presents the relationship between compressive strength and curing time at 7, 28, and 90 days, for several PET proportions and w/c ratios. Generally, the rate of strength, for the concrete-PET and the control concrete, has a similar pattern. The majority of mixes of PET-concrete were able to produce about 75%–90% of their corresponding 28-day strength at 7 days. Accordingly, it is close to controlling concrete.

Even so, it was found that the early development of the PET-concrete strength was somewhat changed from that of the control concrete. In Figure 16, the strength comparison showed that the PET-concrete mixtures developed within (75%–90%) of their 28 days strength in 7 days. In contrast, control concrete developed within (70%–80%). This behavior has also been studied by Tang et al. (2008), who mentioned that the probable cause could be because of the introduction of a PS aggregate, which would reduce the capacity of the specific thermal concrete causing a decreased heat loss to the environmental surroundings through the hydration process. Tang et al. (2008) based his conclusion on the investigation of Wang et al. (2007) who carried out a calorimetric test to calculate the temperature history of freshly concrete made from PS aggregate for 72 h. Overall, it can be an inference that concrete with a PET aggregate can have a superior accelerated early age because of the greater and faster heat produced during hydration.

4 Conclusion

This study investigated the influence of PET aggregate and w/c on the properties of concrete. Based on the results obtained from this experimental study, the following conclusions can be drawn.

1 Increasing the amount of PA as a partial replacement for sand, regardless of the w/c ratio, affects the workability of fresh concrete relative to the control mixture.

2 There is a decrease in the fresh density and dry density of PET-containing concrete with increasing replacement ratio and w/c ratios.

3 Concrete with 50% PA at .40-.55 w/c, had a dry density below 2000 kg/m3. Thus, this concrete can be categorized as lightweight concrete.

4 The percentages of water absorption and porosity in concrete using PET aggregate rise as the replacement ratios and w/c increase.

5 As the PET substitution ratio and w/c ratio increased, the compressive strength of all PET-concrete mixes decreased compared to the control concrete for all curing ages. Therefore, PET-concrete is recommended for non-structural applications (such as pavements and sports stadiums, wall panels, and channel liners), with a replacement ratio of no more than 25%.

6 The reason for the decline of the compressive strength is the reduction of cement hydration due to the following factors: (i) the weakness of the ITZ as a result of the smooth surface and flat shape of the plastic particles; and ii) the hydrophobic nature of the PET particles that has limited the entry of water into the concrete microstructure during the curing process.

7 It can be concluded from the stress-strain curves that with the increase of the PET quantity, the maximum stress increases significantly, and the plasticity behavior is improved due to the high elasticity of the plastic particles, but compared to the conventional concrete, the peak compressive stress was lower.

8 Because of the high porosity of PET-concrete and the lamination structure (angularity) of plastic particles, the UPV decreased at all curing ages as the proportion of PET particles and w/c ratios increased.

5 Recommendations

The following points suggest potential future research on this topic:

1. Studying the relationship between plastic concrete and steel reinforcement.
2. Studying the characteristics of PET and how the source influences concrete behavior.
3. Evaluating and comparing the entire construction monetary cost of making concrete with plastic *versus* traditional conventional concrete.
4. Studying the impact of combining plastic aggregate and fibers on the characteristics of concrete.
5. Studying the long-term durability of concrete with PET flakes.

Data availability statement

The original contributions presented in the study are included in the article/Supplementary Material, further inquiries can be directed to the corresponding authors.

Author contributions

Conception and design of study: YA-K, SQ, and IH; Acquisition of data: YÖ, AFD, MS, and VS; Analysis and/or interpretation of data: SQ. Drafting the manuscript: YA-K, SQ, IH, YÖ, AFD, MS, and VS; Revising the manuscript critically for important intellectual content: AFD, MS, AND VS. Approval of the version of the manuscript to be published: YA-K, SQ, IH, YÖ, AFD, MS, and VS.

Funding

Conflict of interest

The authors declare that the research was conducted in the absence of any commercial or financial relationships that could be construed as a potential conflict of interest.

Publisher's note

All claims expressed in this article are solely those of the authors and do not necessarily represent those of their affiliated organizations, or those of the publisher, the editors and the reviewers. Any product that may be evaluated in this article, or claim that may be made by its manufacturer, is not guaranteed or endorsed by the publisher.

References

Aci-122r (2002). *Guide to thermal properties of concrete and masonry systems*. Michigan, PA: ACI- Institute.

Aci-211-1-91 (2002). *Standard practice for selecting proportions for normal, heavyweight, and mass concrete (Reapproved 2002)*. ACI- Institute.

Aci-318-19 (2019). *Building Code requirements for structural concrete (ACI 318-19) and commentary (ACI 318r-19)*. ACI Committee 318.

Ahmed, H. U., Mohammed, A. A., Rafiq, S., Mohammed, A. S., Mosavi, A., Sor, N. H., et al. (2021). Compressive strength of sustainable geopolymer concrete composites: A state-of-the-art review. *Sustainability* 13, 13502. doi:10.3390/su132413502

Ahmad, J., Majdi, A., Babeker Elhag, A., Deifalla, A. F., Soomro, M., Isleem, H. F., et al. (2022). A step towards sustainable concrete with substitution of plastic waste in concrete: Overview on mechanical, durability and microstructure analysis. *Crystals* 12, 944. doi:10.3390/cryst12070944

Akçaözoğlu, S., Atiş, C. D., and Akçaözoğlu, K. (2010). An investigation on the use of shredded waste PET bottles as aggregate in lightweight concrete. *Waste Manag.* 30, 285–290. doi:10.1016/j.wasman.2009.09.033

Akçaözoğlu, S., Akçaözoğlu, K., and Atiş, C. D. (2013). Thermal conductivity, compressive strength and ultrasonic wave velocity of cementitious composite containing waste PET lightweight aggregate (WPLA). *Compos. Part B Eng.* 45, 721–726. doi:10.1016/j.compositesb.2012.09.012

Akeed, M. H., Qaidi, S., Ahmed, H. U., Faraj, R. H., Mohammed, A. S., Emad, W., et al. (2022). Ultra-high-performance fiber-reinforced concrete. Part IV: Durability properties, cost assessment, applications, and challenges. *Case Stud. Constr. Mater.* 17, e01271. doi:10.1016/j.cscm.2022.e01271

Al-Tayeb, M. M., Aisheh, Y. I. A., Qaidi, S. M. A., and Tayeh, B. A. (2022). Experimental and simulation study on the impact resistance of concrete to replace high amounts of fine aggregate with plastic waste. *Case Stud. Constr. Mater.* 17, e01324. doi:10.1016/j.cscm.2022.e01324

Albano, C., Camacho, N., Hernández, M., Matheus, A., and Gutierrez, A. (2009). Influence of content and particle size of waste pet bottles on concrete behavior at different w/c ratios. *Waste Manag.* 29, 2707–2716. doi:10.1016/j.wasman.2009.05.007

Ali, S. S., Elsamahy, T., Al-Tohamy, R., Zhu, D., Mahmoud, Y. a.-G., Koutra, E., et al. (2021). Plastic wastes biodegradation: Mechanisms, challenges and future prospects. *Sci. Total Environ.* 780, 146590. doi:10.1016/j.scitotenv.2021.146590

Almeshal, I., Al-Tayeb, M. M., Qaidi, S. M. A., Abu Bakar, B. H., and Tayeh, B. A. (2022). Mechanical properties of eco-friendly cements-based glass powder in aggressive medium. *Mater. Today Proc.* 58, 1582–1587. doi:10.1016/j.matpr.2022.03.613

Astm-C138 (2015). *Unit weight, yield, and gravimetric air content of concrete*. West Conshohocken, PA: ASTM International.

Astm-C142 (2015). *Slump of hydraulic cement concrete*. West Conshohocken, PA: ASTM International.

Astm-C192/C192m (2009). *Standard practice for making and curing concrete test specimens in the laboratory*. West Conshohocken, PA: ASTM International.

Astm-C39 (2012). *Standard test method for compressive strength of cylindrical concrete specimens*. Chủ biên.

Astm-C496 (2008). *ASTM C496/C496M-04e1 standard test method for splitting tensile strength of cylindrical concrete specimens*. Annu B ASTM Stand.

Astm-C597 (2009). *597, Standard test method for pulse velocity through concrete*. West Conshohocken, PA: ASTM International.

Astm-C642 (2015). *Standard test method for density, absorption, and voids in hardened concrete*. West Conshohocken, PA: ASTM International.

Astm-International (2015). *ASTM-C494: Standard specification for chemical admixtures for concrete*. West Conshohocken, PA): Astm-International.

Azhdarpour, A. M., Nikoudel, M. R., and Taheri, M. (2016). The effect of using polyethylene terephthalate particles on physical and strength-related properties of concrete; a laboratory evaluation. *Constr. Build. Mater.* 109, 55–62. doi:10.1016/j.conbuildmat.2016.01.056

Babafemi, A. J., Šavija, B., Paul, S. C., and Anggraini, V. (2018). Engineering properties of concrete with waste recycled plastic: A review. *Sustainability* 10, 3875. doi:10.3390/su10113875

Barreto, E. D. S., Stafanato, K. V., Marvila, M. T., De Azevedo, A. R. G., Ali, M., Pereira, R. M. L., et al. (2021). Clay ceramic waste as pozzolan constituent in cement for structural concrete. *Materials* 14, 2917. doi:10.3390/ma14112917

Cao, M., and Khan, M. (2021). Effectiveness of multiscale hybrid fiber reinforced cementitious composites under single degree of freedom hydraulic shaking table. *Struct. Concr.* 22, 535–549. doi:10.1002/suco.201900228

Choi, Y.-W., Moon, D.-J., Chung, J.-S., and Cho, S.-K. (2005). Effects of waste PET bottles aggregate on the properties of concrete. *Cem. Concr. Res.* 35, 776–781. doi:10.1016/j.cemconres.2004.05.014

Cosqc (1984a). *IQS No. 5: Portland cement*. Baghdad, Iraq: Central Organization for Standardization and Quality Control.

Cosqc (1984b). *IQS No. 45: Aggregate form natural sources for concrete and building construction*. Baghdad, Iraq: Central Organization for Standardization and Quality Control.

De Azevedo, A. R., Marvila, M. T., Ali, M., Khan, M. I., Masood, F., and Vieira, C. M. F. (2021). Effect of the addition and processing of glass polishing waste on the durability of geopolymeric mortars. *Case Stud. Constr. Mater.* 15, e00662. doi:10.1016/j.cscm.2021.e00662

Emad, W., Mohammed, A. S., Bras, A., Asteris, P. G., Kurda, R., Muhammed, Z., et al. (2022). Metamodel techniques to estimate the compressive strength of UHPFRC using various mix proportions and a high range of curing temperatures. *Constr. Build. Mater.* 349, 128737. doi:10.1016/j.conbuildmat.2022.128737

Faraj, R. H., Ahmed, H. U., Rafiq, S., Sor, N. H., Ibrahim, D. F., and Qaidi, S. M. A. (2022). Performance of self-compacting mortars modified with nanoparticles: A systematic review and modeling. *Clean. Mater.* 4, 100086. doi:10.1016/j.clema.2022.100086

Farhana, Z., Kamarudin, H., Rahmat, A., and Al Bakri, A. (2015). "The relationship between water absorption and porosity for geopolymer paste," in *Materials science forum: Trans tech publ*, 166–172.

Fediuk, R., and Ali, M. (2022). Recyclable materials for ecofriendly technology. *Materials* 15, 7133. doi:10.3390/ma15207133

Hannawi, K., Prince, W., and Kamali-Bernard, S. (2010). Effect of thermoplastic aggregates incorporation on physical, mechanical and transfer behaviour of cementitious materials. *Waste Biomass Valorization* 1, 251–259. doi:10.1007/s12649-010-9021-y

He, X., Yuhua, Z., Qaidi, S., Isleem, H. F., Zaid, O., Althoey, F., et al. (2022). Mine tailings-based geopolymers: A comprehensive review. *Ceram. Int.* 48, 24192–24212. doi:10.1016/j.ceramint.2022.05.345

Heredia, N. V. (2018). *Incorporation of waste polyethylene terephthalate (PET) into concrete using statistical mixture design*. Newfoundland: Masters, Memorial University of Newfoundland.

Khan, M. A. (2021). Towards progressive debonding in composite RC beams subjected to thermo-mechanical bending with boundary constraints–A new analytical solution. *Compos. Struct.* 274, 114334. doi:10.1016/j.compstruct.2021.114334

Khan, M. A. (2022). Bond parameters for peeling and debonding in thin plated RC beams subjected to mixed mode loading–Framework. *Adv. Struct. Eng.* 25, 662–682. doi:10.1177/13694332211065184

Khan, M. A. (2023). "Integrating BIM with ERP systems towards an integrated multi-user interactive database: Reverse-bim approach," in *Recent trends in construction technology and management* (Springer), 209–220.

Khan, M. A., Irfan, S., Rizvi, Z., and Ahmad, J. (2019). A numerical study on the validation of thermal formulations towards the behaviour of RC beams. *Mater. Today Proc.* 17, 227–234. doi:10.1016/j.matpr.2019.06.423

Khan, M., Imam, M. K., Irshad, K., Ali, H. M., Hasan, M. A., and Islam, S. (2021a). Comparative overview of the performance of cementitious and non-cementitious nanomaterials in mortar at normal and elevated temperatures. *Nanomaterials* 11, 911. doi:10.3390/nano11040911

Khan, M., Sutanto, M. H., Napiah, M. B., Zoorob, S. E., Al-Sabaeei, A. M., Rafiq, W., et al. (2021b). Investigating the mechanical properties and fuel spillage resistance of semi-flexible pavement surfacing containing irradiated waste PET based grouts. *Constr. Build. Mater.* 304, 124641. doi:10.1016/j.conbuildmat.2021.124641

Khan, M., Cao, M., Chu, S., and Ali, M. (2022a). Properties of hybrid steel-basalt fiber reinforced concrete exposed to different surrounding conditions. *Constr. Build. Mater.* 322, 126340. doi:10.1016/j.conbuildmat.2022.126340

Khan, M., Cao, M., Xie, C., and Ali, M. (2022b). Effectiveness of hybrid steel-basalt fiber reinforced concrete under compression. *Case Stud. Constr. Mater.* 16, e00941. doi:10.1016/j.cscm.2022.e00941

Khan, M., Lao, J., and Dai, J.-G.The Hong Kong Polytechnic University, Hong Kong, China (2022c). Comparative study of advanced computational techniques for estimating the compressive strength of UHPC. *J. Asian Concr. Fed.* 8, 51–68. doi:10.18702/acf.2022.6.8.1.51

Khan, M. I., Sutanto, M. H., Yusoff, N. I. M., Zoorob, S. E., Rafiq, W., Ali, M., et al. (2022d). Cementitious grouts for semi-flexible pavement surfaces—a review. *Materials* 15, 5466. doi:10.3390/ma15155466

Khoshkenari, A. G., Shafigh, P., Moghimi, M., and Mahmud, H. B. (2014). The role of 0–2 mm fine recycled concrete aggregate on the compressive and splitting tensile strengths of recycled concrete aggregate concrete. *Mater. Des.* 64, 345–354. doi:10.1016/j.matdes.2014.07.048

Kılıç, A., Atiş, C. D., Yaşar, E., and Özcan, F. (2003). High-strength lightweight concrete made with scoria aggregate containing mineral admixtures. *Cem. Concr. Res.* 33, 1595–1599. doi:10.1016/s0008-8846(03)00131-5

Kore, S. D. (2018). Sustainable utilization of plastic waste in concrete mixes-a review. *J. Build. Mater. Struct.* 5, 212–217. doi:10.34118/jbms.v5i2.59

Kou, S., Lee, G., Poon, C., and Lai, W. (2009). Properties of lightweight aggregate concrete prepared with PVC granules derived from scraped PVC pipes. *Waste Manag.* 29, 621–628. doi:10.1016/j.wasman.2008.06.014

Kumar, S., Singh, E., Mishra, R., Kumar, A., and Caucci, S. (2021). Utilization of plastic wastes for sustainable environmental management: A review. *ChemSusChem* 14, 3985–4006. doi:10.1002/cssc.202101631

Lesovik, V., Tolstoy, A., Fediuk, R., Amran, M., Ali, M., and De Azevedo, A. R. (2022). Improving the performances of a mortar for 3D printing by mineral modifiers. *Buildings* 12, 1181. doi:10.3390/buildings12081181

Maglad, A. M., Zaid, O., Arbili, M. M., Ascensão, G., Şerbănoiu, A. A., Grădinaru, C. M., et al. (2022). A study on the properties of geopolymer concrete modified with nano graphene oxide. *Buildings* 12, 1066. doi:10.3390/buildings12081066

Neville, A. M., and Brooks, J. J. (2010). *Concrete technology*. Pearson Education Limited.

Plastic-Europe (2019). *An analysis of European plastics production, demand and waste data*, 147. Plastics–the facts.

Qaidi, S., Al-Kamaki, Y. S. S., Al-Mahaidi, R., Mohammed, A. S., Ahmed, H. U., Zaid, O., et al. (2022a). Investigation of the effectiveness of CFRP strengthening of concrete made with recycled waste PET fine plastic aggregate. *PLOS ONE* 17, e0269664. doi:10.1371/journal.pone.0269664

Qaidi, S., Najm, H. M., Abed, S. M., Özkılıç, Y. O., Al Dughaishi, H., Alosta, M., et al. (2022b). Concrete containing waste glass as an environmentally friendly aggregate: A review on fresh and mechanical characteristics. *Materials* 15, 6222. doi:10.3390/ma15186222

Qaidi, S. M. A., Tayeh, B. A., Isleem, H. F., De Azevedo, A. R. G., Ahmed, H. U., and Emad, W. (2022c). Sustainable utilization of red mud waste (bauxite residue) and slag for the production of geopolymer composites: A review. *Case Stud. Constr. Mater.* 16, e00994. doi:10.1016/j.cscm.2022.e00994

Qaidi, S. M. A., and Al-Kamaki, Y. S. S.University of Duhok (2021). State-of-the-Art review: Concrete made of recycled waste PET as fine aggregate. *J. Duhok Univ.* 23, 412–429. doi:10.26682/csjuod.2020.23.2.34

Rahmani, E., Dehestani, M., Beygi, M., Allahyari, H., and Nikbin, I. (2013). On the mechanical properties of concrete containing waste PET particles. *Constr. Build. Mater.* 47, 1302–1308. doi:10.1016/j.conbuildmat.2013.06.041

Rilem-Lc2 (1978). Recommendation: Functional classification of lightweight concrete. *Mater. Struct.* 5, 173–175.

Room, S., Ali, M., Alam, M. A., Khan, U., Ammad, S., and Saad, S. (2021). "Assessment of lightweight Aggregate concrete using textile washing stone," in Proceeding of the 2021 Third International Sustainability and Resilience Conference: Climate Change, Sakheer, Bahrain, November 2021 (IEEE), 327–333.

Shah, S. P., and Wang, K. (2004). "Development of 'green'cement for sustainable concrete using cement kiln dust and fly ash," in Proceedings of the International Workshop on Sustainable Development and Concrete Technology, Beijing, China, May 2004 (Beijing, China: Iowa State University, Ames), 15–23.

Tang, W. C., Lo, Y., and Nadeem, A. (2008). Mechanical and drying shrinkage properties of structural-graded polystyrene aggregate concrete. *Cem. Concr. Compos.* 30, 403–409. doi:10.1016/j.cemconcomp.2008.01.002

Tayeh, B. A., Akeed, M. H., Qaidi, S., and Bakar, B. H. A. (2022a). Influence of microsilica and polypropylene fibers on the fresh and mechanical properties of ultra-high performance geopolymer concrete (UHP-GPC). *Case Stud. Constr. Mater.* 17, e01367. doi:10.1016/j.cscm.2022.e01367

Tayeh, B. A., Akeed, M. H., Qaidi, S., and Bakar, B. H. A. (2022b). Influence of sand grain size distribution and supplementary cementitious materials on the compressive strength of ultrahigh-performance concrete. *Case Stud. Constr. Mater.* 17, e01495. doi:10.1016/j.cscm.2022.e01495

Tayeh, B. A., Akeed, M. H., Qaidi, S., and Bakar, B. H. A. (2022c). Influence of the proportion of materials on the rheology and mechanical strength of ultrahigh-performance concrete. *Case Stud. Constr. Mater.* 17, e01433. doi:10.1016/j.cscm.2022.e01433

Topçu, İ. B., and Uygunoğlu, T. (2007). Properties of autoclaved lightweight aggregate concrete. *Build. Environ.* 42, 4108–4116. doi:10.1016/j.buildenv.2006.11.024

Wang, K., Ge, Z., Grove, J., Ruiz, J. M., Rasmussen, R., and Ferragut, T. (2007). *Developing a simple and rapid test for monitoring the heat evolution of concrete mixtures for both laboratory and field applications.*

Xie, C., Cao, M., Guan, J., Liu, Z., and Khan, M. (2021). Improvement of boundary effect model in multi-scale hybrid fibers reinforced cementitious composite and prediction of its structural failure behavior. *Compos. Part B Eng.* 224, 109219. doi:10.1016/j.compositesb.2021.109219

Zulkernain, N. H., Gani, P., Chuan, N. C., and Uvarajan, T. (2021). Utilisation of plastic waste as aggregate in construction materials: A review. *Constr. Build. Mater.* 296, 123669. doi:10.1016/j.conbuildmat.2021.123669

Finite element, analytical, artificial neural network models for carbon fibre reinforced polymer confined concrete filled steel columns with elliptical cross sections

Haytham F. Isleem[1]*, Daudi Salezi Augustino[2], Ahmed Salih Mohammed[3], Ahmed M. Najemalden[4], P. Jagadesh[5], Shaker Qaidi[6,7] and Mohanad Muayad Sabri Sabri[8]

[1]Department of Construction Management, Qujing Normal University, Qujing, China, [2]Department of Structural and Construction Engineering, University of Dar es Salaam, Dar es Salaam, Tanzania, [3]College of Engineering, University of Sulaimani, Sulaymaniyah, Iraq, [4]Highways and Bridges Engineering Department, Technical College of Engineering, Duhok Polytechnic University, Duhok, Iraq, [5]Department of Civil Engineering, Coimbatore Institute of Technology, Coimbatore, India, [6]Department of Civil Engineering, College of Engineering, University of Duhok, Duhok, Iraq, [7]Department of Civil Engineering, College of Engineering, Nawroz University, Duhok, Iraq, [8]Peter the Great St. Petersburg Polytechnic University, St. Petersburg, Russia

In the present era of architecture, different cross-sectional shapes of structural concrete elements have been utilized. However, this change in shape has a significant effect on load-carrying capacity. To restore this, the use of column confinements with elliptical sections has gained attention. This paper aim to investigate the effect of elliptical shape sections of confined concrete reinforced with Carbon Fiber Reinforced Polymer (CFRP) and steel tube on axial load-carrying capacity. This study is achieved using following tools Finite Element (FE) in Abaqus and Artificial Neural Networks (ANN) modeling. The study involved a 500-mm-high column with three sets of aspect ratios: 1.0, 1.5, and 2.0. In each aspect ratio, three different layers of CFRP were used, i.e., .167, .334, and .501-mm. Analytical results showed that with the increase in aspect ratio from 1 to 2, there is a decrease in ultimate axial load of about 23.2% on average. In addition, the combined confining pressure of steel tube and CFRP increases with a decrease in dilation angle as the number of CFRP layers increases. The failure mode for the column with a large aspect ratio is local buckling at its mid-height along the minor axis. The result showed a good correlation between FE and experimental results of ultimate stress and strains, with a mean squared error of 2.27 and .001, respectively. Moreover, ANN and analytical models showed a delightful correlation of R^2 of .97 for stress models and .88 for strain models, respectively. The elliptical concrete section of the column confined with steel tubes can be adopted for a new architectural type of construction; however, with more than three aspect ratios, the wrapping of the section with CFRP jackets is highly recommended.

1 Introduction

The durability of concrete has been a major concern for concrete structural elements exposed to chloride and salty environments for many years. Solution for the above problem is to pour the concrete in confining jackets, which control the exposure of concrete to an aggressive environment. Numerous studies have investigated concrete columns enclosed by different materials (Guo et al., 2009; Isleem et al., 2021) . These jackets are Poly Vinyl Chloride (PVC), Fiber Reinforced Polymer (FRP), steel tubes, and different fibers, among others. Under axial compression, the use of PVC increases the ductility of the concrete column by 1.28 to 2.35 times the unconfined equivalent concrete but the loss in confining strength of PVC when the temperature rises (Woldemariam et al., 2019). To overcome the above-stated problem, the introduction of high-strength steel tubes on behalf of PVC tubes is reported in the literature. However, when a specimen is exposed to a high corrosion environment, several researchers introduce the FRP as a wrapping element which not only increases strength but also enhances both the elastic stiffness and post-strain hardening (Zeng et al., 2021).

The introduction of FRP composites in the civil engineering sector offers numerous benefits in comparison to conventional building materials. Even engineers and researchers have observed a rise in the use of FRP composites in civil engineering applications, both in existing and retrofitted reinforced structures (Zeng et al., 2020; Abdel et al., 2022). The addition of different types of fibers to the specimen improves the concrete's post-cracking behavior, energy absorption capacity, and toughness nature as reported in the literatures (Khan and Ali, 2016; Amin and Tayeh, 2020; Zeyad et al., 2022a; Khan and Ali, 2022). Several researchers recommend using agricultural and non-agricultural industrial waste for concrete production to improve its quality on pre-loading and post-loading behavior (Amin et al., 2021; Azevedo et al., 2022; Jagadesh et al., 2022; Saad et al., 2022). According to the literature (Elchalakani et al., 2020; Zeng et al., 2020), the use of FRP as wrapping materials for column specimens increases their load-carrying capacity and other associated properties. It can be concluded that the different types of fiber or fiber composite materials, such as FRP, that use an integral part, show no better results when compared to the use of FRP as an external wrapping material. The usage of Carbon Fiber Reinforced Polymer (CFRP) in columns will enhance the material's ductility when subjected to lateral loads is reported by Zeng

et al. (2020). A 1.0 mm CFRP layer showed a 27% increase in the axial capacity of the column compared to a column without CFRP jackets (Abdel et al., 2022).

In column specimens, the confinement effect of core concrete depends on the material strength and section size (Sun et al., 2022). The elliptical section reduces the axial capacity, leading to local buckling at the mid-height. Effects on several parameters, like longitudinal reinforcement, hoop reinforcement, slenderness ratio, and so on, also affect the load-carrying capacity of column specimens (Isleem et al., 2022a; Elchalakani et al., 2020). Studies have been conducted both numerically and experimentally on composite columns like concrete-filled PVC tubes (Isleem et al., 2022b) and concrete-filled steel tubes (He et al., 2019).

(Abadel et al., 2022) Inferred in 2022 that the use of both welded wire mesh and CFRP in retrofitting columns is cost-effective; however, the use of CFRP increases ductility as compared to welded wire jackets. This ductility in the structural column increases the column's post-load carrying capacity after initial elastic stiffness. (Gemi et al., 2021) suggested in 2021 that the use of different wrappings such as Glass Fiber Reinforced Polymer (GFRP) composite on beams improved energy dissipation and load-carrying capacity to 394% and 237%, respectively. Using FRP wrapping on pultruded beams infilled with reinforced concrete significantly improved ductility, load capacity, and energy dissipation capacity. In 2022, (Gemi et al., 2022), observed that GFRP and CFRP increased the initial stiffness with a full wrapping effect of 44.2% and 65.4%, respectively. In structural concrete members such as beams, the introduction of an opening tremendously affects the shear capacity, which steel rebar alone cannot restore (Augustino et al., 2022a). Restoring this capacity through external strength is limited by the type of opening. The strengthening technique using CFRP increased load-carrying capacity and ductility for openings with a diameter-to-beam depth ratio (D/H) of less than 3 is reported by Aksoylu et al. (2020). From the above discussion, it can be concluded that the introduction of FRP (like CFRP, GFRP, etc.) results not only in increasing the load-carrying capacity of specimens and their associated properties like ductility, energy dissipation, and so on, but also protects the inner specimen from harmful outer agents.

The confined concrete column dilates as plasticity increases. This lateral volumetric change of strain after the composite has yielded results in high confining pressure on the confining material, which tends to
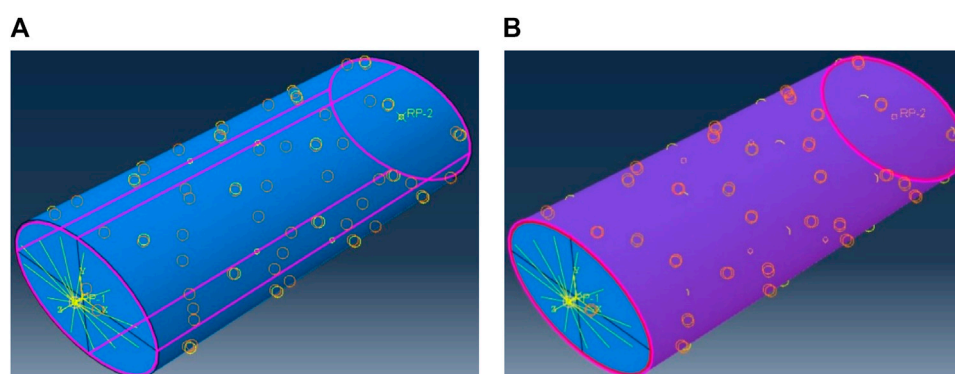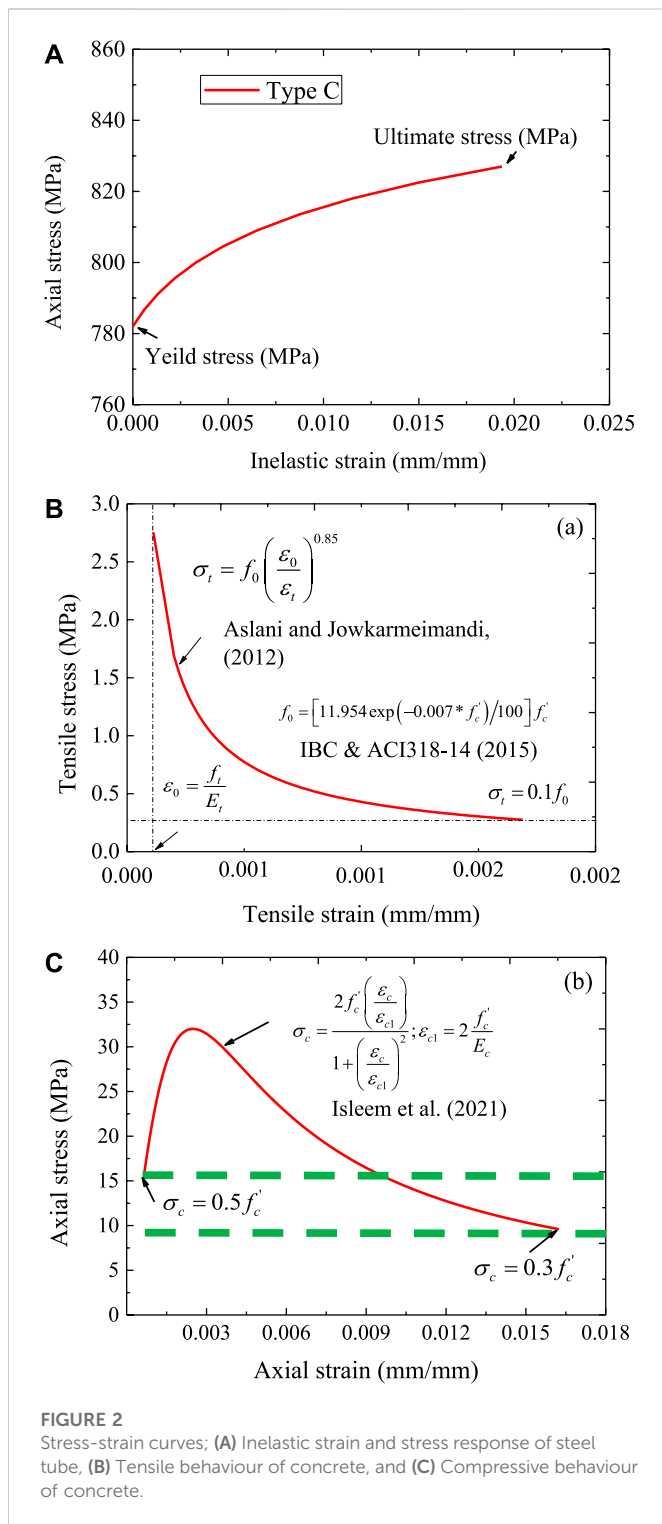

FIGURE 1
Tie constraints used assembling concrete, steel tube, and CFRP; **(A)** between concrete and steel tube, and **(B)** between steel tube and CFRP.

FIGURE 2
Stress–strain curves; **(A)** Inelastic strain and stress response of steel tube, **(B)** Tensile behaviour of concrete, and **(C)** Compressive behaviour of concrete.

incompressible (Abaqus et al., 2004). This indicates that at high confining pressure, the dilation angle reduces.

The increase in compressive strength has less ductility compared to normal concrete, leading to less lateral expansion of concrete and a small confining pressure (Jiang et al., 2007; Augustino et al., 2022b). Regardless of whether FRP-confined concrete columns are loaded monotonically or cyclically, the stress-strain curve envelopes follow the same trend (Ozbakkaloglu and Akin, 2012). This trend indicates that the effectiveness of confining FRP jackets depends on the strength of individual jackets and the thickness of layers. CFRP jackets in the industry can provide the safety level of the elliptical section on its local buckling as the aspect ratio increases. The usage of steel tubes not only results in higher load-bearing capacity of columns, but the introduction of CFRP as a wrapping element on steel tubes leads to further increase in the load-bearing capacity of composite columns. Several experimental and numerical modeling studies (Liu et al., 2017; Cai et al., 2019) have been conducted on the behavior of elliptical concrete-filled steel tubes and reported that the influence of elliptical shape on load carrying capacity of column. Elchalakani et al. (2020) tested 15 solid, circular, GFRP-reinforced concrete columns and reported an increase in ductility for both axial and eccentric loading conditions.

Composite tubes like concrete-filled steel tubes and steel-embedded concrete specimens have increased usage in civil construction applications due to their auspicious performance resulting from the composite action between the individual components (Isleem et al., 2022a). Different geometrical sections provide typical features that bring many advantages and disadvantages, enabling columns to be oriented to carry the external load most efficiently (Lam and Testo, 2008). To provide structural engineers with viable options, the effect on the elliptical cross-sections of various parameters such as confined concrete strength, tube thickness, aspect ratio, etc. was investigated in this study.

Most experimental tests use resources, which necessitated the use of an artificial intelligence algorithm to predict parameters. However, caution is required, such as data partitioning, training, and testing to avoid the overfitting/underfitting of results (Matlab, 2004; Althoey et al., 2022). A comparison of experimental with analytical studies to ensure the quality of analytical results has been reported by (Khan et al., 2021) in 2021. To reduce the cost of experimental work, the time required to experiment, and the manpower involved with it, researchers are pushed to conduct analytical studies (Khan and Ali, 2020). In recent days, researchers have recommended analytical methods to understand the behavior (load-carrying capacity, ultimate strain, etc.,) of composite members (Khan and Ali, 2020b). The experimental setup of the confined concrete column using steel tube and CFRP is too demanding and requires more resources to be deployed. The use of finite element (FE), analytical, and ANN modeling could be an alternative approach to the experimental investigation of these composites.

1.1 Novelty of research

In literature, the effect of aspect ratio on concrete-filled steel columns is limited. Even though several works discuss the effect of aspect ratio on the different types of column specimens (steel columns, concrete columns, and concrete columns wrapped in FRP) with different geometrical natures (circular, rectangular, and square).

advance the second linear phase of the composite (Lin et al., 2014). The axial behaviour of composite columns is influenced by the concrete strength is noted by Khan et al. (2020); Zeyad et al. (2022b). In most instances, the dilatancy of concrete decreases as its grade increases (Chung et al., 2002). In the plastic flow of concrete, the concrete-damaged plasticity utilizes materials with almost the same dilation angle throughout the confinement. This is done through a default eccentricity of .1 in Abaqus; however, a small dilation angle approaching zero indicates that the inelastic deformation is

FIGURE 3
Effect of aspect ratio and confining pressure on dilation angle; **(A)** Aspect ratio of 1.0, **(B)** Aspect ratio of 1.5, **(C)** Aspect ratio of 2.0 and **(D)** Aspect ratio of 1.0,1.5 and 2.0.

TABLE 1 Mechanical properties of CFRP (Zhang et al., 2022; Jiang et al., 2014).

E1 (MPa)	E2 (MPa)	E3 (MPa)	Nu12	Nu13	Nu23	G12 (MPa)	G13 (MPa)	G23 (MPa)
229600	2900	2900	.26	.28	.26	3920	1,130	3920

However, according to the knowledge of the authors, there is no FEM simulation related to the CFRP-wrapped, confined concrete-filled steel columns with elliptical cross sections. Hence, in this study, the effect of aspect ratio on the CFRP-wrapped confined concrete-filled steel columns with elliptical cross-section is investigated using FE analysis, and ANN modeling is investigated with the help of existing experimental results from the literature.

2 Methodology

2.1 Finite element modeling (FEM)

2.1.1 Material properties and interface modeling

The FEM was developed using Abaqus software with inputs from experimental results (Zheng et al., 2021). The column had a height of

500 mm with variable cross-sections (2a × 2 b) of 194 × 194, 230 × 154, and 252 × 126 mm, representing an aspect ratio of 1.0, 1.5, and 2.0, respectively. Aspect ratios 1, 1.5, and 2.0 were designated by letters A, B, and C, followed by numbers 1, 2, and 3, referring to the number of CFRP layers used. The layers of CFRP were attached to the steel tube using tie constraints. The steel tube confined inside the concrete is the modelled in ABAQUS tool as a tie constraint Figure 1. For all of these constraints, the steel tube was set as the master surface due to its high strength compared to the strength of the concrete and CFRP.

An extra repeated model was run in each set of CFRP layers and labeled with Romanic numbers, I and II. Since steel tubes are ductile, their plastic failure was established based on their yield strength. Concrete was modeled with compressive strength, Young's modulus, and peak strain of 32 MPa, 24.8 GPa, and .0022, respectively. These parameters were used to establish the post-behavior of concrete using stress-inelastic crushing and cracking strains curves, as shown

TABLE 2 Geometry of steel tube and CFRP [Zhang et al., 2022].

Specimen	CFRP	Steel tube			
	t_{CFRP} (mm)	2a (mm)	2b (mm)	t_s (mm)	Aspect ratio, a/b
E-A-0-I	–	194	194	3	1.0
E-A-0-II	–	194	194	3	1.0
E-A-1-I	.167	194	194	3	1.0
E-A-1-II	.167	194	194	3	1.0
E-A-2-I	.334	194	194	3	1.0
E-A-2-II	.334	194	194	3	1.0
E-A-3-I	.501	194	194	3	1.0
E-A-3-II	.501	194	194	3	1.0
E-B-0-I	–	230	154	3	1.5
E-B-0-II	–	230	154	3	1.5
E-B-1-I	.167	230	154	3	1.5
E-B-1-II	.167	230	154	3	1.5
E-B-2-I	.334	230	154	3	1.5
E-B-2-II	.334	230	154	3	1.5
E-B-3-I	.501	230	154	3	1.5
E-B-3-II	.501	230	154	3	1.5
E-C-0-I	–	252	126	3	2.0
E-C-0-II	–	252	126	3	2.0
E-C-1-I	.167	252	126	3	2.0
E-C-1-II	.167	252	126	3	2.0
E-C-2-I	.334	252	126	3	2.0
E-C-2-II	.334	252	126	3	2.0
E-C-3-I	.501	252	126	3	2.0
E-C-3-II	.501	252	126	3	2.0

in Eq. 2.1 and Eq. 2.2. The behavior of the steel tube exhibited a bilinear stress-strain curve; an example from existing models is provided in Figure 2A. The incremental compressive stress can be calculated using the expression provided in Figure 2C, in which the stress at the elastic stage is considered to be 50% of the standard cylinder compressive strength. Figure 2B provides a mathematical equation to generate the tensile stress train response of unconfined concrete; however, the failure of concrete was controlled as CFRP failed.

$$\varepsilon^{in} = \varepsilon - \frac{\sigma_c}{E_0} \qquad (2.1)$$

$$\varepsilon^{cr} = \varepsilon - \frac{\sigma_t}{E_0} \qquad (2.2)$$

Where ε^{in} is the inelastic crushing strain, ε is the total strain in tension or compression, σ_c is the compressive stress at the yield, E_0

is the initial modulus of elasticity for the undamaged material, i.e., at the linear elastic zone of stress-strain curves, and σ_t is the tensile strength of concrete. After defining the yield stress-inelastic strain pair of variables, the damage variables of concrete, both in tension and compression, need to be defined as well in Eq. 2.3.

$$d_{c,t} = 1 - \frac{\sigma}{\sigma_{peak}} \qquad (2.3)$$

In these equations, σ_{peak} is a peak tensile or compressive stress of the concrete test specimen, $d_{c,t}$ is a damage parameter in compression or tension. It ranges from zero for undamaged material, i.e., just before peak stress, to one for completely damaged material in the descending part of the stress-strain curve. Using damage parameters, elastic strain, and inelastic strain, the plastic strains are established as in Eq. 2.4 and Eq. 2.5.

TABLE 3 Material properties of concrete, steel tubes, and CFRP used in modeling.

Specimen	Concrete		Ultimate stress and strain of a confined column		Confining pressure of steel tube and CFRP	
	f_{co}, MPa	ε_{co}	Stress, f_{cu}, MPa	Strain, ε_{cu}	Steel tube, f_{ls}, MPa	CFRP, f_{lf}, MPa
			Experimental results			
E-A-0	32	.002492	81.4307	.0443	24.926	.0000
E-A-1	32	.002492	101.9913	.0218	24.926	7.3524
E-A-2	32	.002492	120.8273	.0283	24.926	14.7048
E-A-3	32	.002492	135.4023	.0355	24.926	22.0572
E-B-0	32	.002492	68.8466	.0173	26.942	.0000
E-B-1	32	.002492	95.5084	.0145	26.942	7.8083
E-B-2	32	.002492	105.4617	.0187	26.942	15.6167
E-B-3	32	.002492	117.1038	.0226	26.942	23.4250
E-C-0	32	.002492	64.1334	.0115	29.976	.0000
E-C-1	32	.002492	88.4239	.0086	29.976	8.7331
E-C-2	32	.002492	91.8310	.0102	29.976	17.4661
E-C-3	32	.002492	93.6748	.0115	29.976	26.1992
			Finite element results			
E-A-0	32	.002492	87.5259	.0438	24.926	.0000
E-A-1	32	.002492	101.6816	.0222	24.926	7.3524
E-A-2	32	.002492	122.0474	.0280	24.926	14.7048
E-A-3	32	.002492	146.4600	.0351	24.926	22.0572
E-B-0	32	.002492	80.2077	.0138	26.942	.0000
E-B-1	32	.002492	96.4553	.0147	26.942	7.8083
E-B-2	32	.002492	107.0162	.0190	26.942	15.6167
E-B-3	32	.002492	122.2655	.0228	26.942	23.4250
E-C-0	32	.002492	73.0063	.0108	29.976	.0000
E-C-1	32	.002492	90.6650	.0086	29.976	8.7331
E-C-2	32	.002492	91.7701	.0100	29.976	17.4661
E-C-3	32	.002492	95.4834	.0150	29.976	26.1992

$$\varepsilon^{pl} = \varepsilon^{in} - \frac{d_c}{1-d_c}\frac{\sigma}{E_O} \quad (2.4)$$

$$\varepsilon^{pl} = \varepsilon^{cr} - \frac{d_c}{1-d_c}\frac{\sigma}{E_O} \quad (2.5)$$

In the concrete model, the dilation angles were varied, and the effect of confining pressure was assessed as shown in Figure 3, in which eccentricity, viscosity, a ratio of biaxial and uniaxial compressive stress, and K were maintained as default values (3DS, 2011; Tao and Chen, 2015). The CFRP had thicknesses of .167, .334, and .501 mm, with engineering constants shown in Table 1. The details of the column specimens and parameters used in modeling are shown in Tables 2, 3.

2.1.2 Loading and boundary conditions

The column was loaded axially, necessitating the boundary condition. To maintain homogeneity of the composite specimens during loading, steel tube, CFRP, and concrete were coupled using kinematic coupling at the top and bottom to the created reference points in ABAQUS. All displacements and rotation degrees of freedom for the composite specimens were displaced by this coupling. At reference points, the axial displacement and axial load were prescribed and extracted in ABAQUS as shown in Figure 4. Since the column becomes more fragile as its aspect increases, the E-C, E-B, and E-A columns were assigned displacements of 0.04 H, 0.03 H, and 0.02 H, respectively.
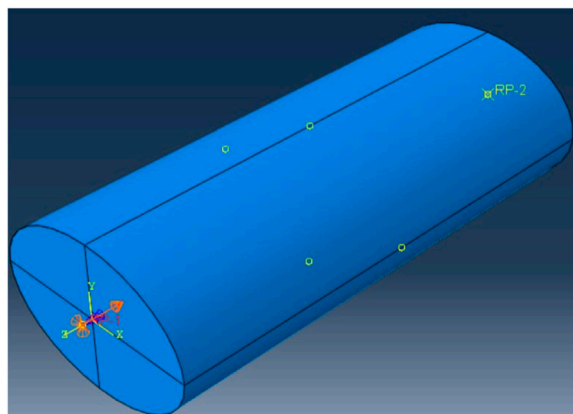
FIGURE 4
Reference points and prescribed displacement.

2.1.3 Analysis, finite element type, and meshing

Abaqus/Explicit was used in the analysis step. This was because of some advantages of this solver: it has a stable time increment and saves the storage capacity of computers as it does not permit iterations. It uses the stable known result or parameter from the previous step and generates the next output through a central difference integration scheme (3DS, 2011). This integration scheme utilizes very small time increments, resulting in a long computation time. To limit this, mass scaling was introduced at the beginning of the analysis step at a factor of 10. The Abaqus/Explicit is normally used to model the dynamic problem; however, step smoothing was used to minimize the velocity in the model, hence low kinetic energy. The kinetic energy of the whole

model (ALLKE) was 5% of the total internal energy of the whole model (ALLIE), as recommended for static analysis (3DS, 2011). During discretization of modeling in ABAQUS, steel tubes and CFRP were assigned four nodes-shell elements (SC4R) with homogeneous and composite characteristics. Concrete was modeled using a solid, homogenous element called the hexagon (C3D8R). All elements had the same mesh size of 25 mm, with any variations being avoided since the small mesh sizes control the time increment in ABAQUS. Figure 5 shows the mesh of concrete, steel tube, and CFRP with their respective finite elements.

3 Results and discussion

3.1 Failure modes and behavior of confined concrete

Figures 6, 7 depict the strain variation in the column without and with CFRP, respectively. The results show that the tensile strain decreases in the steel tube as the aspect ratio increases. The variation in compressive strains and stresses in confined concrete is also affected by the aspect ratio; however, with an aspect ratio of 1, the variations are evenly distributed. This is associated with a slender section as the aspect ratio increases to 3. At an aspect ratio of 2, the shorter dimension (major axis) of the elliptical section contracted significantly, resulting in lateral concrete budging. This results in high axial compressive stress in the minor axis of the section, leading to high confining pressure. As the aspect ratio went to 3, there was uneven strain variation in the shorter diameter of the section, leading to an abrupt reduction in axial stresses, resulting in local buckling of the column in that minor axis. This phenomenon has been reported in the literature (Zeng et al., 2021).
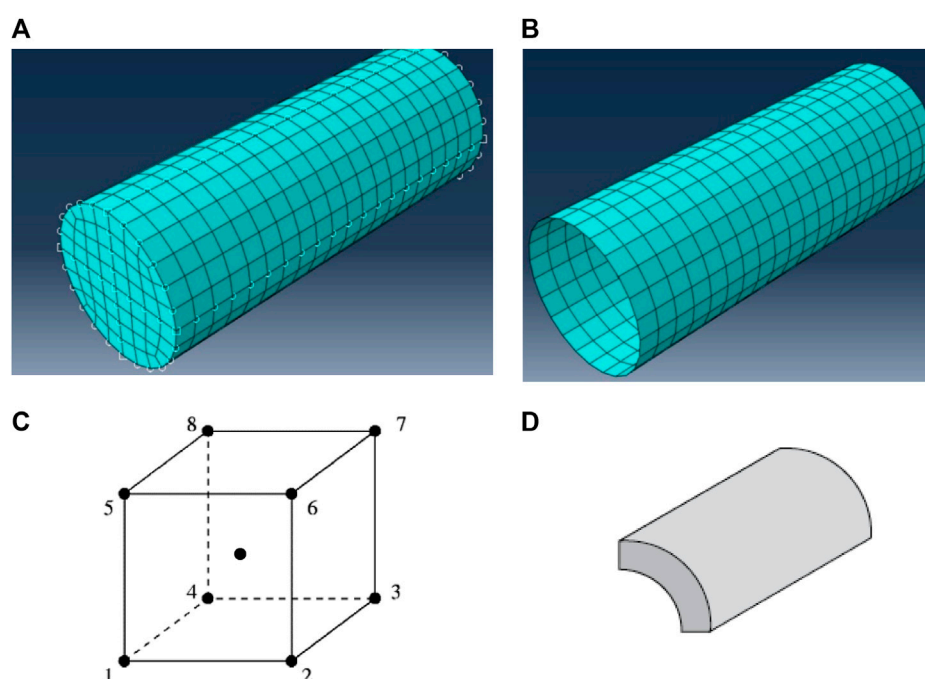

FIGURE 5
Meshing and finite elements used in modelling; **(A)** Structural mesh of concrete, **(B)** Structured mesh of steel tube and CFRP, **(C)** C3D8R element, the single integration point and **(D)** 3 mm shell element (SC4R): Note: These figures are from Abaqus (2014).
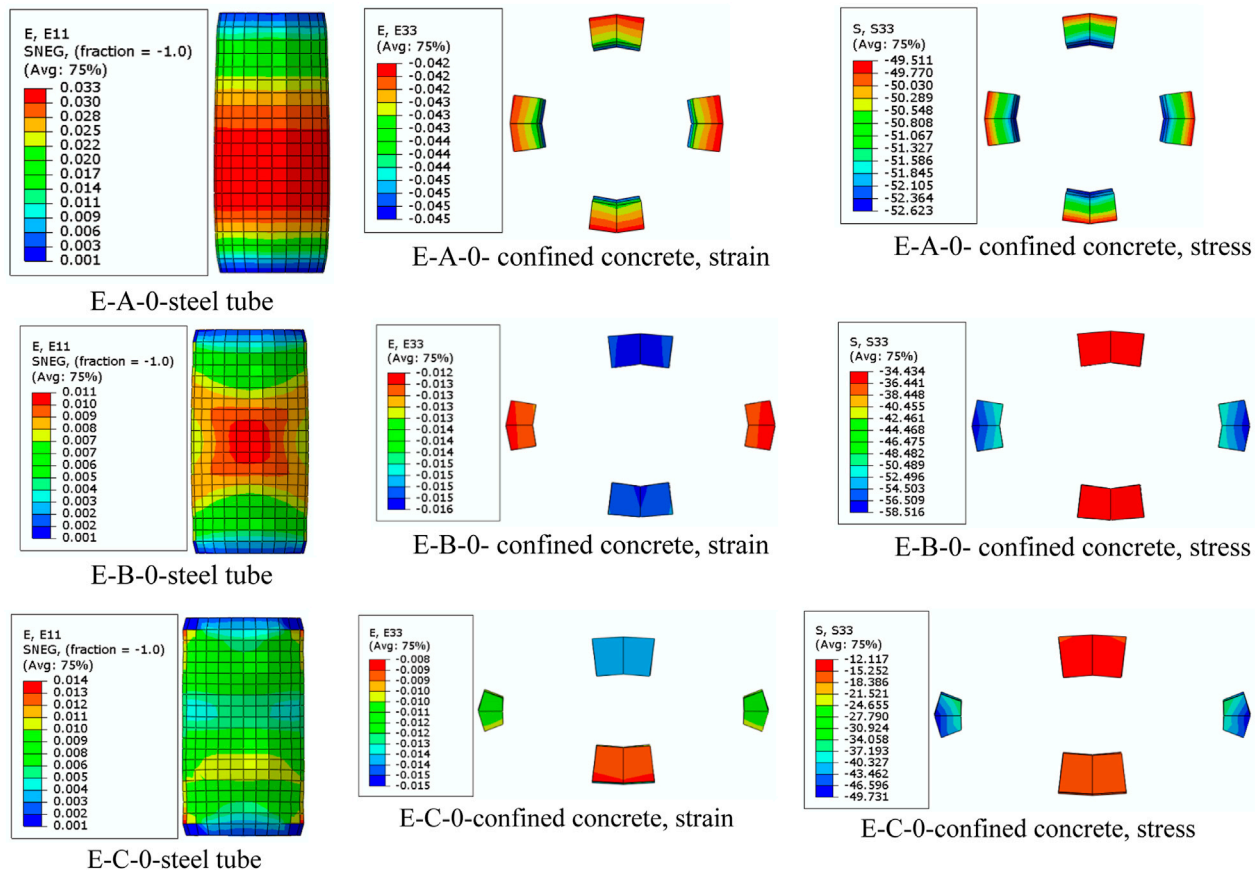
FIGURE 6
Strain variation in the column without CFRP.

When a layer of CFRP was tied along the steel tube, there was a sharing of axial strains; however, for two and three layers of CFRP, the material failed slightly before compared to the specimen with steel tube alone. In general, the addition of CFRP layers delays the early failure of the elliptical section, hence improving the load-carrying capacity of the column. Concrete failure in the confinement was controlled by the failure criteria of the stress-strain curves of CFRP wraps. In elliptical sections as the number of CFRP layers and aspect ratio increased, both the steel tube and the CFRP layer failed at the mid-height of the column with a well developed of failure shape as X structure. Specimens with the high aspect ratio of 3, also with CFRP layers as two and three, and the steel tube showing no hoop strains at mid- height of the column indicate that the hoop stress is mainly carried by CFRP. This typically denotes the rupture mechanism of CFRP in a steel tube. Compared to E-C columns, the x-shaped columns for aspect ratio 2 (E-B columns) showed high strain re-distribution stress in steel tubes from the center, resulting in high axial stress in concrete.

Figures 8, 9 show the results of hoop stress in variation columns without and with CFRP, respectively. In comparison to E-B-0 and E-C-0, the E-A-0 column had high hoop tensile stress in the steel tube below the mid-height, resulting in high compressive stresses at the base. The E-B-0 showed homogeneity in the budging of the specimen at mid-height compared to the E-C-0, which showed less stress at mid-height, indicating less capability of withstanding loads. In addition, the

use of a combined steel tube and CFRP layer showed high hoop strain and stress, denoting high confining pressure with less axial deformation of concrete compared to the column with only steel tubes. This composite plays a virtual role in reducing the buckling of the columns with elliptical sections.

3.2 The confining effect of Carbon Fibre Reinforced Polymer on ultimateaxial loads

Figures 10–12 show the load-strain curves for columns with aspect ratios of 1, 1.5, and 2, respectively. The confined concrete column, E-A-0, had high axial loads of 2588 N compared to E-B-0 and E-C-0, with axial loads of 2311 and 1987 N, respectively. The axial load decreases as the aspect ratio increases. This might have been associated with the confinement efficiency being reduced as the column sections became more elliptical, i.e., aspect ratios of 2 and 3. A similar decrease in axial loads was observed by Zeng et al. (2021) in 2021 and Chen et al. (2021) also in 2021. Columns without CFRP with an aspect ratio of 3 (E-C-0) reduced the axial load to 23.2% of column E-A-0. The results also show that axial loads increased as the number of CFRP layers increased due to the increased ductility of the specimen before ultimate failure. Columns E-A-1, E-A-2, and E-A-3 had an axial load of 3006.8, 3609.1, and 4331 N, being 16.2, 39.4, and 67.3% higher than columns without CFRP (E-A-0). Columns
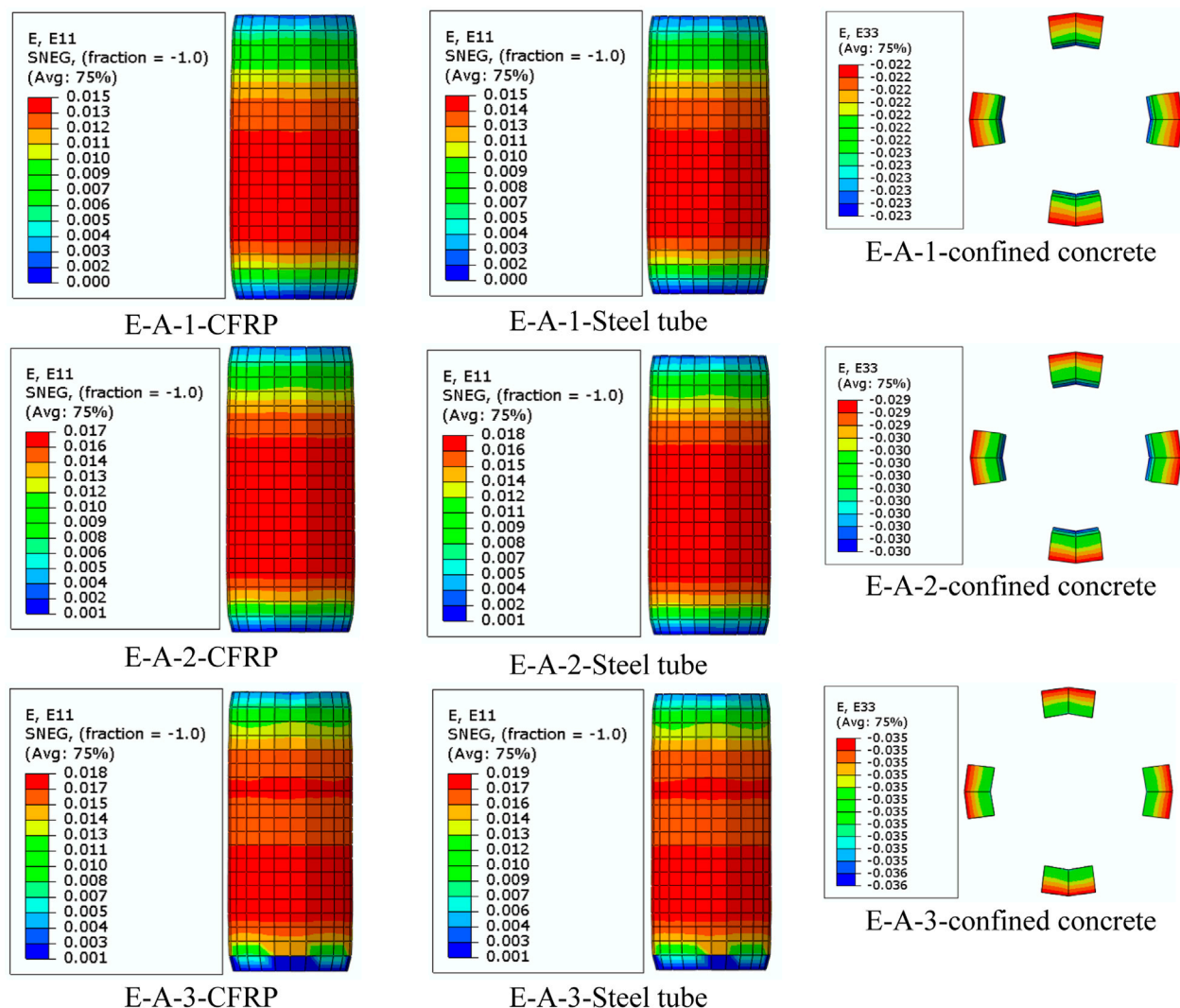
FIGURE 7
(Continued).

E-B-1, E-B-2, and E-B-3 had an axial load of 2684.4, 2978.3, and 3402.7 N being 15.9, 28.8, and 47.2% high than columns without CFRP (E-B-0). In addition, columns E-C-1, E-C-2, and E-C-3 had an axial load of 3006.8, 3609.1, and 4331 N, being 16.2, 39.4, and 67.3% higher than columns without CFRP (E-C-0). These results are in agreement with the test result by Zeng et al., in 2022, where the loads of the columns are the same as the FE result. The addition of CFRP increased the post-behavior of the majority of fiber-reinforced structural elements, particularly deep concrete beams, and confined concrete [10]. This result in high ultimate loads due to strain hardening and ductility as fiber layers increased, leading to bilinear load-strain curves (Abdel et al., 2022; Lin et al., 2004) of specimens. At the second linear part of the load-strain curve, composite with CFRP layers, concrete behaved plastically, with the majority of load transfer occurring via reinforcing composites.

3.3 Correlation of FEM and experimental results

Figure 13 depicts the statistical assessment of FEM and experimental strain and stress results using mean square error. The results show a good correlation of mean squared error (MSE) of .001 and 2.27 for strains and stress, respectively, with a maximum strain for the composite of .025. The results also show a strong correlation between the ultimate axial load for steel-tubed columns and multiple CFRP layers. For columns with only steel tubes, the ultimate axial load appeared to be slightly different; however, the yield loads had a strong correlation with steel specimen. This is because as concrete dilates, localized failure of the column with steel tube alone occurs due to less confining pressure.
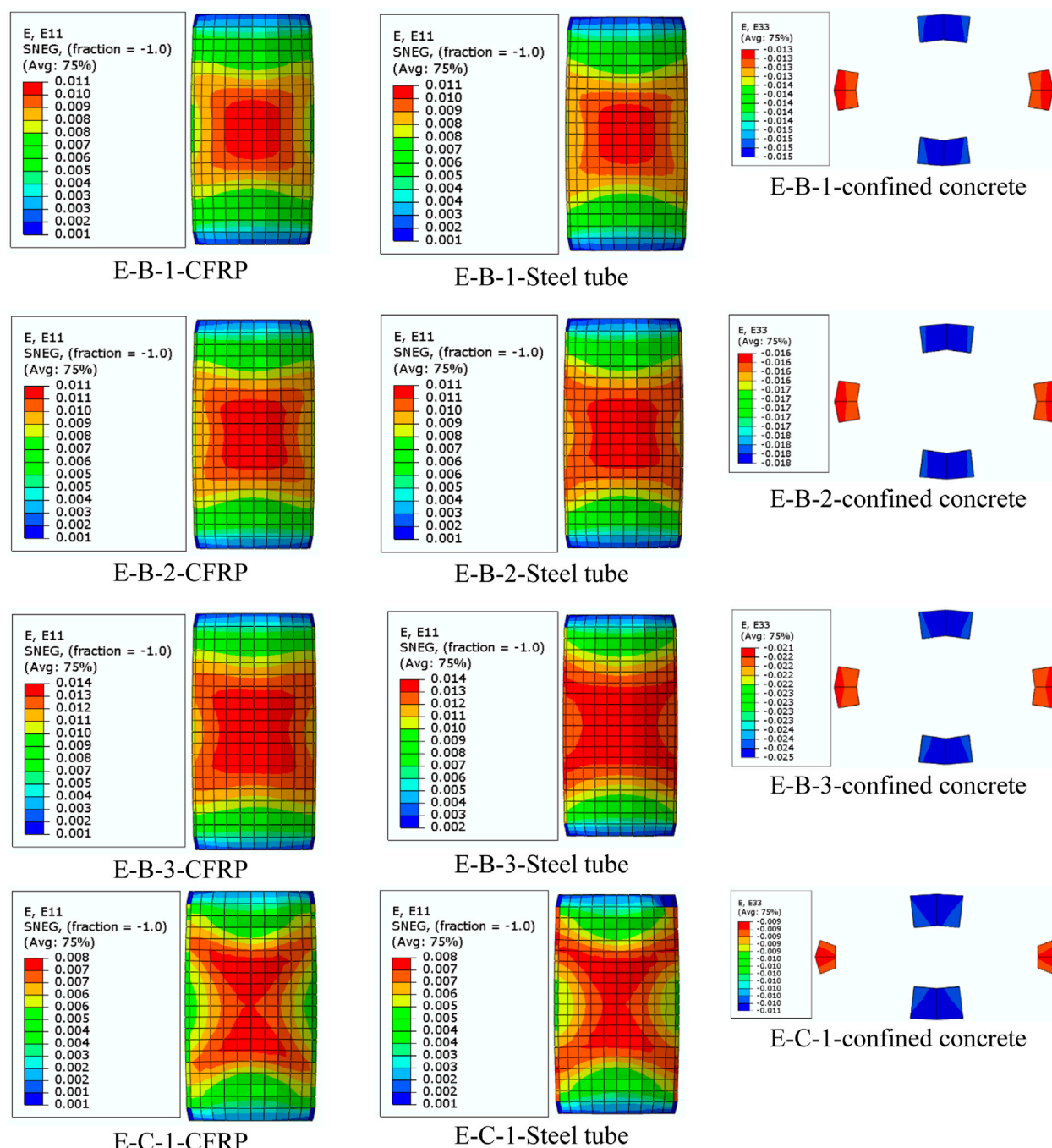
FIGURE 7b
(Continued).

3.4 Artificial neural network (ANN) technique

3.4.1 Model formulation

The ANN technique is widely used for many purposes, such as classification, pattern recognition, and modeling. In particular, the use of ANN for predicting the compressive strength and strain of FRP-confined concrete has been studied (i.e., Cascardi et al., 2017). However, the use of ANN for CFRP-confined concrete columns with elliptical cross-sections has not yet been explored. Therefore, the aim of this is to use the ANN toolbox provided in MATLAB (MATLAB, 2012) to estimate the axial compressive stress and strain capacities of confined concrete that exhibit hardening behavior as the number of CFRP increases. The number of experimental and FEM data used to train and test the ANN model was 24 in total. In the development processes of the ANN model, an appropriate selection of the input variables is a very important process. The axial load capacity of CFRP-confined structures depends on the geometric dimensions (i.e., elliptical dimension of column, thickness of steel tube, layers of CFRP) and the properties of the confining material (i.e., CFRP and steel tube).
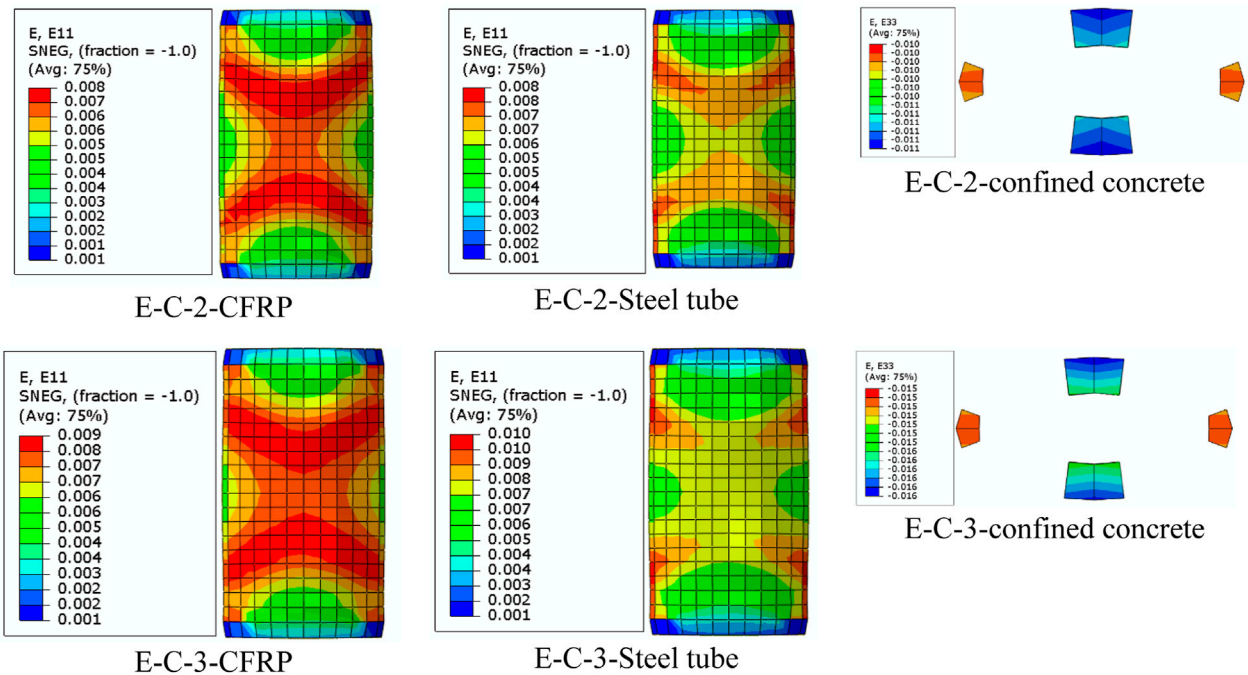
FIGURE 7c
(Continued) Strain variation in the column with CFRP; along the CFRP, steel tube, and in concrete.
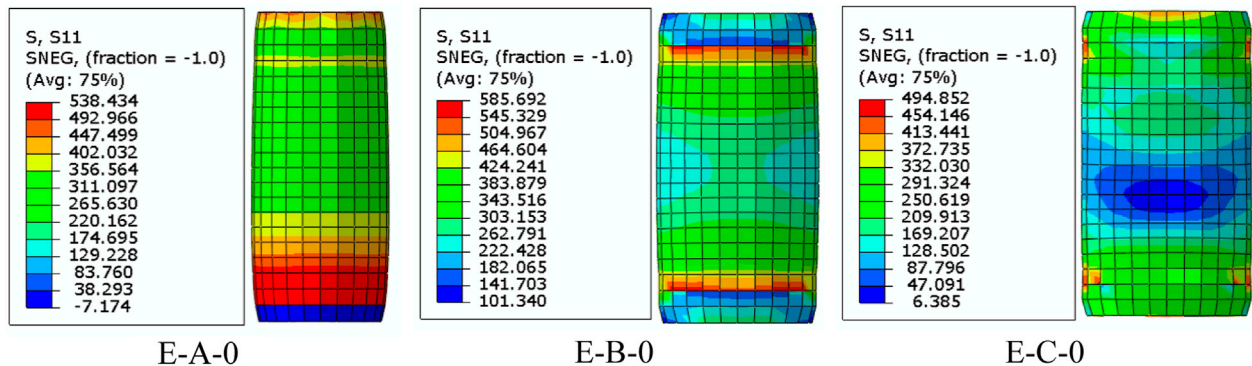
FIGURE 8
Hoop stress variation in columns without CFRP along the steel tubes.

As a result, the input variables, which appear to have significant effects on the axial load capacity and strain, were taken into account with the following factors: 1) x_1 represented by Eq. 3.1 is the aspect ratio of an elliptical column, 2) x_2 represented by Eq. 3.2 is a non-dimensional factor to account for the effect of the confinement by a steel tube, and 3) x_3 represented by Eq. 3.3 is a non-dimensional factor to account for the effect of the confinement by the CFRP layer, and 5) f_{co} is the compressive strength of concrete.

$$x_1 = 2a/2b \qquad (3.1)$$

$$x_2 = f_{ls}/f_{co} \qquad (3.2)$$

$$x_3 = f_{lf}/f_{co} \qquad (3.3)$$

The output variables were: 1) y_1 is the ultimate stress of the ratio of composite-to-compressive strength of concrete as in Eq. 3.4, and 2) y_2 is the ratio of ultimate strain-to-strain of concrete for the confined concrete column loaded with axial compression loads, as shown in Eq. 3.5:

$$y_1 = f_{cu}/f_{co} \qquad (3.4)$$

$$y_2 = \varepsilon_{cu}/\varepsilon_{co} \qquad (3.5)$$

The database was randomly divided into training (60%), validation (20%), and testing (20%). Choosing the appropriate number of hidden neurons and the number of hidden layers is a
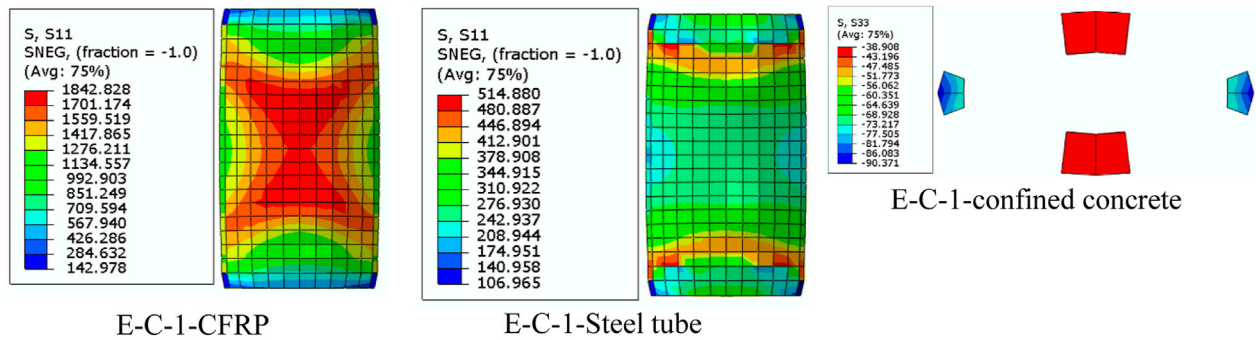
FIGURE 9
Hoop stress variation in columns with CFRP, E-C-1; along the CFRP, steel tube, and in concrete.
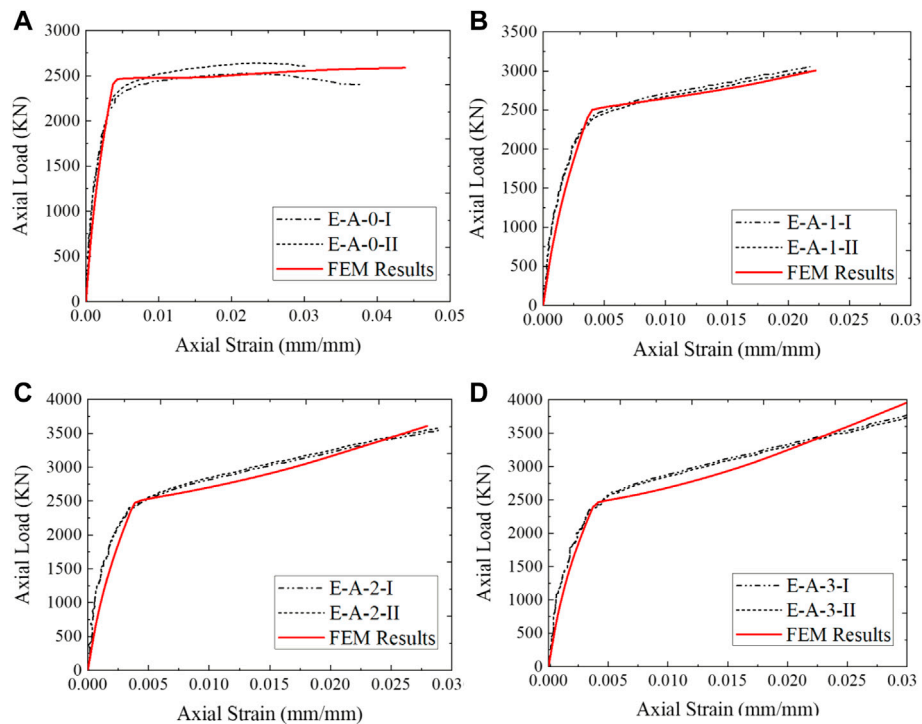
FIGURE 10
Load-strain curve for columns with aspect ratio 1; **(A)** No CFRP layer, **(B)** One layer, **(C)** Two layers, and **(D)** Three layers.

major parameter in obtaining an accurate ANN model. The number of hidden layers and the number of nodes in hidden layers are usually determined via trial-and-error procedures or using suggested rules (Amani and Moeini, 2012). Therefore, one layer of hidden nodes was based on previous suggestions (Isleem et al., 2022b), and the optimum model parameters (i.e., the number of hidden nodes and the rate of learning) were found by a proposed training approach. This can be accomplished using one of several available approaches, in which the network was trained with a set of random values for the initial weight, hidden node number, and learning rate. The Levenberg–Marquardt denoted by Trainlm (Demuth and Beale, 1998) was selected as the

training function. The performance function is MSE, and the transfer functions in both hidden and output layers are Purelin transfer functions. It is to be noted that the default transfer functions in the ANN toolbox are Tansig (Demuth and Beale, 1998). By transforming the data in the first and last ANN layers using the function (Eqs 3.6 and Eq. 3.7) and choosing Purelin transfer functions, the ANN model reveals an acceptable performance:

$$x = [x_1, x_2, x_3]^T \qquad (3.6)$$

$$y = [y_1, y_2]^T \qquad (3.7)$$
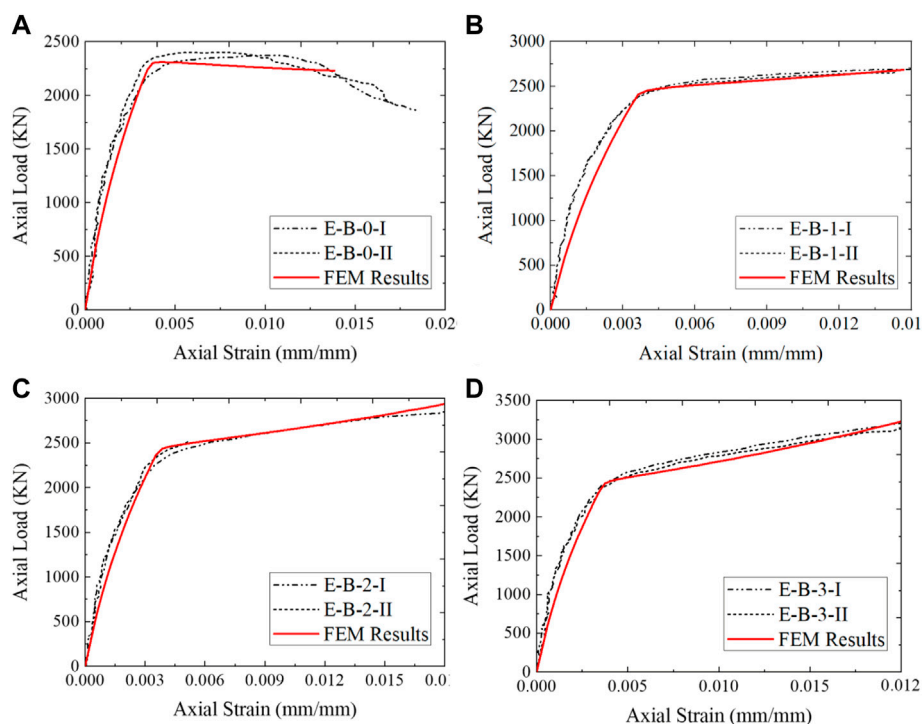
FIGURE 11
Load-strain curve for columns with aspect ratio 1.5; **(A)** No CFRP layer, **(B)** One layer, **(C)** Two layers, and **(D)** Three layers.
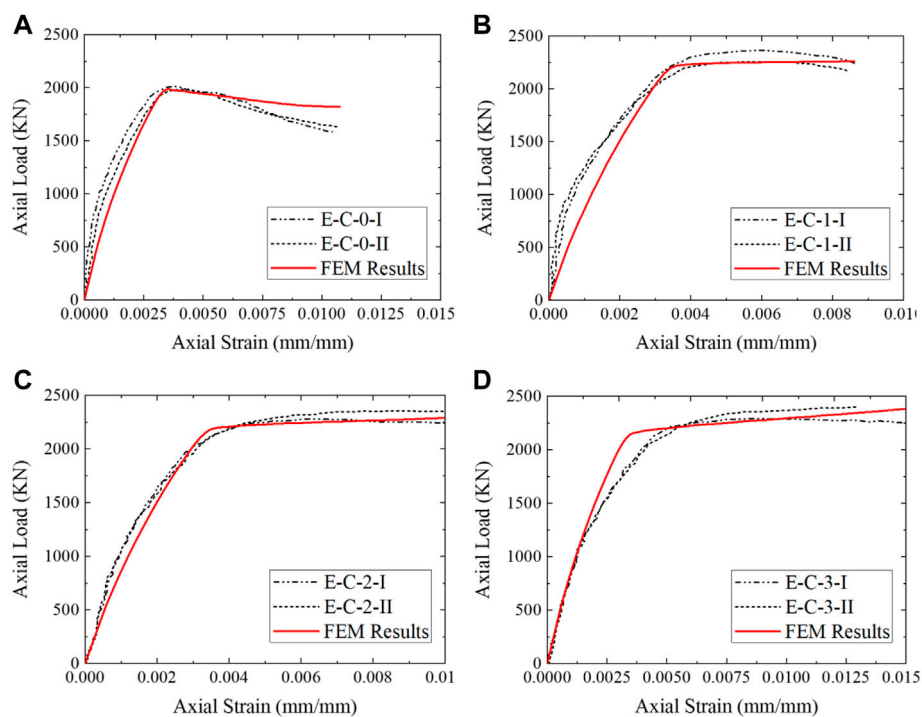
FIGURE 12
Load-strain curve for columns with aspect ratio 2; **(A)** No CFRP layer, **(B)** One layer, **(C)** Two layers, and **(D)** Three layers.
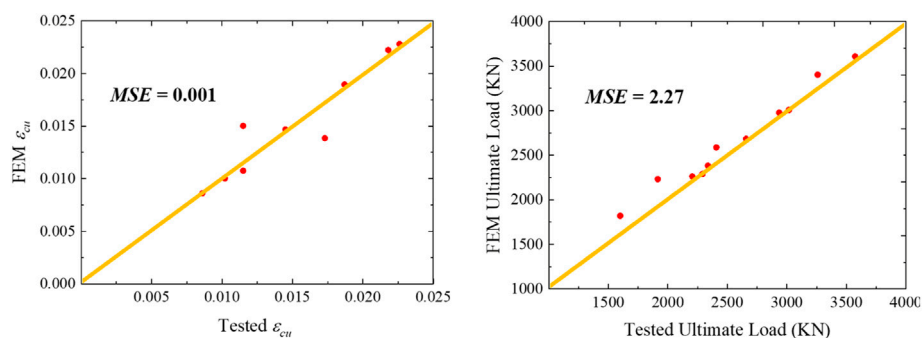
FIGURE 13
Statistical assessment of FEM and experimental results.
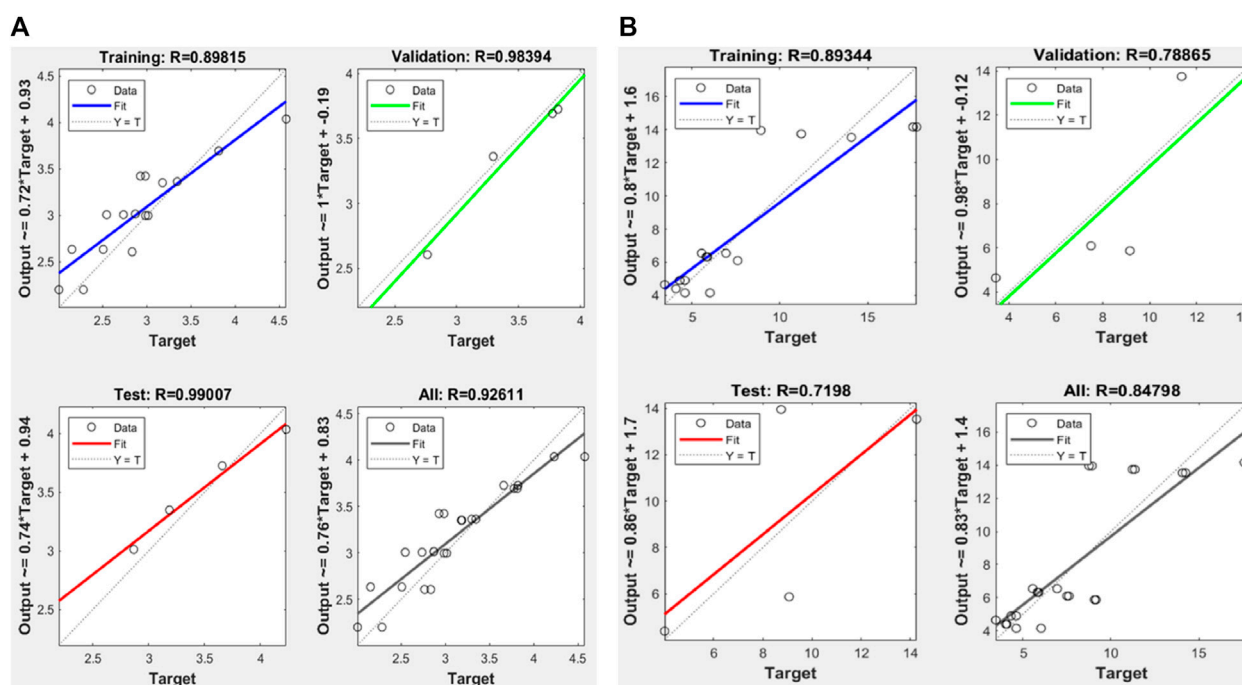
FIGURE 14
Performance of trained data in ANN; **(A)** stress ratios and **(B)** strain ratios.

TABLE 4 The scale of input data.

Input/0utput	$2a/2b$	f_{ls}/f_{co}	f_{lf}/f_{co}	f_{cu}/f_{co}	$\varepsilon_{cu}/\varepsilon_{co}$
Maximum	2.05	.937	.819	4.577	17.78
Minimum	1.0	.779	0.0	2.0	3.45
Mean	1.52	.853	.373	3.098	8.168
Standard deviation	.438	.066	.286	.636	4.26

Once the ANN model is built and the first and last data layers are chosen and normalized, the network can now be trained. The performance of the system on the test data is used to measure the success of the learning process. These test data are usually not involved in the training process; rather, they are used in determining the generalization capability of the trained network, which ensures that

FIGURE 15
Mean squared error for trained data.

FIGURE 16
The performance of the analytical model against experimental data; **(A)** stress ratios and **(B)** strain ratios.
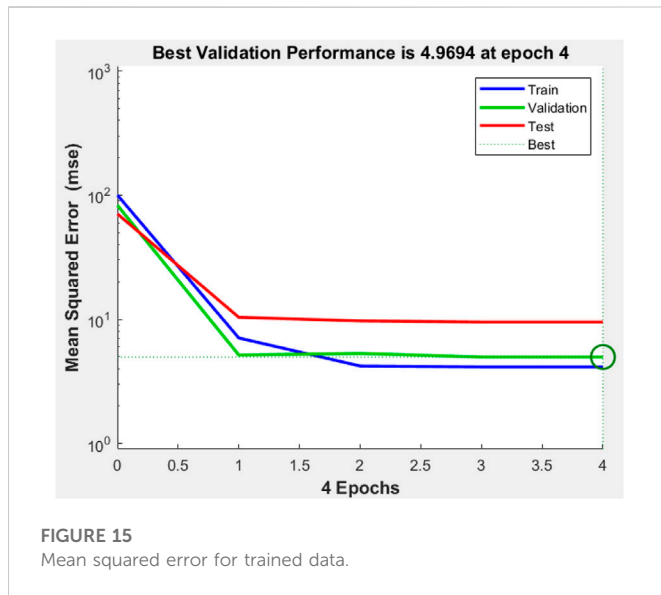
the trained data are not memorized during the learning process (Awolusi et al., 2019). On the other hand, the validation data set is used to evaluate the performance of trained data in each epoch sequentially. Based on the overall model performance and the least mean square error achieved across a wide range of training parameters, the optimal number of hidden nodes was found to be three, and the optimal number of iterations (epochs) in performing the training was found to be four. Using these resulting parameters in a training approach, the most accurate results can then be obtained. Figure 14 clearly shows the result of R^2 for the train, validate, and test data, which have the best correlation of test data, indicating the best training has been achieved. The performance and accuracy of trained data were assessed using the mean square error. Figure 15 shows that the data in training, validation, and testing had a close mean square error. In Eqs 3.8–3.15, the predictions from the ANN model in practical form were generated, in which the inputs (x) and outputs (y) were scaled using the minimum and maximum values provided in Table 4, w is the order of weight for hidden and output neurons, w_1 and w_2, respectively; a is the linear function that combines the intercept/bias in the hidden and output layers, $w_2{}^\sigma$ is the weight of the output layer resulting from the stress ratio, $w_2{}^\varepsilon$ is the weight of the output layer resulting from the strain ratio, The b_1 and b_2 are the matrices containing the bias of the hidden and output layers.

$$\left[\left(\frac{y - y_{min}}{y_{max} - y_{min}} - 0.5 \right) \times 2 \right] = w \left[\left(\frac{x - x_{min}}{x_{max} - x_{min}} - 0.5 \right) \times 2 \right] + a$$
(3.8)

$$w = w_2 \times w_1 \tag{3.9}$$

$$a = w_2 \times b_1 + b_2 \tag{3.10}$$

$$w_2 = \begin{bmatrix} w_2{}^\sigma \\ w_2{}^\varepsilon \end{bmatrix} \tag{3.11}$$

$$w_1 = \begin{bmatrix} -0.871 & 3.402 & -0.699 \\ 1.803 & 0.427 & 0.2 \\ -2.868 & -0.471 & 1.957 \end{bmatrix} \tag{3.12}$$

$$w_2 = \begin{bmatrix} 0.535 & 0.031 & 0.639 \\ 0.922 & -0.912 & 0.4254 \end{bmatrix} \tag{3.13}$$
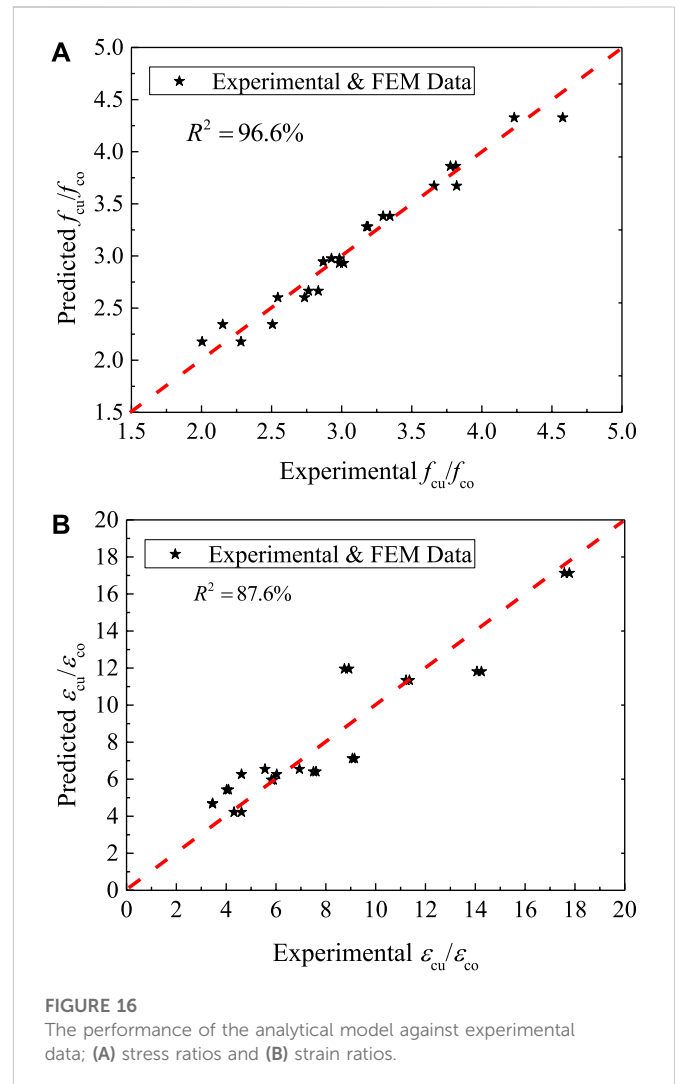
$$b_1 = \begin{bmatrix} 1.128 \\ -1.213 \\ 1.429 \end{bmatrix} \tag{3.14}$$

$$b_2 = \begin{bmatrix} -0.942 \\ -1.330 \end{bmatrix} \tag{3.15}$$

3.5 Analytical axial stress and strain models

The analytical models were developed based on the ratio of minor and major dimensions of the elliptical section, 2a, and 2b, respectively, and the factor to account for the effect of the combined confinement by a steel tube and CFRP against the strength of confining concrete, f_{co}. The total confined pressure due to the steel tube and CFRP is given in Eq. 3.8.

$$f_l = f_{ls} + f_{lf} \tag{3.16}$$

where f_l is the total confining pressure of steel tube and CFRP, f_{ls} and f_{lf} are the confining pressures produced by steel tubes and CFRP, respectively. The confining pressure of a steel tube and CFRP are given

in Eq. 3.9 and Eq. 3.10, respectively, according to ASTM, 2008, and Wang et al., 2012.

$$f_{ls} = 0.5\rho_{st}f_{yt} \tag{3.17}$$

$$f_{lf} = 0.5\rho_f f_{yf} \tag{3.18}$$

Where ρ_{st} and ρ_f are the volumetric ratios of steel tube and CFRP, respectively, f_{yt} and f_{yf} are the yield strengths of steel tube and CFRP, respectively. The volumetric ratios of materials used in this study are given in Eq. 3.11 and Eq. 3.12.

$$\rho_{st} = \left[\frac{1.5\left(0.5\left(2a + 2b\right)\right) - \sqrt{0.5\left(2a \times 2b\right)}}{0.5\left(2a \times 2b\right)}\right]t_s \tag{3.19}$$

$$\rho_f = \left[\frac{1.5\left(0.5\left(2a + 2b + 2t_s\right)\right) - \sqrt{0.5\left(\left(2a + t_s\right) \times \left(2b + t_s\right)\right)}}{0.5\left(\left(2a + t_s\right) \times \left(2b + t_s\right)\right)}\right]t_{CFRP} \tag{3.20}$$

Where, t_s is the thickness of the steel tube and t_{CFRP} is the thickness of the CFRP layer. Considering all Eqs 3.8–3.12, the stress and strain models were formulated as in Eq. 3.13 and Eq. 3.14, respectively. These models considered the ratio of the ultimate stress or strain (f_{cu}, ε_{cu}) of the column to the strength or strain of the confined concrete. The strength and strain (f_{co}, ε_{co}) of the confined concrete are the maximum strength and strain at the first bilinear load-strain curves.

$$\frac{f_{cu}}{f_{co}} = 1 - 1.189\left(\frac{2a}{2b}\right)^{0.359} exp\left(\left(\frac{f_{ls} + f_{lf}}{f_{co}}\right)^{0.841}\right) + 5.489\left(\frac{f_{ls} + f_{lf}}{f_{co}}\right) \tag{3.21}$$

$$\frac{\varepsilon_{cu}}{\varepsilon_{co}} = 2.89\left[1 + 1.163\left(\frac{2a}{2b}\right)^{-2.629} exp\left(\left(\frac{f_{ls} + f_{lf}}{f_{co}}\right)^{-2.211}\right)\right]\left(\frac{f_{ls} + f_{lf}}{f_{co}}\right) \tag{3.22}$$

The evaluation of the analytical stress ratio and strain ratio was based on regression analysis. The values were compared to experimental ratios. There was a strong correlation between the experiment and the analytical results, with an R^2 of .9657 for the stress ratio and .8755 for the strain ratio in Figure 16. This relationship shows that the sum of the square of the differences between the point and the regression line is small, leading to the least mean square error as in ANN. The t-test was also conducted to assess the difference in mean values between experimental and analytical stress ratios and strain ratios, considering unequal variances. The t-values were .006 for stress ratios and .06 for strain ratios, both of which were less than the t-critical of 1.68. These results indicate no statistical differences between experimental and analytical ratios (Ross, 2004).

4 Conclusions and recommendation

The following conclusions were drawn in this study.

- The axial load-carrying capacity is affected as the column becomes more elliptical. A high aspect ratio of 3 results in local buckling of the mid-height with a lower axial compression load of 1987 N. With the increase in the aspect ratio of the column section, the CFRP was highly stressed, with a well-developed x-shape of stress variation at the mid-height of the column. This indicates the possibility of CFRP rupture in the minor axis of the cross-section with a relatively high axial load of the column 67.3% for a column specimen of aspect ratio as 3, with CFRP versus the same column without CFRP.

- The increase in the number of layers of CFRP resulted in bilinear load-strain curves. The second linear part of the load-strain curve is due to the high confinement pressure contributed by CFRP resulting from the dilation of concrete in its plastic stage. The combined effect of steel tube and CFRP results in high confining pressure, leading to a small dilation angle. This indicates the plastic flow of the concrete was high, resulting in high confining pressure and an increased axial load-strain ratio.

- The artificial neural network and analytical model developed predict stress and strain ratios well. ANN had R^2 values of .926 and .848. These compared well with analytical R^2 values of .966 and .876 for stress and strain ratios, respectively.

On the point of application, these composite columns are used for architectural purposes and also applications where the specimens with a high eccentrically load. For the same specimen conditions, this research can be further extended to the eccentrical loading conditions, with higher concrete strength, different slenderness ratios, and different types of FRP. This kind of future research will solve structural engineers' analysis problems. Xie et al., 2021.

Data availability statement

The original contributions presented in the study are included in the article/Supplementary material, further inquiries can be directed to the corresponding author.

Author contributions

Conceptualization: HI, Investigation: HI, DA, and PJ, Methodology: HI and DA, Project administration: HI and DA, Resources: HI, DA, and MS, Software: HI and DA, Supervision: HI, Validation: DA and PJ, Visualization DA, SQ, AN, AM, and PJ, Writing—Original draft: DA and PJ, Writing—review and editing: DA, SQ, AN, AM, and PJ, Funding: MS, AM, and AN.

Conflict of interest

The authors declare that the research was conducted in the absence of any commercial or financial relationships that could be construed as a potential conflict of interest.

Publisher's note

All claims expressed in this article are solely those of the authors and do not necessarily represent those of their affiliated

organizations, or those of the publisher, the editors and the reviewers. Any product that may be evaluated in this article, or claim that may be made by its manufacturer, is not guaranteed or endorsed by the publisher.

References

3DS, 2011 3Ds (2011). *Abaqus 6.11 theory manual.* Providence, RI, USA": Dassault Systèmes Simulia Corp.

Abadel, A. A., Masmoudi, R., and Iqbal Khan, M. (2022). Axial behavior of square and circular concrete columns confined with CFRP sheets under elevated temperatures: Comparison with welded-wire mesh steel confinement. *Structures* 45, 126–144. doi:10.1016/J.ISTRUC.2022.09.026

Abaqus (2014). Analysis USER's guide volume V: Prescribed conditions. CONSTRAINTS Interact. https://www.academia.edu/28334906/Abaqus_Analysis_Users_Guide.

Abdel, A. A., Khan, M. I., and Masmoudi, en R. (2022). Experimental and numerical study of compressive behavior of axially loaded circular ultra-high-performance concrete-filled tube columns. *Case Stud. Constr. Mat.* 17, 01376. doi:10.1016/J.CSCM.2022.E01376

Aksoylu, C., Yazman, Ş., Özkılıç, Y. O., Gemi, L., and Arslan, M. H. (2020). Experimental analysis of reinforced concrete shear deficient beams with circular web openings strengthened by CFRP composite. *Compos. Struct.* 249, 112561. doi:10.1016/j.compstruct.2020.112561

Althoey, F., Akhter, M. N., Nagra, Z. S., Awan, H. H., Alanazi, F., Khan, M. A., et al. (2022). Prediction models for marshall mix parameters using bio-inspired genetic programming and deep machine learning approaches: A comparative study. *Case Stud. Constr. Mat.* 18, 01774. doi:10.1016/j.cscm.2022.e01774

Amani, J., and Moeini, R. (2012). Prediction of shear strength of reinforced concrete beams using adaptive neuro-fuzzy inference system and artificial neural network. *Sci. Iran.* 19 (2), 242–248. doi:10.1016/j.scient.2012.02.009

Amin, A., and Tayeh, B. A. (2020). Investigating the mechanical and microstructure properties of fiber reinforced lightweight concrete under elevated temperatures. *case Stud. Constr. Build. Mater.* 13, 00459. doi:10.1016/j.cscm.2020.e00459

Amin, A., Zeyad, A. M., Tayeh, B. A., and Agwa, I. S. (2021). Effects of nano cotton stalk and palm leaf ashes on ultrahigh performance concrete properties incorporating recycled concrete aggregates. *Constr. Build. Mater.* 302, 124196. doi:10.1016/j.conbuildmat.2021.124196

Astm (2008). *Standard test method for tensile properties of polymer matrix composite materials.* West Conshohocken: D3039/D3039M-08.

Augustino, D. S., Kabubo, C., Kanali, C., and Ocharo, R. (2022a). The orientation effect of opening and internal strengthening on shear performance of deep concrete beam using recycled tyre steel fibres. *Results Eng.* 15, 100561. doi:10.1016/j.rineng.2022.100561

Augustino, D. S., Onchiri, R. O., Kabubo, C., and Kanali, C. (2022b). Mechanical and durability performance of high-strength concrete with waste tyre steel fibres. *Adv. Civ. Eng.* 32. 4691972, doi:10.1155/2022/4691972

Awolusi, T. F., Oke, O. L., Akinkurolere, O. O., Sojobi, A. O., and Aluko, O. G. (2019). Performance comparison of neural network training algorithms in the modeling properties of steel fiber reinforced concrete. *Heliyon* 5 (1), 01115. doi:10.1016/j.heliyon.2018.e01115

Azevedo, A. R. G., Amin, M., Hadzima-Nyarko, M., Agwa, I. S., Zeyad, A. M., Tayeh, B. A., et al. (2022). Possibilities for the application of agro-industrial wastes in cementitious materials: A brief review of the Brazilian perspective. *Clean. Mater.* 3, 100040. doi:10.1016/j.clema.2021.100040

Cai, Y., Quach, W-M., and Young, B. (2019). Experimental and numerical investigation of concrete-filled hot-finished and cold-formed steel elliptical tubular stub columns. *Thin-Walled Struct.* 145, 106437. doi:10.1016/j.tws.2019.106437

Cascardi, A., Micelli, F., and Aiello, M. A. (2017). An Artificial Neural Networks model for the prediction of the compressive strength of FRP-confined concrete circular columns. *Eng. Struct.* 140, 199–208. doi:10.1016/J.ENGSTRUCT.2017.02.047

Chen, G., Wang, Y., Yu, T., Wan, B., Zhang, B., and Liu, en Q. (2021). Behavior and design-oriented model for elliptical FRP-confined concrete under axial compression. *Eng. Struct.* 249, 113387. doi:10.1016/j.engstruct.2021.113387

Chung, H., Yang, K., Lee, Y., and Eun, H. (2002). Stress–strain curve of laterally confined concrete. *Eng. Struct.* 24, 1153–1163. doi:10.1016/s0141-0296(02)00049-4

Demuth, H., and Beale, M. (1998). *Neural network toolbox for use with matlab. User's guide.* Natick, MA, USA: The MathWorks, Inc.

Elchalakani, M., Dong, M., Karrech, A., Mohamed Ali, M. S., and Huo, J-S. (2020). Circular concrete columns and beams reinforced with GFRP bars and spirals under axial, eccentric, and flexural loading. *J. Compos Constr.* 24, 04020008. doi:10.1061/(asce)cc.1943-5614.0001008

Gemi, L., Madenci, E., and Özkılıç, Y. O. (2021). Experimental, analytical and numerical investigation of pultruded GFRP composite beams infilled with hybrid FRP reinforced concrete. *Eng. Struct.* 244, 112790. doi:10.1016/J.ENGSTRUCT.2021.112790

Gemi, L., Madenci, E., Özkılıç, Y. O., Yazman, Ş., and Safonov, A. (2022). Effect of fiber wrapping on bending behavior of reinforced concrete filled pultruded GFRP composite hybrid beams. *Polym. (Basel)* 14 (18), 3740. doi:10.3390/polym14183740

Guo, Y., Huang, P., Yang, Y., and Li, L. (2009). Experimental studies on axially loaded concrete columns confined by different materials. *KEM* 402, 513–518. doi:10.4028/www.scientific.net/KEM.400-402.513

He, L., Lin, S., and Jiang, H. (2019). Confinement effect of concrete – filled steel tube columns with infill concrete of different strength grades. *Front. Mater.* 6. doi:10.3389/fmats.2019.00071

Isleem, H. F., Jagadesh, P., Ahmad, J., Qaidi, S., Althoey, F., Najm, H. M., et al. (2022b). Finite element and theoretical investigations on PVC-CFRP confined concrete columns under axial compression. *Front. Mater.* 9, 1055397. doi:10.3389/fmats.2022.1055397

Isleem, H. F., Peng, F., and Tayeh, B. A. (2022a). Confinement model for LRS FRP-confined concrete using conventional regression and artificial neural network techniques. *Compos. Struct.* 279, 114779. doi:10.1016/J.COMPSTRUCT.2021.114779

Isleem., H. F., Muhammad, A., Wesam, S. A., Shah., M. K, Zeb., S., Ali Musarat, M., et al. (2021). Axial compressive strength models of eccentrically-loaded rectangular reinforced concrete columns confined with FRP. *Mater. (Basel)* 14 (13), 3498. doi:10.3390/ma14133498

Jagadesh, P., Nagarajan, V., Karthik Prabhu, T., and Arunachalam, K., "Effect of nano-titanium dioxide on mechanical properties of fly ash and ground granular blast furnace slag based geopolymer concrete" Journal of building engineering, Vol.61, 105235, 2022. doi:10.1016/j.jobe.2022.105235

Jiang, S. F., Ma, S. L., and Wu, Z. Q. (2014). Experimental study and theoretical analysis on slender concrete-filled CFRP-PVC tubular columns. *Constr. Build. Mat.* 53, 475–487. doi:10.1016/j.conbuildmat.2013.11.089

Jiang, T., and Teng, J. G. (2007). Analysis-oriented stress–strain models for FRP – confined concrete. *Eng. Struct.* 29, 2968–2986. doi:10.1016/j.engstruct.2007.01.010

Khan, M., and Ali, M. (2020). Cracking behaviour and constitutive modelling of hybrid fibre reinforced concrete. *J. Build. Eng.* 30, 101272. doi:10.1016/j/jobe.2020.101272

Khan, M., and Ali, M. (2016). Use of glass and nylon fibers in concrete for controlling early age micro cracking in bridge decks. *Constr. Build. Mater.* 125, 800–808. doi:10.1016/j.conbuildmat.2016.08.111

Khan, M., Ali, M., and Xie, C. (2022). Effectiveness of hybrid steel basalt fiber reinforced concrete under compression. *case Stud. Constr. Mater.* 16, 00941. doi:10.1016/j.cscm.2022.e00941

Khan, M., Cao, M., and Ali, M. (2020). Cracking behaviour and constitutive modelling of hybrid fibre reinforced concrete. *J. Build. Eng.* 30, 101272. doi:10.1016/J.JOBE.2020.101272

Khan, M., Cao, M., Chaopeng, X., and Ali, M. (2021). Experimental and analytical study of hybrid fiber reinforced concrete prepared with basalt fiber under high temperature. *Fire Mater.* 46 (1), 205–226. doi:10.1002/fam.2968

Lam, D., and Testo, N. (2008). "Structural design of concrete filled steel elliptical hollow sections," in *Composite construction VI* Colorado USA.

Lin, H. J., and Liao, C. I. (2004). Compressive strength of reinforced concrete column confined by composite material. *Compos. Struct.* 65 (2), 239–250. doi:10.1016/j.compstruct.2003.11.001

Liu, F., Wang, Y., and Chan, T-M. (2017). Behaviour of concrete-filled cold-formed elliptical hollow sections with varying aspect ratios. *Thin-Walled Struct* 110, 47–61. doi:10.1016/j.tws.2016.10.013

Matlab (2012). *MATLAB and statistics toolbox release 2012b.* Natick, MA, USA: The MathWorks, Inc.

Ozbakkaloglu, T., and Akin, E. (2012). Behavior of FRP-confined normal- and high-strength concrete under cyclic axial compression. *J. Compos. Constr.* 16 (4), 451–463. doi:10.1061/(asce)cc.1943-5614.0000273

Ross, S. M. (2004). *Introduction to probability and statistics for engineers and scientists.* Third edit. Berkeley: Elsevier Academic Press.

Saad, M., Agwa, I. S., Abdelsalam, B., and Amin, M. (2022). Improving the brittle behavior of high strength concrete using banana and palm leaf sheath fibers. *Mech. Adv. Mater. Struct.* 29 (4), 564–573. doi:10.1080/15376494.2020.1780352

Sun, Z., Zou, Y., Wang, C., Pan, J., Wang, L., and Chen, M. (2022). Study on confinement mechanism of core concrete in steel tubular-corrugated steel plate confined concrete columns. *J. Build. Eng.* 52, 104497. doi:10.1016/j.jobe.2022.104497

Tao, Y., and Chen, J. F. (2015). Concrete damage plasticity model for modeling FRP-to-concrete bond behavior. *J. Compos. Constr.* 19 (1), 04014026. doi:10.1061/(asce)cc.1943-5614.0000482

Wang, Z., Wang, D., Smith, S. T., and Lu, en D. (2012). CFRP-confined square RC columns. I: Experimental investigation. *J. Compos. Constr.* 16 (2), 150–160. doi:10.1061/(asce)cc.1943-5614.0000245

Woldemariam, A. M., Oyawa, W. O., and Nyomboi, T. (2019). Structural performance of uPVC confined concrete equivalent cylinders under axial compression loads. *Buildings* 9 (4), 82. doi:10.3390/buildings9040082

Xie, C., Cao, M., Khan, M., Yin, H., and Guan, J. (2021). Review on different testing methods and factors affecting fracture properties of fiber reinforced cementitious composites. *Constr. Build. Mater.* 273, 121766. doi:10.1016/j.conbuildmat.2020.121766

Zeng, J. J., Da Liang, S., Li, Y. L., Guo, Y. C., and Shan, G. Y. (2021). Compressive behavior of FRP-confined elliptical concrete-filled high-strength steel tube columns. *Compos. Struct.* 266 (100), 113808. doi:10.1016/j.compstruct.2021.113808

Zeyad, A. M., Hakeem, I. Y., Amin, M., Tayeh, B. A., and Agwa, I. S. (2022a). Effect of aggregate and fibre types on ultra-high-performance concrete designed for radiation shielding. *J. Build. Eng.* 58, 104960. doi:10.1016/J.JOBE.2022.104960

Zeyad, A. M., Hakeem, I. Y., Amin, M., Tayeh, B. A., and Agwa, I. S. (2022b). Effect of aggregate and fibre types on ultra-high-performance concrete designed for radiation shielding. *J. Build. Eng.* 58, 104960. doi:10.1016/j.jobe.2022.104960

Check for updates

Effect of thermal cycles on the engineering properties and durability of sustainable fibrous high-strength concrete

Ibrahim Y. Hakeem[1]*, MD. Akter Hosen[2], Mana Alyami[1],
Shaker Qaidi[3,4]*, Yasin O. Özkılıç[5], Ali Alhamami[1] and
Mohammad Alharthai[1]

[1]Department of Civil Engineering, College of Engineering, Najran University, Najran, Saudi Arabia,
[2]Department of Civil and Environmental Engineering, College of Engineering, Dhofar University, Salalah,
Oman, [3]Department of Civil Engineering, College of Engineering, University of Duhok, Duhok, Iraq,
[4]Department of Civil Engineering, College of Engineering, Nawroz University, Duhok, Iraq, [5]Department of
Civil Engineering, Faculty of Engineering, Necmettin Erbakan University, Konya, Türkiye

In this research, the effect of heat−cool cycles (HCCs) on high-strength concrete (HSC) containing steel fibres (SFs), polypropylene fibres (PPFs), and date palm fibres (DPFs), which were named fibrous high-strength concrete (FHSC), was studied. To produce FHSC, three doses of 0.2, 0.6, and 1 percent of each fibre were used. All samples were tested after 28 days of normal water curing and 270 days of exposure to HCCs (continuing the authors' project and research published at 28 and 180 days). This entails heating for 2 days at 60 C in the oven and cooling for another 2 days at room temperature for 270 days. The experiment's findings revealed that fibre reinforcement in concrete enhances its strength and durability. By incorporating the three types of fibres into high-strength concrete, with and without HCCs, the modulus of rupture was significantly increased. In both conditions, including with or without the implementation of HCCs, incorporating the three fibre types into the HSC showed a significant increase in toughness. As a result, natural date palm fibres can produce sustainable FHSC that can withstand harsh environmental conditions. Moreover, compared to the previous study conducted by the authors at 180 days, there is a slight severity in both the pattern of decrease and increase of the studied characteristics at 270 days caused by the effect of thermal cycles and fibres.

KEYWORDS

fibrous concrete, date palm fibre, engineering characteristics, durability, thermal cycles, energy absorption capacity

1 Introduction

Concrete constructions are often subjected to a wide range of environmental conditions during their lifecycle (Khan et al., 2022a; Hakeem et al., 2022c; Zhang et al., 2022). As a result, the resilience of a concrete building is evaluated by how well it can withstand particular exposure circumstances without requiring costly rehabilitation or maintenance (Ma et al., 2017;

Abbreviations: DPFs, date palm fibres; FHSC, fibrous high-strength concrete; HCCs, heat−cool cycles; HSC, high-strength concrete; PPFs, polypropylene fibres; SFs, steel fibres; SPs, super plasticizers; UPV, ultrasonic pulse velocity.

Althoey and Hakeem, 2022; Hakeem et al., 2022d). Concrete is described as a composite material that can last for many decades, if not hundreds, with little or no maintenance (Saeed et al., 2022a; Hakeem et al., 2022b; Qaidi et al., 2022b; Zeybek et al., 2022). Standard concrete is composed of cement, coarse aggregate, and fine aggregate without reinforcing steel (Hakeem et al., 2022a; Althoey et al., 2022b). Modifications to the components and mixture design of ordinary cement concrete can be made to develop several forms of concrete that are acceptable for a variety of environmental circumstances and structural loads (Anas et al., 2022c; Anas et al., 2022f). Several behaviour-related challenges are presented in order to highlight the poor behaviour of ordinary concrete even more (Koushkbaghi et al., 2019; Ahmad et al., 2020; Khan et al., 2021).

The development of ultra-high-performance concrete in the 1990s was a significant advancement in the production of concrete (Ahmad et al., 2016; Qaidi et al., 2022a; Saeed et al., 2022b). This revolutionary concrete was distinguished by its high compressive and tensile strengths and its ductility and fracture toughness (Richard and Cheyrezy, 1995). Furthermore, fibres are being used as discrete three-dimensional reinforcement to address the limitations of ordinary cement concrete and as a replacement for ultra-high-performance concrete (Bajaber and Hakeem, 2021). Fibre-reinforced concrete incorporates fibre into its mix to improve load resistance (Anas et al., 2022a; Anas et al., 2022b). Various types of fibre-reinforced concrete have been created, each with

distinct and important advantages because of its various advantages, including good ductility, tensile strength, and fatigue resistance. Fibre-reinforced concrete has a broad variety of applications, including industrial floors, building pavements, slope stabilisation, impact-resistant structures, and tunnel linings (Kaur and Talwar, 2017; Ahmed et al., 2021; Çelik et al., 2022).

The use of proper fibre type can postpone or minimize the beginning and propagation of fractures in concrete under compressive and tensile loads (Bingöl and Balaneji, 2019; Anas et al., 2022e). Available commercial reinforcements are divided into many groups and have characteristics that make them appropriate for certain purposes. Steel fibre (Iqbal et al., 2019), polypropylene fibre (Hussain et al., 2020), carbon fibre (Nassiri et al., 2021), glass fibre (Peled et al., 2005), carbon nanotubes (Hawreen et al., 2019), basalt fibre (Geng et al., 2022), organic fibres (Ahmad et al., 2020), and other materials are examples. When it refers to the mechanical behaviour of concrete, SF is, by far, the best fibre when compared to other industrial fibres. SF has a high tensile strength of more than 1,200 MPa and an elastic modulus of around 200 GPa (Najm et al., 2022b; Nanayakkara et al., 2022). The research has developed a paradigm that supports the feasibility of SF as an outstanding reinforcing material with good tensile, compressive, modulus of rupture, and shear strengths (Alabduljabbar et al., 2019; Tayeh et al., 2022b; Tayeh

TABLE 1 Chemical characteristics of cement.

Composite	Mass (%)
Cao	63.83
SiO_2	19.7
Al_2O_3	6.25
Fe_2O_3	3.45
SO_3	2.25
K_2O	1.08
MgO	0.97
LOI	1.52
Insoluble	0.95

TABLE 2 Physical characteristics of cement.

Composite	Mass
C2S	12.10%
C3S	59%
C3A	10.60%
C4AF	10.40%
Fineness	4,100 cm^2/g
Specific gravity	3.15

TABLE 3 Physical characteristics of the aggregates.

Type of aggregate	Characteristics			
	Fineness modulus	Specific gravity	Water sorptivity (%)	Bulk unit weight (kg/m^3)
Coarse	7.34	2.77	0.69	1630.00
Fine	2.23	2.67	1.31	1535.74

TABLE 4 Steel fibre's physical characteristics.

Length (cm)	6
Diameter (cm)	0.075
Tensile strength (GPa)	0.625
Unit weight (g/cm^3)	7.85
Aspect ratio	80

TABLE 5 Polypropylene fibre's physical characteristics.

Length (cm)	1.2
Diameter (cm)	0.0025
Young modulus (GPa)	5.4
Unit weight (g/cm^3)	0.91
Tensile strength (GPa)	0.550
Elongation at breaking (%)	30

TABLE 6 Date palm fibre's physical characteristics.

	Type of DPF			
Characteristics	Raw fibres	1.5% Sodium-hydroxide treated	3.0% Sodium-hydroxide treated	6.0% Sodium-hydroxide treated
Length (cm)	9	8	8	8
Diameter (cm)	0.09	0.065	0.061	0.069
Strain	0.044	0.058	0.062	0.055
Elongation (%)	4	6	6	5
Tensile strength (GPa)	0.100	0.174	0.234	0.181

TABLE 7 Fibrous high-strength concrete mix proportion (kg/m³).

Mix ID	Cement	Aggregate		SP	Water	Fibre		
		Coarse	Fine			SF	PPF	DPF
Control	400.0	1105.4	736.93	2.0	176.4	—	—	—
DPF-0.2	400.0	1105.4	736.93	2.0	176.4	—	—	8.0
DPF-0.6	400.0	1105.4	736.93	2.0	176.4	—	—	24.0
DPF-1.0	400.0	1105.4	736.93	2.0	176.4	—	—	40.0
PFF-0.2	400.0	1105.4	736.93	2.0	176.4	—	8.0	—
PFF-0.6	400.0	1105.4	736.93	2.0	176.4	—	24.0	—
PFF-1.0	400.0	1105.4	736.93	2.0	176.4	—	40.0	—
SF-0.2	400.0	1105.4	736.93	2.0	176.4	8.0	—	—
SF-0.6	400.0	1105.4	736.93	2.0	176.4	24.0	—	—
SF-1.0	400.0	1105.4	736.93	2.0	176.4	40.0	—	—

FIGURE 1
Influence of HCCs on the compressive strength of FHSC.

FIGURE 2
Relationship between the volume and compressive strength of SF, PPF, and DPF. **(A)** Relationship between the volume and compressive strength of SF. **(B)** Relationship between the volume and compressive strength of PPF. **(C)** Relationship between the volume and compressive strength of DPF.

properties when compared to well-known composites like palm and glass, palm and bamboo, and glass made using the same processes (Nanayakkara and Xia, 2019; Najm et al., 2022a). The tensile strength of these glass and palm composites was investigated by Priya et al. (2005). More fabric was added to these composites, which increased their mechanical properties. The matrix and reinforcement were revealed to have good chemical resistance and interfacial bonding. Mishra et al. (2003) used chemically altered sisal fibres as reinforcement in the polyester matrix, in addition to glass fibres, to enhance the mechanical characteristics of the hybrid composites (Anas et al., 2022d; Anas et al., 2022g). The test results reveal that hybrid composites absorb less water than unhybridized composites (Althoey et al., 2022b; Hakeem et al., 2022c).

Civil engineering infrastructures have been built in hot and cold weathering zones such as the desert region. In such cases, the concrete is not only fractured by hot and cold processes, but it is also harmed by shrinkage cracking. As a result, the purpose of this research is to investigate the effect of HCCs on HSC containing various fibres comprising natural SF, PPF, and DPF in different volumetric ratios. Fibre implantation is the most widely used method for enhancing the structural behaviour of concrete (Cao et al., 2018b; Parvez et al., 2019; Khan and Ali, 2020; Xie et al., 2021). Fibres reduce the incidence of cracking, improve early strength under impact loads, and increase the structure's toughness. As a result, the primary goal of this work is to investigate the impacts of three different forms of fibres (steel, polypropylene, and date palm) in HSC without HCCs (curing for 28 days) and with HCCs (treatment for 270 days) and to continue the authors' project and the paper published in 28 and 180 days (Hakeem et al., 2023).

2 Materials and methodology

2.1 Materials

2.1.1 Cement
The FHSC samples used in this study were prepared using normal Portland cement (Type I). Table 1 and Table 2 include information regarding the chemical and physical properties of cement, respectively.

2.1.2 Aggregates
The coarse aggregate in the FHSC was crushed stone with a maximum size of 20 mm. As a fine aggregate, natural dune sand was used, with the bulk of its particles passing through a 4.75-mm sieve. Table 3 shows the physical properties of coarse and fine aggregates.

2.1.3 Fibres
2.1.3.1 Steel fibres
The SFs were bundled with hooks and adhesives at both ends. These bundles of SFs were used to produce FHSC. The physical properties of SF are given in Table 4. The range of fibres required to make FHSC varies from 0 to 1 percent of the concrete volume.

2.1.3.2 Polypropylene fibres (PPFs)
In comparison to SF and DPF concrete, PPFs were used to produce FHSC. The physical properties of PPF were given by the supplier, as shown in Table 5.

et al., 2022c; Unis Ahmed et al., 2022). The experimental results of the modulus of the rupture test, as reported by Azad et al. (2013), show that the samples can withstand higher loads until they reach the cracking load; nevertheless, once they reach the peak load, a softening mode of collapse can be seen, demonstrating significant ductility. Furthermore, it has been established that the introduction of SF enhances the resistance of reinforced concrete beams to shear failure, minimizing the need for stirrups (Khan and Ali, 2019; Lantsoght, 2019; Khan et al., 2020; Khan et al., 2022b).

Mohanty et al. (2002) revealed that the water sorptivity rates of these concrete samples were low when compared to unpalmed and classified composites. An investigation of the modulus of rupture, tensile, and dielectric properties of composites indicated similar findings for these
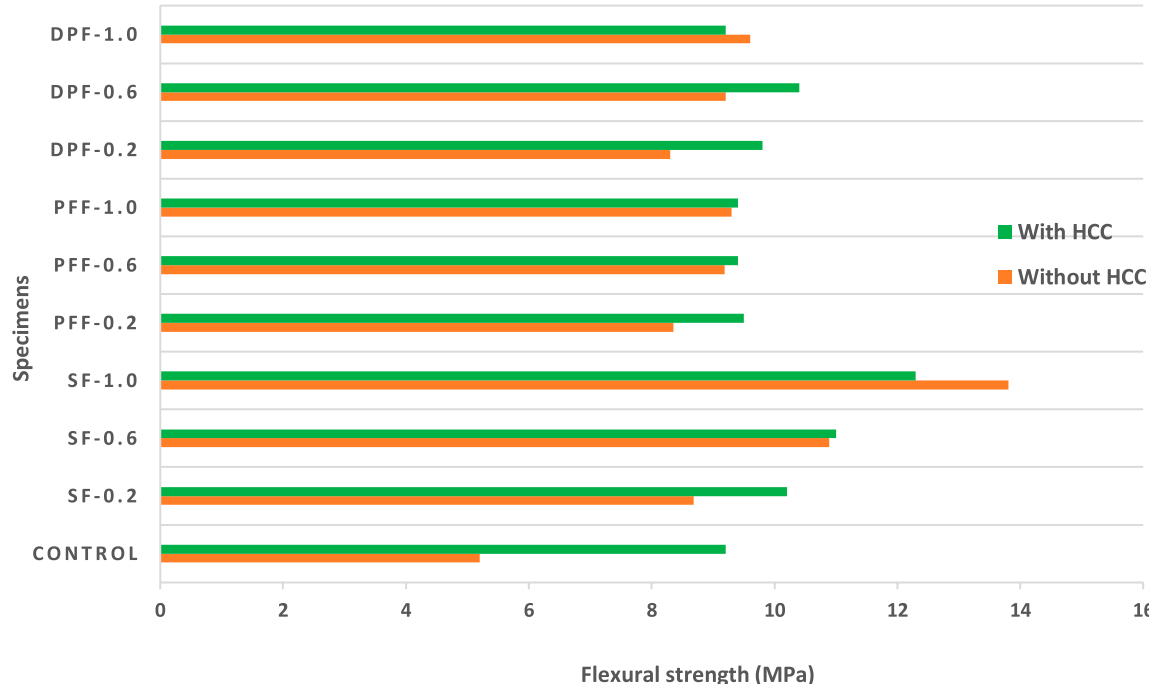
FIGURE 3
Impact of HCCs on the modulus of rupture of FHSC.

2.1.3.3 Date palm fibres

DPFs were obtained from 15- to 25-year-old date palm trees in and around Najran, Saudi Arabia (Althoey et al., 2022a). These trees constitute one of the most accessible diversities and are responsible for a significant volume of agro-waste.

The DPFs were chemically cured using different doses of sodium hydroxide to increase their compatibility with other concrete components and to eliminate any possible impurities from the surface of the fibres. The main effect of this approach is the disruption of hydrogen bonding within the network structure, which is shown here with increasing surface roughness (Kabir et al., 2012). Aqueous sodium hydroxide is used in this case to dissolve oils, wax, and lignin from the cell walls. As a result, alkaline treatment often influences the cellulose fibril, degree of polymerization, and, hence, the extraction of lignin and other non-cellulosic substances. The DPFs were treated by immersing them in a sodium hydroxide solution. Individually, the fibres were immersed in 1.5, 3.0, and 6.0 percent sodium hydroxide solutions. The fibres were submerged in the solution at room temperature for 24 h. Due to the maximum tensile strength of the fibres, the treatment with 3 percent sodium hydroxide was selected based on the impact on the fibres. The physical properties of the DPFs are listed in Table 6.

2.1.4 Superplasticizer

Superplasticizers (SPs) are well-known as effective water reducers in the production of HSC. In this investigation, Glenium®110M, which is based on polycarboxylate ether, was used as a superplasticizer for water reducers in the production of FHSC.

2.3 Methodology

2.3.1 Mix design and sample preparation

The behaviour of the fibres was evaluated using a variety of experiments that focused on particular characteristics of the FHSC. For FHSC, SF, PPF, and DPF were mixed with concrete in variable proportions of 0.2, 0.6, and 1.0 percent by concrete volume, respectively, as shown in Table 7.

The testing procedure was performed to determine the various hardened characteristics of the FHSC-utilising cylinders (150 mm diameter x 300 mm height), cubes (100 mm), and prisms (100 mm × 100 mm x 500 mm).

2.3.2 Thermal cycle procedure

After 28 days of water curing, the samples were placed in an oven and subjected to HCC. An HCC comprised 2 days of heating at 60 ˚C followed by 2 days of cooling at room temperature 25+- 5 ˚C (one-cycle) for 270 days (continuing the authors' project and research published at 28 and 180 days) (Hakeem et al., 2023). This heat–cool cycle was selected to imitate the daily change in ambient temperature in many parts of Saudi Arabia throughout the summertime. There was enough distance between the samples to allow for a regular flow of hot air during heating and easy heat dissipation during cooling. The compressive strength, modulus of rupture, toughness, ultrasonic pulse velocity, and water sorptivity of the samples were evaluated after 270 days of exposure.

FIGURE 4
Relationship between the volume and modulus of rupture of SF, PPF, and DPF. **(A)** Relationship between the volume and modulus of rupture of SF. **(B)** Relationship between the volume and modulus of rupture of PPF. **(C)** Relationship between the volume and modulus of rupture of DPF.
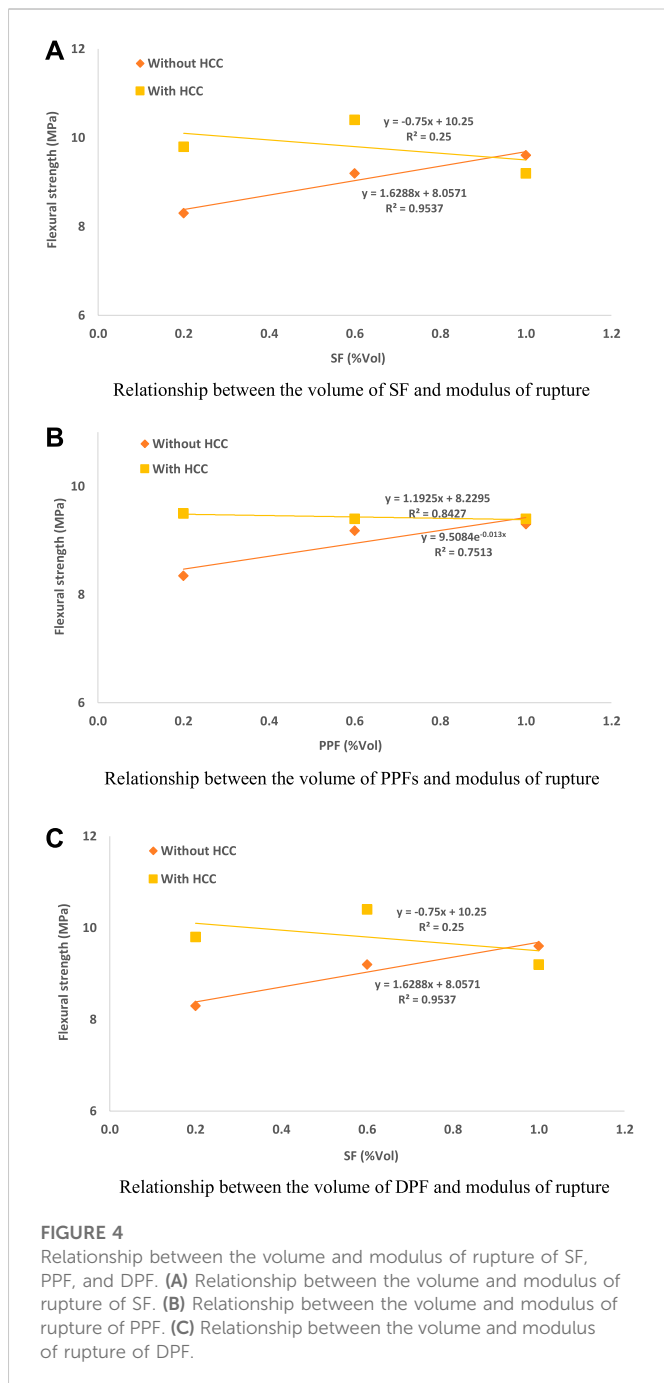
2.3.3 Investigation of structural properties

2.3.3.1 Compressive strength test
The compressive strength test for FHSC was performed in accordance with ASTM C109 (ASTM, 2020). After 28 days of hydration with regular drinking water, cube specimens (100 mm) were evaluated.

2.3.3.2 Modulus of rupture test
A centre-point loading setup was used to evaluate the modulus of rupture of FHSC prism specimens according to ASTM C293 (International, 2016b). This test was carried out using a Universal Instron machine with a loading capacity of 400 kN and a constant loading rate of 0.0167 mm/s. The displacement was measured using an LVDT mounted in the middle of the FHSC prism samples. The

displacement and applied load were automatically recorded in the data logger while the test was being performed on the prism samples.

2.3.3.3 Toughness
The energy retained by the unit cross-sectional area at any displacement terminal point is used to describe the toughness (capacity to absorb energy) of the FHSC samples (Hosen et al., 2022). The toughness of the samples was measured using the area under the load against deflection graphs up to the samples' rupture.

2.3.3.4 Ultrasonic pulse velocity test
To confirm the uniformity and stability of the FHSC samples, the ultrasonic pulse velocity (UPV) test was performed (Hosen et al., 2021). The test was carried out using the FHSC samples in line with ASTM C597 (International, 2016a).

2.3.3.5 Water sorptivity test
The development of surrounding small holes caused by excessive water is an indication of higher-grade concrete. As a consequence, concrete quality parameters such as unit weight, stiffness, and durability are commonly estimated using the water sorptivity test (also known as water absorption). The water sorptivity test for FHSC was made in line with BS 2011 Part 122 (Institution, 1998) using cylindrical specimens (150 mm in height and 75 mm in diameter) after satisfying the curing period requirement of 28 days.

3 Results and discussion

3.1 Compressive strength

Figure 1 presents the experimental results of compressive strength for FHSC samples without HCCs (curing for 28 days) and with HCCs (treatment for 270 days). The compressive strength steadily increased with increasing the fibre content for the FHSC samples without using HCCs, as shown in Figure 1. In contrast, the compressive strength of PPF- and DPF-reinforced concrete samples was somewhat decreased with increasing volume content of fibres when HCCs were used (Hakeem et al., 2023). As a result, the compressive strength might indeed be determined by the strength of the aggregates (Cao et al., 2018b; Khan et al., 2022c; Hosen et al., 2022), notwithstanding the little influence of HCCs on strength (Hakeem et al., 2023). Moreover, compared to the authors' previous study (Hakeem et al., 2023) at 180 days, there is a slight increase in compressive strength at 270 days, which is due to the effect of fibres.

Figures 2A–C show the relationship between compressive strength and the volume of SF, PPF, and DPF without HCCs (curing for 28 days) and with HCCs (treatment for 270 days). Strong R^2 values were found for the FHSC samples in this relationship.

3.2 Modulus of rupture

The modulus of rupture behaviour of fibre-reinforced concrete is essential to safeguard structures from extreme environmental
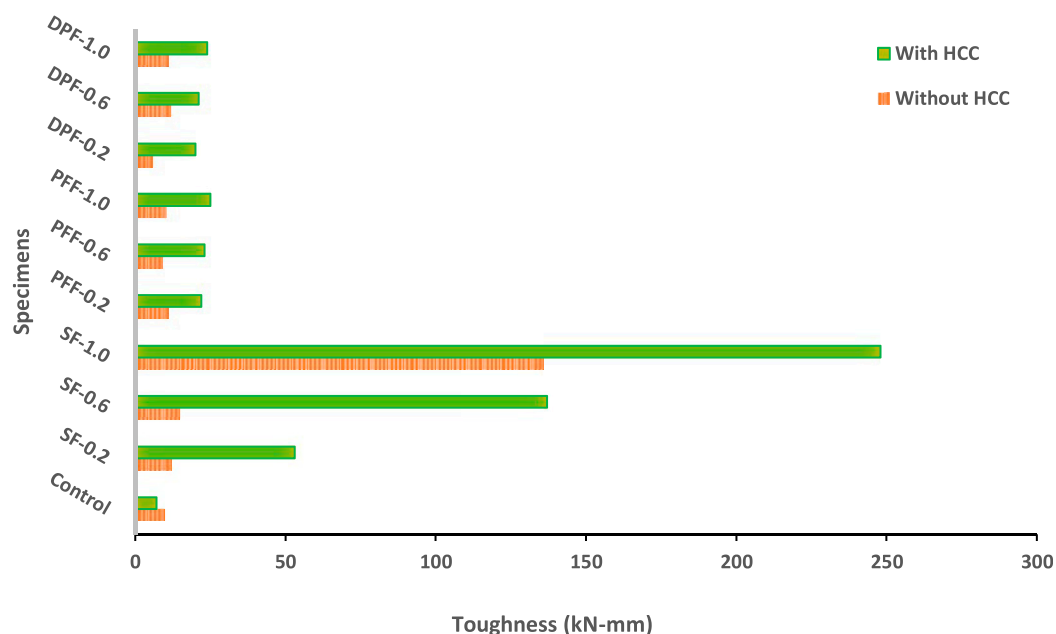
FIGURE 5
Behaviour toughness of FHSC with-and-without HCCs.
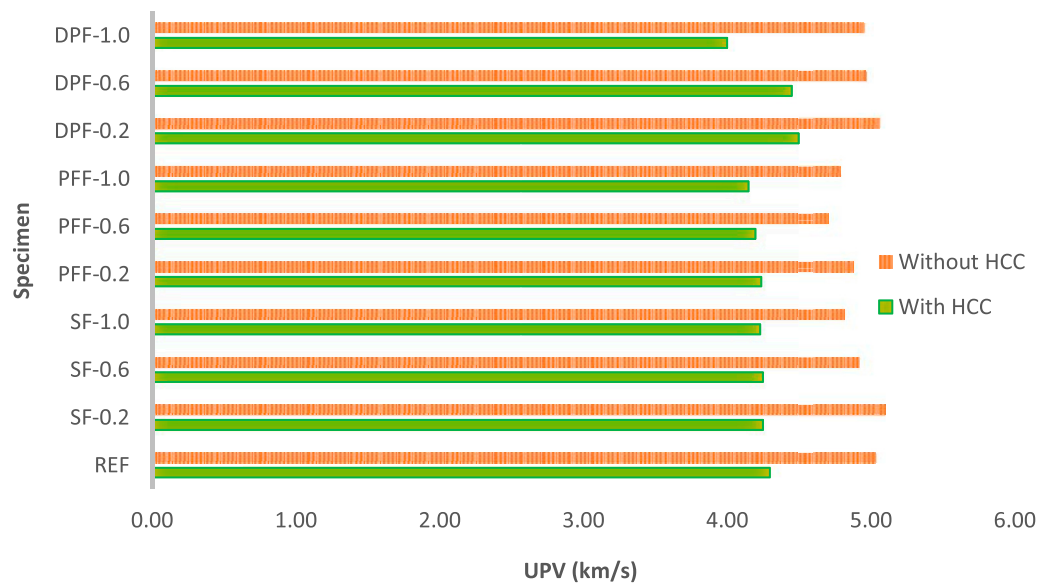
FIGURE 6
Deviations of UPV with and without HCCs for FHSC.

actions comprising excessive temperatures and freeze–thaw cycles (Cao et al., 2018a; Khan et al., 2018; Meskhi et al., 2022). Figure 3 illustrates the development of FHSC and the modulus of rupture. The introduction of SF, PPF, and DPF was increased from 0 to 1 percent and the modulus of rupture was increased by up to 33, 2, and 1 percent, respectively, above the control samples when HCCs were applied. SF considerably increased the modulus of rupture in both conditions as compared to PPF and DPF. Because of their increased capacity to survive extreme weathering impact and flexural rigidity, SFs could be able to delay or resist the formation of initial cracks in the cross-section of the samples (Tayeh et al., 2022a; Qaidi et al., 2022e). DPFs, on the other side, outperformed PPFs in terms of modulus of rupture behaviour due to their longer fibre length (Hakeem et al., 2023).

FIGURE 7
Relationship between the volume and UPV of SF, PPF, and DPF. **(A)** Relationship between the volume and UPV of SF. **(B)** Relationship between the volume and UPV of PPF. **(C)** Relationship between the volume and UPV of DPF.
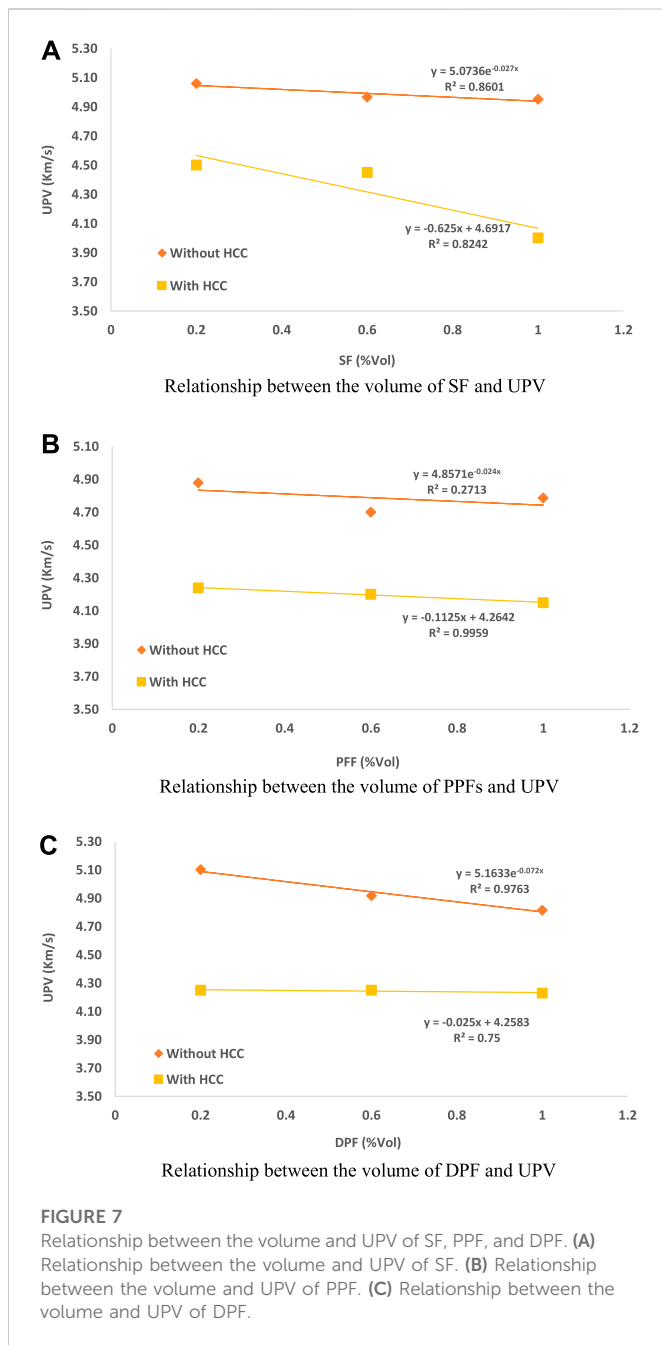
Kriker et al. (2005), on the other hand, studied the mechanical and physical properties of four distinct types of DPFs. The strength, toughness, microstructure, and continuity index of DPF-reinforced concrete are all reported as a function of curing in hot and water (Tayeh et al., 2022a; Qaidi et al., 2022c; Qaidi et al., 2022d; Qaidi et al., 2022e). It was observed that increasing the amount and length of fibre reinforcement enhanced the post-crack modulus of rupture and toughness coefficients but lowered the compressive strengths and initial crack in both water and hot, dry curing (Hakeem et al., 2023). Moreover, compared to the authors' previous study (Hakeem et al., 2023) at 180 days, there is a slight reduction in the modulus of rupture at 270 days,

which is due to the influence of thermal cycle exposure on the concrete.

Figures 4A–C show the relationship between the volume of SF, PPF, and DPF and the modulus of rupture without HCCs (curing for 28 days) and with HCCs (treatment for 270 days). This relationship indicated that without using HCCs, the FHSC samples linearly improved in the modulus of rupture.

3.3 Toughness

The toughness (energy absorption capabilities) of the FHSC samples without HCCs containing SF, PPF, and DPF was compared to the control sample. As the volume of fibre reinforcement in the concrete mixtures was increased, the toughness and load-bearing capacity improved (Hakeem et al., 2023).

The toughness of the FHSC samples without HCCs (curing for 28 days) and with HCCs (treatment for 270 days) are illustrated in Figure 5. According to the evaluation of the ruptured failure samples, the failure was caused by the crack-bridging interaction between the grout and fibres in the matrix (Abd et al., 2022; He et al., 2022; Ibrahim et al., 2022; Abd et al., 2023). As a result of the increased stiffness of the SF, its toughness in both circumstances, with and without HCCs, is greater than that of the PPF- and DPF-reinforced concrete samples. As a result, it is indicated that concrete containing SF is better suitable for hard weathering action than PPF and DPF concrete samples (Hakeem et al., 2023). Moreover, compared to the authors' previous study (Hakeem et al., 2023) at 180 days, there is a slight increase in toughness at 270 days, which is due to the effect of fibres.

3.4 Ultrasonic pulse velocity

Figure 6 presents the UPV of the HSC without HCCs (curing for 28 days) and with HCCs (treatment for 270 days) containing SF, PPF, and DPF. The SF, PPF, and DPF were introduced in increasing proportions to the HSC, which served to lessen ultrasonic wave pass-through further and more efficiently without the HCC (Hakeem et al., 2022b). HCCs had no effect on the FHSC as fibre amounts increased. This was to confirm that the FHSC was uniform and stable (Hakeem et al., 2023). Moreover, compared to the authors' previous study (Hakeem et al., 2023) at 180 days, there is a slight decrease in UPV at 270 days, which is due to the influence of thermal cycle exposure on the concrete.

Figures 7A–C illustrate the relationship between the volume of SF, PPF, and DPF and the UPV without HCCs (curing for 28 days) and with HCCs (treatment for 270 days).

3.5 Water sorptivity

The pore structure of concrete is widely known to have a significant impact on the material's durability. The quantity of water absorbed by immersion offers an estimate of the overall pore
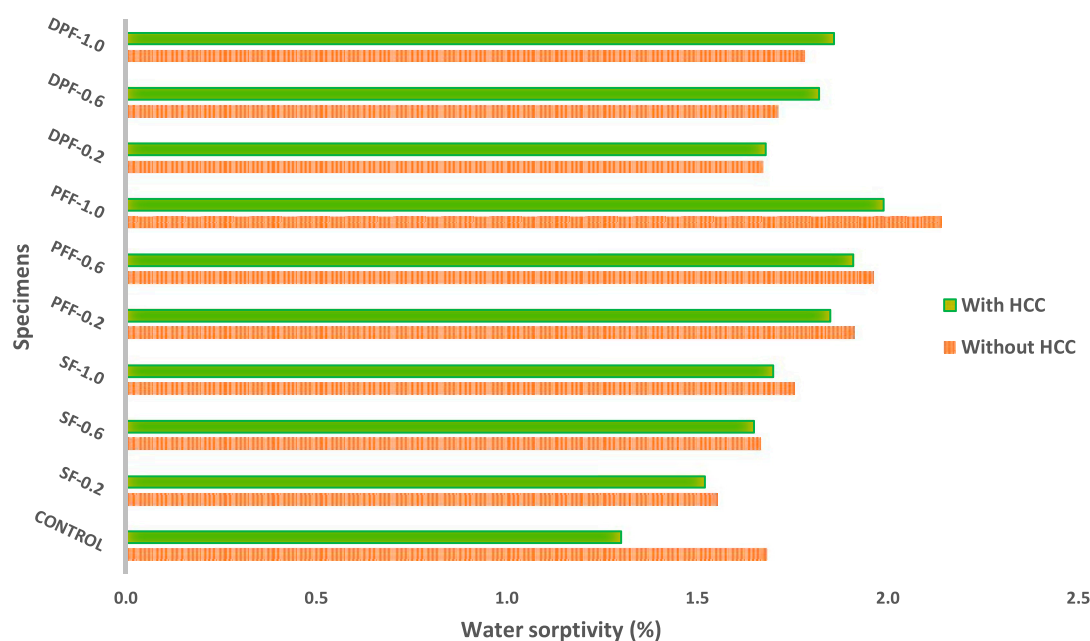
FIGURE 8
Variation of water sorptivity of FHSC.

volume of the concrete (De Schutter and Audenaert, 2004). In cases of applied HCC and without HCC, the water sorptivity of the FHSC samples was greater than that of the control concrete (Hakeem et al., 2023). Increasing the volume of fibre in the concrete increased the water sorptivity, as seen in Figure 8. Because the fibres flowed around the mortar and formed an interaction with it, they enhanced the micropores within the concrete. As a result, the water sorptivity of fibre reinforced was greatly enhanced as compared to the control sample. Nevertheless, the water sorptivity of FHSC was much lower, despite the fact that the water sorptivity of good-grade concrete should be less than 10 percent by weight (Neville, 1995; Hakeem et al., 2023). Moreover, compared to the authors' previous study (Hakeem et al., 2023) at 180 days, there is a slight decrease in water sorptivity at 270 days, which is due to influence of thermal cycle exposure on the concrete.

Figures 9A–C shows a substantial relationship between the water sorptivity and the volume of SF, PPF, and DPF content without HCCs (curing for 28 days) and with HCCs (treatment for 270 days).

4 Conclusion

In continuation of the authors' project and the paper published in 28 and 180 days (Hakeem et al., 2023), the effect of HCC for 270 days on concrete comprising SF, PPF, and DPF was studied in order to develop HSC. For the production of FHSC, different percentages (0, 0.2, 0.6, and 1.0 percent) of SF, PPF, and DPF were used. Mechanical and durability properties comprising compressive strength, modulus of rupture, toughness, ultrasonic pulse velocity, and water sorptivity were investigated. Based on the laboratory findings, the following concluding observations can be made:

1. The compressive strength of FHSC was dramatically increased by increasing the quantity of fibre volume fraction without using HCC. In contrast, performing HCC on samples comprising PPF and DPF lowered their compressive strength. Nevertheless, the SF-encompassing samples demonstrated a significant improvement in this condition as well, owing to the fibres' higher compressive load-bearing capacity.
2. The modulus of rupture enhanced significantly when SF, PPF, and DPF were added to HSC without HCC (curing for 28 days) and with HCC (treatment for 270 days). As the percentages of SF, PPF, and DPF were increased from 0 to 1 percent, the modulus of rupture increased by up to 33, 2, and 1 percent, respectively, above the control samples when HCC was applied.
3. In all conditions, with and without the application of HCC, the introduction of SF, PPF, and DPF into HSC demonstrated a significant increase in toughness compared with the control sample.
4. The inclusion of SF, PPF, and DPF in HSC improved UPV when compared to the control sample without HCC. The application of HCC to the FHSC samples had no effect.
5. As a result, natural DPF can be used to make a sustainable FHSC that can resist harsh weather conditions.
6. Moreover, compared to the authors' previous study at 180 days, there is a slight increase in compressive strength and toughness and a slight decrease in the modulus of rupture, ultrasonic pulse velocity, and water sorptivity at 270 days.

5 Recommendations

Further studies have to focus on the structural characteristics of SF-, PPF-, and DPF-comprising high-strength concrete, considering

A
y = 0.225x + 1.6517
R² = 0.9067

y = 1.6424e^{0.0794x}
R² = 0.9788

Relationship between the volume of SF and water sorptivity

B
y = 1.8401e^{0.1414x}
R² = 0.915

y = 1.8138e^{0.0912x}
R² = 0.9949

Relationship between the volume of PPFs and water sorptivity

C
y = 0.2523x + 1.5072
R² = 0.9935

y = 0.225x + 1.4883
R² = 0.9382

Relationship between the volume of DPF and water sorptivity
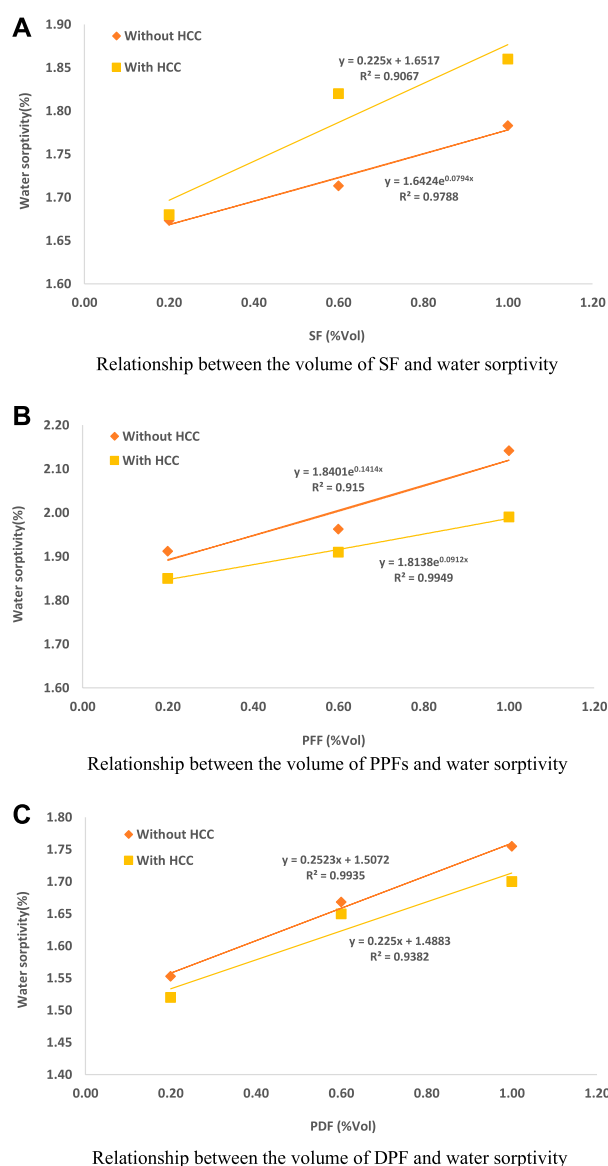
FIGURE 9
Relationship between the volume and water sorptivity of SF, PPF, and DPF. **(A)** Relationship between the volume and water sorptivity of SF. **(B)** Relationship between the volume and water sorptivity of PPF. **(C)** Relationship between the volume and water sorptivity of DPF.

the full-scale structural elements under monotonic and fatigue loading.

Data availability statement

The original contributions presented in the study are included in the article/Supplementary Material; further inquiries can be directed to the corresponding authors.

Author contributions

Conception and design of the study: MH, SQ, IH, MA, and AA; acquisition of data: YÖ, MoA; analysis and/or interpretation of data: MA, MoA, AA; drafting the manuscript: MH, SQ, IH, YÖ, MA, MoA and AA; revising the manuscript critically for important intellectual content: MA, MoA, AA; and approval of the version of the manuscript to be published: MH, SQ, IH, YÖ, MA, MoA and AA.

Acknowledgments

Conflict of interest

The authors declare that the research was conducted in the absence of any commercial or financial relationships that could be construed as a potential conflict of interest.

Publisher's note

All claims expressed in this article are solely those of the authors and do not necessarily represent those of their affiliated organizations, or those of the publisher, the editors, and the reviewers. Any product that may be evaluated in this article, or claim that may be made by its manufacturer, is not guaranteed or endorsed by the publisher.

References

Abd, S. M., Mhaimeed, I. S., Tayeh, B. A., Najm, H. M., and Qaidi, S. (2022). Flamingo technique as an innovative method to improve the shear capacity of reinforced concrete beam. *Case Stud. Constr. Mater.* 17, e01618. doi:10.1016/j.cscm.2022.e01618

Abd, S. M., Mhaimeed, I. S., Tayeh, B. A., Najm, H. M., and Qaidi, S. (2023). Investigation of the use of textile carbon yarns as sustainable shear reinforcement in concrete beams. *Case Stud. Constr. Mater.* 18, e01765. doi:10.1016/j.cscm.2022.e01765

Ahmad, S., Hakeem, I., and Maslehuddin, M. (2016). Development of an optimum mixture of ultra-high performance concrete. *Eur. J. Environ. Civ. Eng.* 20, 1106–1126. doi:10.1080/19648189.2015.1090925

Ahmad, W., Farooq, S. H., Usman, M., Khan, M., Ahmad, A., Aslam, F., et al. (2020). Effect of coconut fiber length and content on properties of high strength concrete. *Materials* 13, 1075. doi:10.3390/ma13051075

Ahmed, H. U., Mohammed, A. A., Rafiq, S., Mohammed, A. S., Mosavi, A., Sor, N. H., et al. (2021). Compressive strength of sustainable geopolymer concrete composites: A state-of-the-art review. *Sustainability* 13, 13502. doi:10.3390/su132413502

Alabduljabbar, H., Alyousef, R., Alrshoudi, F., Alaskar, A., Fathi, A., and Mustafa Mohamed, A. (2019). Mechanical effect of steel fiber on the cement replacement materials of self-compacting concrete. *Fibers* 7, 36. doi:10.3390/fib7040036

Althoey, F., and Hakeem, I. Y. (2022). "Development of green and sustainable ultra-high-performance concrete composite reinforced with date palm fibers," in Proceedings of the IOP Conference Series: Earth and Environmental Science, United Kingdom, May 27, 2022 (IOP Publishing), 012021.

Althoey, F., Hakeem, I. Y., Hosen, M., Qaidi, S., Isleem, H. F., Hadidi, H., et al. (2022a). Behavior of concrete reinforced with date palm fibers. *Materials* 15, 7923. doi:10.3390/ma15227923

Althoey, F., Zaid, O., De-Prado-Gil, J., Palencia, C., Ali, E., Hakeem, I., et al. (2022b). Impact of sulfate activation of rice husk ash on the performance of high strength steel fiber reinforced recycled aggregate concrete. *J. Build. Eng.* 54, 104610. doi:10.1016/j.jobe.2022.104610

Anas, S., Alam, M., Isleem, H. F., Najm, H. M., and Sabri, M. M. S. (2022a). Ultra high performance concrete and C-frp tension Re-bars: A unique combinations of materials for slabs subjected to low-velocity drop impact loading. *Front. Mater.* 9, 1061297. doi:10.3389/fmats.2022.1061297

Anas, S., Alam, M., Isleem, H. F., Najm, H. M., and Sabri Sabri, M. M. (2022b). Role of cross-diagonal reinforcements in lieu of seismic confining stirrups in the performance enhancement of square RC columns carrying axial load subjected to close-range explosive loading. *Front. Mater.* 9, 1002195. doi:10.3389/fmats.2022.1002195

Anas, S., Alam, M., and Shariq, M. (2022c). Behavior of two-way RC slab with different reinforcement orientation layouts of tension steel under Drop Load Impact. *Mater. Today Proc.* article in press. doi:10.1016/j.matpr.2022.08.509

Anas, S., Alam, M., and Shariq, M. (2022d). Damage response of conventionally reinforced two-way spanning concrete slab under eccentric impacting drop weight loading. *Def. Technol.* 19, 12–34. doi:10.1016/j.dt.2022.04.011

Anas, S., Alam, M., and Umair, M. (2022e). Air-blast and ground shockwave parameters, shallow underground blasting, on the ground and buried shallow underground blast-resistant shelters: A review. *Int. J. Prot. Struct.* 13, 99–139. doi:10.1177/20414196211048910

Anas, S., Alam, M., and Umair, M. (2022f). Performance based strengthening with concrete protective coatings on braced unreinforced masonry wall subjected to close-in explosion. *Mater. Today Proc.* 64, 161–172. doi:10.1016/j.matpr.2022.04.206

Anas, S., Shariq, M., Alam, M., and Umair, M. (2022g). Evaluation of critical damage location of contact blast on conventionally reinforced one-way square concrete slab applying CEL-FEM blast modeling technique. *Int. J. Prot. Struct.* 13, 672–715. doi:10.1177/20414196221095251

Astm (2020). "Standard test method for compressive strength of hydraulic cement mortars," in *C109/C109M-20b* (Pennsylvania, United States: ASTM International).

Azad, A. K., Ahmad, S., and Hakeem, I. (2013). Effect of cyclic exposure and fibre content on tensile properties of ultra-high-performance concrete. *Adv. Cem. Res.* 25, 273–280. doi:10.1680/adcr.12.00039

Bajaber, M., and Hakeem, I. (2021). UHPC evolution, development, and utilization in construction: A review. *J. Mater. Res. Technol.* 10, 1058–1074. doi:10.1016/j.jmrt.2020.12.051

Bingöl, A. F., and Balaneji, H. H. (2019). Determination of sulfate resistance of concretes containing silica fume and fly ash. *Iran. J. Sci. Technol. Trans. Civ. Eng.* 43, 219–230. doi:10.1007/s40996-018-0160-x

Cao, M., Li, L., and Khan, M. (2018a). Effect of hybrid fibers, calcium carbonate whisker and coarse sand on mechanical properties of cement-based composites. *Mater. Construcción* 68, e156. doi:10.3989/mc.2018.01717

Cao, M., Xie, C., Li, L., and Khan, M. (2018b). The relationship between reinforcing index and flexural parameters of new hybrid fiber reinforced slab. *Comput. Concr. Int. J.* 22, 481–492.

Çelik, A. İ., Özkılıç, Y. O., Zeybek, Ö., Karalar, M., Qaidi, S., Ahmad, J., et al. (2022). Mechanical behavior of crushed waste glass as replacement of aggregates. *Materials* 15, 8093. doi:10.3390/ma15228093

De Schutter, G., and Audenaert, K. (2004). Evaluation of water absorption of concrete as a measure for resistance against carbonation and chloride migration. *Mater. Struct.* 37, 591–596. doi:10.1617/14045

Geng, K., Chai, J., Qin, Y., Li, X., Duan, M., and Liang, D. (2022). Exploring the brittleness and fractal characteristics of basalt fiber reinforced concrete under impact load based on the principle of energy dissipation. *Mater. Struct.* 55, 78–16. doi:10.1617/s11527-022-01891-2

Hakeem, I, Hosen, M. A., Alyami, M., Qaidi, S., and Özkılıç, Y. (2023). *Influence of heat-cool cyclic exposure on the performance of fiber-reinforced high-strength concrete* sustainability. doi:10.3390/su15021433

Hakeem, I. Y., Althoey, F., and Hosen, A. (2022a). Mechanical and durability performance of ultra-high-performance concrete incorporating SCMs. *Constr. Build. Mater.* 359, 129430. doi:10.1016/j.conbuildmat.2022.129430

Hakeem, I. Y., Amin, M., Abdelsalam, B. A., Tayeh, B. A., Althoey, F., and Agwa, I. S. (2022b). Effects of nano-silica and micro-steel fiber on the engineering properties of ultra-high performance concrete. *Struct. Eng. Mech.* 82, 295–312.

Hakeem, I. Y., Amin, M., Zeyad, A. M., Tayeh, B. A., Maglad, A. M., and Agwa, I. S. (2022c). Effects of nano sized sesame stalk and rice straw ashes on high-strength concrete properties. *J. Clean. Prod.* 370, 133542. doi:10.1016/j.jclepro.2022.133542

Hakeem, I. Y., Rahman, M. K., and Althoey, F. (2022d). Experimental investigation of hybrid beams utilizing ultra-high performance concrete (UHPC) as tension reinforcement. *Materials* 15, 5619. doi:10.3390/ma15165619

Hawreen, A., Bogas, J., and Kurda, R. (2019). Mechanical characterization of concrete reinforced with different types of carbon nanotubes. *Arabian J. Sci. Eng.* 44, 8361–8376. doi:10.1007/s13369-019-04096-y

He, X., Yuhua, Z., Qaidi, S., Isleem, H. F., Zaid, O., Althoey, F., et al. (2022). Mine tailings-based geopolymers: A comprehensive review. *Ceram. Int.* 48, 24192–24212. doi:10.1016/j.ceramint.2022.05.345

Hosen, M. A., Shammas, M. I., Shill, S. K., Al-Deen, S., Jumaat, M. Z., and Hashim, H. (2022). Ductility enhancement of sustainable fibrous-reinforced high-strength lightweight concrete. *Polymers* 14, 727. doi:10.3390/polym14040727

Hosen, M. A., Shammas, M. I., Shill, S. K., Jumaat, M. Z., Alengaram, U. J., Ahmmad, R., et al. (2021). Investigation of structural characteristics of palm oil clinker based high-strength lightweight concrete comprising steel fibers. *J. Mater. Res. Technol.* 15, 6736–6746. doi:10.1016/j.jmrt.2021.11.105

Hussain, I., Ali, B., Akhtar, T., Jameel, M. S., and Raza, S. S. (2020). Comparison of mechanical properties of concrete and design thickness of pavement with different types of fiber-reinforcements (steel, glass, and polypropylene). *Case Stud. Constr. Mater.* 13, e00429. doi:10.1016/j.cscm.2020.e00429

Ibrahim, A. M., Abd, S. M., Hussein, O. H., Tayeh, B. A., Najm, H. M., and Qaidi, S. (2022). Influence of adding short carbon fibers on the flexural behavior of textile-reinforced concrete one-way slab. *Case Stud. Constr. Mater.* 17, e01601. doi:10.1016/j.cscm.2022.e01601

Institution, B. S. (1998). *Testing concrete-Part 122*. United Kingdom: Method for Determination of Water Absorption. BS 1881-122:2011.

International, A. (2016a). "C293/C293M-16," in *Standard test method for flexural strength of concrete (using simple beam with center-point loading)* (Pennysylvania, United States: ASTM International).

International, A. (2016b). *Standard test method for pulse velocity through concrete*. West Conshohocken, PA: ASTM. C597-16.

Iqbal, S., Ali, I., Room, S., Khan, S. A., and Ali, A. (2019). Enhanced mechanical properties of fiber reinforced concrete using closed steel fibers. *Mater. Struct.* 52, 56–10. doi:10.1617/s11527-019-1357-6

Kabir, M., Wang, H., Lau, K., and Cardona, F. (2012). Chemical treatments on plant-based natural fibre reinforced polymer composites: An overview. *Compos. Part B Eng.* 43, 2883–2892. doi:10.1016/j.compositesb.2012.04.053

Kaur, P., and Talwar, M. (2017). Different types of Fibres used in FRC. *Int. J. Adv. Res. Comput. Sci.* 8, 272–275. doi:10.26483/ijarcs.v8i7.4239

Khan, M., and Ali, M. (2019). Improvement in concrete behavior with fly ash, silica-fume and coconut fibres. *Constr. Build. Mater.* 203, 174–187. doi:10.1016/j.conbuildmat.2019.01.103

Khan, M., and Ali, M. (2020). Optimization of concrete stiffeners for confined brick masonry structures. *J. Build. Eng.* 32, 101689. doi:10.1016/j.jobe.2020.101689

Khan, M., Cao, M., Ai, H., and Hussain, A. (2022a). Basalt fibers in modified whisker reinforced cementitious composites. *Period. Polytech. Civ. Eng.* 66, 344–354. doi:10.3311/ppci.18965

Khan, M., Cao, M., Hussain, A., and Chu, S. H. (2021). Effect of silica-fume content on performance of CaCO3 whisker and basalt fiber at matrix interface in cement-based composites. *Constr. Build. Mater.* 300, 124046. doi:10.1016/j.conbuildmat.2021.124046

Khan, M., Cao, M., Xie, C., and Ali, M. (2022b). Effectiveness of hybrid steel-basalt fiber reinforced concrete under compression. *Case Stud. Constr. Mater.* 16, e00941. doi:10.1016/j.cscm.2022.e00941

Khan, M., Lao, J., and Dai, J.-G. (2022c). Comparative study of advanced computational techniques for estimating the compressive strength of UHPC. *J. Asian Concr. Fed.* 8, 51–68. doi:10.18702/acf.2022.6.8.1.51

Khan, M., Rehman, A., and Ali, M. (2020). Efficiency of silica-fume content in plain and natural fiber reinforced concrete for concrete road. *Constr. Build. Mater.* 244, 118382. doi:10.1016/j.conbuildmat.2020.118382

Khan, U. A., Jahanzaib, H. M., Khan, M., and Ali, M. (2018). "Improving the tensile energy absorption of high strength natural fiber reinforced concrete with fly-ash for bridge girders," in *Key engineering materials* (Switzerland: Trans Tech Publ), 335–342.

Koushkbaghi, M., Kazemi, M. J., Mosavi, H., and Mohseni, E. (2019). Acid resistance and durability properties of steel fiber-reinforced concrete incorporating rice husk ash and recycled aggregate. *Constr. Build. Mater.* 202, 266–275. doi:10.1016/j.conbuildmat.2018.12.224

Kriker, A., Debicki, G., Bali, A., Khenfer, M., and Chabannet, M. (2005). Mechanical properties of date palm fibres and concrete reinforced with date palm fibres in hot-dry climate. *Cem. Concr. Compos.* 27, 554–564. doi:10.1016/j.cemconcomp.2004.09.015

Lantsoght, E. O. (2019). How do steel fibers improve the shear capacity of reinforced concrete beams without stirrups? *Compos. Part B Eng.* 175, 107079. doi:10.1016/j.compositesb.2019.107079

Ma, C.-K., Apandi, N. M., Sofrie, C. S. Y., Ng, J. H., Lo, W. H., Awang, A. Z., et al. (2017). Repair and rehabilitation of concrete structures using confinement: A review. *Constr. Build. Mater.* 133, 502–515. doi:10.1016/j.conbuildmat.2016.12.100

Meskhi, B., Beskopylny, A. N., Stel'makh, S. A., Shcherban', E. M., Mailyan, L. R., Beskopylny, N., et al. (2022). Insulation foam concrete nanomodified with microsilica and reinforced with polypropylene fiber for the improvement of characteristics. *Polymers* 14, 4401. doi:10.3390/polym14204401

Mishra, S., Mohanty, A., Drzal, L., Misra, M., Parija, S., Nayak, S., et al. (2003). Studies on mechanical performance of biofibre/glass reinforced polyester hybrid composites. *Compos. Sci. Technol.* 63, 1377–1385. doi:10.1016/s0266-3538(03)00084-8

Mohanty, A. K., Misra, M., and Drzal, L. (2002). Sustainable bio-composites from renewable resources: Opportunities and challenges in the green materials world. *J. Polym. Environ.* 10, 19–26. doi:10.1023/a:1021013921916

Najm, H. M., Nanayakkara, O., Ahmad, M., and Sabri Sabri, M. M. (2022a). Colour change of sustainable concrete containing waste ceramic and hybrid fibre: Effect of temperature. *Materials* 15, 2174. doi:10.3390/ma15062174

Najm, H. M., Nanayakkara, O., and Sabri, M. M. S. (2022b). Destructive and non-destructive evaluation of fibre-reinforced concrete: A comprehensive study of mechanical properties. *Materials* 15, 4432. doi:10.3390/ma15134432

Nanayakkara, O., Najm, H. M., and Sabri, M. M. S. (2022). Effect of using steel bar reinforcement on concrete quality by ultrasonic pulse velocity measurements. *Materials* 15, 4565. doi:10.3390/ma15134565

Nanayakkara, O., and Xia, J. (2019). Mechanical and physical properties of mortar of partially replaced fine aggregates with sawdust. *Acad. J. Civ. Eng.* 37, 308–313.

Nassiri, S., Alshareedah, O., Rodin, H., and Englund, K. (2021). Mechanical and durability characteristics of pervious concrete reinforced with mechanically recycled carbon fiber composite materials. *Mater. Struct.* 54, 107–118. doi:10.1617/s11527-021-01708-8

Neville, A. M. (1995). *Properties of concrete*. London United States: Longman.

Parvez, I., Shen, J., Khan, M., and Cheng, C. (2019). Modeling and solution techniques used for hydro generation scheduling. *Water* 11, 1392. doi:10.3390/w11071392

Peled, A., Jones, J., and Shah, S. P. (2005). Effect of matrix modification on durability of glass fiber reinforced cement composites. *Mater. Struct.* 38, 163–171. doi:10.1617/14091

Priya, S. P., Ramakrishna, H., Rai, S., and Rajulu, A. V. (2005). Tensile, flexural, and chemical resistance properties of waste silk fabric-reinforced epoxy laminates. *J. Reinf. plastics Compos.* 24, 643–648. doi:10.1177/0731684405045024

Qaidi, S. M. A., Mohammed, A. S., Ahmed, H. U., Faraj, R. H., Emad, W., Tayeh, B. A., et al. (2022c). Rubberized geopolymer composites: A comprehensive review. *Ceram. Int.* 48, 24234–24259. doi:10.1016/j.ceramint.2022.06.123

Qaidi, S. M. A., Sulaiman Atrushi, D., Mohammed, A. S., Unis Ahmed, H., Faraj, R. H., Emad, W., et al. (2022d). Ultra-high-performance geopolymer concrete: A review. *Constr. Build. Mater.* 346, 128495. doi:10.1016/j.conbuildmat.2022.128495

Qaidi, S. M. A., Tayeh, B. A., Zeyad, A. M., De Azevedo, A. R. G., Ahmed, H. U., and Emad, W. (2022e). Recycling of mine tailings for the geopolymers production: A systematic review. *Case Stud. Constr. Mater.* 16, e00933. doi:10.1016/j.cscm.2022.e00933

Qaidi, S., Najm, H. M., Abed, S. M., Ahmed, H. U., Al Dughaishi, H., Al Lawati, J., et al. (2022a). Fly ash-based geopolymer composites: A review of the compressive strength and microstructure analysis. *Materials* 15, 7098. doi:10.3390/ma15207098

Qaidi, S., Najm, H. M., Abed, S. M., Özkılıç, Y. O., Al Dughaishi, H., Alosta, M., et al. (2022b). Concrete containing waste glass as an environmentally friendly aggregate: A review on fresh and mechanical characteristics. *Materials* 15, 6222. doi:10.3390/ma15186222

Richard, P., and Cheyrezy, M. (1995). Composition of reactive powder concretes. *Cem. Concr. Res.* 25, 1501–1511. doi:10.1016/0008-8846(95)00144-2

Saeed, A., Najm, H. M., Hassan, A., Qaidi, S., Sabri, M. M. S., and Mashaan, N. S. (2022a). A comprehensive study on the effect of regular and staggered openings on the seismic performance of shear walls. *Buildings* 12, 1293. doi:10.3390/buildings12091293

Saeed, A., Najm, H. M., Hassan, A., Sabri, M. M. S., Qaidi, S., Mashaan, N. S., et al. (2022b). Properties and applications of geopolymer composites: A review study of mechanical and microstructural properties. *Materials* 15, 8250. doi:10.3390/ma15228250

Tayeh, B. A., Akeed, M. H., Qaidi, S., and Bakar, B. H. A. (2022a). Influence of sand grain size distribution and supplementary cementitious materials on the compressive strength of ultrahigh-performance concrete. *Case Stud. Constr. Mater.* 17, e01495. doi:10.1016/j.cscm.2022.e01495

Tayeh, B. A., Akeed, M. H., Qaidi, S., and Bakar, B. H. A. (2022b). Influence of the proportion of materials on the rheology and mechanical strength of ultrahigh-performance concrete. *Case Stud. Constr. Mater.* 17, e01433. doi:10.1016/j.cscm.2022.e01433

Tayeh, B. A., Akeed, M. H., Qaidi, S., and Bakar, B. H. A. (2022c). Ultra-high-performance concrete: Impacts of steel fibre shape and content on flowability, compressive strength and modulus of rupture. *Case Stud. Constr. Mater.* 17, e01615. doi:10.1016/j.cscm.2022.e01615

Unis Ahmed, H., Mahmood, L. J., Muhammad, M. A., Faraj, R. H., Qaidi, S. M. A., Hamah Sor, N., et al. (2022). Geopolymer concrete as a cleaner construction material: An overview on materials and structural performances. *Clean. Mater.* 5, 100111. doi:10.1016/j.clema.2022.100111

Xie, C., Cao, M., Guan, J., Liu, Z., and Khan, M. (2021). Improvement of boundary effect model in multi-scale hybrid fibers reinforced cementitious composite and prediction of its structural failure behavior. *Compos. Part B Eng.* 224, 109219. doi:10.1016/j.compositesb.2021.109219

Zeybek, Ö., Özkılıç, Y. O., Karalar, M., Çelik, A. İ., Qaidi, S., Ahmad, J., et al. (2022). Influence of replacing cement with waste glass on mechanical properties of concrete. *Materials* 15, 7513. doi:10.3390/ma15217513

Zhang, N., Yan, C., Li, L., and Khan, M. (2022). Assessment of fiber factor for the fracture toughness of polyethylene fiber reinforced geopolymer. *Constr. Build. Mater.* 319, 126130. doi:10.1016/j.conbuildmat.2021.126130

frontiers | Frontiers in Materials

Check for updates

Bio-deposition approaches for sustainable execution of recycled aggregates in concretes

Muhammad Arslan Ahmad[1,2†], Bing Liu[3†], Qiuwei Li[1], Muhammad Adeel[4], Jinlong Zhang[1], Yingwu Zhou[5*] and Xu Deng[1*]

[1]Shenzhen Key Laboratory of Marine Bioresource and Eco-environmental Science, College of Life Sciences and Oceanography, Shenzhen University, Shenzhen, China, [2]College of Physics and Optoelectronic Engineering, Shenzhen University, Shenzhen, China, [3]School of Traffic and Environment, Shenzhen Institute of Information Technology, Shenzhen, China, [4]BNU-HKUST Laboratory of Green Innovation, Advanced Institute of Natural Sciences, Beijing Normal University at Zhuhai, Zhuhai, China, [5]College of Civil and Transportation Engineering, Shenzhen University, Shenzhen, China

Our study offers a quantitative framework for microbial-induced calcium carbonate precipitation (MICP) to uplift the properties of recycled aggregate concrete (RAC). In this regard, a marine alkalophilic bacterium *Bacillus sp.* B6 was employed, and its growth and mineralization efficiency under seawater conditions was investigated. Optimization of MICP was achieved with different nutrient sources and bacterial introduction methods (dip and spray). The efficiency of treated recycled aggregates (RA) was determined by using scanning electron microscopy (SEM) and energy dispersive X-ray (EDX) in combination with basic technologies of density improvement and water absorption. The results show that the optimal nutrient sources of carbon and nitrogen are glucose ($7 \, g \, L^{-1}$) and tryptone ($5 \, gL^{-1}$), respectively. Spray treated recycled aggregate (RA) is reported to be efficient with a reduction in water absorption (~19%), and improvement in bulk (~2.4%) and apparent density (~1.7%). The effectiveness of the MICP treatment process is confirmed with SEM and EDX observations, indicating the filling of microcracks with calcium carbonates. As such, the mechanical properties of RAC with spray treated RA significantly increase by up to ~24% in compressive strength as compared to the control treatment. Current findings will help revitalize the construction industry by utilizing the MICP-treated RA and minimizing the load on natural aggregates.

KEYWORDS

self-healing, recycled aggregates, microbial induced calcium precipitation, marine bacteria, spray treatment, mechanical properties

1 Introduction

The construction industry makes a significant contribution to waste material production i.e. 1.3 billion tonnes per year (Ghaffar et al., 2020) and CO_2 emissions of up to 60% (Müller et al., 2013). It is estimated that around 70% of the human population will be in urban areas by 2050 and construction waste will increase to 2.2 billion tonnes by 2025 (Environment, 2018). Concrete is the major pillar of the modern construction industry, and demand for concrete is ever-growing, reaching up to 30 billion tons per year globally (Monteiro et al., 2017). Additionally, developing countries are financing huge in building concrete infrastructures and *per capita* production of concrete is higher than any other construction material. On the other hand, developed countries face the challenge of refurnishing or upgrading aged infrastructures (Monteiro et al., 2017). In this regard, investigation on minimizing the

carbon footprints, reuse of construction waste, developing sustainable construction materials (Melton, 2022), and evaluating the consequences of construction waste on the environment (Zhao et al., 2020) is the prime focus in the construction industry.

Globally, natural aggregates (NA) consumption was 48.3 billion tons in 2015, and the demand is increasing by 1% per year (The Freedonia Group, 2019). Furthermore, it also has been predicted that the NA demand in the coming two or three decades will be doubled due to the current increasing rate of concrete production. An effective way to combat the depletion of NA would be choosing alternative construction material with construction and demolition (C&D) waste without sacrificing the performance of concrete (Zhao et al., 2020). Mistri et al. (2020) reported that around 40% of total municipal solid waste comes from C&D, which has been a serious problem for the environment and living biota. Generally, C&D waste materials disposed of in landfills cover huge land areas (Xiao, 2018) and contaminate soil and water resources. Apparently, converting C&D wastes into sustainable construction material will reduce the growing stress on NA resources, (Mukharjee and Barai, 2014), landfill area, soil and water contamination (Wang B. et al., 2021; Mistri et al., 2021).

The quality of recycled aggregate (RA) is based on the sources of involved materials (Kou and Poon, 2015) and their characteristics (Mistri et al., 2019). In addition, attached mortar (AM) on the surface of RA is weaker and more porous as compared to the old parent rock (Behera et al., 2014). Moreover, RA has notably high water absorption (around 3%–12%) as opposed to NA (<1%), which ultimately affects the hardened and fresh properties of recycled aggregate concrete (RAC) (Khan et al., 2018). Micro-pores and micro-cracks on RA result in weak interfacial properties (Kisku et al., 2017). It is found that RAC with 100% RA has 30% less compressive strength as compared to natural aggregate concrete (Pradhan et al., 2017). Most RAC originating from C&D waste material generally have lower grades as they already serve their services. Thus, pre-processing and proper characterization are imperative to achieve better quality RAC.

Recent research found that RAC can be strengthened cost-effectively and environmentally friendly manner without the removal of AM (Wang et al., 2017; Zeng et al., 2019; Ouyang et al., 2022). Strengthening AM fills the micro-cracks and pores of RAC, which leads to improvements in mechanical properties and less water absorption (Kaur et al., 2020). The application of microbial-induced calcium carbonate precipitation (MICP) by the bio-mineralization process has emerged as a highly effective and innovative method in improving the properties related to concrete infrastructure (Wang et al., 2017; Cao et al., 2018; 2020; Joshi et al., 2019; Zhan et al., 2019; Feng et al., 2020). This methodology is also called bio-deposition, as bacteria are used on the surface or inside the concrete structure to precipitate the $CaCO_3$ through the bio-mineralization process. The basic principle of the bio-mineralization process is that the bacterial vegetative cells produce CO_3^{2-} via a series of metabolic processes, and at the end CO_3^{2-} reacts with Ca^{2+} to produce $CaCO_3$ precipitation as shown in Eq. 1. Furthermore, it is important to assure the viability of bacterial spores (Huang et al., 2022).

$$Ca^{2+} + CO_3^{2-} \rightarrow CaCO_3 \qquad (1)$$
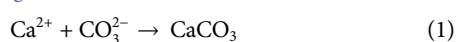
Recently, some researchers have tried to apply MICP to improve RA properties. Several scientists (Lu et al., 2022; Ouyang et al., 2022) investigated RA modification by applying MICP, and their results

confirmed the effectiveness and feasibility of microbial modification. Wang et al. (2017) applied MICP and found that water absorption of RAC for 6–8 mm aggregate range was improved by 14.5%, while a 13.9% increase was observed for the 12–16 mm aggregate range. This water absorption improvement could be due to calcite precipitation induced by bacteria inside the RAC pores. However, overall MICP efficiency on RAC is dependent on many factors, including types of cementitious media, bacterial culture concentration, method of application (i.e. spraying or immersion), environmental conditions, aggregates size, etc.

The long-term durability concerns have limited the use of RA in concrete structures. However, RAC is an emerging topic in the construction industry due to the depletion of NA resources and the rapid increase in construction waste (Beattie et al., 2022; Rosa et al., 2022). So far, there is no detailed research and mechanistic understanding of improving RA strength by MICP and its application in RAC under seawater conditions. Previously, the majority of studies aiming at improving RA properties using MICP techniques were supplemented with additional calcium sources which compromise the economic viability of RAC (Wu et al., 2018; Zeng et al., 2019; Zhan et al., 2019; Feng et al., 2020). Moreover, those studies only investigated the effect of MICP on RA via dip or immersion method that was particularly made for laboratory-based bio-deposition.

To the best of our knowledge, no study has been conducted so far on the commercial generation of RAC with MICP that can be applied for to the construction of infrastructure in seawater. Therefore, this study was designed for the effective application of MICP in the modification of RA and production of sustainable RAC for the marine environment. In this regard, a marine alkalophilic bacterium *Bacillus sp.* B6 which was isolated previously and stored in our lab was employed, and its growth and mineralization efficiency under seawater conditions was investigated and optimized. Modification of RA was carried out by applying MICP under the proposed growth conditions and various exposure methods (dip and spray) were applied for introducing MICP on RA, and the efficiency of RA was visualized by using scanning electron microscopy (SEM) and energy dispersive X-ray (EDX) in combination with basic technologies of density improvement and water absorption. Finally, the modified RA was used to develop the concrete specimen and its compressive strength was tested. The compressive strength and micro properties of the RAC were observed to predict the MICP mechanism. Our results form the basis for optimizing the culturing condition and identifying the feasibility of using RA with spray treatment to enhance the MICP. The current study provides novel and valuable information for our mechanistic understanding and improved properties of RA and RAC. The developed method is expected to boost RA utilization in the concrete industry, leading toward the sustainable construction era.

2 Experimental program

2.1 Recycled aggregates

The RAs used in this work were recycled aggregates obtained from a demolished building waste landfill site in

FIGURE 1
Visualization of recycled aggregates used in our experiment.
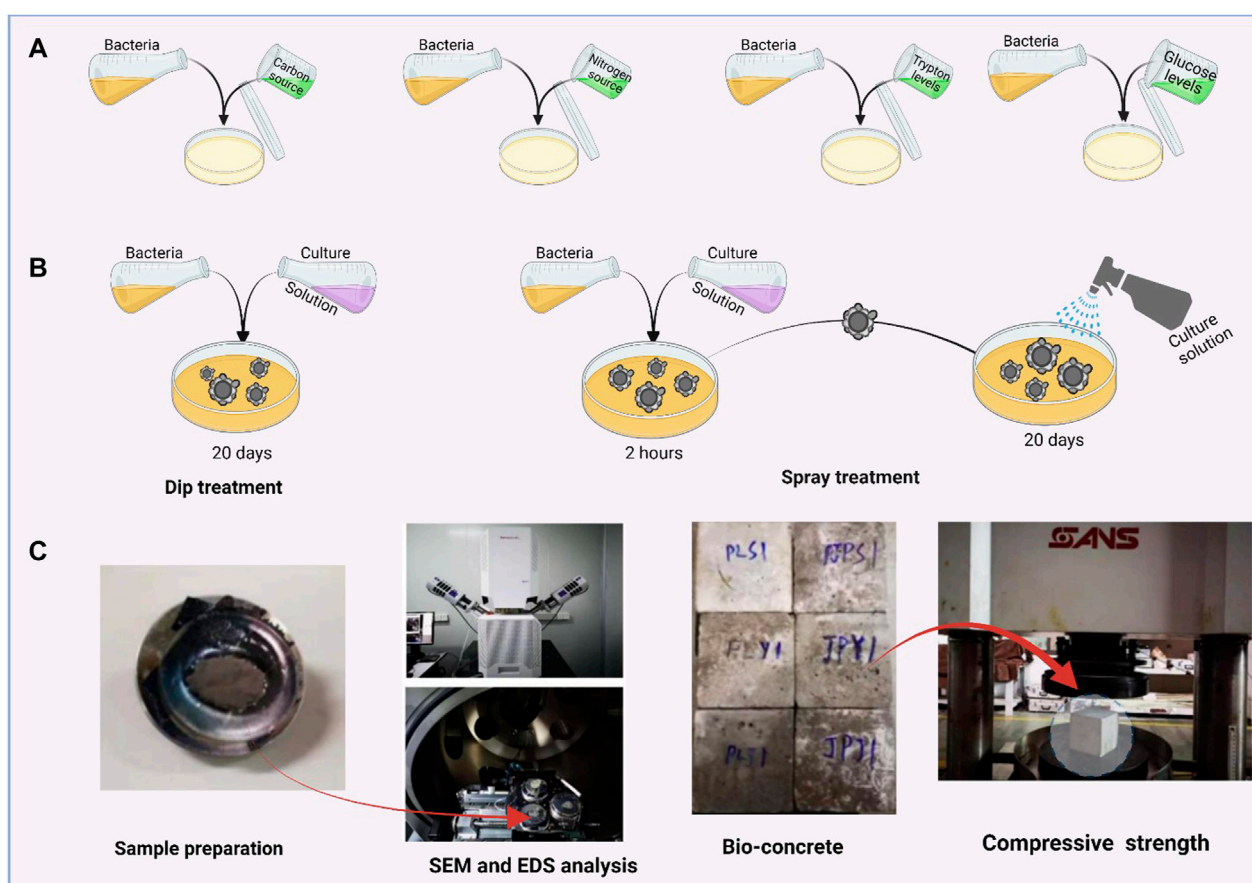
FIGURE 2
Schematic illustration of experimental procedures **(A)** Optimization of bacterial growth under different sources of carbon and nitrogen **(B)** Bio deposition of recycled aggregates *via* dip and spray treatments **(C)** SEM-EDX analysis of treated aggregates, formation of the concrete specimen and testing of flexural strength.

Shenzhen, China and shown in Figure 1. RAs were divided into two particle sizes, i.e. 5–10 mm and 10–20 mm. A constant weight of RA was achieved by drying at 80°C and repeatedly cleaning with tap water to remove the impurities.

2.2 Bacterial strain and optimum cultivation

Bacillus sp. B6, which was screened from the coastal sediments of mangrove forests in Futian, Shenzhen, and recognized as alkalophilic

TABLE 1 Composition of sea water environment.

Reagents	Composition	Quantity
A	tryptone	5 g
	glucose	7 g
	KH_2PO_4	1 mL
	ASW-A solution	652 mL
B	ASW-B solution	197 mL
C	CAPS	22.13 g
	Deionized water	150 mL

TABLE 2 Composition of ASW-A solution.

Reagents	Quantity
NaCl	29.9076 g
Na_2SO_4	5.01 g
KCl	0.8462 g
$NaHCO_3$	0.245 g
KBr	0.1224 g
H_3BO_3	0.0324 g
NaF	0.0038 g
Deionized water	1,000 mL

TABLE 3 Composition of ASW-B solution.

Reagents	Concentration
$MgCl_2 \cdot 6H_2O$	2.2984 g
$CaCl_2 \cdot 2H_2O$	0.4457 g
$SrCl_2 \cdot 6H_2 0$	0.0388 g
Deionized water	1,000 mL

Bacillus, was used in this study. The optimum condition for culture growth was obtained *via* various carbon and nitrogen sources, later best source of carbon and nitrogen was further applied to detect their suitable concentration for bacterial growth. The bio-deposition treatments on RA were selected on the basis of best-grown culture. Figure 2 shows the overall schematic illustration of the experimental procedure adopted for this study.

2.3 Seawater mineralization solution

The composition of the seawater mineralization solution is shown in Table 1. The pH of the solution was adjusted to 10.5 by NaOH to provide an alkaline environment for microbial mineralization and deposition.

Artificial sea water solution A (ASW-A) and artificial sea water solution B (ASW-B) solution refer to basic seawater mineralization

TABLE 4 Treatment design of experiment.

Treatment	Dip	Spray
Blank	Deionized water	Deionized water
Nutrient	Nutrient solution	Nutrient solution
Mixed	Nutrient solution + Bacteria	Nutrient solution + Bacteria

medium and their composition is provided below in Table 2 and Table 3.

2.4 Bacterial deposition treatment on RA

RAs were treated by using two methods, i.e. dip and spray treatments. In dip treatment, RAs were soaked in seawater mineralization solution containing B6 at a concentration of 1×10^8 cells mL^{-1}. The blank treatment group contains only deionized water without the addition of bacteria, the nutrient group contains nutrient solution without bacteria, and the mixed group contains both bacteria and nutrient solution. The soaking time for dip treatment was 20 days, and the ambient temperature was 27°C. For spraying treatment, RAs were firstly soaked in seawater mineralization solution containing B6 for 120 min to allow B6 cells to stick to the surface of RA. After that, RAs were taken out and sprayed with the same mineralization culture solution every 12 h. The spray time was 20 days and the ambient temperature was controlled at 27 C. Further information regarding experimental treatments for both dip and spray methods is provided in Table 4.

2.5 Effect of bacterial deposition

The treatment efficiency was quantified regarding water absorption, bulk density, and apparent density. High-resolution SEM-EDX analysis of RA under different treatment methods was performed to show the precipitation for filling of pores and cracks in RA and change in their elemental composition.

2.5.1 Water absorption

Both treatments and all three groups were subjected to water absorption test. Water absorption refers to the percentage of weight of water in the saturated state of RA to the weight of RA in the state of net dry weight. The experiment was carried out in accordance with the relevant regulations in "Recycled Coarse Aggregate for Concrete" (GB/T 25,177-2010). A portion of cleaned and dried RA (about 500 g) was placed in a white square box and soaked in water. The water surface should be about 5 mm higher than the surface of the RA sample. After soaking for 24 h, take it out of the box, and dry the surface of the aggregate by air blower to achieve saturated surface dry state. The mass was immediately weighed, recorded as G1. Then the sample was placed in a blast drying oven with a temperature of 105 C to dry to constant weight, which is the aggregate in the state of net dry weight. The sample was weighed after cooling to room temperature, recorded as G2. All the measurement was repeated three times. Water absorption rate is determined based on following formula as shown in Eq. 2.

Cement water ratio	Cement (g)	Water (g)	Sand (g)	RA (g)
0.5	538	274.3	576	1,070

FIGURE 3
Detection of nutrient sources **(A)** different sources of carbon **(B)** different levels of glucose **(C)** different sources of nitrogen and **(D)** different levels of tryptone, at different time interval.
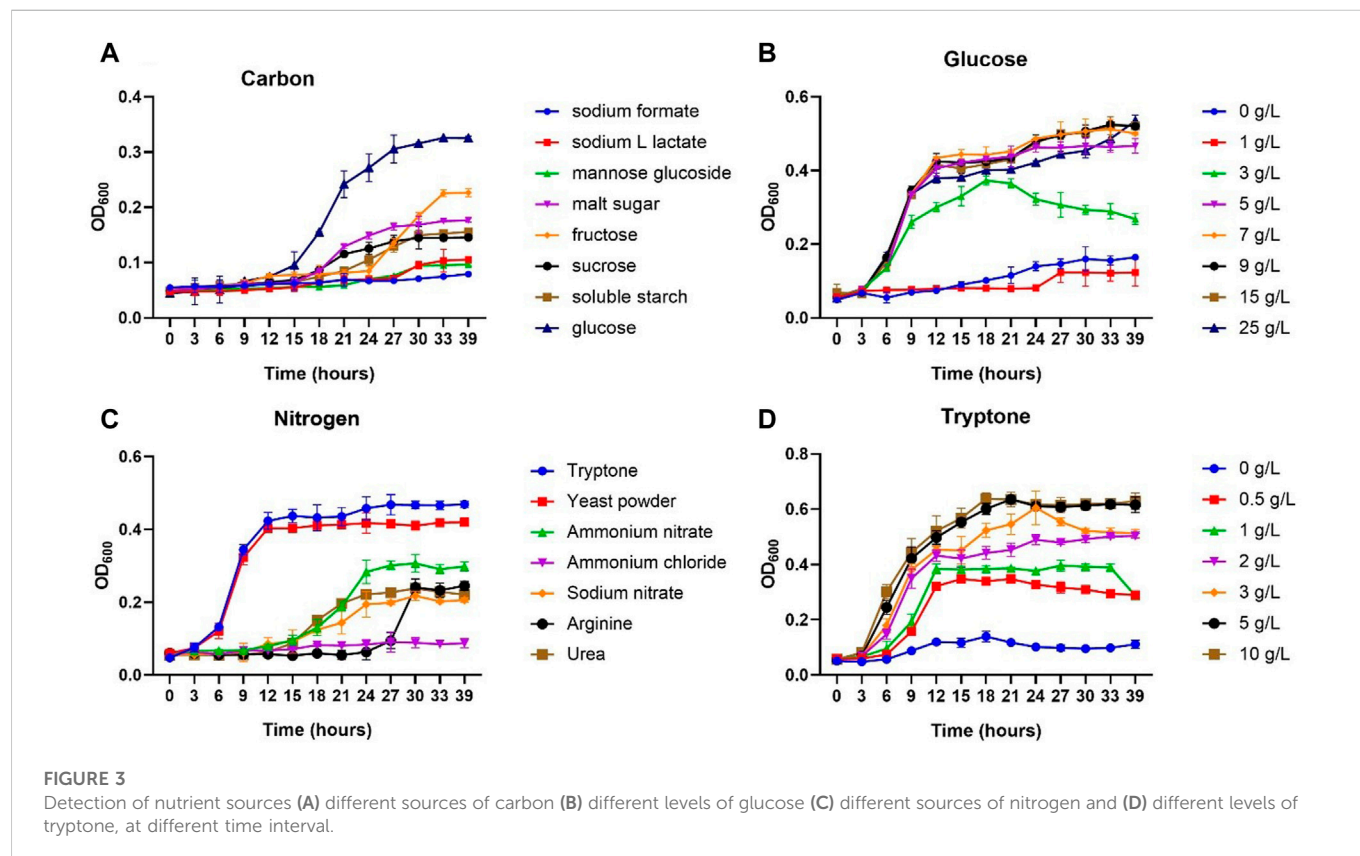
$$\text{Water absorption rate} = (G1 - G2)/G2 \times 100 \qquad (2)$$

2.5.2 Bulk density

Bulk density refers to the mass of recycled aggregate per unit volume in the bulk state. The experiment was carried out according to the relevant regulation in "Recycled Coarse Aggregates for Concrete" (GB/T 25,177-2010). Cleaned and dried RA was poured evenly into a 500 mL volumetric cylinder, assuring aggregates were fallen naturally without touching the volumetric cylinder. After the cylinder was full, it was weighed and its mass and recorded as mt. Then the mass of the volume cylinder was weighed out and recorded as mv. The bulk density is measured based on the following formula as shown in Eq. 3, where V is the volume of the cylinder.

$$\text{Bulk density } (kg/m^3) = (mt - mv)/V \qquad (3)$$

2.5.3 Apparent density

Apparent density refers to the mass per unit volume of recycled aggregate after the voids in the container and aggregate are removed. The cleaned and dried recycled aggregate was soaked into a 500 mL volumetric cylinder and shaken to remove air bubbles. After the bubbles were drained, water was poured into the volumetric

cylinder and the apparent density was measured based on the relevant regulations described in "Recycled Coarse Aggregate for Concrete" (GB/T 25,177-2010).

2.5.4 Characterization of the biogenic precipitation

The morphology of the precipitates on the surface of the aggregates was investigated by use of a scanning electron microscope (SEM, JEOL JSM-7600F). Coating of dry samples with carbon layer was done before the examination. Furthermore, EDX measurement was also performed to double check the chemical composition of particles that were present on aggregate surface.

2.6 Production of RAC

Ordinary Portland cement (P.O. 42.5) produced by Fenyi Conch Cement Co., Ltd and China ISO standard sand provided by Xiamen Aisio Co., Ltd. were used to produce the concrete specimen. The MICP-treated RAs were deployed into RAC test blocks, and the size of
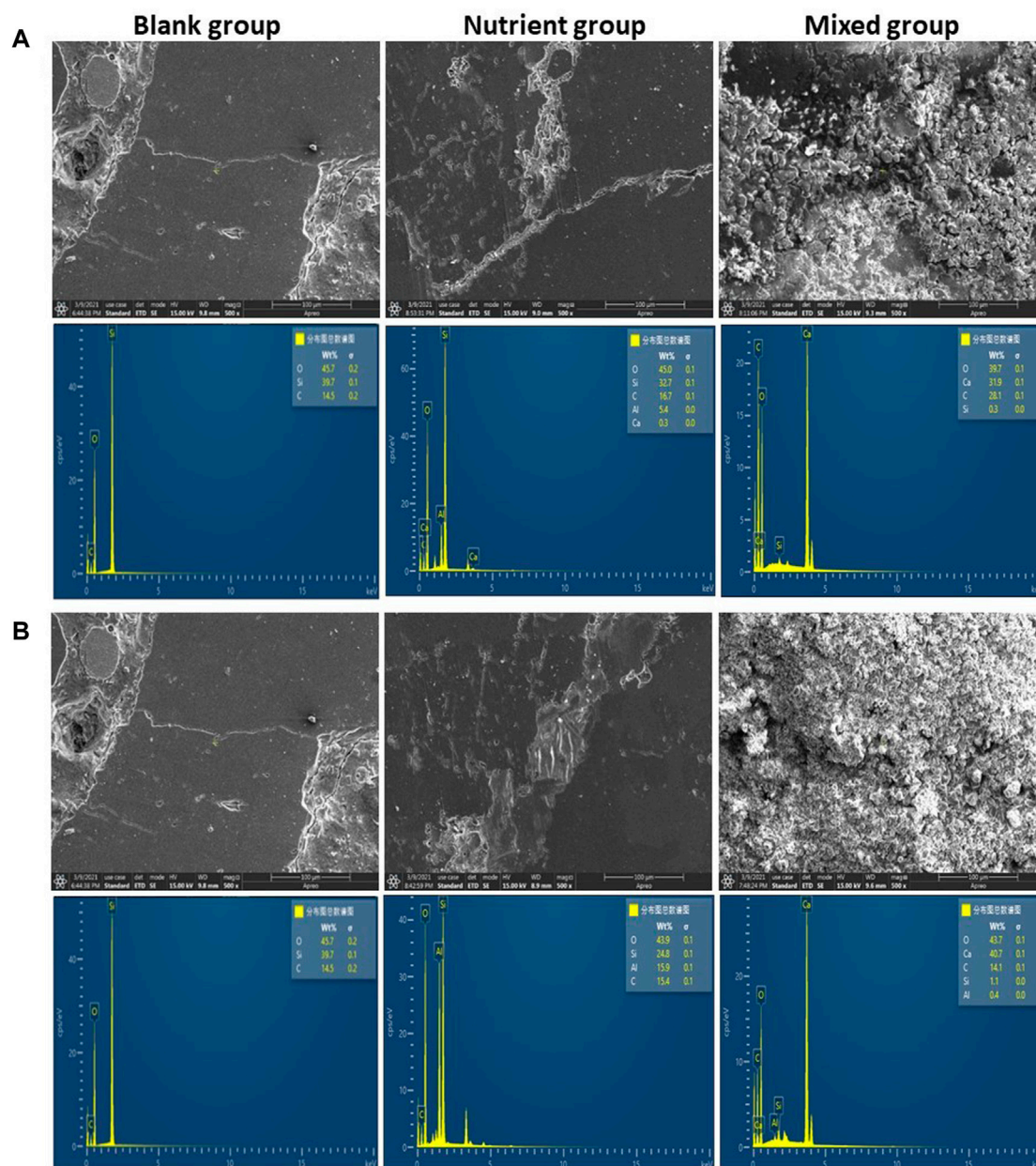
FIGURE 4
SEM-EDX images of RA exposed to blank (deionized water only), nutrient (nutrient solution only) and mixed group (nutrient solution + B6): **(A)** presents the dip treatment and **(B)** presents the spray treatments.

the test block was kept 10 cm × 10 cm × 10 cm. A total of 9 different types of RAC were prepared, each of which was set up in three parallel groups. The changes in mechanical properties were observed by comparing the compressive strength of the test block types treated in different ways. The material used in the formulation of RAC is provided in Table 5.

2.6.1 Compressive strength of RAC

Compressive strength refers to the maximum pressure that the recycled concrete can withstand per unit area. The experiment was carried out with reference to the "Inspection Method of Cement Mortar Strength" (GB/T 17671-1999), with the following steps. Remove the test block from the curing room

and clean the surface. Place the test block on the table of the pressure testing machine, and align the center intersection of the concrete with the center of the ball axis of the lower table. Adjust the upper plate to about 2 cm away from the test block. Adjust the loading speed of the press on the system to 0.5 MPa–0.8 MPa. Start the press, when the test block begins to approach failure and begins to deform rapidly, the system will stop pressurizing on its own, and record the failure load FC, accurate to 1 kN, based on following formula as shown in Eq. 4.

$$RC = FC/A \qquad (4)$$

RC is the compressive strength (MPa), FC is the maximum load (N) at failure and A is the area of the pressed part in mm^2.
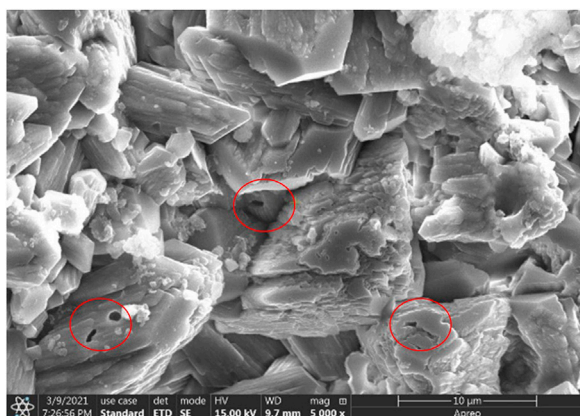
FIGURE 5
High resolution SEM microscopic morphology showing traces of bacterial cell.

2.7 Statistical analysis

All the experiments were performed in triplicates. The data were analyzed by analysis of variance (ANOVA) and the means were compared by Tukey's test ($p < 0.05$) using the GraphPad Prism software (version 5.0). Error bars on each graph show the standard deviation.

3 Results and discussion

3.1 Effects of nutrient sources on optimal bacterial growth

Microbes play a major role in mineralization and precipitation through different metabolic activities involving various pathways in the presence of specific organic and/or inorganic nutrients in the surrounding environment (Garg et al., 2022). Almost all the microbes in the natural environment are able to induce the mineralization process, however, their efficiency of mineralization differs. In our previous work, we screened a marine bacterium *Bacillus sp. B6* from the coastal sediments of mangrove forests and evaluated its calcium precipitation activity (CPA). Our result disclosed that B6 possesses high CPA, higher than most of the reported mineralization strains, indicating the potential for self-healing of concrete damage and modification of RA (Zhang et al., 2019).

On the other hand, even if one kind of bacterial strain has strong CPA, the quantity of bacterial cells is also a crucial influential factor for the effective modification of RA. In this regard, we identified the best source and optimal concentration of carbon (Figure 3A, B) and nitrogen (Figure 3C, D) nutrients for the growth of B6 bacterium in the seawater environment. Six sugars (glucose, maltose, fructose, mannose, sucrose soluble starch) and two organic acid salts (sodium formate and sodium L-lactate) were used as carbon sources to explore the effects of different carbon sources on the growth of B6 as shown in Figure 3A. It was found that the plateau OD_{600} values of

mannose and sodium formate were the lowest. Additionally, L-sodium lactate had little effect on the growth of B6. The OD_{600} values of sucrose, soluble starch, maltose, fructose, and glucose in the plateau phase were relatively higher, indicating that the growth of vegetative cells was promoted to a certain extent. Among them, the OD_{600} value of glucose was the highest, reaching up to 0.33, and the lag period of glucose was also the shortest among the carbon sources. Therefore, glucose was identified as the dominant carbon source in B6 mineralized growth cultures. Furthermore, we tested the role of glucose on bacterial culture at different concentrations as shown in Figure 3B. We found that when glucose concentration is higher than 5 gL^{-1}, the growth of vegetative cells is relatively vigorous. With the further increase of concentration, the OD_{600} value of the plateau phase is in the range of 0.52–0.53, and the difference is not large. In order to save costs, the glucose concentration at 7 gL^{-1} is found to be the dominant carbon source concentration.

Similarly, we tested the effects of three organic nitrogen sources, yeast powder, tryptone, and urea, and four inorganic nitrogen sources including sodium nitrate, ammonium nitrate, ammonium chloride, and arginine, on the growth cycle of B6. Among them, tryptone was the best nitrogen source, and the OD_{600} value in the plateau phase was 0.47. As such, tryptone was chosen as the nitrogen source for the mineralization and growth of the B6 bacteria. Later, we applied different tryptone concentrations to isolate the optimum level of tryptone for B6 bacterial growth. A concentration level of 5 gL^{-1} was chosen as an effective tryptone concentration of nitrogen source.

Carbon and nitrogen sources are critical factors controlling the growth and $CaCO_3$ precipitation (Zhang et al., 2019). CO_3^{2-} in $CaCO_3$ originates from enzymes and the synthesis of these enzymes depends on carbon and nitrogen metabolism (Bergh et al., 2020). Furthermore, carbon and nitrogen metabolism are interconnected, requiring shared functioning between these elements. The increase in the growth of bacteria increases the probability of mineralization to a certain extent, and maintaining a high cell number contributes to a high rate of mineralization deposition (Zhang et al., 2017). The rapid bacterial growth and reproduction of bacterial cells mean that bacteria synthesize a large number of intermediate metabolites with carbon/nitrogen sources by cellular respiration, so cellular respiration is strong, which helps to generate energy (Zhang et al., 2016a). Cell metabolism entails energy, and metabolism enhancement helps bacteria produce calcium carbonate as a metabolite and consequently improves the overall efficiency of mineralization (Zhang et al., 2016b; Seifan et al., 2018).

3.2 Evaluation of treatment method for bio deposition

3.2.1 Visualization of microbial deposition and characterization

The microstructure of RA treated with/without bacteria under different methods is shown in Figure 4. As shown in Figures 4A,B, the surface of RA treated in the mixed group was covered with a lot of particles from the dip and spray treatments, and the density of precipitates in the spraying group is higher than that in the dip group, almost covering the whole scanning area. However, the
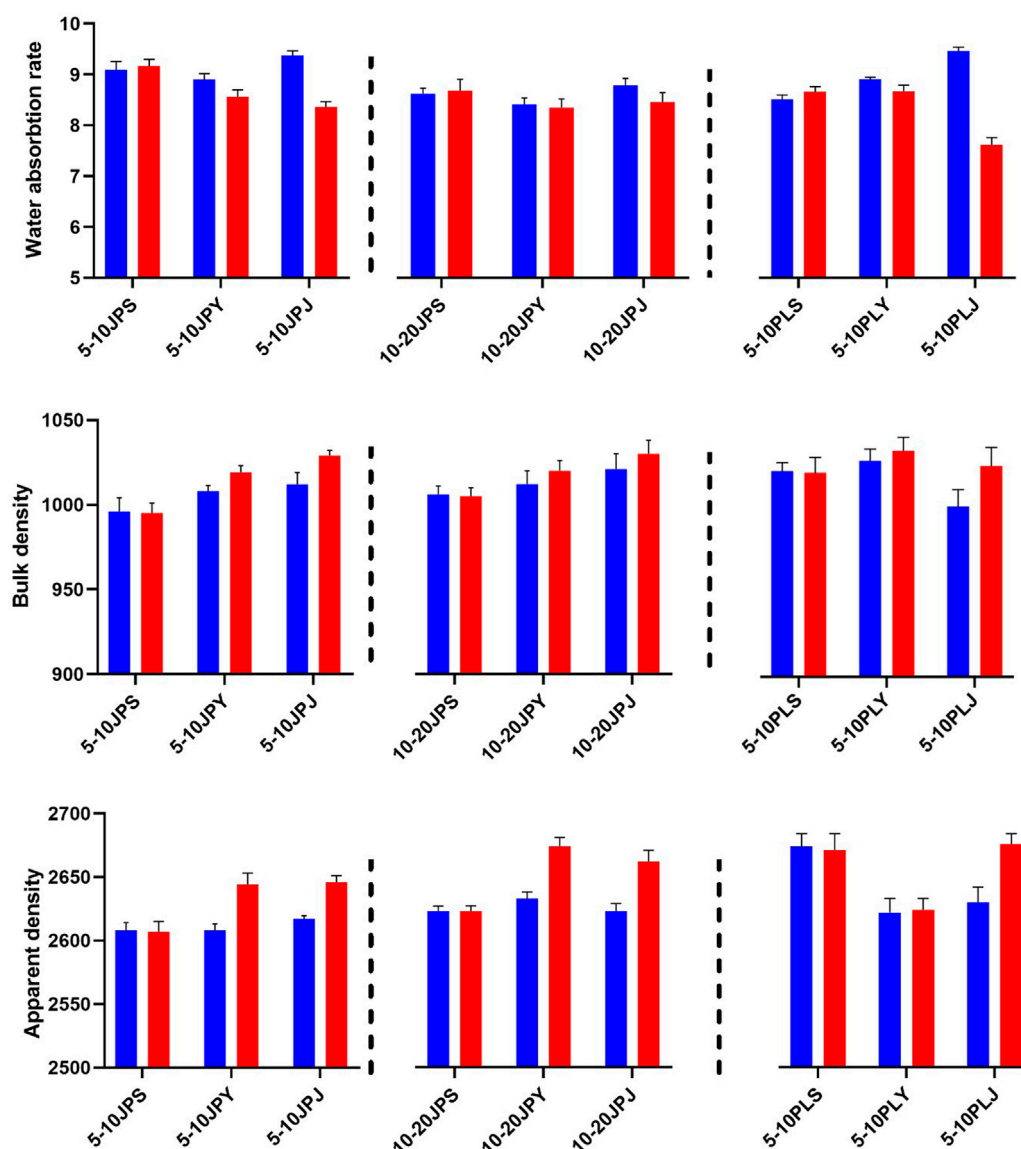
FIGURE 6
Effect of dip and spray treatment on water absorption, bulk density and apparent density. For all the samples, "JP" presents dip treatment, "PL" presents spray treatment. The last letter S, Y, and J presents blank (distilled water only), nutrient (nutrient solution only) and mixed (nutrient + B6) group, respectively. 5−10 and 10−20 are the size of recycled aggregates in millimeter (mm). The color of bar presents before and after treatment for blue and red, respectively.
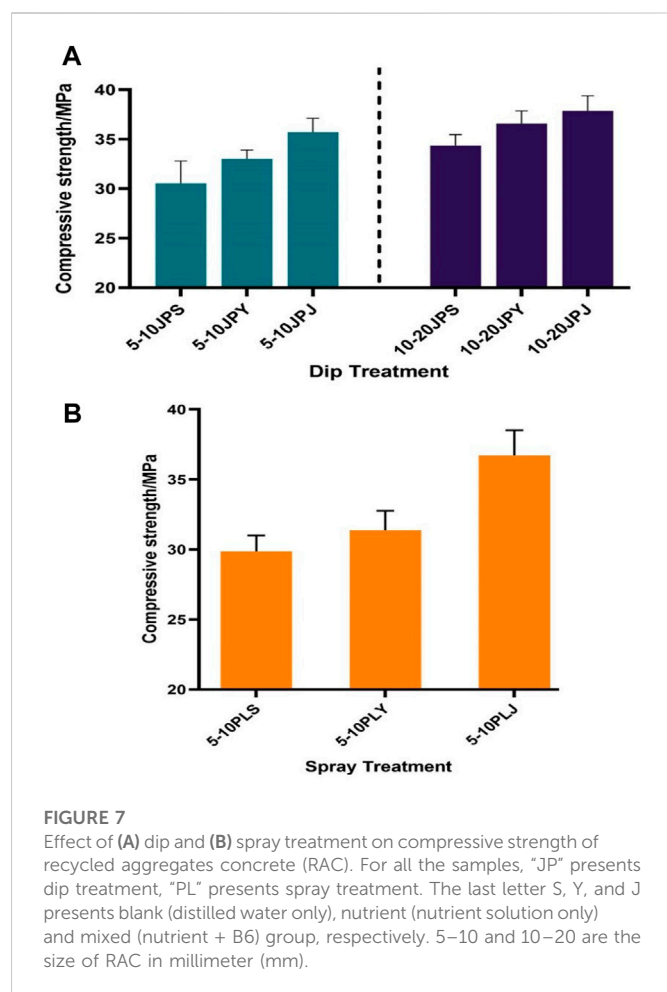
cracks and pores of RA in the nutrient group were only partially filled with a little substance no matter what treatment method was applied. Compared with the mixed group, almost no precipitation was observed on the surface of RA in the blank group. These results may suggest the contribution of bacteria in substance precipitation. The formation of precipitates in the nutrient group may also be due to certain unexpected bacteria as all the mineralization process in our experiment was not sterile cultivation. Moreover, the EDX analysis in Figure 4 disclosed that the main elements of the precipitates in the mixed group are C, O, and Ca, and the mass ratio of each element is close to 3:12:10.

Combined with the higher resolution SEM microscopic morphology result in Figure 5, it can be inferred that the

precipitate is calcium carbonate in calcite type. In addition, it can be noted that the contribution of B6 in the production of calcium carbonate can be further confirmed by the trace of bacterial cells, which is clearly visible and marked with a red circle in Figure 5.

3.2.2 Microbial community with nutrients modestly improves the duration indexes

The dense calcium carbonate layer on the surface of RA has a positive impact on improving the physical properties of RA and RAC. Herein, we evaluated the response of different duration indexes such as water absorption, bulk density, apparent density exposed to dip and spray treatment. Figure 6 shows the water

FIGURE 7
Effect of **(A)** dip and **(B)** spray treatment on compressive strength of recycled aggregates concrete (RAC). For all the samples, "JP" presents dip treatment, "PL" presents spray treatment. The last letter S, Y, and J presents blank (distilled water only), nutrient (nutrient solution only) and mixed (nutrient + B6) group, respectively. 5−10 and 10−20 are the size of RAC in millimeter (mm).

absorption, bulk density and apparent density of RA before and after microbial modification in different treatment groups. For RA with diameter size 5–10 mm in the mixed group, the decline in water absorption was recoded ~11% for dip treatment and ~19% for spray treatment. No significant reduction in water absorption was observed with the increase in size of RA (diameter size 10–20 mm) with dip treatment. Moreover, it can be seen that in the absence of B6, no visible change of water absorption of RA was achieved under any treatment. Therefore, the reduction in water absorption of treated RA can be due to the presence of the MICP that plugged the microcracks (Zeng et al., 2019). Previously, Wu et al. (2018) adopted the bacterial respiration technique to produce calcium carbonate precipitation and reported a decline in water absorption of RA by 10, 13, and 23% for particle sizes of 20, 10, and 5 mm, respectively. This can be associated with the increase in micro-hardness of the interfacial transition zone of RA after microbial treatment. It was possible to obtain a reduction in water absorption of aggregate (Qiu et al., 2014), and the effect would be more visible in the case of RA with small size originating from inferior quality concrete.

In addition, the effect of MICP treatment on the bulk and apparent density of RA in different groups is similar to that on water absorption as shown in Figure 6. Compared with the blank group, the bulk density of the mixed group for dip treatment was ~1.7% and 2.4% increase for spray treatment in case of RA diameter size range 5–10 mm. Similarly, the increase in apparent density was

recorded after treatment for RA (diameter size 5–10 mm) ~1.5% in the case of the mixed group for dip treatment and ~1.7% for spray treatment. Singh et al. (2018) investigated the modification effect of ureolytic/non-ureolytic bacteria on the interfacial transition zone of RA and reported the increase in bulk density of microbial-treated aggregates, which is in line with our experiment. The dense calcium carbonate layer formed on RA as shown in SEM results effectively reduce the water absorption and improve the bulk and apparent density of aggregate. Thus, the proposed modification techniques seem promising for the performance enhancement in terms of duration indexes of RA.

3.3 Proposed MICP treatment process for RAC production

We constructed the RAC based on the above-mentioned comparison of the effects on water absorption decrease and improvement in bulk and apparent densities of treated RA. The size of the RAC blocks was 10 cm × 10 cm × 10 cm, and a total of 9 blocks were prepared according to our desired research plan in Section 2.5. Each of the three groups was set in parallel, and the mechanical properties were observed by comparing the compressive strength of the test blocks.

The development of the compressive strength of concrete at age of 28 days made of RA exposed to dip or spray treatment was determined as shown in Figure 7. It was found that for RAC made of B6 dip-treated RA (5–10 mm), the compressive strength increased ~16.7% as compared with the blank group. But for the same treatment, when the size of RA was 10–20 mm, the increase in the compressive strength of RAC was only ~8.9% as compared to the blank group. This can be associated with the result of the higher water absorption in larger sizes of RA as previously stated in Section 3.1 and 3.2. Earlier Yu et al. (2019) also reported a decrease in compressive strength with the increase in RA size. In addition, the small particle size of RA may provide a larger specific surface area, which is more suitable for the adhesion of microorganisms followed by an increase in the compressive strength of RAC.

It is worth mentioning that by use of B6 spray-treated RA of the same size (5–10 mm), the compressive strength of RAC increased ~24.1% compared with the blank group, higher than the 16.7% achieved by dip-treatment. The higher efficiency of spray treatment can actually be explained by the above SEM result that more substances were precipitated on RA under spray treatment. The reason why spray treatment is superior to dip treatment is probably that, compared with immersing aggregates totally under the water, spraying allows bacterial cells growing on the surface of the aggregates to acquire more oxygen from the air, thus achieving higher respiration efficiency. This is good because a better result can be obtained by using a lesser amount of microbes and nutrient culture *via* spray treatment. Treatment of RA can be economized by spraying bacterial culture onto the surface of RA at regular intervals and thus achieving long-lasting concrete structures on an industrial scale. Zhan et al. (2019) reported a ~32% increase in the compressive strength of mortar containing recycled fine aggregates and treated with MICP under different sources of calcium. All the previous reported studies adopted different experimental conditions and the overall efficiency of the MICP

TABLE 6 Important findings from studies regarding MICP treatment on properties of RA and RAC.

Reporting authors	Important experimental conditions	Findings
Current study	RA size (5–10 mm) and (10–20 mm)	Reduction in water absorption ~19%
	Bacillus sp. B6 (1×10^8 cells mL^{-1})	Concrete samples incorporating treated RA had 24.1% increase in compressive strength
	Dip and Spray techniques for bacterial introduction	
Ouyang et al. (2022)	RA size 4.75–9.5 mm	Reduction in water absorption 10.60%
	Bacillus pasteurii	Increase in compressive strength 15%
	Additional calcium source	The RAC prepared from the treated RA and supplemented with 0.2 mol/L calcium ion shows best mechanical properties
Zhan et al. (2019)	RA size ≤0.15 mm	Water absorption decreased from 4·35% to 2·62%
	Sporosarcina pasteurii (2×10^9 cells mL^{-1})	Mortar samples incorporating treated RA had 31·2% increase in compressive strength
	Additional calcium sources i.e. calcium chloride and calcium nitrate	
Wang et al. (2021b)	RA size 9.5–31.5 mm	Reduction in water absorption by 33%
	Bacillus mucilaginosus	Increase in weight by 12%
Zhao et al. (2021)	RA size 0.2–100 mm	Increase in weight and decrease in water absorption of treated RA was approximately 4.83% and 35.93% respectively
	Sporosarcina pasteurii	Increase in flexural strength of mortar specimen is 23.3%
Feng et al. (2020)	RA size 0.2–100 mm	Reduction in water absorption by 31.4%
	Sporosarcina pasteurii	Increase in flexural strength of mortar cast is 84.5% and compressive strength 14.3% respectively
	Additional calcium source	
Singh et al. (2018)	RA size 1–20 mm	Reduction in water absorption (43% in non-ureolytic and 64% in ureolytic bacterial strain
	Ureolytic bacteria, B. megaterium	Performance of B. megaterium proved to be better for calcification
	Non-ureolytic bacteria B. cohnii	
	Additional Nano silica	
Wang et al. (2017)	RA size 6–20 mm	Increase in weight 2.5%
	Bacillus sphaericus	Decrease in water absorption 1% Increase in compressive strength 16%
Zeng et al. (2019)	RA size 10–20 mm *S. pasteurii* Additional calcium sources	Decrease in water absorption 10%
		Increase in compressive strength 6.2%
Wu et al. (2018)	RA size 5–10 mm and 10–20 mm *Bacillus pseudofirmus* Additional calcium sources	Reduction in water absorption 23% Increase in compressive strength 35%

on RAC depends on different factors, so the results are not comparable. As our results and experimental programs are novel, for reference we provide comprehensive information on previously published literature on RA treated with MICP in Table 6.

The approach adopted in this study holds more practical and economic benefits, especially for developing infrastructure in a seawater environment with spray-treated MICP RAC. It is evident that the MICP modification *via* spray treatment has a beneficial effect on the physical properties of RA and RAC. The development of RAC through the suggested treatment method will help to reduce the application of natural aggregates, decrease the overall cost and

protect the environment from the hazardous effects of the construction industry. Furthermore, this approach can be adopted to develop infrastructure in a sea environment, stream restoration and reduced the carbon footprints of the construction industry as shown in Figure 8.

The proposed treatment process in this study can be used as a reference in engineering applications. However, due to the limited influencing factors taken into consideration in this study, whether the parameters reported here are optimal for other experimental conditions might require further verification. To meet the requirements of application in engineering practice, it is essential to continue optimizing the
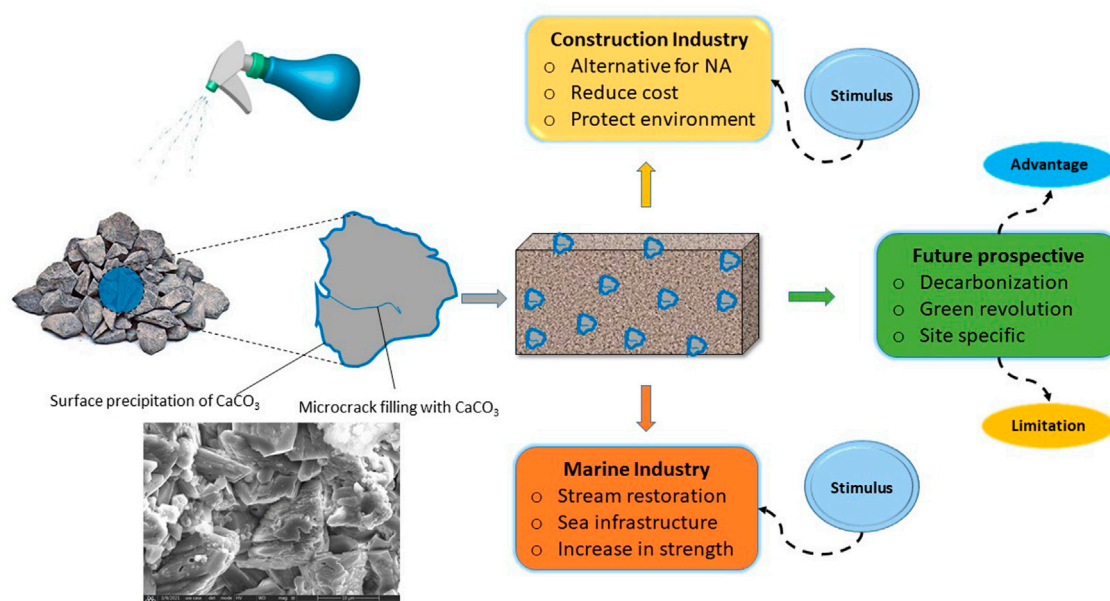
FIGURE 8
Schematic illustration of evaluation of RA treated with MICP, emerging role in construction industry/marine industry with future goals and prospects.

proposed MICP treatment process under different environment scenarios. For example, the current study proves that spraying culture medium on the surface of RA instead of soaking the RA in culture medium is more efficient and economical treatment method. The indentification of bacteria with higher natural MICP ability, cheaper nutrients, industrial wastewater containing calcium sources and testing of proposed approaches in changing environment is worth more in-depth exploration for future studies.

4 Conclusion

With the development of the sustainable cement industry, the self-healing properties of concrete have received widespread attention. As such, current findings will help to revitalize the construction industry by utilizing the self-healing RA to produce RAC and minimize the load on natural aggregates. Herein, the optimization of the MICP treatment process with different nutrient sources for seawater environment was achieved, improving the properties of RA. In particular, dip and spray methods were employed to test the modification effects on RA and RAC. Based on the experimental results, the following conclusions can be summarized.

- The carbon and nitrogen sources in seawater environments were optimized to cultivate bacteria with excellent growth ability that

can effectively facilitate the MICP process on RA in seaside environments.
- The optimal nutrient sources of carbon and nitrogen were detected as glucose (7 gL^{-1}) and tryptone (5 gL^{-1}) respectively.
- The physical properties of RA, treated with spray treatment are significantly improved as compared to the untreated and dip treatment, especially for aggregates with a smaller particle size (5–10 mm). Visual observation with SEM elucidates micro mechanism and the role of the MICP in treated RA. Furthermore, the in-depth understanding of MICP process is carried out *via* the elemental composition of precipitate with EDX.
- The results show that bacterial-treated RA supplemented with nutrients *via* spray treatment significantly affects RAC's mechanical properties by improving compressive strength.
- Although this research provides a way forward for developing sustainable RAC with microbial-treated RA. Still, efforts should be made to identify the novel bacterial strains with higher MICP and ensure the working of the proposed approach in different environmental conditions. More studies should be planned to achieve healing effectiveness on larger RA.

Data availability statement

The original contributions presented in the study are included in the article/supplementary material, further inquiries can be directed to the corresponding authors.

Author contributions

MAA and BL: Conceptualization, Data curation, Writing–original draft. Formal analysis. QL: Methodology, Software. MA: Formal analysis. JZ: Investigation, Visualization. YZ: Supervision, Review and Editing. XD: Funding acquisition, Supervision, Writing–review and editing. All authors read and approved the manuscript.

Funding

Conflict of interest

The authors declare that the research was conducted in the absence of any commercial or financial relationships that could be construed as a potential conflict of interest.

Publisher's note

References

Beattie, R. E., Su, B., Thill, R., and Hristova, K. R. (2022). Recycled concrete aggregates are an economic form of urban riparian erosion management with limited impacts on freshwater chemistry and microbial diversity. *J. Hazard. Mater.* 434, 128934. doi:10.1016/j.jhazmat.2022.128934

Behera, M., Bhattacharyya, S. K., Minocha, A. K., Deoliya, R., and Maiti, S. (2014). Recycled aggregate from C&D waste and its use in concrete – a breakthrough towards sustainability in construction sector: A review. *Constr. Build. Mater.* 68, 501–516. doi:10.1016/j.conbuildmat.2014.07.003

Bergh, J. M., Miljević, B., Šovljanski, O., Vučetić, S., Markov, S., Ranogajec, J., et al. (2020). Preliminary approach to bio-based surface healing of structural repair cement mortars. *Constr. Build. Mater.* 248, 118557. doi:10.1016/j.conbuildmat.2020.118557

Cao, M., Khan, M., and Ahmed, S. (2020). Effectiveness of calcium carbonate whisker in cementitious composites. *Period. Polytech. Civ. Eng.* doi:10.3311/PPci.14288

Cao, M., Li, L., and Khan, M. (2018). Effect of hybrid fibers, calcium carbonate whisker and coarse sand on mechanical properties of cement-based composites. *Mater. Construcción* 68, e156. doi:10.3989/mc.2018.01717

Environment, U. N. (2018). Global status report 2018. *UNEP - U. N. Environ. Programme*. Available at: http://www.unep.org/resources/report/global-status-report-2018 (Accessed March 23, 2022).

Feng, Z., Zhao, Y., Zeng, W., Lu, Z., and Shah, S. P. (2020). Using microbial carbonate precipitation to improve the properties of recycled fine aggregate and mortar. *Constr. Build. Mater.* 230, 116949. doi:10.1016/j.conbuildmat.2019.116949

Garg, R., Garg, R., and Eddy, N. O. (2022). Microbial induced calcite precipitation for self-healing of concrete: A review. *J. Sustain. Cement-Based Mater.* 0, 1–14. doi:10.1080/21650373.2022.2054477

GB/T 17671-1999 (n.d.) Chinesestandard (2022). Available at: https://www.chinesestandard.net/PDF.aspx/GBT17671-1999 (Accessed June 9, 2022).

Ghaffar, S. H., Burman, M., and Braimah, N. (2020). Pathways to circular construction: An integrated management of construction and demolition waste for resource recovery. *J. Clean. Prod.* 244, 118710. doi:10.1016/j.jclepro.2019.118710

Huang, R., Lu, Y., Ahmad, M., Zhang, J., and Deng, X. (2022). The viability of spores is the key factor for microbial induced calcium carbonate precipitation. *Appl. Microbiol. Biotechnol.* 107, 543–552. doi:10.1007/s00253-022-12319-w

Joshi, S., Goyal, S., Mukherjee, A., and Reddy, M. S. (2019). Protection of concrete structures under sulfate environments by using calcifying bacteria. *Constr. Build. Mater.* 209, 156–166. doi:10.1016/j.conbuildmat.2019.03.079

Kaur, N. P., Majhi, S., Dhami, N. K., and Mukherjee, A. (2020). Healing fine cracks in concrete with bacterial cement for an advanced non-destructive monitoring. *Constr. Build. Mater.* 242, 118151. doi:10.1016/j.conbuildmat.2020.118151

Khan, M., Cao, M., and Ali, M. (2018). Effect of basalt fibers on mechanical properties of calcium carbonate whisker-steel fiber reinforced concrete. *Constr. Build. Mater.* 192, 742–753. doi:10.1016/j.conbuildmat.2018.10.159

Kisku, N., Joshi, H., Ansari, M., Panda, S. K., Nayak, S., and Dutta, S. C. (2017). A critical review and assessment for usage of recycled aggregate as sustainable construction material. *Constr. Build. Mater.* 131, 721–740. doi:10.1016/j.conbuildmat.2016.11.029

Kou, S., and Poon, C. (2015). Effect of the quality of parent concrete on the properties of high performance recycled aggregate concrete. *Constr. Build. Mater.* 77, 501–508. doi:10.1016/j.conbuildmat.2014.12.035

Lu, C.-H., Bu, S., Shahin, M. A., Zheng, Y., and Cheng, L. (2022). Mitigation of alkali-silica reaction by microbially induced CaCO3 protective layer on aggregates. *Constr. Build. Mater.* 328, 127065. doi:10.1016/j.conbuildmat.2022.127065

Melton, L. (2022). How to grow cement. *Nat. Biotechnol.* 40, 286. doi:10.1038/s41587-022-01264-8

Mistri, A., Bhattacharyya, S. K., Dhami, N., Mukherjee, A., and Barai, S. V. (2020). A review on different treatment methods for enhancing the properties of recycled aggregates for sustainable construction materials. *Constr. Build. Mater.* 233, 117894. doi:10.1016/j.conbuildmat.2019.117894

Mistri, A., Bhattacharyya, S. K., Dhami, N., Mukherjee, A., and Barai, S. V. (2019). Petrographic investigation on recycled coarse aggregate and identification the reason behind the inferior performance. *Constr. Build. Mater.* 221, 399–408. doi:10.1016/j.conbuildmat.2019.06.085

Mistri, A., Dhami, N., Bhattacharyya, S. K., Barai, S. V., Mukherjee, A., and Biswas, W. K. (2021). Environmental implications of the use of bio-cement treated recycled aggregate in concrete. *Resour. Conservation Recycl.* 167, 105436. doi:10.1016/j.resconrec.2021.105436

Monteiro, P. J. M., Miller, S. A., and Horvath, A. (2017). Towards sustainable concrete. *Nat. Mater* 16, 698–699. doi:10.1038/nmat4930

Müller, D. B., Liu, G., Løvik, A. N., Modaresi, R., Pauliuk, S., Steinhoff, F. S., et al. (2013). Carbon emissions of infrastructure development. *Environ. Sci. Technol.* 47, 11739–11746. doi:10.1021/es402618m

Mukharjee, B. B., and Barai, S. V. (2014). Influence of incorporation of nano-silica and recycled aggregates on compressive strength and microstructure of concrete. *Constr. Build. Mater.* 71, 570–578. doi:10.1016/j.conbuildmat.2014.08.040

Ouyang, J., Liu, K., Sun, D., Xu, W., Wang, A., and Ma, R. (2022). A focus on Ca2+ supply in microbial induced carbonate precipitation and its effect on recycled aggregate. *J. Build. Eng.* 51, 104334. doi:10.1016/j.jobe.2022.104334

Pradhan, S., Kumar, S., and Barai, S. V. (2017). Recycled aggregate concrete: Particle Packing Method (PPM) of mix design approach. *Constr. Build. Mater.* 152, 269–284. doi:10.1016/j.conbuildmat.2017.06.171

Qiu, J., Tng, D. Q. S., and Yang, E.-H. (2014). Surface treatment of recycled concrete aggregates through microbial carbonate precipitation. *Constr. Build. Mater.* 57, 144–150. doi:10.1016/j.conbuildmat.2014.01.085

Rosa, L., Becattini, V., Gabrielli, P., Andreotti, A., and Mazzotti, M. (2022). Carbon dioxide mineralization in recycled concrete aggregates can contribute immediately to carbon-neutrality. *Resour. Conservation Recycl.* 184, 106436. doi:10.1016/j.resconrec.2022.106436

Seifan, M., Sarmah, A., Samani, A., Ebrahiminezhad, A., Younes, G., and Berenjian, A. (2018). Mechanical properties of bio self-healing concrete containing immobilized bacteria with iron oxide nanoparticles. *Appl. Microbiol. Biotechnol.* 102, 4489–4498. doi:10.1007/s00253-018-8913-9

Singh, L. P., Bisht, V., Aswathy, M. S., Chaurasia, L., and Gupta, S. (2018). Studies on performance enhancement of recycled aggregate by incorporating bio and nano materials. *Constr. Build. Mater.* 181, 217–226. doi:10.1016/j.conbuildmat.2018.05.248

The Freedonia Group (2019). Global construction aggregates. *Free. Group*. Available at: https://www.freedoniagroup.com/industry-study/global-construction-aggregates-3742.htm (Accessed March 23, 2022).

Wang, B., Yan, L., Fu, Q., and Kasal, B. (2021a). A comprehensive review on recycled aggregate and recycled aggregate concrete. *Resour. Conservation Recycl*. 171, 105565. doi:10.1016/j.resconrec.2021.105565

Wang, J., Vandevyvere, B., Vanhessche, S., Schoon, J., Boon, N., and De Belie, N. (2017). Microbial carbonate precipitation for the improvement of quality of recycled aggregates. *J. Clean. Prod*. 156, 355–366. doi:10.1016/j.jclepro.2017.04.051

Wang, R., Jin, P., Ding, Z., and Zhang, W. (2021b). Surface modification of recycled coarse aggregate based on Microbial Induced Carbonate Precipitation. *J. Clean. Prod*. 328, 129537. doi:10.1016/j.jclepro.2021.129537

Wu, C.-R., Zhu, Y.-G., Zhang, X.-T., and Kou, S.-C. (2018). Improving the properties of recycled concrete aggregate with bio-deposition approach. *Cem. Concr. Compos*. 94, 248–254. doi:10.1016/j.cemconcomp.2018.09.012

Xiao, J. (2018). "Recycled aggregate concrete," in *Recycled aggregate concrete structures springer tracts in civil engineering*. Editor J. Xiao (Berlin, Heidelberg: Springer), 65–98. doi:10.1007/978-3-662-53987-3_4

Yu, F., Sun, D., Wang, J., and Hu, M. (2019). Influence of aggregate size on compressive strength of pervious concrete. *Constr. Build. Mater*. 209, 463–475. doi:10.1016/j.conbuildmat.2019.03.140

Zeng, W., Zhao, Y., Poon, C. S., Feng, Z., Lu, Z., and Shah, S. P. (2019). Using microbial carbonate precipitation to improve the properties of recycled aggregate. *Constr. Build. Mater*. 228, 116743. doi:10.1016/j.conbuildmat.2019.116743

Zhan, M., Pan, G., Wang, Y., Fu, M., and Lu, X. (2019). Recycled aggregate mortar enhanced by microbial calcite precipitation. *Mag. Concr. Res*. 72, 622–633. doi:10.1680/jmacr.18.00417

Zhang, J., Mai, B., Cai, T., Luo, J., Wu, W., Liu, B., et al. (2017). Optimization of a binary concrete crack self-healing system containing bacteria and oxygen. *Materials* 10, 116. doi:10.3390/ma10020116

Zhang, J., Wang, C., Wang, Q., Feng, J., Pan, W., Zheng, X., et al. (2016a). A binary concrete crack self-healing system containing oxygen-releasing tablet and bacteria and its Ca2+-precipitation performance. *Appl. Microbiol. Biotechnol*. 100, 10295–10306. doi:10.1007/s00253-016-7741-z

Zhang, J., Wu, R., Li, Y., Zhong, J., Deng, X., Liu, B., et al. (2016b). Screening of bacteria for self-healing of concrete cracks and optimization of the microbial calcium precipitation process. *Appl. Microbiol. Biotechnol*. 100, 6661–6670. doi:10.1007/s00253-016-7382-2

Zhang, J., Xie, L., Huang, X., Liang, Z., Liu, B., Han, N., et al. (2019). Enhanced calcite precipitation for crack healing by bacteria isolated under low-nitrogen conditions. *Appl. Microbiol. Biotechnol*. 103, 7971–7982. doi:10.1007/s00253-019-10066-z

Zhao, Y., Peng, L., Feng, Z., and Lu, Z. (2021). Optimization of microbial induced carbonate precipitation treatment process to improve recycled fine aggregate. *Clean. Mater*. 1, 100003. doi:10.1016/j.clema.2021.100003

Zhao, Z., Courard, L., Groslambert, S., Jehin, T., Léonard, A., and Xiao, J. (2020). Use of recycled concrete aggregates from precast block for the production of new building blocks: An industrial scale study. *Resour. Conservation Recycl*. 157, 104786. doi:10.1016/j.resconrec.2020.104786

Influence of ternary hybrid fibers on the mechanical properties of ultrahigh-strength concrete

Suhad Abed[1], Rafal Hadi[2], Akram Jawdhari[3],
Hadee Mohammed Najm[4], Shaker Mahmood[5,6]*, Munder Bilema[7]
and Mohanad Muayad Sabri Sabri[8]

[1]Department of Highways and Airports Engineering, College of Engineering, University of Diyala, Diyala,
Iraq, [2]Department of Civil Engineering, Bilad Alrafidain University College, Diyala, Iraq, [3]Department of
Mechanical and Civil Engineering, Purdue University- Northwest, Hammond, IN, United States,
[4]Department of Civil Engineering, Zakir Husain Engineering College, Aligarh Muslim University, Aligarh,
India, [5]Department of Civil Engineering, College of Engineering, University of Duhok, Duhok, Iraq,
[6]Department of Civil Engineering, College of Engineering, Nawroz University, Duhok, Iraq, [7]Department of
Civil Technology, College of Science Technology- Qaminis, Qaminis, Libya, [8]Peter the Great St.
Petersburg Polytechnic University, St Petersburg, Russia

Ultra-high performance concrete (UHPC), an advanced class of fiber-reinforced
cementitious material with extraordinary mechanical properties, low permeability,
shrinkage and creep, and high energy absorption capacity, has seen steady
increase in use, with applications covering construction of new members and
retrofit of existing ones. Fibers are added in the UHPC mix to bridge cracks, carry
tensile stresses, and contribute greatly to member ductility and load capacity.
Hybrid fibers comprising micro and macro types are beneficial where the first type
resists microcracking and the second targets macrocracking. This study
investigates the effects of blending three fiber types, namely, hooked-end steel
(referred to as type 1, representing macro fibers class), straight-end steel (type 2,
intermediate size fibers), and carbon (type 2, micro size fiber), on the mechanical
properties of UHPC. Experimental tests were performed to characterize the
following mechanical properties: flowability, compressive strength, tensile
strength, flexural strength, modulus of elasticity, and dry shrinkage. The
primary variable in the tests was the blending of different fiber types, using
either a unary form of type 1, a binary form of type 1 and 3 or type 2 and 3,
and a ternary mix of all three types, at 1.56% dosage by volume. The mix with
ternary fibers yielded a compressive strength, tensile strength, flexural strength,
and modulus of elasticity that is 14%−17%, 14%−16.8%, 43.66%−22.16%, and 12%−
16%, larger than the same respective properties of the mix with unary fibers. In
addition, ternary fibers increased the cohesiveness of the mix by 17% and 26%
compared to unary fibers.

KEYWORDS

UHPC, fiber-reinforced concrete, reactive powder concrete, fibers, fiber reinforced
polymer

1 Introduction

Ultra-high performance concrete (UHPC), also known as reactive powder concrete
(RPC) and ultra-high performance fiber-reinforced concrete (UHPFRC) (Ter Maten, 2011;
Qaidi et al., 2022a; Tayeh et al., 2022c), is an advanced class of fiber-reinforced cementitious
material obtained through the removal of coarse aggregate, optimization of particle

gradation, use of admixtures and microfibers (Ter Maten, 2011; Saeed et al., 2022; Zeybek et al., 2022). It consists of fine powders such as cement, quartz, fine sand, and mineral additives such as fly ash, silica fume, and ground granulated blast-furnace slag, used due to their pozzolanic properties and filling capacity (Shakor et al., 2019a; Puzatova et al., 2022; Vinod et al., 2022). With a low w/c ratio [typically less than 0.25 (Graybeal, 2014; Sanjuán and Andrade, 2021)], superplasticizers are also used to ensure good flow, consolidation, and workability of UHPC (Caluk et al., 2019; Tayeh et al., 2022a; Qaidi et al., 2022f). Discontinuous fiber reinforcement, typically made from steel with diameters of 0.5 mm, lengths of 12.5 mm, and dosage of 2%–4% by volume, are incorporated in UHPC mix to provide bond at the micro level and minimize micro-cracking (Harris and Roberts-Wollmann, 2005). The mechanical properties of UHPC include a compressive strength (f_c') of more than 150 MPa, and tensile strength exceeding 5 MPa with a strain-hardening response resembling metallic ductility. UHPC has low permeability, shrinkage, and creep; good durability, and high energy absorption capacity.

While the high initial cost prohibits its application in mass construction, UHPC has been used mainly in applications that maximize its attributes, including in members subjected to harsh environments, as a repair overlay for bridge decks and corroded steel girders ends; in construction of link slabs, hybrid members containing UHPC in highly stressed regions such as beam mid-spans and column plastic hinges; and as grout material for joints between adjacent precast girders or between a precast slab and steel girder (Grünewald, 2004; Qaidi et al., 2022f; He et al., 2022). Nonetheless, with the development of open-source mixes which help to reduce the unit price, establishment of design codes and guidelines, abundance of research studies and filed applications, and presence of educational programs introducing various design and construction aspects to professional engineers and contractors, UHPC is becoming increasingly used in the construction of full members such as beams (Standard, 2017; Qaidi S. M. et al., 2022; Tayeh et al., 2022d; Qaidi et al., 2022f), thin shells (Ter Maten, 2011; Shakor et al., 2019b), concrete sandwich panels (Qaidi et al., 2022c), marine structures, piers, and sewage treatment units (Tayeh et al., 2022b; Qaidi et al., 2022c; Qaidi et al., 2022d; Qaidi et al., 2022e; Faraj et al., 2022; He et al., 2022).

Fibers have a crucial role within UHPC, mainly acting as stitches, bridging cracks and transferring load across their faces, thus increasing the member's ductility and load capacity (Emad et al., 2022; Faraj et al., 2022). Some of UHPC mechanical properties, particularly the post-cracking tensile stress-strain response, are dependent on fiber properties such as type, content, aspect ratio (length/diameter), combined stiffness (for fiber cocktail), and method of placement during casting (Ter Maten, 2011; Qaidi et al., 2021a; Almeshal et al., 2022). Multiple studies investigated key parameters related to the use of single-type fibers in UHPC. For example, Biolzi et al. (1997) studied the effects of three contents for steel fibers, namely: 2%, 4%, and 6% by volume, on UHPC's compressive strength, direct tensile strength, and elastic modulus. Gao (2007) compared the dynamic load performance of plain and fiber-reinforced UHPC (Ali et al., 2022a; Ali et al., 2022b).

While single-type fibers are predominantly used, multiple studies have found that using a mixture of fiber lengths and

types, results in better ductility and strength. Fiber cocktails enable better-cracking resistance where short fibers act to bridge microcracks while long ones restrain macrocracks. Different fiber types have been found to result in different attributes, namely, a) steel fibers to increase fracture energy and strength, b) Polypropylene (PP) fibers to increase fire resistance and reduce spalling and early shrinkage, and c) glass fibers to reduce internal stresses in fresh UPHC. The study by Rossi et al. (1987) was one of the first to propose the mix of multi-type fibers with the product dubbed multi-modal fiber-reinforced concrete. Few studies investigated the effects of blending multi-type fibers in UHPC. Raza et al. (2021) examined three types of single fiber-reinforced UHPC, namely: steel fiber (SF), glass fiber (GF), and carbon fiber (CF), and three blended fiber mixes, namely: SF-GF, GF-CF, and CFSF. A constant volume fraction of 2% was used for all fiber combinations. The study concluded that using a hybrid mix of 1% SF and 1% CF yielded the maximum overall mechanical performance among all combinations. Shaheen and Shrive (2006) compared CF- and SF-reinforced UHPC and found the former to result in significantly higher fracture toughness, and compressive and splitting tensile strength than the latter (Cao et al., 2018b; Khan et al., 2018; Ahmad et al., 2020).

Despite the limited studies, there is a need to examine further the effects of multi-type and blended fibers on the behavior of UHPC (Cao et al., 2018a; Khan et al., 2021; Khan et al., 2022). This study aims to examine whether higher mechanical and durability properties in UHPC can be obtained if a blend of multiple fiber types representing a range of micro and macro types with different dimensions, end conditions, and textures are used instead of single fiber type. Three types of fibers were used in the study: hooked-end steel fibers as macro class, straight-end steel fibers as intermediate class, and carbon fibers as micro reinforcement. Experimental tests were performed to characterize the common mechanical properties: flowability, compressive strength, tensile strength, flexural strength, modulus of elasticity, and dry shrinkage.

2 Experimental work

To understand the effects of blended micro and macro fiber bundles on the behavior of UHPC, five mixes were chosen and tested comprising diverse types of fibers (carbon fibers and straight steel fibers as microfiber and steel fiber with hooked-ends as macro fiber) (Figure 1) in its single and hybrid states with different volumetric percentages (V_f). The properties of the fibers used are presented in Table 1. They include a) hooked-end steel fibers (after this referred to as type 1) with a length (L) and diameter (D) of 50 and 0.75 mm, respectively, representing the macro reinforcement; b) straight-end steel fibers (after this referred to as type 2) with L and D of 15 and 0.2 mm, respectively, as an intermediate size micro reinforcement; and carbon fibers (after this referred to as type 3) with L and D of 8 and 0.007 mm, as a smaller size micro reinforcement. The volume fraction of steel fibers used in this study was 1.33% depending on the published earlier study (Ahmed and Abd, 2018; Al-Tayeb et al., 2022; Akeed et al., 2022c; Emad et al., 2022; Faraj et al., 2022), while the carbon fiber ratio chosen was based on a general review of the literature.

The UHPC was produced using exceptionally fine materials including ordinary Portland cement (type I), river silica sand, and
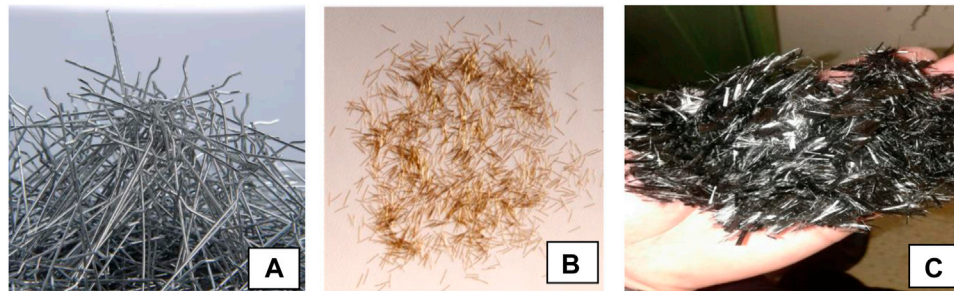
FIGURE 1
(A) Steel fibers with hooked ends, **(B)** steel fibers with straight ends, and **(C)** carbon fibers.

TABLE 1 Fiber properties.

Type of fibers	Steel fibers (hooked-ends)	Steel fibers (straight ends)	Carbon fibers
Length (mm)	50	15–16	8
Diameter (mm)	0.75	0.2 ± 0.02	7 ± 2 microns
Density (kg/m^3)	7,800	7,800	1,700
Aspect ratio (L/D)	50	40–80	1,140
Tensile strength (MPa)	1,345	2,000	3,500

silica fume, in addition to the use of a chemical additive superplasticizer (Gleinum 51) to reduce the w/c ratio to 20%. All the properties of the materials used are shown in Table 2, the sieve analysis of silica sand is shown in Table 3, and the details of the proportions of the mixture materials are shown in Table 4. Mixes 1 and 2 contain 1.33% of uni-type fibers, the former with type 1 and the latter with type 2, Table 4. Mix 3 contains a blend, of 1.33% of type 1% and 0.2% of type 3 fibers. Mix 4 features 1.33% of type 2 fibers and 0.2% of type 3, while mix 5 has a combination of 0.66% of type 1, 0.66% of type 2, and 0.2% of type 3 fibers. The effects of the hybrid fibers were characterized through material tests on several mechanical properties: compressive strength, tensile strength, flexural strength, and modulus of elasticity. Table 5 summarizes the various characterization tests performed on the mixes, showing the specimen configuration and dimensions for each test, along with the standard followed in each test.

To ensure that the fine particles overlap with each other and blend properly, the dry materials (cement, silica sand, and silica fume) were mixed for 3 min in a small rotary mixer. The superplasticizer was then diluted with the required water quantity and the final solution was added to the dry ingredients, where mixing was then continued for additional 2 min to obtain a homogeneous mixture. Finally, the fibers were distributed uniformly and gradually to prevent them from balling and agglomeration, while maintaining a uniform distribution over the mixture during the mixing period.

Before pouring the UHPC mix, the molds for material tests (i.e., cylinders, cubes, and prisms) were prepared by coating their inner surfaces with a thin layer of oil to facilitate specimen removal after the concrete hardens. The specimens were lightly tapped by a metal rod to reduce air voids and ensure good compaction. Figure 2 shows a representative sample of the freshly cast specimens in molds. The specimens were levelled using a trowel and then left to cure for 24 h. They were removed from the models and placed in a curing basin filled with water (Figure 3) until the required tests were performed at 7 and 28 days. A total of 90 specimens with different shapes (i.e., cubes, cylinders, and prisms) were prepared and tested for the 5 mixes in Table 4, at the ages of 7 and 28 days.

3 Experimental tests

3.1 Flow table test

A flow test, following ASTM C-1437 (ASTM, 2007) standards, was conducted (Figure 4) to measure the workability of the five UHPC mixes used in the study. The flow is defined as the average increase in the base diameter, measured at least in four different diameters at approximately equidistant intervals, and is expressed as a percentage of the original base diameter.

$$Flow = \left[\frac{D_{avg} - D_o}{D_o}\right]*100$$

Where:

D_{avg} = Average base diameter measured after the mold is lifted and the mortar spreads.
D_o = Original base diameter of the mold.

TABLE 2 Material properties used in the current study.

Properties		Cement	Iraqi specification No. 5/1984	Silica sand	Silica fume	Superplasticizer
Form		Powder	—	Fine granules	Powder	Viscous liquid
Color		Dark gray	—	Light brown	Light gray	Light brown
Relative density		1,440 kg/m²	—	1,600	—	1.1 @ 20 Co
pH		—	—	—	—	6.6
Viscosity		—	—	—	—	128 ± 30 CPS@ 20 Co
Specific gravity		—	—	2.63	—	—
Surface area m²/kg		405	Minimum (230)	—	24,000-28,000	—
SiO₂	% (weight)	21.44	—	—	≥90	—
SO₃		2.7	Maximum (2.8)	—	≤0.2	—
CaO		61.19	—	—	≤0.8	—
C3A		5.73	—	—	—	—
C3S		42.83	—	—	—	—
C2S		29.4	—	—	—	—
C4AF		11.19	—	—	—	—

Sitting time:
  Initial (min.)
  Final (hr.)
		135
		3:25
			Minimum (45)
			Maximum (10)
				—	—	—

Compressive strength (MPa):
  3- days
  7- days
		24.4
		32.3
			Minimum (15)
			Minimum (23)
				—	—	—

TABLE 3 Sieve analysis of silica sand.

Sieve size	Passing %
600 μm	93
300 μm	23
150 μm	4.5
Pan	0

3.2 Compressive strength test

Compression tests were conducted according to BS 1881 (BS, 1989) on cubes with a side length of 100 mm using a hydraulic testing machine with a capacity of 2,000 kN, at a loading rate of 0.25 ± 0.05 MPa per second, as shown in Figure 5.

3.3 Splitting tensile strength test

Splitting tensile tests were performed according to ASTM C496 (Standard, 2017), on cylinders with diameters (D) and lengths (L) of 150 and 300 mm, respectively. Figure 6 shows a cylinder undergoing

testing by a universal testing machine with a capacity of 2,000 kN. The splitting tensile strength was calculated using the following formula:

$$f sp = \frac{2 P}{\pi \times D \times L}$$

Where:
f_{sp}: Splitting tensile strength (MPa).
P: Applied load in (N).
D: Cylinder diameter (mm).
L: Cylinder length (mm).

3.4 Flexural strength test

To characterize the UHPC modulus of rupture (f_r), prisms with dimensions of 100 mm × 100 mm × 500 mm were prepared according to ASTM C78-22 specification (ASTM, 2010) and tested under two-point loading with a clear span of 450 mm, Figure 7. The following equation is used to determine f_r:

$$f_r = P \times L/b \times h^2$$

Where:

P = maximum applied load in N, L = prism span (450 mm), b = prism width (100 mm), and h: prism depth (100 mm).

TABLE 4 Mix proportions for the 5 UHPC mixes.

Mix code	Cement kg/m³	SS kg/m³	SF %	w/c %	SP (%)	Hooked-end Steel fiber	Straight ends Steel fiber	Carbon fiber
M 1	1,000	1,000	25	20	3	1.33%	—	—
M 2	1,000	1,000	25	20	3	—	1.33%	—
M 3	1,000	1,000	25	20	3	1.33%	—	0.2%
M 4	1,000	1,000	25	20	3	—	1.33%	0.2%
M 5	1,000	1,000	25	20	3	0.66%	0.66%	0.2%

SS, Silica Sand; SF, Silica Fume; SP, Superplasticizer; w/c, Water to cement ratio.

TABLE 5 Characterization tests performed on the mixtures.

Mechanical property	Specimen		Testing standard
	Shape	Dimension (mm)	
Compressive strength	Cube	$L = 100$	BS 1881-1989
Splitting strength	Cylinder	$L = 200$	ASTM C469-14
		$D = 100$	
Flexure strength	Prism	$L_1 = 500$	ASTM C78-22
		$L_2 = 100$	
		$L_3 = 100$	
Flow test	—	—	ASTM C1437-20
Modulus of Elasticity	Cylinder	$L = 300$	ASTM C496-14
		$D = 150$	

L, length of cube or height of cylinder; D, diameter of cylinder; L_1, length of prism; L_2, width of prism; L_3, height of prism.

FIGURE 2
Cast specimens in cube and cylinder molds.

FIGURE 3
Specimens being cured in wet conditions.

3.5 Modulus of elasticity test

The modulus of elasticity (E_c) is a major parameter affecting the design and analysis of a UHPC member and is typically related to the square root of the compressive strength (f_c') in an empirical relation (Russell et al., 2013). E_c of the examined mixes was characterized experimentally by testing three 150 mm × 300 mm cylinders per mix, each instrumented with 2 strain gages placed within the middle third length of the cylinder in the axial direction (Figure 8). Averaging the two gage readings from all three cylinder tests, E_c for each mix was found using the following equation adopted from the ASTM C469/C479M-14 (ASTM, 2002) standards:

FIGURE 4
A sample of the flow table test.

FIGURE 6
A sample of the tensile splitting test.

FIGURE 5
A sample of compressive strength test.

FIGURE 7
A sample of the flexural strength test.

S_1 = Stress corresponding to a longitudinal strain (ε_1) of 50 millionth,

ε_2 = Longitudinal strain produced by stress S_2.

3.6 Drying shrinkage test

Prismatic 40 mm × 40 mm × 160 mm specimens were used to measure the length change of the concrete sample due to the effects of

$$E_C = \frac{S_1 - S_2}{\varepsilon_2 - 0.00005}$$

Where:

S_2 = Stress corresponding to 40% of the ultimate capacity, in MPa,

FIGURE 8
A sample of modulus of elasticity test.

FIGURE 9
Drying shrinkage test.

drying shrinkage, following specifications of ASTM C157/C157M-14 (Standard, 2014). For each mix, two specimens were tested under room temperature conditions, taking the average of the two as the mix drying shrinkage. A comparator length tool (Figure 9) was used to measure the change in length with time, while the following equation was utilized to determine the shrinkage at any age:

$$\Delta L_x = [(CRD - initial~CRD)/~G] \times 100$$

Where:

ΔL_x = Length change at any age.

CRD = Difference between comparator reading and reference bar at any age.

G = Specimen length.

4 Results and discussion

This section discusses the results of the various material tests conducted to characterize the effects of hybrid fibers on the mechanical performance of UHPC. The results are divided into six sections, each discussing the results of one of the material characterization tests addressed in Section 3.

4.1 Flow table test

The results of the flow table test are presented in Table 6 and Figure 10. The results show a decrease in the flow ability of the

TABLE 6 Flow table test results.

Mixes type	Flow table test/cm
M 1	21
M 2	23
M 3	19
M 4	20.5
M 5	17

UHPC mix, as the fiber percentage increases from 1.33% to 1.53% (15% increase). Previous studies (Boulekbache et al., 2010; Sahoo et al., 2019; Akeed et al., 2022a) have shown that the reduction in flowability associated with the use of fiber reinforcements can be attributed to: 1) the large length and surface area of the fibers compared to the aggregates causing an increase in the cohesive forces between the two constituents; 2) fibers effects on altering the granular skeleton structure of the mix and hindering its flow; 3) fiber reinforcements tend to flow perpendicular to the paste; thus they generate resisting forces and moments to the flow velocity of the fresh mixture (Ahmed H. U. et al., 2022; Abd et al., 2022; Akeed et al., 2022b; Abd et al., 2023).

4.2 Compressive strength test

Figure 11 and Table 7 present the results of the compressive strength (f_c') of UHPC for the five different mixes with various fiber blends, at three ages, 7, 28, and 56 days. Comparing mixes 1 and 2, both with 1.33% single-type fibers but featuring type 1 for the former
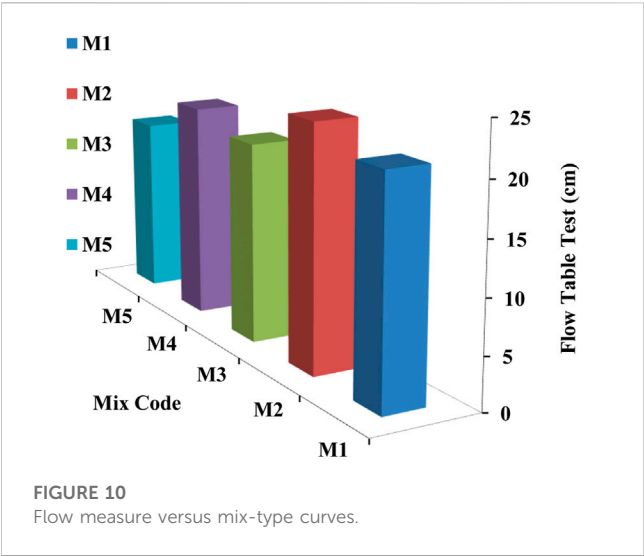
FIGURE 10
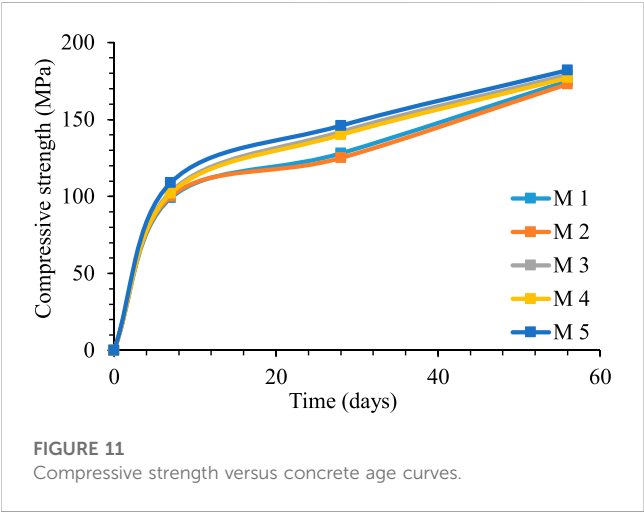Flow measure versus mix-type curves.

FIGURE 11
Compressive strength versus concrete age curves.

and type 2 for the latter, f_c' seems invariable for all ages (Ali et al., 2022a; El Ouni et al., 2022; Raza et al., 2022). Using a blend of two types of fibers as the case in mixes 3 and 4 seems to result in a negligible increase in f_c' at 7 and 56 days but a noticeable 11.5% increase at 28 days, on average, when compared to f_c' of mixes 1 and 2. On the other hand, the triple fiber type (mix 5) with fiber composition of 0.66% type

1, 0.66% type 2, and 0.2% type 3 results in a 5%–15% increase in f_c' compared to that of the single fiber type mixes (mixes 1 and 2), and 2%–6% compared to the double fiber type mixes (mixes 3 and 4). Incorporating hybrid fibers into the mix optimizes the benefits of each fiber type due to the different material properties for each type as well as different lengths. With microfibers bridging microcracks and macro ones targeting macrocracks, cracks with different sizes can be controlled, eventually improving compressive strength (Aisheh et al., 2022; Ahmed S. N. et al., 2022).

All mixes accrue an increase in f_c' with age, sharply during the first 7 days from casting and at a much slower rate afterwards. Aside from the similarity in trend with conventional concrete and natural hydration process, the presence of parts unique to UHPC, such as superplasticizers and silica fume, also contribute to compressive strength growth with time. For example, silica fume is known to react chemically with calcium hydroxide, thus increasing the strength and reducing the voids inside the concrete (Sahoo et al., 2019; Ahmed et al., 2021; Akeed et al., 2022d; Akeed et al., 2022e).
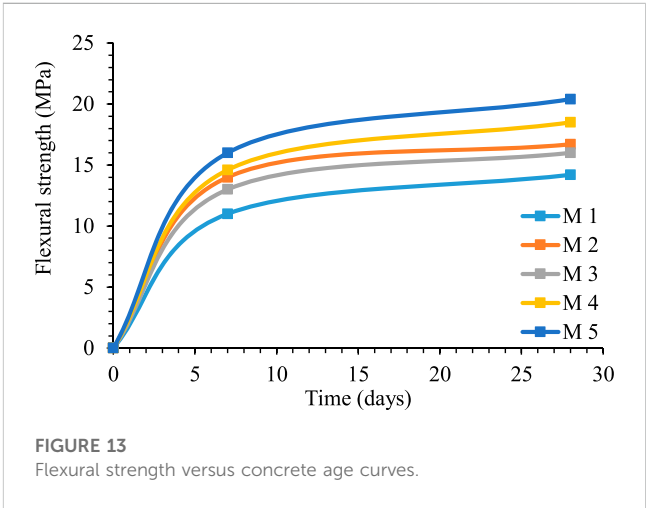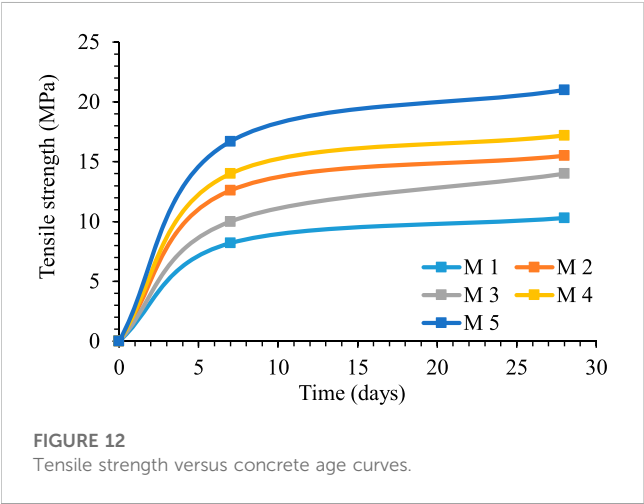
4.3 Splitting tensile strength test

Although the tensile strength (f_t) of UHPC is higher than that of conventional concrete, it is subpar to the compressive strength. Thus, tensile splitting tests were also performed to examine the effects of hybrid fiber types in improving the tensile strength of UHPC. Table 8 and Figure 12 present the f_t values for the five different mixes at the ages of 7 and 28 days. f_t of mix 2 was 50%–54% larger than that of mix 1, likely because of the larger tensile strength of the straight steel fibers (type 2) compared to the hooked-end ones (type 1). Both mix 1 and 2 contain single-type fibers. Mix 3 with 1.33% type 1 fibers and 0.2% type 3 (total fiver volume = 1.53%) had a 22%–36% larger f_t than mix 1 with 1.33% type 1 fibers. Despite having 13% fewer fibers, mix 2 (with single-type 2 fibers) had f_t 11%–26% larger than that mix 3. Comparing mix 4 and 2, both containing type 2 fibers but a small 0.2% of carbon fibers (type 3) is added to the former, mix 4 had 11% larger f_t. Of the five proportions, mix 5 features the largest f_t, 16.7 MPa at 7 days and 21 MPa at 28 days. This was a 100% increase over mix 1, 32%–35% over mix 2, 50%–67% over mix 3, and 19%–22% over mix 4. In all mixes, f_t increased with age resonating with the trend observed for the tests on compressive strength.

TABLE 7 Results of the compressive strength test.

Mix code	Compressive strength (MPa) at 7-days	Compressive strength (MPa) at 28-days	Compressive strength (MPa) at 56-days
M 1	99	128	175
M 2	100	125	173
M 3	103	142	179
M 4	102	140	177
M 5	109	146	182

TABLE 8 Splitting tensile strength results.

Mix code	Splitting tensile Strength (MPa) at 7-days	Splitting tensile Strength (MPa) at 28-days
M 1	8.2	10.3
M 2	12.6	15.5
M 3	10	14
M 4	14	17.2
M 5	16.7	21

FIGURE 12
Tensile strength versus concrete age curves.

FIGURE 13
Flexural strength versus concrete age curves.

4.4 Flexural strength test

Table 9 and Figure 13 present the results of the effect of using hybrid fibers on the flexural strength (f_b) of UHPC, at the ages of 7 and 28 days. It can be seen that blending carbon fibers (type 3) with hooked-end steel fibers (type 1) as in mix 3 or straight-end steel fibers (type 2) as in mix 4 results in an increase in f_b by about 12.67% and 10.78%, respectively, compared to mix 1 and 2 with single-type fibers. Using the three-type fiber blend resulted in the largest f_b, 20.5 MPa at 28 days. This improvement is due to the increase in the bonding strength between the fibers and the concrete mixture, and thus an increase in the material's ductility. Furthermore, due to the presence of fibers in the mix, higher energy input is required to extend the crack further, and the crack-tip region will be restrained,

which can be attributed to the closing pressure on crack surfaces induced by the bridging fibers (Ter Maten, 2011).
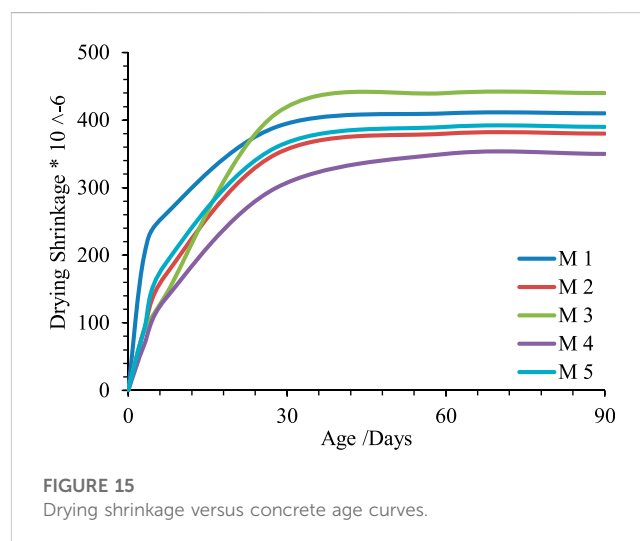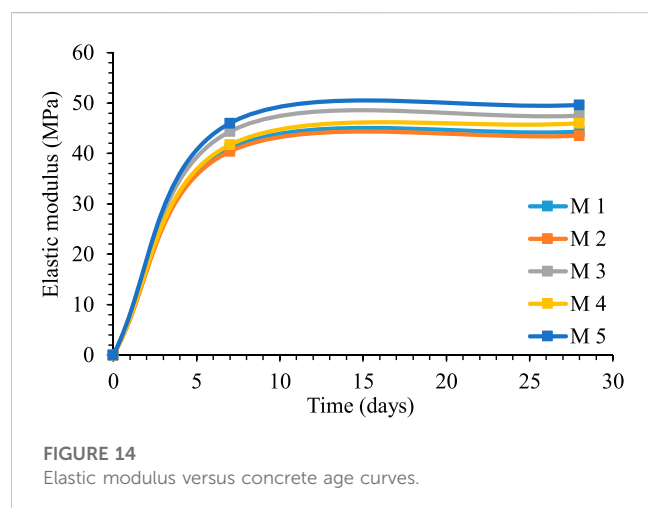
4.5 Modulus of elasticity test

Table 10 and Figure 14 present the results of the UHPC elastic modulus (E) for the five mixes, at two ages 7 and 28 days. The results show the hybrid fibres' clear role in increasing the mix's stiffness. When carbon fibers were used with hooked-end steel fibers (mix 3), E increased by about 7.18% compared to mix 1 (type 1 fibers only) and 5.7% compared to mix 2 (type 1 fibers only). Mix 5 (with a blend of all three fiber types) resulted in the highest E 49.63 MPa, at 28 days of age. E of concrete is directly affected by the compressive

TABLE 9 Flexural strength results.

Mix code	Flexural strength (MPa) at 7-days	Flexural strength (MPa) at 28-days
M 1	11	14.2
M 2	14	16.7
M 3	13	16
M 4	14.6	18.5
M 5	16	20.4

TABLE 10 Results for modulus of elasticity test.

Mix code	Modulus of elasticity (GPa) at 7-days	Modulus of elasticity (GPa) at 28-days
M 1	41	44.32
M 2	40.4	43.53
M 3	44.34	47.5
M 4	41.7	46
M 5	46	49.63

FIGURE 14
Elastic modulus versus concrete age curves.

FIGURE 15
Drying shrinkage versus concrete age curves.

strength of concrete (Tomosawa et al., 1990) where fibers have an essential role in reducing the concrete cracking strains due to the crack bridging effects, and ultimately increasing the stiffness.

4.6 Drying shrinkage test

The results of the drying shrinkage test for the five mixes versus age in days are presented in Figure 15. The shrinkage was measured at five ages, namely, 3, 7, 28, 56, and 90 days. In line with other mechanical tests, Figure 15 confirms the advantages of hybrid fibers where mix 5 (with triple fiber type) yielded the smallest values for dry shrinkage.

The functions of the fibers in cement-based composites can be classified into two categories: shrinkage crack control and mechanical property enhancement. For shrinkage crack control, generally lesser amounts of low-modulus and low-strength fibers are added to restrain the early-age shrinkage and suppress shrinkage cracking. Short straight steel fibers can serve as bridging mechanisms during cracking. Therefore, the use of short steel fibers, especially those with a high aspect ratio, is beneficial in that case.

4.7 Discussion on the role of fibers

In conventional applications of fiber cementitious composites, the fibers' function becomes visible after a major crack has formed in

the composite (Shah, 1990). At this stage, there are one or few major cracks and the overall composite behaviour is characterized by strain softening after the peak load is reached. The incorporation of fibers significantly increases the total energy consumption and overall toughness of the composite. In such cases, and where fiber rupture does not govern, the gradual fiber debonding and pullout failures can consume a great amount of energy. On the other hand, with an increase in fiber volume fraction, microcracks formed in the matrix may be stabilized due to the interaction between the matrix and fibers through bonding, hence postponing the formation of the first major crack in the matrix. Thus, the apparent tensile strength of the matrix can be increased (Shah, 1990). Moreover, when a sufficient volume fraction of small-diameter steel, glass, or synthetic fibers is incorporated into the cement-based matrix, the fiber/matrix interaction can lead to strain hardening and multiple cracking behaviours, changing the failure mode from quasi-brittle to ductile.

As a result, the composite's toughness and matrix tensile strength can be significantly improved. One of the mechanisms for slowing the growth of a transverse crack in unidirectional fiber composites can be attributed to the development of longitudinal cylindrical shear microcracks located at the boundary between the fiber and the bulk matrix, which allows the fibers to debond while transferring the force across the faces of the main crack. In addition to enhancing the toughness and tensile strength, the addition of fibers can also improve the bending resistance of cement-based composites. However, adding fibers has only a minor influence on

the compressive strength of cement-based composites. At a small fiber volume fraction, there is almost no effect. Hence, it is not worthwhile to incorporate fibers to enhance compressive strength. The enhancing order of fibers on the mechanical properties of cement-based composites is toughness, followed by flexural strength, tensile strength, and compressive strength (Shah, 1990).

Microfibers are efficient in restraining microcracks and macro fibers in restraining macroscopic cracks. From the materials point of view, the fibers that are commonly used in fiber-reinforced cement-based composites are carbon, glass, polymeric (e.g., acrylic, aramid, nylon, polyester, polyethylene), natural (e.g., wood cellulose, sisal, coir), and steel (high tensile and stainless). Several types of fibers have different values of young's modulus, tensile strength, surface textures, and elongation abilities. These properties affect the bond between the fibers and the matrix, the ability to bridge cracks, the improvement of matrix properties, and, by extension, how fiber-reinforced cement-based composites behave.

5 Conclusion

This study conducted tests on 90 small-scale specimens with different shapes and functions to characterize the effects of blended micro- and macro-size fibers on the mechanical properties of ultra-high performance concrete (UHPC). The fibers studied were hooked-end steel (referred to as type 1, representing macro class), straight-end steel (type 2, intermediate size), and carbon (type 2, micro size). Five mixes were cast and differing by the type and blend of fibers, namely, a) with type 1 unary fibers, b) with type 2 unary fibers, c) with type 1 and 3 binary fiber blend, d) with type 2 and 3 binary fiber blend, and e) with all three fibers. A fiber dosage of 1.56% by volume was used for blended fiber mixes. The characterization tests were performed on the following mechanical properties: flowability, compressive strength, tensile strength, flexural strength, modulus of elasticity, and dry shrinkage. Based on the results, the following conclusions were made:

1. Using ternary fiber cocktail instead of unary type 1 fibers resulted in a 20% decrease in the flowability of the UHPC mix.
2. The compressive strength (f_c'), at ages of 7 and 28 days, does not seem to vary for mixes with unary fibers (type 1 or type 2). f_c' for the mixes with a blend of two types of fibers (type 1 and 3 or type 2 and 3) was slightly larger than that of the unary-fiber mixes at ages of 7 and 56 days, but 11.5% larger at 28 days. The ternary-fiber mix resulted in f_c' of 5%–15% and 2%–6% more than that of the unary-fiber and binary-fiber mixes, respectively.
3. The ternary fiber cocktail improved the UHPC tensile strength by 14% and 16.8%, compared to the mixes featuring unary and binary fibers. This is because of the multiple roles of different fiber classes in bridging various crack sizes.

4. The ternary fiber cocktail resulted in 22.16%–43.66% increase in flexural strength (an indicator of higher ductility) compared to the mixes featuring unary fibers.
5. The modulus of elasticity was increased by 12%–14% when ternary fiber cocktail was used *in lieu* of unary type 1 fibers.
6. The triple-fiber cocktail also resulted in smaller drying shrinkage than the other fiber blends. It is hypothesized that lesser amounts of low-modulus and low-strength fibers results in better restraint of the early-age shrinkage and shrinkage cracking.

Data availability statement

The original contributions presented in the study are included in the article/Supplementary Material, further inquiries can be directed to the corresponding author.

Author contributions

Conception and design of the study: SA, RH, AJ, HN, SM, MB, and MS; acquisition of data: SA, RH, AJ, and HN; analysis and/or interpretation of data: SM, MB, and MS; drafting the manuscript: SA, RH, AJ, HN, SM, MB, and MS; revising the manuscript critically for important intellectual content: SA, RH, AJ, HN, SM, MB, and MS; and approval of the version of the manuscript to be published: SA, RH, AJ, HN, SM, MB, and MS.

Funding

Conflict of interest

Publisher's note

References

Abd, S. M., Mhaimeed, I. S., Tayeh, B. A., Najm, H. M., and Qaidi, S. (2022). Flamingo technique as an innovative method to improve the shear capacity of reinforced concrete beam. *Case Stud. Constr. Mater.* 17, e01618. doi:10.1016/j.cscm.2022.e01618

Abd, S. M., Mhaimeed, I. S., Tayeh, B. A., Najm, H. M., and Qaidi, S. (2023). Investigation of the use of textile carbon yarns as sustainable shear reinforcement in concrete beams. *Case Stud. Constr. Mater.* 18, e01765. doi:10.1016/j.cscm.2022.e01765

Ahmad, W., Farooq, S. H., Usman, M., Khan, M., Ahmad, A., Aslam, F., et al. (2020). Effect of coconut fiber length and content on properties of high strength concrete. *Materials* 13, 1075. doi:10.3390/ma13051075

Ahmed, B. K., and Abd, S. M. (2018). Eliminating the shrinkage of high strength concrete by using super absorbent polymer (SAP). *Diyala J. Eng. Sci.* 11, 8–13. doi:10.24237/djes.2018.11402

Ahmed, H. U., Mohammed, A. A., Rafiq, S., Mohammed, A. S., Mosavi, A., Sor, N. H., et al. (2021). Compressive strength of sustainable geopolymer concrete composites: A state-of-the-art review. *Sustainability* 13, 13502. doi:10.3390/su132413502

Ahmed, H. U., Mohammed, A. S., Faraj, R. H., Qaidi, S. M. A., and Mohammed, A. A. (2022a). Compressive strength of geopolymer concrete modified with nano-silica: Experimental and modeling investigations. *Case Stud. Constr. Mater.* 16, e01036. doi:10.1016/j.cscm.2022.e01036

Ahmed, S. N., Hamah Sor, N., Ahmed, M. A., and Qaidi, S. M. A. (2022b). Thermal conductivity and hardened behavior of eco-friendly concrete incorporating waste polypropylene as fine aggregate. *Mater. Today Proc.* 57, 818–823. doi:10.1016/j.matpr.2022.02.417

Aisheh, Y. I. A., Atrushi, D. S., Akeed, M. H., Qaidi, S., and Tayeh, B. A. (2022). Influence of steel fibers and microsilica on the mechanical properties of ultra-high-performance geopolymer concrete (UHP-GPC). *Case Stud. Constr. Mater.* 17, e01245. doi:10.1016/j.cscm.2022.e01245

Akeed, M. H., Qaidi, S., Ahmed, H. U., Emad, W., Faraj, R. H., Mohammed, A. S., et al. (2022a). Ultra-high-performance fiber-reinforced concrete. Part III: Fresh and hardened properties. *Case Stud. Constr. Mater.* 17, e01265. doi:10.1016/j.cscm.2022.e01265

Akeed, M. H., Qaidi, S., Ahmed, H. U., Faraj, R. H., Mohammed, A. S., Emad, W., et al. (2022c). Ultra-high-performance fiber-reinforced concrete. Part IV: Durability properties, cost assessment, applications, and challenges. *Case Stud. Constr. Mater.* 17, e01271. doi:10.1016/j.cscm.2022.e01271

Akeed, M. H., Qaidi, S., Ahmed, H. U., Faraj, R. H., Majeed, S. S., Mohammed, A. S., et al. (2022b). Ultra-high-performance fiber-reinforced concrete. Part V: Mixture design, preparation, mixing, casting, and curing. *Case Stud. Constr. Mater.* 17, e01363. doi:10.1016/j.cscm.2022.e01363

Akeed, M. H., Qaidi, S., Ahmed, H. U., Faraj, R. H., Mohammed, A. S., Emad, W., et al. (2022d). Ultra-high-performance fiber-reinforced concrete. Part I: Developments, principles, raw materials. *Case Stud. Constr. Mater.* 17, e01290. doi:10.1016/j.cscm.2022.e01290

Akeed, M. H., Qaidi, S., Ahmed, H. U., Faraj, R. H., Mohammed, A. S., Emad, W., et al. (2022e). Ultra-high-performance fiber-reinforced concrete. Part II: Hydration and microstructure. *Case Stud. Constr. Mater.* 17, e01289. doi:10.1016/j.cscm.2022.e01289

Al-Tayeb, M. M., Aisheh, Y. I. A., Qaidi, S. M. A., and Tayeh, B. A. (2022). Experimental and simulation study on the impact resistance of concrete to replace high amounts of fine aggregate with plastic waste. *Case Stud. Constr. Mater.* 17, e01324. doi:10.1016/j.cscm.2022.e01324

Ali, B., Azab, M., Ahmed, H., Kurda, R., El Ouni, M. H., and Elhag, A. B. (2022a). Investigation of physical, strength, and ductility characteristics of concrete reinforced with banana (Musaceae) stem fiber. *J. Build. Eng.* 61, 105024. doi:10.1016/j.jobe.2022.105024

Ali, B., Farooq, M. A., El Ouni, M. H., Azab, M., and Elhag, A. B. (2022b). The combined effect of coir and superplasticizer on the fresh, mechanical, and long-term durability properties of recycled aggregate concrete. *J. Build. Eng.* 59, 105009. doi:10.1016/j.jobe.2022.105009

Almeshal, I., Al-Tayeb, M. M., Qaidi, S. M. A., Abu Bakar, B. H., and Tayeh, B. A. (2022). Mechanical properties of eco-friendly cements-based glass powder in aggressive medium. *Mater. Today Proc.* 58, 1582–1587. doi:10.1016/j.matpr.2022.03.613

Astm, C. (2010). "Standard test method for flexural strength of concrete (using simple beam with third-point loading)," in *American society for testing and materials)*, 19428–12959.()

Astm, C. (2007). *Standard test method for flow of hydraulic cement mortar*, C1437.

Astm, C. (2002). Standard test method for static modulus of elasticity and Poisson's ratio of concrete in compression. *Annu. book ASTM Stand.* 4, 469.

Biolzi, L., Guerrini, G. L., and Rosati, G. (1997). Overall structural behavior of high strength concrete specimens. *Constr. Build. Mater.* 11, 57–63. doi:10.1016/s0950-0618(96)00026-8

Boulekbache, B., Hamrat, M., Chemrouk, M., and Amziane, S. (2010). Flowability of fibre-reinforced concrete and its effect on the mechanical properties of the material. *Constr. Build. Mater.* 24, 1664–1671. doi:10.1016/j.conbuildmat.2010.02.025

Bs, P. (1989). *Method for determination of compressive strength of concrete cubes*.

Caluk, N., Mantawy, I., and Azizinamini, A. (2019). Durable bridge columns using stay-in-place UHPC shells for accelerated bridge construction. *Infrastructures* 4, 25. doi:10.3390/infrastructures4020025

Cao, M., Li, L., and Khan, M. (2018a). Effect of hybrid fibers, calcium carbonate whisker and coarse sand on mechanical properties of cement-based composites. *Mater. Construcción* 68, e156. doi:10.3989/mc.2018.01717

Cao, M., Xie, C., Li, L., and Khan, M. (2018b). The relationship between reinforcing index and flexural parameters of new hybrid fiber reinforced slab. *Comput. Concr. Int. J.* 22, 481–492.

El Ouni, M. H., Shah, S. H. A., Ali, A., Muhammad, S., Mahmood, M. S., Ali, B., et al. (2022). Mechanical performance, water and chloride permeability of hybrid steel-polypropylene fiber-reinforced recycled aggregate concrete. *Case Stud. Constr. Mater.* 16, e00831. doi:10.1016/j.cscm.2021.e00831

Emad, W., Mohammed, A. S., Bras, A., Asteris, P. G., Kurda, R., Muhammed, Z., et al. (2022). Metamodel techniques to estimate the compressive strength of UHPFRC using various mix proportions and a high range of curing temperatures. *Constr. Build. Mater.* 349, 128737. doi:10.1016/j.conbuildmat.2022.128737

Faraj, R. H., Ahmed, H. U., Rafiq, S., Sor, N. H., Ibrahim, D. F., and Qaidi, S. M. A. (2022). Performance of self-compacting mortars modified with nanoparticles: A systematic review and modeling. *Clean. Mater.* 4, 100086. doi:10.1016/j.clema.2022.100086

Gao, X. (2007). *Mix design and impact response of fibre reinforced and plain reactive powder concrete*. RMIT University.

Graybeal, B. (2014). *Design and construction of field-cast UHPC connections*. Washington, DC: United States. Federal Highway Administration.

Grünewald, S. (2004). *Performance-based design of self-compacting fibre reinforced concrete*.

Harris, D. K., and Roberts-Wollmann, C. L. (2005). *Characterization of the punching shear capacity of thin ultra-high performance concrete slabs*. Charlottesville, VA: Virginia Center for Transportation Innovation and Research.

He, X., Yuhua, Z., Qaidi, S., Isleem, H. F., Zaid, O., Althoey, F., et al. (2022). Mine tailings-based geopolymers: A comprehensive review. *Ceram. Int.* 48, 24192–24212. doi:10.1016/j.ceramint.2022.05.345

Khan, M., Cao, M., Chu, S., and Ali, M. (2022). Properties of hybrid steel-basalt fiber reinforced concrete exposed to different surrounding conditions. *Constr. Build. Mater.* 322, 126340. doi:10.1016/j.conbuildmat.2022.126340

Khan, M., Cao, M., Hussain, A., and Chu, S. H. (2021). Effect of silica-fume content on performance of CaCO3 whisker and basalt fiber at matrix interface in cement-based composites. *Constr. Build. Mater.* 300, 124046. doi:10.1016/j.conbuildmat.2021.124046

Khan, U. A., Jahanzaib, H. M., Khan, M., and Ali, M. (2018). "Improving the tensile energy absorption of high strength natural fiber reinforced concrete with fly-ash for bridge girders," in *Key engineering materials* (Switzerland: Trans Tech Publ), 335–342.

Puzatova, A., Shakor, P., Laghi, V., and Dmitrieva, M. (2022). Large-scale 3D printing for construction application by means of robotic arm and gantry 3D printer: A review. *Buildings* 12, 2023. doi:10.3390/buildings12112023

Qaidi, S. M. A., Dinkha, Y. Z., Haido, J. H., Ali, M. H., and Tayeh, B. A. (2021a). Engineering properties of sustainable green concrete incorporating eco-friendly aggregate of crumb rubber: A review. *J. Clean. Prod.* 324, 129251. doi:10.1016/j.jclepro.2021.129251

Qaidi, S. M. A., Tayeh, B. A., Zeyad, A. M., De Azevedo, A. R. G., Ahmed, H. U., and Emad, W. (2022a). Recycling of mine tailings for the geopolymers production: A systematic review. *Case Stud. Constr. Mater.* 16, e00933. doi:10.1016/j.cscm.2022.e00933

Qaidi, S. M., Atrushi, D. S., Mohammed, A. S., Ahmed, H. U., Faraj, R. H., Emad, W., et al. (2022b). Ultra-high-performance geopolymer concrete: A review. *Constr. Build. Mater.* 346, 128495. doi:10.1016/j.conbuildmat.2022.128495

Qaidi, S., Yahia, A., Tayeh, B. A., Unis, H., Faraj, R., and Mohammed, A. (2022c). 3D printed geopolymer composites: A review. *Mater. Today Sustain.* 20, 100240. doi:10.1016/j.mtsust.2022.100240

Qaidi, S. M. A., Sulaiman Atrushi, D., Mohammed, A. S., Unis Ahmed, H., Faraj, R. H., Emad, W., et al. (2022d). Ultra-high-performance geopolymer concrete: A review. *Constr. Build. Mater.* 346, 128495. doi:10.1016/j.conbuildmat.2022.128495

Qaidi, S. M. A., Tayeh, B. A., Ahmed, H. U., and Emad, W. (2022e). A review of the sustainable utilisation of red mud and fly ash for the production of geopolymer composites. *Constr. Build. Mater.* 350, 128892. doi:10.1016/j.conbuildmat.2022.128892

Qaidi, S. M. A., Tayeh, B. A., Isleem, H. F., De Azevedo, A. R. G., Ahmed, H. U., and Emad, W. (2022f). Sustainable utilization of red mud waste (bauxite residue) and slag for the production of geopolymer composites: A review. *Case Stud. Constr. Mater.* 16, e00994. doi:10.1016/j.cscm.2022.e00994

Raza, S. S., Ali, B., Noman, M., Fahad, M., and Elhadi, K. M. (2022). Mechanical properties, flexural behavior, and chloride permeability of high-performance steel fiber-reinforced concrete (SFRC) modified with rice husk ash and micro-silica. *Constr. Build. Mater.* 359, 129520. doi:10.1016/j.conbuildmat.2022.129520

Raza, S. S., Qureshi, L. A., Ali, B., Raza, A., and Khan, M. M. (2021). Effect of different fibers (steel fibers, glass fibers, and carbon fibers) on mechanical properties of reactive powder concrete. *Struct. Concr.* 22, 334–346. doi:10.1002/suco.201900439

Rossi, P., Acker, P., and Malier, Y. (1987). Effect of steel fibres at two different stages: The material and the structure. *Mater. Struct.* 20, 436–439. doi:10.1007/bf02472494

Russell, H. G., Graybeal, B. A., and Russell, H. G. (2013). *Ultra-high performance concrete: A state-of-the-art report for the bridge community"*. United states. McLean, Virginia: Federal Highway Administration. Office of Infrastructure.

Saeed, A., Najm, H. M., Hassan, A., Sabri, M. M. S., Qaidi, S., Mashaan, N. S., et al. (2022). Properties and applications of geopolymer composites: A review study of mechanical and microstructural properties. *Materials* 15, 8250. doi:10.3390/ma15228250

Sahoo, K. K., Sarkar, P., and Davis, R. (2019). Mechanical properties of silica fume concrete designed as per construction practice. *Proc. Institution Civ. Engineers-Construction Mater.* 172, 20–28. doi:10.1680/jcoma.16.00085

Sanjuán, M. Á., and Andrade, C. (2021). Reactive powder concrete: Durability and applications. *Appl. Sci.* 11, 5629. doi:10.3390/app11125629

Shah, S. P. (1990). *Toughening of cement-based materials with fiber reinforcement*, MRS Online Proceedings Library (OPL. 211.

Shaheen, E., and Shrive, N. G. (2006). Optimization of mechanical properties and durability of reactive powder concrete. *ACI Mater. J.* 103, 444.

Shakor, P., Nejadi, S., Paul, G., and Malek, S. (2019a). Review of emerging additive manufacturing technologies in 3D printing of cementitious materials in the construction industry. *Front. Built Environ.* 4, 85. doi:10.3389/fbuil.2018.00085

Shakor, P., Nejadi, S., Paul, G., Sanjayan, J., and Nazari, A. (2019b). Mechanical properties of cement-based materials and effect of elevated temperature on three-dimensional (3-D) printed mortar specimens in inkjet 3-D printing. *ACI Mater. J.* 116, 55–67.

Standard, A. (2014). *C157,"Standard test method for length change of hardened hydraulic-cement mortar and concrete"*. West Conshohocken, PA, United States: Annual Book of ASTM Standards. 4.

Standard, A. (2017). *C496/C496M-17 Standard test method for splitting tensile strength of cylindrical concrete specimens*. West Conshohocken PA: ASTM International.

Tayeh, B. A., Akeed, M. H., Qaidi, S., and Bakar, B. H. A. (2022a). Influence of microsilica and polypropylene fibers on the fresh and mechanical properties of ultra-high performance geopolymer concrete (UHP-GPC). *Case Stud. Constr. Mater.* 17, e01367. doi:10.1016/j.cscm.2022.e01367

Tayeh, B. A., Akeed, M. H., Qaidi, S., and Bakar, B. H. A. (2022b). Influence of sand grain size distribution and supplementary cementitious materials on the compressive strength of ultrahigh-performance concrete. *Case Stud. Constr. Mater.* 17, e01495. doi:10.1016/j.cscm.2022.e01495

Tayeh, B. A., Akeed, M. H., Qaidi, S., and Bakar, B. H. A. (2022c). Influence of the proportion of materials on the rheology and mechanical strength of ultrahigh-performance concrete. *Case Stud. Constr. Mater.* 17, e01433. doi:10.1016/j.cscm.2022.e01433

Tayeh, B. A., Akeed, M. H., Qaidi, S., and Bakar, B. H. A. (2022d). Ultra-high-performance concrete: Impacts of steel fibre shape and content on flowability, compressive strength and modulus of rupture. *Case Stud. Constr. Mater.* 17, e01615. doi:10.1016/j.cscm.2022.e01615

Ter Maten, R. (2011). *Ultra high performance concrete in large span shell structures*.

Tomosawa, F., Noguchi, T., and Onoyama, K. (1990). "Investigation of fundamental mechanical properties of high-strength concrete," in *Summaries of technical papers of annual meeting of* Architectural Institute of Japan*)*, 497–498.()

Vinod, S., Shakor, P., Sartipi, F., and Karakouzian, M. (2022). Object detection using ESP32 cameras for quality control of steel components in manufacturing structures. *Arabian J. Sci. Eng.*, 1–18. doi:10.1007/s13369-022-07562-2

Zeybek, Ö., Özkılıç, Y. O., Karalar, M., Çelik, A. İ., Qaidi, S., Ahmad, J., et al. (2022). Influence of replacing cement with waste glass on mechanical properties of concrete. *Materials* 15, 7513. doi:10.3390/ma15217513

Behavior of geomaterial composite using sugar cane bagasse ash under compressive and flexural loading

Harshal Nikhade[1,2], Ram Rathan Lal Birali[1], Khalid Ansari[2],
Mohammad Arsalan Khan[3,4]*, Hadee Mohammed Najm[3],
S. M. Anas[5]*, Mohammad Mursaleen[6]*, Mohd Abul Hasan[7] and
Saiful Islam[7]

[1]Department of Civil Engineering, Kavikulguru Institute of Technology and Science, Ramtek, India,
[2]Department of Civil Engineering, Yeshwantrao Chavan College of Engineering, Nagpur, India,
[3]Department of Civil Engineering, Zakir Husain College of Engineering and Technology, Aligarh Muslim
University, Aligarh, India, [4]Geomechanics and Geotechnics Group, Kiel University, Kiel, Germany,
[5]Department of Civil Engineering, Jamia Millia Islamia, New Delhi, India, [6]China Medical University
Hospital, China Medical University (Taiwan), Taichung, Taiwan, [7]Civil Engineering Department, College of
Engineering, King Khalid University, Abha, Saudi Arabia

The sugar industry produces a huge quantity of sugar cane bagasse ash in India. Dumping massive quantities of waste in a non-eco-friendly manner is a key concern for developing nations. The main focus of this study is the development of a sustainable geomaterial composite with higher strength capabilities (compressive and flexural). To develop this composite, sugarcane bagasse ash (SA), glass fiber (GF), and blast furnace slag (BF) are used. Ash generated from burning sugar cane in the sugar industry is known as sugar cane bagasse. To check the suitability of this secondary waste for use in civil engineering and to minimize risk to the environment in the development of sustainable growth, a sequence of compressive and flexural strength tests was performed on materials prepared using sugar cane bagasse ash (SA) reinforced by glass fiber (GF) in combination with blast furnace slag (BF) and cement (CEM). The effects of the mix ratios of glass fiber to bagasse ash (0.2%–1.2%), blast furnace slag to the weight of bagasse ash (10%), cement binding to bagasse ash (10%–20%), and water to sugar cane bagasse ash (55%) regarding the flexural strength, compressive strength, density, tangent modulus, stress–strain pattern, and load–deflection curve of the prepared materials were studied. According to the findings, compressive strength achieved a maximum strength of 1055.5 kPa and ranged from 120 to 1055.5 kPa, and the flexural strength achieved a maximum strength of 217 kPa and ranged from 80.1 to 217 kPa at different mix ratio percentages. The value of the initial tangent modulus for the cube specimens ranged between 96 and 636 MPa. For compression specimens with 20% cement, the density decreased from 1320.1 to 1265 kg/m^3, and the flexural strength decreased from 1318 to 1259.6 kg/m^3. With limitation in lower percentages of C/SA, the specimen cannot sustain its shape even after curing period. In comparing the previous research with the present experimental work, it was observed that the material proposed here is lightweight and can be utilised as a filler substance in weak compressible soils to improve their load-bearing capacity.
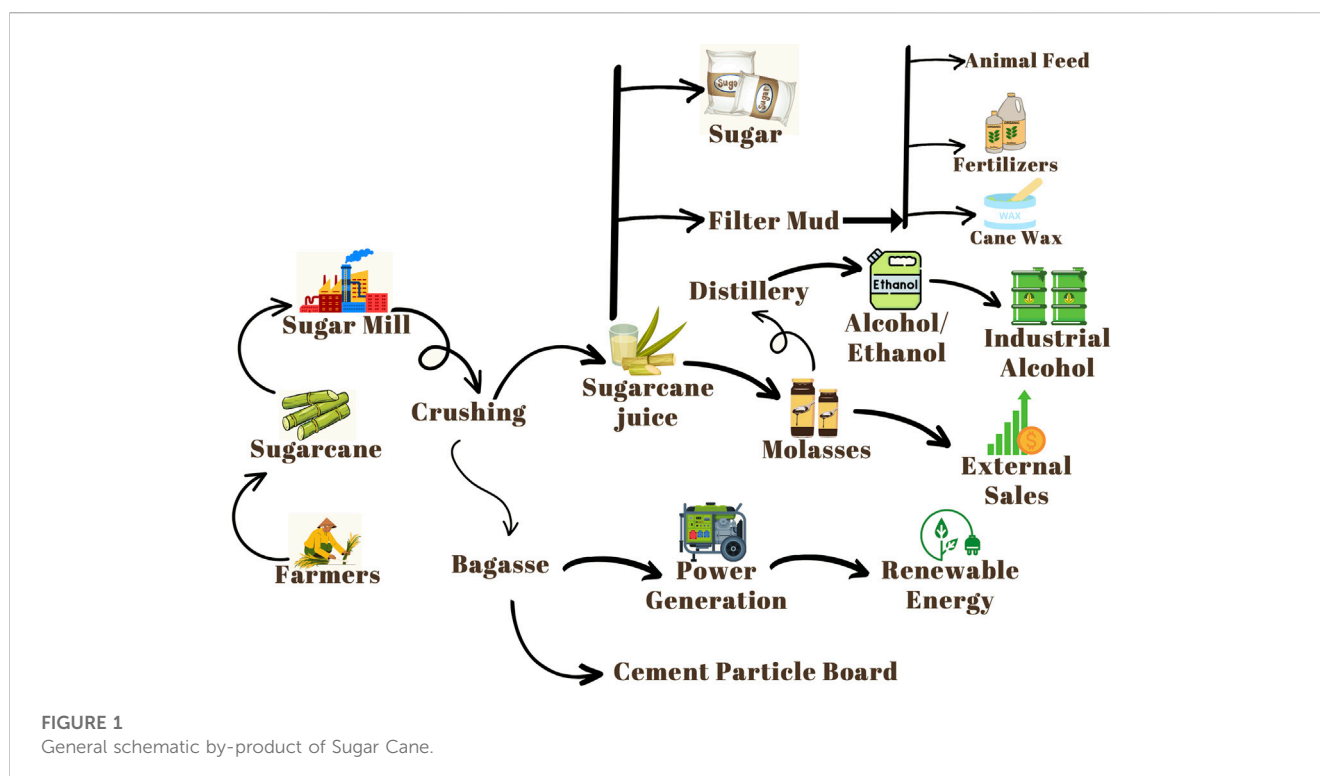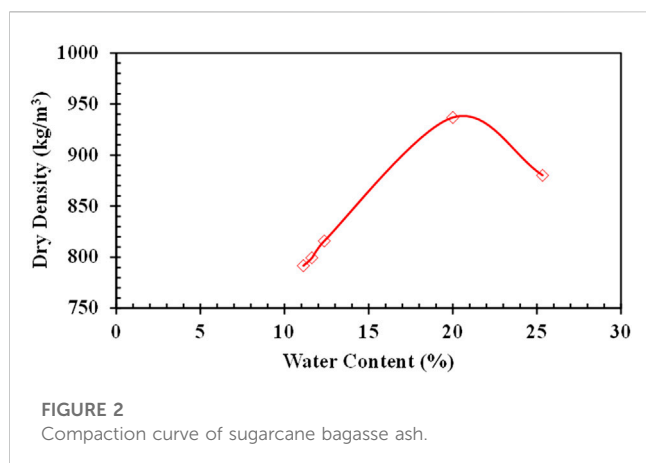
1 Introduction

The most common building material used globally is cement. Cement production is influenced by a nation's level of industrialization and modernization (Stafford et al., 2016). However, it generates a significant amount of carbon dioxide, almost 8% of the world's total, production, and for manufacturing purposes, it uses a lot of resources, including raw materials and energy (Anjos et al., 2020). As a result, academics are interested in long-term research on the cement industry to utilize various agricultures wastes and create cement-based sustainable materials (Talero et al., 2007; Rubenstein, 2012; Saleh et al., 2020) without compromising cement's durability, cost, or mechanical strength. It is possible to cut carbon dioxide emissions by up to 40%–50% (Cordeiro and Kurtis, 2017; Martirena and Monzó, 2018). Various common supplemental cementitious materials, such as blast furnace slag, fly ash, metakaolin, and natural pozzolans, have been used to lower the clinker-to-cement ratio (Bahurudeen et al., 2015; Cordeiro et al., 2018; Rajasekar et al., 2018). Recent research has looked at pozzolanic geomaterials, such as industrial and agricultural wastes (Cordeiro et al., 2011; Cordeiro et al., 2016; Andreão et al., 2019).

Cementitious compounds can be improved by using blast furnace slag and pozzolanic materials to combine their distinct physical and chemical properties (Khan et al., 2021). A secondary surface for hydrate precipitation and nucleation is provided by blast furnace slag (Bentz et al., 2017); however, the dilution effect (Rodríguez de Sensale and Rodríguez Viacava, 2018) can reduce the mechanical strength of this material, making it operate like a quasi-inert material at a high concentration (Bahurudeen and Santhanam, 2015). For the cement industry, the mixture of blast furnace slag and pozzolan is a desirable alternative. Since pozzolan can improve mechanical performance at advanced ages (Cordeiro et al., 2018).

Bagasse is the fibrous byproduct that remains after the sugarcane juice has been extracted (Deepika et al., 2017). Sugarcane businesses produce sugarcane bagasse ash (SA) as a byproduct of the auto-combustion procedure in cogeneration boilers (Rao et al., 2021) as shown in Figure 1. Bagasse was first primarily utilized in the manufacture of paper (Kuruba et al., 2020). Due to its sufficient calorific content, bagasse is used as a fuel feedstock in the cogeneration boilers of the sugar industry to produce electricity (Bartošek, 2014). Nearly all of the sugar facilities in India and other nations that produce sugar have quickly built cogeneration systems due to the significant money generation connected to this process (Bartošek, 2014). Bagasse is a suitable feedstock for cogeneration boilers; however, disposing of the leftover ash causes serious environmental issues (Rodrigues, 2011). The discharge of bagasse ash causes serious contamination to nearby water bodies and land because of the light unburned fibre debris that is present and excessive black color (Andreão et al., 2020). A significant proportion of this agro-waste is being dumped in nearby regions more and more, which has a negative impact on the ecosystem and lacks disposal land (Bahurudeen et al., 2015). The main components of raw SA are coarse/fine fibrous unburned particles and fine burnt particles (Bahurudeen and Santhanam, 2015). This ash is irregularly shaped and primarily amorphous silica-rich after suitable processing to remove unburned components, with lesser amounts of aluminum, alkali, iron, and magnesium (Setayesh Gar et al., 2017). The analysis of the literature reveals that processed SA may be viewed as a supplementary cementitious material (SCM), and it is generally acknowledged that the fineness of SA enhances its pozzolanic properties (Le et al., 2018; Zareei et al., 2018).

FIGURE 1
General schematic by-product of Sugar Cane.

FIGURE 2
Compaction curve of sugarcane bagasse ash.

Alkali-activated materials (AAMs) have seen an increase in use as a Portland cement substitute in recent decades due to their advantages as a greener method. In-depth analyses of AAMs' effectiveness when it comes to mechanical strength, microstructure and durability have revealed results on par with or even better than those of ordinary Portland cement (OPC) (van Deventer et al., 2014). Alkaline activators and decent starting materials are used to create inorganic binders at the proper temperature. As activated solutions in the binder material, potassium/sodium hydroxides and/or sodium/potassium silicates are often favored (Duxson et al., 2006). Slag, fly ash, and coal bottom ash are examples of industrial by-products that include aluminosilicate and are widely utilized as precursors (Mugahed et al., 2022). Alkali hydroxide and/or alkali silicate solutions react chemically with solid aluminosilicate particles in the mixtures to generate binding gels. Two reaction products that differ from Portland cement in terms of their level of hydration are produced in AAMs, depending on the chemical components present in the starting materials. The reaction result may be N-A-S-H gels for low-calcium precursors such as fly ash (or similar ashes), and C-A-S-H gels for high-calcium precursors such as GBFS (Rakhimova and Rakhimov, 2014). Two important factors that significantly affect the compressive strength of a binder are the SiO_2/Na_2O molar ratio (also known as the silicate modulus, or Ms) and the Na_2O molar concentration of the liquid. Based on the results of the experiments (Zhang et al., 2022a), the fresh mixtures can be classified as Bingham fluids, and the addition of the right amount of nano-SiO_2 (NS) and water-reducing admixture can improve the mixtures' rheology and flowability. However, adding too much PVA fiber and NS has an negative effect on the mixtures' workability. According to reports, increasing the sodium oxide dose or the silicate modulus of the activator has led to better strength by improving raw material dissolution. Alkali-activated materials can be heat cured to increase their early strength and possibly reduce their shrinkage (Thomas et al., 2017). However, specimens with restricted fractures that were healed in water at room temperature showed a decrease of mechanical strength (Kirschner and Harmuth, 2004).

Furthermore, tiny particulates that might cause serious air pollution are present in the areas of sugar facilities. The majority of sugar factories are situated in villages, and SA (remaining sugarcane bagasse ash) from the factories is immediately deposited onto the arable land in these communities (Deepika et al., 2017). It is essential to discover another application for bagasse ash other than disposal. Bagasse ash has been suggested as a suitable ingredient for blended cement manufacture in earlier studies (Ganesan et al., 2007). Ashes with reactive silica are produced by the cogeneration boiler's carefully regulated combustion process (Cetin et al., 2004). According to research using differential scanning calorimetry (DSC), enhanced production of calcium-silicate-hydrate (C-S-H) gel occurred when SA is present (Singh et al., 2000). However, the use of unprocessed SBS as a cementitious material is hindered by the greater loss on ignition (LOI) value of around 20 percent and the lower specific gravity of about 1.9. Therefore, the majority of researchers agree that treating SA is preferred over increasing its pozzolanicity (Cordeiro et al., 2009).

In comparing SBS-blended concrete to regular Portland cement (OPC) concrete, it has demonstrated increased strength, decreased permeability, and low heat of hydration (Ganesan et al., 2007; Bahurudeen et al., 2015). Due to a lack of proper knowledge of the material and scalable methodologies, the manufacturing of building materials using bagasse ash has been prohibited (Mangi et al., 2020). Most past research studies have concentrated on using bagasse ash in concrete, and on the basis of thorough experimental plans, acceptable processing technology for blended cement manufacture has been recommended (Frías et al., 2011). Numerous studies have been conducted to determine the potential utility of SA in the major nations that produce sugar, including Brazil, India, and Thailand (Chusilp et al., 2009; Wen et al., 2022). The appropriate performance assessment and processing of bagasse ash for different building materials, such as alkali-activated concrete, paver blocks, and unburned bricks, were not sufficiently studied in previous research investigations. To gain a scientific understanding and make the most use of SA, performance evaluation in various applications is also required in addition to material characterization.

Sustainable concrete is popular as a building material because of its higher flexural and compressive strengths and lower cost. Due to its limited elasticity and resistance to fracture, it is naturally vulnerable. Metal or non-metal fibers have been put into concrete to address these issues. Fiber-reinforced concrete cracks cannot form or spread if the fibers are distributed randomly. Because of this, concrete is now far more robust and malleable (Wen et al., 2022). Structures prone to earthquakes, tunnel linings, and explosions have all made use of this material (Khawaja et al., 2021). Fibers are made of polyvinyl alcohol (PVA), polypropylene (PP), hooked-end steel fiber (HKs), crimped steel fiber (CRs), and others (Najm et al., 2022a). Metallic fibers (HKs and CRs) are the bestbecause of their strong compressive, tensile, twisting, and bridging strengths. PVA-reinforced concrete offers higher pull-out loads and flexural strength than concrete reinforced with metallic fibers. The inclusion of fiber also highly contributes to enhancing the fracture (Xu et al., 2018) and fire resistance (Yashwanth et al., 2017) and seismic load (Channa et al., 2022). According to the findings (Zhang et al., 2022b), the geopolymer mortar had considerable mass loss when exposed to temperatures between 25°C and 250°C, however, only a little amount of mass loss was observed between 250°C and 700°C and none at all between 700°C and 800°C. Under wet-thermal and chloride salt conditions, fiber-reinforced cementitious composites' fracture characteristics were enhanced by polyvinyl alcohol (PVA) and nano-SiO_2 (NS). PVA fibre and NS enhanced the porosity, microcracks, and interfacial transition zone of fiber-reinforced cementitious composites at the microscopic level. The fracture characteristics considerably improved at 1.2% and 0.5%, respectively, of PVA fibre and NS contents (Zhang et al., 2022c) When the structure of PVA and fiber-reinforced
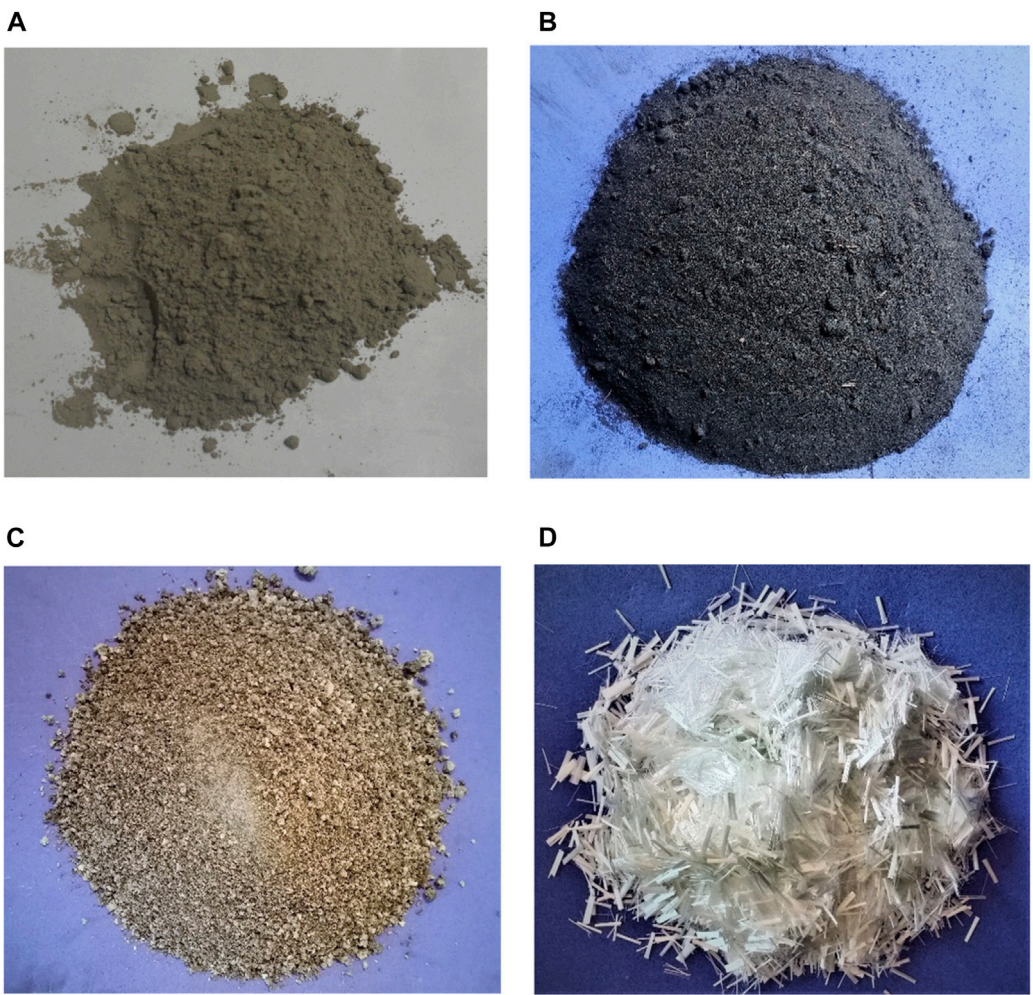
FIGURE 3
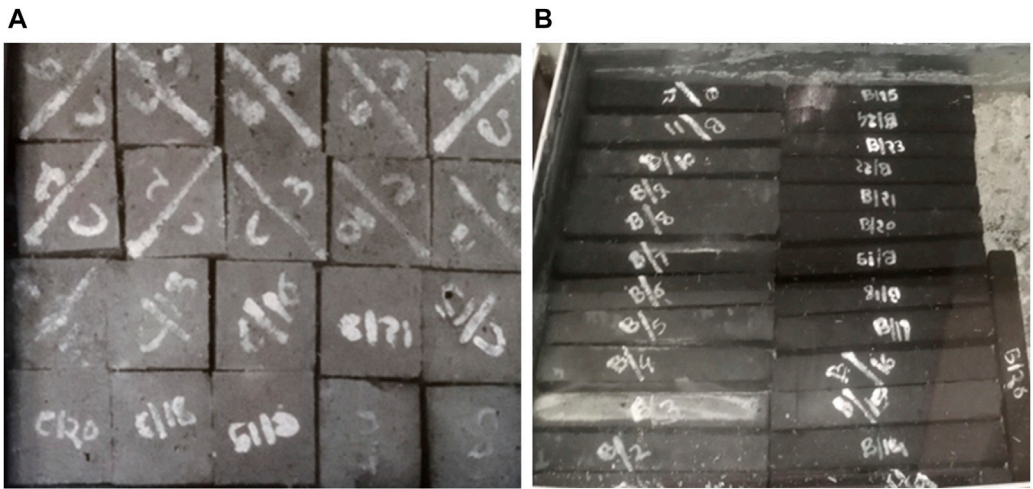Materials used **(A)** OPC (53 Grade); **(B)** SA; **(C)** BFS; **(D)** GF.

FIGURE 4
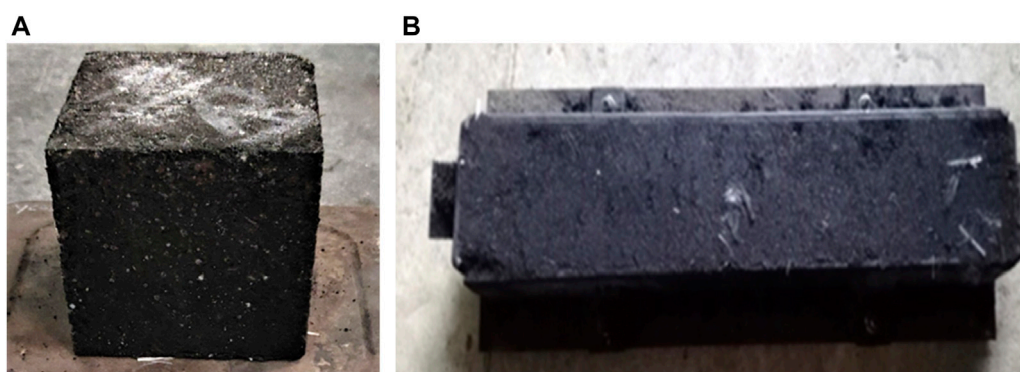Curing of **(A)** cube specimen; **(B)** beam specimen.

FIGURE 5
(A) Cube specimen (100 mm × 100 mm × 100 mm). **(B)** Beam specimen (400 mm × 50 mm × 50 mm).

TABLE 1 Mix ratios and quantity of materials used for preparing cube and beam specimens.

No.	Mix ratio (%)	Weight of SA WSA (gm)	Weight of BF slag W BF slag (gm)	Weight of glass fiber W GF (gm) 10% cement	Weight of cement 10% Wc (gm)	Weight of cement 15% Wc (gm)	Weight of cement 20% Wc (gm)	Water, V_w (mL) (55%)	Curing duration in days
1	0.2	859.05	85.90	1.72	85.90	128.5	171.81	429.52	7, 14, 28
2	0.4	857.0	85.70	3.43	85.70	128.5	171.4	428.50	7, 14, 28
3	0.6	854.94	85.49	5.15	85.49	128.24	170.98	427.47	7, 14, 28
4	0.8	852.88	85.29	6.86	85.29	127.93	170.57	426.44	7, 14, 28
5	1.0	850.91	85.09	8.10	85.09	127.63	170.18	425.45	7, 14, 28
6	1.2	848.34	84.83	10.11	84.83	127.20	169.66	424.16	7, 14, 28

cementitious composite samples heated to 600°C and 800°C became loose and more microcracks formed, it was determined that the macro-mechanical properties had reduced (Zhang et al., 2022d).

According to the literature review, there have been various initiatives to use waste materials for sustainable development, such as coal ash, bottom ash, and stone dust in cement (Ram Rathan Lal and Badwaik, 2016; Ram Rathan Lal and Nawkhare, 2016). Very few works carried out with sugar cane bagasse ash in this direction. Consequently, the main goal of this work was to evaluate the effects of various quantities of geomaterial composites with glass fibres on the mechanical properties and classify them into geomaterials per the design standards for usability. Therefore, a detailed investigation into the compressive, flexural, density, tangent modulus, stress–strain pattern, and load–deflection curve of newly prepared materials was conducted. This in-depth analysis of sugar cane bagasse ash and blast furnace slag was done with the goal of finding the ideal ratio in terms of mechanical qualities and cost, reducing environmental stress, and pursuing sustainable growth. In the numerous studies in the literature, experimental works have been used to predict the behavior of sugar cane bagasse ash (Channa et al., 2022). However, there has been no experimental work to evaluate the effect of using sugar cane bagasse ash (SA) and blast furnace slag (BF) reinforced by glass fiber (GF) on the mechanical properties of mortar, which is crucial to calibrate under different loadings (compressive and flexural) and can

be used as an indication for future studies based on sugar cane bagasse ash. In addition, several scholars used different variants of concrete in their numerical and experimental research works performed under quasi-static, static, and extreme loading conditions (Khan and El Rimawi, Forthcoming; Khan and Ali, 2016; Khan et al., 2017a; Khan et al., 2017b; Khan et al., 2017c; Khan et al., 2018; Khan and Ali, 2019; Ahmed et al., 2021; Anas et al., 2021; Anas et al., 2022a; Ahmed et al., 2022; Anas et al., 2022b; Khan et al., 2022; Mansouri et al., 2022; Qaidi et al., 2022; Anas et al., 2023; Iman et al., 2023).

2 Materials and methods

The performance of sugar cane bagasse ash reinforced with glass fiber (GF) in comparison to blast furnace slag (BF) and cement is examined in the current study. The compressive and flexural strength, density, tangent modulus, stress–strain pattern, and load–deflection curve of concrete are evaluated.

2.1 Materials

The research materials used consist of ordinary Portland Cement (OPC) 53 grade, sugar cane bagasse ash (SA), blast

TABLE 2 Material testing mechanisms.

Tests	Equipment	Sample	Curing condition	Formula
Slump	Abram cone	Fresh concrete	Quickly after mixing	-
Compressive Strength (ASTM C39)	(2000 KN) Compressive testing machine at axial	Hardened concrete	28 Days	$CS = \frac{P}{A}$
Flexural Strength (ASTM C78)	Two-point load test	Hardened concrete	28 Days	$FS = \frac{PL}{bd^2}$

CS, compressive strength, A = cross-sectional area, FS, flexural strength, P = maximum load from load deflection curve, L = span length, b = width of specimen, d = depth of specimen.
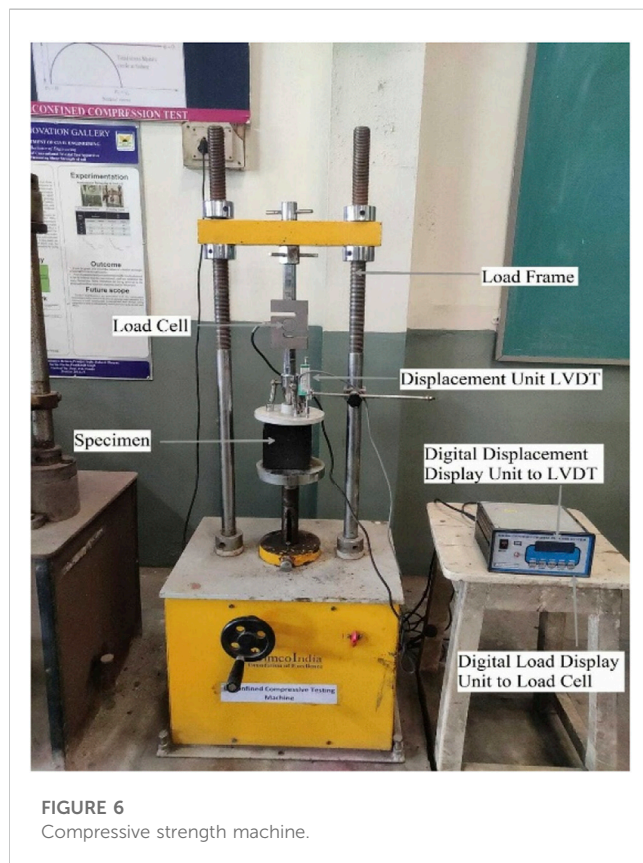

FIGURE 6
Compressive strength machine.

furnace slag (BFS), and glass fiber (GF). Bagasse ash was collected in a dry state from the Khambata Sugar Cane Factory, Bhandara (District), India. Blast furnace slag was collected in dry conditions from Varthi Steel Industries, Bhandara (District), India, and glass fiber was obtained from Jaipurkar Construction Pvt. Ltd., Nagpur (District), India.

The sugarcane bagasse ash used in this investigation had a chemical make-up of 45% cellulose, 27% hemicellulose, 20% lignin, and 8% ash, obtained from the Soil Science and Chemistry Department, Nagpur University, India. In the laboratory, the sugar cane bagasse ash's material characteristics were calculated. According to the Unified Soil Classification System (USCS), the sugar cane bagasse ash is categorized as analogous to fine sand and silt. Sugar cane bagasse ash may also be classified as non-plastic material that affects the granulometric behavior of clay particles (ASTM C1585-13, 2013). In accordance with the ASTM D 698 (ASTM D1557, 2021), the standard proctor experiment was used to determine the compaction characteristics of the material. The dry density of the sugar cane bagasse ash was 940 kg/m³, and the moisture content was 20%. The compaction curve of the SA is plotted in Figure 2.

The blast furnace slag was determined to have a fineness modulus of 2.89, as per IS 383–1970 (BIS:383, 1970), and classified into a medium sand category. Glass fiber was used in the experiment for reinforcing the prepared material. Alkali-resistant (AR) glass fiber (dimensions: length of 12 mm and diameter of 19 μm) was used in the present work for an X-ray

TABLE 3 Density of beam materials after 7, 14, and 28 days for 10%, 15%, and 20% cement to SA materials.

| Mix ratio	7 Days			14 Days			28 Days		
	Cement %			Cement %			Cement %		
	10%	15%	20%	10%	15%	20%	10%	15%	20%
0.2	1187.2	1225.4	1261.5	1237.2	1269.0	1291.0	1265.8	1292.1	1318.0
0.4	1172.1	1209	1241.9	1226.6	1255.0	1280.0	1257.1	1280.0	1305.0
0.6	1167.0	1198.3	1228.2	1217.8	1243.6	1268.9	1243.0	1268.2	1292.7
0.8	1153.1	1187	1217.9	1205.0	1231.8	1255.7	1231.3	1255.9	1280.0
1.0	1143.3	1173.9	1205.0	1192.3	1217.8	1242.0	1219.8	1243.0	1268.9
1.2	1136.9	1165.7	1197.4	1185	1205.0	1231.1	1207	1231.7	1259.6
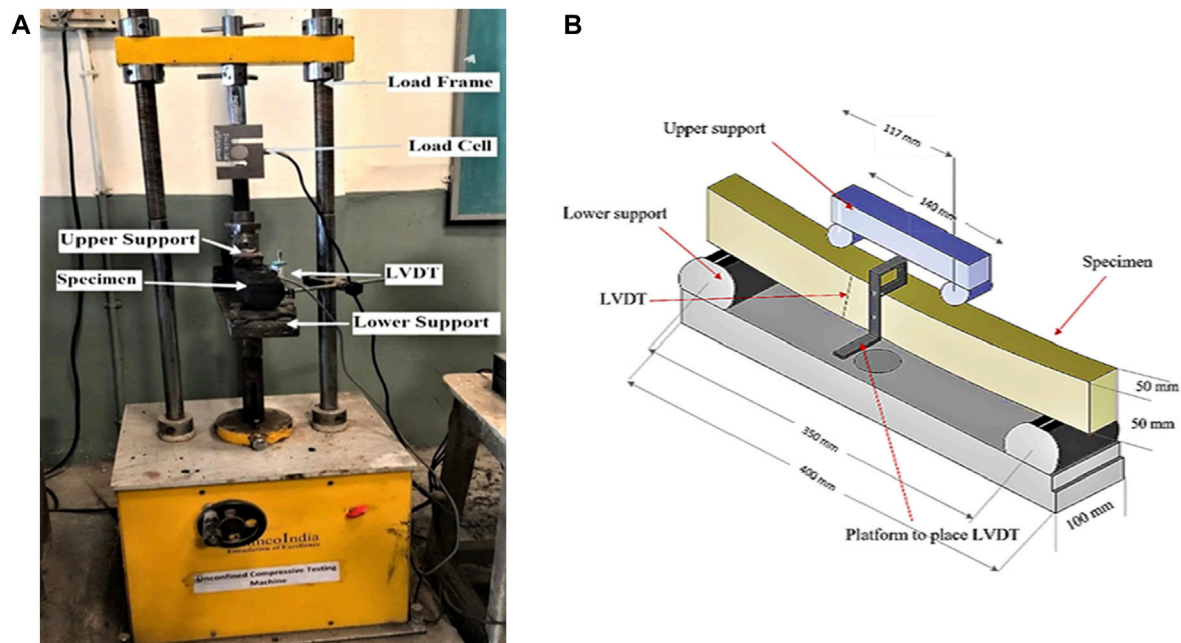
FIGURE 7
Dimensions of the fabricated tool for flexural test. **(A)** Real Dimensions; **(B)**Sketch Dimension.

fluorescence (XRF) trial and was executed using an X-ray fluorescence spectrometer at the Indian Bureau of Mines, Nagpur. As per ASTM C618 (ASTM C618-17a, 2017), sugar cane bagasse ash is classified as a Class F type of material, and blast furnace slag is classified as a Class C type of material. Figure 3 shows the materials used in the research work: OPC (53 grade), sugar cane bagasse ash, blast furnace slag, and glass fiber.

2.2 Preparation of specimen

The quantities of various constituents of the mix were calculated based on a method used by previous researchers (Nikhade and Lal, 2021). The weight ratio of glass fibre to sugarcane bagasse ash is known as the mix ratio %. In the current study, the dry weight of SA is calculated using formula $WSA = \gamma_{dmax} \times VSA$, where γ_{dmax} maximum dry unit weight of sugar cane bagasse ash and VSA is volume of SA, $VSA = V-VBF-VGF$, V the total volume to specimen (1000 cm^3), and VBF is taken 70 cm^3 and volume of VGF glass fiber is taken 2.3 cm^3 to achieve the mix ratio 0.2%.The ratios were 0.2, 0.4, 0.6, 0.8, and 1.0% for the cube specimens and 0.2, 0.4, 0.6, 0.8, 1.0, and 1.2% for the beam specimens. To achieve a mix ratio of 0.2, the volume of the blast furnace was 70 cm^3 and that of the glass fiber was 2.3 cc. After mixing the materials, i.e., the SA, BF slag, GF, and cement, the materials were formed into a homogeneous slurry with an optimum moisture content of 20%, and the water to sugar cane bagasse ash ratio was maintained at 55% for the present work.

2.3 Curing method adopted

Curing is a process used to control the hydration that occurs in concrete due to the presence of Portland cement. The majority of the time, it entails controlling the loss of moisture and, in some instances, temperature (ASTM Standards C-293, 2002). Examples of curing techniques include using shade during concrete work, covering concrete surfaces with hessian or gunny bags, water spraying, the ponding process, immersion in water, membrane curing, and steam curing (Maroliya, 2012). Immersion curing was chosen for this project (Figure 4) at room temperature (25°C–30°C), where the samples were submerged entirely in water. This is a suitable approach that satisfies all curing requirements, including hydration promotion, shrinkage elimination, and heat absorption during hydration.

2.4 Mix proportions

In the container, the required amounts of SA, BF slag, and cement were obtained and mixed thoroughly with the required amount of water. After that, glass fiber was added to the mix to prevent it from clustering. The casting of the specimens was performed immediately after the mixing was completed. A total of 135 cube specimens (100 mm × 100 mm × 100 mm) and 162 beam specimens (400 mm × 50 mm × 50 mm) were prepared. After 24 h, the specimens were taken out from the molds, and air dried again for a period of 24 h, as shown in Figure 5A, B. The mix ratios and material amounts needed to make the cube and beam specimens are shown in Table 1.
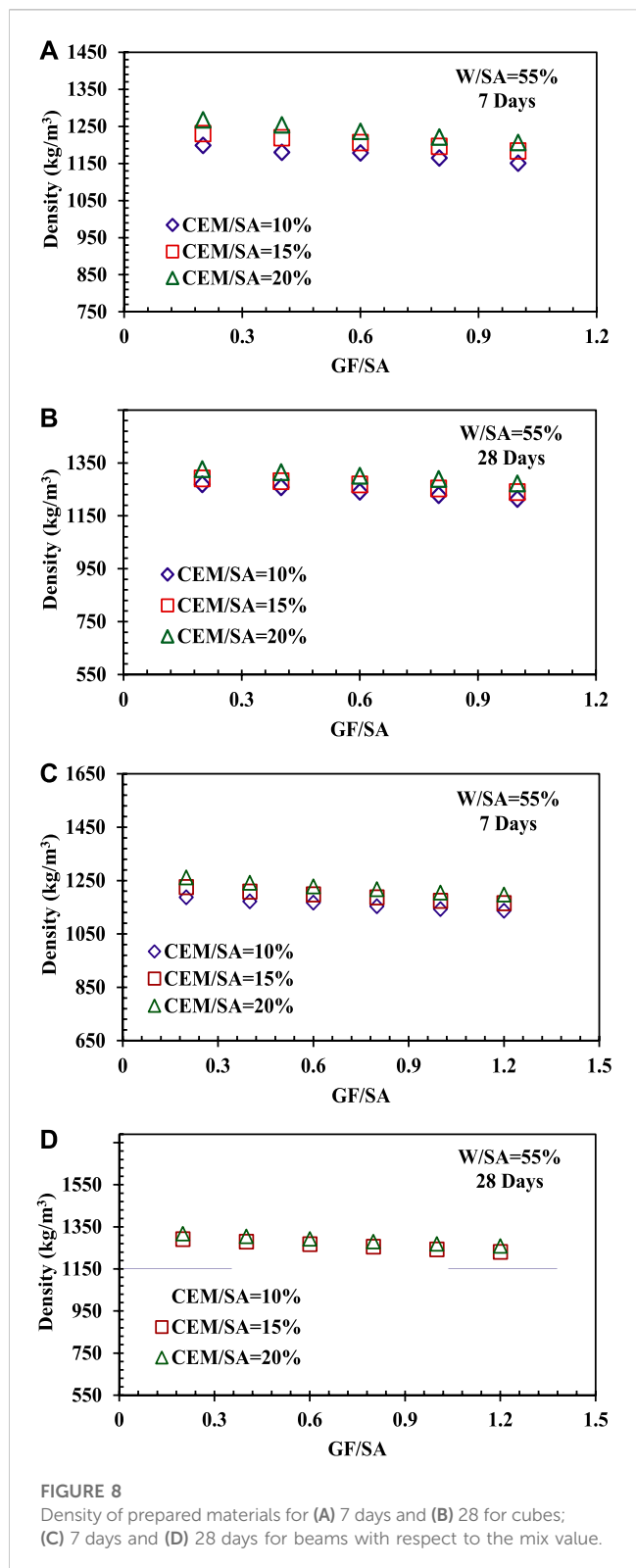
2.5 Tests on mechanical properties

2.5.1 Compressive strength test

The compressive strength of a geomaterial is defined as its ability to withstand failure when subjected to compressive pressures. The
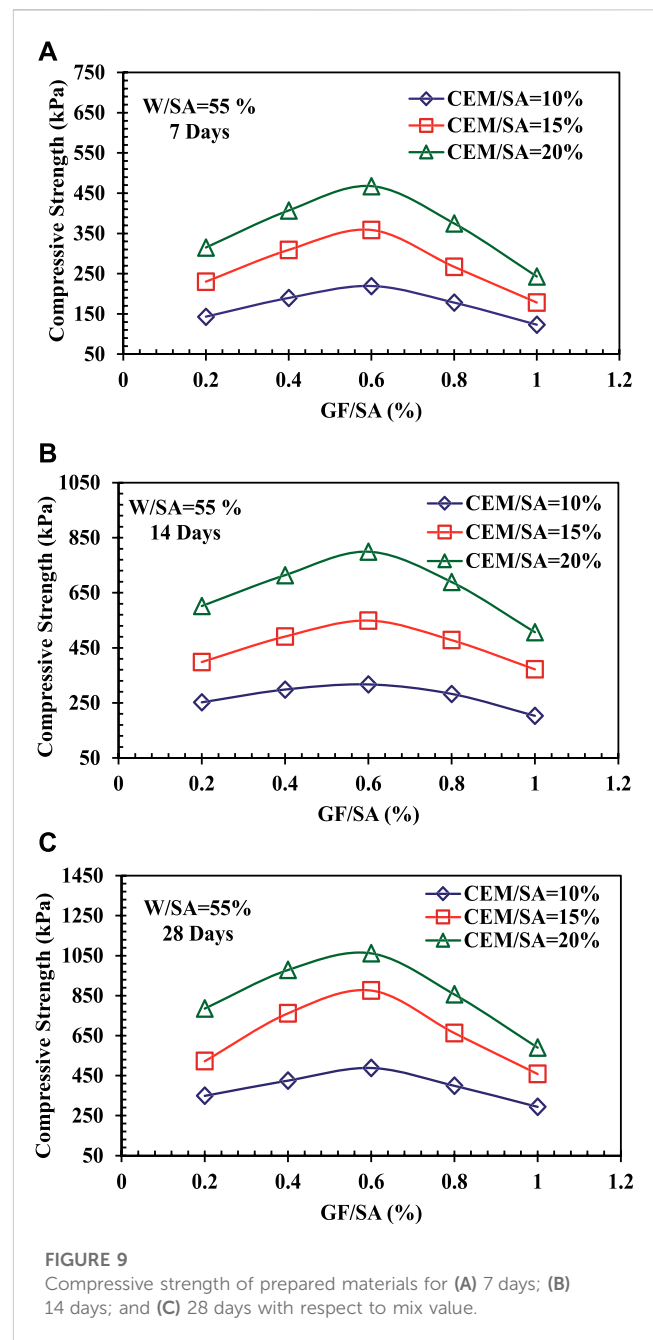
load applied at the point of failure is divided by the cross-sectional area of the sample to determine the hardened concrete's compressive strength (Table 2). The samples were tested using a compressive strength testing device in accordance with ASTM C39 after 28 days of curing (ASTM C39, 2016) (Figure 6).

2.5.2 Flexural strength test

As per ASTM C78, this flexural strength test was performed (ASTM C78, 2016). Figure 7A, B shows the experimental setup of a 2-point bending problem fabricated for flexural testing; the base support was 100 mm wide and 400 mm long, and it was attached to a metal block. Three hundred 50 mm was the effective length between the metal blocks arranged in a grid.
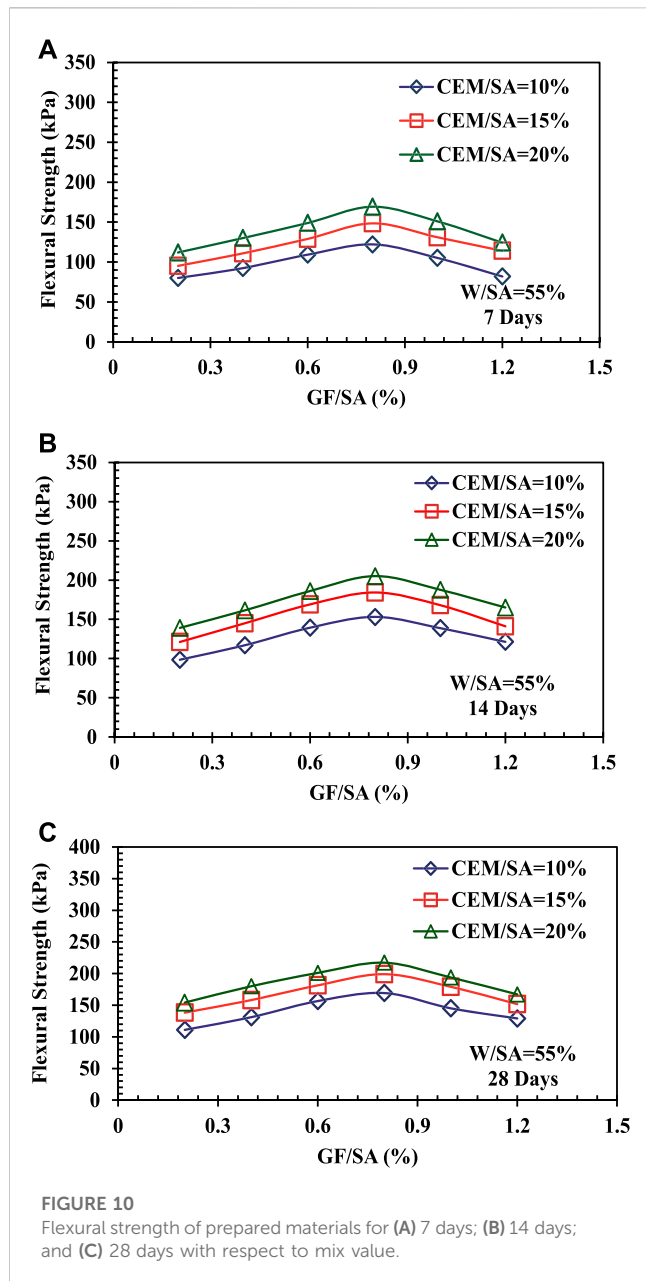
FIGURE 10
Flexural strength of prepared materials for **(A)** 7 days; **(B)** 14 days; and **(C)** 28 days with respect to mix value.

FIGURE 11
Stress−strain curve of SA and BF slag reinforced with glass fiber under compressive stress for mix ratios of 0.4% for **(A)** 7, **(B)** 14, and **(C)** 28 days.

2.6 Tests on microstructural analysis

2.6.1 Scanning electron microscopy

Scanning electron microscopy (SEM) uses image analysis to measure and evaluate minute details by repeatedly scanning the surface of a material with a concentrated electron beam. The signals generated when electrons collide with atoms in a sample reveal clues about the surface's topography and composition. Using an SEM, one can look into component failures, find particles, and examine substance–substrate interactions (ASTM C78, 2016). A JEOL JSM6380 LV scanning electron microscope with an accelerating voltage of 30.0 kV was used for this work. The materials were gold-plated in order to conduct energy dispersive spectroscopy (EDS).
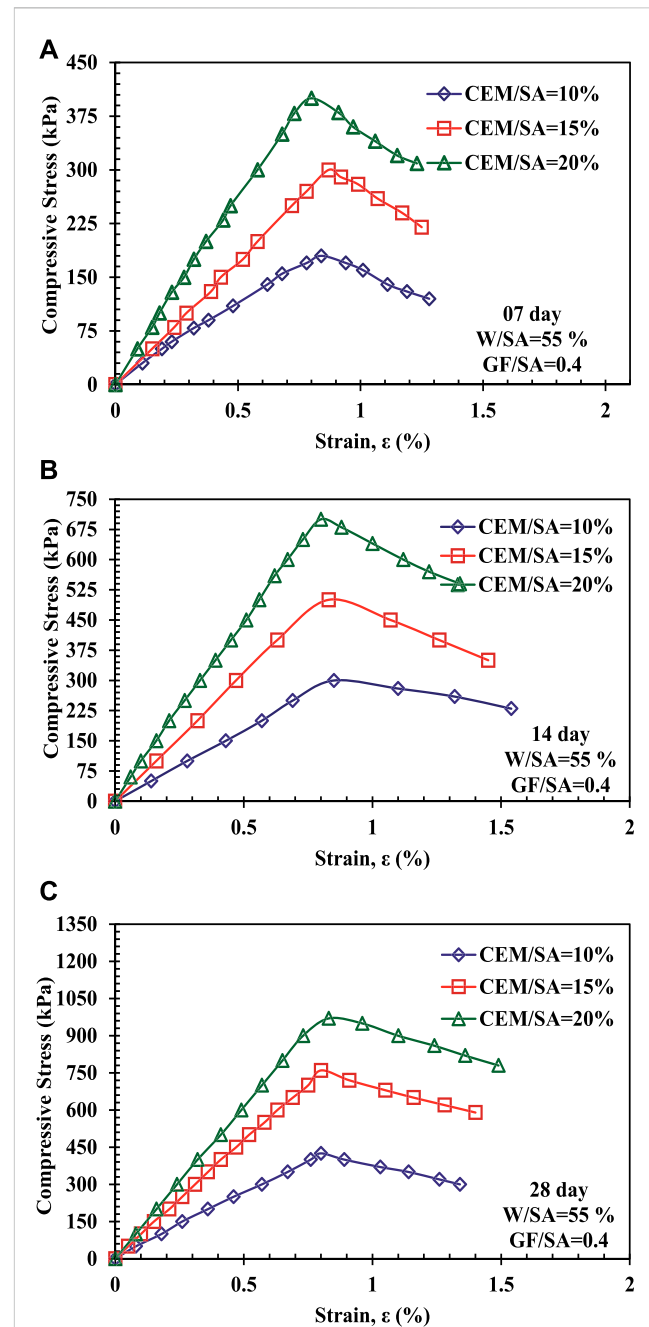
2.6.2 X-ray diffraction

In order to learn about and identify the atomic and crystallographic nature of a material, X-ray diffraction (XRD) is performed as a microstructural analysis test. Exiting X-rays are irradiated onto a sample, and their intensities and scattering angles are measured. The material's composition is ascertained by examining the position, angle, and intensities of the scattered intensity peaks, which are presented as a function of the scattering angle. In geological research, XRD is frequently
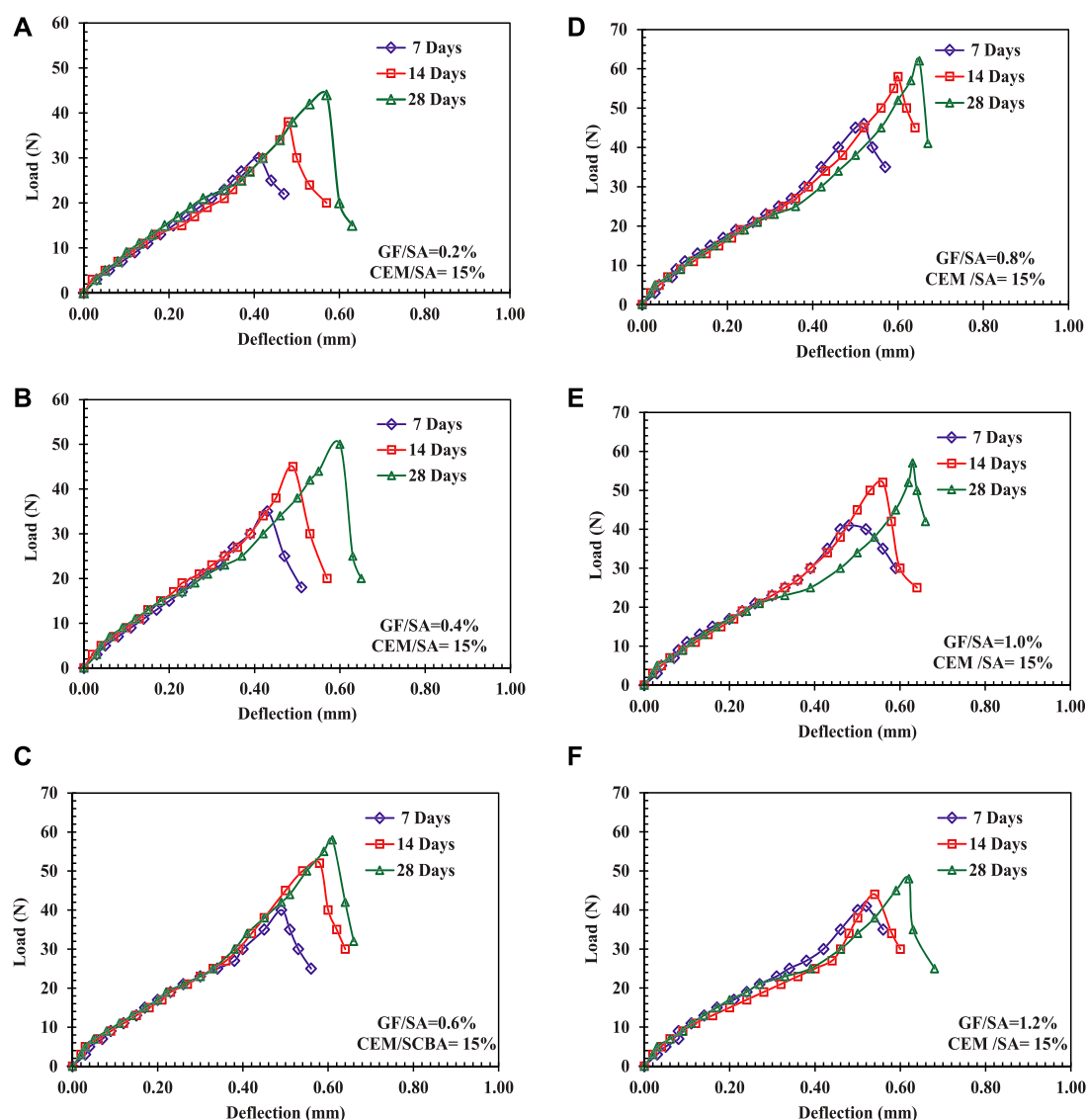
FIGURE 12
Load vs. deflection curve of prepared materials for all curing periods at GF/SA mix ratios of **(A)** 0.2%; **(B)** 0.4%; **(C)** 0.6%; **(D)** 0.8%; **(E)** 1.0%; **(F)** 1.2%, and CEM/SA ratio of 15%.
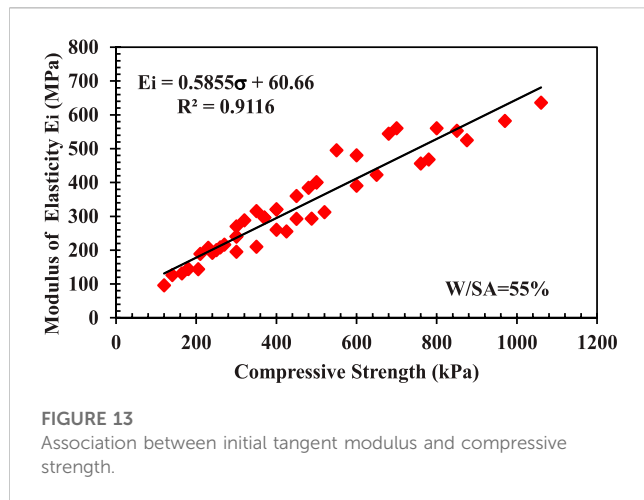
combined with other microstructural techniques, such as electron microprobe microscopy, scanning electron microscopy and optical light microscopy particularly when the sample to be investigated is a combination. XRD data can be used to identify each mineral present in the sample and their relative abundance (Maroliya, 2012).

3 Result and discussion

The failure pattern, stress and strain pattern, density, initial tangent modulus, compressive strength, flexural strength, and load–deflection curve pattern of the cube and beam specimens were evaluated, and the results obtained are discussed.

3.1 Density of specimen

The cube and beam specimens were weighed after air drying, and the densities were calculated before the compressive strength tests. It was observed that for all mix ratio percentages, the density of the materials decreased with increases in the mix ratio percentages for all curing periods, as shown in Figure 8. For each mixing ratio, the density of the compression cube specimens increased with the percentage of the cement to sugar cane bagasse ash ratio increasing from 0% to 20%. The density of the material used for the cube specimens varied from 1140.0 kg/m³ to 1320.1 kg/m³ and for the beams, it varied from 1136.9 to 1318 kg/m³. The density of the materials was higher at a 0.2% mix ratio and lower at a 1.2% mix ratio. At a

FIGURE 13
Association between initial tangent modulus and compressive strength.

3.2 Compressive strength

The compressive strengths of the GF-reinforced SA and BF slag-based specimens were remarkably influenced by the curing time, mix rate, and ratios of the cement to SA. The peak magnitude achieved in the compressive stress curve was taken as the compressive strength. It was found that the addition of GF to SA improved the compressive strength until an optimum percentage of fiber mix. For each of the mix ratios and curing periods, the specimens with a 0.6% mix ratio had the maximum compressive strength. Similar behavior was observed for the blast furnace slag material prepared by Nikhade et al. (Mandal et al., 2018; Nikhade and Lal, 2023). The value of compressive strength ranged from 120 kPa to 1055.5 kPa. The compressive strength of the material after 7 days of curing was 140.0 kPa at a mix ratio of 0.2% and increased up to 219.3 kPa with a mix ratio of 0.6%. Further increases in the mix ratio caused the compressive strength to decrease. The percentage increase in the compressive strength after 7 days of curing was 36.16%. Figure 9 demonstrates the variation in the compressive strength of the materials after 7 days, 14 days, and 28 days with respect to the mix value. A non-linear pattern was observed between the compressive strength and the mix ratio percentage for the curing period of 7–28 days. The strength values obtained in the study are higher than those in the study by Nikhade et al. (Nikhade and Lal, 2021), i.e., 100–500 kPa, which fall under the category of lightweight filler materials and between those in the study by Mandal D. (Mandal et al., 2018), i.e., 159 kPa–2500 kPa.

10% cement-to-bagasse ash mix ratio, the density of the material used to prepare the cube specimens ranged from 1195.7 kg/m³ to 1140.0 kg/m³ and the percentage change at 7 days of curing was 4.65%. For the beam material, the density varied from 1187.2 kg/m³ to 1136.2 kg/m³, and the percentage change in density at 7 days of curing was 4.29%. Table 3 summarizes the density of the beam materials after 7, 14, and 28 days for 10%, 15%, and 20% ratios of cement-to-SA materials. The density of the materials obtained in the present study lies within the range of lightweight filler materials, i.e., between 700 kg/m³ and 1100 kg/m³, as indicated by Nikhade et al. (Nikhade and Lal, 2021). The density of the materials was higher than in the study by Horvath (Osei et al., 2020), of which it was in the range of 12–32 kg/m³.

3.3 Flexural strength

The flexural strength of the prepared materials was also significantly influenced by the curing period, mix ratio, and
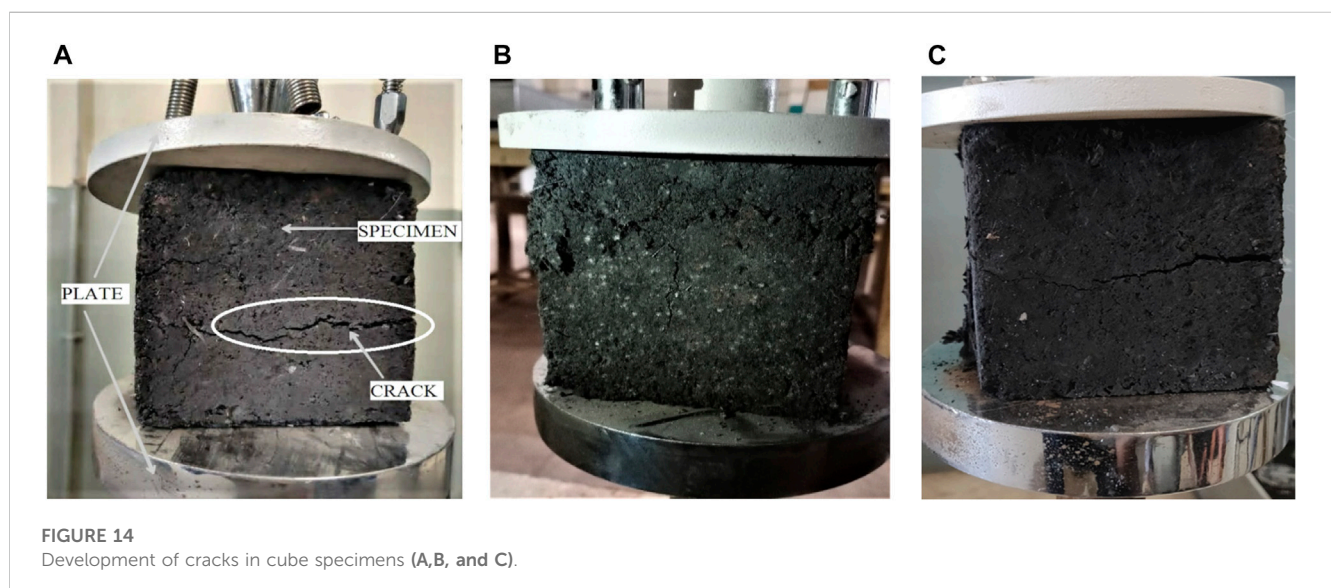

FIGURE 14
Development of cracks in cube specimens (A,B, and C).

FIGURE 15
Development of cracks in beam specimens **(A–D)**.

percentage of GF used for the preparation of beam specimens for flexural tests. The flexural strength was obtained at the maximum failure load from the load–deflection curve. In all the specimens, the fracture occurred within the middle third of the span. The flexural strength was calculated according to ASTM C1609. The lowest value of flexural strength was 80.1 kPa, obtained at 7 days for the 0.2% mix ratio. The highest value of flexural strength was 217.2 kPa, obtained at 28 days for the mix ratio of 0.8%. Figure 10 shows the variation in the flexural strength with respect to the mix ratio. A non-linear relationship was found between the mix ratio and the flexural strength for all mix ratios and curing periods. However, the flexural strength increased with an increase in the percentage of glass fiber up to a certain extent. The highest or optimum value of the mix ratio was found to be 0.8%, at which the flexural strength was the maximum in all cases (Najm et al., 2022b; Najm and Ahmad, 2022; Nanayakkara et al., 2022).

3.4 Stress–strain curve

The significance of the stress–strain diagram is that the elastic modulus is calculated at a point on the ascending branch of the diagram. Figure 11 shows the stress–strain diagram for a mix ratio of 0.2% for 7, 14, and 28 days at the water-to-SA ratio of 55%

plotted under a sustained strain rate of 1.00 mm/min in proportion to the BF slag reinforced with glass fiber at different mix ratios. For all specimens, a non-linear connection between stress and strain was found. It was observed that the CEM/SA at 20% had a higher stiffness compared to that at 10% and 15%. The material behavior of the geomaterial changed from ductile to brittle in nature for all the curing periods and mix ratios tested.

3.5 Load and deflection curve

The load–deflection curve was plotted for the cement-to-SA ratios of 10%, 15%, and 20%. The graph grows linearly up to the cracking load and then falls rapidly. The maximum load was found to increase with the curing periods for all specimens. The mid-span deflection at failure varied from 0.12 to 0.84 mm. Figure 12 shows the load–deflection relationships for GF/SA with 0.2%–1.2% mix ratios and the cement-to-SA ratio fixed at 15%. It was observed that the stiffness increased with the curing period and mix ratio, and higher stiffness at a 0.8% mix ratio was observed. The stiffness of the geomaterial for the cement-to-SA ratio of 20% was significantly higher than the other two combinations of cement percentages, i.e., 10% and 15%.
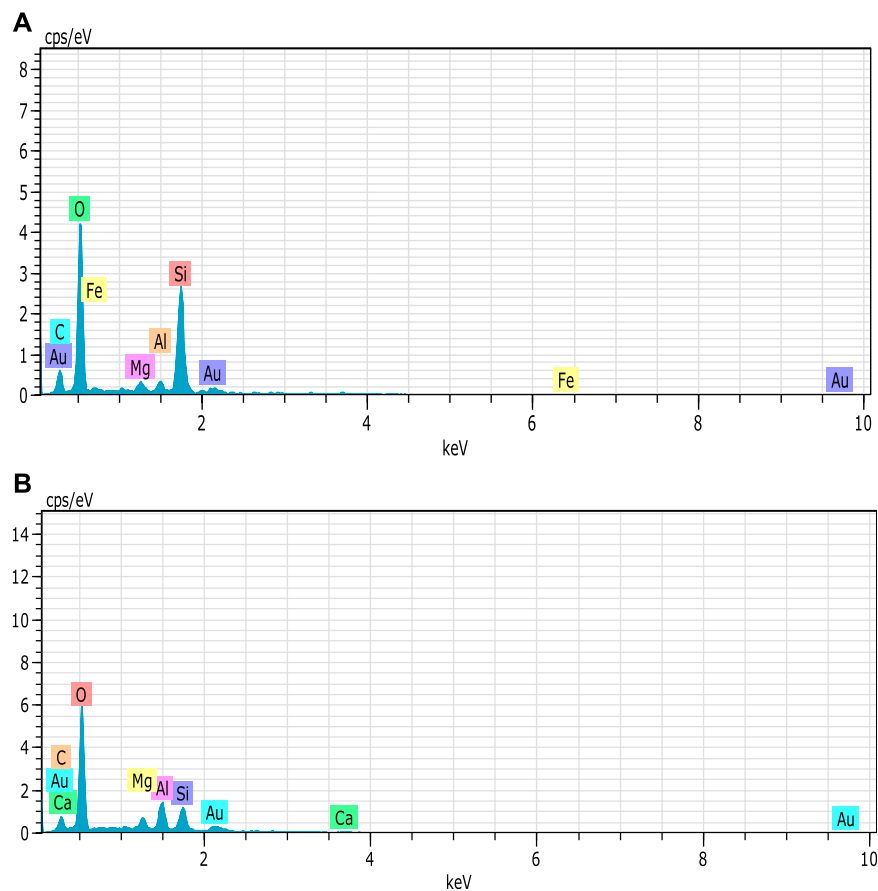
FIGURE 16
EDS patterns of **(A)** sugar cane bagasse ash; **(B)** blast furnace slag.

3.6 Initial tangent modulus

The initial tangent modulus (E_i) is a significant parameter that represents the rigidity of the prepared material. It was calculated as the incline of the tangent line to the rise of the stress–strain pattern. The (E_i), magnitude ranged from 96 to 636 MPa. The values obtained lie in the range of the lightweight filler category of materials, i.e., 79–555 MPa, as prepared by Liu et al. (Liu et al., 2006). The values are greater than those of the geofoam blocks prepared by Horvath (Horvath, 1998), i.e., in the range of 2.2–11.4 MPa. Figure 13 shows the association between the initial tangent modulus and the compressive strength. The connection between the (E_i) and the compressive strength (σ) is effectively represented by a linear relationship as follows.

3.7 Failure pattern

The failure patterns indicate that the cube specimens went through lateral expansion (bulging) before developing cracks in distinct planes, as shown in Figure 14A–C and Figure 15A–D. In the present experimental study, for most of the cube specimens, horizontal cracks occurred at locations around the bottom third of the specimen. Specimens tested for compression failed within an axial strain range of 0.6%–1.21%. For the beam specimen under

flexural loading, vertical flexural crack developed at the pure flexural region (the span between two-point loads). All the specimens failed at deflection ranging from 0.16 to.

3.8 Microstructural analysis

The energy dispersive spectroscopy (EDS) test was performed on SA and BF slag materials to determine the phase composition materials. The minerals present in the sugar cane bagasse ash were identified using the database of JCPDS. The predominant minerals present in the SA and BF slag were quartz (81.13%), potassium carbonate (11.18%), cristobalite (4.0%), gumbelite (56.12%), and dolomite (32.12%). The EDS patterns of the SA and BF slag show the presence of oxygen, silica, and copper, as shown in Figure 16A, B. The SA materials consisted of irregularly shaped particles, the BF slag consisted of rounded, semi-spherical, and irregularly shaped particles and the glass fiber consisted of rounded-shape particles, as shown in Figure 17A–C. Finally, more or less similar mechanical and microstructural behaviors of waste material replacements reinforced by different types of fibers have been reported by several researchers (Horvath, 1998; Liu et al., 2006; Matsuda et al., 2008; Landa-Ruiz et al., 2021; Althoey et al., 2022; Najm et al., 2022b; Memon et al., 2022; Nanayakkara et al., 2022; Prabhath et al., 2022).
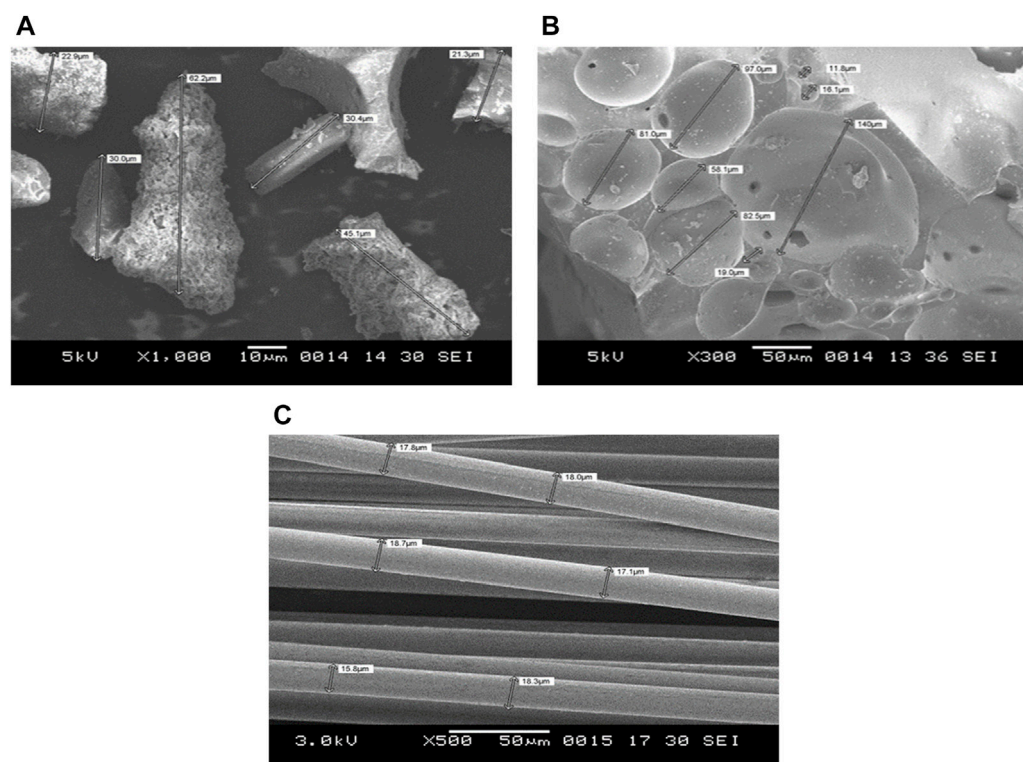
FIGURE 17
Microstructures of **(A)** SBCA; **(B)** BFS; **(C)** GF.

4 Limitation and future scope

Since a lower percentage of C/SA results in a specimen that does not retain its shape even after the curing period, and this value was used as 10% while making specimens for the compressive and flexural tests. Because of this restriction, no samples with cement contents less than 10% could be cast and analyzed. Further utilization of larger specimens is impossible because of the loading frame and testing instrument with the maximum size. Based on future research, the shear strength of a material can be determined under various compression and flexure loading conditions.

Additionally, the inclusion of nano-material admixtures (Khan et al., 2021) may further me used to enhance the properties and how the application of external strengthening (Khan, 2021a; Khan, 2021b; Khan, 2022) will affect failure modes may also be studied.

5 Conclusion

Sustainable concrete is popular as a building material because of its higher flexural and compressive strengths and lower cost. Due to its limited elasticity and resistance to fracture, it is naturally vulnerable. Metal and non-metal fibers have been put into concrete to address these issues. However, This study's primary goal was to evaluate the performance of various quantities of glass-fiber-reinforced geomaterial composites on the mechanical properties and classify

them into geomaterials per the design standards for usability. Therefore, a detailed investigation into the compressive strength, flexural strength, density, tangent modulus, stress–strain pattern, and load–deflection curve of newly prepared materials were analyzed. The intention of such a detailed examination of sugar cane bagasse ash and blast furnace slag was to obtain the optimum contents in terms of mechanical properties to reduce environmental stress, and to approach sustainable development. So, in order to comprehend the behaviour of geomaterials created utilizing bagasse ash, an experimental investigation was carried out. From the observations, the findings are as follows.

– The density of the cube specimens decreased with increases in the mix ratios with values ranging from 0.2% to 1.0%. For the compression specimens with 20% cement and a water-to-SA ratio of 55%, the density decreased from 1320.1 to 1265 kg/m^3 (about 4.35%).

– The density of the beam specimens decreased with increases in the mix ratio values from 0.2% to 1.2%. For the flexural specimens with 20% cement content, the density decreased from 1318 to 1259.6 kg/m^3. The percentage decrease was about 4.43%.

– As the curing time went on, the compressive strength increased. The maximum compressive strength of 1055.5 kPa was found at 28 days for a mix ratio of 0.6% with a 20% CEM/SA ratio and a 55% W/SA ratio. The lowest compressive strength of 120 kPa was found at 7 days for a mix ratio of 1.0% and a CEM/SA ratio of 10%.

– Additionally, it was discovered that the flexural strength increased as the curing time increased. The highest flexural strength of

217.2 kPa was observed for the specimen with a mix ratio of 0.8% cured for 28 days, and a CEM/SA ratio kept at 20%. The lowest flexural strength of 80.10 kPa was observed for specimens with a mix ratio of 0.2% cured for 7 days with a CEM/SA ratio of 10%.

– The uniaxial compressive stress–strain curve shows non-linear behavior and increases in the compressive strength and stiffness were observed with an increase in the curing period. The failure strain ranged from 0.6% to 1.21% for a W/SA ratio of 55%.

– A non-linear relationship between the flexural load and the mid-span deflection was also observed. The curve increased linearly up to the failure load and then fell rapidly. The mid-span deflection at failure varied from 0.16 to 0.79 mm.

– The initial tangent modulus was found to vary linearly with compressive stress. The compressive stress varied non-linearly with the mix ratio; therefore, the initial tangent modulus varied non-linearly with the mix ratio. The value of the initial tangent modulus for the cube specimens ranged from 96 to 636 MPa for a W/SA ratio of 55%.

The obtained compressive strength in this research is more than 50 kPa as reported by Matsuda et al. (2008) (Matsuda et al., 2008), would resist liquefaction during an earthquake. Therefore, the newly developed SA reinforced glass fiber material satisfy the criteria and it can be used as fill materials which can solve the problem of environmental pollution with an eye on sustainable development. The materials prepared in this study are under the lightweight category of materials. Therefore, given the observations and the recommendations of the design standards, the geomaterial composite prepared in this study is suitable as a lightweight geomaterial.

Data availability statement

The raw data supporting the conclusion of this article will be made available by the authors, without undue reservation.

Author contributions

Conceptualization, HN and RL; data curation, HN, RL, KA, HMN, MM, MK, SA, MAH, and SI; formal analysis, HN, RL, KA, HMN, MM, MK, SA, MAH, and SI; funding acquisition, MAH, SA, MM, and SI; investigation, HN and RL; methodology, HN, RL, KA, and HMN; resources, KA, HMN, MM, MK, SA, MAH, and SI; software, HN, KA, and MK; supervision, RL; validation, RL, HMN, SA, MAH, and SI; visualization, HMN, SA, MAH, and SI; writing–original draft, HN and KA; writing–review and editing, MK, RL, HN, and HMN. All authors have read and agreed to the published version of the manuscript.

Conflict of interest

The authors declare that the research was conducted in the absence of any commercial or financial relationships that could be construed as a potential conflict of interest.

Publisher's note

All claims expressed in this article are solely those of the authors and do not necessarily represent those of their affiliated organizations, or those of the publisher, the editors and the reviewers. Any product that may be evaluated in this article, or claim that may be made by its manufacturer, is not guaranteed or endorsed by the publisher.

References

Ahmed, H. U., Mohammed, A. A., Serwan, R., Mohammed, A. S., Mosavi, A., Sor, N. A. H., et al. (2021). Compressive strength of sustainable geopolymer concrete composites: A state-of-the-art review. *Sustainability* 13 (24), 13502. doi:10.3390/su132413502

Ahmed, H. U., Mohammed, A. S., Faraj Rabar, H., Qaidi, S. M. A., and Mohammed, A. A. (2022). Compressive strength of geopolymer concrete modified with nano-silica: Experimental and modeling investigations. *Case Stud. Constr. Mater.* 16, e01036. doi:10.1016/j.cscm.2022.e01036

Althoey, F., Awoyera, P. O., Inyama, K., Khan, M. A., Mursaleen, M., Hadidi, H. M., et al. (2022). Strength and microscale properties of bamboo fiber-reinforced concrete modified with natural rubber latex. *Front. Mater* 9, 1064885. doi:10.3389/fmats.2022.1064885

Anas, S. M., Alam, M., and Shariq, M. (2023). Damage response of conventionally reinforced two-way spanning concrete slab under eccentric impacting drop weight loading. *Def. Technol.* 19, 12–34. doi:10.1016/j.dt.2022.04.011

Anas, S. M., Alam, M., and Umair, M. (2021). Experimental and numerical investigations on performance of reinforced concrete slabs under explosive-induced

air-blast loading: A state-of-the-art review. *Structures* 31, 428–461. doi:10.1016/j.istruc.2021.01.102

Anas, S. M., Alam, M. I., Haytham, F., Najm, H. M., and Sabri, M. M. S. (2022). Role of cross-diagonal reinforcements in lieu of seismic confining stirrups in the performance enhancement of square RC columns carrying axial load subjected to close-range explosive loading. *Front. Mater.* 9. Article in press. doi:10.3389/fmats.2022.1002195

Anas, S. M., Alam, M. I., Haytham, F., Najm, H. M., and Sabri, M. M. S. (2022). Ultra high performance concrete (UHPC) and C-frp tension Re-bars: A unique combinations of materials for slabs subjected to low-velocity drop impact loading. *Front. Mater.* 9. Article in press. doi:10.3389/fmats.2022.1061297

Andreão, P. V., Suleiman, A. R., Cordeiro, G. C., and Nehdi, M. L. (2020). Beneficiation of sugarcane bagasse ash: Pozzolanic activity and leaching behavior. *Waste Biomass Valor* 11, 4393–4402.

Andreão, P. V., Suleiman, A. R., Cordeiro, G. C., and Nehdi, M. L. (2019). Sustainable use of sugarcane bagasse ash in cement-based materials. *Green Mater* 7, 61–70. doi:10.1680/jgrma.18.00016

Anjos, M. A. S., Araújo, T. R., Ferreira, R. L. S., Farias, E. C., and Martinelli, A. E. (2020). Properties of self-leveling mortars incorporating a high-volume of sugar cane bagasse ash as partial Portland cement replacement. *J. Build. Eng.* 32, 101694. doi:10.1016/j.jobe.2020.101694

ASTM C1585-13 (2013). *Standard test method for measurement of rate of absorption of water by hydraulic cement concretes*. West Conshohocken, PA, USA: ASTM. doi:10.1520/C1585-13.2

ASTM C39 (2016). *ASTM standard C39/C39m-16, standard test method for compressive strength of cylindrical concrete specimens*. West Conshohocken, PA, USA: ASTM.

ASTM C618-17a (2017). *Standard specification for coal fly ash and raw or calcined natural pozzolan for use in concrete*. West Conshohocken, PA, USA: ASTM, 1–5.

ASTM C78 (2016). *Standard test method for flexural strength of concrete*. West Conshohocken, PA, USA: ASTM.

ASTM D1557 (2021). *Standard test methods for laboratory compaction characteristics of soil using modified effort (56,000 Ft-lbf/ft3 (2,700 kN-m/m3))*, 3. West Conshohocken, PA, USA: ASTM, 1–10.

ASTM Standards C-293 (2002). *Standard test method for flexural strength of concrete (using simple beam with center-point loading)*. West Conshohocken, PA, USA: ASTM.

Bahurudeen, A., Kanraj, D., Gokul Dev, V., and Santhanam, M. (2015). Performance evaluation of sugarcane bagasse ash blended cement in concrete. *Cem. Concr. Compos.* 59, 77–88. doi:10.1016/j.cemconcomp.2015.03.004

Bahurudeen, A., and Santhanam, M. (2015). Influence of different processing methods on the pozzolanic performance of sugarcane bagasse ash. *Cem. Concr. Compos.* 56, 32–45. doi:10.1016/j.cemconcomp.2014.11.002

Bartošek, J. (2014). Czech cane sugar factories II. *List. Cukrov. Repar.* 130, 328–334.

Bentz, D. P., Ferraris, C. F., Jones, S. Z., Lootens, D., and Zunino, F. (2017). Limestone and silica powder replacements for cement: Early-age performance. *Cem. Concr. Compos.* 78, 43–56. doi:10.1016/j.cemconcomp.2017.01.001

BIS:383 (1970). *Specification for coarse and fine aggregates from natural sources for concrete*. New Delhi, India: Indian Standard, 1–24.

Cetin, E., Moghtaderi, B., Gupta, R., and Wall, T. F. (2004). Influence of pyrolysis conditions on the structure and gasification reactivity of biomass chars. *Fuel* 83, 2139–2150. doi:10.1016/j.fuel.2004.05.008

Channa, S. H., Mangi, S. A., Bheel, N., Soomro, F. A., and Khahro, S. H. (2022). Short-term analysis on the combined use of sugarcane bagasse ash and rice husk ash as supplementary cementitious material in concrete production. *Environ. Sci. Pollut. Res.* 29, 3555–3564. doi:10.1007/s11356-021-15877-0

Chusilp, N., Jaturapitakkul, C., and Kiattikomol, K. (2009). Effects of LOI of ground bagasse ash on the compressive strength and sulfate resistance of mortars. *Constr. Build. Mater.* 23, 3523–3531. doi:10.1016/j.conbuildmat.2009.06.046

Cordeiro, G. C., Filho, R. D. T., and De Almeida, R. S. (2011). Influence of ultrafine wet grinding on pozzolanic activity of submicrometre sugar cane bagasse ash. *Adv. Appl. Ceram.* 110, 453–456. doi:10.1179/1743676111Y.0000000050

Cordeiro, G. C., and Kurtis, K. E. (2017). Effect of mechanical processing on sugar cane bagasse ash pozzolanicity. *Cem. Concr. Res.* 97, 41–49. doi:10.1016/j.cemconres.2017.03.008

Cordeiro, G. C., Paiva, O. A., Toledo Filho, R. D., Fairbairn, E. M. R., and Tavares, L. M. (2018). Long-term compressive behavior of concretes with sugarcane bagasse ash as a supplementary cementitious material. *J. Test. Eval.* 46, 20160316–20160573. doi:10.1520/JTE20160316

Cordeiro, G. C., Tavares, L. M., and Toledo Filho, R. D. (2016). Improved pozzolanic activity of sugar cane bagasse ash by selective grinding and classification. *Cem. Concr. Res.* 89, 269–275. doi:10.1016/j.cemconres.2016.08.020

Cordeiro, G. C., Toledo Filho, R. D., Tavares, L. M., and Fairbairn, E. D. M. R. (2009). Ultrafine grinding of sugar cane bagasse ash for application as pozzolanic admixture in concrete. *Cem. Concr. Res.* 39, 110–115. doi:10.1016/j.cemconres.2008.11.005

Deepika, S., Anand, G., Bahurudeen, A., and Santhanam, M. (2017). Construction products with sugarcane bagasse ash binder. *J. Mater. Civ. Eng.* 29, 04017189. doi:10.1061/(asce)mt.1943-5533.0001999

Duxson, P., Lukey, G. C., and van Deventer, J. S. J. (2006). Thermal evolution of metakaolin geopolymers: Part 1—physical evolution. *J. Non. Cryst. Solids* 352, 5541–5555. doi:10.1016/j.jnoncrysol.2006.09.019

Frías, M., Villar, E., and Savastano, H. (2011). Brazilian sugar cane bagasse ashes from the cogeneration industry as active pozzolans for cement manufacture. *Cem. Concr. Compos.* 33, 490–496. doi:10.1016/j.cemconcomp.2011.02.003

Ganesan, K., Rajagopal, K., and Thangavel, K. (2007). Evaluation of bagasse ash as supplementary cementitious material. *Cem. Concr. Compos.* 29, 515–524. doi:10.1016/j.cemconcomp.2007.03.001

Horvath, J. S. (1998). *The compressible-inclusion function of EPS geofoam: Analysis and design methodologies; research report No. CE/GE-98-1; manhattan college*. Bronx, NY, USA: Civil Engineering Department. doi:10.13140/RG.2.2.26209.35685

Iman, M., Mortazavi, S. J., Manfredi, M., Awoyera, P. O., Mansouri, E., Khaki, A., et al. (2023). Development of new material models for thermal behavior of cold-formed G-450 and G-550 steels in OpenSees software. *J. Archit. Eng.* 29 (2). doi:10.1061/JAEIED.AEENG-1491

Khan, M. A., El Rimawi, J. A., and Silberschmidt, V. (2017). Numerical representation of multiple premature failures in steel-plated RC beams. *Int. J. Comput. Methods* 14 (4), 1750035. doi:10.1142/S0219876217500359

Khan, M. A., and El Rimawi, J. A. (Forthcoming). "On peeling-versus-shear failures in prematurely collapsing RC beams strengthened in flexure," in *Practice periodical on structural design and construction*. (ASCE). doi:10.1061/PPSCFX/SCENG-1224

Khan, M., and Ali, M. (2019). Improvement in concrete behavior with fly ash, silica-fume and coconut fibres. *Constr. Build. Mater.* 203, 174–187. doi:10.1016/j.conbuildmat.2019.01.103

Khan, M., and Ali, M. (2016). Use of glass and nylon fibers in concrete for controlling early age micro cracking in bridge decks. *Constr. Build. Mater.* 125, 800–808. doi:10.1016/j.conbuildmat.2016.08.111

Khan, M., Cao, M., and Ali, M. (2018). Effect of basalt fibers on mechanical properties of calcium carbonate whisker-steel fiber reinforced concrete. *Constr. Build. Mater.* 192, 742–753. doi:10.1016/j.conbuildmat.2018.10.159

Khan, M., Lao, J., and Dai, J-G. (2022). Comparative study of advanced computational techniques for estimating the compressive strength of UHPC. *J. Asian Concr. Fed.* 8 (1), 51–68. doi:10.18702/acf.2022.6.8.1.51

Khan, M. A. (2022). Bond parameters for peeling and debonding in thin plated RC beams subjected to mixed mode loading – framework. *Adv. Struct. Eng.* 25 (3), 662–682. doi:10.1177/13694332211065184

Khan, M. A., El Rimawi, J., and Silberschmidt, V. (2017). Relative behaviour of premature failures in adhesively plated RC beam using controllable and existing parameters. *J. Compos. Struct.* 180, 75–87. doi:10.1016/j.compstruct.2017.08.006

Khan, M. A., Imam, M. K., Irshad, K., Ali, H. M., Hasan, M. A., and Islam, M. (2021). Comparative overview of the performance of cementitious and non-cementitious nanomaterials in mortar at normal and elevated temperatures. *Nanomaterials* 11 (4), 911. doi:10.3390/nano11040911

Khan, M. A., Silberschmidt, V., and El Rimawi, J. (2017). Controlled failure warning and mitigation of prematurely failing beam through adhesive. *J. Compos. Struct.* 161, 119–131. doi:10.1016/j.compstruct.2016.11.049

Khan, M. A. (2021). Toward key research gaps in design recommendations on flexurally plated RC beams susceptible to premature failures. *J. Bridge Eng.* 26, 9. doi:10.1061/(ASCE)BE.1943-5592.0001772

Khan, M. A. (2021). Towards progressive debonding in composite RC beams subjected to thermo-mechanical bending with boundary constraints – a new analytical solution. *J. Compos. Struct.* 274, 114334. doi:10.1016/j.compstruct.2021.114334

Khawaja, S. A., Javed, U., Zafar, T., Riaz, M., Zafar, M. S., and Khan, M. K. (2021). Eco-friendly incorporation of sugarcane bagasse ash as partial replacement of sand in foam concrete. *Clean. Eng. Technol.* 4, 100164. doi:10.1016/j.clet.2021.100164

Kirschner, A. V., and Harmuth, H. (2004). Investigation of geopolymer binders with respect to their application for building materials. *Ceram. Silik.* 48, 117–120.

Kuruba, E. K., Rao, P. V. K. J., Khokhar, D., and Patel, S. (2020). Technologies for preparation of solid and granular jaggery: A review. *Curr. J. Appl. Sci. Technol.* 39, 105–113. doi:10.9734/cjast/2020/v39i3030978

Landa-Ruiz, L., Landa-Gómez, A., Mendoza-Rangel, J. M., Landa-Sánchez, A., Ariza-Figueroa, H., Méndez-Ramírez, C. T., et al. (2021). Physical, mechanical and durability properties of ecofriendly ternary concrete made with sugar cane bagasse ash and silica fume. *Crystals* 11 (9), 1012. doi:10.3390/cryst11091012

Le, D. H., Sheen, Y. N., and Lam, M. N. T. (2018). Fresh and hardened properties of self-compacting concrete with sugarcane bagasse ash–slag blended cement. *Constr. Build. Mater.* 185, 138–147. doi:10.1016/j.conbuildmat.2018.07.029

Liu, H. L., Deng, A., and Chu, J. (2006). Effect of different mixing ratios of polystyrene pre-puff beads and cement on the mechanical behaviour of lightweight fill. *Geotext. Geomembr.* 24, 331–338. doi:10.1016/j.geotexmem.2006.05.002

Mandal, D., Ram Rathan Lal, B., and Shankar, K. (2018). "Compressive strength behaviour of glass fibre reinforced blast furnace slag-based material," in Proceedings of the 11th International Conference on Geosynthetics, Seoul, Korea, 16–21 September 2018, 1874–1880.

Mangi, S. A., Memon, Z. A., Khahro, S. H., Memon, R. A., and Memon, A. H. (2020). Potentiality of industrial waste as supplementary cementitious material in concrete production. *Int. Rev. Civ. Eng.* 11, 214–221. doi:10.15866/irece.v11i5.18779

Mansouri, E., Manfredi, M., and Hu, J-W. (2022). Environmentally friendly concrete compressive strength prediction using hybrid machine learning. *Sustainability* 14 (20), 12990. doi:10.3390/su142012990

Maroliya, M. K. (2012). A qualitative study of reactive powder concrete using X-ray diffraction technique. *IOSR J. Eng.* 2, 12–16. doi:10.9790/3021-02911216

Martirena, F., and Monzó, J. (2018). Vegetable ashes as supplementary cementitious materials. *Cem. Concr. Res.* 114, 57–64. doi:10.1016/j.cemconres.2017.08.015

Matsuda, H., Shinozaki, H., Ishikura, R., and Kitayama, N. (2008). "Application of granulated blast furnace slag to the earthquake resistant Earth structure as a geo-material," in *Proceedings of the 14th world conference on earthquake engineering beijing China*.

Memon, S. A., Javed, U., Shah, M. I., and Hanif, A. (2022). Use of processed sugarcane bagasse ash in concrete as partial replacement of cement: Mechanical and durability properties. *Buildings* 12 (10), 1769. doi:10.3390/buildings12101769

Mugahed, A., Shan-Shan, H., Onaizi, A. M., Murali, G., and Abdelgader, H. S. (2022). Fire spalling behavior of high-strength concrete: A critical review. *Constr. Build. Mater.* 341, 127902. doi:10.1016/j.conbuildmat.2022.127902

Najm, H. M., and Ahmad, S. (2022). The use of waste ceramic optimal concrete for A cleaner and sustainable environment—a case study of mechanical properties. *Civ. Environ. Eng. Rep.* 32, 85–115. doi:10.2478/ceer-2022-0030

Najm, H. M., Nanayakkara, O., Ahmad, M., and Sabri Sabri, M. M. (2022). Mechanical properties, crack width, and propagation of waste ceramic concrete subjected to elevated temperatures: A comprehensive study. *Materials* 15, 2371. doi:10.3390/ma15072371

Najm, H. M., Nanayakkara, O., and Sabri, M. M. S. (2022). Destructive and non-destructive evaluation of fibre-reinforced concrete: A comprehensive study of mechanical properties. *Materials* 15, 4432. doi:10.3390/ma15134432

Nanayakkara, O., Najm, H. M., and Sabri, M. M. S. (2022). Effect of using steel bar reinforcement on concrete quality by ultrasonic pulse velocity measurements. *Materials* 15, 4565. doi:10.3390/ma15134565

Nikhade, H. R., and Lal, B. (2021). Experimental studies on sugar cane bagasse ash based geomaterials. *Int. J. Eng. Manag. Res.* 11, 1–3. doi:10.31033/ijemr.11.5.1

Nikhade, H. R., and Lal, B. (2023). "Studies on sugar cane bagasse ash and blast furnace slag-based geomaterial," in *Indian geotechnical and geoenvironmental engineering conference* (Singapore: Springer), 25–32.

Osei, D. Y., Mustapha, Z., and Zebilila, M. D. (2020). Compressive strength of concrete using different curing methods. *J. Soc. Dev. Sci.* 10, 30–38. doi:10.22610/jsds.v10i3(s).2983

Prabhath, N., Kumara, B. S., Vithanage, V., Samarathunga, A. I., Sewwandi, N., Maduwantha, K., et al. (2022). A review on the optimization of the mechanical properties of sugarcane-bagasse-ash-integrated concretes. *J. Compos. Sci.* 6 (10), 283. doi:10.3390/jcs6100283

Qaidi, S. M. A., Tayeh, B. A., Isleem, H. F., AzevedoAfonso, R. G. D., Unis, H. A., et al. (2022). Sustainable utilization of red mud waste (bauxite residue) and slag for the production of geopolymer composites: A review. *Case Stud. Constr. Mater.* 16, e00994. doi:10.1016/j.cscm.2022.e00994

Rajasekar, A., Arunachalam, K., Kottaisamy, M., and Saraswathy, V. (2018). Durability characteristics of ultra high strength concrete with treated sugarcane bagasse ash. *Constr. Build. Mater.* 171, 350–356. doi:10.1016/j.conbuildmat.2018.03.140

Rakhimova, N. R., and Rakhimov, R. Z. (2014). A review on alkali-activated slag cements incorporated with supplementary materials. *J. Sustain. Cem. Mater.* 3, 61–74. doi:10.1080/21650373.2013.876944

Ram Rathan Lal, B., and Badwaik, V. N. (2016). Experimental studies on bottom ash and expanded polystyrene beads–based geomaterial. *J. Hazard. Toxic, Radioact. Waste* 20 (2), 04015020. doi:10.1061/(asce)hz.2153-5515.0000305

Ram Rathan Lal, B., and Nawkhare, S. S. (2016). Experimental study on plastic strips and EPS beads reinforced bottom ash based material. *Int. J. Geosynth. Ground Eng.* 2 (3), 25–12. doi:10.1007/s40891-016-0066-2

Rao, M. S. C., Vijayalakshmi, M. M., and Praveenkumar, T. R. (2021). Behaviour of green concrete (blended concrete) using agro-industrial waste as partial replacement of cement along with nanoparticles. *Appl. Nanosci.* 1, 1–9. doi:10.1007/s13204-021-01917-1

Rodrigues, J. A. R. (2011). Do engenho à biorrefinaria: A usina de açúcar como empreendimento industrial para a geração de produtos bioquímicos e biocombustíveis. *Quim. Nova* 34, 1242–1254. doi:10.1590/S0100-40422011000700024

Rodríguez de Sensale, G., and Rodríguez Viacava, I. (2018). A study on blended Portland cements containing residual rice husk ash and limestone filler. *Constr. Build. Mater.* 166, 873–888. doi:10.1016/j.conbuildmat.2018.01.113

Rubenstein, M. (2012). Emissions from the cement industry. *State Planet* 11, 1–9.

Saleh, H. M., Salman, A. A., Faheim, A. A., and El-Sayed, A. M. (2020). Sustainable composite of improved lightweight concrete from cement kiln dust with grated poly(styrene). *J. Clean. Prod.* 277, 123491. doi:10.1016/j.jclepro.2020.123491

Setayesh Gar, P., Suresh, N., and BindiganavileSugar, V. (2017). Sugar cane bagasse ash as a pozzolanic admixture in concrete for resistance to sustained elevated temperatures. *Constr. Build. Mater.* 153, 929–936. doi:10.1016/j.conbuildmat.2017.07.107

Singh, N. B., Singh, V. D., and Rai, S. (2000). Hydration of bagasse ash-blended Portland cement. *Cem. Concr. Res.* 30, 1485–1488. doi:10.1016/S0008-8846(00)00324-0

Stafford, F. N., Raupp-Pereira, F., Labrincha, J. A., and Hotza, D. (2016). Life cycle assessment of the production of cement: A Brazilian case study. *J. Clean. Prod.* 137, 1293–1299. doi:10.1016/j.jclepro.2016.07.050

Talero, R., Rahhal, V., Potapov, V. V., Serdan, A. A., Kashpura, V. N., Gorbach, V. A., et al. (2007). AN2521 application note:19 V–75 W laptop adapter with tracking boost PFC pre-regulator, using the L6563 and L6668. *Constr. Build. Mater.* 1, 2–6.

Thomas, R. J., Lezama, D., and Peethamparan, S. (2017). On drying shrinkage in alkali-activated concrete: Improving dimensional stability by aging or heat-curing. *Cem. Concr. Res.* 91, 13–23. doi:10.1016/j.cemconres.2016.10.003

van Deventer, J. S. J., Nicolas, R. S., Ismail, I., Bernal, S. A., Brice, D. G., and Provis, J. L. (2014). Microstructure and durability of alkali-activated materials as key parameters for standardization. *J. Sustain. Cem. Mater.* 4, 116–128. doi:10.1080/21650373.2014.979265

Wen, C., Zhang, P., Wang, J., and Hu, S. (2022). Influence of fibers on the mechanical properties and durability of ultra-high-performance concrete: A review. *J. Build. Eng.* 52 (2022), 104370. doi:10.1016/j.jobe.2022.104370

Xu, Q., Ji, T., Gao, S. J., Yang, Z., and Wu, N. (2018). Characteristics and applications of sugar cane bagasse ash waste in cementitious materials. *Materials* 12, 39. doi:10.3390/ma12010039

Yashwanth, M. K., Avinash, G. B., Raghavendra, A., and Kumar, B. G. N. (2017). An experimental study on alternative cementitious materials: Bagasse ash as partial replacement for cement in structural lightweight concrete. *Indian Concr. J.* 91, 51–58.

Zareei, S. A., Ameri, F., and Bahrami, N. (2018). Microstructure, strength, and durability of eco-friendly concretes containing sugarcane bagasse ash. *Constr. Build. Mater.* 184, 258–268. doi:10.1016/j.conbuildmat.2018.06.153

Zhang, P., Gao, Z., Wang, J., Guo, J., and Wang, I. (2022). Influencing factors analysis and optimized prediction model for rheology and flowability of nano-SiO2 and PVA fiber reinforced alkali-activated composites. *J. Clean. Prod.* 366 (2022), 132988. doi:10.1016/j.jclepro.2022.132988

Zhang, P., Han, X., Hu, S., Wang, J., and Wang, T. (2022). High-temperature behavior of polyvinyl alcohol fiber-reinforced metakaolin/fly ash-based geopolymer mortar. *Compos. Part B Eng.* 244 (2022), 110171. doi:10.1016/j.compositesb.2022.110171

Zhang, P., Peng, Y., Guan, J., and Guo, J. (2022). Fracture behavior of multi-scale nano-SiO2 and polyvinyl alcohol fiber reinforced cementitious composites under the complex environments. *Theor. Appl. Fract. Mech.* 122 (2022), 103584. doi:10.1016/j.tafmec.2022.103584

Zhang, P., Zhang, P., Wu, J., Zhang, Y., and Guo, J. (2022). Mechanical properties of polyvinyl alcohol fiber-reinforced cementitious composites after high-temperature exposure. *Gels* 8 (10), 662. doi:10.3390/gels8100662

Check for updates

*CORRESPONDENCE
Mohammad Arsalan Khan,
✉ mohd.arsalan.khan@hotmail.co.uk
S. M. Anas,
✉ mohdanas43@gmail.com
Mohammad Mursaleen,
✉ mursaleenm@gmail.com

Corrigendum: Behavior of geomaterial composite using sugar cane bagasse ash under compressive and flexural loading

Harshal Nikhade[1,2], Ram Rathan Lal Birali[1], Khalid Ansari[2], Mohammad Arsalan Khan[3,4]*, Hadee Mohammed Najm[3], S. M. Anas[5]*, Mohammad Mursaleen[6]*, Mohd Abul Hasan[7] and Saiful Islam[7]

[1]Department of Civil Engineering, Kavikulguru Institute of Technology and Science, Ramtek, India, [2]Department of Civil Engineering, Yeshwantrao Chavan College of Engineering, Nagpur, India, [3]Department of Civil Engineering, Zakir Husain College of Engineering and Technology, Aligarh Muslim University, Aligarh, India, [4]Geomechanics and Geotechnics Group, University of Kiel, Kiel, Germany, [5]Department of Civil Engineering, Jamia Millia Islamia, New Delhi, India, [6]China Medical University Hospital, China Medical University (Taiwan), Taichung, Taiwan, [7]Civil Engineering Department, College of Engineering, King Khalid University, Abha, Saudi Arabia

KEYWORDS

glass fiber, bagasse ash, blast furnace slag, mechanical strength, sustainable geomaterial

---

A Corrigendum on

Behavior of geomaterial composite using sugar cane bagasse ash under compressive and flexural loading

by Nikhade H, Birali RRL, Ansari K, Khan MA, Najm HM, Anas SM, Mursaleen M, Hasan MA and Islam S (2023). Front. Mater. 10:1108717. doi: 10.3389/fmats.2023.1108717

In the published article, there was an error in **Affiliations** 6 and 7. Instead of "China Medical University Hospital, Taiwan, Taichung, China"; and "King Khalid University, Abha, Saudi Arabia," it should respectively be "China Medical University Hospital, China Medical University (Taiwan), Taichung, Taiwan"; and "Civil Engineering Department, College of Engineering, King Khalid University, Abha, Saudi Arabia."

The authors apologize for this error and state that this does not change the scientific conclusions of the article in any way. The original article has been updated.

Publisher's note

All claims expressed in this article are solely those of the authors and do not necessarily represent those of their affiliated organizations, or those of the publisher, the editors and the reviewers. Any product that may be evaluated in this article, or claim that may be made by its manufacturer, is not guaranteed or endorsed by the publisher.

Check for updates

Machine learning-based evaluation of parameters of high-strength concrete and raw material interaction at elevated temperatures

Gongmei Chen[1]*, Salman Ali Suhail[2], Alireza Bahrami[3]*,
Muhammad Sufian[4] and Marc Azab[5]

[1]School of Architecture and Civil Engineering, Changchun Sci-Tech University, Changchun, China,
[2]Department of Civil Engineering, University of Lahore (UOL), Lahore, Pakistan, [3]Department of Building
Engineering, Energy Systems and Sustainability Science, Faculty of Engineering and Sustainable
Development, University of Gävle, Gävle, Sweden, [4]School of Civil Engineering, Southeast University,
Nanjing, China, [5]College of Engineering and Technology, American University of the Middle East, Egaila,
Kuwait

High-strength concrete (HSC) is vulnerable to strength loss when exposed to high temperatures or fire, risking the structural integrity of buildings and critical infrastructures. Predicting the compressive strength of HSC under high-temperature conditions is crucial for safety. Machine learning (ML) techniques have emerged as a powerful tool for predicting concrete properties. Accurate prediction of the compressive strength of HSC is important as HSC can experience strength losses of up to 80% after exposure to temperatures of 800°C−1000°C. This study evaluates the efficacy of ML techniques such as Extreme Gradient Boosting, Random Forest (RF), and Adaptive Boosting for predicting the compressive strength of HSC. The results of this study demonstrate that the RF model is the most efficient for predicting the compressive strength of HSC, exhibiting the R^2 value of 0.98 and lower mean absolute error and root mean square error values than the other applied models. Furthermore, Shapley Additive Explanations analysis highlights temperature as the most significant factor influencing the compressive strength of HSC. This article provides valuable insights into the timely and effective determination of the compressive strength of HSC under high-temperature conditions, benefiting both the construction industry and academia. By leveraging ML techniques and considering the critical factors that influence the compressive strength of HSC, it is possible to optimize the design and construction process of HSC and enhance its resilience to high-temperature exposure.

1 Introduction

In recent years, the construction sector has developed considerable interest in using high-strength concrete (HSC) for applications like high-rise buildings, offshore structures, and bridges. The primary utilization of HSC in buildings is structural framing, including columns and beams that are major load-bearers. Therefore, adequate measures against fire safety are vital safety prerequisites in building design. With enhanced applications of HSC, there is rising concern about HSC's behavior in fire, which can damage structures (Figure 1). The phenomenon of spalling at higher temperatures is the primary reason for this concern (Khaliq and Kodur, 2018; Xiong and Liew, 2020; Kushnir et al., 2021; Lalu et al., 2021; Li et al., 2021). Usually, the structural elements of normal-strength concrete show considerable performance under exposure to fire. However, a distinct difference is reported in the literature between HSC and normal-strength concrete after exposure to fire (Bilodeau et al., 2004; Laneyrie et al., 2016; Ozawa et al., 2017; Cao et al., 2018). Moreover, the explosive spalling that occurs in HSC under exposure to rapid fire is also of significant concern (Alfahdawi et al., 2019; Xiong and Liew, 2020; Afzal and Khushnood, 2021; Li et al., 2021; Khan et al., 2022c). The HSC's fire response tracing demands the application of precise modeling which can adequately account for the HSC's structural response and material properties like spalling on exposure to real fire scenarios. This rising concern about the HSC's behavior in fire requires adequate fire safety measures and the application of precise modeling that can account for the HSC's structural response and material properties upon exposure to real fire scenarios.

The development of HSC in the cementitious material field occurred between the 1950s and 1960s, and its compressive strength was designated over 40 MPa (Carrasquillo et al., 1981). HSC has very little impermeability, high density, and high durability, making for wide application in the construction sector in skyscrapers, long-span bridges, and piers. The design method of HSC is comparatively more complex than standard strength concrete, demanding in-depth knowledge of the mechanical and chemical characteristics of its ingredients, more experience, and multiple trials to attain concrete of the required properties. One of the key factors in the design of

HSC structures is the compressive strength (Duan et al., 2013). Deficiency in the compressive strength of HSC may result in severe structural failures and difficult repairs, as HSC is primarily designed to bear excessive compressive forces (Al-Shamiri et al., 2019). Incorporation of different materials such as fibers (Xie et al., 2021; Shi et al., 2022; Sun et al., 2023), hinges (Huang et al., 2022; Huang et al., 2023a), and special cements (Wang et al., 2022) has also been reported to enhance the properties of cementitious composites. Moreover, researchers are more attentive nowadays to sustainable supplementary cementitious materials for sustainable development (Cao et al., 2019; Arshad et al., 2020; Khan et al., 2021; Ahmad et al., 2023; Lao et al., 2023a; Lao et al., 2023b; Qian et al., 2023; Riaz Ahmad et al., 2023). The timely and precise determination of the compressive strength of HSC can save costs and time, as it is the requirement of various design standards and codes. The complexity of HSC structures requires significant expertise, and accurate determination of the compressive strength is crucial to prevent structural failure.

Applying machine learning (ML) approaches can effectively solve complex issues in different engineering fields (Dong et al., 2023b; Huang et al., 2023b). ML approaches can predict the output depending on the input variable dataset (Huang et al., 2021; Wang et al., 2022; Zhang et al., 2023). Both individual and ensemble ML approaches are employed. The Decision Tree (DT) is classified as an individual approach, whereas the Random Forest (RF), eXtreme Gradient Boosting (XGBoost), and Adaptive Boosting (AdaBoost) are categorized as ensemble ML techniques. It has been frequently reported in the literature that ensemble ML approaches tend to perform better than individual ones, possibly due to the ability of ensembles to reduce the variance and bias of individual models, capture a broader range of patterns and relationships within the data, and improve generalization to new and unseen examples. Ensembles can also be useful in cases where individual models are prone to overfitting or have limitations in their predictive capacity. Overall, ensemble approaches have become increasingly popular in ML due to their potential to increase prediction accuracy and robustness and their versatility for use across different application domains (Wang et al., 2022). ML techniques are used to investigate the mechanical properties of concrete (Chaabene et al., 2020; Khan et al., 2022d). Additionally, research works were conducted on multiple types of concrete, such as phase change material-integrated concrete (Marani and Nehdi, 2020), high-performance concrete (HPC) (Castelli et al., 2013), recycled aggregate concrete (RAC) (Zhang et al., 2020), and self-healing concrete (Ramadan Suleiman and Nehdi, 2017), to estimate their characteristics. Han et al. (2019) utilized ML techniques to predict the compressive strength of HPC by considering various parameters such as cement, aggregates, sand, water, ground granulated blast-furnace slag, and age. Their algorithm achieved high accuracy in the HPC's strength estimation. ML approaches, especially ensemble techniques, have been increasingly applied to solve complex issues and improve prediction accuracy and robustness in various engineering fields, including the investigation of mechanical properties of different types of concrete; further research is needed to explore the effects of fire exposure on the HSC's performance and its interactions with various parameters.

The mechanical characteristics of HSC have been extensively evaluated in numerous studies. However, the laboratory processes

FIGURE 1
Fire consequences (Wróblewski and Stawiski, 2020).

for casting, curing, and testing specimens require considerable effort, time, and cost. Hence, applying ML, such as advanced approaches, for assessing the characteristics of HSC may solve these issues and decrease experimentation costs (Dong et al., 2023a; Asghari et al., 2023; Sami et al., 2023). Accordingly, this research applies three different ensemble ML approaches—XGBoost, Adaboost, and RF—for the compressive strength prediction of HSC. These ensemble algorithms are better than individual algorithms for predicting the compressive strength of HSC at high temperatures (Ahmad et al., 2021). For predicting the compressive strength of HSC *via* the application of ML algorithms, the considered input parameters include cement (kg/m^3), fly ash (kg/m^3), nano-silica (kg/m^3), water (kg/m^3), super plasticizer (kg/m^3), fine and coarse aggregates (kg/m^3), silica fume (kg/m^3), and temperature (°C). These parameters are taken as predictor variables for the compressive strength of HSC. Moreover, the employed algorithms' performance is also evaluated with the help of comparison and statistical analysis. Depending on the evaluated performance, a better algorithm is recommended to determine the strength of HSC. Furthermore, the basic constituents' influence on the strength of HSC is yet to be explored. Thus, the influence of HSC's raw ingredients—the input parameters—on the strength under compressive loading—its output parameter—is evaluated and explained in detail by Shapley Additive Explanations (SHAP) analysis. The integration of SHAP with the utilized ML models will gain detailed information on HSC mix design with respect to its strength parameters through complex non-linear behavior. It will aid in developing sustainable and fire-resistant HSC mixes.

2 Research significance

The manufacturing and testing of HSC for evaluating its superior properties involve costly and time-consuming laboratory procedures such as specimen casting, curing, and testing. Modern ML techniques have recently been employed to tackle these challenges in predicting the mechanical behavior of HSC. This study utilizes ensemble ML approaches—including XGBoost, Adaboost, and RF—to predict the compressive strength of HSC. It investigates the effect and interaction of raw ingredients through the SHAP analysis, using nine input factors as predictor variables. The models are executed using Python programming language, and k-fold cross-validation is utilized to verify test data. The SHAP analysis is used to examine the contribution of each input factor to the compressive strength of HSC. The study aims to enhance the efficiency, effectiveness, and cost-effectiveness of designing fire-resistant structures and can serve as a foundation for future HSC research at high temperatures.

3 Standard machine learning models

3.1 Extreme Gradient Boosting (XGBoost) algorithm

An XGBoost model is a reliable tool for scientists in the data science field because of an efficient ensemble tree-based model

(Chen and Guestrin, 2016). The structure of Adaboost, which employs various functions for predicting the output by Eq. 1, is the base of Extreme Adaboost (Friedman, 2001).

$$\bar{y}_i = y_i^0 + \eta \sum_{K=1}^{n} f_k(U_i) \qquad (1)$$

Here, the predicted outcome is demonstrated by $\bar{y}_i$ having ith data with U_i, which is a variable vector; n denotes the number of predictors as per independent tree structures for each f_k (k = 1-n); y_i^0 is the primary hypothesis; η denotes the learning rate to increase the algorithm's performance and connect supplementary trees to avoid overfitting. The main limitation of ML is developing a model with minimum overfitting. In XGBoost, the complementary evaluation of the training phase is done.

According to Eq. 1, on the kth level, the kth predictor is linked with the algorithm and kth y_i^{-k} prediction is evaluated by the estimated outcome $y_i^{-(k-1)}$ in the subsequent phase. The established f_k for the kth predictor is given in Eq. 2.

$$y_i^{-k} = y_i^{-(k-1)} + \eta f_k \qquad (2)$$

f_k denotes the weight of the leaves, established by limiting the objective function of the kth tree (Eq. 3).

$$f_{obj} = \gamma Z + \sum_{a=1}^{Z} \left[g_a \omega_a + \frac{1}{2}(h_a + \lambda)\omega_a^2 \right] \qquad (3)$$

Here, the leaf nodes' quantum is depicted by Z, the constant coefficient by λ, the factor of complexity by c, and leaf weight (1—Z) by ω_a^2. c and λ are the governing parameters employed for improving the model in order to avoid over-fitting; g_a and h_a are the summed parameters against the entire database connected with the gradient leaf of the initial and previous loss function, respectively. To build the kth tree, a leaf is additionally distributed in various leaves. The gain factors are utilized to apply this system, provided in Eq. 4.

$$G = \frac{1}{2}\left[\frac{O_L^2}{P_L + \lambda} + \frac{O_R^2}{P_R + \lambda} + \frac{(O_L + O_R)^2}{P_L + P_R + \lambda} \right] \qquad (4)$$

The gain factors are represented with G, left and right leaf, P_L and O_L, and P_R and O_R. The standards for division are usually supposed during the approximation of the gain factor toward '0'. c and λ are governing parameters indirectly based on gain factors. For example, the gain factor may be significantly reduced with a greater regularization factor, ultimately avoiding the convolution process of a leaf. However, in this case, the model's performance in selecting the training data can also be decreased. The XGBoost basic step-wise structure is presented in Figure 2.

3.2 Adaptive Boosting (Adaboost) algorithm

One of the supervised ML approaches is the AdaBoost Regressor, which utilizes an ensemble technique. This approach involves reallocation of weights for each instance, where higher weights are assigned to those that have been incorrectly identified. These techniques are typically employed in supervised learning to reduce bias and variance and improve the performance of weak learners. Furthermore, this approach uses bulk quantities of DTs during data training. The mistakenly characterized recorded data are assigned a high priority weight for developing the initial model/
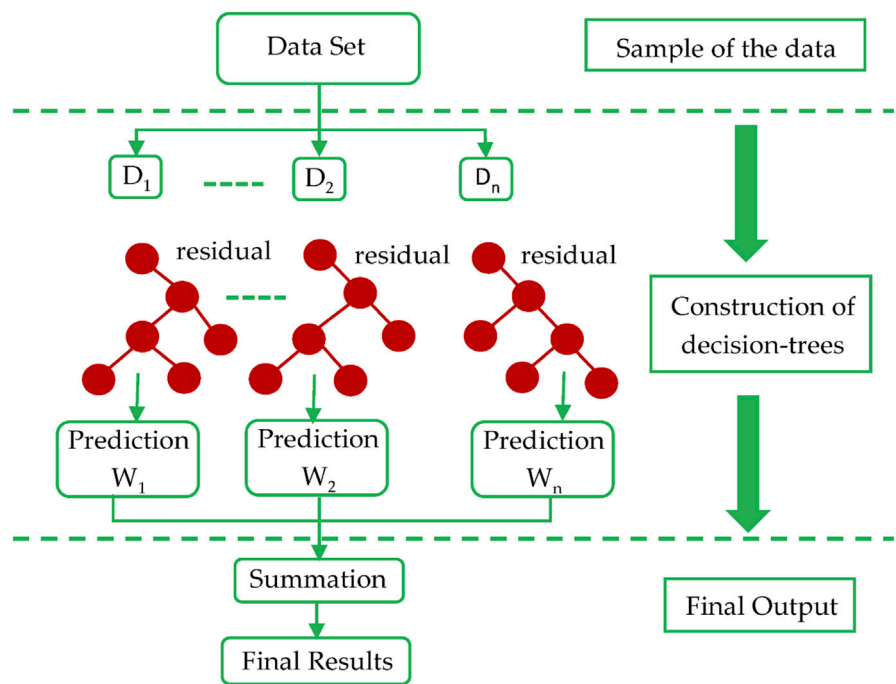
FIGURE 2
Structure of the XGBoost algorithm (Amjad et al., 2022).

DT. These data entries are selected as input for the other algorithms. This process is repeated until the desired quantity of basic learners is fulfilled. In terms of binary classification issues, AdaBoost is better at enhancing the performance of DT and may be applied to boost the efficacy of ML techniques. The Adaboost basic step-wise structure is shown in Figure 3.
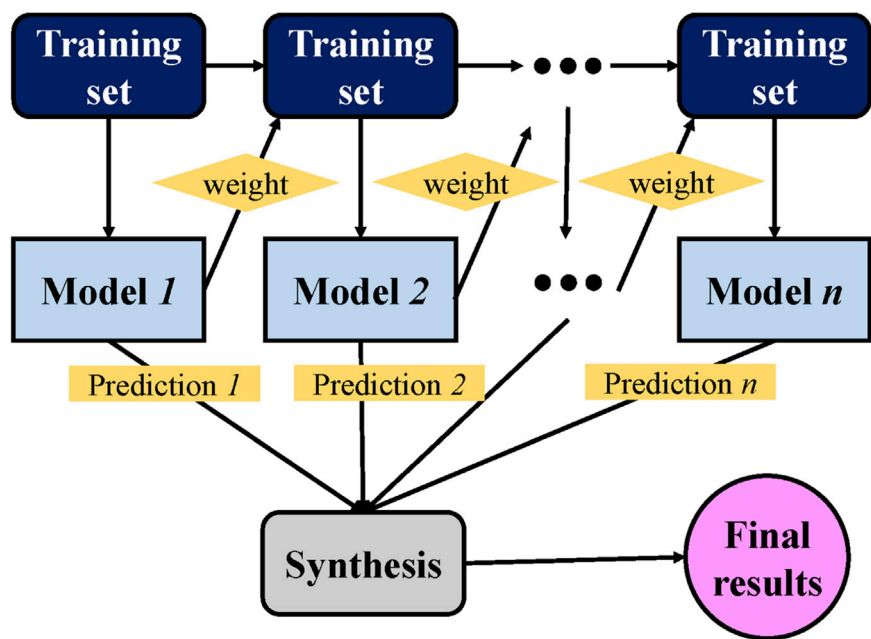

FIGURE 3
Structure of the Adaboost algorithm (Wang et al., 2021).

3.3 Random Forest (RF) algorithm

The RF algorithm has been extensively investigated by numerous researchers as a technique for classification and regression (Han et al., 2019; Zhang et al., 2019). The concrete compressive strength is predicted by using RF (Shaqadan, 2016). The key distinction between DT and RF lies in the number of trees. While DT builds a single independent tree, RF creates multiple trees, referred to as "forests". Unrelated data are randomly selected and assigned to these trees. Each of these trees comprises columns and rows with data, determining the column and row dimensions. Discrete steps are taken for each tree's growth. This data frame includes two-thirds of randomly selected data for every tree: RF. The prediction variables are selected randomly, and the fine splitting of these variables performs node splitting. In the case of all trees, the lingering data are used to predict the outlier error. Consequently, the ultimate out-of-bag error rate is evaluated by merging errors out of each tree. Every tree offers regression, and the forest with the most votes is adopted from the entire forest. The value of the vote may be 0's and 1's. The attained proportion of 1's stipulates the probability of prediction. RF is an efficient ensemble model, comprising necessary variable importance measures (VIMs) with vigorous resistance against rarer model variables and overfitting. DT is utilized for RF as a base estimator. Satisfactory outcomes may be attained by RF algorithms having variable settings (Xu et al., 2021). RF permits base predictor amalgamations and variable settings to be decreased to 1. The RF step-wise structure is shown in Figure 4.

3.4 Shapley Additive Explanations (SHAP)

This study also uses the SHAP analysis (Lundberg, 2021) to assess the global feature influences and corresponding dependencies/interactions of all selected features on the compressive strength of HSC, thus expanding the model's description. In this technique, the description in the case of estimation for every instance is explained with the help of contribution computations by selected features through SHAP values. The value involvement for each feature against all the probable combinations is averaged to attain the SHAP values. The features with more influence have more definite the SHAP values. The average is taken for the SHAP values of every feature from the dataset to accomplish global feature influences. These values are then sorted in descending order of importance; the plotting is carried out afterward. A unique point in the aforesaid plot shows the SHAP value for individual features and instances. X-axis depicts the SHAP values, whereas feature importance is shown on the y-axis. A higher y-axis value displays a greater feature influence. Furthermore, their significance is illustrated by color scale. SHAP plots of feature dependence demonstrate the feature's interaction and respective effect on the compressive strength of HSC. It can yield improved data compared to partial dependence traditional graphs (Lundberg et al., 2020). In this SHAP analysis, particularly the feature importance "j" against the algorithm's output f; $\phi^j(f)$ is allocated weight to sum the involvement of features for the model output, $f(x_i)$, to attain
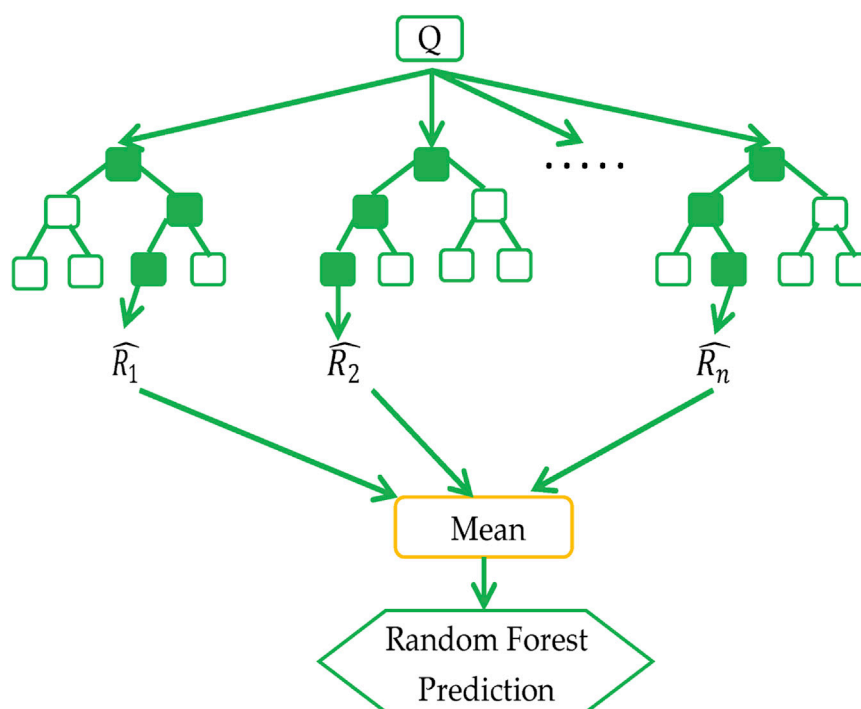

FIGURE 4
Structure of the Random Forest algorithm (Amjad et al., 2022).

the possible combinations of overall features (Molnar, 2020). $\phi^j(f)$ is devised by Eq. 5.

$$\phi^j(f) = \sum_{S \subseteq \{x^1,\ldots,x^p\}/\{x^j\}} \frac{|S|!(p-|S|-1)!}{p!} \left(f(S \sqcup \{x^j\}) - f(S)\right)$$

(5)

where x_j = feature j, p = feature number in model, and S = feature subset. The SHAP method employed in this study determines the feature importance by quantifying estimation errors when a particular value of the feature is perturbed. The weight allocation to a feature during the value dispersion is based on the sensitivity of the prediction error. The performance of trained ML algorithms is described through the SHAP analysis. It applies a supplementary feature attribution approach (linear input parameter summation) to illustrate an interpretable algorithm. An algorithm with input variables x_i; i ranges between $1-k$; k shows input variables quantity and h (x_s) depicts a descriptive algorithm having x_s in the form of simple input. Eq. 6 is proposed for depicting a unique algorithm $f(x)$.

$$f(x) = h(x_s) = \varnothing_0 + \sum_{i=1}^{p} \varnothing_i x_s^i$$

(6)

where $\varnothing_0$ = constant with no information (means no input); p = the number of input features; $x = m_x(x_s)$ indicates a connection between both x and x_s input variables. Lundberg and Lee (2017) proposed Eq. 6, where the prediction value $h()$ was increased by $\varnothing_0, \varnothing_1,$ and $\varnothing_3$ relations along with decreased $\varnothing_4$ in the form of $h()$ value, which were also reported in Figure 5. The solution to Eq. 6, which is a single value, incorporates three essential characteristics: missingness, consistency, and local accuracy. The attribution is confirmed by consistency without decrement, assigned to the particular feature having more influence. In the case of missingness, this certifies that there is no importance value which is allocated to missing features—represented by $\varnothing_i = 0$ applied through $x_s^i = 0$. Regarding local accuracy, the feature attribution summation is verified as an output function. This necessitates the use of an algorithm for a similar outcome f

for x_s, which serves as a simplified input. $x = m_x x_s$ signifies the local accuracy attainment.

4 Dataset description

The database is developed from the literature (Fu et al., 2005; Cülfik and Özturan, 2010; Ergün et al., 2013; Bastami et al., 2014; Chen et al., 2015; Xiong et al., 2016; Mousa, 2017). For predicting the compressive strength of HSC, the considered input dataset is presented in Figure 6. The available literature was used to obtain data on the compressive strength of HSC, which were then compiled into a database. The input parameters are cement (kg/m³), fly ash (kg/m³), nano-silica (kg/m³), water (kg/m³), super plasticizer (kg/m³), fine aggregates (kg/m³), coarse aggregates (kg/m³), silica fume (kg/m³), and temperature (°C) (Figure 6); these parameters are taken as predictor variables for the compressive strength of HSC. This strength is predicted by applying Anaconda Software's Python and Spyder Scripting. Figure 7 illustrates the relative frequency dispersion of the output parameter, i.e., the compressive strength.

5 Results and analysis

5.1 Extreme Gradient Boosting (XGBoost)

Figure 8 displays a comparison between the experimental and predicted values of the compressive strength of HSC using XGBoost, which depicts the highly precise prediction of the compressive strength of HSC. The R^2 value of 0.94 is within a reasonable range, indicating the adequacy of XGBoost. Figure 9 shows the error distribution for the compressive strength of HSC utilizing XGBoost between the estimated and experimental values. The error of the compressive strength of HSC is 4.65 MPa on average. Around 61.2% of the values are below 5 MPa, while there is a 35.48% range from 5 to 10 MPa, with only 3.22% exceeding 10 MPa.
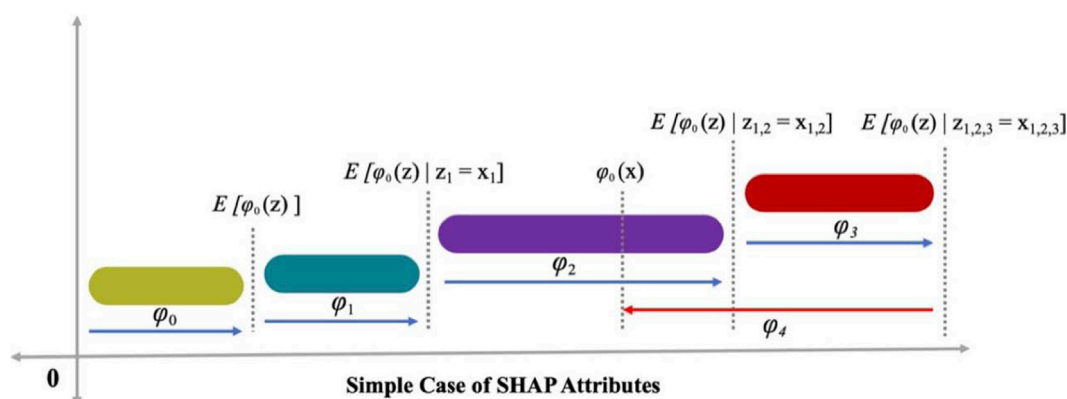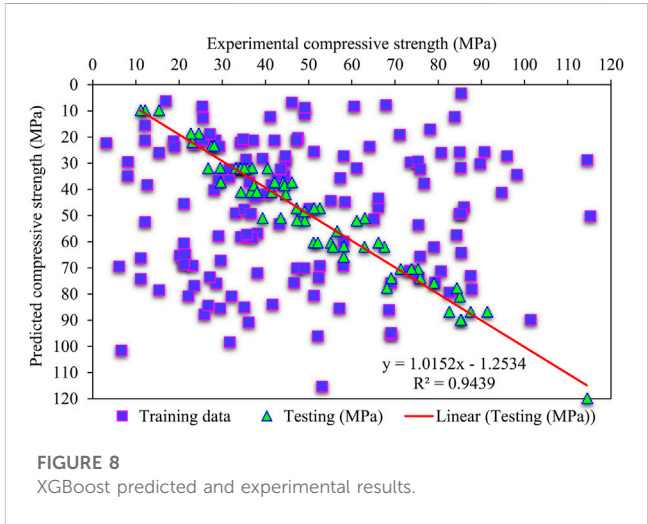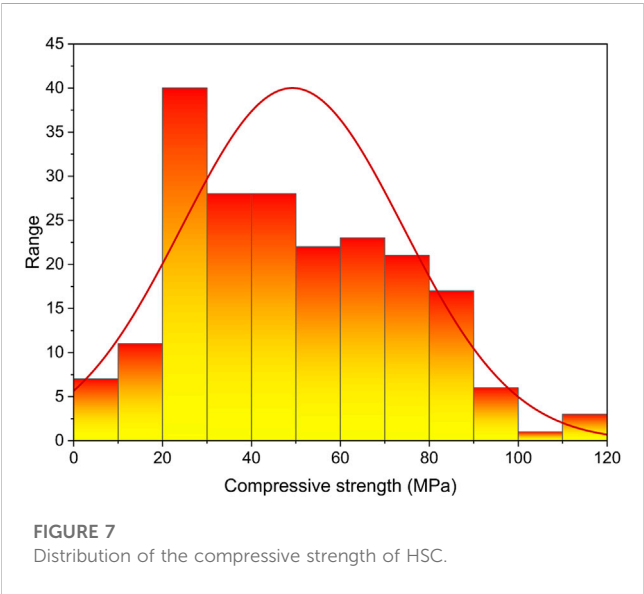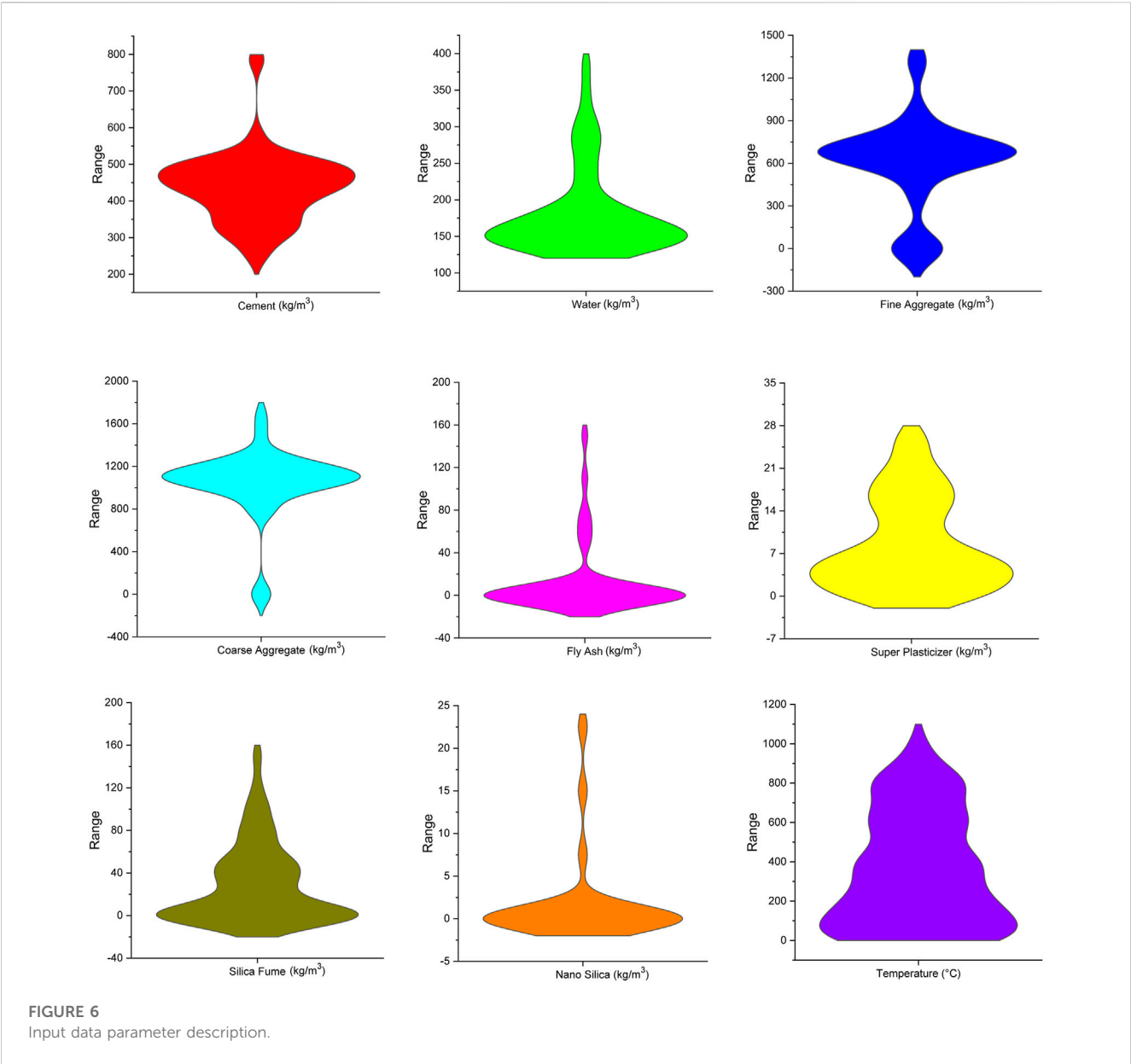

FIGURE 5
Attributes of SHAP (Shen et al., 2022).

FIGURE 6
Input data parameter description.

FIGURE 7
Distribution of the compressive strength of HSC.

FIGURE 8
XGBoost predicted and experimental results.

FIGURE 9
XGBoost estimated and experimental values distribution with errors.

FIGURE 11
Adaboost predicted and experimental results.
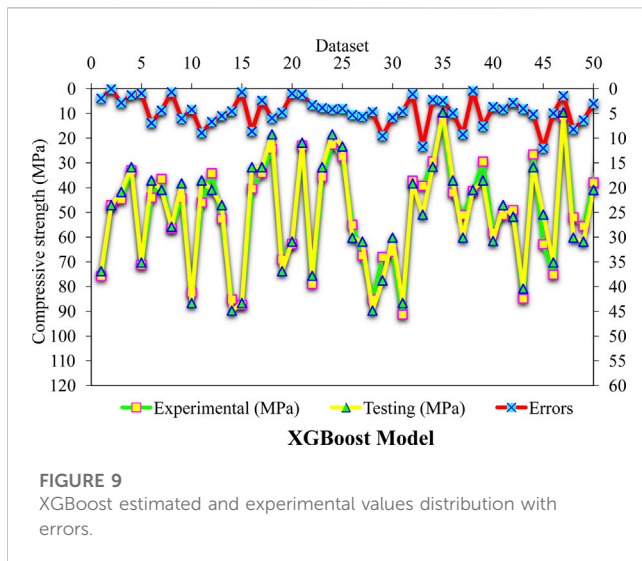
Moreover, further statistics such as highest, mean, median, lowest, first, and third quartile values in the case of experimental and predicted results from the test database are demonstrated in Figure 10. It can be seen in the graphical data that there is a difference between predicted and actual outcomes. Based on the box plot, it appears that the median of the actual values is 51.34 MPa, while the median of the predicted values is 50.86 MPa. The fact that these two values are close suggests that the model can predict the target variable relatively accurately.

5.2 Adaptive Boosting (Adaboost)

Figure 11 provides the predicted and actual values for the compressive strength of HSC utilizing the Adaboost algorithm, in which the R^2 value of 0.90 depicts results with comparatively more precision than XGBoost. The error distribution for experimental and Adaboost-predicted values in the case of the compressive strength of HSC is presented in Figure 12. Here, 59.67% of values lie below 5 MPa, 17.74% lie in the range 5–10 MPa, and 22.58% are
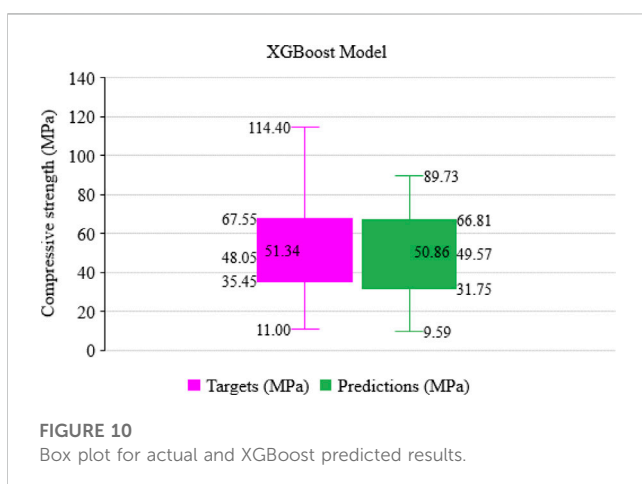

FIGURE 10
Box plot for actual and XGBoost predicted results.
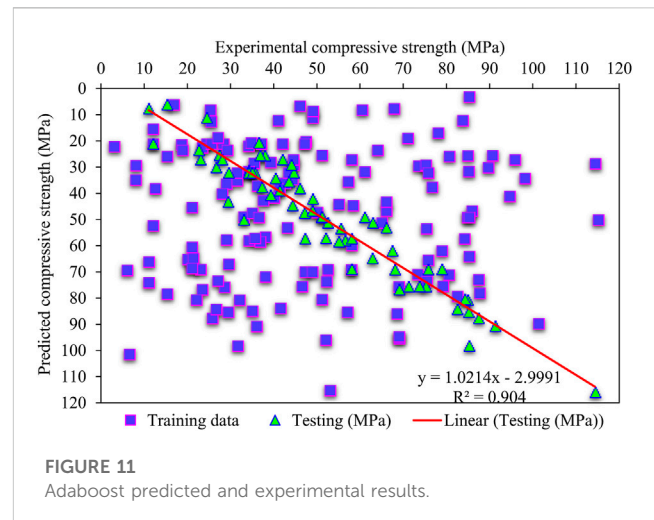
above 10 MPa; the lesser R^2 and greater error value represent the poorer accuracy of Adaboost than that of XGBoost.

The box plot (Figure 13) shows the statistical evaluation, such as minimum, mean, maximum, median, and first and third quartile values, for estimated and experimental outcomes from the test database. The box plot indicates that the median value of the actual data is 51.34 MPa, whereas the predicted data have a median of 49.44 MPa. The close proximity of these two median values implies that the model makes relatively accurate predictions of the target variable. One can observe the variance between the anticipated and factual outcomes by examining the numerical values on the graph. It may be noted from the graph data that there is more difference between predicted and actual outcomes than in XGBoost.

5.3 Random Forest (RF)

Figure 14 illustrates the experimental and RF-estimated values regarding the compressive strength of HSC. The R^2 value of 0.98 for RF depicts comparatively more accurate outcomes than the other models considered. Furthermore, the predicted results for the compressive strength of HSC for RF are precise out of the ensemble models employed. Figure 15 presents the dispersal among RF-estimated and experimental outcomes and error values for the compressive strength of HSC. Notably, 95.16% of the entire error values are below 5 MPa, and 4.83% of remaining values are from 5–10 MPa; notably, no value is above 10 MPa. The higher R^2 values of the RF algorithm for the compressive strength of HSC demonstrates better accuracy. Thus, more accurate prediction results can be achieved by utilizing RF than the other models.

In addition, Figure 16 displays the statistical analysis in the form of a box plot, which exhibits the minimum, mean, median, maximum, first quartile, and third quartile values for both the actual and RF-predicted values. According to the box plot, the median value for the actual dataset is 51.34 MPa, while the median value for the predicted dataset is 51.89 MPa. This suggests that the model performs reasonably well in predicting the target variable, as the difference between the two median values is small. The output for the RF model in the case of predicted and actual values is closer, unlike XGBoost and Adaboost.
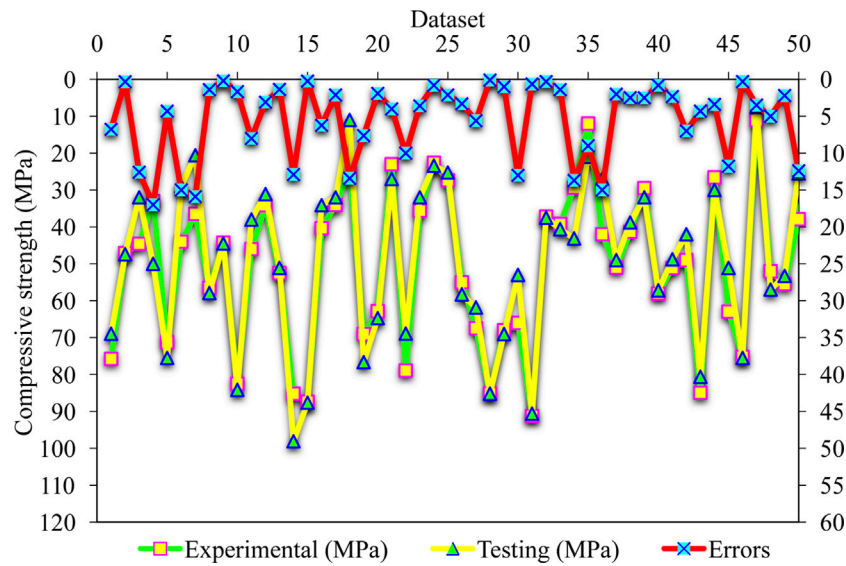
FIGURE 12
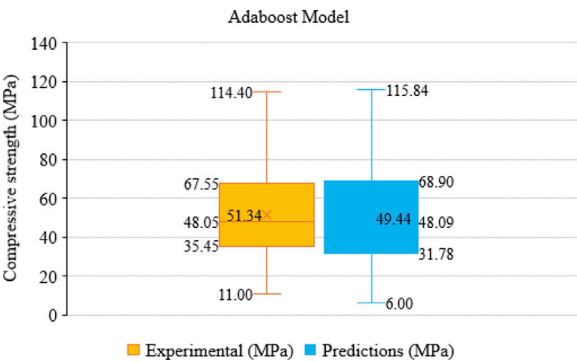Adaboost estimated and experimental values distribution with errors.

FIGURE 13
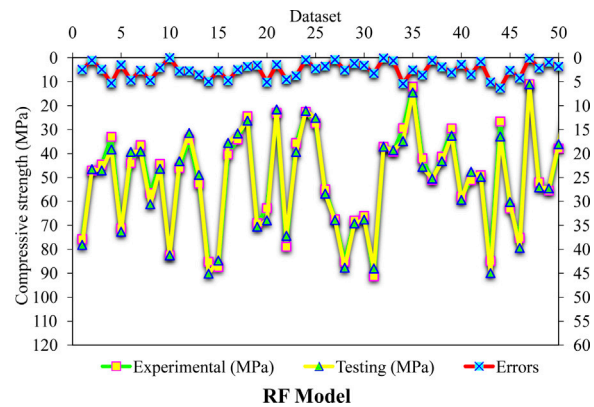Box plot for Adaboost predicted and actual results.

FIGURE 15
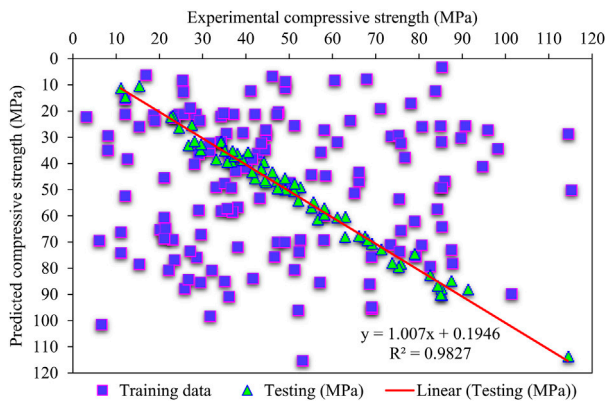RF estimated and experimental values distribution with errors.

FIGURE 14
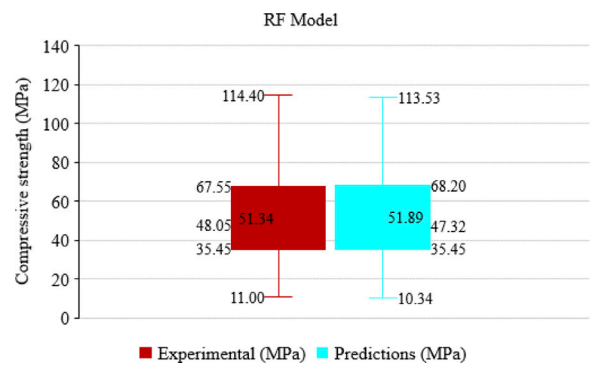RF predicted and experimental results.

FIGURE 16
Box plot for actual and RF predicted results.

TABLE 1 Statistical analysis for XGBoost, Adaboost, and RF algorithms.

Statistical checks	Techniques		
	XGBoost	Adaboost	RF
R^2	0.94	0.90	0.98
MAE (MPa)	4.7	5.7	2.5
RMSE (MPa)	5.4	7.5	3.0
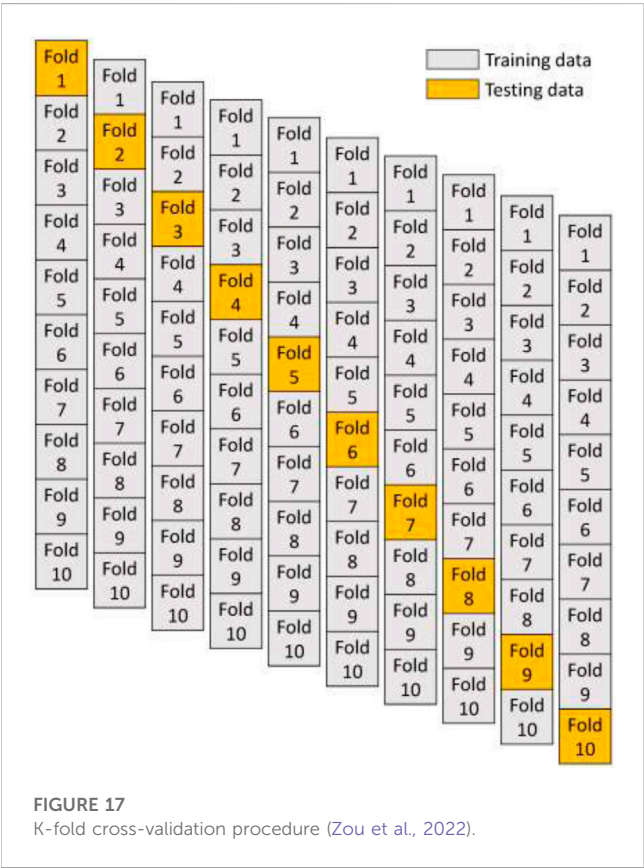
FIGURE 17
K-fold cross-validation procedure (Zou et al., 2022).

FIGURE 18
Statistical analysis: (A) XGBoost; (B) Adaboost; (C) RF.

5.4 Comparison of models

This study employs the k-fold approach to validate the implemented algorithm. In the literature (Amin et al., 2022a; Khan et al., 2022a; 2022b; Zou et al., 2022), the statistical analysis is reported to assess the model's performance. Usually, data splitting into ten subgroups is carried out for the random dispersion to perform the k-fold process for cross-validation; this approach is repeated ten times to achieve outcomes in a satisfactory range, as shown in Figure 17. Table 1 presents the statistical checks of all the used algorithms. For RF, the R^2 value is 0.98; in Adaboost, the R^2 value is 0.90; for XGBoost, it is 0.94 (Figures 18A–C). The R^2 value for the RF model is higher with lower error values compared to the other considered algorithms to estimate the compressive strength of HSC.

The compressive strength of HSC is predicted by applying ensemble ML techniques in the current work for reliable and efficient outcomes. The R^2 value of RF as 0.98 depicts a more accurate prediction for the compressive strength of HSC. Figures 19A–C show the RF model's superiority for predicting the compressive strength of HSC using a single optimized algorithm from 20 sub-models. Hence, it is concluded that RF has more accuracy and less error than all other algorithms.

5.5 Improved machine learning models' explainability

The current research work indicates an enhanced explanation of the ML algorithms employed along with the interactions of input
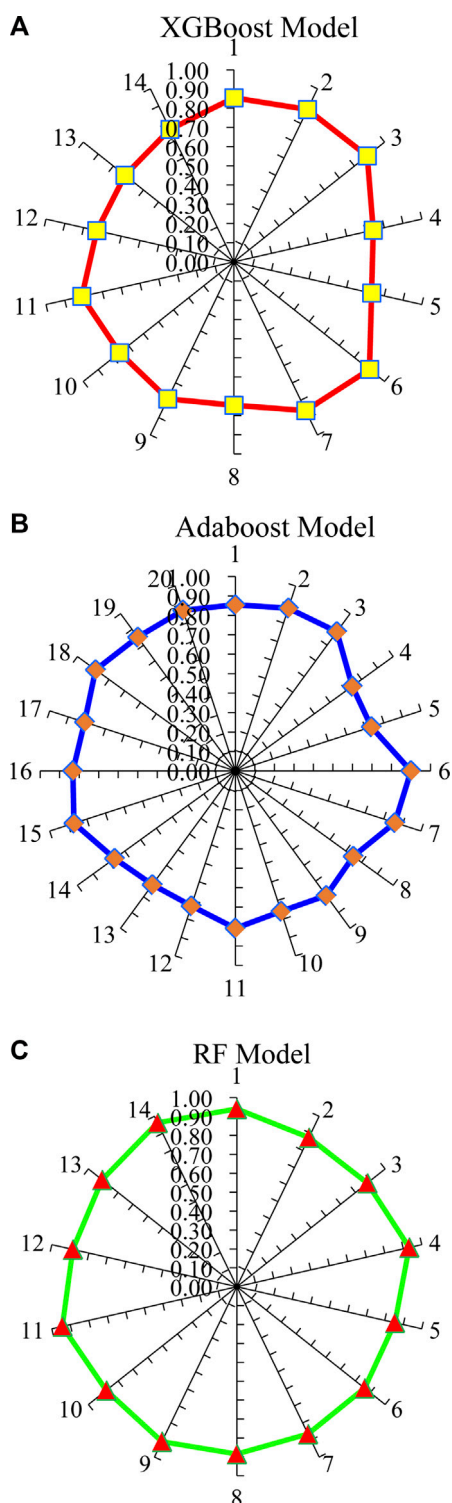
FIGURE 19
Results of sub-models: **(A)** XGBoost; **(B)** Adaboost; **(C)** RF.

here the algorithm is demonstrated for the compressive strength of HSC through the SHAP analysis. The correlation of features with the SHAP values for the strength of HSC is presented in Figure 20. It is notable that the temperature feature is extremely higher in terms of the SHAP values. This depicts that temperature significantly influences the compressive strength of HSC. Increased temperature tends to cause a reduction in the compressive strength. Fine and coarse aggregates also considerably influence the compressive strength of HSC, followed by temperature. As the greater quantity of aggregates offers more matrix interface, this loses its bonding upon heating, resulting in shrinkage cracks and ultimately reducing the compressive strength. Afterward, there is a cement feature which positively influences the compressive strength of HSC. Increasing cement content will thus enhance the compressive strength of HSC. Water indirectly influences the compressive strength of HSC. The strength of the composite is reduced due to a higher water–cement ratio and increased pore water pressure, resulting in excessive cracking and explosive spalling. Increased water content would result in decreased strength of HSC. Fly ash positively influences the strength of HSC as further hydration is achieved. Similarly, super plasticizers, silica fume, and nano-silica also have slight but positive influences on the compressive strength of HSC.

The interaction of the features with the compressive strength of HSC is illustrated in Figure 21. Figure 21A depicts the cement feature interaction, which directly influences the strength of HSC. The negative influence of water is observed for the compressive strength of HSC (Figure 21B). In this case, the inverse relation with the compressive strength of HSC is noted. The fine aggregate feature dependency is shown in Figure 21C: the impact of fine aggregates on silica fume also demonstrates a negative influence, resulting in decreased compressive strength of HSC. Thereafter, both positive and negative influences are witnessed in the coarse aggregate feature and are dependent on content (Figure 21D). Therefore, up to optimal content, coarse aggregates would contribute to the compressive strength of HSC and thence reduce the strength. The fly ash, super plasticizer, and silica fume interaction plots are presented in Figures 21E–G. In these three plots, the direct/ positive influence of all said features is depicted for the compressive strength of HSC. However, in the case of the temperature feature plot (Figure 21H), an inverse relation of temperature is reported with the compressive strength of HSC.

6 Discussion

The use of advanced predictive modeling techniques has become significantly popular in recent years (Chen et al., 2022; Wang et al., 2022; Amin et al., 2023; Nazar et al., 2023a; 2023b). Numerous studies have employed ML algorithms such as Gene Expression Programming, Bagging Regressor, AdaBoost, and RF to predict the compressive, splitting-tensile, and shear strengths of various composites, including geopolymer concrete, recycled aggregate concrete, ultra-high-performance concrete, and rice husk ash concrete. Table 2 summarizes these studies, highlighting the ML algorithms used and the properties predicted for various cementitious composites. The comparison allows for an assessment of the efficiency and reliability of the algorithms employed in this study compared to other literature

features. The SHAP analysis on the entire dataset presents an improved feature that influences global representation due to mergence with local SHAP explanations. The RF algorithm offers the most accurate prediction for the compressive strength of HSC, so
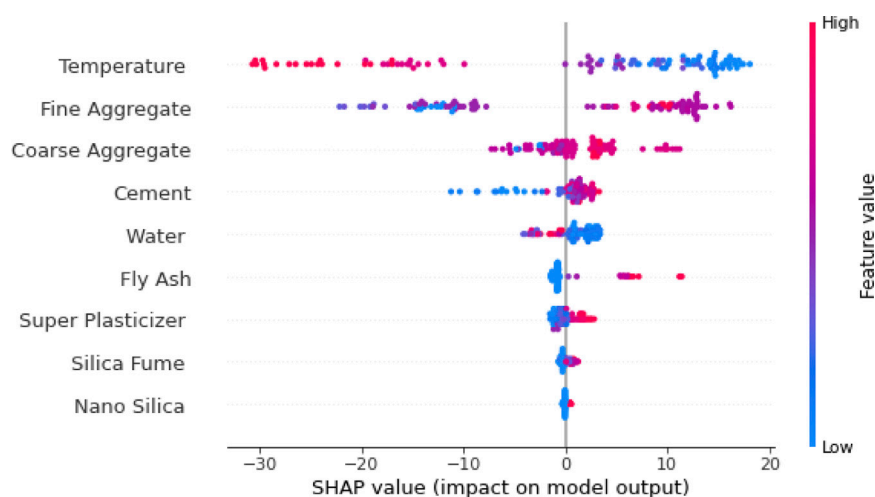
FIGURE 20
SHAP plot.

studies. The RF model in this study produces the R^2 value of 0.98, indicating a high level of precision in predicting the compressive strength of HSC. Overall, Table 2 signifies that the RF model provides relatively accurate predictions, consistent with the literature. It is worth noting that, after RF, the XGBoost and GB algorithms exhibit greater precision than the other algorithms. In our study, XGBoost also performed well after RF, with the R^2 value of 0.94, and AdaBoost demonstrated the acceptable R^2 value of 0.90. Thus, the use of ML algorithms indicates significant potential for predicting the mechanical properties of various cementitious composites. The results of this study demonstrate the effectiveness of the RF, XGBoost, and AdaBoost algorithms in predicting the compressive strength of HSC, with RF showing the highest level of precision. These findings suggest that ML techniques can be a valuable tool in the field of concrete, offering a reliable and efficient method for predicting the properties of HSC.

7 Conclusion

In the construction industry, the utilization of ML methodologies is increasingly recognized as a promising approach for predicting the concrete's mechanical characteristics. The current study's primary aim is to assess the precision of ML techniques to estimate the compressive strength of HSC at elevated temperatures. To predict the compressive strength of HSC using ML algorithms, various input parameters are considered predictor variables. The following points are concluded.

- The R^2 value of 0.98 for the RF algorithm depicts its precision in predicting the compressive strength of HSC. However, in ensemble XGBoost and Adaboost ML algorithms, the R^2 values are 0.94 and 0.90, respectively, showing lesser accuracy in predicting the compressive strength of HSC.

- By utilizing 20 sub-algorithms within a range of 10–200 estimates, the optimal compressive strength of HSC is predicted. The RF ensemble model is comparatively more accurate in predicting the compressive strength of HSC than the other algorithms considered.

- It is revealed from the k-fold test results that the RF and XGBoost algorithms show lesser RMSE and MAE values and greater R^2 values in case of the compressive strength of HSC than the other algorithms. At the same time, RF has the highest prediction accuracy to predict the strength of HSC.

- The efficiency of the models employed is also assessed with the help of statistical measures such as MAE and RMSE. Higher coefficient of determination values and lower error values indicate that RF is more accurate than XGBoost and AdaBoost in predicting the compressive strength of HSC.

- From all the applied ML approaches, RF is the most accurate approach for precise prediction of the compressive strength of HSC.

- According to the SHAP analysis, temperature features have the greatest impact on the strength of HSC, followed by the contributions of fine and coarse aggregates, cement, water, fly ash, super plasticizer, and silica fume. However, nano-silica has the least influence on the prediction of the compressive strength of HSC.

- The compressive strength of HSC is positively and negatively affected by cement and temperature, respectively, as extracted from the feature interaction plot.

- Further investigation is required to examine the load–slip modeling of HSC, specifically regarding the age of the matrix and strength.

To improve the effectiveness of HSC modeling with respect to the age of the matrix and strength, future studies could focus
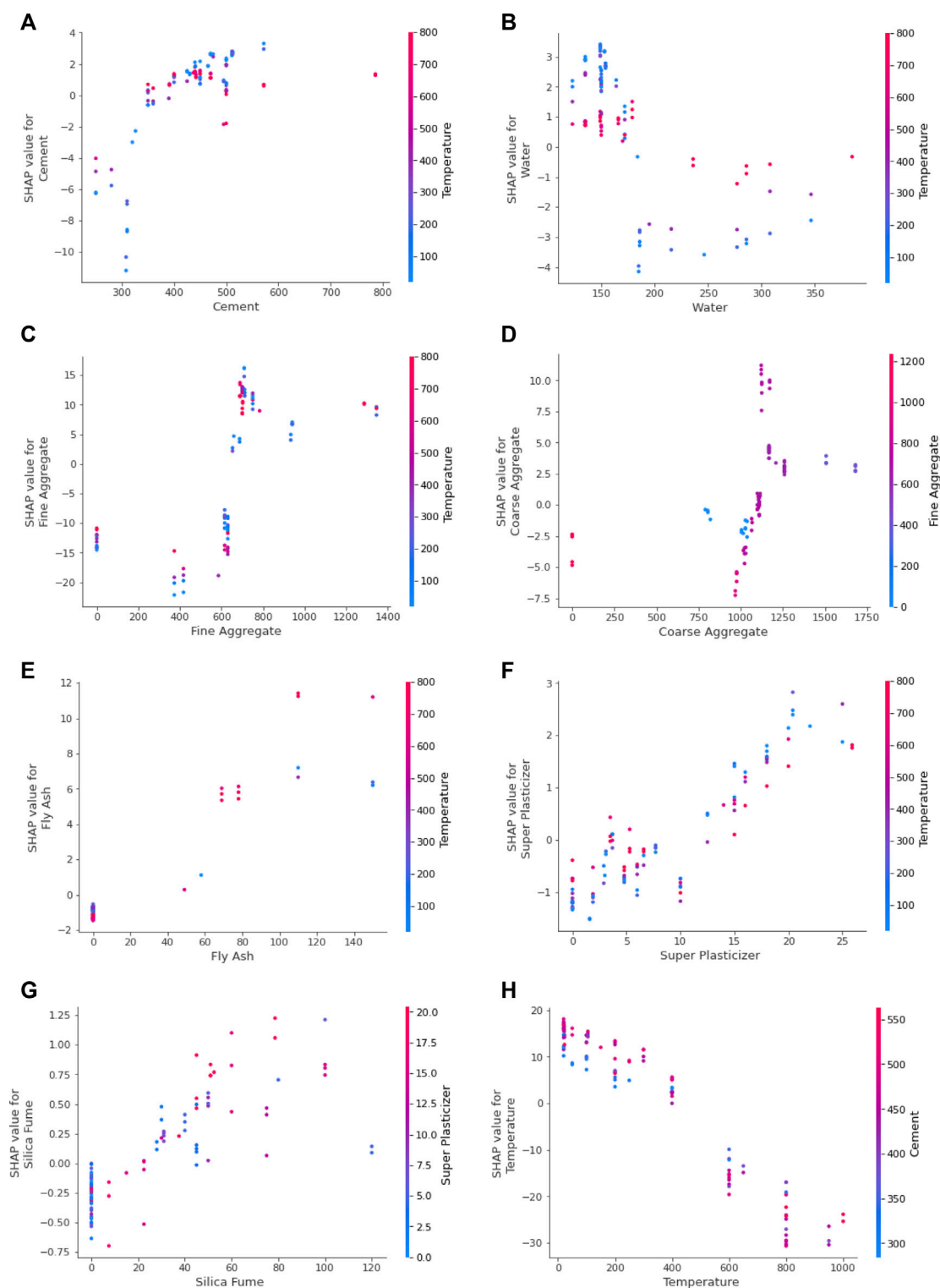
FIGURE 21
Feature interaction plot: **(A)** cement, **(B)** water, **(C)** fine aggregate, **(D)** coarse aggregate, **(E)** fly ash, **(F)** super plasticizer, **(G)** silica fume, and **(H)** temperature.

on employing deep learning algorithms due to their ability to handle complex and non-linear relationships. Additionally, the use of deep learning in conjunction with metaheuristic

optimization techniques can further increase the accuracy of predictions and enhance the overall modeling process. It is also recommended that a larger and more comprehensive dataset be

TABLE 2 Summary of prediction models in the current study and in the literature.

References	Material description	ML approaches	R^2
Current study	High-strength concrete (HSC)	Random Forest (RF)	0.98
Current study	High-strength concrete (HSC)	Extreme Gradient Bosting (XGBoost)	0.94
Current study	High-strength concrete (HSC)	Adaptive Boosting (Adaboost)	0.90
Ahmad et al. (2021)	High-strength concrete (HSC)	Decision Tree (DT)	0.83
Ahmad et al. (2021)	High-strength concrete (HSC)	Artificial Neural Network (ANN)	0.82
Zou et al. (2022)	Geopolymer concrete	Decision Tree (DT)	0.88
Ahmad et al. (2021)	Fly ash concrete	Decision Tree (DT)	0.83
Khan et al. (2022b)	Waste marble powder concrete (WMC)	Adaptive Boosting (AdaBoost)	0.91
Amin et al. (2022a)	Recycled coarse aggregate concrete (RCAC)	Gradient Bosting (GB)	0.94
Khan et al. (2022a)	Fly ash concrete	Bootstrap Aggregation (BA)	0.93
Amin et al. (2022b)	Geopolymer concrete	Multiple Layer Perceptron Neural Network (MLPNN)	0.81
Amin et al. (2022b)	Geopolymer concrete	Support Vector Machine (SVM)	0.78

utilized to train and test the deep learning models to achieve better results.

Data availability statement

The original contributions presented in the study are included in the article/Supplementary material; further inquiries can be directed to the corresponding authors.

Author contributions

GC: conceptualization, methodology, resources, writing—original draft, and project administration. SS: investigation, software, methodology, and writing—review and editing. AB: conceptualization, methodology, investigation, software, validation, formal analysis, resources, writing—original draft, writing—review and editing, and project administration. MS:

methodology, investigation, validation, and writing—review and editing. MA: validation, formal analysis, resources, and writing—review and editing.

Conflict of interest

The authors declare that the research was conducted in the absence of any commercial or financial relationships that could be construed as a potential conflict of interest.

Publisher's note

All claims expressed in this article are solely those of the authors and do not necessarily represent those of their affiliated organizations, or those of the publisher, the editors, and the reviewers. Any product that may be evaluated in this article, or claim that may be made by its manufacturer, is not guaranteed or endorsed by the publisher.

References

Afzal, M. T., and Khushnood, R. A. (2021). Influence of carbon nano fibers (CNF) on the performance of high strength concrete exposed to elevated temperatures. *Constr. Build. Mater.* 268, 121108. doi:10.1016/j.conbuildmat.2020.121108

Ahmad, A., Ostrowski, K. A., Maślak, M., Farooq, F., Mehmood, I., and Nafees, A. (2021). Comparative study of supervised machine learning algorithms for predicting the compressive strength of concrete at high temperature. *Materials* 14, 4222. doi:10.3390/ma14154222

Ahmad, M. R., Das, C. S., Khan, M., and Dai, J.-G. (2023). Development of low-carbon alkali-activated materials solely activated by flue gas residues (FGR) waste from incineration plants. *J. Clean. Prod.* 397, 136597. doi:10.1016/j.jclepro.2023.136597

Alfahdawi, I. H., Osman, S., Hamid, R., and Al-Hadithi, A. I. (2019). Influence of PET wastes on the environment and high strength concrete properties exposed to high temperatures. *Constr. Build. Mater.* 225, 358–370. doi:10.1016/j.conbuildmat.2019.07.214

Al-Shamiri, A. K., Kim, J. H., Yuan, T.-F., and Yoon, Y. S. (2019). Modeling the compressive strength of high-strength concrete: An extreme learning approach. *Constr. Build. Mater.* 208, 204–219. doi:10.1016/j.conbuildmat.2019.02.165

Amin, M. N., Ahmad, W., Khan, K., Ahmad, A., Nazar, S., and Alabdullah, A. A. (2022a). Use of artificial intelligence for predicting parameters of sustainable concrete and raw ingredient effects and interactions. *Materials* 15, 5207. doi:10.3390/ma15155207

Amin, M. N., Khan, K., Ahmad, W., Javed, M. F., Qureshi, H. J., Saleem, M. U., et al. (2022b). Compressive strength estimation of geopolymer composites through novel computational approaches. *Polymers* 14, 2128. doi:10.3390/polym14102128

Amin, M. N., Iftikhar, B., Khan, K., Javed, M. F., Abuarab, A. M., and Rehman, M. F. (2023). Prediction model for rice husk ash concrete using AI approach: Boosting and bagging algorithms. *Structures* 50, 745–757. doi:10.1016/j.istruc.2023.02.080

Amjad, M., Ahmad, I., Ahmad, M., Wróblewski, P., Kamiński, P., and Amjad, U. (2022). Prediction of pile bearing capacity using XGBoost algorithm: Modeling and performance evaluation. *Appl. Sci.* 12, 2126. doi:10.3390/app12042126

Arshad, S., Sharif, M. B., Irfan-Ul-Hassan, M., Khan, M., and Zhang, J.-L. (2020). Efficiency of supplementary cementitious materials and natural fiber on mechanical performance of concrete. *Arabian J. Sci. Eng.* 45, 8577–8589. doi:10.1007/s13369-020-04769-z

Asghari, Y., Sadeghian, G., Mohammadyan-Yasouj, S. E., and Mirzaei, E. (2023). Forecast of modern concrete properties using machine learning methods, *Artificial intelligence in mechatronics and civil engineering: Bridging the gap*, 167–205.

Bastami, M., Baghbadrani, M., and Aslani, F. (2014). Performance of nano-silica modified high strength concrete at elevated temperatures. *Constr. Build. Mater.* 68, 402–408. doi:10.1016/j.conbuildmat.2014.06.026

Bilodeau, A., Kodur, V., and Hoff, G. (2004). Optimization of the type and amount of polypropylene fibres for preventing the spalling of lightweight concrete subjected to hydrocarbon fire. *Cem. Concr. Compos.* 26, 163–174. doi:10.1016/s0958-9465(03)00085-4

Cao, M., Mao, Y., Khan, M., Si, W., and Shen, S. (2018). Different testing methods for assessing the synthetic fiber distribution in cement-based composites. *Constr. Build. Mater.* 184, 128–142. doi:10.1016/j.conbuildmat.2018.06.207

Cao, M., Xie, C., Li, L., and Khan, M. (2019). Effect of different PVA and steel fiber length and content on mechanical properties of CaCO₃ whisker reinforced cementitious composites. *Mater. Construcción* 69, e200. doi:10.3989/mc.2019.12918

Carrasquillo, R. L., Nilson, A. H., and Slate, F. O. (1981). Properties of high strength concretto short-term loads. *J. Proc.* 78, 171–178. doi:10.14359/6914

Castelli, M., Vanneschi, L., and Silva, S. (2013). Prediction of high performance concrete strength using genetic programming with geometric semantic genetic operators. *Expert Syst. Appl.* 40, 6856–6862. doi:10.1016/j.eswa.2013.06.037

Chaabene, W. B., Flah, M., and Nehdi, M. L. (2020). Machine learning prediction of mechanical properties of concrete: Critical review. *Constr. Build. Mater.* 260, 119889. doi:10.1016/j.conbuildmat.2020.119889

Chen, T., and Guestrin, C. (2016). "Xgboost: A scalable tree boosting system," in Proceedings of the 22nd acm sigkdd international conference on knowledge discovery and data mining, August 2016, 785–794.

Chen, L., Fang, Q., Jiang, X., Ruan, Z., and Hong, J. (2015). Combined effects of high temperature and high strain rate on normal weight concrete. *Int. J. Impact Eng.* 86, 40–56. doi:10.1016/j.ijimpeng.2015.07.002

Chen, J., Tong, H., Yuan, J., Fang, Y., and Gu, R. (2022). Permeability prediction model modified on kozeny-carman for building foundation of clay soil. *Buildings* 12, 1798. doi:10.3390/buildings12111798

Cülfik, M. S., and Özturan, T. (2010). Mechanical properties of normal and high strength concretes subjected to high temperatures and using image analysis to detect bond deteriorations. *Constr. Build. Mater.* 24, 1486–1493. doi:10.1016/j.conbuildmat.2010.01.020

Dong, H., Linghu, J., and Nie, Y. (2023a). Integrated wavelet-learning method for macroscopic mechanical properties prediction of concrete composites with hierarchical random configurations. *Compos. Struct.* 304, 116357. doi:10.1016/j.compstruct.2022.116357

Dong, Z., Quan, W., Ma, X., Li, X., and Zhou, J. (2023b). Asymptotic homogenization of effective thermal-elastic properties of concrete considering its three-dimensional mesostructure. *Comput. Struct.* 279, 106970. doi:10.1016/j.compstruc.2022.106970

Duan, Z. H., Kou, S. C., and Poon, C. S. (2013). Prediction of compressive strength of recycled aggregate concrete using artificial neural networks. *Constr. Build. Mater.* 40, 1200–1206. doi:10.1016/j.conbuildmat.2012.04.063

Ergün, A., Kürklü, G., Serhat, B. M., and Mansour, M. Y. (2013). The effect of cement dosage on mechanical properties of concrete exposed to high temperatures. *Fire Saf. J.* 55, 160–167. doi:10.1016/j.firesaf.2012.10.016

Friedman, J. H. (2001). Greedy function approximation: A gradient boosting machine. *Ann. statistics* 29, 1189–1232. doi:10.1214/aos/1013203451

Fu, Y., Wong, Y., Poon, C. S., and Tang, C. (2005). Stress–strain behaviour of high-strength concrete at elevated temperatures. *Mag. Concr. Res.* 57, 535–544. doi:10.1680/macr.2005.57.9.535

Han, Q., Gui, C., Xu, J., and Lacidogna, G. (2019). A generalized method to predict the compressive strength of high-performance concrete by improved random forest algorithm. *Constr. Build. Mater.* 226, 734–742. doi:10.1016/j.conbuildmat.2019.07.315

Huang, S., Huang, M., and Lyu, Y. (2021). Seismic performance analysis of a wind turbine with a monopile foundation affected by sea ice based on a simple numerical method. *Eng. Appl. Comput. fluid Mech.* 15, 1113–1133. doi:10.1080/19942060.2021.1939790

Huang, H., Li, M., Yuan, Y., and Bai, H. (2022). Theoretical analysis on the lateral drift of precast concrete frame with replaceable artificial controllable plastic hinges. *J. Build. Eng.* 62, 105386. doi:10.1016/j.jobe.2022.105386

Huang, H., Li, M., Yuan, Y., and Bai, H. (2023a). Experimental research on the seismic performance of precast concrete frame with replaceable artificial controllable plastic hinges. *J. Struct. Eng.* 149, 04022222. doi:10.1061/jsendh.steng-11648

Huang, Y., Huang, J., Zhang, W., and Liu, X. (2023b). Experimental and numerical study of hooked-end steel fiber-reinforced concrete based on the meso-and macro-models. *Compos. Struct.* 309, 116750. doi:10.1016/j.compstruct.2023.116750

Khaliq, W., and Kodur, V. (2018). Effectiveness of polypropylene and steel fibers in enhancing fire resistance of high-strength concrete columns. *J. Struct. Eng.* 144, 04017224. doi:10.1061/(asce)st.1943-541x.0001981

Khan, M., Cao, M., Xie, C., and Ali, M. (2021). Efficiency of basalt fiber length and content on mechanical and microstructural properties of hybrid fiber concrete. *Fatigue and Fract. Eng. Mater. Struct.* 44, 2135–2152. doi:10.1111/ffe.13483

Khan, K., Ahmad, A., Amin, M. N., Ahmad, W., Nazar, S., and Arab, A. M. A. (2022a). Comparative study of experimental and modeling of fly ash-based concrete. *Materials* 15, 3762. doi:10.3390/ma15113762

Khan, K., Ahmad, W., Amin, M. N., Ahmad, A., Nazar, S., Alabdullah, A. A., et al. (2022b). Exploring the use of waste marble powder in concrete and predicting its strength with different advanced algorithms. *Materials* 15, 4108. doi:10.3390/ma15124108

Khan, M., Cao, M., Chaopeng, X., and Ali, M. (2022c). Experimental and analytical study of hybrid fiber reinforced concrete prepared with basalt fiber under high temperature. *Fire Mater.* 46, 205–226. doi:10.1002/fam.2968

Khan, M., Lao, J., and Dai, J.-G. (2022d). Comparative study of advanced computational techniques for estimating the compressive strength of UHPC. *J. Asian Concr. Fed.* 8, 51–68. doi:10.18702/acf.2022.6.8.1.51

Kushnir, A. R., Heap, M. J., Griffiths, L., Wadsworth, F. B., Langella, A., Baud, P., et al. (2021). The fire resistance of high-strength concrete containing natural zeolites. *Cem. Concr. Compos.* 116, 103897. doi:10.1016/j.cemconcomp.2020.103897

Lalu, O., Darmon, R., and Lennon, T. (2021). "Spalling of high strength concrete in fire," in *IOP conference series: Materials science and engineering* (Bristol, England: IOP Publishing), 012027.

Laneyrie, C., Beaucour, A.-L., Green, M. F., Hebert, R. L., Ledesert, B., and Noumowe, A. (2016). Influence of recycled coarse aggregates on normal and high performance concrete subjected to elevated temperatures. *Constr. Build. Mater.* 111, 368–378. doi:10.1016/j.conbuildmat.2016.02.056

Lao, J.-C., Huang, B.-T., Xu, L.-Y., Khan, M., Fang, Y., and Dai, J.-G. (2023a). Seawater sea-sand Engineered Geopolymer Composites (EGC) with high strength and high ductility. *Cem. Concr. Compos.* 138, 104998. doi:10.1016/j.cemconcomp.2023.104998

Lao, J.-C., Xu, L.-Y., Huang, B.-T., Zhu, J.-X., Khan, M., and Dai, J.-G. (2023b). Utilization of sodium carbonate activator in strain-hardening ultra-high-performance geopolymer concrete (SH-uhpgc). *Front. Mater.* 10, 1–12. doi:10.3389/fmats.2023.1142237

Li, L., Khan, M., Bai, C., and Shi, K. (2021). Uniaxial tensile behavior, flexural properties, empirical calculation and microstructure of multi-scale fiber reinforced cement-based material at elevated temperature. *Materials* 14, 1827. doi:10.3390/ma14081827

Lundberg, S. M., and Lee, S.-I. (2017). A unified approach to interpreting model predictions. *Adv. neural Inf. Process. Syst.* 30. Available at: https://arxiv.org/abs/1705.07874.

Lundberg, S. M., Erion, G., Chen, H., Degrave, A., Prutkin, J. M., Nair, B., et al. (2020). From local explanations to global understanding with explainable AI for trees. *Nat. Mach. Intell.* 2, 56–67. doi:10.1038/s42256-019-0138-9

Lundberg, S. (2021). *A game theoretic approach to explain the output of any machine learning model*. San Francisco: Github.

Marani, A., and Nehdi, M. L. (2020). Machine learning prediction of compressive strength for phase change materials integrated cementitious composites. *Constr. Build. Mater.* 265, 120286. doi:10.1016/j.conbuildmat.2020.120286

Molnar, C. (2020). *Interpretable machine learning*. NC, United States: Lulu. com.

Mousa, M. I. (2017). Effect of elevated temperature on the properties of silica fume and recycled rubber-filled high strength concretes (RHSC). *HBRC J.* 13, 1–7. doi:10.1016/j.hbrcj.2015.03.002

Nazar, S., Yang, J., Amin, M. N., Khan, K., Ashraf, M., Aslam, F., et al. (2023a). Machine learning interpretable-prediction models to evaluate the slump and strength of fly ash-based geopolymer. *J. Mater. Res. Technol.* 24, 100–124. doi:10.1016/j.jmrt.2023.02.180

Nazar, S., Yang, J., Javed, M. F., Khan, K., Li, L., and Liu, Q.-F. (2023b). An evolutionary machine learning-based model to estimate the rheological parameters of fresh concrete. *Structures* 48, 1670–1683. doi:10.1016/j.istruc.2023.01.019

Ozawa, M., Sakoi, Y., Fujimoto, K., Tetsura, K., and Parajuli, S. S. (2017). Estimation of chloride diffusion coefficients of high-strength concrete with synthetic fibres after fire exposure. *Constr. Build. Mater.* 143, 322–329. doi:10.1016/j.conbuildmat.2017.03.117

Qian, L.-P., Ahmad, M. R., Lao, J.-C., and Dai, J.-G. (2023). Recycling of red mud and flue gas residues in geopolymer aggregates (GPA) for sustainable concrete. *Resour. Conservation Recycl.* 191, 106893. doi:10.1016/j.resconrec.2023.106893

Ramadan Suleiman, A., and Nehdi, M. L. (2017). Modeling self-healing of concrete using hybrid genetic algorithm–artificial neural network. *Materials* 10, 135. doi:10.3390/ma10020135

Riaz Ahmad, M., Khan, M., Wang, A., Zhang, Z., and Dai, J.-G. (2023). Alkali-activated materials partially activated using flue gas residues: An insight into reaction products. *Constr. Build. Mater.* 371, 130760. doi:10.1016/j.conbuildmat.2023.130760

Sami, B. H. Z., Sami, B. F. Z., Kumar, P., Ahmed, A. N., Amieghemen, G. E., Sherif, M. M., et al. (2023). Feasibility analysis for predicting the compressive and tensile strength of concrete using machine learning algorithms. *Case Stud. Constr. Mater.* 18, e01893. doi:10.1016/j.cscm.2023.e01893

Shaqadan, A. (2016). Prediction of concrete mix strength using random forest model. *Int. J. Appl. Eng. Res.* 11, 11024–11029.

Shen, Z., Deifalla, A. F., Kamiński, P., and Dyczko, A. (2022). Compressive strength evaluation of ultra-high-strength concrete by machine learning. *Materials* 15, 3523. doi:10.3390/ma15103523

Shi, T., Liu, Y., Hu, Z., Cen, M., Zeng, C., Xu, J., et al. (2022). Deformation performance and fracture toughness of carbon nanofiber-modified cement-based materials. *ACI Mater. J.* 119.

Sun, L., Wang, C., Zhang, C., Yang, Z., Li, C., and Qiao, P. (2023). Experimental investigation on the bond performance of sea sand coral concrete with FRP bar reinforcement for marine environments. *Adv. Struct. Eng.* 26, 533–546. doi:10.1177/13694332221131153

Wang, C., Xu, S., and Yang, J. (2021). Adaboost algorithm in artificial intelligence for optimizing the IRI prediction accuracy of asphalt concrete pavement. *Sensors* 21, 5682. doi:10.3390/s21175682

Wang, Q., Hussain, A., Farooqi, M. U., and Deifalla, A. F. (2022). Artificial intelligence-based estimation of ultra-high-strength concrete's flexural property. *Case Stud. Constr. Mater.* 17, e01243. doi:10.1016/j.cscm.2022.e01243

Wróblewski, R., and Stawiski, B. (2020). Ultrasonic assessment of the concrete residual strength after a real fire exposure. *Buildings* 10, 154. doi:10.3390/buildings10090154

Xie, C., Cao, M., Khan, M., Yin, H., and Guan, J. (2021). Review on different testing methods and factors affecting fracture properties of fiber reinforced cementitious composites. *Constr. Build. Mater.* 273, 121766. doi:10.1016/j.conbuildmat.2020.121766

Xiong, M.-X., and Liew, J. R. (2020). Buckling behavior of circular steel tubes infilled with C170/185 ultra-high-strength concrete under fire. *Eng. Struct.* 212, 110523. doi:10.1016/j.engstruct.2020.110523

Xiong, Y., Deng, S., and Wu, D. (2016). Experimental study on compressive strength recovery effect of fire-damaged high strength concrete after realkalisation treatment. *Procedia Eng.* 135, 476–481. doi:10.1016/j.proeng.2016.01.158

Xu, Y., Ahmad, W., Ahmad, A., Ostrowski, K. A., Dudek, M., Aslam, F., et al. (2021). Computation of high-performance concrete compressive strength using standalone and ensembled machine learning techniques. *Materials* 14, 7034. doi:10.3390/ma14227034

Zhang, J., Ma, G., Huang, Y., Aslani, F., and Nener, B. (2019). Modelling uniaxial compressive strength of lightweight self-compacting concrete using random forest regression. *Constr. Build. Mater.* 210, 713–719. doi:10.1016/j.conbuildmat.2019.03.189

Zhang, J., Huang, Y., Aslani, F., Ma, G., and Nener, B. (2020). A hybrid intelligent system for designing optimal proportions of recycled aggregate concrete. *J. Clean. Prod.* 273, 122922. doi:10.1016/j.jclepro.2020.122922

Zhang, C., Yin, Y., Yan, H., Zhu, S., Li, B., Hou, X., et al. (2023). Centrifuge modeling of multi-row stabilizing piles reinforced reservoir landslide with different row spacings. *Landslides* 20, 559–577. doi:10.1007/s10346-022-01994-5

Zou, Y., Zheng, C., Alzahrani, A. M., Ahmad, W., Ahmad, A., Mohamed, A. M., et al. (2022). Evaluation of artificial intelligence methods to estimate the compressive strength of geopolymers. *Gels* 8, 271. doi:10.3390/gels8050271

Study on the effect of mineral admixtures on working and mechanical properties of the grouting material

Quanjun Shen[1], Ruishuang Jiang[2,3]*, Bori Cong[1], Baolin Guo[2,3], Hongfa Shang[1] and Xiaoge Ji[1]

[1]Shangdong Hi-Speed Group Innovation Research Institute, Jinan, China, [2]Shandong Transportation Institute, Jinan, China, [3]Shandong Engineering Laboratory of Bridge-Tunnel Performance Evaluation and Durability Promotion, Jinan, China

Aiming at the existing grouting material, there are a series of problems such as poor fluidity of the grouting, rapid loss of fluidity, non-compactness of the grouting after hardening, gaps or holes, and the like. In this paper, fly ash, limestone powder, and silica fume are used to replace cement, and the influence of mineral admixtures on the fluidity, rheological properties, and strength of the grouting material are systematically studied. The experiment found that: fly ash, limestone powder, and silica fume can all improve the fluidity of the grouting material, and the effect of fly ash is the best. Compared with pure cement grouting, the initial fluidity and 60 min fluidity of the grouting material mixed with 40 wt% fly ash were reduced by 35.5% and 53.8% respectively. Fly ash and limestone powder mixed into the grouting material will significantly improve the rheological properties, while silica fume will reduce the flow properties of the grouting. The addition of fly ash and limestone powder will reduce the mechanical properties of the grouting material, while silica fume can improve the mechanical properties of the grouting material. Compared with pure cement grouting, the 28 days compressive strength with 4 wt% limestone powder grouting material is reduced by 4.5%, and the flexural strength is reduced by 6%; the 28 days compressive strength with 4 wt% silica fume grouting material is increased by 6.5%, the flexural strength increased by 1%.

KEYWORDS

mineral admixture, working performance, mechanical properties, bleeding, dosage, grouting material

1 Introduction

In recent years, the construction of highway bridges in our country has developed rapidly. The design and construction of long-span prestressed concrete bridges have become a popular trend. Prestressed concrete technology has the advantages of using high strength materials, promoting the lightweight structure, with large span ability, and effectively avoid concrete cracking. However, all the advantages of the prestressed concrete bridge structure must be based on the integrity of the bond between the prestressed reinforcement and the structural concrete. According to the different characteristics of fabrication, design and construction, the prestressed concrete structure can be divided into pre-tensioning method and post-tensioning method. At present, the post-tensioning method has been widely used in the construction of highway bridges. The cantilever construction, site pouring and span construction mainly adopt the post-tensioning method. Duct grouting is an

important part of post-tensioning prestressed structure construction. It plays an important role in protecting prestressed reinforcement from harmful ion erosion. Moreover, it directly affects the overall stiffness and strength of the prestressed concrete component, making the prestressed reinforcement and surrounding concrete joint as a whole. To improve and ensure the quality of prestressed duct grouting, the quality of grouting material is the premise. It is necessary to choose the raw materials and optimize the mix ratio design. The performance of the grouting material is directly related to the durability of the post-tensioning prestressed concrete structure (Feng and Wang, 2012; Song et al., 2014a; Ba, 2018; Zhang et al., 2020; Tan et al., 2022).

Prestressed duct grouting material as an important construction material for prestressed structures, scholars have done a lot of research on it. Li (2011) prepared a new grouting material made of ordinary Portland cement and rapid hardened sulphoaluminate cement as the compound system, adding retarder (tartaric acid and boric acid) and early strength admixture (lithium carbonate). Due to the characteristics of high early strength and rapid hardening. Compared with the conventional grouting material, the prepared grouting material has higher early strength and better working performance. However, it is difficult to control the setting time, so it is proposed that the cementing material of prestressed grouting should not choose thioaluminate cement, but mainly ordinary silicic acid cement. Song et al. (2014b) improved the physical properties of grouting material by changing mixing parameters and replacing cement varieties. Cheng et al. (2014) explored the influence of volume deformation and submicrostructure of prestressed pore by adding plastic expansion agent. Li (Li et al., 2018) studied the influence of ultrafine calumonite on the performance of the grouting material. The study shows that the increase of the calcium increases the strength and setting time of the grouting material.

Xiang et al. (2018) studied the influence of limestone powder on the performance of the grouting material. The results show that in a certain range, the fluidity of the grouting material is gradually increased with the increase of limestone powder. Moreover, it has a positive effect on improving the strength of the grouting material and can inhibit the contraction of the grouting material in the later stage. Through microscopic testing and characterization, it is known that the strength increase is mainly due to the physical filling effect of limestone powder, which makes the interior more dense. The pozzolanic activity of limestone powder and other mineral admixture will also lead to the increase of the grouting material strength. Ma et al. (2021) studied the influence of gypsum on the fluidity, mechanical properties and shrinkage rate of the grouting material. The results show that when the gypsum ($CaSO_4$) exists simultaneously with the water-reducing agent, the adsorption and steric hindrance will improve the initial fluidity of the grouting material. At the same time, $CaSO_4$ can promote the generation of calcium sulfoaluminate in the hydration products, which improve the strength of the grouting material. In addition, the increase in the amount of calcium can fill the gap between hydration products, making the grouting material more dense and improve the stability of the grouting material. Masbin et al. formulated a prestressed grouting agent from fly ash, silicon ash, water-reducing agent, expansion agent, cellulose and defoaming agent (Shu et al., 2021a). The effects of various raw materials on the variability of compressive strength were studied through the test system. And the mix ratio was optimized by applying the Logit model. The test results show that the dosage of water-reducing agent and defoaming agent will increase the variability of the compressive strength of the grouting material. While silica fume, expansion agent

and cellulose will inhibit the variability of the compressive strength to some extent. The compressive strength of the optimized grouting material can reach more than 60 MPa in 7 days and 74 MPa in 28 days. Moreover, the data error of the same group is within 10%, and the variability is significantly reduced. Shu et al. (2021b) used fly ash (FA) or steel slag powder (SS) as raw material, and studied the influence of FA and SS on the fluidity and mechanical properties of grouting material. The results show that the optimal amounts of FA and SS were 40% and 20%. The grouting material containing 40% FA or 20% SS have good mobility and mechanical properties. Guan and Zhong (2013) deeply studied the physical and mechanical properties, rheological properties and microstructural changes of ultrafine high-performance grouting cement. The study shows that when the fly ash is mixed into the ultrafine cement, the fluidity of the grouting material can be greatly improved. Because the pozzolanic activity of the fly ash, it can improve the hardening strength of the late grouting material stage. The interior can be more dense, and the impermeability of the slurry can be enhanced.

Liu et al. (2023) prepared nano-silica (NS) -modified aqueous epoxy resin (WEP) by *in situ* polymerization and mixed it into the grouting material. The characteristics and microstructure of composite grouting material and the microscopic coordination mechanism of each slurry composition is analyzed. The results show that increasing the NS concentration in WEP can shorten the setting time and improve the stability of the composite grouting material. When the NS content in WEP was 4%, the compressive strength of the specimens increased by 33.71% at 3 days and 39.03% at 28 days. The composite material of NS and WEP can promote the production of the hydration products C-S-H and C-A-S-H, and promote the fine crystallization of the hydration products. Hydrated crystals were grown on NS of the WEP surface, thereby bridging the resin film and cement particles. Zhang et al. (2021) used polypropylene fiber (PP), polyvinyl fiber (PVA) and basalt fiber (BF) as a mixture of the grouting material, studied the fiber on the basic mechanical properties, toughness and the best content and length of each fiber. The results show that fiber is the ideal material to improve the toughness of the grouting material. The best content of each fiber in the grouting material is 0.5% (PP), 0.3% (BF) and 0.1% (PVA), and the best length is 9 mm (PP), 3 mm (BF) and 3 mm (PVA). The best content of each fiber in grouting material is 0.5% (PP), 0.3% (BF) and 0.1% (PVA), and the best length is 9 mm (PP), 3 mm (BF) and 3 mm (PVA).

Sun et al. (2020) introduced thioaluminate cement, hydroxypropyl methyl cellulose, lithium carbonate and calcium formate in the cementing system, and prepared the prestressed duct grouting material for railway that meets the requirements of JTG/TF 50-2011 "Technical Specification for Construction of Highway Bridge and Culverts" under the condition of −5°C. Yang et al. (2019) studied the effect of expansion agent on the limiting expansion rate of grouting material. The result shows that the rate of limiting expansion increased with the increase of expansion agent. In a certain dosage range, the expansion agent has an obvious effect on increasing the early limiting expansion rate of grouting material. Wang and Zhang (2017) developed a duct grouting material, which has high fluidity, small flow loss, micro expansion and no bleeding occur. They selected polycarboxylicacid water reducer, plastic expansion agent, defoaming agent as chemical admixture. By performing orthogonal test to optimize the raw materials and the mix ratio. The prepared duct grouting material meets the requirements of JTG/TF 50-2011 "Technical Specification for Construction of Highway Bridge and Culverts." He et al. (2023) proposed that the combination of superabsorbent polymer (SAP) and
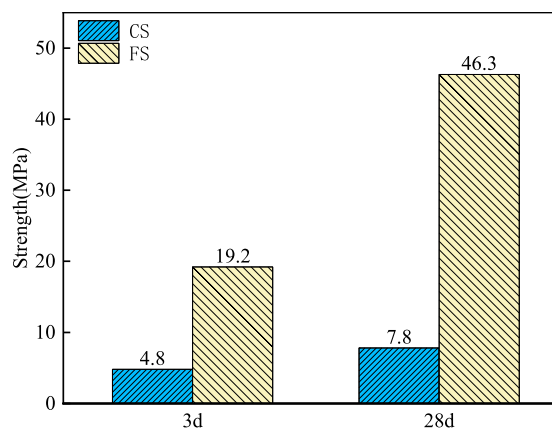
FIGURE 1
Mechanical properties of the selected cement.

the expansion agent can effectively reduce the shrinkage deformation of ultra-high strength cement-based grouting materials (UHS-CGM) in dry environment. Moreover, the effects of different SAP sizes and dosage on the compressive strength, inhibitory expansion rate, internal relative humidity (IRH) and hydration characteristics of UHS-CGM containing MgO expansion agent (MEA) were studied. And the composition and content of hydration products are analyzed by TG and XRD by SEM. The results show that SAP improved the hydration degree of UHS-CGM and the expansion efficiency of MEA, significantly improved the inhibitory expansion rate of UHS-CGM under standard curing and sealed curing. While reduced the compressive strength of UHS-CGM, which increased with the increasing size and dose of SAP.

At present, there is a comprehensive study on the addition of adding appropriate admixture to the grouting material and the optimization of the mix ratio of raw materials. But the existing research on the rheology or working performance of the grouting is less. Studying the rheological characteristics of grouting can provide a basis for adjusting the ratio of the grouting and controlling the preparation process of materials. Thus, improving the construction performance of the material and its physical and chemical properties as well as application effect. This paper combined with the test system of fly ash, limestone powder, silicon ash mineral admixture on the grouting material flowability, rheology, mechanical properties of the law, in order to improve the working performance and mechanical properties of the grouting material.

2 Experiment

2.1 Raw materials

The cement is P·O 42.5 cement from Shanshui Dongyue with a density of 3.10 g/cm³ and a specific surface area of 380 m²/kg. The fly ash is Beijing-taipei Grade I fly ash with a density of 2.2 g/cm³, a fineness of 5.9% and a loss on ignition of 2.1%, water requirement ratio 95%; Limestone powder; Sika water reducing agent, white powder, water reducing rate 27%, air content 2.4% (water reducing rate and air content 1%), expansion agent. The 3 and 28 days

compressive strength (CS) and flexural strength (FS) of the main cement materials used in this experiment are shown in Figure 1.

2.2 Specimen preparation

In the traditional sense, the vast majority of prestressed duct grouting materials is pure cement slurry. Only a certain amount of water reducing agent, expansion agent and thickening agent are added to prepare the duct grouting materials on site. The mixing is not sufficient and the influence of various factors makes the quality of the duct grouting materials can not be guaranteed. Thus, there are a series of problems such as poor fluidity, fast flow loss, large drainage rate of serous slurry, stratified segregation, uncompaction after slurry hardening, void or holes (Zhang et al., 2019; Chen et al., 2020; Ma et al., 2022; Mou et al., 2022; Wang et al., 2022). Therefore, this study is based on the literature review and previous experiments (Xie et al., 2020; Khan et al., 2021; Khan et al., 2022a; Khan et al., 2022b; Sha et al., 2023). The key parameters of water-binder ratio, water-reducing agent and expansion agent are determined in Table 1. On the basis of these parameters, the working state of the grouting material can be adjusted by adjusting the composition of the cementitious material and adding admixtures until the grouting material with excellent performance can be prepared. First, the test raw materials will be proportionally prepared dry mixture, and pre-mixing. Then first add water to the mixing pot, then add the dry mixture, then start the mixing device, from low-speed mixing (500 r/min, stirring 1 min) to high-speed full mixing (2,000 r/min, stirring 9 min, blade linear speed of 15 m/s).

The working performance (fluidity) of the mixed grouting was tested first, and then the grouting was poured into a 40 mm × 40 mm × 160 mm cement mortar triple die for molding. The grouting level was slightly higher than the test model height for the first time, to be the surface of the "Plastic" state after the collection. After the specimens for mechanical properties testing were finished, polyethylene film was applied to the surface of the specimens (as shown in Figure 2) and the molds were removed after indoor curing at a temperature of 20°C ± 2°C or 1 day, remove the mold and move to the concrete standard curing room for standard curing, until the specified age to take out the mechanical properties of the test.

2.3 Testing methods

2.3.1 Working performance
2.3.1.1 Liquidity
The working performance (fluidity) of the grouting material was tested in accordance with the "Test code for cement and cement concrete for highway engineering" (JTG E 30) (JTGE30-2005.2005-03-03, 2005) (as shown in Figure 2).

2.3.1.2 Rheological properties
The rheological properties of mortar were tested by BML rheometer.

2.3.2 Mechanical properties
The compressive strength and flexural strength of the grouting material at 3, 7, and 28 days were measured by automatic pressure testing machine for cement mortar strength. The test method was carried out according to "Testing method for strength of cement

TABLE 1 Mix ratio parameter.

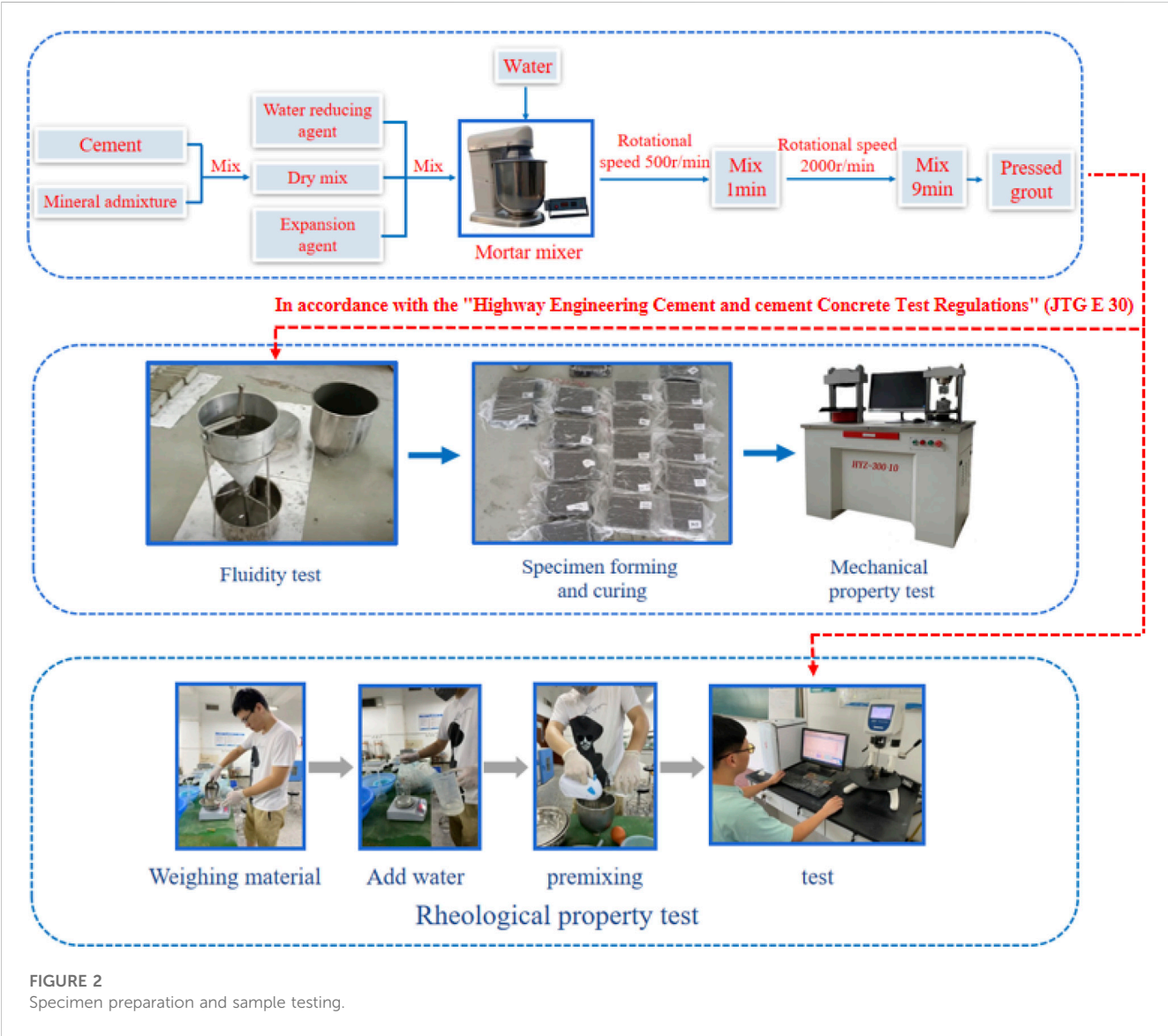| Water binder ratio	Water-reducing admixture (%)	Swelling agent (%)
0.28	0.3	0.03

FIGURE 2
Specimen preparation and sample testing.

mortar (ISO method)" (GB/T 17671) (Standardization Administration of China, 2009).

3 Results and discussions

3.1 The influence of mineral admixture on the working performance of the grouting material

3.1.1 Effect of fly ash on the fluidity of the grouting material

In order to study the effect of the content of fly ash on the working performance of the grouting, the same content of fly ash was used to replace 10 wt%, 20 wt%, 30 wt%, 40 wt%, 50 wt% of the cement. The test mix ratio and fluidity test results are shown in Table 2 and Figure 3.

Figure 3 reflects the effect of the amount of fly ash on the performance of the grouting material. It can be seen from Figure 3 that the fluidity of the grouting decreases with time. As the time increased from 0 to 60 mins, the fluidity of pure cement grouting increased from 31 to 52 s, and the fluidity increased by 67.7%. The fluidity of the grouting material mixed with 50 wt% fly ash increased from 23 to 24 s, and the fluidity increased by 4.35%. It can be seen that the addition of fly ash can significantly reduce the time loss of the grouting material. When the content of fly ash in the grouting material increases from 0 wt% to 40 wt%, the initial fluidity of the grouting material tends to decrease. However, when the content of

TABLE 2 Single test material amount (kg/m3).

Number	Cement	Fly ash	Water
SP1	1,660	0	465
SP2	1,494	166	465
SP3	1,328	332	465
SP4	1,162	498	465
SP5	996	664	465
SP6	830	830	465

TABLE 3 Single test material amount (kg/m³).

Number	Cement	Lime plaster	Water
SP1	1,660	0	465
SP7	1,577	83	465
SP8	1,494	166	465
SP9	1,328	332	465

FIGURE 3
Test results of the effect of fly ash on the working performance of the grouting material.

FIGURE 4
Test results of the effect of limestone powder on the working performance of the grouting material.

fly ash is 50 wt%, the initial fluidity of the grouting material increases. When the content of fly ash in the grouting material increases from 0 wt% to 50 wt%, the initial fluidity of the grouting material decreases from 31 to 23 s, a decrease of 25.8%, and the 60 min fluidity of the grouting material decreases from 52 to 24 s, a decrease of 53.8%. In summary, the addition of fly ash can effectively improve the working performance of the grouting material and reduce the loss of fluidity over time, but the dosage should not be too high.
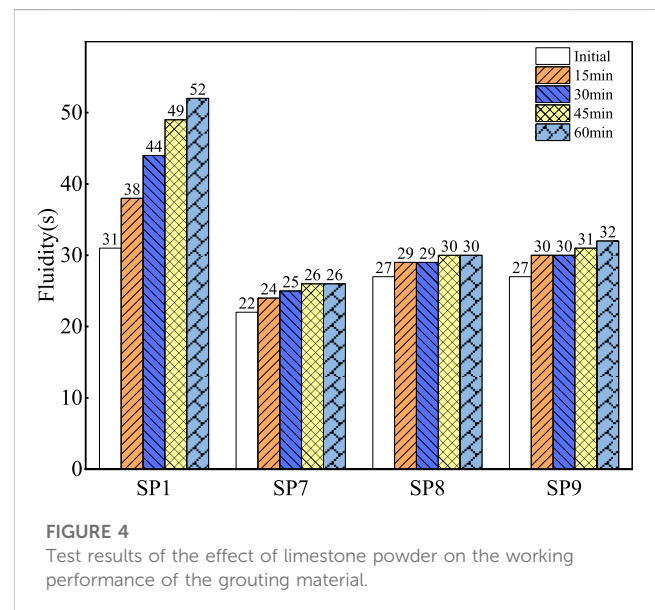
3.1.2 Effect of limestone powder on the fluidity of the grouting material

In order to study the effect of limestone powder on the working performance of the grouting material, an equal content of limestone was used to replace 5 wt% 10 wt%, and 20 wt% cement. The test mix ratio and fluidity test results are shown in Table 3 and Figure 4.

Figure 4 reflects the effect of adding limestone powder on the working performance of the grouting material. It can be seen from Figure 4 that the fluidity of the grouting decreases with time. The content of limestone powder increased from 0 wt% to 5 wt%, and the initial fluidity of the grouting material decreased from 31 to 22 s, a decrease of 29%. As the time increased from 0 to 60 mins, the fluidity of the grouting material decreased from 52 to 26 s, a decrease of 50%.

It can be seen that the incorporation of limestone powder can effectively improve the working performance of the grouting material and greatly reduce the loss of the fluidity of the grouting material over time. However, when the limestone powder content increased from 5 wt% to 20 wt%, the initial fluidity of the grouting material increased from 22 to 27 s, an increase of 23%. The fluidity of the grouting increased from 26 to 32 s at 60 min, an increase of 23%. In summary, limestone powder can significantly improve the fluidity of the grouting material and reduce the loss of fluidity of the grouting material over time. However, excessive limestone powder will inhibit the working performance of the grouting material, resulting in a decrease in the fluidity of the grouting material.

3.1.3 Effect of silica fume on the grouting material fluidity

In order to study the influence of silica fume on the performance of grouting material, an equal content of silica fume was used to replace 4 wt%, 5 wt%, and 6 wt% cement. The test mix ratio and fluidity test results are shown in Table 4 and Figure 5.

Figure 5 reflects the effect of silica fume on the performance of the grouting material. It can be seen from Figure 5 that with 4 wt% silica fume, the initial fluidity of the grouting decreased from 31 to 26 s, a decrease of 16%. And the 60 min fluidity decreased from 52 to 31 s, a decrease of 41%. Silica fume can improve the working

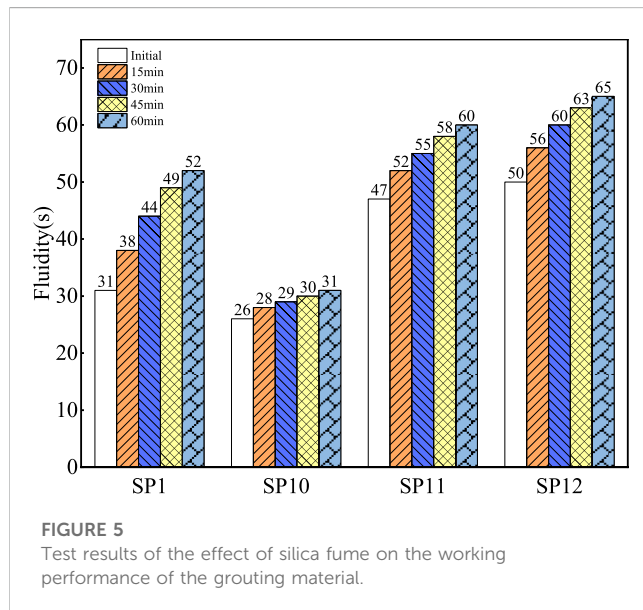| Number	Cement	Silica fume	Water
SP1	1,660	0	465
SP10	1593.6	66.4	465
SP11	1,577	83	465
SP12	1560.4	99.6	465

FIGURE 5
Test results of the effect of silica fume on the working performance of the grouting material.

performance of the grouting, and can significantly reduce the loss of the fluidity of the grouting material over time. When the content of silica fume increased from 4 wt% to 6 wt%, the initial fluidity of the grouting material increased from 26 to 50 s, an increase of 92%. The fluidity of the grouting material increased from 31 to 65 s at 60 min, an increase of 109%. The working performance of the grouting material is very sensitive to the change of the silica fume content, and excessive silica fume will seriously inhibit the working performance of the grouting material. Therefore, the content of silica fume in the grouting material needs to be strictly controlled, otherwise the working performance of the grouting material will be severely inhibited.

3.1.4 Effect of fly ash, limestone powder and silica fume on rheological properties of the grouting material

Figure 6 is the relationship curve between shear stress and shear rate of pure cement grouting and mixed with different amounts of fly ash, silica fume and limestone powder grouting material drawn using the data measured by the rheometer. It can be seen from Figure 6 that there is an obvious positive correlation between the shear stress and the shear rate of the grouting material. From the curve of shear stress and shear rate of cement paste, it can be seen that when the shear rate is low, the shear stress increases rapidly. But with the further increase of the shear rate, the growth rate of the

shear stress gradually slows down. The rheological curve of pure cement grouting material can fit well with the modified Binghan model, where R2 can reach 0.97. The relationship between shear stress and shear rate can be described by fitting Eq. 1.

$$\tau = -0.0033\gamma^2 + 0.40\gamma + 41.30, \quad R^2 = 0.97 \quad (1)$$

When 10 wt% fly ash was added to the grouting material, the rheological properties of the grouting material changed significantly. When the shear rate is constant, the shear stress of the grouting mixed with 10 wt% fly ash is significantly smaller than that of the pure cement grouting. There is also an obvious positive correlation between the shear stress and the shear rate of the grouting material mixed with 10 wt% fly ash. Similar to the pure cement grouting material, the rheological curve of the grouting material mixed with 10 wt% fly ash can also fit the modified Binghan model very well, in which R2 can reach 0.99. Therefore, the relationship between the shear stress and the shear rate of the grouting material mixed with 10 wt% fly ash can be described by the fitting Eq. 2.

$$\tau = -0.0023\gamma^2 + 0.33\gamma + 33.30, \quad R^2 = 0.99 \quad (2)$$

When adding 10 wt% limestone powder to the grouting material, the rheological properties of the grouting material also changed significantly. When the shear rate is constant, the shear stress of the grouting material mixed with 10 wt% limestone powder is smaller than the shear stress of the pure cement grouting material and the grouting material mixed with 10 wt% fly ash. The shear stress and shear rate of the same grouting material mixed with 10.0 wt% limestone powder also have a significant positive correlation. The rheological curve of the grouting material can also fit well with the modified Binghan model, where R2 can reach 0.99. Therefore, the relationship between the shear stress and the shear rate of the grouting material mixed with 10 wt% fly ash can be described by the fitting Eq. 3.

$$\tau = -0.0012\gamma^2 + 0.30\gamma + 30.57, \quad R^2 = 0.99 \quad (3)$$

When adding 5 wt% silica fume to the grouting material, the rheological properties of the paste changed significantly. When the shear rate is constant, the shear stress of the grouting material mixed with 5 wt% silica fume is significantly greater than that of the pure grouting material, grouting material mixed with 10 wt% fly ash and grouting material mixed with 10 wt% limestone powder. The rheological curve of the grouting material can also fit well with the modified Binghan model, where R2 can reach 0.99. Therefore, the relationship between the shear stress and the shear rate of the grouting material mixed with 10 wt% fly ash can be described by the fitting Eq. 4.

$$\tau = -0.0045\gamma^2 + 0.47\gamma + 53.40, \quad R^2 = 0.99 \quad (4)$$

Combining the above four fitting equations, it can be known that mixing fly ash and limestone powder into grouting material will significantly improve the rheological properties of grouting material. When 10 wt% fly ash is added to the grouting material, the apparent viscosity and yield stress of the grouting material are reduced from 0.40 Pa·s and 41.3 Pa to 0.33 Pa·s and 33.3 Pa, reduced by 17.5% and 19.4%. This may be due to the fact that the spherical structure of fly ash reduces the friction between grouting material. Compared with the pure cement grouting the apparent viscosity and yield stress are
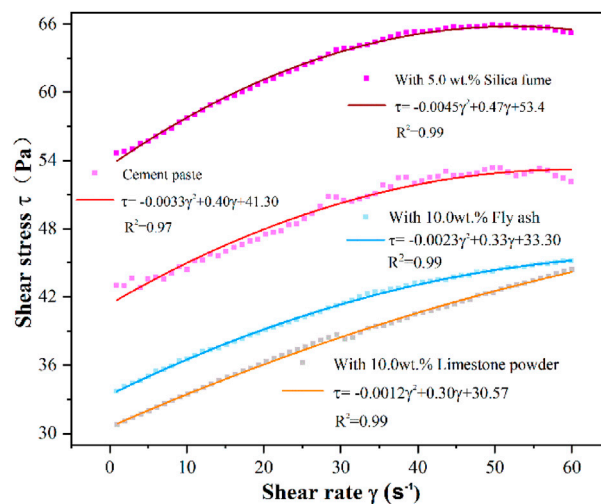
FIGURE 6
Effect of fly ash, silica fume and limestone powder on rheological properties of the grouting material.

reduced by 25% and 26% when 10 wt% of limestone powder is added to the grouting material. However, when adding 5 wt% silica fume, the apparent viscosity and yield stress of the grouting increased significantly. Compared with the pure cement grouting, the apparent viscosity and yield stress of the grouting increased from 0.40 Pa·s and 41.3 Pa to 0.47 Pa·s and 53.4 Pa, which increased by 17.5% and 30%. Therefore, the incorporation of fly ash and limestone powder can improve the working performance of the grouting material, while silica fume can reduce the rheological properties of the grouting material.

3.2 Effect of mineral admixture on mechanical properties of the grouting material

3.2.1 Effect of fly ash on mechanical properties of the grouting material

Figure 7A reflects the 3, 7, and 28 days flexural strength of pure cement grouting material and grouting material mixed with different proportions of fly ash. It can be seen from Figure 7A that the 3, 7, and 28 days flexural strength of pure cement grouting material (SP1) is higher than that grouting material with fly ash. Compared with pure cement grouting material, when the fly ash content is 10 wt%, 20 wt%, 30 wt%, 40 wt% and 50 wt%. The 3 days flexural strength of the grouting material is reduced by 13.33%, 28.33%, 38.33%, 48.33% and 55%, respectively; The 7 days flexural strength of the grouting material is reduced by 12.79%, 23.26%, 32.56%, 40.70% and 47.67%, respectively; The 28 days flexural strength of the grouting material is reduced by 11.65%, 23.30%, 32.04%, 39.81% and 48.54%, respectively; It can be seen that with the increase of the amount of fly ash, the flexural strength of the grouting material gradually decreases, and the influence of the addition of fly ash on the early strength of the grouting material is more significant.

Figure 7B reflects the 3, 7, and 28 days compressive strength of pure cement grouting material and grouting material mixed with different proportions of fly ash. It can be seen from Figure 7B that the 3, 7, and 28 days compressive strength of pure cement grouting material (SP1) is higher than that grouting material with fly ash. Compared with pure cement grouting material, when the fly ash content is 10 wt%, 20 wt%, 30 wt%, 40 wt% and 50 wt%. The 3 days compressive strength of the grouting material is reduced by 10.54%, 18.50%, 27.17%, 35.36% and 41.90%, respectively; The 7 days compressive strength of the grouting material is reduced by 11.58%, 20.36%, 28.74%, 37.92% and 44.91%, respectively; The 28 days compressive strength of the grouting material is reduced by 9.13%, 19.66%, 28.02%, 36.22% and 43.81%, respectively; It can be seen that with the increase of the content of fly ash, the compressive strength of the grouting material gradually decreases.

In summary, the addition of fly ash will reduce the mechanical properties of the grouting material, but when the content is small (less than 10%), it has little effect on the mechanical properties. And the mechanical properties of the grouting material increase significantly with age.

3.2.2 Effect of limestone powder on mechanical properties of the grouting material

Figure 8A reflects the 3, 7 and 28 days flexural strength of pure cement grouting material and grouting material mixed with different proportions of limestone powder. It can be seen from Figure 8A that the 3 days, 7, and 28 days flexural strength of pure cement grouting material (SP1) is higher than that grouting material with limestone powder. Compared with pure cement grouting material, when the limestone powder content is 5 wt%, 10 wt%, and 20 wt%. The 3 days flexural strength of the grouting is reduced by 5.00%, 20.00% and 31.67%, respectively; The 7 days flexural strength of the grouting is reduced by 3.59%, 10.38% and 24.75%, respectively; The 28 days flexural strength of the grouting is reduced by 5.82%, 15.53% and
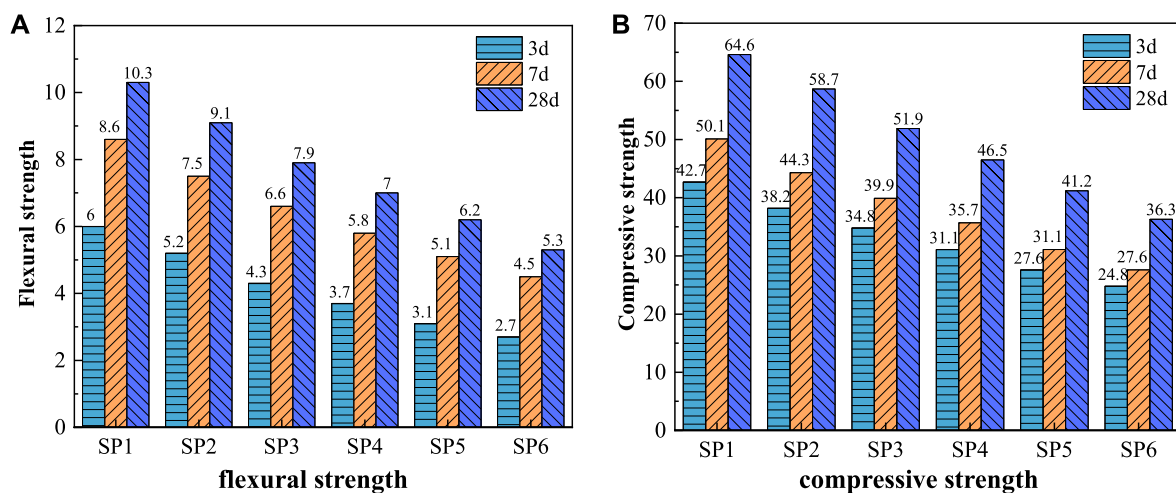
FIGURE 7
Mechanical properties of the grouting material mixed with fly ash. **(A)** flexural strength; **(B)** compressive strength.
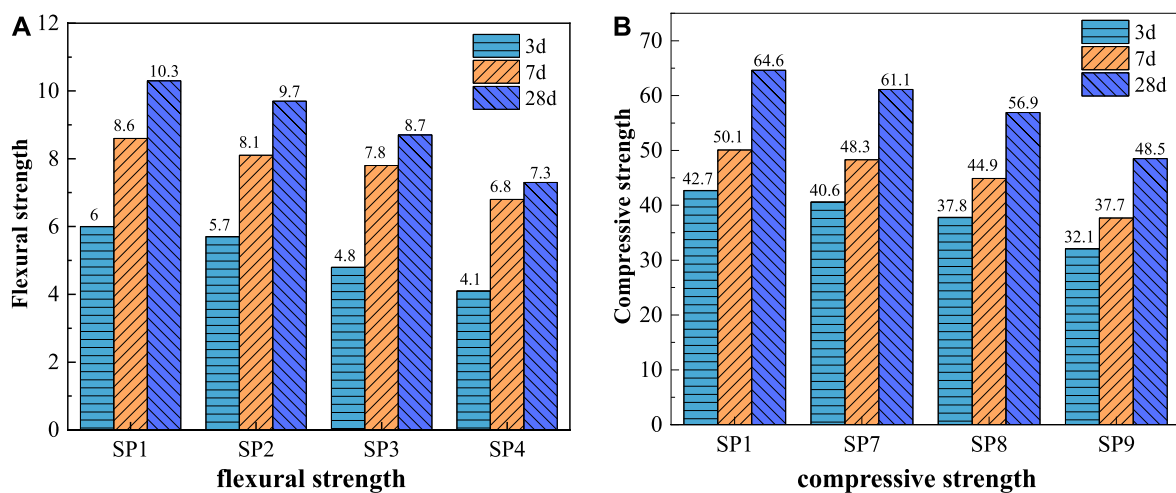

FIGURE 8
Mechanical properties of the grouting material mixed with limestone powder. **(A)** flexural strength; **(B)** compressive strength.

29.13%, respectively; It can be seen that with the increase of the amount of limestone powder, the flexural strength of the grouting material gradually decreases. However, when the amount of limestone powder is less (5 wt%), the flexural strength of the grouting material is only reduced by about 5%.

Figure 8B reflects the 3, 7, and 28 days compressive strength of pure cement grouting material and grouting material mixed with different proportions of limestone powder. It can be seen from Figure 8B that the 3, 7, and 28 days compressive strength of pure cement grouting material (SP1) is higher than that grouting material with limestone powder. Compared with pure cement grouting material, when the limestone powder content is 5 wt%, 10 wt%, and 20 wt%. The 3 days compressive strength of the grouting is

reduced by 4.92%, 11.48% and 24.82%, respectively; The 7 days compressive strength of the grouting is reduced by 3.59%, 9.30% and 24.75%, respectively; The 28 days compressive strength of the grouting is reduced by 5.42%, 11.92% and 24.92%, respectively; It can be seen that with the increase of the content of limestone powder, the compressive strength of the grouting material gradually decreases.

In summary, the addition of limestone powder will reduce the mechanical properties of the grouting material, but when the content is small (5%), it has little effect on the mechanical properties of the grouting material. The mechanical properties of the grouting material will increase significantly with age.
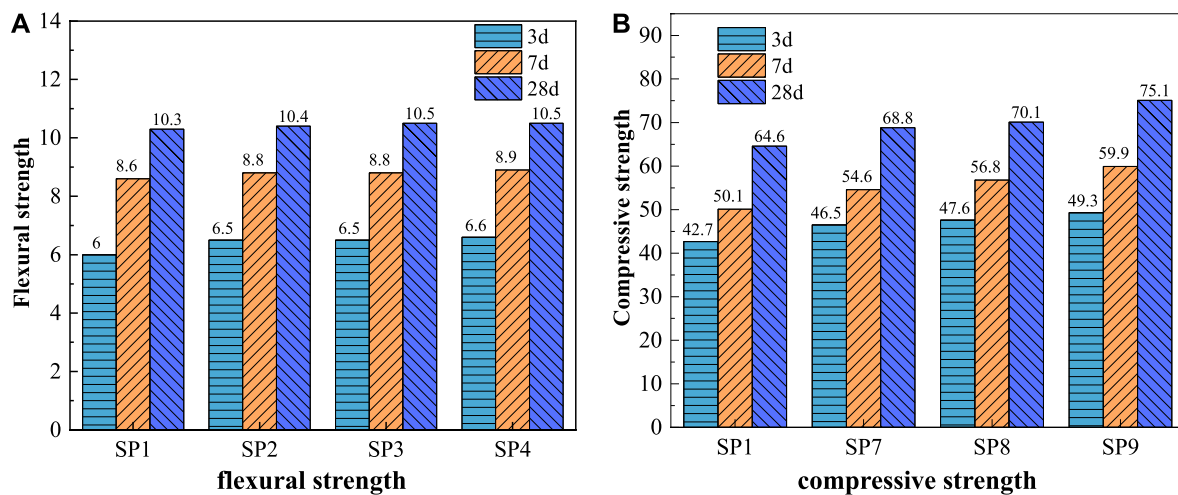
FIGURE 9
Mechanical properties of the grouting material mixed with silica fume. **(A)** flexural strength; **(B)** compressive strength.

3.2.3 Effect of silica fume on mechanical properties of the grouting material

Figure 9A reflects the 3, 7, and 28 days flexural strength of pure cement grouting material and grouting material mixed with different proportions of silica fume. It can be seen from Figure 9A that the 3, 7, and 28 days flexural strength of pure cement grouting material (SP1) is lower than that grouting material with silica fume. Compared with pure cement grouting material, when the silica fume content is 4 wt%, 5 wt%, and 6 wt%. The 3 days flexural strength of the grouting material is increased by 8.33%, 8.33% and 10.00%, respectively; The 7 days flexural strength of the grouting is increased by 2.33%, 2.33% and 3.49%, respectively; The 28 days flexural strength of the grouting is increased by 0.97%, 1.94% and 1.94%, respectively; It can be seen that the increase of silica fume content can promote the development of the early flexural strength of the grouting material, but has little effect on the later strength of the grouting material.

Figure 9B reflects the 3, 7, and 28 days compressive strength of pure cement grouting material and grouting material mixed with different proportions of silica fume. It can be seen from Figure 9B that the 3, 7, and 28 days compressive strength of pure cement grouting material (SP1) is lower than that grouting material with silica fume. Compared with pure cement grouting material, when the silica fume content is 4 wt%, 5 wt%, and 6 wt%. The 3 days compressive strength of the grouting material is increased by 8.90%, 11.48% and 15.46%, respectively; The 7 days compressive strength of the grouting material is increased by 8.98%, 13.37% and 16.36%, respectively; The 28 days compressive strength of the grouting material is increased by 6.50%, 8.51% and 16.25%, respectively; It can be seen that as the content of silica fume increases, the compressive strength of the grouting material increases gradually.

In summary, silica fume can improve the mechanical properties of grouting material, and with the increase of silica fume content, the effect of improving the compressive strength of grouting material is more significant.

4 Discussion

At the present stage, the adjustment of the water binder ratio of the grouting material is limited between 0.26 and 0.28. Which can effectively avoid the bleeding phenomenon of the grouting material and improves the early strength of the grouting material (Song et al., 2014b; Gao et al., 2022). With the decrease of the water binder ratio of the grouting material. The requirements of all kinds of new grouting material are getting higher and higher, which promotes the grouting matierial construction technology constantly updated and improved (Shi, 2020). Grouting materials mixed with appropriate amount of admixtures, such as fly ash, silica fume, limestone powder, etc., can fully meet the needs of mechanical properties and working properties in the current construction. Therefore, the demand for the admixture of the grouting matierial is getting lower and lower. In some special cases that must be mixed with admixture. It should be considered to use good compatibility with the grouting or cement, low chloride, nitrite content, can ensure good grouting mobility, no bleeding and can meet the requirements of mechanical strength specification and construction (Cheng et al., 2014; Yang, 2020). Mineral admixture should be grade I fly ash, slag or silica fume, and the quality should meet the standard requirements. Mineral admixture should be selected according to the engineering needs, and the materials conducive to improve the fluidity and stability of the grouting material should be selected (Xiang et al., 2018). The mixing water shall not contain substances harmful to prestressed tendons or cement. Test and construction of the water source must be tested in the water source and can be used only after meeting the requirements.

5 Conclusion

This paper systematically studies the influence of different contents of fly ash, limestone powder and silica fume on the

working performance and mechanical properties of the grouting material, and the main conclusions are as follows:

(1) Fly ash and limestone powder can effectively improve the working performance of the grouting and reduce the loss of fluidity of the grouting material over time, and the effect of fly ash is the most significant. Compared with the pure cement grouting material, the initial fluidity and 60 mins fluidity of the grouting material mixed with 40 wt% fly ash are reduced by 35.5% and 53.8%. The initial fluidity and 60 mins fluidity of the grouting material mixed with 5 wt % limestone powder decrease by 30% and 41%. But when the fly ash content is 50 wt% and the limestone powder content is 10 wt%, the working performance of the grouting material begins to decrease.

(2) Adding 4 wt% silica fume can improve the working performance of the grouting material, and the initial fluidity and 60 min fluidity of the grouting are reduced by 16% and 41%. However, as the content of silica fume increases, the working performance of the grouting will be significantly reduced, and the fluidity of the grouting will be increased over time.

(3) Fly ash and limestone powder mixed into grouting will significantly improve the rheological properties of the grouting material, but silica fume will reduce the rheological properties of grouting material. Compared with the pure cement grouting material, the apparent viscosity and yield stress of the grouting material mixed with 10 wt% fly ash decreased by 17.5% and 19.4%, respectively; The apparent viscosity and yield stress of the grouting mixed with 10 wt % limestone powder decreased by 25% and 26%, respectively. But mixed with 5 wt% silica fume, the apparent viscosity and yield stress of the grouting increase significantly. Compared with the pure cement grouting material, the apparent viscosity and yield stress of the grouting material mixed with 5 wt% silica fume increase by 17.5% and 30%, respectively.

(4) The addition of fly ash and limestone powder will reduce the mechanical properties of the grouting material. Compared with the pure cement grouting material, the 28 days compressive strength of the grouting material with 10 wt% fly ash is reduced by 9% and the flexural strength is reduced by 12%; The 28 days compressive strength of the grouting material with 4 wt% limestone powder is reduced by 4.5% and the flexural strength is reduced by 6%. With the increase of the content

of fly ash and limestone powder, the mechanical properties of the grouting material tended to decrease gradually.

(5) The addition of silica fume can improve the mechanical properties of the grouting material. Compared with pure cement grouting, the 28 days compressive strength of 4 wt% silica fume grouting material is increased by 6.5%, and the 28 days flexural strength is increased by 1%. With the increase of silica fume content, the mechanical properties of the grouting material tend to increase gradually, especially the increase of compressive strength is the most obvious.

Data availability statement

The original contributions presented in the study are included in the article/Supplementary Material, further inquiries can be directed to the corresponding author.

Author contributions

All authors listed have made a substantial, direct, and intellectual contribution to the work and approved it for publication.

Conflict of interest

The authors declare that the research was conducted in the absence of any commercial or financial relationships that could be construed as a potential conflict of interest.

Publisher's note

All claims expressed in this article are solely those of the authors and do not necessarily represent those of their affiliated organizations, or those of the publisher, the editors and the reviewers. Any product that may be evaluated in this article, or claim that may be made by its manufacturer, is not guaranteed or endorsed by the publisher.

References

Ba, W. (2018). Research on formulation and performance of high-performance pore grouting agent. *Highw. Traffic Technol. Appl. Technol. Ed.* 14 (04), 132–135.

Chen, J., Liu, F., Bai, X., Wang, D., and Wang, J. (2020). Effect of aerogels on properties of sleeve grouting materials. *Tianjin Constr. Sci. Technol.* 30 (6), 49–50.

Cheng, P., Song, X., Li, B., and Hu, S. (2014). Effect of plastic expansion agent on the volume deformation and submicroscopic structure of pre-stressed duct grouting materials. *Bull. Chin. Ceram. Soc.* 33 (6), 1329–1335.

Feng, X., and Wang, W. (2012). Influence of rotational speed on slurry properties of prestressed channels. *J. China & Foreign Highw.* 32 (05), 173–176.

Gao, Y., Ma, P., Kang, S., Cheng, B., Yang, W., Gu, X., et al. (2022). Dynamic evolution of the plastome in the Elm family (Ulmaceae). *Metal. Mine* 51 (1), 14–20. doi:10.1007/s00425-022-04045-4

Guan, X., and Zhong, Q. (2013). Research on the performance of micro-fine cement-based grouting material and its engineering application. *Saf. Coal Mines* 44 (6), 142–145.

He, X., Yang, J., Niu, M., Zhang, G., and Li, G. (2023). Study on expansion effect and hydration characteristics of ultra-high strength cement-based grouting materials based on humidity compensation. *Case Stud. Constr. Mater.* 18, e01941. doi:10.1016/j.cscm.2023.e01941

Jtge30-2005.2005-03-03 (2005). *Test code for cement and cement concrete for highway engineering*. British Columbia, Canada: Abe books.

Khan, M., Cao, M., Ai, H., and Hussain, A. (2022). Basalt fibers in modified whisker reinforced cementitious composites. *Period. Polytech. Civ. Eng.* 66 (2), 344–354. doi:10.3311/ppci.18965

Khan, M., Cao, M., Ai, H., and Hussain, A. (2022). Basalt fibers in modified whisker reinforced cementitious composites. *Period. Polytech. Civ. Eng.* 66 (2), 344–354. doi:10.3311/ppci.18965

Khan, M., Cao, M., Xie, C., and Ali, M. (2021). Efficiency of basalt fiber length and content on mechanical and microstructural properties of hybrid fiber concrete. *Fatigue & Fract. Eng. Mater. Struct.* 44 (8), 2135–2152. doi:10.1111/ffe.13483

Li, H., Guan, X., Zhang, X., Ge, P., Hu, X., and Zou, D. (2018). Influence of superfine ettringiteon the properties of sulphoaluminate cement-based grouting mate-rials. *Constr. Build. Mater.* 166 (166), 723–731. doi:10.1016/j.conbuildmat.2018.02.013

Li, Q. (2011). *Research on the properties of super early-strength cement-based grouting*. Harbin, China: Harbin Institute of Technology.

Liu, W., Sun, Y., Meng, X., and Qin, Y. (2023). Experimental analysis of Nano-SiO2 modified waterborne epoxy resin on the properties and microstructure of cement-based grouting materials. *Energy* 268, 126669. doi:10.1016/j.energy.2023.126669

Ma, J., Cheng, Z., Ke, L., Yang, L., Yuan, D., Yang, Y., et al. (2022). Effects of coal gasifier slag on properties of mortar. *Jiangxi Build. Mater.* (05), 27–28+31.

Ma, Z., Xu, D., Feng, L., Chang, Q., and Fu, P. (2021). Effect of gypsum on the properties of pre-stressed duct grouting material. *Concrete* (8), 155–159.

Mou, C., Cheng, K., Liu, R., Jia, E., Sun, H., Niu, T., et al. (2022). Cooperative optimization of mineral admixtures of cement-based grouting materials for semi-flexible pavement. *Bull. Chin. Ceram. Soc.* 41 (3), 1102–1112.

Sha, F., Fan, R., Gu, S., and Xi, M. (2023). Strengthening effect of sulphoaluminate cementitious grouting material for water-bearing broken rocky stratum. *Constr. Build. Mater.* 368, 130390. doi:10.1016/j.conbuildmat.2023.130390

Shi, Y. (2020). Application and mechanism analysis of CSA expansion agent in grouting material. *New Build. Mater.* 47 (11), 134–137.

Shu, B., Zhou, M., Yang, T., Li, Y., Song, P., Chen, A., et al. (2021). Performance study and engineering application of grouting materials with a large content of solid waste. *Constr. Build. Mater.* 312, 125464. doi:10.1016/j.conbuildmat.2021.125464

Shu, B., Zhou, M., Yang, T., Li, Y., Song, P., Chen, A., et al. (2021). Performance study and engineering application of grouting materials with a large content of solid waste. *Constr. Build. Mater.* 312, 125464. doi:10.1016/j.conbuildmat.2021.125464

Song, X., Li, B., and Chen, M. (2014). Study on the influencing factors of properties of pre-stressed duct grouting material. *Concrete* (09), 138–141.

Song, X., Li, B., and Chen, M. (2014). Study on the influencing factors of properties of pre-stressed duct grouting material. *Concrete* (09), 138–141.

Standardization Administration of China (2009). *Testing method for strength of cement mortar (ISO method)*. Beijing, China: State Administration of Market Supervision and Administration; Standardization Administration of China.

Sun, Y., Huo, M., and Chen, X. (2020). Experimental study on a prestressed passage grouting material for negative temperature railway. *New Build. Mater.* 47 (9), 123–126.

Tan, X., Wu, X., Yang, J., Zhao, J., Zeng, H., and Liang, C. (2022). Effects of granite waste powder on the performance of cement mortar. *China Concr. Cem. Prod.* (10), 96–100.

Wang, H., Wang, C., Li, W., Zhang, B., Jiang, B., Yin, H., et al. (2022). Study on the preparation and performance of high strength grouting materials. *China Concr. Cem. Prod.* (9), 66–69.

Wang, L., and Zhang, S. (2017). Research of high fluidity grouting material of post-tensioned prestressed girder. *Constr. Technol.* 46 (5), 59–65121.

Xiang, J., Liu, L., Cui, X., He, Y., Zheng, G., and Shi, C. (2018). Effect of limestone on rheological, shrinkage and mechanical properties of alkali–Activated slag/fly ash grouting materials. *Constr. Build. Mater.* 191 (166), 1285–1292. doi:10.1016/j.conbuildmat.2018.09.209

Xie, C., Xie, C., Cao, M., Si, W., and Khan, M. (2020). Experimental evaluation on fiber distribution characteristics and mechanical properties of calcium carbonate whisker modified hybrid fibers reinforced cementitious composites. *Constr. Build. Mater.* 265, 120292. doi:10.1016/j.conbuildmat.2020.120292

Yang, H., Wu, W., Chen, D., Ye, X., Guo, Z., and Yao, T. (2019). Effect of expansive agent on the restrained expansion rate of duct grouting material. *New Build. Mater.* 46 (7), 56–59.

Yang, Y. (2020). Research on grouting defects of prestressed tunnel based on impact-echo method. *Journal of Shenyang Jianzhu University (Nat. sci.)* 36 (03), 457–464.

Zhang, H., Li, G., and Li, X. (2020). Study on the duct grouting materia with orthogonal experiment. *Low. Temp. Archit. Technol.* 42 (02), 21–23+52.

Zhang, P., Su, Y., Fan, J., Feng, H., Shao, J., Guo, H., et al. (2021). Experimental research on the mechanical behavior of grouted sleeves with fiber-reinforced grouting material under cyclic loading. *Structures* 34, 2189–2204. doi:10.1016/j.istruc.2021.08.083

Zhang, X., Wu, M., and Hu, X. (2019). The effect of catalyst on mechanical properties of polyurethane/water glass grouting materials. *Min. Res. Dev.* 39 (10), 31–36.

Frontiers in
Materials

Investigates the discovery and design of materials for future application

A multidisciplinary journal that explores the breadth of materials science, engineering and mechanics - from carbon-based materials to smart materials.

Discover the latest Research Topics

See more →

frontiers

Frontiers in
Materials

frontiers | Research Topics